Universitat Autònoma de Barcelona

Molecular Mechanisms Underlying the Role of SynGAP in Cognition and Synaptopathies

Gemma Gou Alsina

Molecular Mechanisms Underlying the Role of SynGAP in Cognition and Synaptopathies

Gemma Gou Alsina

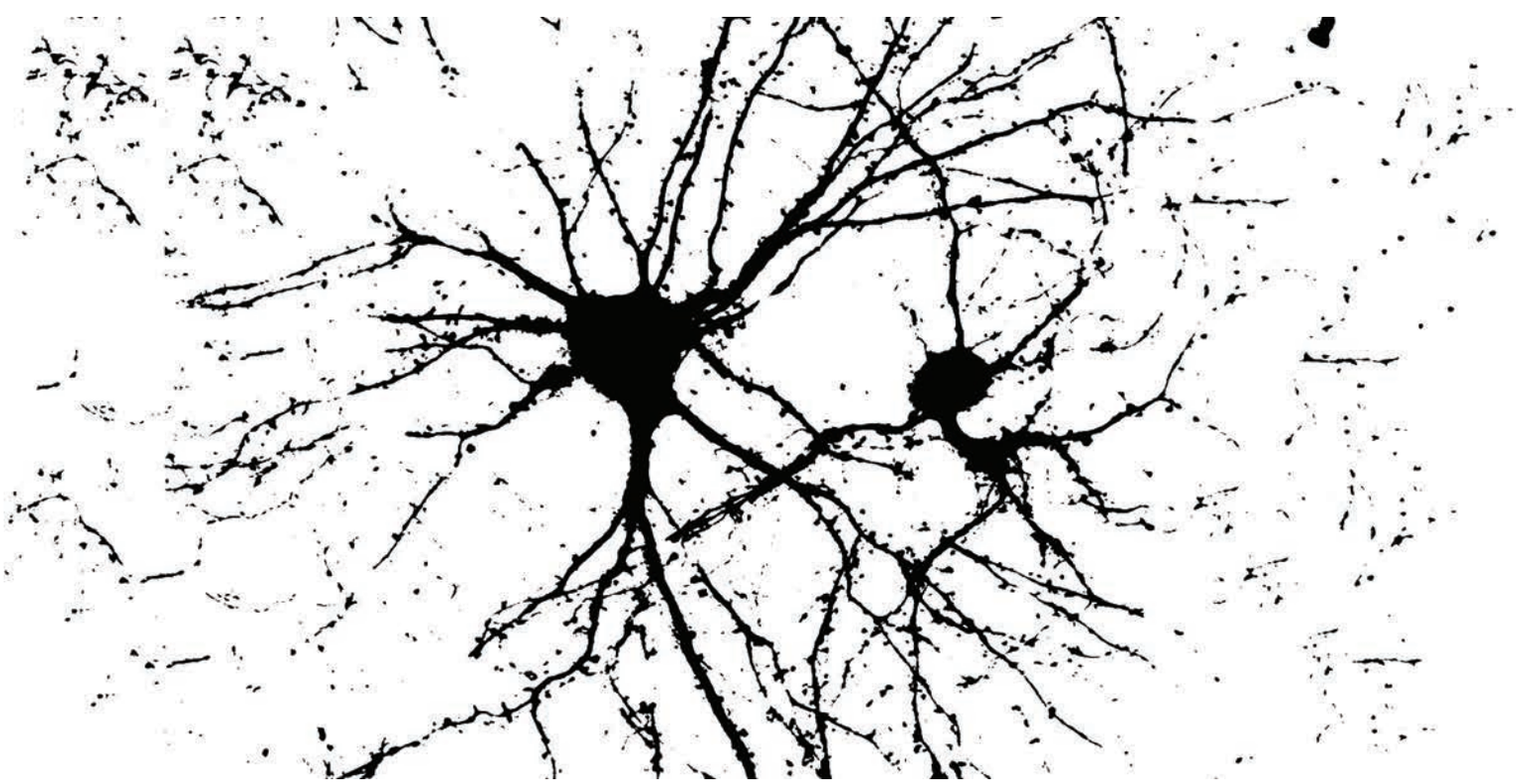

Neuroscience Doctoral Program
Molecular physiology of the Synapse laboratory
IIB & IR Hospital de la Santa Creu i Sant Pau
Universitat Autònoma de Barcelona 2019

Molecular Mechanisms Underlying the Role of SynGAP in Cognition and Synaptopathies

Gemma Gou Alsina, MSc

PhD thesis

Supervised by Àlex Bayés Puig, PhD

Tutored by Carlos Alberto Saura Antolín, PhD

A thesis submitted for the degree of Doctor of Philosophy in Neurosciences

Neuroscience Doctoral Program from Institut de Neurociències (INc)

Molecular Physiology of the Synapse laboratory

IIB & IR Hospital de Sant Pau i de la Santa Creu

Universitat Autònoma de Bercelona

Àlex Bayés Puig Carlos A. Saura Antolín Gemma Gou Alsina

Bellaterra, April 2019

To my parents, Ramon and Mercè

To Magda, Joan, Quim, Josep and Ramon

To all other relatives and friends

To SYNGAP1 patients

“Like the entomologist in search of colourful butterflies, my attention has chased in the gardens of the grey matter cells with delicate and elegant shapes, the mysterious butterflies of the soul, whose beating of wings may one day reveal to us the secrets of the mind.”

Santiago Ramón y Cajal

THESIS FOUNDING

The present thesis has been conducted through the support of the Spanish Government concession *Formación de personal investigador* (FPI) with reference BES-2013-063720 and short-term fellowship fund research exchanges of up to four months in The Scripps Research institute with reference EEBB-I-17-11996, both from *Ministerio de Economía y Competitividad* (MINECO).

CONSIDERATIONS OF THE THESIS STRUCTURE

The present thesis is structured in ten main parts. First, the ‘Summary’ of the results obtained and the corresponding translation in Catalan. Second, there is a general Introduction of the topic divided into six main points to contextualize the data presented in the present thesis. The ‘Objectives’ of the present thesis precede a ‘General Material and Methods’ section. Then, ‘Chapter I’, ‘Chapter II’ and an ‘Annex’ will be presented. In each of these thematic blocks, there is a specific brief ‘Introduction’, ‘Materials and Methods’, ‘Results’ and corresponding ‘Discussion’ sections. It is worth noting that the ‘General Materials and Methods’ section is structured in four core blocks related to biological, genomic, proteomic and downstream bioinformatic analyses of the data. This structure will also be presented in ‘Material and Methods specific to each Chapter or Annex’. The central topic of Chapter I and II is related to the study of SynGAP neurobiology, although with a different perspective. In the first case, refers to the study of SynGAP neurobiology in normal developmental states, whereas in the other case relates to study the role of SynGAP in disease. Subsequently, is presented the ‘Conclusions’ section of the present thesis associated to findings from Chapter I and II. In addition, there is an Annex related to the development of a *Shank2* conditional mouse model for genetic rescue experiments. Finally, a list of articles published resulting from collaborations with other research groups in the context of the present thesis and the ‘Bibliography’ section are also shown.

INDEX

INDEX OF FIGURES

FIGURES FROM INTRODUCTION

FIGURES FROM MATERIALS AND METHODS

FIGURES FROM RESULTS

FIGURES FROM DISCUSSION

INDEX OF TABLES

TABLES FROM INTRODUCTION

TABLES FROM MATERIALS AND METHODS

TABLES FROM RESULTS

ABBREVIATIONS & SYMBOLS

ABBREVIATIONS

aa Amino acid

AAIDD American Association on Intellectual and Developmental Disabilities

AAV Adeno-associated virus

ABP Actin binding protein

ACN Acetonitrile

AcNa Acetate sodium

Actb *β-Actin*

ADHD Attention deficit hyperactivity disorder

ADP Adenosine diphosphate

AGC automatic gain control

AKAPs A-kinase-associated proteins

AKT AKT serine/threonine kinase

AMPA α-amino-3-hidroxi-5-metilo-4-isoxazolpropiónico

AMPAR AMPA receptor

AmpR Ampicillin resistance

ANOVA Analysis of Variance

APA American Psychological Association

AQUA Absolute quantification

ARP Actin-Related Protein

AS Alternative splicing

ASD Autism spectrum disorder

ASN Asparagine

ATP Adenosine triphosphate

AU Arbitrary units

AUC Area under de curve

BA Bicarbonate ammonic

BAC Bacterial artificial chromosome

BGS Brain growth spurt

BLAST Basic local alignment search tool

BP Biologic Process

BSA Bovine serum albumin

CA *Cornus Ammon*

Ca^{2+} Calcium

CaM Calmodulin

CAMK Ca^{2+}/calmodulin-dependent kinase

cAMP Cyclic adenosine monophosphate

CAZ Cytomatrix active zone

CC Coiled coil

CC Cellular Component

cDNA Complementary DNA

CKII Casein kinase 2

CNS Central Nervous System

CNV Copy number variations

COOH Carboxylic acid

Crb Cerebellum

CREB cAMP response element-binding

C-term C-terminal

Ct Cycle quantification value

Ctx Cortex

Cyfip Cytoplasmic FMR1-interacting protein

Da Dalton

DAG Diacylglycerol

DAPI 4′,6-diamidino-2-phenylindole

DAVID Database for Annotation, Visualization and Integrated Discovery

DG *Dentate gyrus*

DGN *Dentate gyrus* granule neurons

DIG Digested

DIV Day *in vitro*

DLG Discs large homolog

DLGAP Disk large associated guanylate-associated protein

DLGAP Disks large-associated protein

DMEM Dulbecco's Modified Eagle's Medium

DNA Deoxyribonucleic acid

dNTP Deoxyribonucleotide triphosphate

DOC Deoxycholate

DSM Diagnostic and Statistical Manual of Mental Disorders

DSMIV-TR Diagnostic and Statistical Manual of Mental Disorders IV- Text Revised

DTA Diphtheria Toxin A

DTT Dithiothreitol

E Elute

E. coli *Escherichia coli*

e.g., *Exempli gratia* (for example)

E/I Excitatory/inhibitory

ECM Extracellular matrix

EDTA Ethylenediaminetetraacetic acid

EGTA Egtazic acid

E-LTD Early long-term depression

E-LTP Early long-term potentiation

EM Electronic microscopy

EMBL-EBI European Bioinformatics Institute

ENSMUST Ensembl Mus Musculus transcript

EPSC Excitatory postsynaptic current

ER Endoplasmic reticulum

ERK Extracellular signal-regulated kinase

ESC Embryonic stem cell

ESI Electrospray ionization

EST cDNA expressed sequence tag

et al. *Et alia* (and others)

EtOH Ethanol

EZ Endocytic zone

FBS Fetal bovine serum

FC Fold Change

FDR False discovery rate

Fig. Figure

Flp Flippase recombinase

Fmol Femtomole

FRT Flp recombinase target

FT Flow-through

FUS Fused in Sarcoma protein

FXS Fragile X-syndrome

FzzR Frizzled receptors

GABA γ-aminobutyric acid

GABAR GABA receptor

GAD Glutamate decarboxylase

GAP GTPase-activating protein

GAPDH Glyceraldehyde-3-phosphate dehydrogenase

GC Genome copies

GC-content Guanine-cytosine content

GDD Global Developmental Delay

GDI Guanine nucleotide dissociation inhibitors

gDNA Genomic DNA

GDP Guanosine diphosphate

GEF Guanine nucleotide exchange factor

GFP Green fluorescent protein

GluA AMPAR subunit

GluD iGluR delta subunit

GluN NMDRA subunit

GluR Glutamate receptors

GO Gene ontology

GSK-3β Glycogen synthase kinase *3β*

GTP Guanosine triphosphate

H Homogenate

h Hour

Hdg Hedgehog

HET Heterozygous

Hip Hippocampus

HOMO Homozygous

HPLC High performance liquid chromatography

hPSD Human post-synaptic densities

IAA Iodoacetamide

IACUC Institutional Animal Care and Use Committee

IB Immunoblot

ID Inner diameter

ID Intellectual disability

i.e *Id est* (that is)

iGluR Ionotropic GluR

IND Induced

IP Immunoprecipitation

I.p Intraperitoneal

IP_3R Inositol triphosphate receptor

IQ Intelligence quotient

IRES Internal ribosome entry site

IU Intensity units

JAK Janus kinase

JNK Jun Nuclear Kinase

KCC2 Neuronal K-Cl cotransporter 2

KCl Potassium chloride

KCNQ Potassium voltage-gated channel

KEGG Kyoto Encyclopedia of Genes and Genomes

KH_2PO_4 Potassium phosphate monobasic

KI Knock-in

KO Knock-out

LB Luria-Bertani broth

LC Liquid chromatography

LC Low-complexity

LC-MS Liquid chromatography- mass spectrometry

LC-MS/MS Liquid chromatography- tandem mass spectrometry

LIMK LIM domain kinase

L-LTD Late long-term depression

L-LTP Late long-term potentiation

LNSXY LoxSTOPNeoR with fragments X and Y

LOF Loss-of-function

logFC Logarithmic fold change

LoxP Locus of Crossover in P1

LR-PCR Long range PCR

LTD Long-term depression

LTP Long-term potentiation

LTQ Linear trap quadrupole

L-VDCC L-type voltage-dependent Ca2+ channels

M Molar

m/z Mass to charge ratio

MAGUK Membrane-associated guanylate kinase

MALDI Matrix-assisted laser desorption

MAPK Mitogen-activated protein kinase kinase

MAPKKK MAP kinase kinase kinase Mitogen-activated protein kinas

Mw Molecular weight

MASC MAGUK associated signaling complex

MASCOT Modular Approach to Software Construction Operation and Test

MECP2 Methyl CpG binding protein 2

MEF Mouse embryonic fibroblasts

MEF-2 Myocyte enhancer factor-2

MEK Mitogen-activated protein kinase kinase

MEKK Mitogen-activated protein kinase kinase kinase

mEPSC Mini excitatory postsynaptic current

mGluR Metabotropic GluR

mGluR-LTD mGluR-dependent long-term depression

min Minute

MPD Multiple phosphorylation domain

mRNA Messenger RNA

MS Mass spectrometry

MS1 First mass spectrometer

MS2 Second mass spectrometer

mTOR Mammalian target of rapamycin

MUPP1 Multiple PDZ domain

Na_2HPO_4 Disodium phosphate

$Na_4P_2O_7$ Sodium pyrophosphate

NaCl Sodium Chloride

NaOH Sodium Hydroxide

NCBI National Centre for Biotechnology Information

NDD Neurodevelopmental disorder

NeoR Neomycin resistance

NF1 Neurofibromatosis type 1

NH_2 Amide

NIH National Institutes of Health

NKCC1 Bumetanide-sensitive sodium-(potassium)-chloride cotransporter 1

NLM National library of medicine

NMDAR N-Methyl-D-aspartic

NMDAR-LTD NMDAR-dependent long-term depression

NMDAR-LTP NMDAR-dependent long-term potentiation

nNOS Neuronal nitric oxide synthase

NRC NMDAR signaling complex

NS-ADID Non-syndromic autosomal dominant intellectual disability

NS-ARID Non-syndromic autosomal recessive intellectual disability

NS-ASD Non-syndromic autism spectrum disorder

NS-ID Non-syndromic Intellectual disability

NSM Non-synaptic membranes

NS-MD Non-sense mediated decay

NS-XLID Non-syndromic X-linked intellectual disability

NT Neurotransmitters

N-term N-terminal

OB Olfactory bulb

OD Optical density

OMIM Online Mendelian Inheritance in Man

ON Overnight

ORF Open reading frame

P Pellet

PAK p21-activated kinase 2

PBM PDZ domain binding motif

PBS Phosphate Buffered Saline

PCA Principal component analysis

pCAMKII phosphorylated CAMKII

PCR Polymerase chain reaction

pErk Phosphorylated Erk

PGK Phosphoglycerate kinase promoter

PH Pleckestrin homology

PI3K Phosphatidylinositol-4,5-bisphosphate 3-kinas

PKC Protein kinase C

PLC Phospholipase C

PMSF Phenylmethane sulfonyl fluoride

PMS Peptide mass spectra

PND Postnatal day

PONDR Predictor of natural disordered regions

PP1 Protein phosphatase 1

PP2B Protein phosphatase 2B (or Calcineurin)

PPI Protein-protein interactions

ppm Parts per million

PSD Postsynaptic density

PSD-95 Postsynaptic density protein 95

PSM Postsynaptic membrane

PSM Peptide spectra matches

pSynGAP phosphorylated SynGAP

PTBP Polypyrimidine tract-binding protein

PTEN Phosphatase and tensin homolog

PTFE Polytetrafluoroethylene

P-TM Pellet from total membrane

PTM Post-translational modifications

PuroR Puromycin

PVDF Polyvinylidene fluoride

qPCR quantitative PCR

RefSeq Reference sequence

RES Rescued

REVIGO Reduce and visualize gene ontology

RIN RNA integrity number

RNA Ribonucleic acid

ROCK Rho-associated protein kinase

rpm Revolutions per minute

RT Room temperature

RT-PCR Reverse transcription PCR

RyR Ryanodine receptors

S Supernatant

SALM Synaptic adhesion-like molecule

SAM Synaptic cell adhesion molecule

SAP102 Synapse-associated protein 102

S-ASD Syndromic autism spectrum disorder

SCN Sodium channel protein

SC Schaeffer collateral

SCZ Schizophrenia

SD Standard deviation

SDS Sodium dodecyl sulphate

SDS-PAGE Sodium dodecyl sulphate polyacrylamide gel electrophoresis

S.E.M Standard error of the mean

SF Stain free

SHANK SH3 and multiple ankyrin repeat domains

S-ID Syndromic Intellectual disability

SLC Solute carrier family 13 member 5

SMART Simple modular architecture research tool

SNP Single nucleotide polymorphisms

SNP Synaptic non-PSD

SOC SOB containing media

SOV Sodium orthovanadate

SPAR Small regulatory polypeptide of amino acid response

SPSS Statistical Package for the Social Sciences

SRM Selected reaction monitoring

S-Syn Supernatant of Synaptosome

STAT Signal transducer and activator of transcription

Str Striatum

STRING Search tool for the retrieval of interacting genes/proteins

SV40 Simian virus 40

S-XLID Syndromic X-linked intellectual disability

SynGAP Synaptic GTPase activating protein

TAE Tris-acetate-EDTA

Taq *Thermo Aquaticus* DNA polymerase

TARPS Transmembrane receptor proteins

TE Tris EDTA

TEMED N, N, N, N-tetramethylethylene

TERM Terminal

TetR Tetracycline resistance

TF Transcription factor

TFA Trifluoracetic acid

Tg Transgenic

Tm Temperature of melting

TM Total membrane

TMX Tamoxifen

TOF Ionization-time-of-flight

TSC Tuberous sclerosis syndrome

T-TBS Tween Tris-buffered saline

UCSC University of Santa Cruz

UPS Ubiquitin-proteasome system

UV Ultra-violet

V/V Volume/Volume

Ver. Version

Vs. *versus* (against)

W Wash

WT Wild-type

SYMBOLS

α Alpha

~ Approximately

β Beta

Χ Chi-Square

δ Delta

γ Gamma

ʎ Lambda

≤ Less of equal than

µ Micron

≥ More or equal than

± Plus-Minus sign

SUMMARY

Summary

Forebrain postsynaptic densities (PSDs), found in dendritic spines, express more than 2,000 different proteins, endowing neurons with the synaptic plasticity mechanisms required for cognition and behaviour. Some of the most abundant PSD proteins are SynGAP and Shanks. In rodents, like in other mammals, the *Syngap1* gene encodes for different isoforms that vary in their N- and C-termini. Mutations in the *SYNGAP1* gene cause autosomal mental retardation type five (MRD5), which is characterized by intellectual disability (ID) and epilepsy, as well as autistic traits in approximately half of the affected individuals, among other impairments.

The first part of the present thesis focused on the study of SynGAP isoforms during mouse neurodevelopment. Their differential abundance in five different brain regions and four developmental stages were systematically investigated using a variety of molecular approaches that allowed for their relative and absolute quantification. Furthermore, their sub-cellular distribution in similar neurodevelopmental stages and expression in human cortices were studied. This work indicated that out of the six previously unreported SynGAP variants identified *in-silico*, three and one were found expressed at the transcript or protein level, respectively. The expression of SynGAP isoforms carrying three out of the four C-terminal variants was also demonstrated in human cortex. Importantly, this work identified differential spatio-temporal regulation and subcellular distribution of SynGAP isoforms containing α1, α2 and β C-term variants. Specifically, the expression of SynGAP-α1 isoforms was found highly restricted to the PSD, while β isoforms predominated in the cytosolic fraction, even at PND56. Isoforms bearing the α2 C-term showed an intermediate pattern, having a primarily cytosolic location until PND21 but being mainly at the PSD afterwards. Interestingly, SynGAP-β and -γ isoforms could have a leading role in early stages of cortical development, as they were found particularly abundant compared to the other ones.

The second part of this thesis addressed the study of the proteomic alterations derived from *Syngap1* haploinsufficiency in the hippocampal PSD. The rescue of these alterations, as well as the effect of SynGAP ablation, both at PND21, was also investigated in two conditional *Syngap1*$^{+/-}$ mouse lines. These analyses revealed that proteins related to small GTPases, translation and energy production among others, were significantly altered in *Syngap1*$^{+/-}$ mice. In addition, ~83% of the alterations observed could be recovered if normal SynGAP levels were restored at PND21. Yet, some alterations persisted or newly arose in *Syngap1*$^{+/-}$ rescued mice. These alterations were mainly associated to protein processing at endoplasmic reticulum, transport of small molecules and proteasomal degradation. Based on gene set enrichment analyses, the molecular alterations observed after SynGAP rescue would be compatible with a less clinically severe scenario. Lastly, the induction of SynGAP deficit at PND21 resulted in a similar number of altered proteins as in embryonic *Syngap1* haploinsufficiency, yet these two scenarios shared few affected proteins, suggesting a developmental role in the molecular alterations observed in the embryonic deficit of SynGAP.

Finally, the present thesis also includes a series of experiments aimed at developing a *Shank2*$^{+/-}$ mouse model for genetic rescue experiments, as mutations in *SHANK* genes are a potential monogenic cause for ASD and other neurodevelopmental disorders, including ID

SUMMARY IN CATALAN

Les densitats postsinàptiques (DPSs) de les sinapsis en espines dendrítiques expressen més de 2.000 proteïnes, dotant a les neurones de plasticitat sinàptica necessària per a la cognició i el comportament. Algunes de les proteïnes més abundants de la DPS són SynGAP i les Shanks. En ratolins, similar a altres mamífers, el gen *Syngap1* codifica per diferents isoformes que varien en el seu N- i C-terminal. Mutacions en *SYNGAP1* humà causa un forma de retard mental autosòmic de tipus 5 (de l'anglès MRD5), el qual es caracteritza per discapacitat intel·lectual (DI), epilèpsia i en aproximadament un 50% dels casos, trets autistes entre altres alteracions.

La primera part d'aquesta tesi es va centrar en l'estudi de les isoformes de SynGAP durant el desenvolupament de ratolí. Usant diferents mètodes, es va quantificar l'abundància relativa i/o absoluta del total de SynGAP i de les isoformes compostes per les variants C-terminal alpha1, alpha2 o beta en cinc àrees cerebrals i quatre estadis diferents del desenvolupament. A més, es va investigar la seva distribució subcel.lular en edats post-natals similars a les anteriors analitzades, alhora que es va confirmar l'expressió d'aquestes isoformes en escorça d'humans. El conjunt d'aquests experiments varen permetre identificar una regulació espacio-temporal i distribució subcel.lular diferencial de SynGAP i les seves isoformes. L'expressió de SynGAP-α1 era restringida a la PSD, mentre que la variant β predominava en el citosol, fins i tot en edat adulta. Les isoformes compostes d'α2 mostraren un patró d'expressió i distribució intermedi al de les altres variants C-terminal. Concretament, SynGAP-α2 predominava en el citosol fins a dia post-natal 21 (DPN21), a partir d'on la seva expressió seria majoritària en la PSD. Atès que en etapes primerenques del desenvolupament SynGAP-β i -γ s'han trobat expressades amb major abundància en comparació a les altres variants, podrien tenir un rol principal en aquests estadis.

La segona part d'aquesta tesi adreçà l'estudi de les alteracions del proteoma de la PSD derivades de l'haploinsuficiència de *Syngap1* en hipocamp. El rescat d'aquestes alteracions va ser també investigat en ratolins modificats genèticament per a *Syngap1*$^{+/-}$, així com els efectes d'una reducció de SynGAP a la DPS, en ambdós casos a DPN21. Aquests estudis revelaren que els nivells de proteïnes relacionades amb la traducció, la producció d'energia, i les 'small GTPases" entre altres anomalies, estarien significament alterades en ratolins *Syngap1*$^{+/-}$. A més, en recuperar l'expressió normal de SynGAP a partir de DPN21, el ~83% de les alteracions observades van ser revertides. No obstant, algunes alteracions romangueren mentre que altres aparegueren com a conseqüència de la reactivació de *Syngap1* en els ratolins rescatats. Aquestes desregulacions feien referència majoritàriament a processos de proteostasis amb un clínica menys severa que en els ratolins no rescatats. La inducció de la reducció de SynGAP a partir del DPN21 també va resultar en canvis dels nivells d'un nombre similar de proteïnes però amb un baix grau de solapament i efecte aparentment menys deleteri que en el cas de ratolins haploinsuficients des de la embriogènesis.

Finalment, es van dur a terme experiments dirigits a desenvolupar ratolins modificats genèticament per a *Shank2*$^{+/-}$ que alhora permetessin estudis de rescat genètic, ja que mutacions en la família de gens *SHANK* en humans son potencials causes d'autisme monogènic i altres desordres del neurodesenvolupament tals com la DI.

INTRODUCTION

The brain is the most complex organ in the body, which together with the spinal cord forms the central nervous system (CNS). Our daily life requires brain-dependent activities including cognitive tasks, executive decisions, learning, memories and emotions. To achieve these high brain functions is essential to relay on 100 billion neurons interconnected into functional neural networks by ~10^{15} specialized cell junctions, called synapses (Herculano-Houzel 2012). Synapses mediate neuronal communication and are the main gatekeepers of information flow within neuronal networks. Indeed, the recently postulated 'Synaptomic theory' posits that a high diversity and variety of synapses are observable in maps of the brain and that these synaptome maps are fundamental to behaviour (Grant 2019). Hence, an in-depth comprehension of synapse formation, diversity and physiology, in healthy and disease, will help understand how sensory inputs are translated into behaviour and cognition.

1. THE SYNAPSE

The reticular theory stated that CNS neurons lacked functional separation, being syncytial in nature. This theory was refuted in the 19th century by Santiago Ramón y Cajal, who stated that nerve cells are discrete units that connect to each other through specific structures to form precise networks[1] (Cowan and Kandel, 2001). However, it was C.S. Sherrington who in 1897 introduced the term "synapse" to refer to these connections. This word originates from the Greek *συνάψις*, which stands for "conjunction" (Foster, Sherrington, and University College 1897).

Early electron microscopy (EM) studies started to unravel the ultrastructure of synapses (Palay and Palade 1955), which suggested that neurons pass signals through these structures. However, synapses not only transmit information between neurons, but also process information by detecting patterns of neural activity that trigger intracellular biochemical pathways, changing the properties of the neuron (Pocklington et al. 2006). Based on the type of synaptic communication, two main types of synapses can be identified: electrical and chemical synapses (Eccles 1982).

1.1 THE ELECTRICAL SYNAPSE

Electric synapses are a type of cellular junction which allow for the pass of ion currents through cells. At electrical synapses, the cytoplasm of adjacent cells is directly connected

[1] Described in the book "Principles of connection specificity" by Ramón y Cajal in 1899.

by clusters of intercellular channels called gap junctions (Fig. I-1A; Bennett and Zukin 2004). They are made by opposed hexameric hemichannels of connexins or similar proteins placed in pre- and postsynaptic cells (Nakase and Naus 2004). Depending on their molecular composition 2nd messengers can also pass through gap junctions. These include, calcium (Ca^{2+}), inositol triphosphate (IP_3) or cyclic adenosine monophosphate (cAMP; Pereda 2014).

In electrical synapses there is no clear structural differentiation between pre- and postsynaptic sides, and the information can flow bidirectionally (Rozental et al. 2001). Nonetheless, vertebrate electrical synapses can be asymmetric, presenting a semi-dense cytoplasmic matrix, which is thought to promote interaction between connexins, and proteins involved in other types of junctions as well as signalling molecules, such as Ca^{2+}/calmodulin-dependent kinase II (CAMKII). Hence, these properties endow electrical synapses with more diversity, complexity and flexibility (Pereda 2014). In addition, electrical synapses coexist with chemical ones (Fukuda and Kosaka 2000), which actually influence them by regulating the traffic of connexins. This cooperative cross-talk promotes the modification of gap junction conductance and the capability of activity dependent plasticity (Pereda 2014). Although, they lack the ability to amplify and transform presynaptic signals, as chemical synapses do, this non-rectifying communication allows efficient detection of simultaneous subthreshold depolarizations within a group of coupled neurons. This property, together with absence of synaptic delay, increase neuronal excitability, promote synchronous firing and allow fast transmission (Silverthorn and Silverthorn 2007; Pereda 2014).

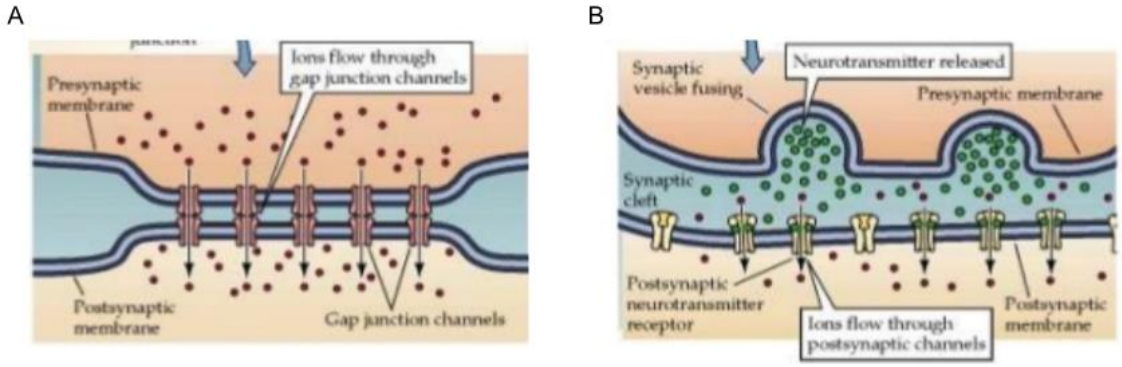

Figure I- 1. Different types of transmission among synapses. (A) Electrical synapse. (B) Chemical synapse. Modified from Purves et al. 2001

1.2 THE CHEMICAL SYNAPSE

The earliest chemical synapses formed directly onto dendritic shafts (Fig. I-1B and I-2A) or other postsynaptic structures such as the cell soma. Thus, presumably they didn't have the finger-like protuberance known as spine. Instead, these synapses were called *en*

passant synapses (Fig. I-2A). Early in animal evolution, chemical synapses became more complex by forming a spine onto the postsynaptic process, which in non-bilaterians very often invaginates the presynaptic element (Fig. I-2B). Later, in bilateral animals, non-invaginating spines became the norm (Fig. I-2C; see section I-2; Petralia et al. 2016).

The prototypical chemical synapse is organized into a presynaptic bouton (typically, an axon terminal) and an apposed postsynaptic element with an intervening synaptic cleft of 10–25 nm in width (Okabe 2007; Westfall 1996). In these connections the incoming electrical signal is 'translated' into a chemical signal in the presynaptic bouton, which secretes a chemical messenger by exocytosis. These messengers or neurotransmitters diffuse across the synaptic cleft and bind to receptors on the postsynaptic membrane (PSM). Their activation initiates signalling cascades that promote postsynaptic events. Consequently, chemical synapses conduct slow (1 ms) and more energetically expense synaptic transmission in just a single direction but allows exciting a much larger postsynaptic cell as compared with electrical synapses. Chemical neurotransmission also can change the sign of the PSM potential offering a richer capacity for information processing (Purves et al. 2007).

1.2.1 TYPES OF CHEMICAL SYNAPSES

In 1959, E.G., Gray was the first to classify synapses. Using their ultrastructural characteristics, he divided synapses into asymmetric (or type I) and symmetric (or type II; Fig. I-3; Gray 1959). Type I synapses presented rounded vesicles and a characteristic electrodense area beneath the PSM, which has since been referred to as the postsynaptic density (PSD, see section I-2.3). Later functional studies identified asymmetric synaptic contacts with excitatory glutamatergic synapses. In contrast, type II synapses were characterized by flatted presynaptic vesicles and a less elaborated ultrastructure. These were afterwards identified as inhibitory synapses as was found that their main neurotransmitters were γ-aminobutyric acid (GABA) and glycine (Peters 1991). Other modulatory synapses such as dopaminergic or serotoninergic ones fell into type II category (Bockstaele and Pickel, 1993).

Based on these criteria, type I synapses account for about 90% of the total population (Sala et al. 2008) and occur mainly onto dendritic spines (see section 2) in principal neurons of the neocortex (Spacek and Hartmann, 1983), hippocampus (Hip) and cerebellum (Crb; Harris and Stevens, 1988). Conversely, type II synapses tend to be more present on dendritic shafts and neuronal cell bodies as *en passant* synapses (Fig. I-2A; Klemann and Roubos 2011). However, in 1968 Colonnier already concluded that not all

synapses fit with this classification. He identified GABA-immunoreactivity in asymmetric synapses and glutamate-immunoreactivity in symmetric ones in various brain areas (Colonnier 1968; Pol 1991; Klemann and Roubos 2011). Hence, Gray's classification didn't cover all synapse spectrums and led many authors to use other categorizations to account for the various morphological subtypes.

Classifications extensively used in the bibliography are based on the type of NTs released and what cellular compartments do contact. The later, includes the typical axondendritic contact, but also axoaxonic, axosomatic or autaptic, which are synaptic contacts of an axon onto its own dendrite (Ikeda and Bekkers 2006). Other classification systems are based in the pre- and postsynaptic neurons involved, like granule cell-pyramidal cell (GC-PC) synapses. Or in morphological features, such as non- or invaginating (Fig. I-2; Zhang et al. 1999; Zhang et al. 1999; Petralia et al. 2015; Nusser 2018), ribbon, calyx, crest or glomerular synapses (Fig. I-2D-E; Harris and Weinberg 2012; Petralia et al. 2016).

Despite 75% boutons make a single synaptic contact, 21% form multiple synapses and 4% lack a postsynaptic partner (Shepherd and Harris 1998; Sorra et al. 2006). Therefore, synapses can also be classified based on the number of contacts they make, such as triad synapses (Fig. I-2F; Laver and Matsubara 2017). Differences in age and evolution are referred to immature/mature and protosynapses, respectively (Benson and Huntley 2012; Ryan and Grant 2009). Depending on the direction of the information flow there are rectifying and non-rectifying synapses (Pereda et al. 2014). The functionality of AMPA receptors (AMPARs) leads to silent *vs.* non-silent synapses (Liao, Hessler, and Malinow 1995; Hanse, Seth, and Riebe 2013). Other cellular structures can also be part of synapses, such as astroglial endfeets. In these occasions we refer to tripartite synapse (Fig. I-3). Additionally, if the extracellular matrix (ECM) is also considered, synapses can be referred to as tetrapartite or as a synaptic quadriga (Halassa, Fellin, and Haydon 2007; Kreutz and Sala 2012; Dityatev and Rusakov 2011).

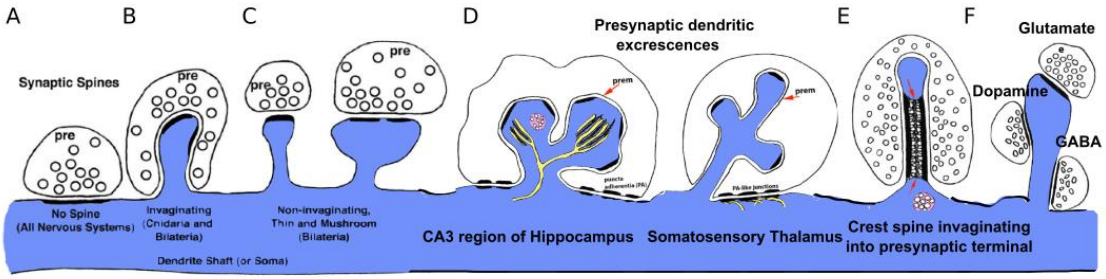

Figure I-2. Types of chemical synapses. Schematic representation of (A) *en passant* synapse. (B-F) Spine synapses being (B) invaginating, (C) (left) thin or (right) mushroom non-invaginating, (D) (left) Cornus Ammon 3 (CA3) hippocampal and (right) thalamic synapses invaginating in presynaptic dendritic excrescences, (E) Crest and (F) multiple dopaminergic, glutamatergic and GABAergic axodendritic or axospinous synapses. Modified from Petralia et al. 2016.

Unlike the diversity of anatomically distinct neurons, much less is known about the diversity of synapses, but it is already clear that not all synaptic proteins are expressed equally at all synapses as some of the protein abundances in different classes of neurons are quite distinct (Wang et al. 2006). Furthermore, remarkable synaptic diversity is also observed among molecularly and morphologically apparently homogeneous synapses (Nusser 2018). To resolve the classification of this enormous diversity, it has been proposed to build a catalogue of synapses based on their postsynaptic proteome or even on their postsynaptic subcomplexes (Grant 2007).

1.2.2 MOLECULAR COMPOSITION OF CHEMICAL SYNAPSES

Molecular evolution studies have identified that the synaptic proteome has increased along animal evolution, particularly in vertebrate species (Emes et al. 2008). This observation has led to hypothesize that the increased capacity of information processing and storage observed in higher organisms can be, at least in part, related with this increased proteomic complexity. In turn, this increased complexity is thought to have evolved around a *core* proto-synapse[2] machinery that can be traced down to unicellular organisms (Emes and Grant 2012). Yet, among vertebrates the synaptic proteome has been shown to be highly conserved, both at the composition and sequence level (Bayés et al. 2017).

The composition and structure of synapses can vary across brain regions and may change during development, maturation, normal aging or in the context of synaptopathies and trauma (Harris and Weinberg 2012). However, generally speaking, the presynaptic bouton presents a membrane specialization composed of Actin filaments referred to as the cytomatrix active zone (CAZ). It hosts ion channels and pumps, cytomatrix proteins like Bassoon and Piccolo (Dresbach et al. 2003), synaptic vesicles of 50-200 nm that contain fast-Acting NTs and other molecules involved in the priming and exocytosis of these synaptic vesicles (e.g., SV2 or Synaptotagmin-1; Galizia, Eisenhardt, and Giurfa 2011; Südhof and Rizo 2011; Südhof 2012; Torres and Inestrosa 2018). Beyond signalling molecules and numerous mitochondria, large dense-cored vesicles containing slow-acting NTs like neuropeptides or amines can be also found (Schweizer 2001). Finally, the presynaptic membrane contains auto- and heteroreceptors (e.g., GABARs) and synaptic adhesion molecules (SAMs) such as Neurexins. At the presynaptic compartment, the most outstanding differences between inhibitory and excitatory synapses is the set of metabolic

[2] A complex of synaptic proteins found in early metazoans without a defined nervous system.

enzymes involved in NT synthesis (Tallafuss, Constable, and Washbourne 2010; Torres et al. 2017).

The synaptic cleft is basically made of standard ECM proteins (e.g., laminin) and specialized SAMs projecting from synaptic membranes, including neuroligin, N-cadherin, SALM, SynCAM or NCAM among other molecules (Harris and Weinberg 2012; Burch, Tao-Cheng, and Dosemeci 2017). These proteins provide a support for trans-synaptic interactions between the CAZ and the PSD. For instance, presynaptic neurexins nucleate an overall trans-synaptic signalling network by interacting with their postsynaptic ligands, such as neuroligins (Harris and Weinberg et al. 2012; Iijima et al. 2016; Südhof 2017). Thus, SAMs not only favour synaptic integrity maintenance, but also the coordination between pre and postsynaptic elements (e.g., the probability of NTs release can be influenced by conformational changes from postsynaptic CAMs; Schweizer 2001).

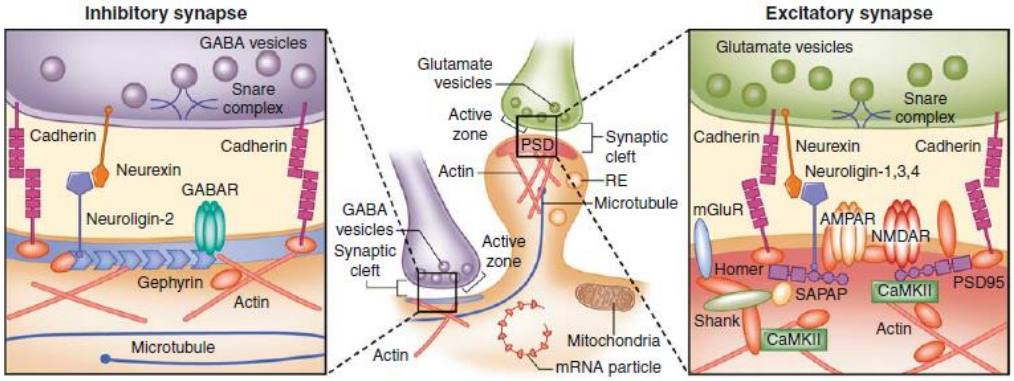

Figure I-3. Molecular composition of chemical synapses. (Left) Inhibitory synapse and (Right) excitatory synapse. Some of their key components are also indicated. Obtained from van Spronsen and Hoogenraad 2010.

The postsynaptic element of excitatory and inhibitory synapses comprises more intrinsic differences than the presynaptic element (Fig. I-3). The former shows the PSD generally placed on the tip of spines, just opposite to the CAZ. The PSD encompasses a wide range of molecules including surface NT receptors or specific SAMs, such as Neuroligin1 (Chubykin et al. 2007; Craig and Kang, 2007), as well as other molecules involved in structural and functional signalling (Schweizer 2001; Emes and Grant 2012). Conversely, inhibitory synapses lack a prominent PSD (Harris and Weinberg et al. 2012), but they can present the so called “free postsynaptic-like densities” which are plaques of intracellular para-membranous electron-dense material that are not aligned with the presynaptic CAZ (Spacek 1982). These synapses present GABA and Glycine receptors mainly anchored by the well-known postsynaptic scaffold Gephyrin. The clustering of this protein is

regulated by Collybistin[3]. Interestingly, this protein as well as Neuroligin-2 are both specific of inhibitory synapses (Sumita et al. 2007; Lepeta et al. 2016).

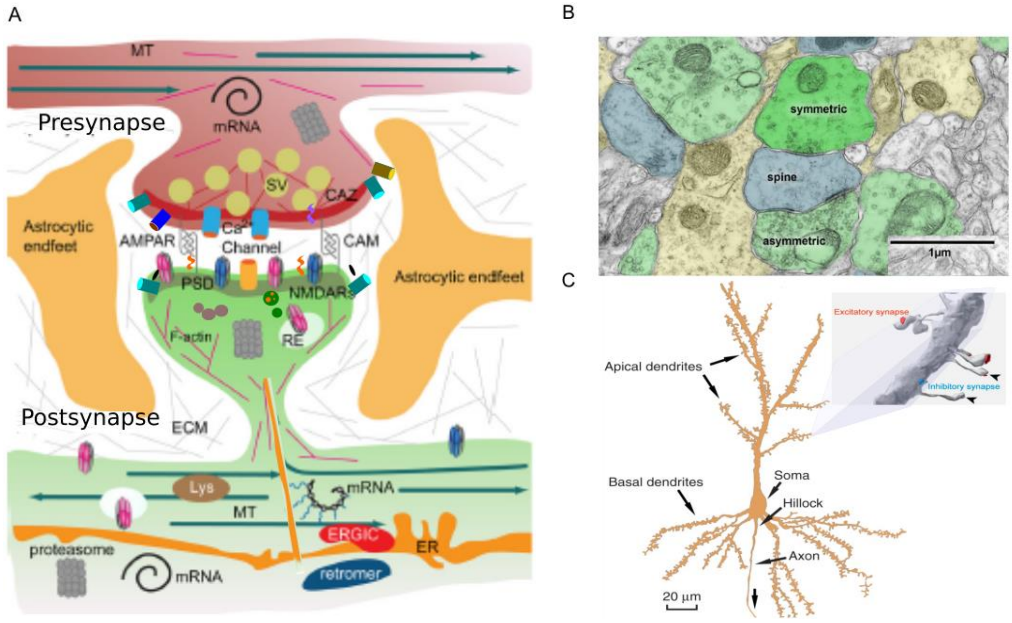

Figure I-4. Elements of excitatory synapse elements. (A) Microsecretory system with local mRNA, polyribosomes (in brown), proteasome machinery (in grey), microtubules (MT) and endoplasmic reticulum (ER) in axonic and dendritic shafts among others. ECM stands for extracellular matrix. (B) EM showing asymmetric type I (light green) and type II (fluorescent green) synapses; dendrites (blue); dendritic spines (grey); astrocytic processes (yellow); uncoloured profiles of axons, and striated ovals are mitochondria. (C) Parts of a pyramidal neuron. PSDs (red) and PSDs facing away from the view (arrowheads). Adapted from (A) Dietrich et al. 2016, (B) The fine structure of the aging brain book and (C) is a composition from Kennedy et al. 2016 and Sheng and Hoongenraad, 2007 for the 3D dendrite reconstruction.

At the edge of synaptic specializations there is a high concentration of Actin binding proteins (ABPs); desmosomes and zonula adherens proteins (Harris and Weinberg et al. 2012; Petralia et al. 2016); NT transporters and extrasynaptic ionotropic and metabotropic receptors. Dendritic spines from glutamatergic synapses present endocytic zones (EZ) located close next to the PSD, these are specialized regions of clathrin-mediated endocytosis (Newpher and Ehlers 2008; Sheng and Kim 2011; Colgan and Yasuda 2014). Noteworthy, metabotropic and ionotropic GABA receptors are present in both pre- and postsynaptic specializations of excitatory synapses (Luján, Shigemoto, and López-Bendito 2005).

Besides the pre- and postsynaptic elements closely associated with the plasma membrane, other cellular structures reside at the synapse. These include a microsecretory system for proteostasis4, present in both the axon terminal and dendritic shaft (Fig. I-4A). Therefore, the turnover of synaptic proteins is controlled by local and somatic *de novo*

[3] Is a a RhoGEF for Cdc42 (Shering and Kim, 2011). For a proper definition see I-2.5.3.2.
[4] Refers to the processes controlling biogenesis, folding, trafficking and degradation of proteins.

messenger ribonucleic acid (mRNA) translation and stability or by protein degradation via the ubiquitin-proteasome system (UPS)[5], lysosomes and autophagosomes. Molecular machines for proteostasis can be shared between synapses in the same dendritic segment (Fig. I-4A), contributing to the assembly of new synapses. Finally, proteins are also transported in and out of synapses through the cytoskeleton or by lateral diffusion at the PSM (Sheng and Hoogenraad 2007; Dieterich and Kreutz 2016).

[5] A pathway for the targeted degradation of proteins, important for regulating protein function.

2. DENDRITIC SPINES

Synaptic spines were discovered in the late 19th century and are defined as a specialized protrusion on the shaft of a certain neurons, normally a dendrite (Hering and Sheng 2001). Although very rarely, they have been shown to project from the neuronal soma (Peters and Kaiserman-Abramof 1970). Since more than 90% of excitatory synapses terminate on dendritic spines in the mammalian brain, synaptic spines are usually referred as dendritic spines (Yuste and Denk 1995; Nimchinsky, Sabatini, and Svoboda 2002)

The average dendritic spine is 0.5 µm in diameter and 0.5-2 µm in length (Hering and Sheng 2001; Nimchinsky, Sabatini, and Svoboda 2002), although large spines from the hippocampal *Cornus Ammon* 3 (CA3) can measure up to 6 µm. Spines present a bulbous head of a variable volume (0.01-1 µm^3), that receives the synaptic input, and a very thin neck (50-400 nm in diameter) that connects it to its parent dendrite (Fig. I-5D; Kwon et al. 2017; Adrian et al. 2014; Maiti et al. 2015). Both the number and the density of dendritic spines located in different cortical areas and species as well within apical and basal dendrites present variations that may reflect unique functional differences (Jacobs et al. 2001; Elston et al. 2011; Benavides-Piccione et al. 2013).

Mitochondria are commonly found in presynaptic boutons yet, their presence at dendritic spines is still a matter of debate. A few articles report mitochondria translocation into the spine after depolarization (Sorra and Harris 2000; Z. Li et al. 2004; Kristen M. Harris and Weinberg 2012; Li et al. 2004; Sheng and Kai et al. Graham et al. 2017; Ranjaru et al. 2019). In addition, large forebrain synapses can also present a structure referred to as spine apparatus[6] at spines, which regulates postsynapitc Ca^{2+} levels, protein synthesis and their post-translational modifications (Harry and Weinberg 2012; Maiti et al. 2015; Petralia 2016).

2.1 TYPES OF DENDRITIC SPINES

Based on Peters and Kaiserman-Abramof (1970) firsts descriptions, which were later extended by Harris et al. (1992), the types of dendritic spines are: (1) filopodia-like spines with no head, (2) long thin spines, (3) thin spines with a relatively slender head and neck, (4) short, stubby spines without a clearly defined neck and (5) large spines with enlarged head regions called mushroom spines (Fig .I-5A). Later, other types have been described, including: the (6) cup-shaped or branched spines (>1 spine head) as well as (7)

[6] Formed by several membranous sacks or cisterns separated by plates of dense material.

discontinuous or perforated spines. These can be further subclassified into (7.a) fenestrated, (7.b) horseshoe or (7.c) segmented, based on their PSD distribution and enlargement after long-term potentiation (LTP; see section I-3). Other, more intricate forms have been identified (Fig. I-5C; Petralia 2016). In the neocortex spines have also been classified based on their life-time into transient and persistent, being persistent spines less motile (Maiti et al. 2015). Yet, most spines change their shape between these categories over periods of minutes or hours. The spine shape, size and volume are intimately linked with synaptic strength and maturity (Sala et al. 2008; Maiti et al. 2015).

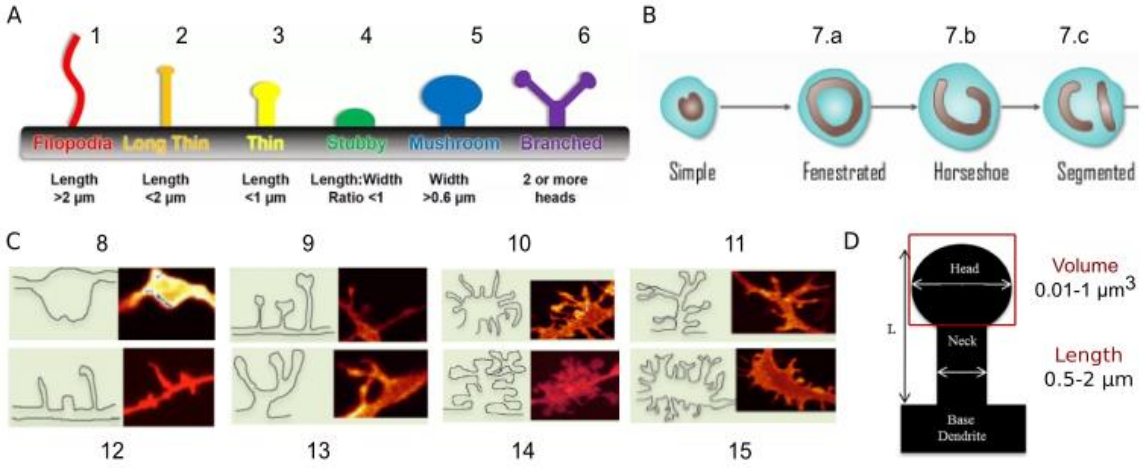

Figure I-5. Types of dendritic spines. (A-B) Types cited in the main text. (C) Other synapse types found in mammals are (8) varicosities, (9) pedunculate, (10) brush ending, (11) racemose, (12) sessile, (13) claw ending, (14) thorny, and (15) coralline excrescence spines. (D) Some dimension of a spine. Modified from (A) Risher et al. 2014 and (B-D) Maiti et al. 2015.

2.2 FUNCTIONAL ROLE OF DENDRITIC SPINES

The appearance of dendritic spines and its variable dimensions confer functional advantages to neurons. Namely, spine neck dimensions influence Ca^{2+} responses by altering diffusional coupling between the dendrite and the spine. In addition, the spine neck can obstruct movements of various molecules between the cytoplasm and the head area and can regulated the number of molecules placed on the cell surface, such as AMPAR (Ashby et al. 2006). Altogether, neck size can affect activation and conductance of PSM receptors, thus the input resistance and transient membrane potential in the spine head (Coss and Perkel 1985; Grunditz et al. 2008). Also, a given spine can receive head and neck synaptic contacts (Fig.I-2F; Chen et al. 2012; Kwon et al. 2017), the latter being typically GABAergic. Inhibitory neck innervation serves to limit both Ca^{2+} influx and postsynaptic potentials to ultimately regulate NMDAR-dependent synaptic integration (Chiu et al. 2013) and complex behaviours (Petralia et al. 2016).

Other remarkable functions are that spines increase the “reach” of the dendrite to connect with potential presynaptic partners (Stepanyants, Hof, and Chklovskii 2002). This is

supported by the searching purpose of spine motility during synaptogenesis (see section I-4; Bonhoeffer and Yuste 2002). Dendritic spines allow to produce a larger depolarization with relatively few channels as compared with the same number of channels placed onto a dendritic shaft (Kwon et al. 2017), and increase the dendritic surface area providing more area to accommodate larger numbers of synapses to amplify presynaptic signals (Scheuss and Bonhoeffer 2014). Therefore, spines allow a thin dendritic shaft to bear more complex circuitry per unit volume of neuropile (Chklovskii, Mel, and Svoboda 2004). The existence of dendritic spines also facilitates to share synaptic plasticity mechanisms specific to co-active spines (Losonczy, Makara, and Magee 2008; Rochefort and Konnerth 2012). All these functions along with the retraction, formation, and morphology changes of spines observed *in vivo* are key components in the rewiring of neural circuits (Arellano et al. 2007; Scheuss and Bonhoeffer 2014). In the absence of spines, the excitatory transmission is highly variable and depend on dendritic location (Gulledge, Carnevale, and Stuart 2012).

In summary, spines are dynamic autonomous microcompartments that biochemically isolate electric signals from the parent dendrite enabling input specific synaptic plasticity and neuronal modulation through its associated molecules and signalling subdomains rather than a mere expansion of postsynaptic surface (Yuste and Denk, 1995; Kennedy 2000; Kwon et al. 2017). They are essential for spiny neurons to detect, uniquely respond to, and store distinct synaptic input endowing the brain the ability to constantly adapt its function to altered environmental requirements (Rafael Yuste 2010; Kasai et al. 2010; Harnett et al. 2012; Kennedy 2016).

2.3 POSTSYNAPTIC DENSITY OF GLUTAMATERGIC SYNAPSES

The most prominent postsynaptic component of vertebrate excitatory glutamatergic synapses is the PSD (Palay 1956; Dosemeci et al. 2016). It is identified as a fuzzy electron-dense structure[7] extending into the cytoplasm beneath the PSM held by cytoplasmic Actin filaments (Emes and Grant 2012). The PSD includes an array of scaffolding proteins that organize and stabilize receptors, ion channels and signalling proteins necessary for synaptic function (Kennedy 1993). Proteins in the PSD show a layered distribution in the axo-dendritic axis when immunolabeled on ultrathin EM sections (Petersen et al. 2003) or investigated by super-resolution light microscopy (Dani et al. 2010). Immediately adjacent to the layer 1 (at the PSM) exists the core of the PSD entitled layer 2 being PSD-95 one of the major components. Below there is layer 3 or a subsynaptic web, ~50 nm thick, called *pallium* or mantle mainly formed by Shanks and Homer proteins (Fig. I-6A). This pallial

[7] Described also as an organelle or morphological and functional specialization of the PSM (Sheng and Kim, 2011) or a dense lamina beneath the PSM (Dosemeci et al. 2016).

layer is more evident after short bouts of stimulation, reflecting the reversible incorporation of additional proteins (Dosemeci et al. 2016; Lautz et al. 2018). Indeed, PSD molecules are dynamically repositioned (Blanpied, Kerr, and Ehlers 2008; Kerr and Blanpied 2012) and exchanged between the spine and the dendritic shaft (Kuriu et al. 2006; Sturgill et al. 2009).

In small synapses, the PSD surface facing the cytosol presents a regular disc-like shape that becomes more complex with increasing synapse size. Many of the largest synapses often have irregular shapes, being composed by “perforated” PSDs, presenting interior holes or be segmented having two completely separated PSDs (Fig.I-3B; Maiti et al. 2015). Despite its heterogenous size, they generally present a diameter between 200-800 nm and a thickness in the 30-60 nm range (Carlin et al. 1980). PSD thickening is sensitive to experimental manipulations (e.g., hypoxia or ischemia; Hu et al. 1998); varies greatly even in synapses from the same brain region (Colonnier 1968); is induced by glutamate depolarization (Kristen M. Harris and Weinberg 2012), and influences subcellular organization of its constituent proteins (Otmakhov et al. 2004; Lautz et al. 2018). Furthermore, the surface area of the PSD highly correlates with spine head volume/size (Racz and Weinberg 2006); total number of presynaptic vesicles; with the specific number of vesicles docked at the CAZ (Harris and Weinberg 2012); postsynaptic receptor abundances (Kasai et al. 2003) and synaptic strength (Racz and Weinberg, 2006).

2.3.1 Functional significance of postsynaptic densities

The generally accepted roles of the PSD are to mediate the apposition of pre- and postsynaptic membranes; to traffic, cluster and facilitate NT receptors anchorage, and to couple their activation to biochemical signalling events (Sheng and Kim, 2011). Nonetheless, more functions can be attributed to the PSD, including modulation of CAMs traffic and controlling the amplitude of excitatory postsynaptic currents (EPSCs). As a result, the composition and organization of the PSD crucially determines the rules by which each excitatory synapse integrates and encodes information through structural and functional plasticity (See section I-3; Grant 2003; Vallejo, Codocedo, and Inestrosa 2017).

2.3.2 MOLECULAR COMPOSITION OF POSTSYNAPTIC DENSITIES

The molecular mass of the average PSD has been estimated to be ~1.1 GDa, which would correspond to ~10,000 copies of a 100 kDa protein (Chen et al. 2005) matching with the identification of a few hundred to 2,000 proteins in PSD fractions by neuroproteomics[8] (Husi et al. 2000; Jordan et al. 2004; Li et al. 2004; Peng et al. 2004; Yoshimura et al. 2004; Trinidad et al. 2008; Bayés et al. 2012). The most abundant protein types at the PSD are Actin-related; kinase/phosphatase regulators and GTPases and its modulators (Fig. I-6B; Sheng and Kim 2011).

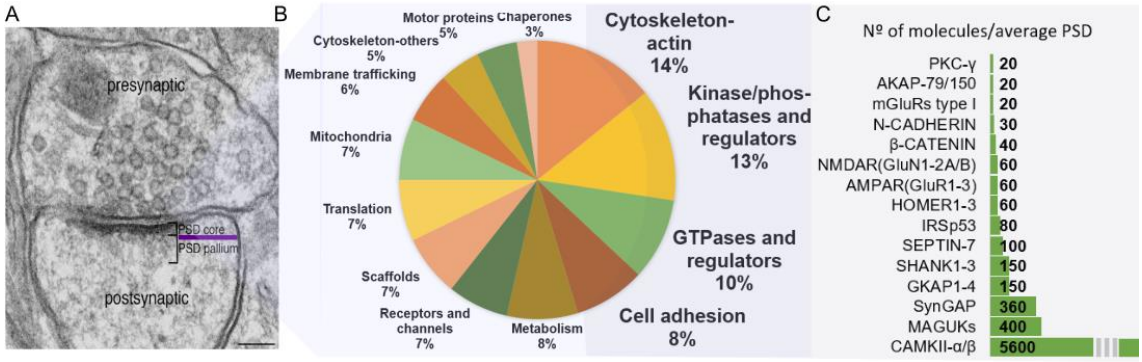

Figure I-6. Molecular composition of forebrain PSDs. (A) Micrography of an average PSD showing its core and *pallium* layers. Scale bar: 0.1 µm. (B) The percentage of PSD proteins identified by MS is classified in functional classes. ~16 % of proteins with miscellaneous functions are not shown. (C) Number of proteins in a given family per averaged size PSD. Adapted from (A) Dosemeci et al. 2016 and (B-C) Sheng and Kim, 2011.

Importantly, less than 10% of these proteins are NT receptors, which highlights that most PSD proteins are not directly involved in electrophysiological functions and instead perform a plethora of signalling and regulatory roles. Furthermore, the most abundant proteins in an average rodent PSD are: CAMKII-α (~2,500 copies), which together with the other isoforms form up to 250 dodecamers (see 2.5.1); ~360 units of 'Synaptic small GTPase activating protein' (SynGAP); ~300 PSD-95; ~90-150 Shank proteins and ~20 SAP102 molecules (Sheng and Hoogenraad 2007; Lowenthal, Markey, and Dosemeci 2015).

2.3.2.1 MEMBRANE BOUND POSTSYNAPTIC PROTEINS

The PSD side facing the plasma membrane encompasses many transmembrane proteins and the phospholipids that they are attached to (Fig. I-7A). These lipids maintain membrane dynamics and fluidity; allow clustering and traffic of proteins; are the source for new signalling lipids (Hering, Lin, and Sheng 2003) and orchestrate NT signalling as they

[8] Neuroproteomics is the study of the proteomes of the nervous system (See section I-6).

place a range of signalling proteins and subdomains like lipid rafts (Allen, Halverson-Tamboli, and Rasenick 2007). Also, embedded within the PSM, there are a wealth of other molecules including Frizzled receptors (FzzR), which are activated by lipid-modified signalling glycoproteins called Wnts (McLeod et al. 2018), voltage gated ion channels and trans-synCAMs, like integrins or leucine repeats rich transmembrane proteins (LRRTMs; Petralia et al. 2005; de Wit et al. 2009; Vallejo, Codocedo, and Inestrosa 2017).

GLUTAMATE RECEPTORS

Glutamate receptors (GluRs) are the cardinal receptors of excitatory synapses (Sheng and Kim, 2011) found at layer 1. Glutamate, which is the main fast excitatory NT in the CNS, and other excitatory amino acids, operate through metabotropic (mGluR) and ionotropic (iGluR) receptors. mGluRs are G-protein-coupled receptors (GPCRs) presenting a seven transmembrane domain structure. They can initiate signalling cascades[9] or cation influx upon glutamate binding. mGluRs are further categorized into Class I, including mGluR1 and mGluR5, and classes II and III (Willard and Koochekpour 2013). In contrast, iGluRs include NMDAR, AMPAR, Delta and Kainate receptor classes. These are respectively composed by GluN, GluA, GluD and GluK subunits, which multimerize to form voltage-gated ion channels (Traynelis et al. 2010).

AMPARs enrichment at the PSDs result from receptor immobilization by more stable PSD proteins, like TARPs[10] (Choquet and Triller 2003; Fukaya et al. 2006). AMPAR subunits (GluA1-4) can be divided into long and short containing C-terminus (C-term) tails (Pandis et al. 2006; W. Lu et al. 2009) and form tetramers with GluA1–4 pairs in various stoichiometries (Hollmann and Heinemann 1994). Indeed, incorporation of GluA2 blocks Ca^{2+} flux through AMPARs, thus GluA2-containing receptors predominate in combination with other subunits (Isaac, Ashby, and McBain 2007) despite homomeric permeable Ca^{2+}AMPARs do exist (Greger et al. 2003; Rossmann et al. 2011). NMDARs are also assembled as tetramers composed of two obligatory GluN1 subunits along with two GluN2 or GluN3 subunits (Lu et al. 2009). The C-term domain of GluR subunits is involved in receptor trafficking and signalling and is the most divergent, accounting for a substantial part of the functional diversity of AMPARs and NMDARs (Paoletti, Bellone, and Zhou 2013). Furthermore, GluRs can be categorized into those that transmit the electrical depolarization (AMPARs) and those that elicited signaling and plasticity mechanisms (NMDARs and mGluRs; Pocklington et al. 2006).

[9] Activation of group I mGluRs mediates slow excitatory neurotransmission in contrast to Groups II/III.
[10] Transmembrane AMPAR regulatory proteins.

Receptor assembly occurs at the ER membrane. Exit from the ER is under stringent quality control, which monitors correct subunit folding and assembly (Greger, Ziff, and Penn 2007). Both GluRs subunits pre-mRNA processing and mRNA editing together with composition of GluRs are not static processes which determines channel conductance properties and gating kinetics as well as regulates vesicular traffic to and from synaptic sites (Nusser 2000; Greger, Ziff, and Penn 2007). Despite both NMDARs and AMPARs are present in high densities at the middle of the PSD but decreasing towards its edges (Nusser 2000), the formers localized more centrally than AMPARs. In fact, extrasynaptic membrane holds AMPARs pools ready for lateral diffusion into and out the synaptic membrane bound to PSD (Derkach et al. 2007), whereas group I mGluR concentrate in an annulus just outside the edge of the PSD (Kennedy 2000; Choquet and Triller 2003).

NEUROTROPHIC FACTOR RECEPTORS

The Ephrin (e.g., EphB), Tyrosine kinase and Fibroblast growth factor receptors are also present at layer 1 of the PSD (Carlisle and Kennedy 2005; Belov and Mohammadi 2013). Neurotrophic factors belong to a class of growth factors (e.g., peptides and small proteins) including the neurothrophin Brain-derived neurotrophic factor (BDNF;Deister and Schmidt 2006; B. Lu, Nagappan, and Lu 2014), Thrombospondins or Neuregulins (Wang et al. 2012). Noteworthy, FzzR/Wnt signalling can be included here too. Importantly, neurotrophic factors triggered signaling act as guidance cues for newborn neurons, and in the mature nervous system, where they are involved in neuronal survival and growth among other functions (McAllister, Katz, and Lo 1999; Poo 2001; Ramos-Quiroga et al. 2014).

2.3.2.2 SCAFFOLDING PROTEINS

Scaffolding proteins mostly reside at the core of the PSD, in the layer 2, coupling membrane proteins with downstream biosynthetic, metabolic and signalling enzymes (Fig. I-7). These adaptor proteins have different domain architectures, promoting protein-protein interactions (PPIs) and can act to allow rapid evolution of new signalling pathways by changing binding specificity and hence interacting partners (Emes and Grant 2012). The most prominent scaffolds are the membrane-associated guanylate kinase (MAGUK)-family members and the disk large associated guanylate-associated protein (DLGAP), which connect GluRs to Shank-Homer family scaffolds (Fig. I-7B).

It is worth noting that ‘Multiple PDZ domain’ or MUPP1 protein, is a 13 PDZ-containing domain scaffold and part of the NMDAR signaling complex (NRC, Krapivinsky et al. 2004),

thus binds many proteins including claudins, tyrosine kinases receptors, SynGAP or RhoGEFs (Penzes et al. 2001; Krapivinsky et al. 2004).

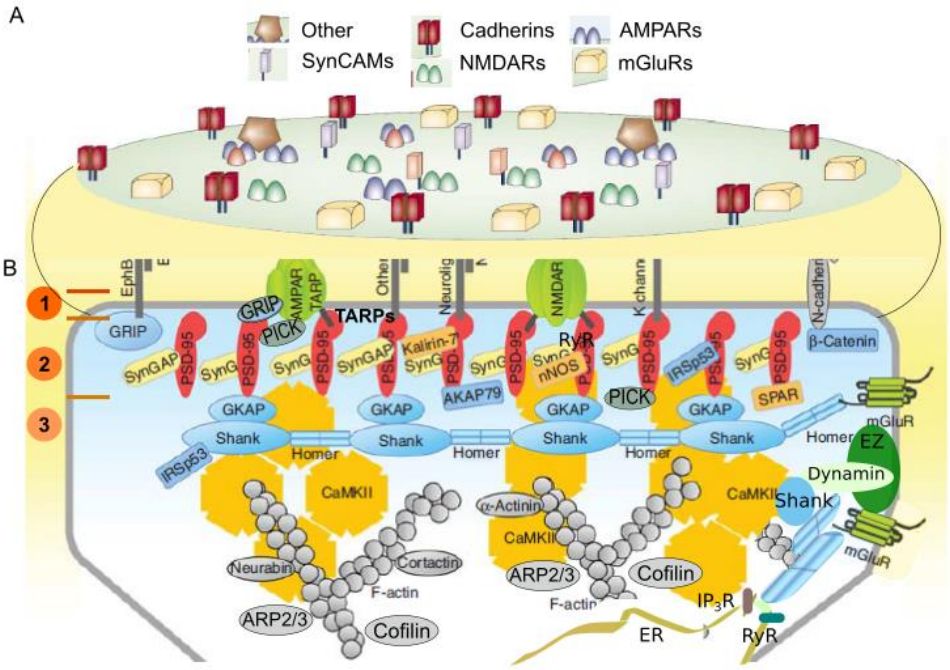

Figure I-7. Schematic organization of a generic PSD of excitatory glutamatergic synapses. (A) Top view of the synapse. (B) Major protein-protein interactions (PPI) of PSD indicated by contacts between the proteins. SynCAMs can include NCAM or Nr-CAM molecules. The left numbers on the side denote the three-layered organization of the core PSD. GKAP is a synonym of DLGAP. Composition from (A) Choquet and Triller, 2003 and (B) Sheng and Kim, 2011 and information added from Petralia et al. 2005.

PSD-95 AND OTHER MAGUKS

MAGUK proteins have no enzymatic activity but contain protein-binding domains such as PDZ[11] domains that mediate PPIs (Good, Zalatan, and Lim 2011; Nourry, Grant, and Borg 2003). MAGUKs include 4 members: PSD-95 (DLG4), PSD-93 (DLG2), SAP102 (DLG3) and SAP97 (DLG1). Specifically, the first three MAGUKs are distributed tangentially along the synaptic membrane (Sans, 2000; Kim and Sheng 2004; Ling et al. 2012; Rasmussen et al. 2017) and interact directly with NMDARs (Sheng and Kim, 2011).

PSD-95 has 5 PPI domains: 3 PDZ, a SH3 and a GK domain. These allow PSD-95 to bind to a wide range of proteins, including receptors and voltage gated channels, TARPs (Lim et al. 2003; Payne 2008) or SynGAP (Kim et al. 1998; Chen et al. 1998). Beyond ease receptor clustering, PSD-95 or the other MAGUKs have the ability to assemble an NMDAR-complex (NRC/MASC[12]; Husi et al. 2000; Grant et al. 2005; Laumonnier, Cuthbert, and Grant 2007), thereby facilitating the functional coupling with downstream

[11] Stands for the first 3 proteins discovered to share PDZ domain: PSD95, Dlg1, and ZO-1. This domain mediate protein interactions (Corbeil et al. 2013).
[12] For NMDAR Complex/MAGUK Associated Signaling Complex, respectively.

signalling molecules such as small GTPases regulators including SynGAP, Kalirin-7 (See 2.5.3; Penzes and Jones 2008) neuronal nitric oxide synthase (nNOS; Aarts et al. 2002), kinases including Fyn, Src, Pyk2 or CAMKII-α (Sheng and Hoogenraad 2007). Conversely, PSD-95 can also recruit other proteins such as A-kinase-associated proteins (AKAPs), which couple GluRs to protein phosphatases (e.g., AKAP79/150 binds calcineurin[13]) to modulate GluR function (Fig. I-7B; Sheng and Kim 2011).

SHANK AND HOMER

PSD-95 interaction with DLGAPs provides a connection between the proteins from layers 1/2 and layer 3. As shown in figure I-7B, DLGAPs binds to Shanks which lies on the cytoplasmic margin of the PSD linking other complexes (Naisbitt et al. 1999; Petralia et al. 2005). Shank family encompasses 3 members (Shank1-3). These are large proteins with multiple PPI domains that couple to the DLGAP/SynGAP–PSD-95–NMDAR complex by interacting with DLGAPs and SynGAP. Shanks can also bind to type I mGluRs through another family of scaffolding proteins, Homer that includes also 3 members (Homer1-3). ABPs and Shanks cooperate to induce accumulation of inositol triphosphate receptors (IP_3Rs), to ultimately promote the maturation of dendritic spines; enlargement of heads and formation of multisynaptic spines (Sala et al. 2001; Shiraishi-Yamaguchi and Furuichi 2007). Conversely, Homers multimerize with themselves (Hayashi et al. 2009), interact with IP_3R, Ryanodine receptors and with Dynamin-3, to link the PSD with endocytic zones (EZs; Sheng and Kim, 2011). Therefore, Homers and Shanks link Ca^{2+} signalling, Actin and small GTPases and its regulators (e.g., Cdc42 and oligophrenin-1) to cytoskeleton remodelling (Shiraishi-Yamaguchi and Furuichi, 2007). Regardless of the mechanism and PPI, Shank and Homer are key in the mGluR signalling complex, which involves 76 proteins (Grant et al. 2005; Lautz et al. 2018).

In summary, scaffolding proteins provide a link between GluRs; SynCAMs, motor proteins and signalling enzymes (Naisbitt et al. 2000); organize interacting proteins and orchestrates the flow of information in a synapse (Good, Zalatan, and Lim 2011). Bearing in mind the list of most abundant PSD proteins (Fig. I-6), the SynGAP-PSD95-DLGAP-SHANK-HOMER platform represents its structural “core” (Sugiyama et al. 2005; Chen et al. 2008; Zeng et al. 2016; Lautz et al. 2018).

[13] Calcineurin is also known as protein phosphatase 2B (PP2B).

2.4 SPINOSKELETON AND ACTIN-BINDING PROTEINS

The cytoskeleton of dendritic spines, termed spinoskeleton, contains proteins such as Fodrin, Actin and Tubulin (Harris and Kater 1994; Koleske 2013). A small fraction of microtubules in mature dendrites transiently enter dendritic spines (Hotulainen and Hoogenraad 2010). Consequently, spine morphogenesis is largely dependent on Actin remodelling, as it is the major component of the spinoskeleton (Kennedy 2000; Dillon and Goda 2005). Hence, complex networks of Actin filaments spreading from the PSD and spine cytoplasm to dendritic shafts interconnect microdomains within the spine and likely coordinate PSD remodelling with membrane traffic and spine growth (Fig. I-8A&C; Hotulainen and Hoogenraad 2010; Colgan and Yasuda 2014).

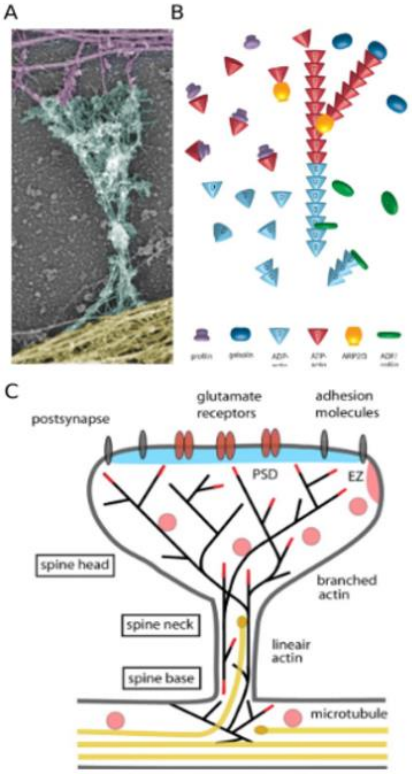

D

Actin-binding proteins		
ABP	**Role**	**References**
Actin-depolymerizing factor (ADF)/Cofilin	Depolymerization/severing. Controls activity-induced synaptic availability of GluRs,exocytosis of synaptic vesicles, and synaptic plasticity. It is inactivated by LIMK and Slingshot	1,2,3
Profilin II	Polymerization	1
F actin-related proteins 2 and 3 (Arp2/3) complex	Branching, nucleation, and crosslink between F-actin, thus increase network expansion	1,2,6,7
WAVE 1	Nucleation-promoting factor	1
N-WASP	Nucleation-promoting factor	1
Cortactin	Nucleation-promoting factor	1
Formin(mDia2)	Nucleation	1
Neurabin I	Bundling	1
Neurabin II/Spinophilin	Bundling	1
Synaptopodin	Bundling	1
CAMKII-β	Bundling	1
α-N-catenin	Bundling. Is acadherin-associated protein that links SynCAMs to the spinoskeleton	1,4,5,9,10
β-catenin	Bundling. Llinks SynCAMs to the spinoskeleton	11
α-actinin	Bundling and links NMDAR to actin spinoskeleton	1,4,5,9,10,11
Developmentally regulated brain protein (Drebrin)	Bundling. Also, Promotes actin nucleating, severin, capping or F-actin crosslinking activity. Also is required to induce the NMDAR and PSD-95 accumulation	1, 8
Gelsolin	Anti-bundling,caping, severing. Thus, prevents monomer exchange of F-actin by end-blocking or capping	1,4
EPS8	Caps barbed ends to stabilize F-actin	1

Figure I-8. The role of ABPs and spinoskeleton dynamics. (A) Platinum replica EM of axonal cytoskeleton (purple), dendritic shaft (yellow) and spine (cyan) from mature hippocampal spines. (B) F-Actin assembly and disassembly by ABPs. The growing/barbed end is extended by addition of Actin-ATP (T, red), Cofilin severs Actin-ADP (light blue) from the older 'pointed' end. (C) Mushroom spine with Actin barbed ends (red lines), MTs (yellow) and organelles. The endocytic zone (EZ) is lateral to PSD in extrasynaptic regions and recycling endosomes (pink) are found in the shaft and spines. The Actin-polymerizing barbed ends are indicated as red lines. (D) Summary of the main roles of some ABPs. References are: 1. Lin and Webb, 2009; 2. Rácz and Weinberg, 2006; 3. Rust, 2015; 4. Hotulainen Hoogenraad, 2010; 5. Paavilainen et al. 2004; 6. Carlisle and Kennedy, 2005; 7; Colgan and Yasuda, 2004; 8. Dun and Chilton, 2010; 9. Tada and Sheng, 2006; 10. Harris and Weinberg, 2012; 11. Sala et al. 2008. (A, C) are extracted from 4 and (B) from 6.

Actin can be found as a soluble globular monomeric and ATP-bound form (G-Actin) or as a polymerized ADP-bound form (F-Actin). The latter is the major structural component of excitatory synapses. Assembly and stabilization of G-Actin into F-Actin supports spine enlargement associated with enhanced synaptic activity. Conversely, its disassembly

promotes spine shrinkage and elimination (Fig. I-8B; Rust 2015). The conversion between G- to F-Actin is a highly dynamic process regulated by ABPs through many different pathways. These pathways can be activated by various surface receptors, specially by NMDARs (Cingolani and Goda, 2008). The compartmentalization of signalling to regulate Actin dynamics is mediated by the discrete localization of ABPs and by multiprotein signalling complexes involving mainly small GTPases and their effectors (Colgan and Yasuda, 2014).

The specific sets of ABPs determine whether spinoskeleton is stabilized to maintain morphology, or whether force is generated to induce membrane deformation and remodelling (Colgan and Yasuda, 2014). As an example, ADF/Cofilin localizes in the spine shell, whereas Cortactin concentrates in the spinoskeleton core. In turn, Cortactin binds Shank and ARP2/3[14], activating and localizing the latter to dendritic spines (Hering and Sheng, 2003; Tadan and Sheng, 2006). Thus, ABPs are crucial not only for the structural plasticity of excitatory synapses, but also for pre- and postsynaptic physiology. Examples of ABPs and its regulation in Actin dynamics are shown in Fig. I-8D.

2.5 SIGNALLING MOLECULES IN DENDRITIC SPINES

Signalling molecules can be found both attached to the PSD or at other spine locations. There are 2 main groups of signalling proteins at dendritic spines: i) kinases and phosphatases and ii) small GTPases and their regulators (Bayés et al. 2012). The PSD is particularly enriched in protein kinases (Sheng and Hoogenraad 2007), since phosphorylation-mediated regulations of synaptic PPIs is a common regulatory strategy in synapses (Huganir and Nicoll 2013). Noteworthy, since CAMKII-α/β and SynGAP represent more than 8% of the PSD mass, they also fulfil a scaffolding role (Rama et al. 2008; Sheng and Kim 2011). Yet, numerous other enzymes are involved in downstream signalling pathways (Kennedy et al. 2005), such as nitric oxide synthase (nNOS), other CAMKs, non-receptor tyrosine kinases like Src and Abl, serine/threonine protein phosphatases (like PP1 or calcineurin) and tyrosine protein phosphatases, including PTENs[15] (Sheng and Hoogenraad 2007; Bayés and Grant 2009; Sheng and Kim 2011). Interestingly, most of these molecules appear to play a role in synaptic plasticity, as does also cAMP response element-binding (CREB), Arc and the synapse-to-nucleus molecule AIDA-1 (Moga et al. 2004; Kaushik et al. 2014).

[14] ARP32/3 is a major component of Actin remodelling of hippocampal spines (Rácz and Weinberg 2008).
[15] PTENs stands for phosphatase and tensin homologs.

2.5.1 Ca^{2+}/CALMODULIN-DEPENDENT PROTEIN KINASE TYPE II

CAMKIIs are serine/threonine kinases activated by Ca^{2+} and Calmodulin, hence their name. The family of CAMKIIs is formed by 4 genes/proteins (α-δ) (Tobimatsu and Fujisawa 1989). CAMKIIs can multimerize into dodecamers[16] (Okamoto, Bosch, and Hayashi 2009; Hell 2014). CAMKII has a broad spectrum of substrates, being expressed at high levels in hippocampal and cortical neurons and synapses (Song, Yan, and Zhang 2004). The biochemical differences observed between the members of CAMKII family are relatively small, but they may result in important functional differences (i.e., activation or autophosphorylation) under conditions in which Ca^{2+} levels are changing rapidly, such as neuronal spikes or brain oscillations (Gaertner et al. 2004). CAMKII-γ and -δ are broadly distributed across the brain but present much lower abundances than CAMKII-α and -β, which are particularly expressed in cortex (Ctx), hippocampus (Hip) and striatum (Str; Yamagata et al. 2009). CAMKII forms dodecamers in forebrain constituted by 9 α and 3 β subunits, whereas this ratio is inverted in cerebellum (Crb; Hell 2014). Several reports showed that the promotor of the CAMKII-α gene restricts its expression at excitatory neurons (Zhang et al. 1999; Knuesel et al. 2005), reason why it has been long considered that CAMKII-α is expressed only in glutamatergic neurons (Jones, Huntley, and Benson 1994; Sík et al. 1998). Yet, more recent works demonstrate its expression in inhibitory neurons such as cerebellar Purkinje cells (Wang et al. 2013). Additionally, CAMKII-α translocate from inhibitory to excitatory synapses depending on the Ca^{2+} levels (Marsden et al. 2010).

CAMKII produces several activity-induced changes at synapses by recruiting other proteins such as Arc, casein kinase 2 (CK2) or proteasomes to spines (Hell 2014). Also, modulates AMPAR (Thein et al. 2014) and small GTPases through its regulators like SynGAP (Zhang et al. 1999; Song, Yan, and Zhang 2004; Okamoto, Bosch, and Hayashi 2009). Moreover, CAMKII is a central organizer of spinoskeleton and acts as an auto-tuning machine to regulate its own localization at the spine. Overall, this protein promotes proper neuronal development, including synaptogenesis and Hip maturity, as well as synaptic plasticity, learning and memory (Hudmon and Schulman 2002; Takai, Sasaki, and Matozaki 2001; Wennerberg 2005; Cherfils and Zeghouf 2013; Chklovskii, Mel, and Svoboda 2004; Okamoto, Bosch, and Hayashi 2009; Hell, 2014).

[16] Alternatively splicing of *CaMKII* mRNA produce at least 30 different proteins (Gaerdner et al. 2004).

2.5.2 THE RAS SUPERFAMILY OF SMALL GTPASES

Small GTPases are exceptionally multispecific guanosine triphosphate (GTP)-binding molecules. One of the largest and better-studied groups of these proteins is the Ras superfamily, which exists in eukaryotes, from yeast to humans, and comprises over 150 members in humans. The Ras oncogenes are the founding members (Takai, Sasaki, and Matozaki 2001; Wennerberg 2005; Cherfils and Zeghouf 2013) and in mammalian neurons locate widespread, being highly represented in the PSD (Dickson 2001; Klooster and Hordijk 2007; Sheng and Kim 2011). Specifically, small GTPases can also be found at intracellular membranes[17], enriched at specialized lipid and/or protein-defined signalling platforms, such as lipid rafts, caveolae or NRC/MASCs (Bos, Rehmann, and Wittinghofer 2007; Klooster and Hordijk 2007; King, Lubeck, and Lapinski 2013; Delint-Ramirez et al. 2010). Interestingly, small GTPases and their modulators represent 10% of total forebrain proteins (Fig. I-6B; Sheng and Kim, 2011) and ~5.4% of MASC has a small GTP-binding domain (Pocklington et al. 2006).

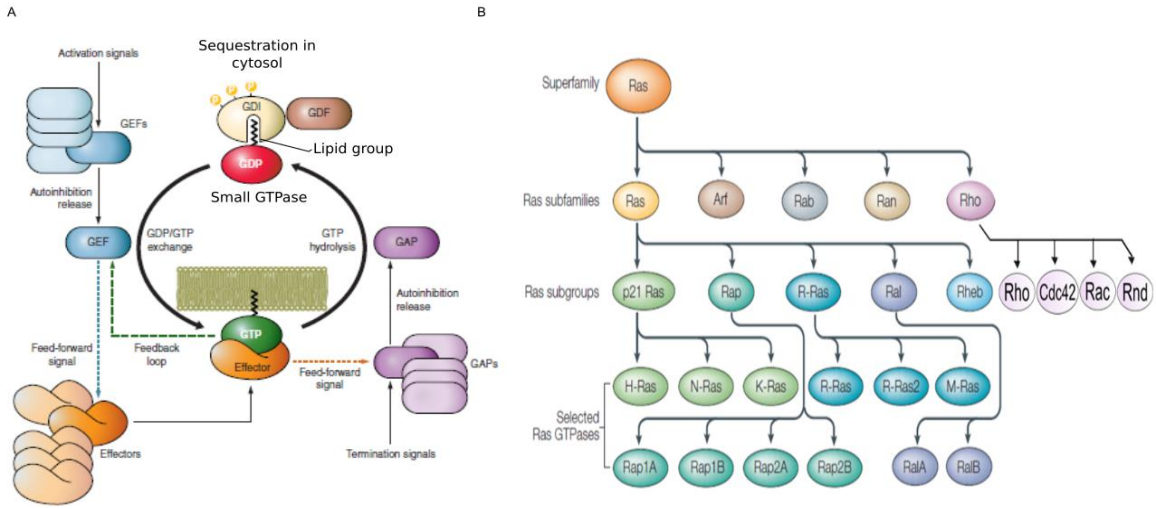

Figure I-9. The basic GDP/GTP switch of the Ras superfamily (A) The GTPase cycle. The activated GTPase can interact with so-called effector targets that ultimately produce a biological consequence. Regulation of cycling is largely accomplished through the coordinated action of its regulators (GEFs, GAPs, and GDIs) whose activity is potentially modulated in response to various signals. The Ras effectors, or immediate downstream signal transducers are proteins that bind preferentially to the GTP-bound form of small GTPases. (B) Overview of Ras superfamily and their subfamilies and subgroups. Also, the main members of Ras subgroups are indicated. Adapted from (A) Cherfils and Zeghouf 2013 and (B) Kennedy et al. 2005.

Because small GTPases can exist in an active GTP-bound and an inactive GDP-bound, they serve as molecular switches (Fig. I-9A; Wennerberg 2005; Bos, Rehmann, and Wittinghofer 2007). In addition, variations in structure, specific subcellular location and interaction with their regulators allow these small GTPases to function as sophisticated

[17] Most small GTPases are modified at their C-term by the addition of prenyl groups, which act as lipid anchors to membranes (Bos et al. 2007).

biotimers[18]. These are remarkably complex and perform a diverse range of cellular processes, ranging from cell proliferation, survival, and differentiation in essentially all cell types, and they also regulate PSD dynamics (See I-3) (Wennerberg 2005; King, Lubeck, and Lapinski 2013). Thus, its dysregulation leads to a wide range of human disorders ranging from cancer to neurodegenerative diseases and RASopathies[19] (Tidyman and Rauen 2009; Klooster and Hordijk 2007; Cromm et al. 2015).

The RAS superfamily is classified in at least 5 major families (Fig. I-9B; Ras, Rab, Rho, Sar1/Arf and Ran) based on their sequence and functional similarities, which in turn are split into subfamilies encompassing different members that have high sequence identity (40–85%), but unique functions and preferred targets (Sheng and Sala 2001). Therefore, it has long been unclear how GTPase signalling specificity is regulated as members share high sequence similarity.

Broadly speaking, the Ras family regulates gene expression as well as synaptic plasticity and neurite development (Bos, Rehmann, and Wittinghofer 2007; Spilker et al. 2008), the Rho family regulates cytoskeletal reorganization and gene expression, the Rab and Sar1/Arf families control vesicle trafficking, whereas the Ran family orchestrates nucleocytoplasmic transport and microtubule organization.

2.5.3 Regulatory proteins of small GTPases

There are 3 main groups of small GTPase regulatory proteins: guanine nucleotide exchange factors (GEFs), GTPase-activating proteins (GAPs) and guanine nucleotide dissociation inhibitors (GDIs; Fig. I-8A). GEFs may be named according to the first signalling cascade they were found to be involved in or the first protein they were shown to regulate. Nevertheless, they usually participate in multiple signalling cascades regulating several small GTPases. This rule also applies for GAPs (Yamashita et al. 2000). Specifically, the PSD from mouse Ctx encompasses a total of 29 GAPs and 30 GEFs (Wilkinson, Li, and Coba 2017).

Once active, small GTPases undergo a conformational change that enables them to interact with downstream effectors[20], ultimately promoting biological responses. Hence, regulatory proteins are key to all those roles mediated by small GTPases since regulatory

[18] Refers to initiate and terminate functions and periods of time for their continuation (Takai et al. 2001).
[19] RASopathies are introduced more extensively in section I-5.
[20] Proteins that typically bind specifically to the GTP-bound form of small GTPases. Thus, these proteins are frequently involved in eliciting a biological response to GTPase activation. Many of them are protein kinases, and probably their interaction with a corresponding active small GTPase can lead to both subcellular redistribution and catalytic activation of the kinase (Bernards and Settleman 2004).

proteins activities assure precise activation levels in neurons and have profound effects on synaptic plasticity (See section I-3; Bos et al. 2007).

2.5.3.1 GUANINE NUCLEOTIDE DISSOCIATION INHIBITORS

Ras, Rho and Rab proteins are prenylated at their C-term, which secures the attachment of their active form to endomembranes (Cherfils and Zeghouf 2013). GDIs remove small GTPase from membranes and relocate them to the cytosol by sequestration of their lipid tail, thus maintaining them as soluble inactive proteins. An example is RabGDI-α which illustrates this additional level of small GTPases control beyond GEFs and GAPs (Seabra, Mules, and Hume 2002; Andre Bernards and Settleman 2004; Klooster and Hordijk 2007).

2.5.3.2 GUANINE NUCLEOTIDE-EXCHANGE FACTORS

GEFs regulates the GDP-GTP cycle of small GTPase by inducing the release of bound GDP and its replacement by GTP (Fig.I-8A; Bernards and Settleman 2004), what renders these molecules into their active form. Beyond their activation by several regulatory signals (e.g., Ca^{2+} or receptor activation), GEF autoinhibition is emerging as a critical mechanism for processing upstream signals so that the appropriate GEF and its cognate downstream pathway are properly selected (Cherfils and Zeghouf 2013). Additionally, GEF function is not limited to the activation of GTPases, but also can determine the signalling output of the activated GTPase by forming a scaffolding platform for specific downstream effectors (Klooster and Hordijk 2007). Some examples are the Rho GEF Kalirin or the Rho and Ras GEFs SOS and RasGRF2 (Bos, Rehmann, and Wittinghofer 2007).

2.5.3.3 GTPASE-ACTIVATING PROTEINS

A hallmark of small GTPases is their very slow intrinsic GTPase activity, which generally does not match the time scale of their cellular functions. To switch off rapidly they require GAPs, which accelerate their intrinsic GTP-hydrolysis activity (Fig.I-8A; Cherfils and Zeghouf 2013). Ras superfamily GAPs share little sequence homology as a result of heterogenous combination of protein domains, which may explain the specificity of GAPs, even within highly homologue small GTPase proteins (Bernards 2003; Bos et al. 2007).

Importantly, GAPs have received considerably less attention than GEFs in the context of GTPase activity regulation. However, several GAPs are implicated in human diseases[21] and some studies have indicated potential function as effectors of activated GTPases

[21] Two widely known human diseases, neurofibromatosis type 1 (NF1) and tuberous sclerosis complex (TSC), are caused by disrupting mutations of these Ras and RhebGAPs encoding genes, respectively.

(Bernards and Settleman 2004). Moreover, the impressive large number of predicted GAPs[22] and the realisation that GAP activity can be enough to promote small GTPases-mediated biological response in the absence of extracellular stimuli (Vincent and Settleman 1999), is changing this preconception.

GAPs can be categorized into subclasses termed after their founding members (King et al. 2013). The first GAP described for the Ras superfamily was p120RasGAP or RASA1[23], which is the prototype of the first class of Ras regulators (Bernards 2003; King et al. 2013). The other 3 RasGAP families are NF1 (Xu et al. 1990); GAP1^{m}[,24] and the SynGAP family. SynGAP was the first member of its family to be described, followed by DAB2ip, RASAL2 and RASAL3 (Sung et al. 2016).

2.5.3.4 SYNAPTIC GTPASE ACTIVATING PROTEIN (SYNGAP)

SynGAP is a bifunctional Ras/RapGAP of 130-143 kDa with activity towards H-Ras and Rap1/2, initially termed p135 SynGAP (Chen et al. 1998; Kim et al. 1998; Krapivinsky et al. 2004; Kennedy et al. 2005; Pena et al. 2008). In 1998, SynGAP was characterized as a major component of the PSD of principal forebrain neurons (Chen et al. 1998; Kim et al. 1998) and as part of the NRC/MASC (Fig. I-10). In addition, SynGAP also regulates Rab5 in developing cerebellar axons (Tomoda et al. 2004), and Rac-1 through Ras activation (Tam et al. 2015; Araki et al. 2015). Thus, SynGAP is key in downstream postsynaptic signalling.

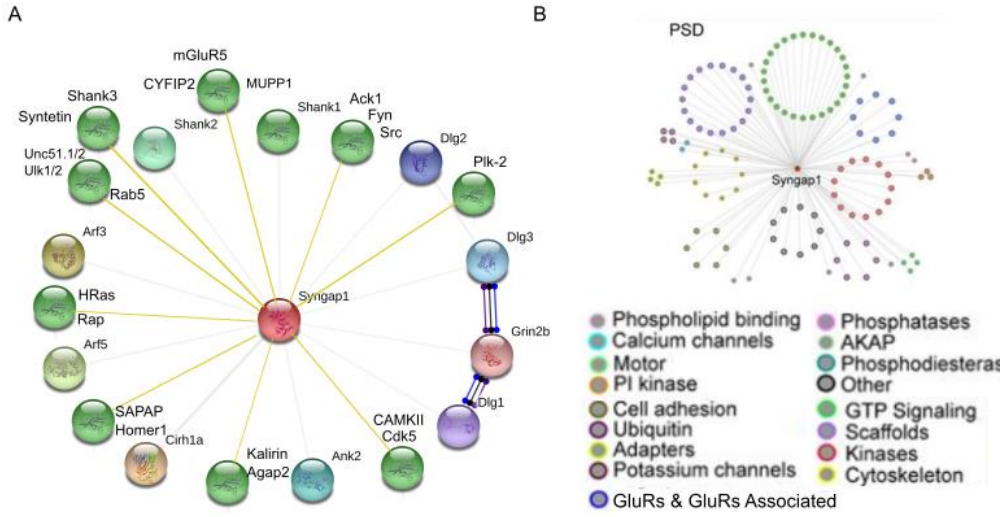

Figure I-10. SynGAP interactome in adult mice (A) Experimental evidence (light grey lines) determined by STRING *Mus Musculus* database set at medium confidence level and other interactions reported (manual text-mining; yellow lines). (B) Functional groups of SynGAP interactome from cortical PSDs extracted from Wilkinson et al. 2017.

[22] Close to 0.5% of human genes predict proteins related to GAPs for small GTPases (Bernards 2003).
[23] Stands for Ras p21 protein activator 1.
[24] RASA1, RASA3, RASA4 and RASAL1 are members of the GAP1^{m} family (King et al. 2013).

The *Syngap1* gene encodes several mRNA isoforms which vary in their 5' and 3' ends. Variation at the 5' is driven by promotor usage and alternative splicing (AS), which is also involved in generating 3' variants. Thus, the *Syngap1* gene in rodents produces different SynGAP isoforms that vary at their N-term (A, B and C variants; Chen et al. 1998; Li et al. 2001; McMahon et al. 2012) and at their C-term[25] (α1, -α2, -β and -γ variants; Li et al. 2001; Fig. I-1). SynGAP thus presents a region common to all its isoforms (a core region), which accounts for most of the total protein. The core region encompasses the following protein domains: a Pleckstrin homology (PH), a C2, a GAP, a proline rich, also known as SH3 domain binding motif and a coiled coil (CC) domain (Fig. I-11; Chen et al. 1998; Kilinc et al. 2018). The three first domains are 23%, 33%, and 47% similar, to those of p120-RasGAP respectively (Oh, Manzerra, and Kennedy 2004). Also, SynGAP can be membrane associated by its N-term (Araki et al. 2015), although the exact mechanism driven this is unclear, whereas the variable sequences of SynGAP may confer distinctive features.

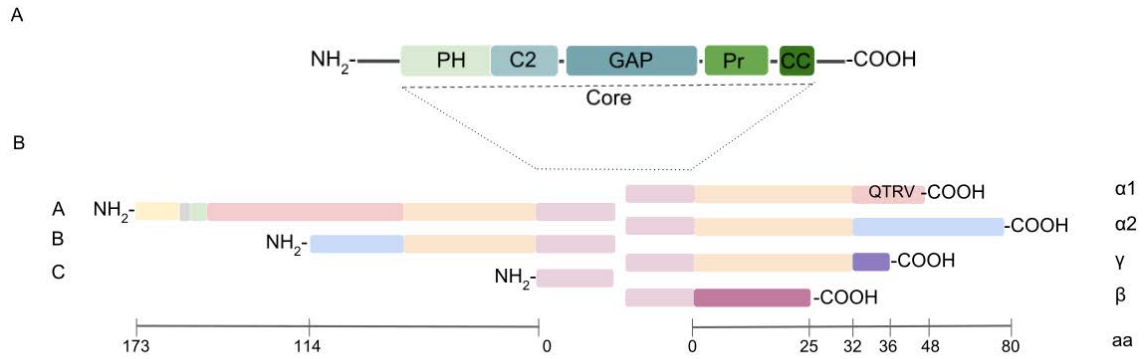

Figure I-11. SynGAP and its isoforms. Schematic illustration of (A) SynGAP domains. (B) Variable regions with its aminoacidic length. Shared sequences are equally coloured.

Although all C-term variants can be found at the PSD (Kim et al. 1998; Chen et al. 1998; Moon et al. 2008; McMahon et al. 2012), SynGAP-α1 is the only one that has a PDZ binding motif (PBM) able to directly bind the three PDZ domains of PSD-95 and other MAGUKs (Chen et al. 1998; Kim et al. 1998) as well as Syntetin, an endocytic vesicular membrane protein with two PDZ domains (Tomoda et al. 2004). In addition, all SynGAP C-term variants are expressed differently at mRNA level (Li et al. 2001), and excluding SynGAP-γ, for which there is not a specific antibody[26], the other variants localize differently

[25] It has been identified 20 different 5' mRNA *Syngap1* variants (Mc. Mahon et al. 2012) and 7 variations in the 3' *SynGAP1* mRNAs (Li et al. 2001), being 4 clustered into the SynGAP-β as they share the same unique sequence with variations in 6 or 3 nucleotides at mRNA level but translate to indistinguishable proteins.
[26] Currently there are no specific known commercial antibodies for unique N-term variants.

at the subcellular level (Li et al. 2001; Tomoda et al. 2004; Moon et al. 2008). Also, SynGAP-α1 and SynGAP-α2 perform distinct roles as they have different GAP activities towards Ras and Rap (See sections I-3 and 4; McMahon et al. 2012). Yet, little is known about the roles of SynGAP-β and -γ; and the N-term variants. SynGAP is expressed in neuronal cell bodies but has been found highly enriched at the PSD of glutamatergic neurons from the olfactory bulb (OB), Hip and Ctx (Chen et al. 1998; Kim et al. 1998; Zhang et al. 1999, Oh et al. 2004; Kim et al. 2005; Ozkan et al. 2014; Luo et al. 2012; Giovanoli et al. 2016; Aceti et al. 2015), whereas Crb express lower levels (Kim et al. 1998). Furthermore, SynGAP is also present at GABAergic neurons from Ctx, Hip and Crb[27] (Zhang et al. 1999; Knuesel et al. 2005; Berryer et al. 2016). Controversially, some articles report no SynGAP immunoreactivity in inhibitory synapses from any neuronal population (Kim et al. 1998), while others find substantial co-localization of SynGAP-β with GAD and Gephyrin (Moon et al. 2008). Finally, SynGAP is not expressed in forebrain glia (Ozkan et al. 2014).

2.5.3.5 REGULATION OF SYNGAP1/SYNGAP

Environmental, epigenetic and genetic control of GAPs expression has been described. Specifically, perinatally exposure to arsenite or prenatal immune activation reduces *Syngap1* expression levels at the brain of rodent pups (Luo et al. 2012; Giovanoli et al. 2016); *Syngap1* transcription can be regulated through the transcription factor MEF-2 (Flavell et al. 2006), and post-transcriptional regulation by miR-101b through Wnt-5 has also been described in Hip (Muro et al. 2015). Also, the usage of *Syngap1* promotor is regulated by synaptic activity and developmental stage (McMahon et al. 2011), whereas RNA binding proteins FUS and ELAVL cooperatively control long *Syngap1-α2* mRNAs stability (Yokoi et al. 2017). Thus, there is a post-transcriptional regulation of *Syngap1* mRNAs variants.

A GAP can interact with itself (e.g., SynGAP can form trimers through its CC domain; Zeng, Bai, and Zhang 2017), with other GAPs (i.e., SynGAP interacts with Agap2) or with GEFs (eg., SynGAP interacts with Kalirin). They also interact with their substrate small GTPases, or with other proteins such serine/threonine kinases or scaffolding proteins. The later brings them together with further sets of substrates (Fig. I-10; Wilkinson, Li, and Coba 2017). For instance, the SynGAP-α1 association with Syntetin in Crb provides a platform to regulate Rab5 (Tomoda et al. 2004; Barnett 2006); MUPP1 place SynGAP close to CAMKII in hippocampal neurons (Krapivinsky et al. 2004), PSD-95 and SAP102

[27] Parvalbumin-positive basket cells that innervate hundreds of neurons (Berryer et al. 2016).

modulates SynGAP association with DLGAPs and NMDAR subunits (Kim et al. 1998; Lautz et al. 2018). Also, interaction with Shanks and Homer1 locates SynGAP at a different PSD layers endowing other functions (Kim et al. 1998; Kozol et al. 2015; Lautz et al. 2018).

Furthermore, PPIs control GAP PTMs, which in turn regulate their activity and cellular distribution. Some of this PTMs include de/phosphorylation, lipid modifications (e.g, prenylation, myristoylation) or SUMOylations [28] (Oh, Manzerra, and Kennedy 2004; Dietrich 2013; K. A. Wilkinson, Nakamura, and Henley 2010; Andre Bernards and Settleman 2004). The function of these PTMs implicate, for instance, proteolytic degradation or the interaction with different phospholipids and their related signaling molecules (Tsai et al. 1989; Tsai, Yu, and Stacey 1990; Hall 1990). One example is in the complex between lipid rafts and PSD-95, which are enriched in Src and Arc but depleted in CaMKII-α and SynGAP (Delint-Ramirez et al. 2010). Thus, sub-membrane domain localization of SynGAP affects its function. Translational and post-translational regulation of precise GAP amounts is another way to control small GTPases (Bernards and Settleman, 2004). SynGAP protein expression is also controlled by Erk and mTOR signalling (See 2.5; Wang et al. 2013).

Moreover, SynGAP location and activity towards Ras and Rap is regulated by CAMKII, Cdk5 or Plk2 phosphitylation (Lee et al. 2011; Song, Yan, and Zhang 2004; Walkup et al. 2015; Araki et al. 2015) as well as by PP2A and calcineurin phosphatases (Araki et al. 2016). Finally, the tyrosine kinases Src, Fyn or Ack1 have also been described to control SynGAP activity (Pei et al. 2001; Masdeu et al. 2016; Masdeu et al. 2017).

2.6 SIGNALLING PATHWAYS IN DENDRITIC SPINES

Spine signalling is key in development, circuit assembly and synaptic plasticity (Wong and Ghosh 2002; Grant 2003; Salinas 2012). Postsynaptic changes involve a hierarchy of highly complex and overlapping signalling cascades encompassing many substrates and their cross-talk (Funk et al. 2012; Sweatt 2001). Altogether, these processes allow local regulation of transcripts and proteins, to ultimately modulate genetic expression and promote biological responses (Coba et al. 2009; Codocedo et al. 2015). Postsynaptic signalling proteins form networks that can be split into pathways, modules (groups of functionally similar proteins), and proteins that are highly connected (hub proteins; Husi et al. 2000). Indeed, a subdivision of biochemical signals at specialized micro-domains within the spine does exist. The spatio-temporal coordination of these complex signalling

[28] The small ubiquitin-like modifier (SUMO) is structurally related to ubiquitin and can be covalently linked to lysine residues. SUMOylation inhibit, modify or enable PPIs (Geiss-Friedlander and Melchior, 2007).

networks endows neurons for the concomitant remodelling of the PSD proteome, being these changes most remarkable in spinoskeleton and membrane trafficking (Colgan and Yasuda 2013). In particular, mouse NRC/MASC contains ~185 proteins contrasting heavily with the 76 or 9 proteins that make up the mGluR and AMPAR signalling complexes, respectively (Grant et al. 2005). The relevance of NRC is underscored by phosphoproteomic experiments showing that the activation of NMDAR in mouse hippocampal slices produced simultaneous changes in phosphorylation of 127 PSD proteins on around 200 sites (Coba et al. 2009) or even ~1,563 phosphorylation sites when considering several brain areas (Trinidad et al. 2008). Importantly, NRC signalling is different in glutamatergic and GABAergic neurons and are specialized in a way that might be unique in time and brain areas (Zhang et al. 1999).

2.6.1 CALCIUM SIGNALLING

Ca^{2+}-mediated signals control many physiological processes in the brain, from neural development and differentiation to synaptic plasticity in mature neurons or even cell death (Sheng and Sala 2001). At the postsynaptic side, cytosolic Ca^{2+} influxes originate from the extracellular space or the ER. The main entrance gate for extracellular Ca^{2+} are NMDAR and L-type voltage-dependent Ca^{2+} channels (L-VDCC), although some types of AMPA and Kainate receptors also display Ca^{2+} permeability. On the other hand, ER Ca^{2+} release is driven by the activation of RyR and IP_3R (Fig. I-12, left panel; Ortuño-Sahagún et al. 2010&2012; Yagami, Kohma, and Yamamoto 2012; Hell et al. 2013).

The dramatic increase of Ca^{2+} activates different postsynaptic enzymes, including different phospholipase C (PLC) and CAMKII proteins, which modulate many other proteins and signalling pathways. The activation of PLC results in the formation of IP_3 and Diacylglycerol (DAG), which act on ER receptors releasing more Ca^{2+}. Furthermore, DAG and Ca^{2+} activate protein kinase C (PKC) that modulates Ras, Raf-1 and Rho, among other proteins (Sweatt 2001). Particularly, PLC-β1 is stimulated by mGluR5 to regulate indirectly CAMKII and SynGAP activity (Oh et al. 2004; Barnes et al. 2015). Also, other sensors, such as Calmodulin, trigger kinase stimulation including CAMKs (John Lisman, Yasuda, and Raghavachari 2012) and phosphatases like Calcineurin (Marsden et al. 2010). Importantly, these events elicit autonomous autophosphorylation of CAMKII, causing its sustained activity and translocation to the PSD where it exerts multiple functions (Shen and Meyer 1999). In line with these events, SynGAP-α1 indirectly binds to CaMKII via PSD-95, MUPP1 or other scaffolding proteins through its PBM (Kim et al. 1998; Chen et al. 1998;

Krapivinsky et al. 2004), while SynGAP-β directly binds the non-phosphorylated form of CaMKII (Li et al. 2001; Oh et al. 2004).

The increase in Ca^{2+} concentration due to synaptic activity results in CAMKII phosphorylation of SynGAP, thus CAMKII regulates SynGAP activity in a PSD-95/GluN2B dependent manner (Kim et al. 2005). However, the effect of SynGAP phosphorylation by CAMKII modulates its GAP activity towards Ras or Rap, yet how does this exactly occur is still a controversial matter (Kim et al. 2001; Oh et al. 2004; Kim et al. 2005; Krapivinsky, et al. 2004; Rumbaugh et al. 2006; Wang et al. 2013; Araki et al. 2015). Also, under depolarizing conditions, SynGAP-α1 and -α2 are phosphorylated and move out of the PSD core, decreasing its small GTPases regulation in the core PSD (Yang et al. 2013; Araki et al. 2015).

Relevant Ca^{2+}-related cascades involved in cytoskeleton reorganization modulated by SynGAP are pCAMKII/RasGEF[29]/Ras-Rac1/Cdc42/PAK3/LIMK-1/Cofilin/Actin (Carlisle et al. 2008; Sheng and Kim 2011; Jeyabalan and Clement 2016); Ras/Tiam1/Rac/RhoA/ROCK2/LIMK/Cofilin (Meng et al. 2002; Sala, Cambianica, and Rossi 2008) or Ras-RalGDS/Ral/Rac/Cdc42/PLC (Colgan and Yasuda 2014). Hence, SynGAP regulates several independent pathways and integrates NMDARs with Ras and Rap associated MAPK and PI3K signalling, respectively (Komiyama et al. 2002; Krapivinsky et al. 2004).

2.6.2 MITOGEN-ACTIVATED PROTEIN KINASE SIGNALLING

The classical mitogen-activated protein kinase (MAPK) pathway begins at the cell membrane, where indirectly small GTPases (mainly Ras, Rac and Rho) or directly protein kinases activate MEKKs, which in turn will stimulate MEKs to finally phosphorylate MAPKs (Fig. I-12, central panel, blue shadow). Activated MAPKs interact with and phosphorylate numerous cytoplasmic substrates, such as non-receptor tyrosine kinases or other kinases[30], and ultimately modulate transcription factors that drive context-specific gene expression (Cargnello and Roux 2011). There are at least 3 distinct MAPK signalling modules, which transduce extracellular signals into the cell and the nucleus to “turn on/off” the expression of specific responsive genes. These modules include: extracellular signal-regulated kinases (Erks), C-Jun N-terminal kinases (JNKs) and p38 kinases (e.g., p38 MAPK; Kim et al. 2003). The small GTPases exert their regulation by promoting Raf relocation to the plasma membrane, allowing activation of Ras/Raf/MEK/Erk/Elk1/SAP-

[29] RasGEFs are SOS1/2 and RasGRF1/2 classes being RTKs the most known activators (Orban 1999).
[30] Sometimes referred to as MAPK-activated protein kinases (MAPKAPK; Gerits et al. 2008).

1/MAPKAPK/CREB; Rap1/BRaf/p38MAPK/Akt/mTOR and Rap2/TNIK/MINK2/JNK/PP2B signalling cascades (Orban, Chapman, and Brambilla 1999; Sheng and Kim 2011; Kumar et al. 2005; Avery, Figueroa, and Vojtek 2007). Strikingly, these signalling networks promote opposite effects in terms of trafficking, clustering and exocytosis or endocytosis of AMPARs (See section I-3; Krapivinsky et al. 2004; Kim et al. 2005; Rumbaugh et al. 2006; McMahon et al. 2012).

2.6.3 PHOSPHATIDYLINOSITOL 3-KINASE SIGNALLING

Tyrosine kinase receptor activation (Fig. I-12, right panel) results in a series of phosphorylations by associated tyrosine kinases of different substrates such as FRS2/3, which provide docking sites for additional signalling proteins like the adapter Grb2, or intermediate factors like Shc and Shp2[31] (Avery et al. 2007). In addition, these kinases auto-phosphorylate, promoting Grb2 binding, which results in accumulation of Grb2.-SOS complexes near the cell membrane and Ras signalling (Fig. I-12, central and right panels). In a nutshell, these events lead to the activation of PI3K/AKT and Ras/Raf/MEK/Erk pathways (Avery et al. 2007). Other receptors can activate intracellular kinases like PKC-dependent activation of Pyk2 and Src that also recruit Grb2-SOS to the membrane leading to Ras activation (Orban et al. 1999; Pei et al. 2001; Sheng and Kim 2011). Since pSynGAP regulates Ras-Erk pathway and binds to the SH2 domains of Src and Fyn, it also plays a role in PI3K signalling (Pei et al. 2001). One defined PI3K cascade modulated by SOS and SynGAP is PKC/Pyk2/Src/Grb2/Ras/Erk /TSC1/Rheb/mTOR (Fig.I-12, right panel; Sheng and Kim, 2011; Wang et al. 2013).

Of note, Ras and Rap can also modulate the pro-survival cascade: PI3K [32] - PIP_3/PDK/AKT/mTOR/ GSK3β (Komiyama et al. 2002; Knuesel et al. 2005; Srivastava et al. 2018) which mainly regulates protein synthesis and transcription (Kumar et al. 2005). Inversely, the PI3K/AKT pathway can regulate Ras, Rap and Rho cascades (Sheng and Kim, 2001). As an example, this cascade regulates the Ras-family small GTPase Rheb, which in turn regulates the mTOR pathway (Bernards and Settleman 2004).

[31] Is an abbreviature of Src homology 2 tyrosine phosphatase 2.
[32] The complete name is phosphatidylinositol 3'-kinase.

2.6.4 CYCLIC ADENOSINE MONOPHOSPHATE/PROTEIN KINASE A SIGNALLING

G protein-coupled receptors (GPCRs) such as mGluRs are bound to heterotrimeric G proteins comprising a GDP-bound Gα and Gβγ subunits. Upon stimulation, Gα exchanges GDP for GTP and dissociates from the Gβγ subunits. Free Gα performs multiple functions depending on the subunits, including RhoGEF activation (Suzuki, Hajicek, and Kozasa 2009). Two main downstream transduction cascades involve IP_3/DAG and PKA (or cAMP dependent serine/threonine protein kinase). Related to protein kinase A (PKA), extracellular signals are converted to intracellular signals through 2nd messengers by G subunits that regulate adenylyl cyclase (AC). ACs use ATP to generate cAMP (cyclic adenosine monophosphate) and can be also activated by Ca^{2+} through Calmodulin. To illustrate the cross-talk between these previously described signalling cascades, PLC can be also modulated by mGluRs activity (Sheng and Kim, 2001) or signalling pathways like AC/cAMP/RapGEF/Rap/Rap as well as AC/cAMP/PKA/Rap1/BRaf/MEK/Erk/RSK2/CREB (Orban, Chapman, and Brambilla 1999; Sweatt 2001). Interestingly, PKA along with PKC pathways provide a link either between NMDAR or mGluRs and Erk activation (Sweatt 2001).

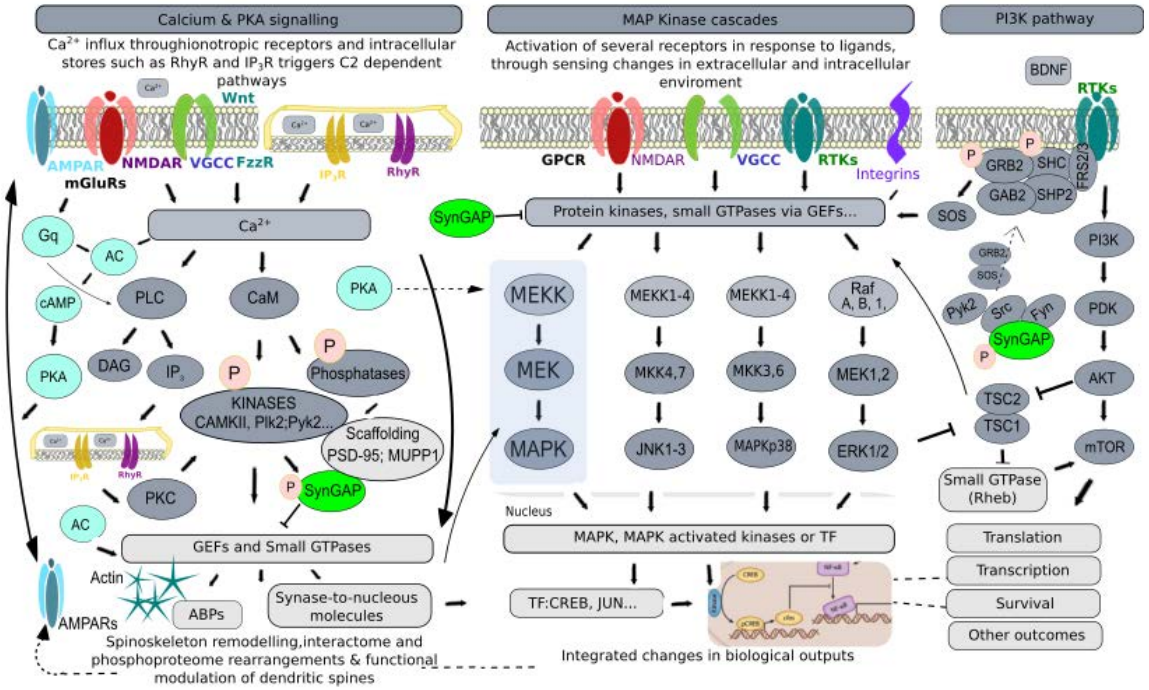

Figure I-12. Signalling pathways in dendritic spines. These pathways start upon membrane receptors activation. The kinases in each tier phosphorylate and activate the kinases located in the next tier downstream. This process is repeated from tier to tier allowing for rapid and regulated transmission. It is unlikely that discrete modules act alone, rather act in parallel and interconnecting within them, to expand signalling networks. Although classical activation of Ras family, via receptor tyrosine kinase (RTKs) and adaptor proteins, does occur in neurons in response to neurotrophic factors, Ras family activation in response to membrane depolarisation or glutamatergic signalling represents a non-classical pathway. Arrows indicate activation whereas "T" inhibition.

3. SYNAPTIC PLASTICITY IN DENDRITIC SPINES

The ability of synapses to modify their structure and transmission efficacy is called synaptic plasticity (Lepeta et al. 2016). It allows synapses to be remodelled, created, and eliminated as a result of synaptic activity (Johansson 2000; Ziv and Brenner 2018) and ultimately, shape neuronal networks (Neves, Cooke, and Bliss 2008; Fauth and Tetzlaff 2016). Synaptic plasticity is critical not only for regulating the flow of information within networks, but also for the development of neural circuits; the acquisition of new information (learning) as well as its storage and recall (memory) or its erase (forgetting; Heidelberger et al. 2014; Bernardinelli, Nikonenko, and Muller 2014). Mushroom spines are AMPAR-rich spines having been strengthened by activity-dependent plasticity and have been called the “memory spines”, since they are found in mature and stable synapses (Sala, Cambianica, and Rossi 2008). In contrast, the young, newly formed thin and filopodia-like spines are the “learning spines”, as they host silent synapses “waiting” for synaptic activity to convert them into more functional synapses (Kasai et al. 2003; Fauth and Tetzlaff 2016). These are more prone to be eliminated over time (Bernardinelli, Nikonenko, and Muller 2014). Despite there is no direct evidence, the conversion of large “memory spine” back into smaller “learning spines”, it is thought to reset the plasticity potential of synapses (Sala, Cambianica, and Rossi 2008).

3.1 TYPES OF SYNAPTIC PLASTICITY

Synaptic plasticity can be split into structural and functional (Colgan and Yasuda 2014). Classic functional plasticity refers to synaptic strength due to quick changes in electrochemical efficacy (Fauth and Tetzlaff 2016). It allows fast adaptations of network activity and can be expressed presynaptically such as changes in the probability of NT release or/and postsynaptically by changes in NT sensitivity as well as the number or unitary conductance of PSM receptors (Heidelberger et al. 2014). Conversely, structural plasticity involves changes in PSD components and spine size and shape. Structural plasticity determines the formation and removal of synapses (Yuste 2010, 2011; Colgan and Yasuda 2014). Although structural plasticity is tightly associated with functional plasticity (Fauth and Tetzlaff et al. 2016), on a longer timescale it may allow more significant and stable rewiring of synaptic networks through both the formation of new connections and the stabilization of the older ones (Bernardinelli, Nikonenko, and Muller 2014).

If the synaptic modification is intrinsic or extrinsic to a given synapse it is referred to as homo- or heterosynaptic plasticity, respectively. Synaptic plasticity can also be distinguished as a function of time: short-term plasticity (persists for seconds to minutes) and long-term plasticity (lasts hours, days or lifetimes). Short- and long-term forms of plasticity are Ca^{2+}-dependent and mediate bidirectional processes that are facilitation/potentiation and depotentiation/depression. Specifically, short-term changes allow for the action-packed regulation of neural information processing, namely postsynaptic potentials and for types of short-term memory. Conversely, in long-term forms brief periods of repetitive synaptic activity lead to sustained changes in synaptic transmission which shapes the responses of sensory cells to its stimuli and mediates learning and long-term memory (Heidelberger et al. 2014).

3.2 MECHANISMS OF SYNAPTIC PLASTICITY

The mixing of a variety of synaptic regulatory mechanisms in different brain areas is likely to provide a rich diversity in the mechanisms by which distinct areas of the brain process and encode information at synapses (Zhang et al. 1999; Crozier et al. 2007; Larsen et al. 2010). Thus, there are several activity-dependent synaptic plasticity mechanisms, being homeostatic (Turrigiano et al. 1998) and Hebbian (Hebb, 1949) the major paradigms (Fig.I-13). One of the homeostatic mechanisms is synaptic scaling, where all synapses in a given neuron are modulated according to the cell average excitability relative to network activity (Ibata, Sun, and Turrigiano 2008; Turrigiano 2008; Goel et al. 2011). Thus, this form of unspecific plasticity induces a negative feedback loop: when neuronal activities are high, overall synaptic efficacies are down-scaled and the other way around (Turrigiano et al. 1998; Turrigiano 2011). Conversely, Hebbian plasticity is a synapse specific correlational form of plasticity that maps the strength of the presynaptic stimulus onto the strength of the postsynaptic transmission (Hebb, 1949; Feldman 2012). Hebbian plasticity alone induces a positive feedback loop and the long-term form can be divided into two main outcomes: LTP and long-term depression (LTD).

Other mechanisms of plasticity are epileptogenesis and metaplasticity. The former depends on mGluR type I activation and protein synthesis (Gall and Lynch 2004; Bardoni and Abekhoukh 2014) whereas metaplasticity occurs when past activity can radically alter the present synaptic properties and thus, change the ability to induce subsequent plasticity (Bliss, Collingridge, and Morris 2014). The combination of specific Hebbian and non-Hebbian modes, like the homeostatic mechanism, leads to a desired and stable neuronal firing rate (Abbott and Nelson 2000; Fauth and Tetzlaff 2016). As a result, synapses important for learning are selectively potentiated and those important for memory are

stabilized by Hebbian LTP, what leads to an increase in spine number and higher neuronal activity within a desirable range. Simultaneously, this increased activity triggers unspecific homeostatic functional and structural plasticity to prune small, non-potentiated synapses or the reverse situation. Hence, these mechanisms adapt the connectivity of the neural network due to individual synapse-specific alterations (Fauth and Tetzlaff et al. 2016).

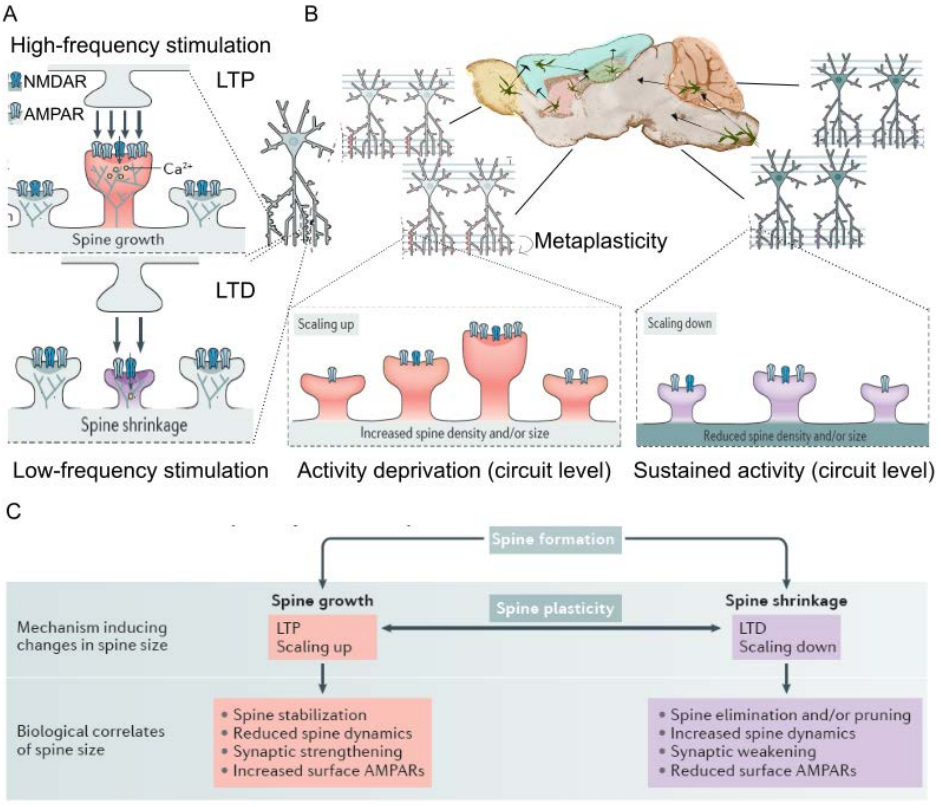

Figure I-13. Synaptic plasticity in dendritic spines. (A) Hebbian and (B) Non-hebbian mechanism including meta- and homeostatic plasticity. Epileptogenic forms are mainly studied in Ctx (blue) and Hip (green), two areas involved in learning and memory. Also, OB (yellow); Crb (orange) and Str (red) have a role in olfactory, motor and memories associated with reinforcement, respectively. (C) Structural plasticity. Modified from Forrest, Parnell, and Penzes 2018 and the *Mus musculus* brain is extracted from http://www.gensat.org.

3.2.1 SYNAPTIC PLASTICITY MEDIATED BY SYNGAP

There are 3 main phases in long-term plasticity: (1) the induction, when pre- and postsynaptic spike patterns are sensed and the nature of the change in synaptic efficacy is signalled (e.g., NTs release and Ca^{2+} levels), (2) the expression which is the actual change in synaptic efficacy (e.g., signalling cascades) at both pre- and/or postsynaptic levels, and (3) the maintenance phase, representing enduring changes and the real substrate of memories (Heidelberger et al. 2014). In addition, an early component (E-LTP/D) and a late component (L-LTP/D) can be distinguished. E-LTP/D lasts less than 4 hours and is independent of protein synthesis, while L-LTP/D lasts more than 4 hours, is protein synthesis dependent and involves synaptic growth (Bliss, Collingridge, and Morris 2014). The molecular details of plasticity are thought to differ between synapse types.

3.2.1.1 NMDAR-DEPENDENT LONG-TERM POTENTIATION

Classical hippocampal LTP at CA3-CA1 synapses originally described by Bliss and Lomo in 1973, is the most robust and widely studied form of LTP (Chater and Goda 2014). However, it can be triggered in a plethora of other brain systems ranging from the spinal cord (Ji et al. 2003) to the neocortex of mammals (Bear and Kirkwood 1993) and non-mammalian species (Heidelberger et al. 2014). LTP can be induced by high frequency stimulation (Harvey and Svoboda 2007) through a variety of electrical, pharmacological and behavioural paradigms (Malenka and Bear, 2004; Artola et al. 2006).

Synaptic activity promotes pCAMKII translocation from the cytosol to the PSD, where it binds and phosphorylates NMDARs (Meng et al. 2003; Barria and Malinow 2005). There, it promotes PSD remodelling by phosphorylation of multiple substrates, including PSD-95, SynGAP, AMPAR subunits. Furthermore, by autophosphorylation CAMKII locks itself in an activated state, which can be reversed by phosphatases (Yoshimura et al. 2002; Bayer and Schulman 2001; Strack et al. 1997). The “slot” model[33] predicts that under basal conditions, all PSD binding slots are filled, and synaptic activity would free them to allow plasticity-associated modifications, including the insertion of new AMPARs[34] (Opazo, Sainlos, and Choquet 2012; Walkup et al. 2016; Lautz et al. 2018; Dosemeci et al. 2015). Indeed, during LTP induction 2% of the total PSD proteome is recruited (Zhang, Neubert, and Jordan 2012), including Shank2, whereas other proteins, such as PSD-95 retains its position (Dosemeci et al. 2015).

Correspondingly, pSynGAP has been proposed to be an important mediator of ‘slot opening’ (Walkup et al. 2016), as its rapid dissociation from the PSD following synaptic activity (Yang et al. 2013; Araki et al. 2015) would leave empty ‘slots’. Furthermore, these transient increases in extra-synaptic pSynGAP can be reversed by phosphatases in response to NMDAR activation (Westphal et al. 1999; Carlisle et al. 2008). As SynGAP dissociates from PSD-95, Homer1 and Shank scaffolds (Lautz et al. 2018) there is an increase in other scaffold interactors resulting in an expansion of the active spine, and a net increase in synaptic strength (Walkup et al. 2016). These events result in an increase in ion flow due to AMPAfication and increased conductivity, to further remove the voltage-dependent blocking of Mg^{2+} from NMDAR channels and elicit small GTPase associated signalling (Kennedy et al. 2005).

[33] The sites at which the receptors are trapped have been referred to as ’slots,’ (Shi et al. 2001) and they are believed to consist principally of PDZ domains of PSD-95 (Opazo et al. 2012; Walkup et al. 2016).
[34] The trafficking of AMPAR to the PSM bound to the PSD, is known as AMPAfication (Heidelberger et al. 2014).

Other events related with LTP are the mobilization of recycling endosomes and vesicles into spines (Park et al. 2006); polyribosome redistribution into enlarged dendritic spines (Ostroff et al. 2002) accompanied by an increase of RNA binding proteins (called RNABPs); poly(A) mRNAs (Zhang, Neubert, and Jordan 2012); F-Actin levels (Lin et al. 2005; Kramár et al. 2006); mitochondria translocation into spines and the appearance of the spine apparatus (Li et al. 2004; Segal 2010; Colgan and Yasuda 2014). Finally, there is an increase of protein synthesis matching with L-LTP leading to an enlargement and morphogenesis of dendritic spines and synapse strengthening (Fig. I-14; Sala, Cambianica, and Rossi 2008).

During the maintenance phase there is a transition from E- to L-LTP whereby deactivated CAMKII may dissociate from PSD and re-associate with the Actin cytoskeleton stabilizing LTP-induced changes (Colgan and Yasuda, 2014). It has been hypothesized that once plasticity (weak or strong) is induced in a synapse, a molecular “tag” identifies this synapse. The synaptic tagging hypothesis states that tags last for a few hours. Synaptic tags promote the capture of newly synthesized proteins transiting in dendrites and use them to convert E-LTP to L-LTP in a synapse-specific manner (Heidelberger et al. 2014). Persistent changes in transcription can be permissive for L-LTP or might be involved in altering the ability of the cell to undergo subsequent metaplasticity. Thus, transcriptional regulation is also important during L-LTP (Sweatt 2001).

Predictably, small GTPases and SynGAP do play a crucial role in synaptic plasticity (Fig. I-14). LTP induction and expression are mediated by cAMP-PKA and Ras/MAPK/Erk cascades (Lisman 1989; Sheng and Kim 2002; Heidelberger et al. 2014), whereas PI3K signalling is required for the expression but not induction of LTP (Sheng and Kim 2002). Notably, activation of p38MAPK signalling has been shown to mediate impairments in LTP (Butler, O’Connor, and Moynagh 2004). Beyond these pathways, SynGAP can also regulate mTOR signaling through the Ras/Erk link to the PI3K cascade (Shi and Gaestel 2002; Heidelberger et al. 2014).

3.2.1.2 NMDAR-DEPENDENT LONG-TERM DEPRESSION

As a concept, LTD of synaptic strength stands for the weakening on synaptic transmission and is supposed to be the correlate of memory erase (Rumbaugh et al. 2006). Despite LTD is as widely expressed as LTP, it was not until 1992 that stimulation protocols to reliably elicit homosynaptic NMDAR-LTD of basal synaptic responses at CA3-CA1 synapses were established (Dudek and Bear 1992).

LTP and LTD share a common intracellular increase in Ca^{2+} levels, but they are separate processes, each controlled by independent pathways (Heidelberger et al. 2014). Mechanistically, the induction of NMDAR-dependent LTD is mediated by low frequency NMDARs stimulation and correlates with a low rise of cytosolic Ca^{2+} (Malenka and Bear 2004) and the activation of phosphatases targeting proteins like PKA, PSD-95 or GluA1 (Chater and Goda 2014). During LTD expression in CA3-CA1 synapses, there is an intervention of a postsynaptic mechanism as LTP, being key the changes in phosphorylation state of AMPARs (See Fig. I-14; Montgomery and Madison 2002). AMPARs phosphorylation state influences their interaction with other proteins, their loss from post- and extrasynaptic membranes, via dynamin- and clathrin-dependent endocytosis (Malenka and Bear 2004; Jurado et al. 2010), along with a reduced conductance (Banke et al. 2000; Bassani et al. 2013). Also, LTD is thought to be mediated by components of the caspase apoptotic pathway that elicit localized upregulation of GSK-3β (Bliss, Collingridge, and Morris 2014) and small GTPases such as Rap and Rab5 (Zhu et al. 2002; Brown et al. 2005). In addition to PI3K (Kim et al. 2011) and JAK/STAT pathways (Nicolas et al. 2012; Chater and Goda 2014), p38 is required in the induction of mGluR-LTD (Corrêa and Eales 2012). Noteworthy, a lack of SynGAP leads to alterations in mGluR-LTD (Barnes et al. 2015).

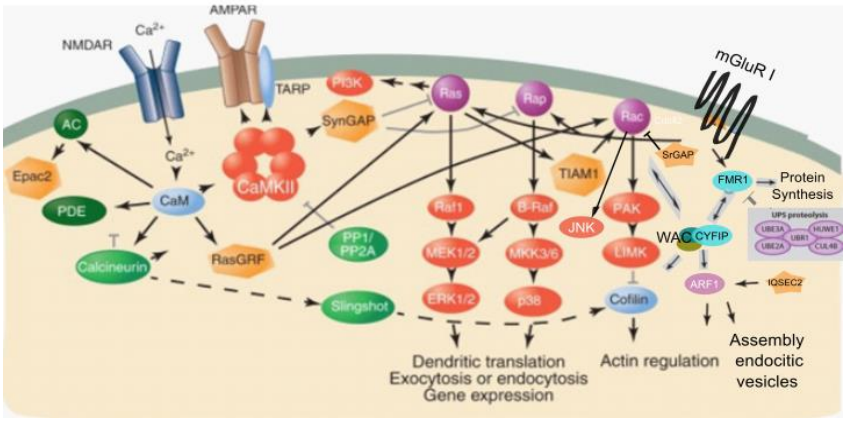

Figure I-14. SynGAP regulation of synaptic plasticity in dendritic spines. Changes in the activity of Ras and Rap are regulated by downstream targets of Ca^{2+}/Calmodulin pathway, including RasGRF, SynGAP, and Adenylyl cyclase. Erk signalling facilitate exocytosis, whereas p38 mediates endocytosis. Yet, intermediate steps in the processes are still unknown. Dashed lines indicate indirect interactions; in grey the inhibitory regulation; arrows with grey background indicate mGluR type I-LTD associated signalling. Irregular shapes show GAPs and GEFs. WAC stands for WAVE complex. Modified from Kennedy et al. 2005.

3.2.1.3 SYNGAP REGULATION OF AMPARS TRAFFICKING

During LTP induction, pCAMKII action and Ras/MEK/Erk and PI3K/AKT pathways drive AMPAR subunits with long C-term (i.e., GluA1/2L) into synapses (Zhu et al. 2002; McCormack, Stornetta, and Zhu 2006; Pavlowsky, Chelly, and Billuart 2012), thus potentiating synaptic strength. In mature cultured neurons, GluN2A-containing NMDARs

promote surface expression of GluA1, whereas GluN2B-NMDARs inhibit its surface expression (Kim et al. 2005). As SynGAP is selectively associated with GluN2B-NMDARs in brain and is required for inhibition of NMDAR-dependent Erk activation (Kim et al. 2005), it operates as a brake of the conversion between silent to non-silent synapses (See 1.2.1; Rumbaugh et al. 2006).

Conversely, LTD is promoted by Rap1/p38 MAPK signalling, leading to synaptic removal of AMPARs with short C-term (GluA2/3; Zhu et al. 2002; McCormack, Stornetta, and Zhu 2006). Among the many molecules signalling downstream of p38MAPK, Rab5 is particularly relevant, as it is essential for early endocytic processes (Shi and Gaestel 2002). Therefore, an attractive hypothesis is that activation of p38 MAPK via Rap1 may accelerate AMPAR endocytosis by stimulating the formation of the GDI-Rab5 complex (Huang et al. 2004; Lim et al. 2016). Then, the RapGAP activity of SynGAP would repress AMPARs endocytosis. Cooperatively, phosphorylation of GluA2/3 would prevent TARPs from AMPAR-induced clustering, further reducing the recycling of AMPAR and synaptic transmission (Matsuda et al. 2000; Chung et al. 2003)

In line with these events, overexpression of either Rap1 or Rap2 causes a decrease in mEPSC (Fu et al. 2007). However, Rap2 mode of action is different from that of Rap1, which has preferential affinity for NMDAR and SPAR (a RapGAP; Husi et al. 2000; Pak et al. 2001), and mediates JNK signalling to control synaptic removal of AMPARs with long C-term during depotentiation[35] (Zhu et al. 2005; Kielland et al. 2009). In a nutshell, Ras proteins have a prominent role in LTP, whereas Rap1 and Rap2 are the main mediators of LTD through different ways, though. SynGAP as a dual GAP regulates all of them (Fig. I- 14 &15).

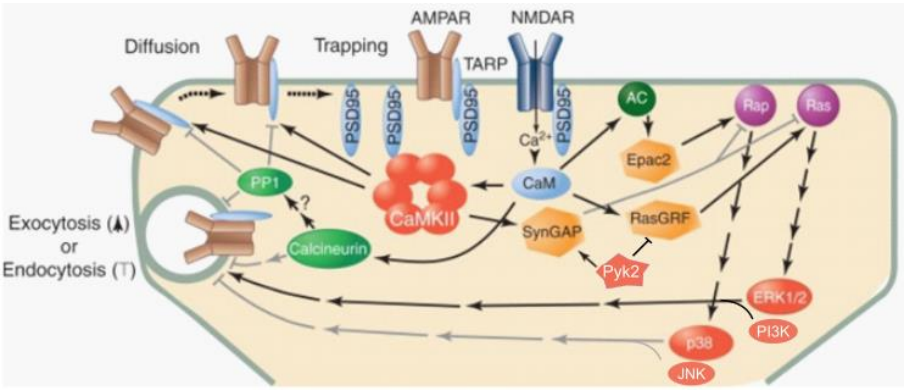

Figure I-15. Synaptic regulation of AMPAR trafficking. Addition of AMPARs to the dendritic plasma membrane by exocytosis, and their removal by endocytosis, occurs at perisynaptic sites in the spine and along the dendritic shaft. Modified from Kennedy 2005.

[35] For instance, low frequency synaptic inputs after LTP induce depotentiation.

3.2.1.4 SYNGAP REGULATION OF DENDRITIC SPINE MORPHOLOGY

The onset of LTP and the concomitant increase in the PSD proteome are coincident with Cdc42 and RhoA activation, ABPs enrichment and spine-volume growth (Hering and Sheng, 2001; Colgan and Yasuda et al. 2014). Thereafter, during maintenance of LTP, there is a growth of new dendritic spines, enlargement of pre-existing ones and, occasionally, the splitting of single PSDs and spines into two functional synapses (R. Yuste and Bonhoeffer 2001; Malenka and Bear 2004; Sala, Cambianica, and Rossi 2008). Actin cytoskeletal reorganization and synthesis of key proteins like CAMKII-α and AMPAR are needed to maintain LTP whereas inhibitors of Actin polymerization impair it (Malenka and Bear 2004). Both Rac1-PAK and RhoA-ROCK pathways are essential for the induction and maintenance of spine enlargement (Araki et al. 2015). Moreover, upon LTP induction Cofilin is transiently activated allowing for spinoskeleton remodelling, thus contributing to structural plasticity. Shortly afterwards, Cofilin is inhibited by phosphorylation, an event which is disrupted in *Syngap1* KO mice that present increased pCofilin levels (Vazquez et al. 2004; Rumbaugh et al. 2006; Carlisle et al. 2008; Barnes et al. 2015; Carlisle et al. 2008). Also, these mice exhibit a significantly abnormal increase in spine head diameter and volume (Vazquez et al. 2004), although no change in spine head size has also been reported (McMahon et al. 2012; Barnes et al. 2015). No differences in spine density in *Syngap1* KO neurons have been found (Vazquez et al. 2004; Rumbaugh et al. 2006; Carlisle et al. 2008; Barnes et al. 2015).

Regarding LTD, the loss of AMPARs and conductance (Spilker et al. 2008) is paralleled by a reduction of scaffold proteins that act as a place holder for AMPARs, like PSD-95 (El-Husseini el et al. 2002; Malinow and Malenka 2002), and a consequent spine head shrinkage and/or retraction of spines associated with Actin depolymerisation (Sala, Cambianica, and Rossi 2008). These effects are mediated by Calcineurin (Horne and Dell'Acqua 2007; Spilker et al. 2008). The fact that SynGAP interacts with Shanks, Homer and mGluR5 (Wilkinson, Li, and Coba 2017; Lautz et al. 2018) and that SynGAP-α1 overexpression triggers a significant spine shrinkage (Rumbaugh et al. 2006), further support its role in LTD.

In summary, SynGAP as a dual GAP, regulates in an isoform specific manner the exo- and endocytosis of AMPARs through ERK/PI3K and p38/JNK, respectively (Fig. I-14&15). Given the fact that: i) both mEPSC and MEF2 activity correlate with the degree of metaplasticity (Zhang et al. 2005; Dietrich 2013), ii) SynGAP control the conversion of silent to non-silent synapses, iii) *Syngap1*$^{+/-}$ mice showed impaired short-term and long-term plasticity, iv) *Syngap1*$^{+/-}$ mice are prone to epileptogenesis, v) SynGAP is part of the

homeostatic compensatory mechanism, and vi) SynGAP promotes enlargement and stabilization of mushroom spines heads, there is no doubt of the key role of SynGAP in several forms of functional and structural synaptic plasticity basic for cognitive functioning.

4. SYNAPSE FORMATION AND MATURATION

Although some mammalian species, like rodents or humans, are born with relatively immature brains (altricial), others are born with more developed brains (precocious). Yet, in both cases, neurons present at birth undergo a period of overproduction of their neurite arborization and of spino- and synaptogenesis. Thus, synaptic density increases importantly early in postnatal development to later be refined by a process called synaptic pruning. The transient period of rapid growth of the sigmoidal curve when brain weight is plotted against age is commonly known as the “brain growth spurt” (BGS; Dobbing and Sands 1978).

4.1 NEURITE EXTENSION

Before the start of synaptogenesis, around postnatal day (PND) 1, neurite extension is a crucial event. The growth cone, a specialized sensing device located at the tip of the outgrowing axon, mediates axonal guidance. Growth cones express a series of guidance receptors like Robo and L1 that can sense a variety of long-range (diffusible) and short-range (surface-bound) guidance cues (Kamiguchi and Lemmon 2000; Huber et al. 2003). These guidance cues can be attractive (e.g., Wnt) or repulsive (e.g., Semaphorin and ephrin) and are secreted in a spatio-temporal manner by intermediate targets and guidepost cells, including astrocytes. As a result, the axon navigates through the labyrinth of the developing CNS to reach its target (Plachez and Richards 2005). In addition, the activation of guidance receptors induces endocytosis of axonal membranes, a process controlled by Rab small GTPases (Zimmer et al. 2003).

Reduced SynGAP expression results in abnormal migration and reduced survival of new-born neurons (Knuesel et al. 2005; Mary Muhia et al. 2012). Accordingly, *Syngap1*$^{-/-}$ mice die between PND2-7 (Komiyama et al. 2002; Kim et al. 2003; Vazquez et al. 2004; Knuesel et al. 2005) and SynGAP amounts inversely correlate with caspase-3 levels, confirming its role in apoptotic pathways (Knuesel et al. 2005). Importantly, in developing neurons SynGAP is distributed in almost all neuronal compartments (see Fig. I-4C), this is in contrast to its high enrichment in PSDs from adult neurons (Knuesel et al. 2005). Also, a lack of SynGAP increases dendritic complexity earlier in neocortex, but not in Hip (Varghese et al. 2017) and promotes a marked reduction of GABAergic boutons of forebrain parvalbumin immunoreactive basket interneurons (Berryer et al. 2013). Finally, SynGAP-α2 was proven to be a negative regulator of axon outgrowth (Tomoda et al. 2004).

4.2 SPINOGENESIS

Most spines serve as recipients for synaptic input, but occasional naked spines can be seen. Filopodia extensions are spine precursors, these are also referred to as protospines. Furthermore, there are spines that appear first as stubbies rather than as long protospines (Yuste and Bonhoeffer, 2004). Only ~0.2% of all filopodia will eventually become spines (Majewska, Newton, and Sur 2006). Noteworthy, these spine precursors coexist with electrical synapses which are widespread at PND5-12 and dramatically decrease by PND16 (Pereda 2014). Between PND0-12 naked spines without PSDs can be identified (Yuste and Bonhoeffer 2001). All these findings lead to establish different models of spinogenesis to explain the protospine diversity found in early stages of development.

The Sotelo model states that spine development is intrinsic and independent of the presynaptic terminal, a cell-autonomous property of the postsynaptic neuron (Fig.I-16a; Sotelo 1978), whereas the Miller & Peters model predicts a sequential three-step growth of spines. The latter is triggered by the axonal terminal whereby (1) spines are made onto the dendritic shaft or immature spines, (2) the presynaptic region of the axon shows a swelling as synaptic vesicles accumulate, and (3) many spines become thin or mushroom-shaped, whereas axonal terminals have well developed varicosities (Fig. I-16b; Miller 1988). Alternatively, the filopodial model states that postsynaptic neurons grow filopodia that actively seek out for presynaptic partners. When these processes contact an axon, a synapse is established (Fig. I-16c; Vaughn, Henrikson, and Grieshaber 1974; Bradley and Berry 1976; Ziv and Smith 1996).

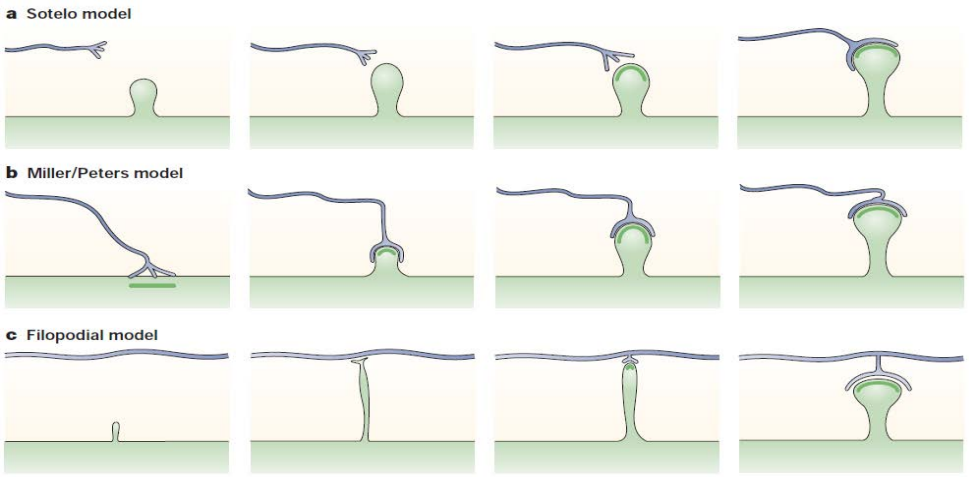

Figure I-16. Models of spinogenesis. Adapted from Yuste and Bonhoeffer 2004.

At day in vitro (DIV) 10, *Syngap1*$^{-/-}$ neurons show more protrusions and mature mushroom spines away from thin filopodia. Thus, SynGAP negatively regulates spine formation and limits spine head expansion and filopodial extension. It is worth noting that these effects

are mediated by the PBM of SynGAP-α1, whereas the GAP domain would only promote a partial head enlargement. Yet, both domains also participate in retarding the widening of spine heads and prolonging the period of filopodial extension (Vazquez et al. 2004; Knuesel et al. 2005; Rumbaugh et al. 2006).

4.3 SYNAPTOGENESIS

Synaptogenesis refers to the biochemical and morphological changes which enable the formation of synapses between neurons. Synaptogenesis is thought to be a protracted phenomenon, taking days or even weeks to complete, whereas spinogenesis can be terminated in minutes. In rodents, synaptogenesis starts at birth after astrocyte appearance (Barker and Ullian 2010), but does not start to be extensive until PND4. It involves (1) synaptic specification and (2) synaptic assembly (Rafael Yuste and Bonhoeffer 2004).

4.3.1 SYNAPTIC SPECIFICATION

For a given neuronal circuit to achieve correct innervation the precise execution of multiple events is required. These include cell fate specification and migration; axon guidance; dendritic growth; synaptic target selection and in most cases, spinogenesis (Colón-Ramos 2009). Synaptic specification in the context of synaptogenesis refers to the selection of the right partner to form a synapse.

The components of the synaptic cleft play an important role during synaptic specification, which explain the high diversity of splice variants of CAMs expressed in a cell specific manner to allow synapse specificity and diversity (Sheng and Kim 2011). For example, Neuroligin-Neurexin interaction determines excitatory or inhibitory synapses specification in an isoform and activity-dependent manner (Graf et al. 2004; Chubykin et al. 2007; Südhof 2017). Also, differentiation of synaptic ultrastructure, the establishment of more permanent intercellular adhesion and the initiation of functional maturation of synaptic transmission processes take place during synapse specification (Kelly and Vernon 1985).

4.3.2 SYNAPTIC ASSEMBLY

After the pre- and postsynaptic contact is made, a gradually mature synapse is formed at both compartments. Synaptic assembly implies the get-together of the complex macromolecular pre-, trans- and post-synaptic machineries (Colón-Ramos 2009), which goes along with the stabilization of the whole structure (Dailey and Smith 1996; Ziv and

Smith 1996; Fiala et al. 1998). Specifically, the dense core vesicles containing Piccolo and Bassoon as well as other protein complexes appear early in axonal processes which travel until they find where new synapses are forming (Zhai et al. 2001; Shapira et al. 2003). Alternatively, postsynaptic proteins can induce presynaptic assembly and drive the formation of new contacts (Giovanoli et al. 2016).

One model of PSD building relies on a Drebrin accumulation on the postsynaptic site, which would promote Actin assembly and the clustering of PSD-95 in the PSD (Takahashi et al. 2003). PSD-95 assembly is spatio-temporally correlated with spine morphogenesis and the clustering of presynaptic vesicle proteins (Marrs, Green, and Dailey 2001). Also, PSD-95 is necessary to stabilize the spine as it contributes to the insertion and activation of GluRs and CAMs (Kim et al. 2006; Gerrow and El-Husseini 2006; Ehrlich et al. 2007). In fact, PSD-95 assembles into supercomplexes composed of over 80 proteins, which together with other building blocks (e.g., complexes or nanodomains) allow the supramolecular organization of proteins and thus, synapse formation (Frank et al., 2017; Frank and Grant 2017). Therefore, PSD-95 can be exploited as a standard marker for excitatory postsynaptic maturation (Kim et al. 2007).

Additionally, Shank and Homer also cooperate to accumulate proteins into the growing PSD, such as DLGAPs or GluN1, and increase the F-Actin content of spines (Sala et al. 2001; Sala, Cambianica, and Rossi 2008), which is also required for postsynaptic clustering (Nonaka et al. 2006). The diversity of synapses arises from the combinatorial expression of a limited number of genes, yet alternative splicing (AS) greatly expands the repertoire of protein involved synapse specification (Südhof 2017). Finally, it is interesting to realise that distinct transcription factors have been shown to independently regulate excitatory and inhibitory synaptogenesis (Gatto and Broadie 2010).

4.3.2.1 SYNGAP ROLE IN FORMATION OF THE POSTSYNAPTIC DENSITY

SynGAP is also implicated in PSD protein clustering and/or movement of PSD proteins into the spine head (Vazquez et al. 2004). Remarkably, a phase-transition model describes how SynGAP anchors and modulates PSD formation and composition both *in vitro* and *in vivo* (Zeng et al. 2016; Araki et al. 2016). In this model, SynGAP forms trimers, mediated by its CC domain, this together with the PBM from SynGAP-α1, would not only facilitates its synaptic localization in basal conditions, but also regulate SynGAP dispersion upon synaptic activation (Zeng et al. 2016). *In vitro,* SynGAP binds to PSD-95 in a 3:2 molar ratio, which leads to the phase separation of these clusters. This mechanism has been proposed to be involved in PSD formation. Finally, Zeng and co-authors predict that

reduced SynGAP levels will prevent to reach the minimum amount of SynGAP required for its anchoring to the PSD and thus, less than half amounts could be targeted to the PSD (Zeng et al. 2016).

However alternative models for PSD formation might exist. These are supported by the fact that, in culture, hippocampal neurons from homozygous (HOMO) *Syngap1*$^{-/-}$ KOs present accelerated ('precocious') spine maturation, early movement of PSD-95 into spine heads and larger PSD-95 clusters (Kim et al. 2003; Vazquez et al. 2004; Rumbaugh et al. 2006). Importantly, SynGAP still associates to the PSD in *Dlg4*$^{-/-}$ (PSD-95) KO mice. Furthermore, as previously mentioned, *Syngap1* KOs do not present changes in spine density (Vazquez et al. 2004; McMahon et al. 2012; Lee et al. 2011; Aceti et al. 2015). Hence, the SynGAP's role in the PSD formation remains unclear.

4.4 SPINE AND SYNAPTIC PRUNING

Once spines and synapses are made, the most remarkable feature is the large reduction in the number of spines and unstimulated synapses. The total spine number in mice peaks near PND21 and declines slowly thereafter until pruning outpaces synapse formation by ~PND30 (I-16; Sala et al. 2003; Aceti et al. 2015; Koeberle et al. 2017). The pruning of synapses occurs in most regions of the mammalian CNS, but the precise timing of spine proliferation and loss varies between species, cortical regions/*laminae*, synapse type, neuron activity and even between genders of the same species. Nonetheless, the overall pattern of development is quite similar (Zhang and Benson 2000). Remarkably, the phagocytic capacity of microglia is particularly important during early brain development and subsequent maturation, paralleling synaptic pruning (Bilimoria and Stevens 2015).

The continuous pruning and creation of synapses might be a process of stochastic inference, in which the network continuously tests and evaluates the "usefulness" of synapses to process or represent external stimuli (Kappel et al. 2015). Thus, synaptic pruning might minimize the resources for synaptic maintenance and increases storage capacity to ultimately, improve mental ability (Aceti et al. 2015; Fauth and Tetzlaff 2016). Therefore, the reduction of the connectivity in the developing brain act as mechanism whereby cortical circuitry is refined through learning rules and/or input competition allowing more efficient processing of adult cognition (Andersen 2003). In *Syngap1*$^{+/-}$ KO mice, spines form early and are pruned prematurely both in neocortex and Hip (Mary Muhia et al. 2012; Clement et al. 2013; Aceti et al. 2015).

4.5 SYNAPTIC MATURATION, MAINTENANCE AND AGING

Synapse maturation and maintenance are key for establishing functional neuronal circuits, despite the exact mechanism driving synaptic maintenance are still under scrutiny. During rodent maturation there is in an increase in spine head size from PND10 to PND21 and a decrease from PND26 (Papa et al. 1995; Nwabuisi-Heath, LaDu, and Yu 2012). Mature synapses display well developed PSDs and several distinct vesicles near the presynaptic CAZ (Petralia, 2005). The extracellular matrix (ECM) also have a role in synapse maturation. Particularly, in mammalian brains a juvenile ECM is synthesized during late embryonic and early postnatal development. During maturation of neuronal circuits, perineuronal nets, formed by diffuse ECM and are progressively condensed, shifting into a net-like structure around synapses (Celio et al. 1998; Carulli, Rhodes, and Fawcett 2007). Astrocyte-derived ECM factors, like Thrombospondins, serve important functions not only during synaptogenesis, but also during synaptic maturation (Christopherson et al. 2005). By PND7, this extensive spine and synapse remodelling coincide with the increase in dendrite density and complexity (Baloch et al. 2009).

Briefly, protein turnover in new synapses is more rapid than in stable ones. Maturation is associated with NMDAR functionality, decrease of spine motility and stabilization of spine shape (Fischer et al. 2000; Segal and Andersen 2000; Sala 2008). Indeed, PSD structure and composition change during synapse maturation. For instance, synapses acquire NMDARs prior to AMPARs throughout an independent localization regulation being the increased ration of NMDAR/AMPARs a hallmark of silent synapses and ongoing synaptic maturation (Grutzendler, Kasthuri, and Gan 2002; Lachamp et al. 2005; Petralia et al. 2005; Swulius et al. 2010; Clement et al. 2012).

Expression levels of many PSD proteins increase with age, peaking between PND14-28 or DIV18-21 in cultured neurons, which correlate with the formation and maturation of synapses (Nwabuisi-Heath et al. 2012). Next, PSD protein levels slowly decrease to reach a *plateau* that persist throughout adulthood but declines in the old brain (Fig. I-16; Rafael Yuste and Bonhoeffer 2004). Some PSD proteins, however, maintain a constant expression level or even show the invers pattern (Sans et al. 2000; Petralia et al. 2005). For instance, the GluN2B/SAP102 complex is increasingly replaced with the GluN2A/PSD-95 tandem in hippocampal and forebrain PSD preparations (Sans et al. 2000; Petralia et al. 2005; Yoshii, Sheng, and Constantine-Paton 2003). Yet, late studies using quantitative gene-tagging revealed a fourfold molar excess of GluN2B over GluN2A in adult forebrain (Frank et al. 2016). Also, SAP102 plays a critical role during synaptic localization of AMPAR at immature synapses, whereas PSD-95 take over this role in mature synapses

(Elias et al. 2006). Finally, in mouse, at least 30% of spine synapses are not replaced and thus, are present for the entire adult life (Grutzendler et al. 2002) which are supported by the existence of synaptic long-lived proteins (Gonzalez-Lozano et al. 2016; Heo et al. 2018).

4.5.1 SynGAP EXPRESSION THROUGHOUT DEVELOPMENT

Syngap1 transcription in the brain starts as early as embryonic day E8.5 (Porter et al. 2005) and peaks at PND14 in Ctx and Hip (Petralia et al. 2005; Barnett et al. 2006; Clement et al. 2012; McMahon et al. 2012). Also, 5' mRNA variants in hippocampal neurons peak at PND14 and are significantly reduced by PND21 (McMahon et al. 2012), whereas 3' variants were equally expressed throughout development (Li et al. 2001). In contrast, SynGAP protein levels can at least be detected by PND2 in Hip (Petralia et al. 2005) and by E16 in Crb (Tomoda et al. 2004). Thereafter, SynGAP expression increases until reaching adult levels at PND35 in Hip and PND10 in Crb. Thus, proper assessment of developmental expression patterns of both SynGAP and its variants in mouse brain still remains elusive.

4.6 CRITICAL PERIODS OF DEVELOPMENT

During the development of an organism, critical and sensitive periods are time windows during which the brain undergoes significant plasticity from the level of individual synapses and neuronal networks up to the level of behaviour (Hensch 2004, 2005; Johnson 2005; Michel and Tyler 2005). Critical periods refer to time span where brain circuit-based phenotypes are made, such as ocular dominance[36] (Fox, Glazewski, and Schulze 2000; Hensch 2004). In addition they provide a framework to map time windows characterised by great changes, relative to other developmental stages, in physiological and behavioural phenotypes (Meredith 2015).

Critical periods are characterised by (1) An opening, closing, and efficacy of intervention, which are different across brain regions, (2) electrical activity has a particular role on the ability to potentiate or depress transmission at individual synapses, (3) there is a need of a precise balance of excitation and inhibition (Hensch, 2004; Hensch and Fagiolini 2005) as during critical periods, inhibition in the CNS is a vital arbiter of neuronal plasticity (Iwai et al. 2003) and (4) they cannot be reactivated in adulthood (Hensch, 2004).

[36] Refers to the tendency to prefer visual input from one eye *vs.* the other.

Particularly in humans, critical periods represent stages in the lifespan of the child where a developmental skill is acquired. Including seeing, hearing, speech or other higher cognitive functions (Fig. I-16; Andersen 2003; Semple et al. 2013). If the child does not receive appropriate stimulation during a given critical period to learn a given skill, it may be difficult, ultimately less successful, or even impossible, to develop some functions later in life (Semple et al. 2013; Leisman, Mualem, and Mughrabi 2015). Therefore, "phenotype" acquisition during critical periods is of highest importance and can influence later development.

4.6.1 SynGAP ROLE IN CRITICAL PERIODS

In Hip and neocortex, SynGAP regulates the pace of dendritic spine structural and functional maturation. Specifically, a reduction of SynGAP levels, disrupts the critical period of neuronal growth by accelerating maturation of spine synapses and altering the dynamics of dendritic structures (Vazquez et al. 2004; Mary Muhia et al. 2012; Clement et al. 2012, 2013; Aceti et al. 2015). Also, SynGAP deficiency during critical periods of mouse development produces multiple behavioural and cognitive aberrant phenotypes (see section I-5; Komiyama et al. 2002; Kim et al. 2003; Guo et al. 2009; Muhia et al. 2009; Muhia et al. 2010; Kilinc et al. 2018). Other examples of the role of SynGAP in critical periods are illustrated in cats, where SynGAP regulates synaptic plasticity during the critical period of visual experience (Kozol et al. 2015; Jaffer et al. 2012). In zebrafish *Syngap1* loss-of-function (LOF) mutations during embryogenesis match with abnormal morphological and behavioural phenotypes (Kozol et al. 2015).

4.6.2 THE GABA EXCITATORY/INHIBITORY SHIFT

During the critical period of synaptogenesis, GABA functionality plays a crucial role in many developmental processes including neuronal differentiation, dendritic arborisation (Tyzio et al. 2007), ionic currents and regulation of network-driven patterns of activity. Because of a higher intracellular chloride concentration ($[Cl^-]i$) in immature neurons, activated GABA-A receptors lead to depolarization and thus excitation, whereas in mature neurons changes in $[Cl^-]i$ promote hyperpolarization. These high $[Cl^-]i$ levels in immature neurons are caused by the high expression of the Cl^- importer (NKCC1) relative to the expression of the Cl^- exporter (KCC2). In rodents, the expression of these 2 transporters reverses from PND14 onwards, while in humans this change occurs around birth (Fig. I-16). Additionally, $[Cl^-]i$ levels are highly labile, being altered transiently or persistently by

enhanced episodes of activity in relation to synaptic plasticity, and a variety of pathological conditions including seizures and brain insults (Ben-Ari et al. 2002; 2012).

The GABA excitatory/inhibitory shift, together with other mechanisms, like a proper synaptic AMPAR/NMDAR ratio (Jeyabalan and Clement 2016), influence the excitatory/inhibitory (E/I) balance. E/I balance is crucial for proper neuronal and network development, as it determines the duration and efficacy of critical periods. Indeed, E/I imbalance is enough to disrupt cognition and sociability (Won et al. 2012; Clement et al. 2012).

4.7 BRAIN DEVELOPMENTAL IN RODENTS AND HUMANS

Brain development and maturation comparisons between species is based upon several indicators of developmental phases including brain growth spurt, timing of neuro- and gliogenesis, neuronal migration biomarkers, synapse formation (Clancy et al. 2007; Workman et al. 2013) or even lifespan correlations (Dutta and Sengupta 2016). In humans, just as in rodents, critical periods occur in a sequential temporal pattern across the brain. As an example, the timing of brain growth spurt differs across different species as do neurogenesis (Dobbing and Sands 1978). Furthermore, synaptic connectivity and synapse plasticity among other events differ slightly in their timing from region-to-region, making precise regional comparisons between brains of differing species challenging (Meredith et al. 2015). Nonetheless, there is also considerable cross-species alignment in terms of key developmental milestones, behavioural phenotypes and regional vulnerability (Fig. I-17; Semple et al. 2013). Therefore, keeping in mind the pronounced differences between rodents and humans, the implications of such measurements at early developmental stages in neurodevelopmental disorder (NDD) rodent models would be significant for *in utero* and neonatal screening and raise possibilities for the timing of therapeutic interventions in the future. Also, the ill adult and aged human brain can benefit of therapies through the correct cross-alignment between species.

Briefly, in contrast with mice, the proliferation of human synapses begins around the 20th gestation week. Synaptic density increases rapidly after birth and by 2 years humans have 50% more synapses than they will have during their adult life. Synaptic elimination and remodelling in humans are more prolonged and continues well into adolescence (Petanjek et al. 2011). Also, activity dependent synaptogenesis influences spine density while aging leads to alterations in spine morphology and reduction of spine density as in mice. Myelination is well underway in rodents by PND10–14 and peaks at approximately PND20, whereas in humans it is not complete until 3–5 years of age (Fig. I-17; Semple et al. 2013).

During the brain growth spurt period, rodents acquire many new motor and sensory abilities while working memory and social behaviours establishment are enhanced at PND20-21 (Fig. I-17. Semple et al. 2013). Crucially, certain behaviours can be temporally correlated with the maturation of specific neuronal regions or processes in humans (Wood, Beyer, and Cappon 2003).

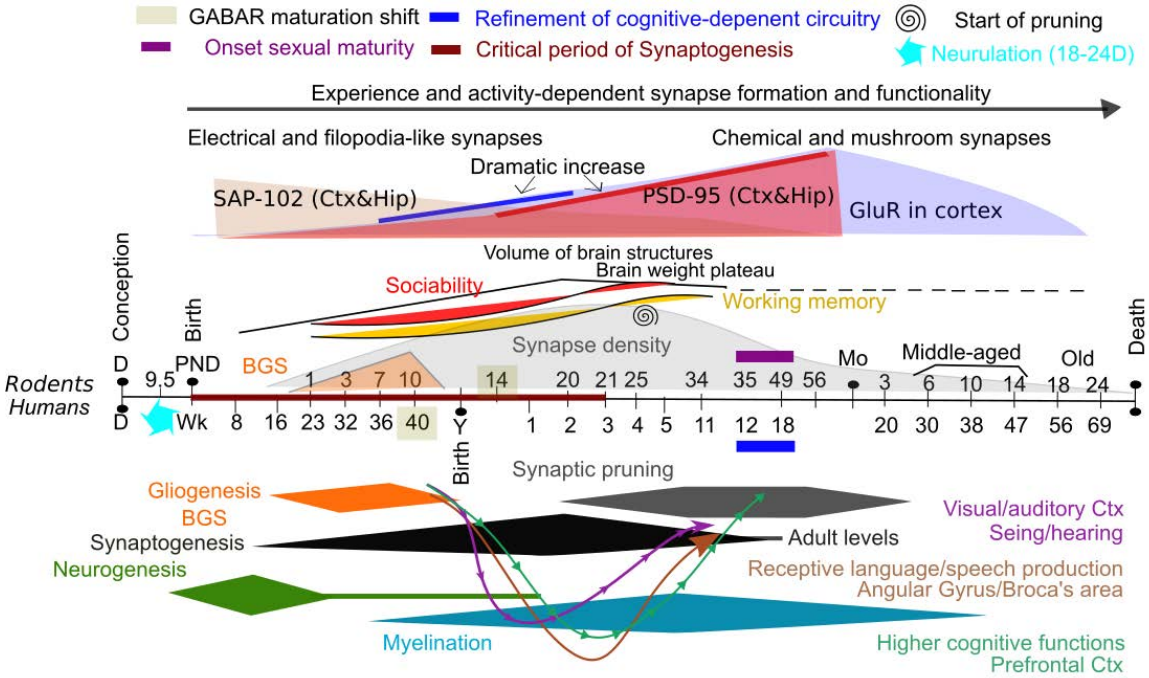

Figure I-17. Human and rodent developmental milestones cross-alignment. In this diagram is shown the rodent age (up) and humans (bottom) comparison of synapse maturation and other key molecular and behavioural milestones. Note that not all features align between species. Days (D), Months (Mo), years (Y), brain growth sprout (BGS), Cortex (Ctx) and Hippocampus (Hip). This figure is a composition from Sans et al. 2000; Petralia et al. 2005; Grantham-McGregor et al. 2007; Semple et al. 2013; www.translatingtime.net and the addition of other features cited in the main text.

5. SYNAPTOPATHIES

Optimal synaptic communication is required for proper brain physiology and perturbations of synapse function and stability match the cognitive decline of normal aging or lead to neurological and neuropsychiatric disorders (Stafstrom and Carmant 2015). Those pathological states of the brain that feature synapse defects at their core have been termed synaptopathies (Brose, O'Connor, and Skehel 2010; Chater and Goda 2014; Lepeta et al. 2016). Particularly, they can arise from any shift in the synaptic connectivity and plasticity expected in a given brain region and developmental time point (Emes and Grant 2012; Forrest, Parnell, and Penzes 2018) or be secondary to changes in additional biochemical processes in the surrounding environment (Grant 2012; Lepeta et al. 2016; van Spronsen and Hoogenraad 2010; Brose, O'Connor, and Skehel 2010).

Synaptopathies encompass childhood onset neurodevelopmental disorders (NDDs) such as autism spectrum disorder (ASD) and intellectual disability (ID); adolescent and young adult onset neuropsychiatric disorders like bipolar disorder and schizophrenia (SCZ), as well as late onset neurodegenerative disorders such as Alzheimer's, Parkinson's diseases and other dementias or addiction, multiple sclerosis and chronic pain (Emes and Grant 2012; Grant 2012; Spronsen and Hoogenraad, 2010; Bliss, Collingridge, and Morris 2014; Grant, Bagni, and O'Dell 2016; Lepeta et al. 2016). Some NDDs have different onset and show associated abnormal spine density mirroring synapse dysfunction and consequent wrong connectivity (Fig. I-18A).

It is hypothesized that genetic and environmental risk factors for synaptopathies converge on a subset of pathways and networks that shift synaptic plasticity and connectivity in a spatio-temporal fashion, thus determining the degree of excitatory input. Both hypoconnected or hyperconnected neurons will impact different cognitive domains (Fig. I-18B). Among genetic factors, an increasing number of disruptive genetic variations affecting the synapse proteome are responsible for these mental disorders (Grant 2007; Forrest, Parnell, and Penzes 2018). Indeed, human PSD (hPSD) mutations cause 133 neurological and psychiatric diseases (Bayés et al. 2012) and 145 MASC genes have been related to 197 CNS conditions (Laumonnier, Cuthbert, and Grant 2007; Bayés and Grant 2016). Although synaptic perturbations are not the only alterations relevant for these diseases, understanding the molecular underpinnings of spine pathology may provide insights into their aetiologies and may reveal new drug targets. Thus, mouse models encompassing these genes can provide a substantial progress in the understanding of mechanisms whereby synaptopathies arise.

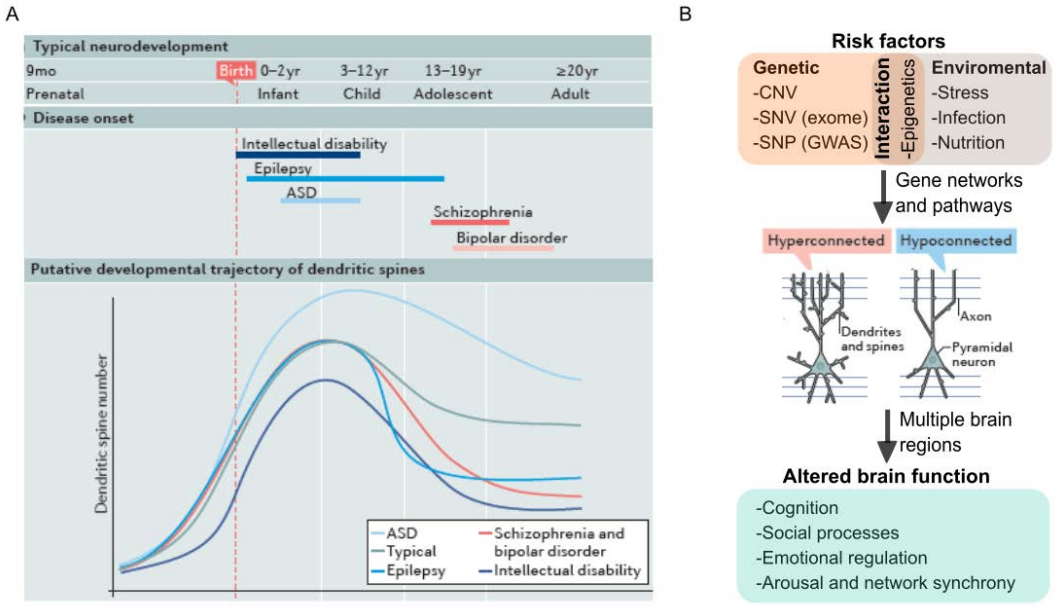

Figure I-17. Neurodevelopment, dendritic spine alterations and risk factors in synaptopathies. (A) Representative synaptopathies onset and associated pathological alterations in dendritic spine number. It is worth noting that various monogenic ID disorders can show the opposite plotted trend (Van bokhoven 2011) and exactly when, where and how spine changes occur is still unknown. (B) Flow-chart of the risk factors (in orange, grey and brown) and their outcomes in synaptopathies (green box). mo, month; CNV, copy number variations; SNP, single-nucleotide polymorphism; SNV, single-nucleotide variation; yr, years. Modified from Forrest et al. 2018.

5.1 NEURODEVELOPMENTAL DISORDERS

NDDs manifest early in development, usually during critical periods (reviewed in section 4.6) and are characterized by missed developmental milestones that produce impairments of personal, social, academic, and/or occupational functioning (Meredith 2015; DSM-V). The prevalence for NDDs in 2010 was estimated to be 1,87%, but likely is much higher as some individual NDDs show higher prevalence (Bromley et al. 2013; H. H. Ropers 2010). Some NDDs show differential prevalence between gender, thus it cannot be excluded a role of sex in diseases vulnerability, presentation, and outcome (Bale et al. 2010).

Currently, NDDs include communication disorders, attention deficit hyperactivity disorder (ADHD), specific learning disorder, motor disorders, ASD and ID with all its non-syndromic and syndromic forms such as fragile X-syndrome (FXS); tuberous sclerosis syndrome (TSC) or Rett syndrome (DSM-V; Zoghbi and Bear 2012). Other diseases such as RASopathies (Sloan and Barres 2014; San Martín and Pagani 2014) together with epilepsy and SCZ are thought to involve a neurodevelopmental dysregulation, so that they can be found classified as NDDs (Lewis and Levitt 2002; Bale et al. 2010; Bozzi, Casarosa,

and Caleo 2012; Xing et al. 2016). Nonetheless, epilepsy and SCZ in DSM-V are defined as chronic neurologic and SCZ & psychotic disorder, respectively.

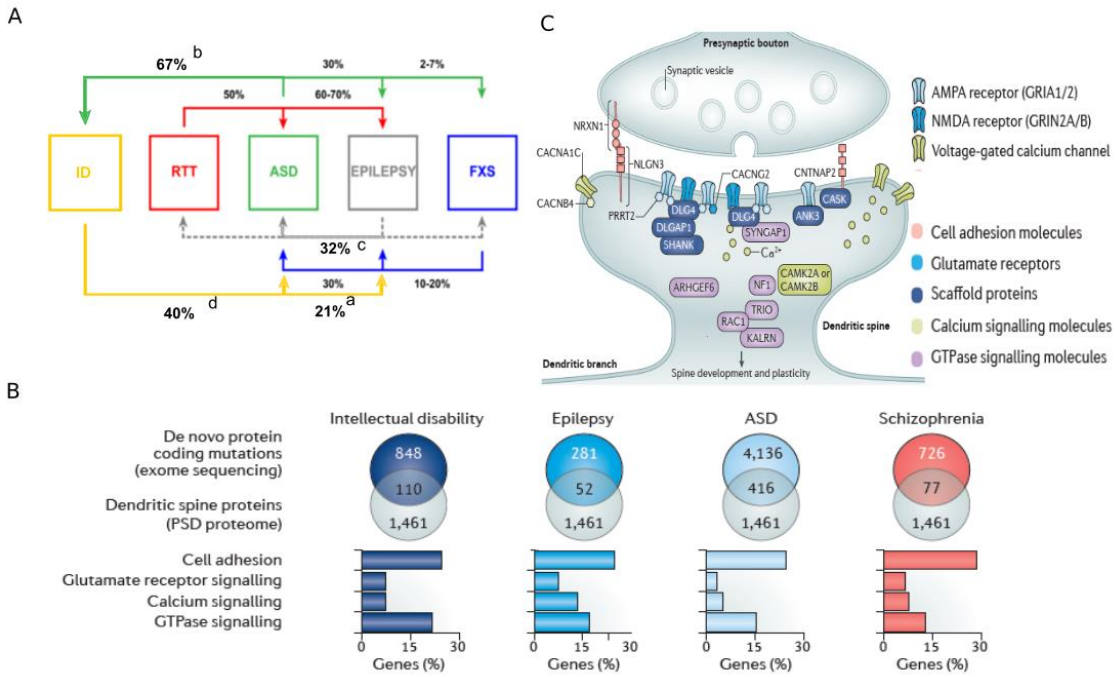

Figure I-19. Genetic relationships and risk factors of NDD.(A) Comorbidities of NDD with E/I imbalance are indicated pair-wise in black. Unknown epilepsy co-occurrences are indicated with a dashed grey line. (B) Scheme of de novo mutations affecting protein coding for each disorder intersected with the human PSD proteome (Bayés et al. 2013). The percentage of PSD-associated mutated genes classified into biological processes relevant to spine structure and function is depicted on the y axis (bottom panels). (C) Localization of genetic risk factors for NDD that regulate spine structure. Functional groups are colour coded. Figure A is modified from [a]Airaksinen et al. 2000; [b]Fombone, 2003; [c]Clarke et al. 2005; [d]Matson and Shoemaker 2009 and [e]Kaufmann et al. 2010; Figure B and C are modified from Forrester et al. 2018.

As suggested before, NDDs considered to be clinically separated (e.g., ID and SCZ), and presumed to have different aetiology, can arise from mutations encompassing the same synaptic complexes and converge to the same pathological mechanisms (Grant 2012; Forrest, Parnell, and Penzes 2018). These overlapping mechanisms might be involved in the high co- or multimorbidity found in NDDs (Fig. I-19A; Gatto and Broadie, 2010; Lepeta et al. 2016). Indeed, reduced cognitive function is a common feature of NDDs (Weldon et al. 2018). Prospective [37] studies of predisposing factors to NDDs found epigenetic modifications due to maternal nutrition, exposure to stress hormones and/or immune activation as important risk factors (Bale et al. 2010; Rai et al. 2013). Conversely, genetic association studies of NDDs, have identified numerous mutations in genes encoding transcriptional and translational regulators (Bale et al. 2010; Iossifov et al. 2014; McCarthy et al. 2014; Gatto and Broadie 2010) and genes encoding for CAMs and small GTPases,

[37] Cohort studies where subjects before the development of the outcome of interest were followed into the future to record any of these assessed outcomes (Henriksson et al. 2018).

Ca^{2+} and GluR signalling proteins (Fig.I-19B&C; Gatto and Broadie 2010, Forrest 2018). Certainly, the high overlap of *de novo* mutated genes related to hPSD in NDDs, disclose that no other known "set of proteins" carry a greater disease burden than does the PSD (Grant et al. 2007; Bayés et al. 2012).

5.2 RASOPATHIES

RASopathies are caused by mutations in genes of the Ras/Raf/MEK/Erk pathway (See section I-2.6.2) and represent one of the most prevalent groups of congenital malformation syndromes affecting approximately 0,1% of the population (Tidyman and Rauen 2016). These disorders include several syndromes such as Neurofibromatosis type I (NFI) or Noonan and Costello syndromes (Sloan and Barres 2014; Aoki et al. 2016). Although they have unique phenotypic features, they also share many overlapping characteristics, including craniofacial dysmorphology, cardiac, cutaneous, skeletal and ocular abnormalities, variable degree of neurocognitive impairment ranging from sever to no ID, hypotonia, impaired growth, a growing ASD comorbidity (Zoghbi and Bear 2012; Alfieri et al. 2014) and in many cases, an increased cancer risk, due to the common Ras/MAPK signalling dysregulation and/or activation (Tidyman and Rauen 2009, 2016). Moreover, mutations affecting this signalling cascade can also occur at mosaic state, resulting in congenital syndromes often distinct from those generated by the corresponding germline mutations (San Martín and Pagani 2014; Hafner and Groesser 2013). These germline or mosaic mutations produce gain-of-function alleles in positive regulators of the Ras/ERK signaling pathway and LOF alleles in negative regulators (San Martín and Pagani, 2014). Some well stablished causal genes are *PTPN1*; *RAF1*; *KRAS* and *NRAS* whereas *RRAS* and *SYNGAP1* are causative of rare new RASopathies (Tidyman and Rauen et al. 2009; 2016).

5.3 SCHIZOPHRENIA

This brain disease typically appears in early adulthood, in the late 2nd to 3rd decade of life. In males the average age of onset is around 5 years earlier (Lewis and Levitt 2002). Yet, behavioural abnormalities can be present as early as 4 weeks of age (Guo et al. 2009). SCZ is estimated to affect 1% of the population (Leucht et al. 2007) with a lifetime risk. The SCZ is characterized by at least one of these symptoms: hallucinations, delusions or disorganized speech (e.g., frequent derailment or incoherence). Other symptoms include grossly disorganized/catatonic behaviour; negative symptoms (i.e., diminished emotional expression) and cognitive deficits. SCZ is ~80% heritable (DSM-V; Lewis and Levitt 2002). Hyperactivity with repetitive and purposeless movements, unable to convey empathy,

anxiety, reduced social interactions with conditioned fear and defects in working memory and one of the major cause of suicide are other featured behaviours in SZC patients (Braga, Petrides, and Figueira 2004; Taylor et al. 2005; Taylor et al. 2005; Guo et al. 2009; Millier et al. 2014). The genetic liability to SCZ appears to be transmitted in a polygenic non-mendelian fashion (Risch and Baron 1984; Risch 2000). *GRIA1*, *MTOR*, *DLG4* and *SYNGAP1* mutations induce susceptibility to suffer SCZ (Magri et al. 2006; Beneyto et al. 2007; Wiedholz et al, 2008; Zhu et al. 2010; Xu et al. 2012; Guo et al. 2009; Tidyman and Rauen 2016).

5.4 EPILEPSY

Epilepsy is one of the most common neurological disorders, characterized by the repeated occurrence of spontaneous excessive hypersynchronous discharge of neurons in the brain (Stafstrom and Carmant 2015). The estimate prevalence of epilepsy with other psychiatric conditions varies greatly around the mean value of 23,5% (Tallez-Zenteno et al. 2007). Epilepsy is classified according to its age of onset, its cause or knowledge of structural and genetic causes as well as the degree of functional impairment. Also, exists subtypes of generalized seizures regarding the presentation like the myoclonic [38] seizures. Significantly, the epileptic encephalopathies including Dravet syndrome are sever brain disorders of early age that manifest with aggressive seizures and electrical epileptogenic activity during brain maturation and progressive cognitive and neuropsychological regression (Suls et al. 2013; epilepsy foundation). Regarding their genetic basis, both monogenic and polygenic mutations can lead to epilepsy (Poduri and Lowenstein 2011). However, many epilepsies have a complex genetic basis with multiple genes contributing to a state of altered cellular excitability shared with ASD and ID (Stafstrom and Carmant 2015). Emerging epilepsies are *SCN2A*, *SCN8A*-, *KCNQ2*, *SLC13A5*-, and *SYNGAP1*-related epilepsies (Grinspan et al. 2018; Vlaskamp et al. 2019).

5.5 AUTISM SPECTRUM DISORDERS

ASD, typically identified before 2-3 years of age (Rice et al. 2012; DSM-IV-TR), are a group of clinically and etiologically heterogeneous pervasive developmental disorders characterized by long-life impairments in social interactions, communication and restricted, repetitive and stereotyped patterns of behaviour (DSM-IV-TR, Rice 2012). Based on DSM-IV-TR, pervasive developmental disorders comprise the autistic disorder first described in 1943 by Leo Kanner (Grice and Buxbaum 2006), Asperger's syndrome

[38] Myoclonic refers to involuntary twitching of a muscle or a group of muscles (Engel 2006).

identified by Hans Asperger in 1944 (Artigas-Pallares and Paula 2012), pervasive developmental disorders not otherwise specified, Rett-Syndrome and childhood disintegrative disorder. Despite all differ from each other in their severity of symptoms, causative factors, language development, deterioration of acquired skills and cognitive development (Lepeta, 2016), they are currently diagnosed as a unique ASD category (DSM-V).

In 2010, 1 in 132 persons in the world (Rice et al. 2012) and 1 in 68-88 children from USA (Gilbert and Man 2017) suffer ASD. Moreover, there are 4-5 ASD diagnosed boys for every girl (Duchan and Patel 2012; Christensen et al. 2016). In addition to the core symptoms, 70% of the cases are accompanied by sensory-perceptual anomalies (Baranek et al. 2006) related to the 5 senses, including environmental hypersensitivity (Monteiro and Feng 2017) or a controversial hyposensitivity in pain (Allely 2013). Also, ASD appear to be comorbid with other conditions such as gastrointestinal dysfunctions ranging from 9 to 91% of ASD cases (Hsiao et al. 2013), neurological impairments including seizures, posture and muscle tone or mild abnormalities in coordination (Matson and Nebel-Schwalm 2007; Santini and Klann 2014; de la Torre-Ubieta et al. 2016), altered connectivity and oscillatory network synchronization (Simon and Wallace 2016), metabolic disorders like Phenylketonuria (Miles 2011), sleep disturbance in 60 % of autistic children (Duchan and Patel 2012; Rice 2012), ADHD in more than 50% of the cases, learning disability around 40% (Bergeron 2016), SCZ in 2,43% (Kohane et al. 2012) and ID in ~67% of ASD patients (Fig. I-18A; Fombonne 2003).

Usually, ASD is classified as non-syndromic (NS-) and syndromic (S-) ASD, or idiopathic *vs.* symptomatic ASD when is un- or known the cause, respectively (Sztainberg and Zoghbi 2016). In idiopathic NS-ASD, autism is the primary diagnosis with no additional symptoms (Ivanov et al. 2015; Sztainberg and Zoghbi 2016), whereas in S-ASD additional phenotypes and/or dysmorphic features are present. Specifically, S-ASD accounts only for 10-20% of ASD cases (Santini and Klann 2014; Varghese et al. 2017). Some examples of S-ASD[39] are Fragile X Syndrome (Verkerk et al. 1991), Rett syndrome (Amir et al. 1999), MECP2 duplication syndrome (Van Esch et al. 2005), Tuberos Sclerosis Complex (Fryer et al. 1987; Kandt et al. 1992), and PTEN macrocephaly syndromes (Butler et al. 2005). Noteworthy, S-ASD unlike idiopathic or NS-ASD, shows a different male/female sex ratio (Ivanov et al. 2015).

[39] However, each of these syndromes have variable clinical symptoms and proportion of individuals with and without autism (Benvenuto et al. 2009; Sztainberg an Zoghbi 2016).

Globally, up to 1,000 genes are involved in ASD (Gilbert and Man 2017) and there is a high heritability (~ 50%; Varghese et al. 2017) further supported by high concordance rates between monozygotic *vs.* dizygotic twins (77-95% *vs.* ~31%; Bourgeron 2016; Monteiro and Feng 2017). However, the contribution of environmental (Hallmayer et al. 2011) and epigenetic risk factors are gaining attention (Hsiao 2013; Gilbert and Man 2014; Ivanov 2015). Many genes involved in S-ASD, NS-ID and epilepsy are also associated with NS-ASD (Santini 2014; Ivanovic 2015). Importantly, rare[40] copy number variations (CNV) of *SYNGAP1* and *SHANK2* has been identified in autism probands[41] (Pinto et al. 2010) and PSD-95 gene variation with ASD (Feyder et al. 2010).

5.5.1 *SHANK2* MOUSE MODELS FOR ASD ASSESSMENT

SHANK mutations are implicated in glutamatergic signalling defects and have been specially associated to ASD (Pinto et al. 2010; Monteiro and Feng 2017). There is a wealth of data regarding *Shank3* pathophysiology, as it is the cause of Phelan-McDermid syndrome, a form of S-ASD (OMIM #606232). Thus, many *Shank3* KO mouse models have been developed (Monteiro and Feng 2017). Nevertheless, much less is known about the role of the other 2 Shanks.

5.6 INTELLECTUAL DISABILITY

The previously known mental retardation or ID, is characterized by significant limitations in both intellectual functioning[42] and adaptive behaviour[43], which covers many every day and social skills (DSM-V). Usually, it is diagnosed before the age of 18, when the intelligence quotient (IQ) is ≤70 and is recognised at least 2 deficits in adaptive behaviours such as delayed language, social skills or self-help skills (DSM-V). However, when children < 5 years fail to meet developmental milestones in intellectual functioning and are unable to undergo systematic assessments, are diagnosed with Global Developmental Delay (GDD) and await reassessment after a period (DSM-V, APA).

ID prevalence ranges between 1-3% (Ropers 2010) and is ~30% more common in males (McLaren and Bryson 1987), although sever ID is more prevalent among females (Kaufmann et al. 2010). 50-60% of patients diagnosed with ID is comorbid with ASD and

[40] DNA mutations with a large effect on disease risk in <1% of general population (Forrest et al. 2018).
[41] In human genetics refers to the patient or member of the family that brings a family under study.
[42] Is the general mental capacity of academic and experimental learning, planning, abstract thinking, judgment and reasoning or problem solving (DSM-V, APA 2013).
[43] Collection of conceptual, social, and practical skills that are learned and performed by people in their everyday lives such as skills for selfcare (San Martín and Pagani 2014).

epilepsy (Fig. I-18A) and multimorbidity with a wide range of psychiatric disorders like RASopathies, SCZ (Deb, Thomas, and Bright 2001; Deb and Bright, 2008), attention deficit hyperactivity disorder (ADHD) or mood disorders (Smith and Matson, 2010; San Martín and Pagani 2014). Beyond cognitive limitations, some have additional problems such as deficits in adaptive coping skills, and excessive maladaptive behaviours like challenging behaviours or dangerous conduct. These categories include aggression in 10-45% of cases, self-injury, sexual offending, fire setting and stealing, although prevalence estimates vary tremendously across studies (Brown, Brown, and Dibiasio 2013; Kilinc et al. 2018). Of note, although ID imposes the leading healthcare cost in the developed world, exceeding cancer and dementia costs, has comparatively received little attention (Ropers 2010).

ID can be split into borderline (IQ 70-85), mild (IQ 50-70), moderate (IQ 35-50), severe (IQ 20-35) and profound (IQ< 20), but in practice, subjects are grouped into mild ID (IQ 50-70) and sever ID (IQ<50; World Human Organization; Ropers and Hamel 2005). Currently, it has been stated that ID must be defined based on adaptative functioning, which determines the level of support required, rather than by an IQ score (DSM-V, APA). In addition, ID is also further classified as ASD into S-ID including syndromic X-linked ID (S-XLID) associated with either malformations or neurological abnormalities and a debatable NS-ID being NS-XLID part of it (Kaufman, Ayub, and Vincent 2010; Afroze and Chaudhry 2013). Furthermore, NS-ID mutations can be autosomal recessive (AR) or dominant (AS) leading to NS-ARID or NS-ADID (Luckasson and Reeve 2001; San Martín and Pagani 2014; Kaufmann et al. 2010; Afroze and Chaudhry 2013). Conversely, AAIDD[44] classified ID based on prenatal causes encompassing RASopathies, inborn errors of metabolism among others and perinatal and postnatal causes which mostly include a large variety of infections and traumatisms in these time periods among other subclassifications (Luckasson and Reeve 2001; San Martín and Pagani 2014).

Interestingly, ~40% of ID cases, being primarily mild, are caused by environmental factors (Rauch et al. 2006; Ropers 2010; van Bokhoven 2011), whereas 40-65% of the moderate to severe cases are due to genetic variations (Kauffman et al. 2010; Hans van Bokhoven, 2011). Up to date, the most important CNV cause of S-ID is Down syndrome (Ropers, 2010) while the most important single-gene cause is Fragile X-syndrome[45] (Ropers and Hamel, 2005). Rho and Ras small GTPases, and its regulators, cause forms of S-ID, such as Neurofibromatosis 1 (NF1; Kaufman et al. 2010; Pavlowsky et al. 2012). Up to ~50

[44] Stands for American Association on Intellectual and Developmental Disabilities.

[45] Alterations in PSD-95 expression have been found in patients with Alzheimer's disease and in mouse models of Fragile X syndrome (FXS; Zelfa et al. 2007).

genes are implicated NS-ID (van Bokhoven, 2011). However, the potential presence of less apparent subtler neurological abnormalities and psychiatric disorders in NS-ID patients and the difficulties in the diagnosis due to the cognitive impairment may lead to incorrect NS-ID classification, thus potentially more genes could be implicated (Ropers and Hamel 2005).

Over the last years, many single gene mutations have been identified as a cause of NS-ID and many of them also cause S-ID (e.g., *MECP2* gen), ASD or other NDD (Kaufmann et al. 2010). To date, 40 genes have been implicated in NS-ARID (Hill et al. 2016), of which 8 are found in NS-ARID consanguineous families like *GRIK2* mutations (Motazacker et al. 2007). Conversely, NS-ADID is likely to be sporadic, mostly resulting from *de novo* truncating mutations being *SYNGAP1* and *SHANK3* causal for this subtype (Hamdan et al. 2009; Hamdan, Daoud, et al. 2011; Hamdan, Gauthier, et al. 2011). Also, rare CNV by deletion and single nucleotide polymorphisms (SNP) in *SHANK2* are reported for NS-ADID (Kaufman et al. 2010; Berkel et al. 2010; Mehregan, Najmabadi, and Kahrizi 2016).

5.6.1 MENTAL RETARDATION AUTOSOMAL DOMINANT 5

MRD5 is caused by *SYNGAP1*$^{+/-}$ mutations on human chromosome 6p21 (OMIM #603384) and is characterized by moderate to severe ID with delayed psychomotor development, apparent in the first years of life. *SYNGAP1* LOF variants are surprisingly common, with the incidence reported as 1–4/10,000 individuals, or ~0.5–1.0% of all reported ID cases, making it one of the most common causes of ID and generalized epileptic encephalopathy in ~100% of the cases (Table I-1; Weldon et al. 2018; Vlaskamp et al. 2019). It can also be associated to various degrees with SCZ ASD; ADHD; seizures; microcephaly and impairments in innate behaviours involving risk-taking, altogether suggesting that there might be thousands of unreported carriers of this mutation worldwide (Weldon et al. 2018; Table I-1). Although during long time *SYNGAP1* LOF has been associated with NS-ID, recently it has been also defined a *SYNGAP1*-association syndrome (Parker et al. 2015).

SYNGAP1 Mutations (MRD5)						
Affected patients	Type of mutation	Gene product	Common phenotypes	Individual phenotypes	Additionl information	Ref.
3/94	*De novo* transverisons and intragenic deletions	Truncated	GDD with delayed motor development, hypotonia, moderate to severe ID, and lenguage impairement	2 epilepsy,1 Strabismums	-	Hamdan et al., 2009
1/100	*De novo* balanced translocation in 6p21 with a breakpoint disrupting *SYNGAP1*	Truncated	-	GDD with delayed motor development, moderate ID, ADHD, speech impairement with connective tissue abnormalities	They postulated that *SYNGAP1* haploinsufficiency might be the main cause of ID and severe speech impairment associated with the novel 6p21.3 deletion described here.	Krepischi et al., 2010
1/996	Microdeletions in 6p21.3	No product	-	ASD and ID	*SHANK2* was also reporeted as novel ASD gene	Pinto et al., 2010
1/10	Microdeletion in 6p21.3	No product	-	Ideopathic ID	*De novo* CNV and point mutations of large effect could explain the majority of all ID cases	Vissers et al., 2010
2	Microdeletion in 6p21.3	No product	ID and generalized epilepsy	ID with drug-resistant seizures, facial dysmorphisms, gut malrotation and abnormal pancreas segmentation	Included in the deletion interval is *SYNGAP1*, as well as the flanking gens *CUTA* and *hPHF1*. All related in brain plasiticty , development and /or organ morphogenesis.	Zollino et al., 2011 and Klitten et al., 2011
5/60	*De novo*	Truncated	Moderate to severe NS-ID, avoidance of other children and impulsivity, ADHD, mood problems such as sullenness and rigidity	2 epilepsy, 2 microcephaly,1 autism	-	Hamdan et al., 2011
2/45	*De novo*	Framshift yielding truncation	Sever NS-ID	-	-	Rauch et al., 2012
21/231	*De novo*	Canonical splice site	Schizophrenia	-	These 231 cases arise from 231 parent-proband trios enriched for sporadic SCZ cases	Xu et al., 2012
5/34	1 inherited from a parent with mosaic mutation, 4 de novo	3 Truncated, 2 missense	GDD	4 moderate to severe NS-ID, 4 epilepsy, 3 ASD, 1 ataxia and 3 behavioral abnormalites	First report of a pathogenic missense mutation. Also, test the functional impact of these muations in cortical organotypic cultures and found inability to abolish Ras related ERK activation.	Berryer et al., 2013
5/500	*De novo*	Truncated	GDD and cognitive regression after seizure onset, Epileptic encephalopathy, myoclonic jerks, severe NS-ID and ASD	1 seizures associated with EEG abnormalities	All patients were initially diagnosed as epileptic encephalopathya. Concluded that epileptic encephalopathy should be part of the phenotypic spectrum associated with *SYNGAP1* mutations	Carvill et al., 2013
1	Microdeletion in 6p21.3	No product	-	GDD, hypotonia, ID, seizures, severe speech impairment, clumsy and uncoordinated, strabismus, recurrent infections, not able to assess the danger but he was sociable	The delation encompasses 4 genes (SYNGAP1, KIFC1, PHF1 and CUTA) considered the 2 first responsible for the phenotype	Writzl and Knegt, 2013
1/106	*De novo*	Truncated	-	Moderate ID. Despite it is not directly reported could be comorbid with autistic traits, epilepsy, microcephaly and hypotonia	Found causative mutations associated genes to defined syndromes in patients deviating from the classic linked phenotype (*DMD, TCF4, MECP2*).	Redin et al., 2014
10	*De novo*	3 Nonsense, 3 frameshift, 1 whole gene deletion, 3 missense and all resulting in SYNGAP1 LOF	GDD, moderate to severe ID, hyper-excitability accompained with significant sleep problems and aggressive/challenging behavior	7 epilepsy,8 hypotonia,5 constipation,7 unsteady gait,2 strabismus,2 dysplasia,7 MR normal imaging,2 microcephaly and myopathic facies	PH and C2 *SYNGAP1* domains were affected in the missese mutations. First time of mention a *SYNGAP1*-associated syndrome and the need to consider SYNGAP1 in the list of differential diagnose for Angelman syndrome patients	Parker et al., 2015
17/251	De novo	-	GDD, with walking achieved in most by age 3 year, speech delay, hypotonia, ataxia, broad-based and clumsy gait.	5 didn't speak by 10 years, 1 seizures,16 myoclonic epilepsy without seizures,8 ASD	Seizures in patients with mutations in exons 4–5 were more pharmacoresponsive than in patients with mutations in exons 8–15	Mignot et al., 2016
1	*De novo*	-		ID, ASD, distinctive dysmorphic features and no seizures		Kimura et al., 2018
53	*De novo* in all	34 truncating, 8 splice-site, and 11 missense/in-frame mutations and 4 microdeletions.	Epilepsy syndrome: 56/57 patients had epilepsy with a median age at seizure onset of 2 years. Also, developmental delay and ID in 96.5% of the cases being moderate to sever ID in more than 81% of them.	-	Different types of seizures 8e.g. EM-myoclonic.atonic seizures, absence seizures, refleix seizures...), photosensitivity in 55% of the cases , ASD in more than 52.6% of the cases, severe behavioural problems (73.2%), 72.2% high pain treshold, 68.4% eating problems 66.7% hypotonia, sleep problesm in 61.8%, ataxia and/or gait abnormalities in 50.9% and in less than 10% other features were eported (e.g., tremor or microcephaly).	Vlaskamp et al. 2019

Table I-1. Review of *SYNGAP1* mutations found in different cohorts of patients. Note that the *SYNGAP1* screening was done in different cohorts of patients including SCZ, epilepsy and ID. GDD stands for global developmental delay and LOF for loss of function.

5.7 PATHOPHYSIOLOGICAL MECHANISMS OF NDDS

Defects in the carefully orchestrated steps required to form functional neural networks, such as neurogenesis, migration, myelination, differentiation, synaptogenesis as well as synaptic function are believed to promote dysfunction at the neuronal and behavioural levels, resulting in NDDs (Lepeta 2016; Gilbert and Man, 2017; Marcello, Di Luca, and Gardoni 2018). A synapse-based theory for cognitive deficits in NDDs has been postulated (Penzes et al. 2011, 2013). Mechanistically, the brain hyperexcitability due to E/I imbalance in neurons result from direct changes in elevated brain activity, altered connectivity and plasticity levels (Stafstrom 2010; Meredith 2015) as well as aberrant development and regulation of the PSD (Sawicka and Zukin 2012). In addition, the E/I imbalance is also strongly influenced by astrocytic dysfunction (Rubenstein and Merzenich 2003; Sloan and Barres 2014). Altogether, drive to cognitive and behavioural disturbances. In support of this notion, LTP and LTD dysregulation contributes or in many cases cause NDDs (Bliss, Collingridge, and Morris 2014) while specific alterations of spine turnover have also been reported in cases of ID or ASD (Cruz-Martín, Crespo, and Portera-Cailliau 2010; Pan et al. 2010; Dubos et al. 2012). Furthermore, dysregulated transcriptional (Chahrour et al. 2008) or translational control (Kelleher and Bear 2008) due to altered MAPK/Erk and PI3K/AKT signalling (Sztainberg and Zoghbi 2016; Gilbert and Man 2017) as well as impaired activity-dependent gene expression (Ebert and Greenberg 2013) are also involved in some NDDs, including ASD and ID (Fig. I-20).

Other pathophysiological mechanism to remark for epilepsy are defects in GABARs subunits and K^+ channels (Stafstrom and Carmant, 2015); electrical coupling, leading to asynchronous neural activity (Hormuzdi et al. 2001; Nakase and Naus 2004) and inborn errors of metabolism (Wolf, Bast, and Surtees 2005; Dulac et al. 2014). In the case of ASD, ~88% of the genes considered to be high-risk for ASD play a role in neurodevelopmental functions such as neurogenesis and differentiation of neuroblasts (Casanova and Casanova 2014), which is supported by excessive neuronal numbers (Gilbert and Man, 2017), altered spine maintenance (Kelleher and Bear 2008; Bourgeron 2009) and altered activity-dependent synaptic pruning (Gilbert and Man, 2017). Also, GABAergic (Tabuchi et al. 2007; Cellot and Cherubini 2014) and electrical neurotransmission are key in ASD (Welsh, Ahn, and Placantonakis 2005).

Glutamatergic synapses are particularly relevant to ID, as 50% of genes mutated in these conditions are expressed at pre- and/or postsynaptic components of excitatory synapsis (Kaufmann et al. 2010; Hamdan, 2011; Pavlowsky et al. 2012). Disrupted synaptic small GTPase signalling and associated abnormal AMPARs trafficking and protein synthesis,

altered cytoskeleton dynamic, UPS-mediated protein degradation and PTMs of histones and DNA methylation[46] has a prominent role in ID (van Bokhoven, 2011; Zoghbi and Bear, 2012; Pavlowsky et al. 2012). Of note, in a brain of a patient with a *SYNGAP1* LOF (MRD5) it has been found in Crb cerebellar Purkinje cell loss with associated astrocytes which was identified also in Ctx or Hip, suggesting a role of immune system alterations in ID (Vlaskamp et al. 2019).

In contrast, SCZ is mainly caused by abnormal function and localization of NMDARs as well as its associated interactors (Magri et al, 2006; Beneyto et al, 2007; Wiedholz et al, 2008; Zhu et al. 2010). Furthermore, GABA and dopamine disturbances, oxidative stress and oligodendrocyte viability also contribute to the functional "dysconnectivity" of neuronal circuits observed in SCZ (Carter 2006; Penzes et al. 2013). Finally, precocious astrocyte development (Sloan and Barres, 2014) along with an impairment in synaptic plasticity (Stornetta and Zhu 2011; Forrest, Parnell, and Penzes 2018) are causal for some RASopathies (Tidyman and Rauen 2009, 2016). Noteworthy, by definition, RASopathies can be part of NDDs mechanisms (e.g., MRD5).

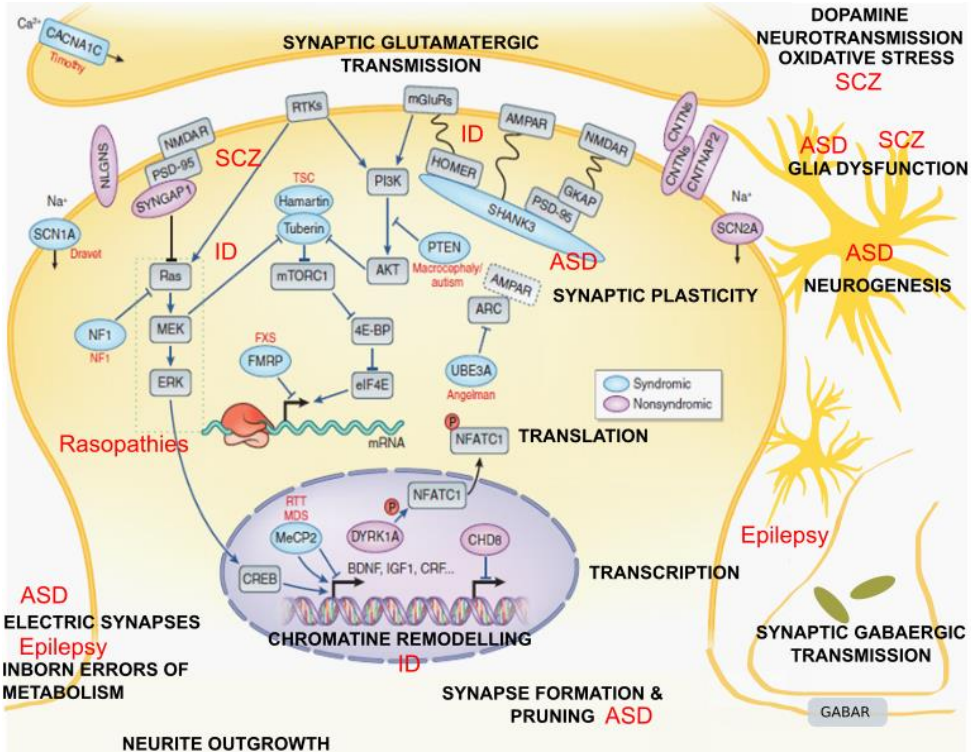

Figure I-20. Pathophysiology mechanisms for some NDDs. Altered events in NDDs are shown in bold. Despite mainly all pathways are in different degrees aberrant in the described diseases, in red is strength the relevance of a given process in a specific disorder. Also, is shown the location and the signalling pathways of proteins encoded by genes that cause the most common S-ASDs (blue) with its associated name (red) and selected genes associated with increased risk of NS-ASD (purple). Modified from Szteinberg and Zoghbi, 2016 and added information is extracted from Xinxing Wang, Kery, and Xiong 2018, Lepeta et al. 2016 and cites from the main text.

[46] ~10-20 ID genes encode regulators of the epigenetic code (van Bokhoven 2011).

5.8 TREATMENTS FOR NDDS

Currently there is no effective treatments to significantly improve core symptoms of ASDs (Xinxing Wang, Kery, and Xiong 2018). However, there are treatments for alleviating concrete ASD endophenotypes such as irritability and stereotypy, despite still there is no drug for sociability impairments. These treatments include Risperidone and/or Aripiprazole administered in combination of behavioural therapies (McPheeters et al. 2011; Won, Mah, and Kim 2013). Nowadays, several candidate ASD drugs for treating social abnormalities have been suggested such as D-cyloserine (a partial agonist of NMDARs) or Rapamicyin (mTOR inhibitor; Fig. I-21; Won, Mah, and Kim 2013).

Regarding SCZ treatments, several antipsychotic drugs such as Clozapine and partial agonist of NMDARs has been proven successful to ameliorate some symptoms (Guo et al. 2009). Conversely, there are several antiepileptic treatments such as Valproate or Topiramate for both general and subtypes of epilepsies (Fig. I-21; Marson and Chadwick 2001), they are usually combined with psychological interventions such as relaxation or cognitive behaviour therapies among others to reduce the seizure frequency and improve the quality of life (Ramaratnam, Baker, and Goldstein 2005). Intriguingly, patients with different *SYNGAP1* mutations showed different resistance to antiepileptic treatments (Mignot et al. 2016).

Animal models of genetic disorders related to ID indicate that intellectual and attention deficit might be rescued by appropriate learning paradigms and pharmacology (San Marín and Pagani, 2014). Of note, these promising results are expected to be the same outcome in humans. Nevertheless, there is no current cure for ID but can be alleviated through therapies including special education programs, life skills training and job coaching (San Martín and Pagani 2014). Importantly, several other potential therapies are put forward like the rescue of the healthy number of copies of the gene in question by reintroduction of functional copies (Kaufmann et al. 2010). This therapeutically intervention can be assessed using conditional genetically modified mice for genetic rescue experiments as a proxy of putative human treatments (See Chapter II and Annex).

Finally, given the fact that most mutations affecting small GTPases lead to hyperactivation of signaling pathways in ID, the inhibitors of small GTPases and its regulators which increase its stability at the membrane or specific drugs that target altered downstream kinases of small GTPases could be other therapeutic strategies (Fig. I-21; Pavlowsky et al. 2012). Yet, one of several limitations for potential therapeutic approaches that need to be solved is associated with the critical periods in which the deficits appear and the window of opportunity that a potential treatment could rescue these deficits.

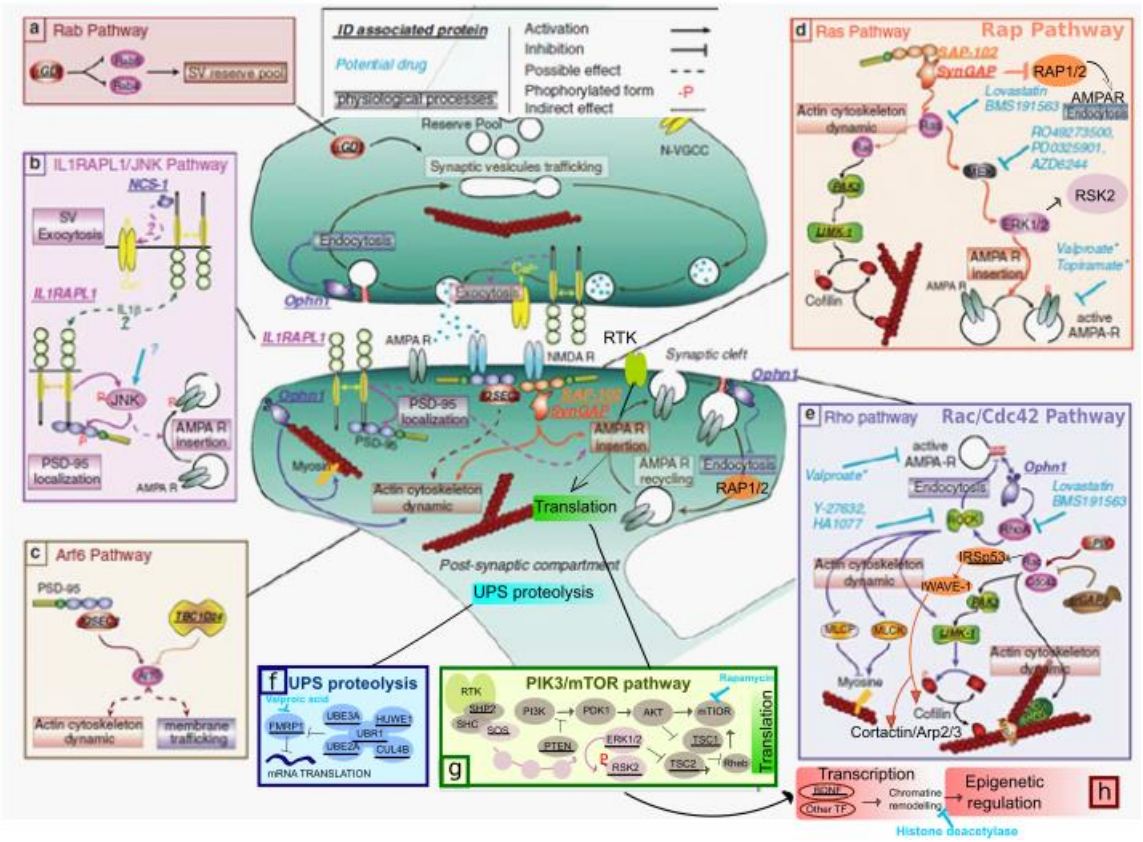

Figure I-21. Synaptic pathways involved in ID and other NDDs as well as possible therapeutic targets. Note that mutations in members of the signalling pathways outlined here, may result in commonly altered processes. In each inset, the molecular details of the pathway are described and the potential drugs for therapeutic (in light blue) and their targets are positioned in the signaling pathway. Modified from Pavlowsky et al. 2012.

5.9 COGNITIVE PHENOTYPE IN *SYNGAP1*$^{+/-}$ MOUSE MODELS

Beyond the previous molecular alterations described in *Syngap1*$^{+/-}$ mutants that server to understand synapse development and plasticity (sections 2, 3 and 4), these mice exhibited dangerous behaviour, a fear remote memory deficit, reduced seizure threshold, enhanced startle reactivity and reduced sensorimotor gating[47] measured by prepulse inhibition[48], lack of social memory and a propensity toward social isolation ranging from hyperactivity, anxiolysis, reduced motor habituation, emotional and social recognition impairments, learning and memory deficits and altered sensitivity to psychomimetic drugs. Indeed, as previously described, several studies led to hypothesize that SynGAP critical windows of neural plasticity prematurely close in *Syngap1*$^{+/-}$ LOF mutations leading to these

[47] Process by which a neural system screens extraneous external (sensory) and internal (cognitive, motor) information from higher order processing and subsequent responses, to enable uninterrupted processing of the most salient aspects of the external and internal environment. It is measured to understand the functional significance of attentional abnormalities (Ahmari et al. 2012).

[48] Prepulse inhibition is a neurological process in which a weaker pre-stimulus (prepulse) inhibits the reaction of an organism to a subsequent strong startling stimulus (pulse). It is used to probe functional status of cortico-striato-pallidal circuitry in humans and rodents (Ahmari et al. 2012).

abnormally brain functioning (Komiyama et al. 2002; Guo et al. 2009; Muhia et al. 2010; Clement et al. 2012; Clement et al. 2013; Ozkan et al. 2014; Aceti et al. 2015; Michaelson et al. 2018). Furthermore, mouse mutants of *Syngap1*$^{+/-}$ phenocopy several features of mouse carrying mutations for synaptic proteins including *CAMKIIα* (Yamasaki et al. 2008); *NMDARs* (Guo et al. 2009; Yamasaki et al. 2008), *FMR1* (Barnes et al. 2015) and *Shank* mutants (Penzes et al. 2013). These parallelisms together with the high multimorbidity conditions seen in MRD5 and other NDDs previously mentioned, strongly supports the view of SynGAP as a hub protein that regulates molecular pathways and neural substrates common among distinct brain disorders. Furthermore, SynGAP normal functioning and/or the alterations driven by *Syngap1* haploinsufficiency could affect differentially various brain areas or have a greater impact during different phases of development as function in a cell-autonomous manner (Clement et al. 2012; Ozkan et al. 2014), thereby accounting for the variability in behavioural endophenotypes. Thus, the proper understanding of the neurobiology of SynGAP will be key to further extend the knowledge about common core mechanism shared with other synaptic key proteins.

6. NEUROPROTEOMICS TO STUDY SYNAPTIC BIOLOGY

The word ‘proteome’ was termed in the nineties (1990) as an analogy of ‘genome’. It was defined as the complete complement of proteins that are expressed by a genome. Thus, proteomics is the science that studies the proteome of a biological system in a given state. Hence, neuroproteomics studies the proteomes of the nervous system (Bayés and Grant 2009). It is also worth noting that disentangling the complex signalling network at spines, or even within some of its subdomains, is technically challenging due to their small size (Colgan and Yasuda, 2014).

PSD enriched fractions are obtained from synaptosome fractions. Synaptosomes are detached, sealed presynaptic nerve terminals, often with portions of the PSM still attached (Whittaker 1984). Based on all the previous information given, PSD is a highly suitable structure for biochemical analysis since it is abundant in the brain and can be enriched using standard biochemical fractionation methods (Carlin et al. 1980). Initially, PSD proteins were separated by SDS-PAGE or 2-dimensional gel electrophoresis, and major bands/spots were sequenced to identify abundant constituents. These biochemical approaches were complemented with the rise of antibodies to PSD components for immunoblotting, peptide sequencing among other approaches. Then, synaptic proteins including PSD-95, Shank, SAP-102 or SynGAP were identified using these methods (Walsh and Kuruc 1992; Lau et al. 1996; Kim et al. 1997; Kim et al. 1998; Chen et al. 1998).

Advances in mass spectrometry (MS) based proteomics in the past 15 years have contributed to a deeper appreciation of the protein networks and the composition of synaptic protein complexes. However, research on protein dynamics underlying core mechanisms of synaptic plasticity in brain lag far behind the previous achievements (Dieterich and Kreutz 2016). The traditional MS approaches can be classified under the umbrella of discovery/shot-gun and targeted proteomics (Sjöström et al. 2015). Discovery based proteomics include electrospray ionization (ESI) to ionize peptides; MS and liquid chromatography coupled to tandem MS (LC-MS or LC-MS/MS), which have identified and relative quantified large numbers of proteins in the PSD fraction or in immunoprecipitated NRC/MASCs (Cheng et al. 2006; Sheng and Hoogenraad 2007). Alternatively, the main feature of a relative recently developed targeted proteomics is the selected reaction monitoring (SRM) workflow which absolute quantification (AQUA) of specific proteins that carry unique peptide sequences (Elschenbroich and Kislinger 2011; Ronsein et al. 2015; Savitski et al. 2015)

OBJECTIVES

The main goals of the present thesis were to:

1. Conduct an *in*-silico analysis of *Syngap1* transcript variants and resulting protein isoforms as well as verify its expression in mouse and/or human tissues.

2. Study the relative and absolute amounts of SynGAP, its C-term variants and interactors expression throughout development in five different mouse brain regions.

3. Quantify relatively the expression of total SynGAP and its C-term variants between five different brain areas in different developmental stages.

4. Assess the subcellular localization of total SynGAP and three of its C-term variants in cortex without premotor/prefrontal region and adult hippocampus.

5. Examine the dynamics of the proteome from hippocampal PSDs due to conditional *Syngap1*$^{+/-}$ haploinsufficiency during mice development.

6. Evaluate the ability to rescue alterations in *Syngap1*$^{+/-}$ hippocampal PSD proteome by complete *Syngap1* reactivation from PND21 onwards.

7. Analyse the proteome alterations in mouse hippocampal PSDs due to *Syngap1*$^{+/-}$ haploinsufficiency induced by PND21 onwards.

8. Develop a *Shank2* conditional KO mice for genetic rescue experiments.

MATERIALS AND METHODS

1. BIOLOGICAL MATERIALS AND METHODS

1.1 ETHICS STATEMENT ON ANIMAL EXPERIMENTATION

The research projects conducted in the present thesis were authorized by the Institutional Animal Care and Use Committee (IACUC) fulfilling the ethical principles required for their approval (according to the current legislation: Decret 214/1997 and RD 53/2013). IACUC obtained authorization from its external board of experts on Animal Experimentation (num.9655). Maintenance, treatment and experimental procedures in mice were conducted at the Animal Facility of the Research Institute of the Hospital de la Santa Creu i Sant Pau. Also, all animal experimentation was done in accordance with the European directive (2010/63/EU) of the European Parliament 'on the protection of animals used for scientific purposes'. Specifically, all experiments were conducted in order to implement the "3R's" policy to reduce as much as possible the number of animals used in each experiment, the animal suffering and discomfort.

1.2 MOUSE HANDLING

Mice were housed at a 12h light/dark cycle with fresh water and food *ad libitum*. Special chow (T.2019.12, Envigo) was administered to pregnant mothers and litter until weaning (PND21), whereas adult mice were fed with regular chow (T.2014.12, Envigo, Europe). Weaned mice were sexed and separated in new cages. The maximum number of animals per cage was 5. Individual animals were identified by an ear hole code. Ear holes were done under general anaesthesia.

1.2.1 ANAESTHESIA

The isofluorane vaporizer was turned on to 5% and the flow-meter was set between 500-1000 mL/min. Forane® (Sigma-Aldrich) was used as a gaseous anaesthetic. Mice were visually monitored and when mice were recumbent and showed no tactile response but constant breath and heartbeat, the flowmeter was set at 100-200 mL/min and vaporizer at 2-3%.

1.2.2 MOUSE STRAINS

Several mouse lines including were used for the experiments designed in the present thesis (Table M-1).

Mouse handling				
Mouse strain	**Short name**	**Source**	**Genetic Background**	**Other information**
C57BL/6J	B6	Jackson Laboratories, Main, USA	B6	
Syngap1 $^{+/-}$ constitutive KO	Constitutive *Syngap1* $^{+/-}$	Prof. Seth Grant, Edimbourgh University	B6	
Tg(CAG-cre/Esr1*)5Amc/J	Cre $^{+/-}$	Jackson Laboratory, Main, USA	B6	
Syngap1 $^{+/-}$ conditional KO for genetic rescue experiments	Rum2	Dr. Gavin Rumbaugh from The Scripps research institute (TSRI)	Cre $^{+/-}$	Clement et al., 2012
Syngap1+/- conditional for KO induction	Rum1	Dr. Gavin Rumbaugh from The Scripps research institute (TSRI)	Cre $^{+/-}$	Clement et al., 2012
Syngap1 $^{+/-}$ conventional KO	Conventional *Syngap1* $^{+/-}$	Dr. Gavin Rumbaugh from The Scripps research institute (TSRI)	B6	Kim et al., 2003
Shank2 conditional KO from clone 8D7	*Shank2* KO 9,000	Facility core IRB Barcelona	FlpO $^{+/-}$ /B6	
Shank2 conditional KO from clone 9D4	*Shank2* KO 10,000	Facility core IRB Barcelona	FlpO $^{+/-}$ /B6	
Shank2 conditional KO from clone 5E10	*Shank2* KO 11,000	Facility core IRB Barcelona	FlpO $^{+/-}$ /B6	
B6N $^{Tyrc-Brd/BrdCrCrl}$	B6 pure albino	Charles River Laboratories, Wilmington, MA, USA	B6 pure albino	
Shank2 KO chimeras	*Shank2* chimera	Facility core IRB Barcelona	FlpO $^{+/-}$ /B6 pure albino	
CAGGs-Flpo-IRES-puro	FlpO $^{+/-}$	Facility core IRB Barcelona	B6	Wu et al., 2009

Table M-1. **Mouse strains used in this thesis.**

1.2.3 MOUSE SACRIFICE

PND0-7 mice were killed by decapitation and mice from PND11 onwards were culled by cervical dislocation minimizing animal suffering.

1.3 TAMOXIFEN PREPARATION AND INJECTIONS

Tamoxifen (TMX; Sigma-Aldrich, St. Louis, MO) was prepared at a final concentration of 20 mg/mL in 10% absolute ethanol (EtOH; ThermoFisher Scientific, Pittsburg, PA) and 90% corn oil (Sigma-Aldrich). First, TMX was dissolved with ethanol and sonicated with an ultrasonic liquid processor (Misonix Inc., NY, USA). Sonication was done with amplitude set to 15% during 5 min with 15 sec 'on/off' cycles. Then samples were vortexed until dissolved and incubated with a thermoblock (Stuart Scientific Ltd., Stone, UK) during 10 min at 37ºC. Finally, corn oil was added to reach the final TMX concentration. TMX was injected intraperitoneally once per day at 5 µL/g of body weight (v:w), starting at PND21 and maintained during 5 consecutive days. Mice were sacrificed at PND56, thus samples were collected 35 days after the first TMX administration (Fig. M-1).

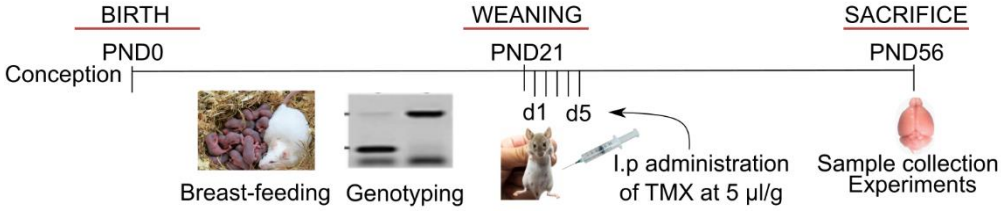

Figure M-1. Tamoxifen administration. Intraperitoneal (I.p) injections of TMX at the dose indicated during 5 consecutive days beginning at weaning (PND21) will induce Cre-dependent recombination for reversion of modified alleles to WT or alternatively, induce the conditional deletion of the targeted modified gene and induce haploinsufficiency.

1.4 TISSUE COLLECTION

1.4.1 MOUSE TAIL BIOPSIES

Tail biopsies were collected for mice genotyping not earlier than PND21. Tail biopsies were collected from anesthetized or sacrificed animals. Tail biopsies consisted ~3 mm long fragments of mouse tail tip, cut with a 10 mm blade scalpel. Histoacryl™ (BBraun Medical Inc., Barcelona) was used to cauterize the wound. Once assured that the tail was not bleeding, mice were placed back on their corresponding chamber.

1.4.2 MOUSE BRAIN AREAS

Mouse head was separated from the rest of the body by severing its neck with dissecting scissors. The head was placed onto a glass petri dish with a filter paper (Merck-Millipore; Darmstadt, Germany) soaked with chilled 1x PBS (0.144 M NaCl; 2.683 Kcl mM; 10.144 mM Na_2HPO_4; 0.735 mM KH_2PO_4). The skin was removed by a cut through the long axis of the head, using 14.5 cm dissecting scissors, whereas the skull and meninges were removed using 11.5 cm Iris scissors and tissue forceps 1:2 (Thermo Scientific). Next, the brain was removed from the skull with the help of curved gerald thump forceps and 2 spatulas (VWR International, Darmstadt, Germany) without compromising its morphology. Tissue was rinsed with chilled 1x PBS and dissected using scalpel blades. For brain dissection of PND0-7 animals a magnifying loupe (Olympus KC 1500 Ledplus; Olympus, UK) was used at 2.5x. 11.5 cm iris scissors were used to remove skull and meninges, whereas thin curved forceps (Fine Science Tools; #11370-42 and 11399-87; Heidelberg, Germany) and plier (Fine Science Tools, #150118-10) were used for dissection. Finally, brain areas were dissected according to Spijker (Spijker 2011) and placed in previously tared 2 mm cryotubes (Nirco, Madrid, Spain). Tissue weight was recorded before snap-freezing in liquid nitrogen. Samples were finally stored in a -80ºC freezer (Thermo Fisher Scientific).

2. MATERIALS AND METHODS FOR GENOMIC SPECIMENS

2.1 RNA EXTRACTION

RNA was isolated using the TRIzol® reagent (Invitrogen, Carlsbad, CA) and purified using the RNeasy Plus Mini Kit (Qiagen, Hilden, Germany). Briefly, 50-100 mg of tissue was mixed with 1 mL TRIZol (Invitrogen life technologies, Thermo-Fisher Scientic) and homogenized with Polytron (VWR). This solution was transferred into RNAse-free 2 mL tubes and incubated for 5 min at room temperature (RT). Then, 200 µL of chloroform (Sigma-Aldrich) were added and the tube was manually shaken during 15 sec. The mixture was incubated for 2-3 min at RT and was centrifuged at 12,000xg (centrifuge Epp 5415D; Eppendorf, Hamburg, Germany) during 15 min at 4ºC. The aqueous phase (~600-700 µL) was placed into a new 2 mL sterile and RNAse-free tube (Eppendorf) and mixed with 500 µL of isopropanol (Sigma-Aldrich). The mix was incubated for 10 min at RT and centrifuged at 12,000xg during 10 min at 4ºC. The pellet was washed with 1 mL of 75% EtOH, vortexed (Vortex, Genie-2; Scientific Industries, USA) to detach it from the bottom of the tube and centrifuged at 7,500xg during 5 min at 4ºC. Finally, the pellet was dried at RT for 10 min and was resuspended with 100-200 µL of RNAse-free water.

2.1.1 RNA PURIFICATION

RNA was purified using EZ-10 DNAaway RNA min-prep kit (BioBasic, Ontario, Canada) following the manufacturer's instructions. 100 µL of RNA containing sample was used in each purification. RNA was eluted with 30 µL of RNAse-free water and incubated 2 min at RT. Finally, samples were centrifuged at 9,000xg during 2 min at RT and were stored at 4ºC for use in the same day or stored at -80ºC.

2.1.2 RNA QUALITY ASSESSMENT

The RNA integrity number (RIN) was assessed for all samples extracted at 100-300 µg/µL work concentration as indicated in section M-2.3. RIN was measured with Bioanalyzer 2100 (DE54107383; Agilent Technologies, CA, USA) and data was processed with the 2100 expert software version (ver.) 2.6 run in a Eukaryote total RNA Nano series II assay class. In general, RINs ranged between 8.5 to 9.60, which were indicative of good RNA quality.

2.2 DNA EXTRACTION

Tissue used to obtain DNA (e.g., tail biopsy) was placed in a 1.5 mL tube. 400 µL of 1x lysis buffer (100 mM Tris pH 8; 5 mM EDTA; 0,2% SDS; 200 mM NaCL, Sigma-Aldrich) was added together with proteinase K (Sigma-Aldrich) at a final concentration of 100 µg/mL. Tissue was then incubated at 55ºC overnight (ON) and centrifuged at 21,000xg (Epp 5417R, Eppendorf) during 15 min at 4ºC. The supernatant was transferred to a new 1.5 mL tub and the pellet discarded. The same volume of isopropanol was added to the simple, tubes were inverted manually several times and centrifuged at 21,000xg during 10 min at 4ºC. The resulting supernatant was removed by decantation and 500 µL of 70% EtOH were added to the pellet. Subsequently, samples were subjected to centrifugation at 21,000xg during 20 min at 4ºC and the supernatant was removed whereas the resulting DNA pellet was dried using a thermoblock (QBD2, Stuart Scientific Ltd.) heated at 60ºC. Once the pellet was considered dry, it was resuspended with 30 µL of sterile Milli-Q water and placed during a minimum of 6 h in the fridge before quantification with Nanodrop 2000 (Thermo-Fisher) to assure its complete resuspension for a reliable quantification.

2.3 DETERMINATION OF DNA AND RNA CONCENTRATION

Unless expressly indicated otherwise, the concentration of DNA or RNA was determined by applying 1.5 µL of sample in a Nanodrop 2000 spectrophotometer (Thermo-Fisher). Absorbance ratios A260/280 and A260/230 were calculated for purity assessment. A minimum of 2 and occasionally 3 measurements were done per each sample and the average number was used to calculate DNA/RNA concentration.

2.4 REVERSE TRANSCRIPTION-POLYMERASE CHAIN REACTION AND CDNA SYNTHESIS

Reverse transcription (RT) followed by polymerase chain reaction (PCR) was used to synthesize and amplify cDNAs from messenger RNA (mRNA). RT-PCR and cDNA synthesis were done using Oligo (dT)23, a mixture of dNTPs (Sigma-Aldrich), and with the RNA polymerase containing kit Easy Script: first strand cDNA synthesis super mix (OriGene Technologies GmbH, Herford, Germany). The thermocycling conditions are detailed in Table M-2.

RT-PCR thermocycling conditions			
Step	Tª (ºC)	Duration	Cycles
1	65	5 min	1
2	4	2 min	1
3	42	16 min	1
4	85	5 min	1
5	4	Infinity	1

Table M-2. RT-PCR thermocycling conditions.

The reaction mix was prepared by adding 1 µL of Oligo (dT) and 8 µL of total RNA at 125 ng/µL for each sample. Then, the mix was heated during 5' at 65ºC in a thermocycler with a hot Bonnet heated lid (PTC-1156 miniCycler; MJ-Research, Bio-Rad). Samples were placed 2 min in ice. Later 10 µL of the reaction mix from the kit and 1 µL of reverse transcriptase (Easy Script RT/RI enzyme mix) was added to reach a final volume of 20 µL. Each 20 µL mixture was heated to 42 ºC during 16 min and to 85 ºC for 5 sec to inactivate the enzyme. Synthesized cDNA was cooled down to 4 ºC and stored at -80ºC for long-term storage. cDNA was used for conventional PCR (Results Chapter II) or quantitative real-time PCR (qPCR; Results Annex). Two negative controls were performed in parallel: i) using no enzyme to identify gDNA contamination and ii) substituting water for RNA to identify possible reactive cross-contaminations.

2.5 CONVENTIONAL POLYMERASE CHAIN REACTION

Conventional PCR was conducted with Taq DNA polymerase (Biotools, B & M Labs, Madrid) for those amplicons up to 1.2 Kba. Larger PCR products were amplified with the Expand high fidelity PCR system (Roche, #04738250001). The PCR reaction mix for each DNA polymerase and the general thermocycling conditions are shown in Table M-3. In addition of DNA polymerase kits, primers (Sigma-Aldrich), dNTP (Promega Biotech Ibérica, Madrid, Spain), sterile Milli-Q water, sterile 0.2 mL tubes and tips were required for PCR. Conventional PCRs were conducted in a Thermocycler C1000 (Touch thermal cycler CFX96 Real-time system; Bio-Rad). The specific thermocycle conditions are specified in each corresponding chapter. A PCR positive control, consisting of DNA and primer pairs producing known DNA fragment and negative controls with sterile water instead of DNA were carried out whenever possible.

A

PCR reaction mix final concentrations			
		Units	µl/rx
gDNA	15-100	ng	1
Primers	15	pmol each	0.75*2
dNTPs	10	pmol	1.25
Buffer	1x buffer 3/Taq with Mg2+	vol	2.5
$MgCl_2$	2.5	mM	-
DNA polymerase*	2.5/0.25	U	0.5/0.2
Reaction vol	25	µl	18.25/18.55

B

PCR thermocycling conditions			
Step	Tª (ºC)	Duration	Cycles
1	94	2 min	1
2.a	94	30 sec	
2.b	50-67*	30 sec	30/35*
2.c	68	5 min	
3	68	5 min	1
4	4	Infinity	1

Table M-3. Conventional PCR conditions. (A) The final concentrations of PCR reaction mix for DNA polymerase Expand high fidelity/Taq DNA polymerase. (B) General thermocycling conditions. * indicates variable changes that will be indicated in each experiment.

2.5.1 PRIMER DESIGN

Primers were selected using Ape software v1.17 (http://jorgensen.biology.utah.edu/wayned/ape) and following several rules including preferred length between 20-25 bp, with C or G endings when possible, checking for secondary structures (www.sigma.com)

and self or other types of complementarities with Primer3 software (www.primer3 plus.com). When possible GC % content was chosen to be greater than 40-45% and PCR conditions were checked in silico (www.basic.northwestern.edu/ biotools/oligocalc.html). Furthermore, the melting temperature (Tm) was selected within the 50-65 ºC range, and the differences between the forward and reverse primer TMs was ideally between 0-3ºC. The primer3 tool (http://bioinfo.ut.ee/ primer3) was used to validate primers. Finally, primer specificity and general features assessment in a given specie were checked using the nucleotide BLAST tool (https://blast.ncbi.nlm.nih.gov/Blast.cgi) from the NCBI (National Center for Biotechnology Information [NCBI] of the National Library of Medicine [NLM] at the National Institutes of Health [NIH]).

2.6 DNA ELECTROPHORESIS

Agarose (Sigma-Aldrich) gels were prepared with 1x TAE (40 mM Tris pH 8.0 [Sigma-Aldrich]; 10 mM EDTA [Merck]; 0.114% acetic acid [Sigma-Aldrich]) at 0,8% when the amplicons were >1 Kba and 1,1% when expected amplified fragments were <1 Kba. Unless otherwise indicated, before agarose gel formation, 1.25 µL of GelRed (Biotium, VWR) at 0.5 µg/mL were added to each 50 mL of agarose. Then, polymerized agarose gels were placed in the adequate electrophoretic cuvette (Mini- and subcell Comb models, Bio-Rad) depending on the gel size. The DNA ladders used were 100 bp or 1KBa (both from Fermentas, Sigma-Aldrich) depending on the expected fragment length.

2.6.1 SAMPLE PREPARATION AND CONDITIONS FOR ELECTROPHORESIS

Routinely 5 µL of PCR products were prepared for electrophoresis by adding 1x loading sample buffer (1x TAE; 30% glycerol; 20% Milli-Q water) and diluted with sterile Milli-Q water up to a final volume of 20 µL.

Unless otherwise indicated, 150 mL-gels were run at 100 V during a minimum of 30 min, whereas 50 mL-gels were run at 70 V, both in buffer 1x TAE (see M-2.6). Gel images were acquired by GelDoc 1000 (Bio-Rad) and processed using Image Lab software (Bio-Rad).

2.7 DNA EXTRACTION FROM AGAROSE GELS

DNA fragments in an agarose gels were visualized in an ultra-violet (UV) transilluminator (220V X-ray film illuminator, 46C, Cultek) and cut with a 10 mm scalpel Blade (Sigma-Aldrich). The Nucleospin Gel and PCR clean-up kit (Macherey-Nagel, Düren, Germany) was used to isolate DNA from agarose following manufacturer's instructions.

3. MATERIALS AND METHODS FOR PROTEIN ANALYSIS

3.1 PROTEIN EXTRACTION

3.1.1 EXTRACTION OF TOTAL HOMOGENATES WITH SODIUM DEOXYCHOLATE

Both mouse and human samples kept at −80 °C were subjected to this procedure. Samples were placed in dry ice before homogenization. Figure M-2 displays a scheme of this purification protocol. Protein extraction buffer was added at a 1:17.5 tissue: extraction buffer ratio (w/v). This buffer consisted of 50 mM Tris-HCl pH 9, 1% deoxycholate (DOC), 50 mM NaF (Merck-Millipore), 20 mM $ZnCl_2$, 1 mM sodium orthovanadate, 1:2,500 phenyl methane sulfonyl fluoride (PMSF), 2 µg/mL aprotinin (Merck-Millipore), 2 µg/mL leupeptin and 1 mM β-glycerophosphate (all from Sigma-Aldrich unless indicated). Brain tissue was homogenized by 20–30 strokes in 1-mL or 7-mL borosilicate Dounce homogenizers (glass-Teflon tissue grinder; Wheaton, Millville, NJ) depending on the volume of buffer required. Homogenised tissue was incubated on ice for 1 h and centrifuged at 21,000×g (model 5417R, Eppendorf) for 30 min at 4 ºC in 1.5 mL centrifuge tubes. The resulting pellet was re-homogenized twice following the same procedure. The 3 resulting supernatants were pooled. In the last re-homogenization cycle half of the initial w/v ratio was used for all tissue types but Ctx and Crb. For protein quantification 1% SDS was added and pellets were resuspended with half ratio tissue/volume resuspension pellet buffer (1% SDS and 50 mM Tris pH 7,4).

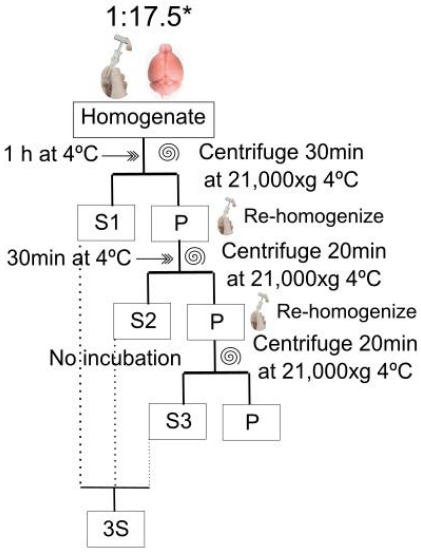

Figure M-2. Extraction protocol with 1% DOC. Work-flow of the method. S stands for supernatant; 3S for pooled S1-S3 and P means pellet. The * indicates that this ratio is subjected to changes depending on the tissue homogenized and the developmental age, which is indicate in the corresponding chapter (i.e., Chapter I).

3.1.2 SUBCELLULAR FRACTIONATION TO OBTAIN POSTSYNAPTIC DENSITIES

PSDs were prepared as a modification of a previously described protocol (Carlin et al. 1980). Essentially, as shown in Fig. M-3A, tissue was chemically and mechanically homogenized in a 9:1 volume: weight ratio using 1 or 7-mL glass-Teflon tissue grinders (borosilicate Dounce homogenizer; Wheaton) with ~40 strokes in a A solution (50 mM Tris pH 7.4, 0.32 M sucrose, 5 mM EDTA, 1mM EGTA, 1µg/mL Aprotinin (Merck-Millipore), 1 µg/mL Leupeptin (Merck-Millipore), PMSF 1/2500, $ZnCl_2$ 20 µM, 50 mM NaF; 1 mM SOV and 2.5 mM Sodium pyrophosphate [unless indicated all from Sigma-Aldrich]) in ice. A first 10 min centrifugation (centrifuge Epp 5417R, Eppendorf) at 1,400xg in 4ºC was conducted. The resulting supernatant was conserved, and pellet was subjected to a second and third re-homogenization with the same centrifugal conditions. Afterwards, the 3 pooled supernatants were centrifuged at 700g for 10 min to discard remaining nuclei and cell debris. Clean supernatant was centrifuged 30 min at 21,00xg at 4ºC. The supernatant represents the cytosolic fraction whereas the pellet obtained contains the membrane fraction (Fig. M-3), which was resuspended with B solution (Sucrose 0.32 M and 50 mM Tris pH 7.4; all from Sigma-Aldrich). This sample was named total membrane (TM) fraction, and the corresponding pellet (P-TM).

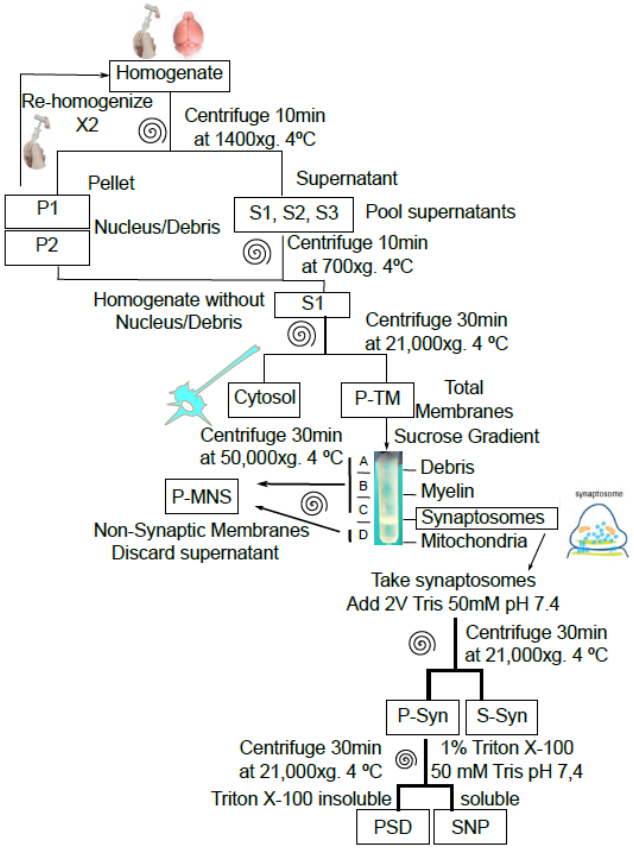

Figure M-3. Synaptosome and PSD fractionation protocol. Flow-chart of the steps and fractions obtained throughout de process. P-TM: Pellet-Total membranes; Syn: Synaptosome; P: Pellet; S: Supernatant; SNP: Synaptic non-PSD.

Sucrose gradient was prepared by dispensing 1mL of E solution (1.2 M sucrose; 50 mM pH 7.4), 1mL D solution (1 M sucrose; 50 mM pH 7.4), 1mL C solution (0.85 M, 50 mM Tris pH 7.4) and ~1 mL B solution with the membrane fraction to 14x89 mm tube (Beckman Coulter, CA, USA) and centrifuged with Sw60 Ti rotor (Beckman Coulter) at 82,500xg for 2 h at 4ºC. The interphase between sucrose 1.2 and 1 M contains the synaptosome fraction. All the other volume was conserved as non-synaptic membranes (NSM). The synaptosome fraction was diluted to reach a final concentration of 10% sucrose with Tris 50 mM pH 7.4 and centrifuged in the rotor Epp 5117R (Eppendorff) at 21,000xg during 30 min. The supernatant fraction was stored and named S-Syn, while the pellet fraction was further resuspended in 80 µL of Tris 50 mM pH 7.4 and 80 µL of 2% Triton X-100 (Sigma-Aldrich; diluted with Tris 50 mM pH 7.4) and maintained on ice during 10 min. Finally, samples were centrifuged at 21,000xg during 30 min. As a result, Triton X-100 soluble fraction (SNP) and Triton X-100 insoluble pellet (PSD enriched) fractions were obtained.

3.2 PROTEIN CONCENTRATION DETERMINATION

Protein concentration was determined using a micro-BCA protein assay kit (Thermo-Fisher Scientific, Waltham, MA, USA). The method used by this kit is based on the Biuret method, where molecules with two or more peptide bonds in alkaline conditions react and reduce Cu2+ ions. This enables selective colorimetric detection of the complex formed between cuprous cation (Cu^{1+}) and bicinchoninic acid. Determination of protein concentration was done using a calibration curve of bovine serum albumin. Samples were incubated in a 96-well plate (Thermo Fisher Scientific) protected with a plastic sealer (cover slips adhesive acetate 128x86mm PA100, Corning) during 1h at 60ºC in a hybridization oven (model 1004, Shell lab). Absorbances for protein concentration were measured at 540 nm wave length in a spectrophotometer (model AD 340; Beckman Coulter).

3.3 SAMPLE PREPARATION FOR PROTEIN ELECTROPHORESIS

Once protein concentration was determined, samples were prepared with Laemmli loading sample buffer 1x (50 mM Tris-HCl, pH 6.8; 2% SDS [Merck-Millipore]; 1% β-mercaptoethanol and 0.04% bromophenol blue) and 10% glycerol (unless indicated, all reagents were purchased at Sigma-Aldrich). Finally, samples were boiled at 95ºC for 5 min. Aliquots were generated and stored at –80ºC until use.

3.4 SDS–POLYACRYLAMIDE GEL ELECTROPHORESIS

Protein samples were loaded and separated by discontinuous polyacrylamide sodium dodecyl sulphate polyacrylamide gel electrophoresis (SDS-PAGE). These gels were

prepared first with a desired % of acrylamide in the gel for protein separation with A solution (acrylamide/bis-acrylamide [Bio-RAD]); B solution (1.5 M Tris-HCl; SDS 0.4% [pH 8.8]); freshly thawn 1% ammonic persulfate (Sigma-Aldrich) and 0.2% TEMED (Sigma-Aldrich). Before polymerization of the separation phase of the gel was achieved, isopropanol (Sigma-Aldrich) was added and removed once solidified the gel. The stacking gel was prepared with A solution; C solution (0.46M Tris-HCl pH 6.8 and 0.4% SDS [Sigma-Aldrich]); Ammonic persulfate and TEMED (both from Sigma-Aldrich). The volumes used for each acrylamide gel are shown in Table M-4.

	Separation phase							Stacking phase	
Acrylamide %	**20**	**16**	**12**	**10**	**8**	**6**	**4**	**4.2**	**Units**
A Solution	2.99	2.43	1.8	1.53	1.33	0.900	0.630	0.252	mL
B Solution	1.08	1.08	1.08	1.08	1.08	1.08	1.08	-	mL
C Solution	-	-	-	-	-	-	-	450	µl
MilliQ water	0.378	0.945	1,575	1,845	2,075	2,475	2,745	1,098	mL
Ammonic persulfate	45	45	45	45	45	45	45	22.5	µl
TEMED	9	9	9	9	9	9	9	2.25	µl
Final volume	**4.509**	**4.509**	**4.509**	**4.509**	**4.509**	**4.509**	**4.509**	**1.825**	**mL**

Table M-4. Volumes for different percentages of acrylamide gels. The volumes are for one acrylamide gel of 0.75 mm thick in each case.

In the case of SDS-PAGE gels prepared for LC-MS/MS analysis of Chapter II and Annex, SDS-PAGE separation phases from conventional 6% acrylamide gels were 2 cm in height and let polymerized ON. In contrast, the stacking phases were prepared and let polymerize 2h before use. Acrylamide gels prepared for these analyses were 0.75 mm thick. Then, samples were run 3 cm within separation phases. The goal of this special SDS-PAGE condition was to concentrate the sample which was afterwards, divided into 6 gel bands ready for sample preparation for LC-MS/MS analyses (Fig. M-4).

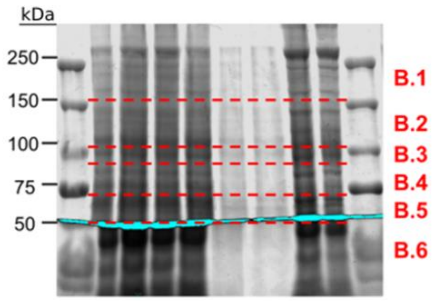

Figure M-4. Representative *Coomassie* stained gel. To conduct *in-gel* protein digestion for LC-MS/MS analyses, conventional acrylamide gels were stained with *Coomassie* prior its cut into 6 bands per lane as shown in this example.

Alternatively, criterion Stain free™ gels (SF gels, Bio-Rad) were prepared according to manufacturer's instructions (see M-3.5.3 for detailed information). These gels allow for protein monitoring throughout immunoblot (IB) to finally be able to correct for protein differences due to technical variability (e.g., differences of loaded samples or in transference). Thus, it allows a reduction of technical variability after protein intensities normalization.

Regardless the type of acrylamide gels prepared, precision plus protein standards all blue or kaleidoscope (both from Bio-Rad) were used as well as a vertical MiniProtean system kit (Bio-rad) and 1x running buffer (0.025 M TRIS pH 8.4; 0.187 M glycine and 0.1% SDS; all from Sigma-Aldrich) to resolve the samples into the appropriate mass weight. Unless indicated, electrophoretic conditions were 25 mAmp per each 0.75 mm wide gel or 50 mAmp per each 1.5 mm wide gel. Gels were run until the loading sample buffer front (blue staining) reach the end of the gel.

3.5 IN-GEL PROTEIN STAINING

3.5.1 *COOMASSIE* STAINING

Proteins resolved in SDS-PAGE gels were stained with 50 mL *Coomassie* solution per gel. This solution was prepared by mixing 80% Brilliant Blue R-250 staining solution (Bio-Rad) and 20% methanol (Panreac*,* Applichem division, Barcelona, Spain). The gel was placed in glass staining dish (Grale Scientific, Melbourne, Australia) and stained ON at RT. Gels were firstly distained with 50 mL of destaining solution (2.5 % acetic acid [Sigma-Aldrich] and 20% methanol [Panreac]) during 10 min in a rocking platform shaker (Stuart Scientific Ltd.,) and later with subsequent treatments of 20% methanol during 1h, until protein bands were clearly visible. Gel images were acquired with ChemiDoc XRS+ (Bio-Rad) or scanned by Umax Colour Scanner (UMAX, Willich, Germany) though MagicScann ver.4.5 UMAX software whereas quantifications were conducted with Image Studio Lite ver. 3.1 (LI-COR Biosciences).

3.5.2 SILVER STAINING

This method was conducted using Silver Stain Plus™ kit (Bio-Rad) accordingly to manufacturer's instructions. Image acquisition and densitometry assessment was done as explained previously in above section M-3.5.1.

3.5.3 CRITERION STAIN FREE PROTEIN STAINING

The technology behind criterion SF gels (Bio-Rad) is based on the activation of proteins separated in acrylamide gels by UV irradiation and the production of a fluorescent signal that is detected by a camera (Bio-Rad). This activation produces UV-induced trihalo compound modification of tryptophan residues contained in proteins after separation by electrophoresis (Kazmin et al. 2002). Importantly, this staining allows correcting for protein

abundance differences in equivalent samples due to technical issues (e.g., different amount of proteins loaded, differences in protein transference). Finally, protein activation, automated image capture and analysis of gels and PVDF membranes transferred with previous activated proteins in SF gels were acquired with ChemiDoc XRS+ system (Bio-Rad). Then, Image Lab software (Bio-Rad) was used to determine the protein densitometry.

3.6 IMMUNOBLOT ANALYSIS

Prior to IB protein concentrations were normalized by silver staining (Silver Stain Plus™ kit, Bio-Rad) of SDS-PAGE gels containing 1.5-2 µg of each sample to ensure that equal amounts of protein were analysed. Also, whenever possible a standard curve with known concentrations of protein were added.

Protein transference was conducted using the MiniProtean kit with a module for transference procedures (Bio-Rad), and 1x chilled transference buffer (20% methanol [Panreac]; 39 mM Glycine; 48 mM TRIS; 0.04% SDS [all from Sigma-Aldrich]). Proteins were transferred into methanol pre-activated polyvinylidene fluoride (PVDF) membranes (Immobilon-P, Merck-Millipore). After transference, PVDF membranes were blocked with 5 mL Odissey blocking solution (LI-COR, Bad Homburg, Germany) or with a blocking solution based on milk protein (5% dehydrated cow milk [Nestlé, Barcelona, Spain]; 1x TBS [50mM Tris·HCl pH7.4; 1,5 M NaCl) and 0.1% sodic azide [all from Sigma-Aldrich]). Subsequently, PVDF membranes were incubated in a roller mixer (Stuart Scientific Ltd) with 3 mL (membrane stripes) or 5 mL (whole membranes) of primary antibody solution ON at 4ºC or 2h at RT depending on the primary antibody used. The list of the antibodies used and their specific incubation conditions, is shown in Table M-6. Both primary and secondary antibodies were prepared with a Tris-buffered solution with tween (T-TBS [50mM Tris·HCl pH7.4; 1,5 M NaCl, 0,1% Tween20; all from Sigma-Aldrich]).

Once the primary antibody incubation was done, four washes with 1x T-TBS of 5 min each were carried out. Then, PVDF membranes were incubated with 5mL of the corresponding secondary antibody IRDye shown in Table M-5 for 1 h at RT and protected from light. In some cases, membranes were reblotted by an ON incubation at 4ºC or 2h at RT depending on the antibody. Images were acquired with an Odissey Scanner (LI-COR Biosciences) and bands from the images were analysed with Image Studio Lite ver. 3.1 software (LI-COR Biosciences). Noteworthy, depending on the IB features, ‘General’ or ‘Individual background subtraction methods were used.

Primary antibodies							
Antibody target (clone)	Cat Number	MW (kDa)	Provider	Host specie	Dilution for IB	Dilution for IP	Incubation Conditions
SynGAP (D78B11)	5540S	~150	Cell Signalling (Izasa)	Rabbit	1:2,000	1:15	4ºC ON or 2h at RT
SynGAP	ab3344	~150	Abcam	Rabbit	1:1,000	_	4ºC ON or 2h at RT
SynGAP	NBP2-27541	~150	Novus Biologicalis	Goat	1:2,500	_	4ºC ON or 2h at RT
SynGAP-α1	06-900	149-160	EMD Millipore	Rabbit	1:1,000	_	4ºC ON
SynGAP-α2 (EPR2883Y)	04-1071	149-160	Merck-Millipore	Rabbit	1:2,000	_	4ºC ON
SynGAP-β	-	149-160	rovided by Dr. Rumbaug	Rabbit	1:1,000	_	4ºC ON
PSD-95	3450	95	Cell Signalling (Izasa)	Rabbit	1:1,000	_	4ºC ON
CAMKII-α	05-532	50	Merck-Millipore	Mouse	1:1,000	_	4ºC ON
Shank2	SC-30192	>110 Kda (138/162/180/202,5)	Santa Cruz	Rabbit	1:1,000	_	4ºC ON
Shank2	USBI041698	>110 Kda (138/162/180/202,5)	United States Biological	Rabbit	1:1,000	_	4ºC ON
Cofilin-1	ab11062	19	Abcam	Rabbit	1:1,000	_	4ºC ON
Dctn2	ab124285	44	Abcam	Rabbit	1:1,000-1:11,000	_	4ºC ON
RhoA	ab187027	22	Abcam	Rabbit	1:1,000-1:11,000	_	4ºC ON
RasH	ab32417	21	Abcam	Rabbit	1:1,000	_	4ºC ON
Fak2	LS-C344504	116	LifeSpanBiosciences	Mouse	1:1,000	_	4ºC ON
Lyn	LS-C145387	59	LifeSpanBiosciences	Mouse	1:1,000	_	4ºC ON
Mrps34	PA5-24471	26	Invitrogen	Rabbit	1:1,000	_	4ºC ON
CK5P3	PA5-54569	57	Invitrogen	Rabbit	1:1,000	_	4ºC ON
Ndrg2	TA311622	41	Quimigen	Rabbit	1:1,000	_	4ºC ON
Mrpl12	TA338337	22	Quimigen	Rabbit	1:1,000	_	4ºC ON
PTN1	04-1140	50	EMD Millipore	Mouse	1:1,000	_	4ºC ON

Secondary antibodies						
Reactivity	Antibody ID	Cat Number	Provider	Host specie	Dilution	Incubation Conditions
Rabbit	IRDye 800CW	926-32212	LI-COR biosciences	Donkey	1:7,500	1h at RT
Mouse	IRDye 680CW	926-68073	LI-COR biosciences	Donkey	1:7,500	1h at RT
Goat	IRDye 800CW	926-32214	LI-COR biosciences	Donkey	1:7,500	1h at RT

Table M-5. Information of primary and secondary antibodies used for Immunoblot and Immunoprecipitation.

3.6.1 IMMUNOBLOT DATA NORMALIZATION

In addition to correct for IB technical variabilities using SF criterion, silver stain procedures or control proteins (e.g., β-Actine), immunoblot data was further normalized to correct for IBs differences between membranes blotted with the same antibody. This allows comparing intensity units (IU) values in the same unit scale before statistical analyses. For this purpose, each individual band IU was divided by the mean of all band intensities in the corresponding membrane whenever was required.

4.BIOINFORMATIC ANALYSES OF DATA

4.1 *IN-SILICO* ANALYSIS OF TRANSCRIPT AND PROTEIN ISOFORMS

Genomic sequences with full annotation, including cDNA, ESTs and protein were retrieved for *Syngap1 and Shank2* from Ensembl (EMBL-EBI; release 91 December for *Synagap1* and release 93 July 2018 for *Shank2* [https://www.ensembl.org]) and GenBank/RefSeq (from NCBI database; [https://www.ncbi.nlm.nih.gov/genbank]).

cDNA sequences were aligned using BLAST (https://blast.ncbi.nlm.nih.gov/Blast.cgi) and UniProt database alignment tools (www.UniProt.org). To match exonic sequences with protein ones, DNA sequences were translated to RNA and protein with the DNA/RNA to protein translator tool (http://www.fr33.net/translator.php). To search which exonic sequences encode SynGAP protein domains, the UniProtKB; Prosite, InterPro and SMART databases annotation were used. Also, protein sequence domains and other features for SynGAP variants were found with SMART, InterPro and Prosite databases, whereas disordered regions were assessed with PONDR on-line tool (www.pondr.com). The specific information about those PTMs other than those reported in the literature were extracted from Prosite, whereas the CC domain and low complexity (LC) regions were obtained from the SMART database.

4.2 DATABASE IDENTIFICATION CODES

Protein identification codes were obtained from LC-MS/MS analyses, but those that were not provided by the corresponding MS software, were converted to different database IDs (e.g., Ensembl gene ID, MGI ID or the gene name) using BioMart from Ensembl database (https://www.ensembl.org/biomart), DAVID (https://david.ncifcrf.gov) and UniProt (www.uniprot.org/uploadlists) conversion tools.

4.3 STATISTICAL ANALYSES

All data were assessed for normal distribution by descriptive statistic measures and applying the Shapiro-Wilk test as a first choice or the Kolmogorov-Smirnov with a Lilliefors correction (K-S) when required. Data normalization was done when needed by transforming data into a base-10 log scale. The equality of variances was assessed by Levene's test. Each test applied to each data analysis is indicated in its corresponding figure legend. GraphPAD Prism version 6.0 (GraphPad, San Diego, CA), SPSS version 24.0 (IBM, CA, USA) or RStudio (Racine 2012) were used to conduct statistical analyses.

All statistical analyses were conducted with a significance level of $\alpha = 0.05$ ($p \leq 0.05$). In some cases, Ignasi J. Gich Saladich (Institut de Recerca de l'Hospital de la Santa Creu I Sant Pau) was asked for statistical advice.

CHAPTER I

CI-INTRODUCTION

The study of SynGAP protein expression in different brain regions and at different developmental stages is particularly interesting, as most reports are focused on gene expression (Li et al. 2001; Porter et al. 2005; Barnett, 2006; Clement et al. 2012; McMahon et al. 2012). In contrast, only qualitative assessments at the protein level throughout development in PSDs from cortex (Ctx; Barnett et al. 2006) as well as in total extracts of hippocampus (Hip; Yang et al. 2004; Petralia et al. 2005) and cerebellum (Crb; Tomoda et al. 2004) have been reported. Given the fact that SynGAP dosage is essential for normal development of human cognition and appears to modify important aspects of neural excitability and sociability (Clement et al. 2012, 2013; Kim et al. 2003; Knuesel et al. 2005; Komiyama et al. 2002; Muhia et al. 2009; Ozkan et al. 2014), a proper assessment of SynGAP abundance and its isoforms during different stages of brain areas development as well as its subcellular distribution in normal conditions will be key to understand the role of SynGAP in the brain. Furthermore, SynGAP isoforms have been suggested to be well conserved in rodents (Kim et al. 1998, Chen et al. 1998, Li et al. 2001), yet this has only been investigated for N-term variants (McMahon et al. 2012). Thus, in the present study, a comparison of the whole protein sequence of SynGAP isoforms between *Rattus norvegicus*, *Mus musculus* and *Homo sapiens* was conducted. Also, as the human isoforms reported at the mRNA levels have not been demonstrated to be expressed at the protein level in human brain, the expression of SynGAP isoforms bearing three C-term variants has also been evaluated.

CI-MATERIALS AND METHODS

1. BIOLOGICAL MATERIALS AND METHODS

1.1 ETHICS STATEMENT FOR HUMAN SAMPLE USE

Adult cortical samples were collected in those cases that a corticectomy of healthy tissue had to be performed to access subcortical pathological tissue that had to be removed by a surgical procedure. Most samples collected originated from neuro-oncological surgery of sub-cortical tumours. To collect these samples, neurosurgeons did not make any change to their procedures that could endanger patient's survival or lead to the loss of cognitive/executive functions. All patients were informed and signed an informed consent.

1.2 MOUSE LINES

Wild-type (WT) mice (*Mus musculus*, strain C57BL/6J) was used (see Table M-1).

1.3. SAMPLE COLLECTION

1.3.1 HUMAN SAMPLES

After resection of Ctx from a young male adult (19 years) and an old male patient (67 years), tissue was wrapped in aluminium foil and snap-frozen in liquid nitrogen without any prior chemical fixation. Samples were stored in -80ºC. All procedures between tissue dissection and snap-freezing were performed in the minimum amount of time possible and maintaining samples in ice, to maximize preservation of its molecular components.

1.3.2 MOUSE SAMPLES

For *Syngap1* mRNA and SynGAP protein expression studies mouse brain regions were collected at postnatal days (PND) 0/1, 4, 11, 21, 56. Tissues were obtained from both sexes at similar ratios until PND21. For older ages, male mice were preferentially used to avoid protein changes due to oestrogens from cycling female. Cortices from 26 months old male mice were provided by Carles Sindreu (Universitat de Barcelona). For protein sub-cellular localization studies Ctx without premotor/prefrontal (PM/PF) area was used. This cortical samples were collected at PNDs 7, 14, 21 and 56 from C57BL/6 mice in similar sex ratios as before. Finally, hippocampus (Hip) for protein subcellular localization studies were taken from PND63 males and females.

2. MATERIALS AND METHODS FOR GENOMIC SPECIMENS

2.1 RNA EXTRACTION, PURIFICATION AND cDNA SYNTHESIS

Frozen Ctx and Hip from PND0/1, 11, 21 and 56 mice were subjected to RNA extraction. Around 40 ng of extracted RNA was subjected to RT-PCR for cDNA synthesis (see general M-2.4). PCR products were prepared and separated by electrophoresis using 6% agarose gel and visualized by GelRed (Biotium, VWR) as previously indicated in general M-2.6.1.

2.2 CONVENTIONAL PCR

A representative figure of the regions chosen for 5' and 3' ends amplification is shown below (Fig. MI-1).

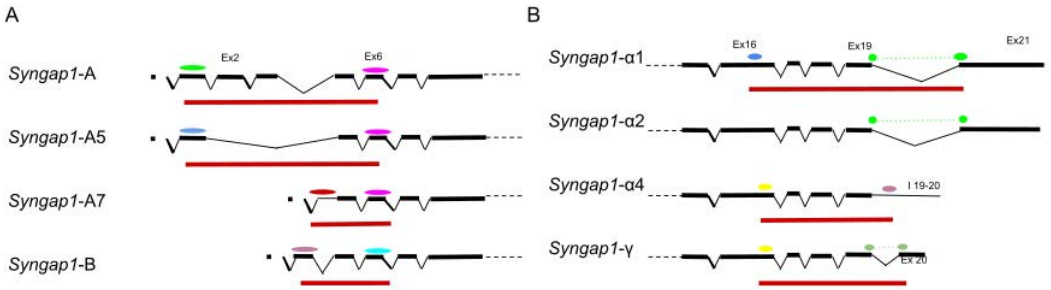

Figure MI-1. Primer pair design for specific amplification of both 5' and 3' variants. Schematic (A) primer pairs hybridization for 5' and (B) 3' variants amplification. Primer locations are indicated by coloured ellipses.

Primer pairs for 5' and 3' end variants are shown in Table MI-1A. The specific thermocycle conditions are indicated in the Table MI-1B.

A

Syngap1 5' and 3' variants identification			
Target	Forward primer	Reverse primer	Fragment size (bp)
SynGAP-A1/2	GTCTCGAGCCTCCATCCATC	GATCTGTCGAAAGCTGCTGG	469
SynGAP-A5	GCCCCCTTCAGAGAATACCAC	GATCTGTCGAAAGCTGCTGG	195
SynGAP-A7	ATGTTCTCGCTGCATCTTCC	GATCTGTCGAAAGCTGCTGG	219
SynGAP-B	CTCTTCTTGCTGCATCTTCC	GATCTGTCGAAAGCTGCTGG	205
SynGAP-α1/2	AGAGGGGCAAGTCTCAACAG	AAGCTGCCTCTCCCCAACTC	728/734
SynGAP-γ	GGGGCAAGTCTCAACAGTTG	ACCTGATGAGGAGCTGAGCG	690
SynGAP-α4	GGGGCAAGTCTCAACAGTTG	CAGACAACGGGATGGCAGATG	834

B

PCR thermocycling conditions			
Step	Tª (ºC)	Duration (min)	Nº of cycles
1	94	5	1
2.a	94	1	
2.b	58*/59**	1	35
2.c	72	1	
3	72	4	1
4	4	Inifinty	1

Table MI-1. **Primer pairs for *Syngap1* variants PCR.** (A) Primer pairs for indicated 5' and 3' *Syngap1* variants. Fragment sizes are indicated in base pairs (bp). (B) Thermocycling conditions. * for 5' *Syngap1* variants and ** for 3' *Syngap1* variants.

3. MATERIAL AND METHODS FOR PROTEIN ANALYSIS

3.1 TOTAL PROTEIN SOLUBILIZATION

For protein expression studies 3S fractions obtained from 1% DOC solubilization of brain tissue were used. This procedure has been previously described (see general M-3.1.1). However, the ratio of tissue weight *vs.* homogenization solution volume varied depending on mouse age as follows: at PND0/1 was 1:5.8, at PND11 1:8.75, whereas at posterior ages it was 1:17.5. The number of biological and technical replicas for each experiment is indicated in the following section MI-3.3.

3.2 SUBCELLULAR FRACTIONATION

For protein subcellular localization studies, the following fractions were analysed: Homogenate without nucleus (S1), Cytosol, non-synaptic membranes (NSM), synaptic not-PSD (SNP) and postsynaptic density (PSD) were collected (see general M-3.1.2).

3.2.1 PROTEIN YIELD CALCULATION

Protein yield is defined as the amount of protein recovered in a given biochemical fraction by the weight of the tissue used in that extraction. The following formulas were used:

$$\text{Total amount of protein (µg)} = \text{final volume(µL)} * \text{protein concentration (µg/µL)}$$

$$\text{Protein Yield} = \text{Total amount of protein (µg)} / \text{tissue weight (mg)}$$

3.3 IMMUNOBLOT ANALYSIS

General immunoblot procedures have been previously described (general M-3.6). In this chapter immunoblot has been used for the studies described below.

3.3.1 ANALYSIS OF SYNGAP ISOFORMS ABUNDANCE AT DIFFERENT DEVELOPMENTAL AGES IN FIVE BRAIN REGIONS.

As previously mentioned, 3S protein fractions were used in this study. The relative abundance of total SynGAP, SynGAP C-term variants, PSD-95 and CAMKII-α was investigated. Silver stained gels were used to correct for possible errors in protein quantification (see general M-3.5.2). In addition, IBs were done with 7.5% acrylamide SF gels (Bio-Rad) to correct for variability occurring during protein transference to PVDF

membranes. Next, IU were normalized as described in M-3.6.1. Information on the number of biological and technical replicas used for IBs in this study is shown in Table MI-2.

Immunoblot information summary										
Study	Samples	N of mice "pooled"	Biological replicates	Technical replicas						Loaded µg
				Total SynGAP	SynGAP-α1	SynGAP-α2	SynGAP-β	PSD-95	CAMKII-α	
Protein abundances at different developmental ages within a brain area (Conventional acyrlamide gels)	3S Ctx PND0/1	4	1	7	-	-	-	-	-	60
	3S Ctx PND11	4	1	5	-	-	-	-	-	40
	3S Ctx PND21	2	1	8	-	-	-	-	-	30
	3S Ctx PND56	2	1	5	-	-	-	-	-	30
	3S Ctx 14 weeks	2	1	4	-	-	-	-	-	30
Protein abundances at different developmental ages within a brain area (SF gels)	3S Ctx PND4	4	1	14	7	7	4	17	11	30/60
	3S Ctx PND11	2	1	20	19	11	12	20	20	30
	3S Ctx PND21	2	1	17	19	10	11	20	19	30
	3S Ctx PND56	2	1	15	17	9	10	16	19	30
	3S Hip PND4	10	1	12	6	6	9	7	7	30
	3S Hip PND11	4	1	16	8	8	12	11	11	30
	3S Hip PND21	5	1	16	8	8	12	12	12	30
	3S Hip PND56	4	1	16	7	8	12	11	11	30
	3S Str PND4	10	1	6	5	5	3	15	3	30
	3S Str PND11	4	1	7	9	7	4	18	10	30
	3S Str PND21	4	1	7	9	8	5	19	11	30
	3S Str PND56	4	1	7	9	7	5	18	11	30
	3S OB PND4	28	1	15	12	10	12	18	7	30/60
	3S OB PND11	28	1	11	6	6	9	18	8	30/60
	3S OB PND21	4	1	16	13	10	11	18	11	30/60
	3S OB PND56	4	1	15	14	11	12	18	9	30/60
	3S Crb PND4	3	1	24	8	9	15	13	4	120
	3S Crb PND11	3	1	24	9	9	14	11	3	120
	3S Crb PND21	2	1	23	9	9	12	11	3	120
	3S Crb PND56	2	1	23	9	8	12	11	3	120

Table MI-2. **Summary of the number of replicas and the amounts of a given sample loaded in the indicated acrylamide gels for IB analyses.** This data corresponds to analyses of the synaptic protein (shown under the label of technical replicas) abundances at different developmental ages in five brain regions (described in the label samples). Cortex (Ctx), Hippocampus (Hip), Striatum (Str), OB (Olfactory Bulb) and Cerebellum (Crb) were analysed.

3.3.2 ANALYSIS OF SYNGAP ISOFORMS ABUNDANCE AT DIFFERENT BRAIN REGIONS AND IN FOUR DEVELOPMENTAL TIME POINTS.

Samples and procedures used in this study are the same as the ones described above (MI-3.3.1) with one exception: SF gels used had 12% acrylamide. Table MI-3 summarises the information related to biological and technical replicas used for IBs in this study.

Immunoblot information summary										
Study	Samples	N of mice "pooled"	Biological replicates	Technical replicas						Loaded µg
				Total SynGAP	SynGAP-α1	SynGAP-α2	SynGAP-β	PSD-95	CAMKII-α	
Protein abundances at different developmental ages between a brain area (SF gels)	3S Ctx PND4	4	1	9	6	6	6	9	6	50
	3S Hip PND4	10	1	9	6	6	6	9	6	50
	3S Str PND4	10	1	9	6	6	6	9	6	50
	3S OB PND4	28	1	9	6	6	6	8	6	50
	3S Crb PND4	3	1	8	6	6	6	8	6	50
	3S Ctx PND11	2	1	15	6	6	6	12	6	30
	3S Hip PND11	4	1	15	6	6	6	12	6	30
	3S Str PND11	4	1	15	6	6	6	12	6	30
	3S OB PND11	28	1	15	6	6	6	12	6	30
	3S Crb PND11	3	1	15	6	6	6	12	4	60
	3S Ctx PND21	2	1	9	6	6	6	6	6	30
	3S Hip PND21	5	1	9	6	6	6	6	6	30
	3S Str PND21	4	1	9	6	6	6	6	6	30
	3S OB PND21	4	1	9	6	6	6	6	6	30
	3S Crb PND21	2	1	9	6	6	6	6	6	60
	3S Ctx PND56	2	1	6	6	6	6	6	9	30
	3S Hip PND56	4	1	6	6	6	6	6	9	30
	3S Str PND56	4	1	6	6	6	6	6	9	30
	3S OB PND56	4	1	6	6	6	6	6	9	30
	3S Crb PND56	2	1	6	6	6	6	6	3	60

Table MI-3. Summary of the number of replicas and the loaded amounts in the protein expression between brain areas in different stages of development. The brain areas studied were Cortex (Ctx), Hippocampus (Hip), Striatum (Str), OB (Olfactory Bulb) and Cerebellum (Crb).

3.3.3 ANALYSIS OF SYNGAP ISOFORMS ABUNDANCE IN MOUSE AND HUMAN CORTICAL SAMPLES.

Samples were prepared as previously described (see general M-3.1.1). Procedures used in this study are the same as the ones described above (MI-3.3.1). However, homogenate samples were used since the solubilization of 1% DOC did not solubilised all SynGAP. In addition, samples that were solubilized and then reconstituted to get a homogenate-like sample were used. This homogenate reconstitution was done by calculating the amount of protein that remained in pellets and S1 fractions from a given sample. Then, the corresponding proportion of these fractions in were added to generate the reconstituted homogenate sample. Table MI-4 summarises the information on biological and technical replicas used for IBs in this study.

Immunoblot information summary										
Study	Samples	N of "pooled" individual	Biological replicates	Technical replicas						Loaded µg
				Total SynGAP	SynGAP-α1	SynGAP-α2	SynGAP-β	PSD-95	CAMKII-α	
Protein abundances at different developmental ages between a brain area (SF gels)	H ans reconstituted H Ctx PND56 (mouse)	2	1	26	9	11	10	20	17	40
	H and reconstituted H Ctx M26 (mouse)	2	1	23	9	11	10	20	18	40
	H or reconstituted H Str PND4 (human)	1	1	24	10	10	11	21	19	40
	H or reconstituted H OB PND4 (human)	1	1	16	9	9	10	20	18	40

Table MI-4. Summary of the number of replicas and the loaded amounts used of cortical mouse and human samples for analyses of synaptic proteins expression. The proteins studied are shown below technical replicas label. H stands for homogenate.

3.3.4 ANALYSIS OF SYNGAP ISOFORMS SUBCELLULAR LOCALIZATION IN CORTEX AT FOUR DEVELOPMENTAL STAGES.

Samples used and the fractionation protocol undertaken have been previously described (see general M-3.1.2). Of note, IBs were conducted after validating the fractionation protocol. Table MI-5 summarises the information on biological and technical replicas used for IBs in this study.

Immunoblot information summary										
Study	Samples	N of mice used	Biological replicates	Technical replicas	Total replicas (biological+technical)					Loaded µg
					Total SynGAP	SynGAP-α1	SynGAP-α2	SynGAP-β	PSD-95	
Subcellular localization experiments in C57BL/6 (Ctx without prefrontal area)	S1 PND7	6	6	≥3	18	6	6	6	6	35
	Cytosol PND7	6	6	≥3	18	6	6	6	6	40
	NSM PND7	6	6	≥3	18	6	6	6	6	50
	SNP PND7	6	6	≥3	18	6	6	6	6	80
	PSD PND7	6	6	≥3	18	6	6	6	6	35
	S1 PND14	6	6	≥3	21	6	6	9	6	40
	Cytosol PND14	6	6	≥3	21	6	6	9	6	50
	NSM PND14	6	6	≥3	21	6	6	9	6	50
	SNP PND14	6	6	≥3	21	6	6	9	6	60
	PSD PND14	6	6	≥3	21	6	6	9	6	25
	S1 PND21	6	6	≥3	18	6	8	8	9	20
	Cytosol PND21	6	6	≥3	18	6	8	8	9	40
	NSM PND21	6	6	≥3	18	6	8	8	9	40
	SNP PND21	6	6	≥3	18	6	8	8	9	60
	PSD PND21	6	6	≥3	18	6	8	8	9	15
	S1 PND56	6	6	≥3	15	11	9	9	6	20
	Cytosol PND56	6	6	≥3	15	11	9	9	6	40
	NSM PND56	6	6	≥3	15	11	9	9	6	40
	SNP PND56	6	6	≥3	15	11	9	9	6	60
	PSD PND56	6	6	≥3	15	11	9	9	6	15

Table MI-5. Summary of the number of replicas and the loaded amounts in the protein subcellular localization analyses. Total protein extracts without nuclei (S1), Cytosol, non-synaptic membranes (NSM), synaptic non-PSD (SNP) and postsynaptic density (PSD) fractions were analysed.

3.3.5 ANALYSIS OF SYNGAP ISOFORMS SUBCELLULAR LOCALIZATION IN ADULT HIPPOCAMPUS.

Samples used and the fractionation protocol undertaken have been previously described (see general M-3.1.2). Tissue was collected from PND63 animals. Of note, IBs were conducted after validating the fractionation protocol. Table MI-6 summarises the information on biological and technical replicas used for IBs in this study.

Immunoblot information summary										
Study	Samples	N of mice used	Biological replicates	Technical replicas	Total replicas (biological+technical)					Loaded µg
					Total SynGAP	SynGAP-α1	SynGAP-α2	SynGAP-β	PSD-95	
	S1 WT	12	6	1 or 2	9	8	8	8	7	20
	Cytosol WT	12	6	1 or 2	9	8	8	8	7	40
	SNP WT	12	6	1 or 2	7	7	7	7	6	60
ular localization experiments	PSD WT	12	6	1 or 2	8	7	7	6	7	15
ap1 PBM+/- (Hip PND63 mice)	S1 HOMO	12	6	1 or 2	8	-	8	8	8	20
	Cytosol HOMO	12	6	1 or 2	8	-	8	8	8	40
	SNP HOMO	12	6	1 or 2	8	-	8	8	8	60
	PSD HOMO	12	6	1 or 2	8	-	8	8	8	15
	S1 WT	12	6	1 or 2	19	5	14	10	20	20
ular abundance comparison	S1 HET	12	6	1 or 2	19	5	14	10	19	20
n *Syngap1* PBM+/- genotypes	S1 HOMO	12	6	1 or 2	19	4	14	10	18	20
(PND63 Ctx)	PSDWT	12	6	1 or 2	29	5	10	14	25	15
	PSD HET	12	6	1 or 2	27	5	10	15	24	15
	PSD HOMO	12	6	1 or 2	29	4	10	14	25	15
	S1 WT	12	6	1 or 2	18	5	14	8	-	20
bcellular abundance	S1 HET	12	6	1 or 2	18	5	10	8	-	20
omparison between	S1 HOMO	12	6	1 or 2	20	4	13	7	-	20
p1 PBM+/- genotypes (PSD-	PSDWT	12	6	1 or 2	15	5	9	14	-	15
95 normalization)	PSD HET	12	6	1 or 2	19	5	10	15	-	15
	PSD HOMO	12	6	1 or 2	18	4	9	13	-	15

Table MI-6. Summary of the number of replicas and the loaded amounts used in the protein subcellular localization analysis in hippocampal samples. Total protein extracts without nuclei (S1), Cytosol, non-synaptic membranes (NSM), synaptic non-PSD (SNP) and postsynaptic density (PSD) fractions were analysed.

3.3.6 NORMALIZATION OF IMMUNOBLOT DATA IN SUBCELLULAR LOCALIZATION STUDIES.

General procedures for normalization of IB data have been previously described (See general M-3.7). Yet, for protein localization studies the procedure was modified as the same amount of protein extracts with different composition (e.g., cytosol *vs.* PSD) would give different intensities in SF gels. Therefore, SF normalization was replaced by a routinely used normalization as follow:

1) Intensity units (IU) of each band was normalized by the amount (µg) of proteins loaded in each lane. Different amounts were loaded according to the age and the fraction assessed to be able to detect the target protein.
2) The average yield (see MI-3.2) of each fraction at each age was multiplied by protein IU to get the total expression of a given protein in each fraction. This calculation corrected for biological variability due to the use of different numbers of brain structures/animals depending on the age.
3) To relatively compare the subcellular amounts and location of the different proteins assessed, all normalized data (IU*Yield) was divided by the values of its corresponding S1 fraction (e.g., [IU*Yield of PSD fraction/IU*Yield of S1]). Importantly, this value allowed to compare subcellular abundance of different proteins.

3.4 DISCOVERY AND TARGETED MASS SPECTROMETRY STUDIES

In this chapter, both discovery and targeted MS approaches were used. An overview of the steps conducted for MS studies aimed to absolutely quantify (AQUA) SynGAP C-term

variants is shown in Fig. MI-7. These steps include an immunoprecipitation (IP) followed to liquid chromatography coupled to tandem mass spectrometry (LC-MS/MS) analysis, which will be further, described in the following sections.

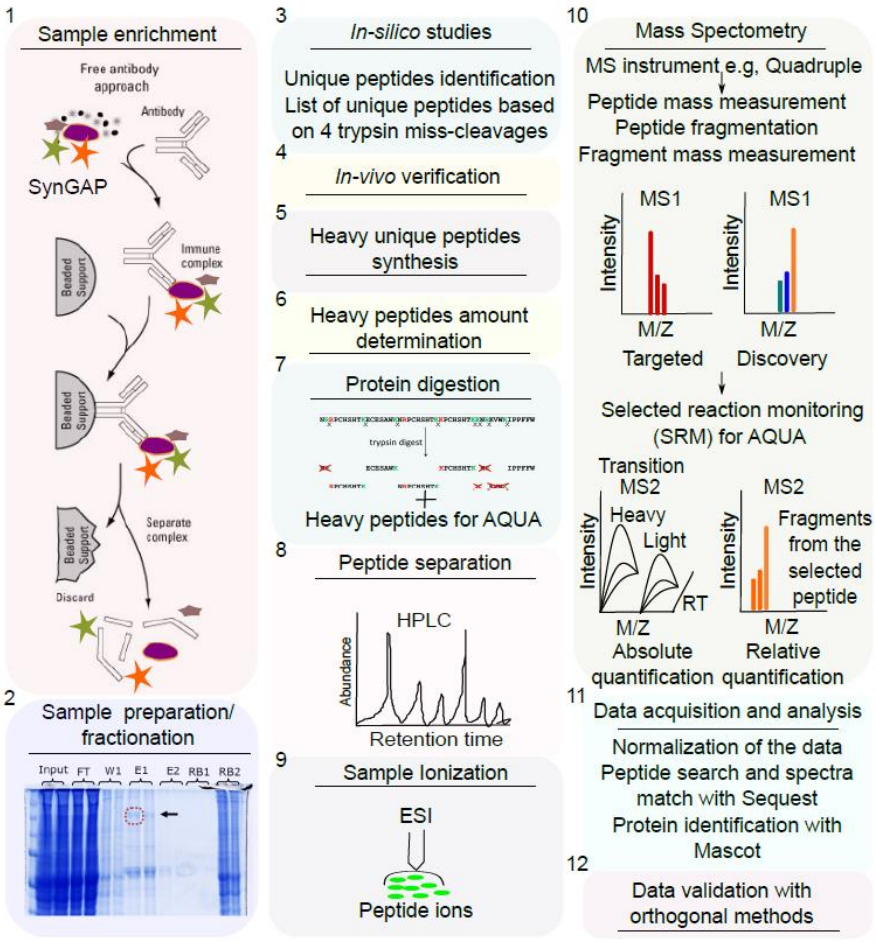

Figure MI-2. Flow-chart of IP coupled to LC-MS/MS studies of SynGAP C-term variants. Both absolute and relative quantification of SynGAP and its C-term variants together with some of its interactors (1, stars) that co-IP with SynGAP (purple oval) in the analysed band (2, red discontinuous square) were conducted. FT: Flow-through, W1: Wash 1, E1: Elute 1, E2: Elute 2, RB1: Boiled resin from the pre-clearing step and RB2: boiled resin after the elution of the resin bound complexes. HPLC: High pressure liquid chromatography; MM/Z: mass to charge ratio; ESI: Electrospray ionization; AQUA: absolute quantification.

3.4.1 SynGAP enrichment

SynGAP enrichment was performed by immunoprecipitation (IP; described below in 3.4.4) from 3S protein fractions obtained from C57BL/6 cortex (see general 3.1.1) prior to LC-MS/MS analysis. The number of animals required for each sample was as follows: 8 for PND0/1, 5 for PND11, 2 for PND21 and 2 for PND56. For the final targeted MS analyses using the serial reaction monitoring (SRM) mode, the number of biological replicas performed was 4 for PND0/1 sample and 3 for all other ages. Then, 3S fractions were concentrated 8x times with an Amicon Ultra-4 column (MWCO 50K; Merck-Millipore). Afterwards, 1/10 volume of a buffer containing 10% Triton X-100 and 0.5 M Tris pH 9,0

(Sigma-Aldrich) was added, the resulting sample was subjected to dialysis and sonication (described below in MI-3-4-3) prior to indirect IP.

3.4.2 PROTEIN DIALYSIS

Dialysis of concentrated samples was needed to prepare them for the indirect IP protocol, since the presence of 1% DOC impaired SynGAP antibody binding (Cell signaling, See Table M-5). Membranes for dialysis (Visking Corporation, Chicago, US) were activated according to manufacturer's instructions. Briefly, membranes were soaked with 1:10 sodium bicarbonate (Sigma-Aldrich) and Milli-Q water (Merck-Millipore) and heated until boiling in a microwave. Next, membranes were stored at 4ºC until use. Two plastic bag pegs at the ends of the membrane were used to close hermetically the bag containing the sample. Then, samples were dialysed ON against the dialysis buffer (50 mM Tris Hcl pH7.4 and 1% Triton X-100) at a v/v ratio of 1:1,000 in constant agitation at 4ºC. The next day, the recovered sample volume was measured and Triton X-100 (Sigma-Aldrich) was adjusted until ~1% as follows:

Dilution factor = Predialysis Volume/ Postdialysis Volume

% of Triton X-100 that needs to be added =1-dilution factor

3.4.3 SAMPLE SONICATION

Dialysed samples were sonicated with an ultrasonic bath Sonicator (Thermo Fisher Scientific) at 5% of its maximum intensity during 45 sec with 1.45 second-long on/off cycles. This resulted in the generation of the final post-dialysis sample.

3.4.4 SYNGAP INDIRECT IMMUNOPRECIPITATION

Before proceeding with the IP, the efficiency of the process and the quality of the postdialysis samples were analysed by SynGAP (Abcam) and PSD-95 (Cell Signaling; see Table MI-5) IBs. This could be performed because small amounts of all fractions generated throughout the whole process were collected and stored.

All biological replicates were adjusted to a concentration of 8 mg/mL. The following average amounts of protein were used for each IP: ~9 mg for PND0/1, ~16 mg for PND11, ~7.8 mg for PND21 and ~6.5 mg for PND56 samples. This allowed to IP similar amounts of SynGAP in all experiments. The estimation of these amounts was done according to previous IB and IP pilot studies.

The immunoprecipitation kit (Pierce® Direct IP Kit, Thermo Fisher Scientific) was used. Columns for IP (x25 spin columns/screw cap; Thermo Fisher Scientific) were prepared as described by the manufacturer. Briefly, a pre-clearing step was carried out, whereby 7.5 µL of A Sepharose resin (Sigma P3391-250MG) with EtOH (Sigma-Aldrich) was prepared by washing with conditioning buffer (50mM Tris pH 7.4 [Sigma-Aldrich]) in a column and centrifuge at 100xg (centrifuge 5417R, Eppendorf) four times at 4ºC. Then, the postdialysis sample was mixed with the dried resin placed in the Pierce column. The columns were incubated 2h at 4ºC in a "wheel" agitator (Stuart) to maintain samples in constant suspension and mixing. Then, the mix was centrifuged at 100xg during 2 min and the input sample was obtained. The resin was boiled with 48 µL of solution prepared with a final composition of 1x loading sample buffer and 10% glycerol (all from Sigma-Aldrich) during 5' at 95ºC to assess unspecific binding whereas input sample was mixed with 1:15 SynGAP antibody whose epitope belongs to a core region (Cell Signaling; #5540S; NEB; see Table M-5) in a 0.5 mL eppendorf ON at 4ºC and mixed in a tube rotator (Stuart). The fact that the antibody is first bound to the protein instead of the resin, is what makes this IP indirect (Fig. MI-2, step 1).

The following day new columns with 7.5 µL of resin were prepared as previously indicated and the sample with SynGAP antibody (Cell Signalling, NEB; see Table M-5) was placed and incubated 3h at 4ºC in the tube rotator. Noteworthy, each sample was divided into four spin-columns to load near 200 µL/column. The flow-through (FT) sample depleted with SynGAP and part of its interactors was recovered by centrifuging the columns at 100xg during 1 min (centrifuge 5417R, Eppendorf). The column with the resin bounded with SynGAP was washed thrice with the dialysis buffer at 100xg during 1min. Before the elution step, columns were prepared by the addition of conditioning buffer, which was removed by centrifugation at 100xg during 1min (centrifuge 5417R, Eppendorf). The elution of SynGAP was done by incubating 15 µL of the acidic elution buffer from the kit during 10 min. This step was repeated twice to generate elutes (E) 1, 2 and 3. Next, columns were also filled with 1x loading sample buffer and 1% glycerol solution up to a final volume of 48 µL and boiled at 95ºC 5 min to assess unspecific interactions. Then the boiled samples were recovered by centrifugation 1 min at 100xg (centrifuge 5417R, Eppendorf). All the other samples obtained were prepared as previously indicated (general M-3.3). Finally, the proper execution of the protocol was assessed through IB before *coomassie* stained gels (see general M-3.5.1) and LC-MS/MS studies were conducted (Fig. MI-2, steps 2-10).

3.4.5 SAMPLE FRACTIONATION AND PROTEIN DIGESTION FOR MS STUDIES

Eluates from the IP procedure were loaded in 6% acrylamide and 1.5 mm wide gels polymerised with 10 well-combs (Bio-Rad). Proteins were separated by SDS-PAGE and were stained with *Coomassie* (Bio-Rad) as previously described. Bands between ~120-200 kDa were excised from acrylamide gels (see Fig. MI-2, step 2) in a transilluminator (22V, Cultex). Excised gel bands were subjected to an in-gel digestion protocol being first reduced with dithiothreitol (10 mM; Sigma-Aldrich) and alkylated with iodoacetamide (55 mM; Sigma-Aldrich), and later digested with trypsin (Promega Biotech Ibérica, Madrid, Spain). This procedure was performed in collaboration with the Proteomics unit from PRBB-CRG under Dr. Sabidó direction.

3.4.6 *IN-SILICO* ANALYSIS OF TARGETED PROTEOMICS DATA

A list of predicted peptides obtained from protein digestions by trypsin, which cuts onto arginine and lysine residues, was generated by the Peptidecutter-ExPASy (https://web.expasy.org/ peptide_cutter) tool. Up to 4 missed cleavages were allowed. This resulted in a list of unique tryptic peptides for each SynGAP N- and C-term variants (Fig. MI-2, step 3).

3.4.7 DISCOVERY PROTEOMICS

Both discovery and targeted approaches were coupled to SynGAP IP and subsequent protein preparation steps before the actual MS analysis. Discovery proteomic (LC-MS/MS) studies were conducted to determine which unique peptides from both N- and C-term variants could be identified and subjected to targeted MS analyses. Around 80% of each trypsin-digested sample (SynGAP IP bands from PND0/1; PND11; PND21 and PND56) were injected in a linear trap quadrupole (LTQ) Orbitrap VelosPro with a short chromatographic method (40min gradient) in a 25 cm 1.9 um column. To avoid carry over, BSA runs were added between samples. BSA controls were included both in the digestion and LC-MS/MS analyses for quality control. This experiment was done twice. The data was searched using an internal version of the search algorithm Mascot (Matrix Science) against a SynGAP (May 2014) homemade database. Also, the Mascot database server search was done with Protein Discoverer ver. 1.4.1.14 (DBVer.:79) using the following search parameters: mass precision of 2ppm; precursor mass range of 250 Da to 5,000 Da; Trypsin with a maximum of 3 misscleavages; the peptide cut off score was set at 10 and peptide without protein cut off at 5. Peptides were filtered based on IonScore>20. The

precursor mass tolerance (MS) was set at 7 ppm and fragment mass tolerance (MS/MS) at 0.5 Da with two variable modifications: oxidation (M) and acetylation (protein N-term), and one fixed modification (C): carbamidomethyl. False discovery rates (FDR) determined by reverse database searches and empirical analyses of the distributions of mass deviation and Mascot Ion Scores were used to establish score and mass accuracy filters. Application of these filters to this dataset were below 1% FDR as assessed by reverse database searching.

Regarding the assessment of the peptide precursor ions, tandem MS experiments directed to scan precursor ions allowed to acquire this type of information. In this experiment MS1 in scanner mode detect all the precursor ions that generate a given fragment. Then precursor ions scanning sets the second analyser to transmit only one specific fragment ion to the detector (Domon and Aebersold 2006). Therefore, depending on the selected fragment ion and the presence of it in different samples (i.e., 3S from different PNDs) assessed it can provide more information regarding the presence of a given peptide than the information from the MS2.

Besides the search within a specific library of unique peptides generated in the *in-silico* studies, a parallel match against the SwissProt mouse database, using an internal version of the search algorithm MASCOT (Hirosawa et al. 1993), was carried out to identify proteins that co-elute with SynGAP in the IP. Proteome Discoverer software (ThermoScientific) has an algorithm whereby redundant proteins are automatically grouped and not displayed separately in the final report. When looking for protein identifications, it is of great importance to assess the number of peptides assigned to a given protein: the more, the better. This software also gives an approximate estimation of protein amount with the parameter “Area” which is the average peak area of the 3 top peptide precursors or peptides for a given protein (TOP3 method). Thus, the relative quantification of peptide precursors was done by the calculation of the area under the curve (AUC) from the peak intensity of the 3 most intense unique peptide precursors identified in MS1 for each protein whenever possible.

3.4.8 TARGETED PROTEOMICS

The general overview of the process conducted for absolute quantification (AQUA) proteomics is shown in Fig. MI-2 (step 4-10). Unique peptides for each isoform were selected before the MS in SRM scanning mode, prioritizing those that were observed in the previous discovery experiments. Then, known amounts (25-500 fmol) of isotopically labelled versions of the targeted peptides ($^{13}C_6$,$^{15}N_2$-Lys and $^{13}C_6$,$^{15}N_4$-Arg AQUA Ultimate

Peptides, Thermo Fisher Scientific) were spiked in the peptide mixture. The unique peptides chosen for each C-term variant were: SynGAP-α1 (GSFPPWVQQTR); SynGAP-α2 (LLDAQER); SynGAP-γ (LLDAQLLIR); SynGAP-β (SIIGSPSLQADAGG GGAASGPPR). Furthermore, two peptides corresponding to the core region of SynGAP were also used (VIQNLANFSK [core1]; SSPAYCTSSSDITEPEQK [core2]). All these peptides were subjected to the following preliminary assessments to choose the adequate amount. In all cases, the amount of each peptide was chosen to be close to the endogenous amount and in the concentration range where a linear response of the peptide was observed.

SRM measurements were performed on a hybrid triple quadrupole mass spectrometer (5500 Q-Trap, AB Sciex) equipped with a reversed-phase chromatography with a 25-cm column (C18, 75-µm inner diameter; 1.9-µm particles; Nikkyo Technos Co., Ltd. Japan) and a 2-cm pre-column (C18, 100-µm, inner diameter; 5-µm particles, Acclaim PepMap 100, Thermo) using a gradient of 5 to 40% acetonitrile (ACN) with 0.1% formic acid (FA) in 60 min at a flow of 0.25 µL/min. Blank runs were performed between the SRM measurements of biological samples to avoid sample carryover. Measurements were done in unscheduled SRM mode with a dwell time of 20 ms and a total cycle time of 1.7 s. For each heavy/light pair 5 transitions were monitored. Transition groups corresponding to the targeted peptides were evaluated with Skyline v2.5 (MacLean et al. 2010) based on co-elution of the transition traces associated with the targeted peptide, both in its light and heavy form; and the correlation between the light SRM relative intensities and the heavy counterpart.

3.4.8.1 NORMALIZATION OF SRM MEASUREMENTS

SRM measurements were corrected to consider SynGAP abundance differences between developmental stages as well as technical differences due to IP variability. This was performed in a two-stage procedure:

1) SRM-derived values were corrected by the total protein used for each IP. For instance, higher amounts of proteins were used in PND0 *vs.* PND56 to IP enough SynGAP and detect it by LC-MS/MS.

2) Protein gel bands were quantified using the Image Studio Lite ver. 5.2 (LI-COR Bioscences) software and the highest value was used to calculate correction factors among the biological replicas in each postnatal age. The corrected values from 1) were then further normalised with these FCs. This step allowed to reduce

variability between IPs as reflected by the different intensities observed in SynGAP protein bands after each IP.

4. BIOINFORMATIC ANALYSES OF DATA

4.1 SEQUENCES OF SYNGAP ISOFORMS USED FOR *IN-SILICO* ANALYSES

The sequences used for *Syngap1*/SynGAP in-silico analyses are indicated in Table MI-6.

Ensembl transcript and protein information						
Isoform	Source	Transcript ID	Accession number	Protein ID	Bp	Aa
Syngap1-A/α1	Ensembl	Syngap1-202	ENSMUST00000177932.6	J3QQ18	3927	1308
Syngap1-A/α2	Ensembl	Syngap1-204	ENSMUST00000194598.5	F6SEU4	6011	1340
Syngap1-A/α2	NCBI	Transcript variant X6	XM_006524240.1	XP_006524303.1	5859	1341
Syngap1-A/α3	Ensembl	MGP_CBAJ_T0046006.1	ENSMUST00000201702.3	-	3921	1303
Syngap1-A/α4	NCBI	Transcript variant X1	XM_006524235	XP_006524298.1	5746	1407
Syngap1-A/α4	NCBI	Transcript variant X2	XM_006524236	XP_006524299.2	5740	1405
Syngap1-A/α4	NCBI	Transcript variant X3	XM_006524237	XP_00652430.1	5704	1393
Syngap1-A/β	Ensembl	Syngap1-207	ENSMUST00000201349.4	A0A0J9YVH8	5824	1282
Syngap1-A/β	NCBI	Transcript variant X12	XM_006524245	XP_006524308.1	4021	1282
Syngap1-A/β	NCBI	Transcript variant X13	XM_006524246	XP_006524308.1	5052	1282
Syngap1-A/β	NCBI	Transcript variant X14	XM_006524247	XP_006524308.1	4021	1282
Syngap1-A/γ	NCBI	Transcript variant X10	XM_006524243	XP_006524306.1	5039	1296
Syngap1-A1/α2	NCBI	N/A	N/A	EDL22526.1	N/A	1325
Syngap1-A5/α4	NCBI	Transcript variant X7	XM_006524241	XP_006524304.1	5517	1331
Syngap1-A6/α4	NCBI	Transcript variant X11	XM_006524244	XP_006524307.1	5510	1290
Syngap1-A7/α4	NCBI	Transcript variant X8	XM_006524242	XP_006524305.1	5510	1321
Syngap1-A8/α4	NCBI	Transcript variant X4	XM_006524238	XP_006524301.1	7402	1379
Syngap1-A9/α4	NCBI	Transcript variant X15	XM_006524248	XP_006524311.1	4420	805
Syngap1-B/α2	Ensembl	Syngap1-201	ENSMUST00000081285.8	A0A140T8K9	4315	1281
Syngap1-B/α4	NCBI	Transcript variant X5	XM_006524239	XP_006524302.1	7710	1348
Syngap1-C/-	McMahon et al.,2012	-	-	-	-	1087

Table MI-7. Detailed information of the transcript variants that encode the same protein isoform in terms of N and C-term sequence.

4.2 DATABASES USED TO PREDICT SYNGAP FEATURES

UniProtKB (Bateman et al. 2017), ScanProsite (de Castro et al. 2006), InterPro (Finn et al. 2017), SMART (Letunic et al. 2004), PONDR-FIT (Xue et al. 2010), Ensembl and GeneBank databases were used.

4.3 STATISTICS AND CORRELATION ANALYSES

In each figure footnote of results is specified the exact statistic test used. In general, one-way or two-way ANOVA with unmatched repeated measures followed by Tukey's or Fisher's Least Significant Difference (LSD) test were applied for protein expression along development analyses. The plots that show the relative percentage of SynGAP C-term variants assessed throughout development were computed by the addition of total fmol per µg of protein without considering the total amounts of the core region.

Finally, the data generated from the relative quantification of protein abundances throughout development at each brain structure studied by IB were further analysed to statistically determine the correlation degree between these proteins: SynGAP-α1, SynGAP-β, PSD-95 and CAMKII-α. Since almost all datasets passed normality test, parametric R Pearson correlation coefficient and associated p-values using paired two-tailed t-test were calculated in all cases by using GrapPad Prism.

CI-RESULTS

1. *IN-SILICO* ANALYSIS OF *SYNGAP1*/SYNGAP ISOFORMS AND VARIANTS

Several bioinformatic analyses were conducted to further explore the diversity both at the molecular and functional levels of *Syngap1* transcripts and protein isoforms.

1.1 PREDICTED AND OBSERVED *SYNGAP1* TRANSCRIPT ISOFORMS AND VARIANTS

In *Mus musculus,* the *Syngap1* gene encompasses 21 exons. It is encoded in chromosome 17, between nucleotide positions 26.941.253-26.972.434 from the forward strand (Fig. RI-1A). The *Syngap1* gene has multiple promotors, and its pre-mRNA undergoes alternative splicing (AS). Together, these two processes result in the expression of different transcript variants, which in turn are translated into distinct SynGAP protein isoforms.

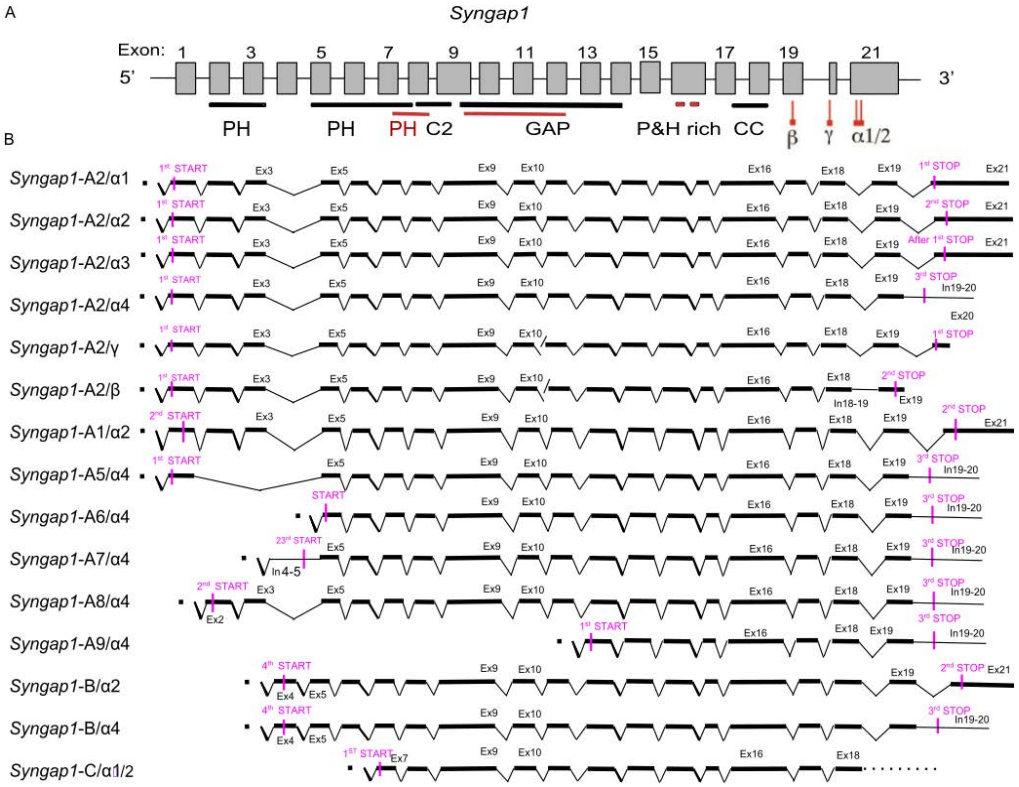

Figure RI-1. *Mus musculus Syngap1* gene and mRNA isoforms. The mouse genomic sequences are retrieved from Ensembl and GeneBank databases. (A) Schematic representation of *Syngap1* gene and the exonic sequences that encode protein domains based on *Syngap1*-A/α2. In red is shown the match with InterPRO features and in black the corresponding protein motives identified using SMART database. Also, exons related to each C-term variant are included. (B) Diagram of mRNA sequences from all 15 different *Syngap1* transcripts. Start and stop codons that yield the different variants at protein level are labelled in pink. If an mRNA variant included fragments of introns is also indicated. The diagram is not in scale.

To search which exons code for SynGAP, protein domains annotations from UniProtKB, ScanProsite and SMART databases as well as manual sequence analyses were used. These searches indicated that exons 2-3 and 5-8 encode for the PH domain, exons 8 and 9 for the C2 domain and exons 9-12 or 9-14, depending on the database, codify for the GAP domain. Furthermore, based on these data, the proline (or SH3 domain binding) and histidine rich motives are encoded by exon 16, whereas the coiled coil (CC) domain arises from sequence within exons 17 and 18 (Fig. RI-1A).

Predicted *Syngap1* transcript sequences from ESTs and manually curated cDNAs from NCBI and Ensembl were explored to look for unreported transcripts. This *in silico* analysis revealed 5 unpublished variants in the 5' variable region that we termed: A5, A6, A7, A8 and A9 since A3 and A4, have already been reported in other vertebrates. Hence, this data rises the number of 5' mRNA variants to 9 in *Mus musculus*. Conversely, 2 previously unreported variants at the 3' end of *Syngap1* mRNAs were also identified, which were termed *Syngap1*-α3 and -α4. Thus, these findings increase the 3' number up to 6 putative variants. Collectively, this *in silico* research disclose 7 previously unreported transcript variants that together with the reported ones, would encode for at least 15 different SynGAP isoforms.

Syngap1 mRNA transcripts that contain the A 5' variant, can be translated into 2 different protein sequences (A1 and A2). Therefore, they are transcribed from the same promoter but are translated using a different start codon. Keeping this in mind, A and A5 5' variants present their starting codon at the 1st exon. The A5 5' variant excludes exons 2, 3 and 4 through alternative splicing (AS). Moreover, A8 variant has its translation start codon in the 2nd exon, A7 in the intron between exon 4 and 5, whereas A6 at exon 5. B-containing transcripts place their start codon in exon 4, which is only present in these isoforms, whereas in transcripts with C and A9 5' variants, start codons are found in the 7th and 12th exons, respectively (Fig. RI-1B). All variants share the transcript sequence that encodes for the core region of SynGAP from exon 7 to exon 18, although *Syngap1*-A9 lacks exons 7 to 11. Finally, in the 3' region, there also are variations among *Syngap1* isoforms. Although transcripts encoding *Syngap1-α1* isoforms found in Ensembl, would include 8 bp from exon 20, it is generally accepted that this exon is in fact completely excluded. Thus, differences between *Syngap1-α1, α2 and α3* arise from exon 21, whereas *Syngap1-α4* includes exon 19 and part of the 19-20 intronic sequence. Of note, *Syngap1-α3* sequence is the only among 3' variants that does not show a different stop codon in the end of its sequence. Finally, exon 20 is exclusive to *Syngap1-γ*, whereas *Syngap1*-β includes a fragment of the 17-18 intron (Fig. RI-1B).

The number of exons coding for each transcript variants varies between 8 in the case of SynGAP-A9/α4 and up to 20 for SynGAP-A/α1. The number of exons contained in each SynGAP transcript is summarized in Table RI-1.

Isoform	Nº of exons	Isoform	Nº of exons	Isoform	Nº of exons
Syngap1-A/α1	20	*Syngap1*-A/β	18	*Syngap1*-A8/α4	17
Syngap1-A/α2	19	*Syngap1*-A1/α2	19	*Syngap1*-A9/α4	8
Syngap1-A/α3	18	*Syngap1*-A5/α4	16	*Syngap1*-B/α2	16
Syngap1-A/α4	18	*Syngap1*-A6/α4	15	*Syngap1*-B/α4	15
Syngap1-A/γ	19	*Syngap1*-A7/α4	15	*Syngap1*-C/--	15

Table RI-1. Number of exons retained in each mRNA variant of *Syngap1.* The identification names are given based on the protein nomenclature. A corresponds to A2 and is used mutually in the literature.

1.2 VALIDATION OF *SYNGAP1* TRANSCRIPTS EXPRESSION THROUGHOUT DEVELOPMENT IN CORTEX AND HIPPOCAMPUS

To establish the regional and developmental expression pattern of *Syngap1* transcripts, total mouse RNA was extracted from Ctx and Hip at PND 0/1, 11, 21 and 56 and cDNA was synthesized. The goal was to experimentally test the expression of all 5' and 3' variants. Because of sequence identity limitations only the following unreported ends: A5, A7 and α4 and the previously known ends: *A1/2*, B, α1/2/3 and γ were investigated by PCR (Fig. RI-2). All unreported and reported 5' ends assessed were found to be expressed in both tissues and at all ages. Similarly, *Syngap1*-α (1-3) and -γ were found also expressed in these two brain areas and in all ages. Conversely, *Syngap1*-α4 was not found expressed in Hip in any age but could be amplified at PND11 and 21 from cortical cDNAs.

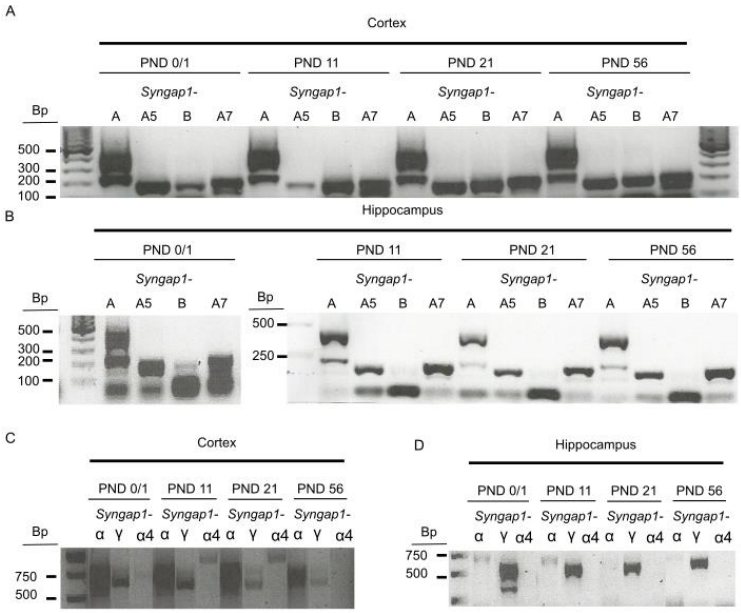

Figure RI-2. Identification of *Syngap1* mRNA variants by PCR throughout development in cortex and hippocampus. (A-B) *Syngap1*-A1/2, -A5, -B and A7 were assessed by PCR. It is shown the PCR fragments obtained by using cDNA from Ctx (A) and Hip (B) at PND 0/1, 11, 21 and 56. (C-D) *Syngap1*-α (1-3); -γ and -α4 expression at PND0/1; 11; 21 and 56 in (C) Ctx and (D) Hip. Negative controls are not shown to simplify the images, but they corroborate no amplicon contamination. Thus, bands detected in the agarose gel are reliable.

1.3 ANALYSIS OF SYNGAP CONSERVATION AMONG RODENTS AND HUMANS

The alignment of *Syngap1* cDNAs from *Mus musculus* and *Rattus norvegicus* (Ensembl codes ENSMUST00000177932.6 and ENSRNOT00000040859.6, respectively) showed 96% sequence coverage and 95% identity. The alignment of the most similar *Syngap1* transcripts from human and mouse (Ensembl codes ENST00000629380.2 and ENSMUST00000194598.5, respectively) displayed a sequence coverage of 58% but an identity of 92%. In addition, when the alignment was done using sequences from the NCBI database, the comparison between mRNA from mouse (Transcript variant NM_001281491.1) and rat (Transcript variant NM_001113409.3) or human (Transcript variant NM_006772.2) showed a 95 and 92% of identity, respectively.

Figure RI-3. Alignment of mammal SynGAP sequences. Alignment of canonical SynGAP sequences from *Rattus norvegicus*, *Mus musculus* and *Homo sapiens* retrieved from UniPROT showed a high conservation between amino acid (aa) sequences with a global identity of 95,46%. Nucleotide changes are denoted in yellow. An * indicates positions which have a single, fully conserved residue, ":" indicates conservation between aa groups of strongly similar properties, whereas "." indicates conservation between aa groups of weakly similar properties. See complete figure footnote overleaf.

Figure RI-3 continuation. Green underlined indicates the canonical N-term variant, no underlining indicates the core SynGAP region and red and blue underlined show α1 and α2 C-term variants. The numbers from the beginning of each row indicate the first aa, whereas the ones located on the right show the number position of the last aa in the corresponding row.

At the protein level, the SynGAP sequence comparison between these three species showed a 95.46% homology between them. Also, there were no major amino acid (aa) substitutions between rodents and human in the PH, C2, GAP or proline rich domains. The protein regions suffering AS also presented a high degree of identity between rodents and humans (Fig. RI-3). Altogether, these comparisons showed that SynGAP is a highly conserved protein among these mammals.

1.4 SEQUENCE COMPARISON OF SYNGAP VARIABLE REGIONS

As mentioned earlier, all SynGAP variants share a core region that represents up to 80% of the total sequence in the longest isoform. Their length varies depending on the isoform, ranging from 805 to 1,379 aa (Table RI-2). SynGAP-C N-term variant defines the start of the core region, thus the other variants (excluding A9), present the N-term variable portions, which can share stretches of sequences between them (Fig. RI-4). The SynGAP-A2 N-term variant is the longest one, being 173 residues long and presenting six fragments (shown with different colours in Fig. RI-4AC) that are differentially used in the other variants. Of the previously unreported N-term variants, A8 misses the first 28 residues from A2 (depicted in yellow, grey and green in Fig. RI-4A&C). SynGAP-A5 misses the third and fourth fragments from A2 (indicated in green and red in Fig. RI-4A&C), A6 lacks the first four sequence fragments from A2 and so does the A7 variant. Also, SynGAP-A7 has a N-term unique sequence (dark green from Fig. RI-4A&C) encoded in intron 4-5. Finally, the SynGAP-A9 variant starts at position 603 relative to A2 sequence.

Ensembl transcript and protein information					
Isoform	**Source**	**Accession number**	**Protein ID**	**Bp**	**Aa**
SynGAP-A/α1	Ensembl	Syngap1-202	J3QQ18	3927	1308
SynGAP-A/α2	Ensembl	Syngap1-204	F6SEU4	6011	1340
SynGAP-A/α3	Ensembl	ENSMUST00000201702.3	MGP_CBAJ_P0046006.	3921	1303
SynGAP-A/α4	NCBI	XM_006524235	XP_006524298.1	5746	1407
SynGAP-A/β	NCBI	XM_006524245	XP_006524308.1	4021	1282
SynGAP-A/γ	NCBI	XM_006524243	XP_006524306.1	5039	1296
SynGAP-A1/α2	NCBI	N/A	EDL22526.1	N/A	1325
SynGAP-A5/α4	NCBI	XM_006524241	XP_006524304.1	5517	1331
SynGAP-A6/α4	NCBI	XM_006524244	XP_006524307.1	5510	1290
SynGAP-A7/α4	NCBI	XM_006524242	XP_006524305.1	5510	1321
SynGAP-A8/α4	NCBI	XM_006524238	XP_006524301.1	7402	1379
SynGAP-A9/α4	NCBI	XM_006524248	XP_006524311.1	4420	805
SynGAP-B/α2	Ensembl	Syngap1-201	A0A140T8K9	4315	1281
SynGAP-B/α4	NCBI	XM_006524239	XP_006524302.1	7710	1348
SynGAP-C/-	McMahon et al.,2012	-	-	-	1087

Table RI-2. Summary of SynGAP isoforms identified. It is shown the isoform name, source of the retrieved and analysed sequence, accession numbers and length of the transcripts/proteins.

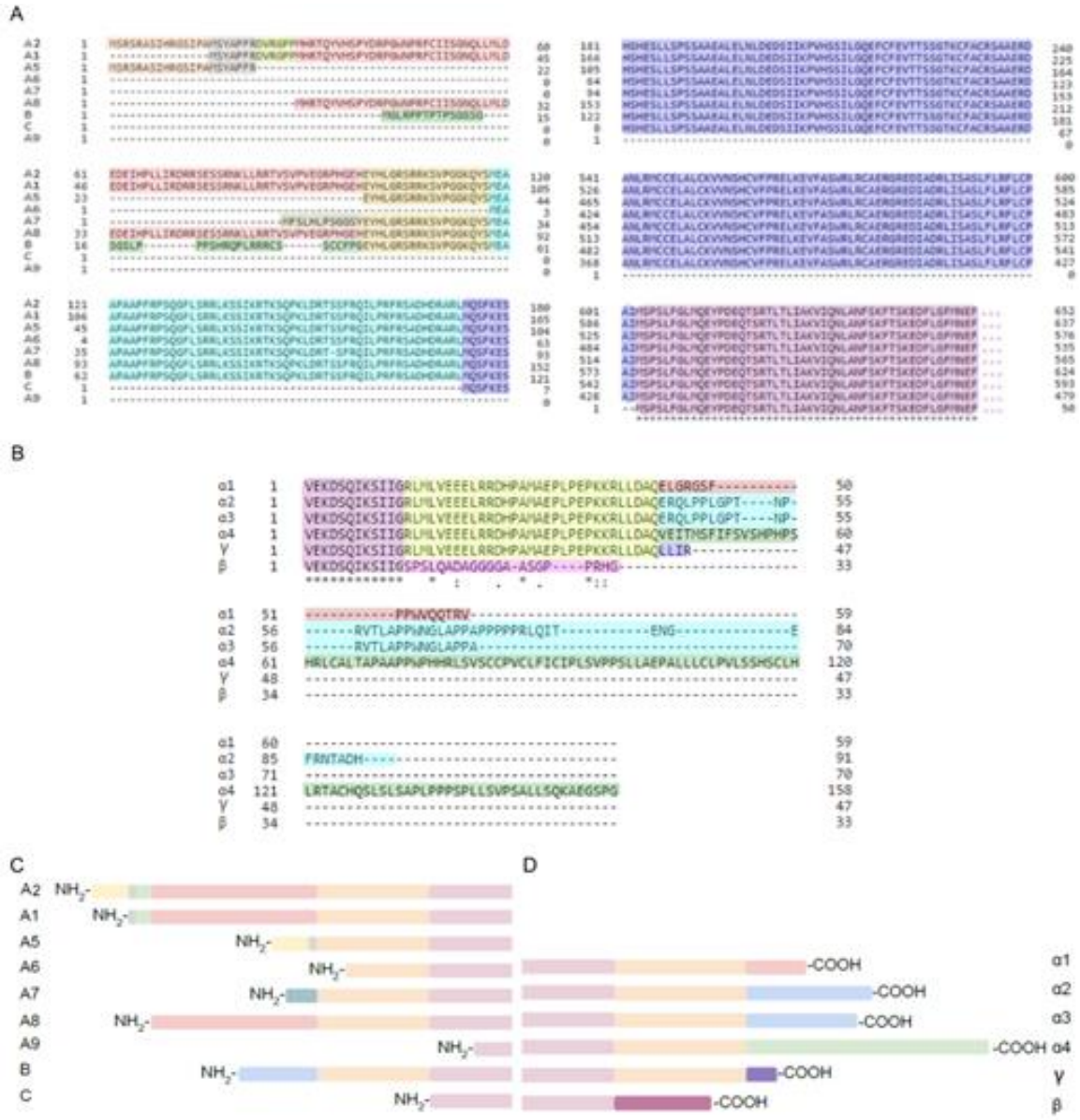

Figure RI-4. Alignment and schematic representation of SynGAP variable regions. (A-B) Variant name is shown in the right. Numbers flanking the sequence indicate starting and ending residues. Sequences presenting 100% identity are labelled with the same colour. (A) Shows N-term variants and (B) C-term variants sequence alignments. Schematic illustration of (C) N-term and (D) C-term variants are also shown. The diagram is not in scale.

Regarding C-term variants, this analysis showed that SynGAP-α1 shares almost all its coding sequence with α2 and α3 and that its unique sequence arises from a splice junction retention during AS. As a result, SynGAP-α1 has 16 unique aa whereas SynGAP-α2 has 48 aa. Also, these studies revealed that SynGAP-α3 is a shorter version of α2. Since the mRNA sequence for *Syngap1*-α3 did not present a stop codon at the end of its sequence and the only predicted stop codon would be the one shared with SynGAP-α1 (see Fig. RI-1), this C-term variant was taken as an artefactual product of bioinformatic predictions. Moreover, SynGAP-α4 has 115 unique residues as compared with the other SynGAP-α and -γ variants (Fig. RI-4B&D). Sequence comparison of these variants indicated that

SynGAP-α4 arises from a partial 5' intronic retention, which leads to a change in the open reading frame (ORF). Moreover, all α and γ variants share a portion of their sequences, but the β variant is completely different. Indeed, the different sequence of SynGAP-β arises from a 13 bp insertion originating at intron 18-19.

1.5 VALIDATION OF SYNGAP ISOFORMS AND VARIANTS EXPRESSION BY LC-MS/MS.

The set of experiments described below were intended to identify the expression of previously un-reported variants at the protein level by LC-MS/MS proteomics.

1.5.1 SYNGAP ISOFORMS AND VARIANTS EXPRESSION IN ADULT CORTICAL SAMPLES

An indirect immunoprecipitation (IP) by using an antibody against a core region of all SynGAP variants followed by an in-gel digestion of the SynGAP immunoprecipitated bands coupled to LC-MS/MS analyses was conducted to determine which SynGAP variants were expressed in adult cortical samples (from 14- week-old mice). This set of experiments allowed to identify unique peptides from SynGAP-A6 and all C-term variants excluding the previously unreported ones (Table RI-3). Also, the most frequently seen unique peptides were those from SynGAP-α2 and -β.

N and C-terminal unique peptides					
Variant	# unique peptides	Identified	Unique peptides	Level of confidence	#PMS
SynGAP-A	5	NO	-		-
SynGAP-A1	4	NO	-		-
SynGAP-A5	10	NO	-		-
SynGAP-A6	5	YES	mEAAPAAPFRPSQGFLSR	Medium	1
SynGAP-A7	5	NO	-		-
SynGAP-A8	2	NO	-		-
SynGAP-A9	4	NO	-		-
SynGAP-B	18	NO	-		-
SynGAP-C	1	NO	-		-
SynGAP-α1	14	YES	GSFPPWVQQTR	Medium	2
SynGAP-α2	12	YES	VTLAPPWNGLAPPAPPPPPR LLDAQER	High	3
SynGAP-α4	10	NO	-		-
SynGAP-γ	5	YES	LLDAQLLIR	High	1
SynGAP-β	13	YES	SIIGSPSLQADAGGGGAASGPPR	High	7

Table RI-3. Unique SynGAP peptides and variants identified in mouse adult Ctx. N- and C-term variants, the number of unique peptides associated to each variant and the identification status based on the Proteome Discoverer software are shown. Also, peptide sequences, the degree of confidence on their identification and the number of times seen, which are expressed in peptide spectral matches (PSMs), are indicated. Peptides identified with low or very low confidence are excluded. Ctx samples were from 14-week-old mice.

Given the fact that a bottom-up proteomics analysis (from peptides to proteins) were performed, the expression of complete SynGAP isoforms could not be identified. Therefore, these analyses were focus on the expression of their N- or C-term variants. Thus, crossing the experimentally derived information on SynGAP isoforms generated in this study with the information from genomic and proteomic databases (e.g., Ensembl,

NCBI) it is likely that the following SynGAP isoforms are expressed in the mouse Ctx: SynGAP-A/α1; -A/α2; -A/γ; -A/β and -A6/α4 (Table RI-4).

Isoforms Identified						
Isoform	Mw (KDa)	Score	Coverage	# Unique Peptides	# Peptides	# PSMs
SynGAP-A/α1	148,1	8621,73	45,90	1	48	281
SynGAP-A/α2	143,4	8507,06	45,76	1	47	274
SynGAP-A/γ	144,8	8500,37	45,49	1	47	275
SynGAP-A/β	141,5	8413,39	45,74	1	46	270
SynGAP-A6/α4	141,1	8371,43	45,55	1	44	256

Table RI-4. List of SynGAP isoforms identified in mouse adult Ctx. Molecular weight (Mw) is indicated in kDa. The main parameters provided by Proteome Discoverer for each isoform are also shown. These include: confidence score, sequence coverage by the peptides identified, number of unique peptides found, total number of unique and common peptides and the peptide spectra matches (PSMs).

1.5.2 SynGAP ISOFORMS AND VARIANTS EXPRESSION IN CORTEX FROM DIFFERENT DEVELOPMENTAL AGES

Using the above-mentioned approaches (see RI-1.2 and 1.5.1), the number of 5' and 3' *Syngap1* variants that could be identified by PCR was very limiting and only one N-term variant could be identified by LC-MS/MS in adult. In addition, since it is possible that some variants predominate in early stages of development, the next aim was to further assess if SynGAP variants were expressed at the protein level in different postnatal ages (PND0/1, 11, 21 and 56) from the developing mouse cortex (Fig. RI-5A).

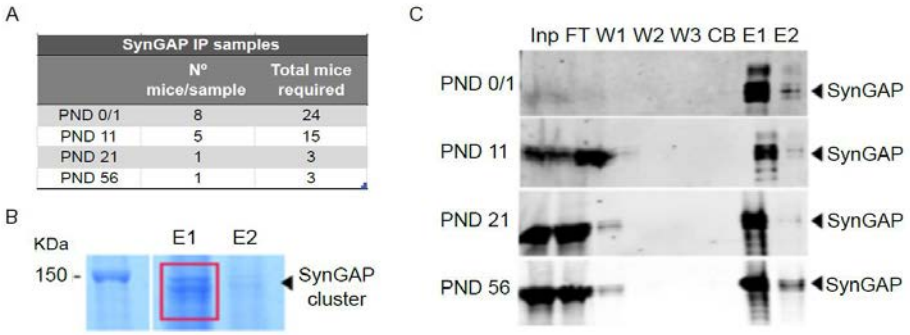

Figure RI-5. SynGAP enrichment throughout IP. (A) Number of mice required per biological replica and total number of mice used for this experiment. (B) A representative *Coomassie* stained acrylamide gel showing the entire volume of the first and second elutes. Note the presence of intense protein bands at the theoretical molecular weight of SynGAP (delimited by a red square). (C) Indirect SynGAP IP using cortical protein extracts from PND0/1, 11, 21 and 56. Note that SynGAP can be detected even if only 2,5% of the eluate volume is loaded. Also, the enrichment procedure was successful even at PND 0/1 when the SynGAP expression is very low. Input (Inp), flow-through (FT), wash (W), conditioning buffer (CB) and elution (E) fractions are also shown.

Importantly, almost all SynGAP could be immunoprecipitated from PND0/1 (Fig. RI-5C, top image). In contrast, there was a remaining amount of SynGAP in the flow-through (FT) fraction in posterior ages, probably because it exceeded the amount of the antibody available to bind SynGAP. Interestingly, SynGAP exhibited a layered pattern indicative of different SynGAP isoforms (Fig. RI-5B&C). Also, LC-MS/MS analyses showed that

SynGAP-β could be identified in all ages, SynGAP-α2 in all but PND11 and the N-term variant A6 was only identified in PND11 (Fig. RI-5).

Age	SynGAP variant	Unique peptide	# PMS
PND 0/1	SynGAP-α2	VTLAPPWNGLAPPAPPPPPR	2
	SynGAP-β	SIIGSPSLQADAGGGGAASGPPR	3
PND 11	SynGAP-A6	mEAAPAAPFRPSQGFLSR	2
	SynGAP-β	SIIGSPSLQADAGGGGAASGPPR	6
PND 21	SynGAP-α2	LQITENGEFR	1
	SynGAP-α2	VTLAPPWNGLAPPAPPPPPR	3
	SynGAP-β	SIIGSPSLQADAGGGGAASGPPR	4
PND 56	SynGAP-α2	VTLAPPWNGLAPPAPPPPPR	3
	SynGAP-β	SIIGSPSLQADAGGGGAASGPPR	7

Table RI-5. N- and C-term SynGAP variants identified throughout development by discovery proteomics. The variants and corresponding unique peptides identified by LC-MS/MS at each PND are shown. Also, the higher number of times seen (#PMS) each variant from two independent experiments is indicated. Those peptides identified with low confidence level were discarded.

A

Amount of peptide precursors ions throughout development				
Age	SynGAP variant	Unique peptide	Precursor	Area
PND 0/1	SynGAP-A6	MEAAPAAPFRPSQGFLSR	995.9938++	1,80E+06
	SynGAP-A6	MEAAPAAPFRPSQGFLSR	664.3316+++	1,89E+06
	SynGAP-α2	VTLAPPWNGLAPPAPPPPPR	1023.0702++	3,59E+06
	SynGAP-α2	VTLAPPWNGLAPPAPPPPPR	682.3825+++	8,03E+06
	SynGAP-α2	LQITENGEFR	603.8093++	2,51E+07
	SynGAP-α2	QLPPLGPTNPR	595.3380++	2,74E+08
	SynGAP-α2	LLDAQER	422.7298++	3,69E+07
	SynGAP-β	SIIGSPSLQADAGGGGAASGPPR	1012.0138++	4,27E+07
	SynGAP-β	SIIGSPSLQADAGGGGAASGPPR	675.0116+++	1,67E+07
PND 11	SynGAP-A6	MEAAPAAPFRPSQGFLSR	995.9938++	9,70E+06
	SynGAP-A6	MEAAPAAPFRPSQGFLSR	664.3316+++	6,19E+06
	SynGAP-α2	VTLAPPWNGLAPPAPPPPPR	1023.0702++	1,59E+07
	SynGAP-α2	VTLAPPWNGLAPPAPPPPPR	682.3825+++	2,87E+07
	SynGAP-α2	LQITENGEFR	603.8093++	2,68E+07
	SynGAP-α2	QLPPLGPTNPR	422.7298++	1,38E+08
	SynGAP-α2	LLDAQER	422.7298++	1,98E+07
	SynGAP-β	SIIGSPSLQADAGGGGAASGPPR	1012.0138++	1,32E+08
	SynGAP-β	SIIGSPSLQADAGGGGAASGPPR	675.0116+++	5,28E+07
PND 21	SynGAP-A6	MEAAPAAPFRPSQGFLSR	995.9938++	1,67E+07
	SynGAP-A6	MEAAPAAPFRPSQGFLSR	664.3316+++	1,19E+07
	SynGAP-α2	LQITENGEFR	603.8093++	3,67E+07
	SynGAP-α2	VTLAPPWNGLAPPAPPPPPR	1023.0702++	6,69E+06
	SynGAP-α2	VTLAPPWNGLAPPAPPPPPR	682.3825+++	1,27E+07
	SynGAP-α2	QLPPLGPTNPR	595.3380++	5,88E+08
	SynGAP-α2	LLDAQER	422.7298++	1,11E+08
	SynGAP-β	SIIGSPSLQADAGGGGAASGPPR	1012.0138++	1,37E+08
	SynGAP-β	SIIGSPSLQADAGGGGAASGPPR	675.0116+++	4,54E+07
PND 56	SynGAP-A6	MEAAPAAPFRPSQGFLSR	995.9938++	6,41E+07
	SynGAP-A6	MEAAPAAPFRPSQGFLSR	664.3316+++	5,03E+07
	SynGAP-α1	GSFPPWVQQTR	651.8331++	1,20E+07
	SynGAP-α2	VTLAPPWNGLAPPAPPPPPR	1023.0702++	9,08E+06
	SynGAP-α2	VTLAPPWNGLAPPAPPPPPR	682.3825+++	1,57E+07
	SynGAP-α2	LLDAQER	422.7298++	3,62E+08
	SynGAP-α2	QLPPLGPTNPR	595.3380++	1,87E+09
	SynGAP-β	SIIGSPSLQADAGGGGAASGPPR	1012.0138++	6,41E+07
	SynGAP-β	SIIGSPSLQADAGGGGAASGPPR	675.0116+++	5,03E+07

B

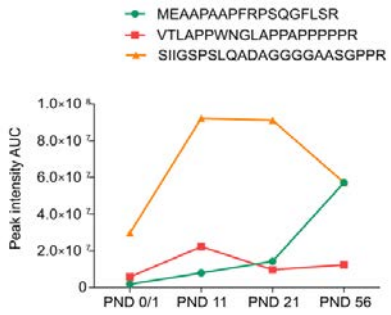

Figure RI-6. Abundance of peptide precursor ion throughout development. (A) List of peptide precursor ions identified in each age. The associated peptide and the mass with plus symbols denoting the charge state are shown. Importantly, the intensity value extracted from peak area-derived MS1 chromatograms for each precursor ion is also reported as a quantitative measure of the precursor abundance relative to each PND assessed. (B) Unique peptide abundance comparison expressed in terms of intensity units obtained from the peak area under de curve (AUC). It is plotted the averaged abundances of SynGAP-A6, -α2 and -β peptide precursors. Noteworthy, a higher amount of protein was used to IP SynGAP from tissue samples collected at PND0/1 and 11 than at older ages. Thus, the expression at these two ages is overestimated.

To further explore which SynGAP variants were expressed in developing cortical samples, especially those previously unreported, unique ion peptide precursors of these variants were evaluated (Fig. RI-6). This analysis allowed to confirm the expression of the N-term A6 and the C-term α2 and β variants at all ages, whereas SynGAP-α1 was also found expressed in young adult animals (PND56). Next, the relative quantification of these peptide ion precursors was conducted and showed how the amounts of each SynGAP variant changed as a function of PND. Although these data were preliminary, they suggested that, for instance, SynGAP isoforms containing β variant might be more abundant than α2 at all ages investigated (Fig. RI-6B), reaching its maximum at PND 21. It is worth mentioning that the expression levels at PND0/1 and 11 are overestimated as higher amounts of proteins than PND21 and 56 were used to conduct the IP. Conversely, the expression of A6-containing SynGAP isoforms might increase progressively and reach similar expression levels to that of SynGAP-β at PND 56 (Fig. RI-6B).

1.6 *IN-SILICO* PREDICTION OF SYNGAP PROTEIN DOMAINS, MOTIFS AND POST-TRANSLATIONAL MODIFICATIONS

The sequences from SynGAP isoforms were evaluated to identify possible unreported protein domains, motives or post-translational modifications using several databases (Table RI-6; Fig. RI-7). In general terms, these studies indicate that SynGAP-A2 and -A1 have the longest PH domain, presenting the same length. In contrast SynGAP-A5, -A6, -A7, -A8, -B and -C have truncated versions of the PH domain and SynGAP-A9 lacks both PH and C2 domains (Table RI-6A).

A

Number of aa in SynGAP domains				
Isoform	PH	C2	GAP	Prich
SynGAP-A2/α1	227	100	338	31
SynGAP-A2/α2	227	100	338	31+7
SynGAP-A2/α3	227	100	338	31
SynGAP-A2/α4	227	100	338	31
SynGAP-A2/γ	227	100	338	31
SynGAP-A2/β	227	100	338	31
SynGAP-A1/α2	227	100	338	31
SynGAP-A5/α4	124	100	338	31
SynGAP-A6/α4	127	100	338	31
SynGAP-A7/α4	127	100	338	31
SynGAP-A8/α4	127	100	338	31
SynGAP-A9/α4	-	-	127	31
SynGAP-B/α2	127	100	338	31
SynGAP-B/α4	127	100	338	31
SynGAP-C/--	78	100	338	31

B

	New Phospho-sites				Other PTMs	
Isoform	PKC	cAMP	CKII	Tyr	Myristilation	ASN Glycosilation
SynGAP-A2/α1	20	1	23	3	37	6
SynGAP-A2/α2	20	1	23	3	37	6
SynGAP-A2/α3	20	1	22	3	36	5
SynGAP-A2/α4	22	1	23	3	37	6
SynGAP-A2/γ	20	1	23	3	37	6
SynGAP-A2/β	20	1	23	3	40	6
SynGAP-A1/α2	20	1	23	3	36	6
SynGAP-A5/α4	21	1	22	2	37	6
SynGAP-A6/α4	20	-	22	2	36	6
SynGAP-A7/α4	21	1	22	2	36	6
SynGAP-A8/α4	22	1	23	3	36	6
SynGAP-A9/α4	11	-	17	-	22	6
SynGAP-B/α4	22	2	22	2	34	6
SynGAP-C/α	15	-	22	2	36	6

C

Predicted and validated SynGAP domains				
Isoform	Nº CC	Nº LC	PBM	Proline rich
SynGAP-A/α1	1*	8	1*	-
SynGAP-A/α2	1*	9	-	1
SynGAP-A/α3	1*	8	-	-
SynGAP-A/α4	1*	10	-	-
SynGAP-A/γ	1*	8	-	-
SynGAP-A/β	1*	9	-	-

D

Putative PTMs				
Isoform	PKC	CKII	Myristilation	ASN Glycosilation
SynGAP-α1	8	17	22	6
SynGAP-α2	8	17	22	6
SynGAP-α3	8	16	21	5
SynGAP-α4	10	17	22	6
SynGAP-γ	8	17	22	6
SynGAP-β	8	17	25	6

Table RI-6. Summary of SynGAP domain composition in different isoforms and predicted PTMs. (A) Each column shows the number of aa associated to a given domain for each isoform (left). The domains PH, C2, GAP were analysed using SMART database and the Proline rich/SH3 domain binding (Prich) motif information was retrieved from UniProt and LMDI Predictor. (B) New phosphorylation sites and other posttranslational modifications (PTMs) for the analysed isoforms (right). The number of times predicted in a given isoform are also indicated. See complete figure footnote overleaf.

Table RI-6 continuation. The identification of these PTMs was done using ScanProsite. (C) The number of CC and low complexity (LC) regions were retrieved from SMART database. The PBM was identified in ScanProsite and both PBM whereas SH3 domain binding motif was identified using the LMDI Predictor. * indicates experimentally validated domains. Of note, SynGAP-β has a shorter CC. (D) Putative PTMs after the GAP domain.

Also, different isoforms might encompass different numbers of phospho-sites for PKC, cAMP-dependent kinases and casein kinase II (CKII). In addition, different numbers of tyrosines that can be phosphorylated and myristylation sites, in both the N- or C-term were identified (Table RI-6B&D. Differences were also found in asparagines (ASN) that can be glycosylated and in the number of low complexity (LC) regions depending on the C-term expressed. Interestingly, SynGAP-α4 presented one more LC regions than SynGAP-α2 and β and two more than α1 and γ. Of the different algorithms used to predict SH3 domain binding motives only one, LMDIPredictor, identified a previously unreported motif specific to the α2 variant, which could be functionally relevant. Finally, the specific location of these modifications along with other features reported in the literature for each SynGAP variant were also annotated (Fig. RI-7).

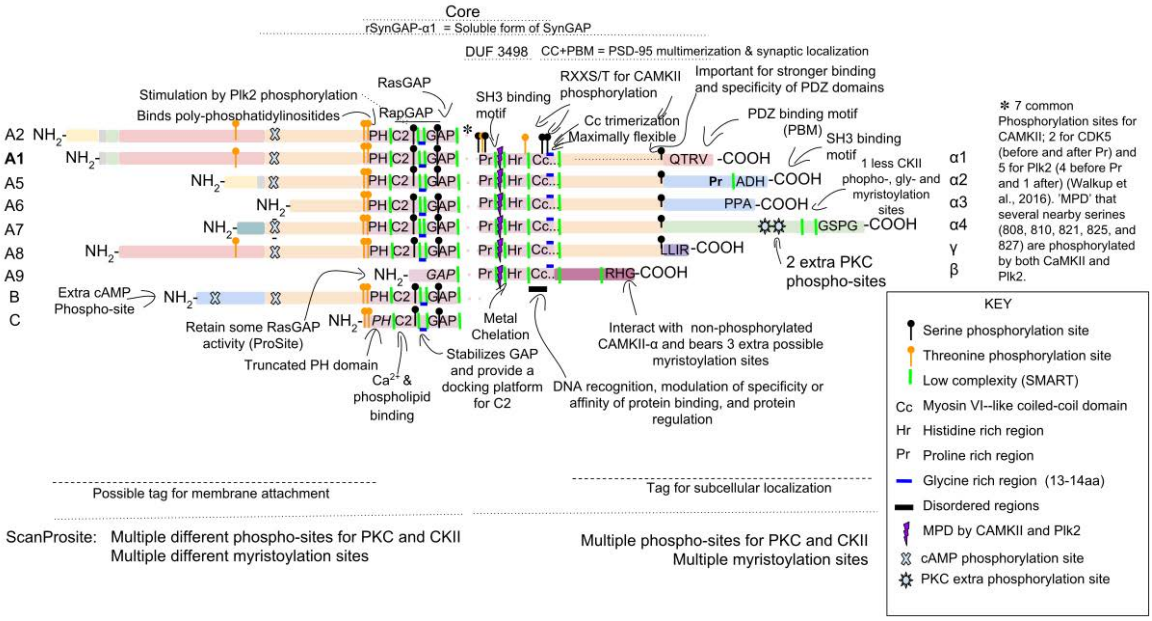

Figure RI-7. Location of reported and unreported protein features of each SynGAP N- and C-term variants. Comprehensive annotation of known domains and motives together with the unreported features identified in this study. SMART, Prosite, InterPro and LMDIPredictor databases were used. Disordered regions were identified with PONDR-FIT. MPD stands for multiple phosphorylated domain; PBM: PDZ binding motif. Only domains with high probability of occurrence were included.

2. RELATIVE QUANTIFICATION OF SYNGAP AND OTHER SYNAPTIC PROTEINS IN DIFFERENT BRAIN AREAS AND AT DIFFERENT AGES

Total extracts of proteins (3S) solubilized with 1% DOC-containing buffer were recovered at PND4,11, 21 and 56 from Ctx, Hip, Str, OB and Crb to study the expression of SynGAP, some of its C-term variants and two interactors (PSD-95 and CAMKII-α) by IB.

2.1 SPATIO-TEMPORAL REGULATION OF TOTAL SYNGAP PROTEIN LEVELS

The analysis of SynGAP expression, showed that total SynGAP followed different patterns of expression in both temporal and spatial domains (Fig. RI-8). Specifically, the intra-structure comparison indicated that SynGAP adult levels were reached by PND 11 in Crb; PND 21 in Ctx and Hip, and PND56 in Str and OB (Fig. RI-8A). Also, a dramatic increase in SynGAP between PND4 and 11 was seen in Ctx, Hip and Str, whereas in Crb there was a slighter but significant increase in its expression. This trend was maintained between PND11 and 21 in Ctx and Hip, but not in Str, OB and Crb. Indeed, in Crb there was a biphasic expression where SynGAP expression levels were stabilized between PND11 and PND21.

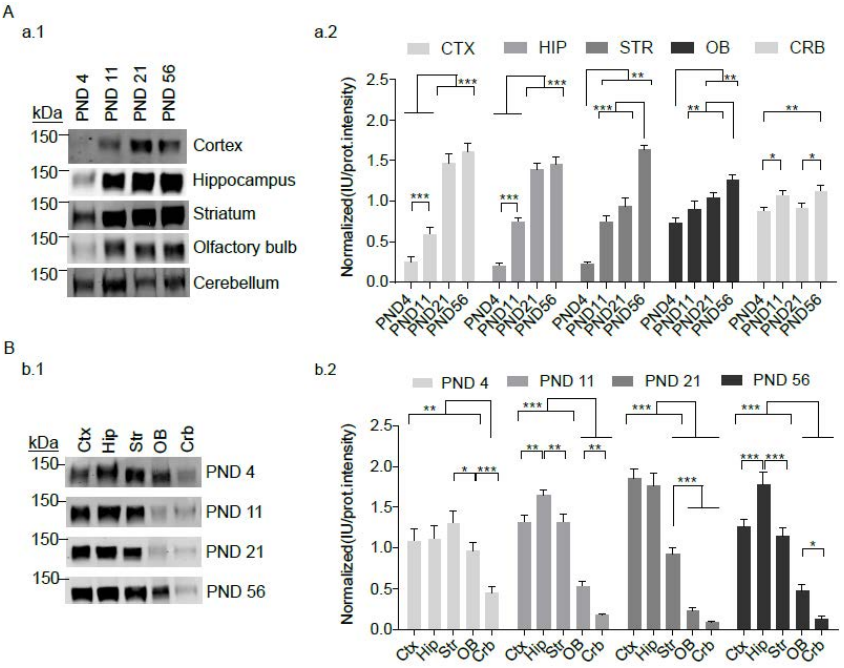

Figure RI-8. Total SynGAP expression throughout development in different mouse brain areas. (A) Intra-structure comparison. (a.1) Representative IB were 30 µg of total extract protein was loaded for Ctx, Hip, Str and OB, whereas 120 µg were loaded for Crb. The same amounts of proteins were used for all ages. (a.2) Bar plot showing pan-SynGAP expression in all brain areas. (B) SynGAP inter-structure expression at different ages. (b.1) Representative IB and (b.2) bar plot showing pan-SynGAP expression at all ages. Raw data was first corrected for the amount of protein transferred to the IB membrane and later normalised by the mean intensity of all SynGAP bands. All data followed normal distribution and one-way ANOVA followed by Tukey's post-hoc test was applied. * $p < 0.05$; ** $p < 0.01$ and *** $p < 0.001$.

The inter-structure comparison showed that at PND4, the Crb expressed the lowest amount of total SynGAP as compared with the other brain regions, while OB only reached significant differences when compared with Str (Fig. RI-8B; Fig. RI-9A). At PND11, Crb remained as the region with the lowest SynGAP levels while SynGAP expression in OB lagged behind that of Ctx, Hip and Str. Furthermore, Hip was the structure that expressed more SynGAP. This trend mirrored the adult one, since at PND56 the expression pattern was the same. However, at PND21 there was a slightly different expression pattern as Ctx and Hip expressed the same SynGAP levels while OB and Crb levels were not different and in Str, SynGAP was significantly less expressed than in Ctx and Hip (Fig. RI-8B; Fig. RI-9B).

A

SynGAP PND56 *vs.*			
Structure	**PND4**	**PND11**	**PND21**
Ctx	6.5	2.7	1.1
Hip	7.3	2	1
Str	7.2	2.7	1.3
OB	1.7	1.4	1.2
Crb	1.2	1	1.1

B

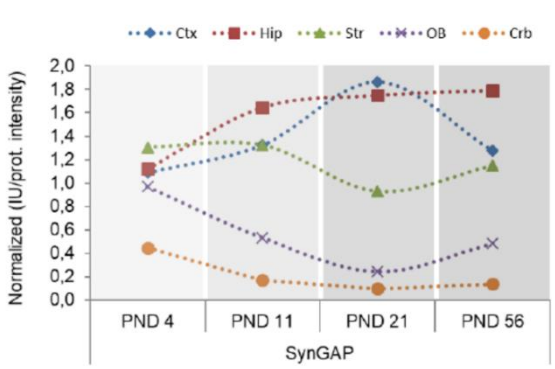

Figure RI-9. Fold changes of SynGAP expression in adult compared to a given age and relative inter-structure comparison of SynGAP levels. (A) Table showing SynGAP expression fold change (FC) at PND56 relative to a given age and for each structure assessed. Numbers close to 1 indicate similar expression, whereas higher numbers indicate higher expression at PND56. (B) Relative SynGAP levels between structures at PND4, 11, 21 and 56. Note that relative expression can only be compared for each given age.

2.2 SPATIO-TEMPORAL REGULATION OF SYNGAP C-TERM VARIANTS

Subsequently, the expression pattern of SynGAP C-term variants was determined and compared with that of total SynGAP. These could only be achieved for those variants whose antibody was available (SynGAP-α1, α2 and β). The comparison of the expression levels of these variants in Ctx showed that the maximum expression of SynGAP-α1 was at PND56, whereas for SynGAP-α2 and -β this maximum was achieved at PND21. These two variants presented a dramatic increase between PND4 and PND11. Moreover, only cortical SynGAP-β levels at PND21 were significantly higher than PND56. Indeed, by PND11 adult levels were reached (Fig. RI-10A). Despite all variants globally followed a similar expression pattern in Hip, there were two important events: 1) SynGAP-α1 exhibited a marked increase between PND4 and PND11 and 2) SynGAP-β levels at PND21 didn't significantly differ from those at PND56 (Fig. RI-10B). Moreover, in Str SynGAP-α1 presented constant SynGAP expression from PND11 until PND21, while it showed a very pronounced peak of expression between PND21 and 56. In this case, SynGAP-α2 followed the same pattern. Furthermore, SynGAP-β in the Str had expression

pattern different from those in the Ctx and Hip. Here, at PND11 SynGAP-β was expressed at the same levels as at PND21, and there was no higher expression at PND21 compared to PND56 (Fig. RI-10C).

Interestingly, the expression pattern of SynGAP variants in OB and Crb was quite different as compared with the other brain areas assessed. Namely, in OB SynGAP-α1 also acquired adult levels at PND56, although the FC between PND21 and PND56 were less pronounced than the ones observed for Ctx and Hip (Fig. RI-10F). In contrast, in Crb SynGAP-α1 followed a two-step increase while adult levels were reached between PND11-21. In the case of SynGAP-α2, it showed adult levels between PND21-56 in OB, whereas in Crb, these were achieved at PND56. Indeed, in Crb SynGAP-α2 expression followed a progressive increase with stabilization between PND11 and PND21. Strikingly, SynGAP-β was found regulated equally in OB and Crb throughout development as no expression differences between PNDs were found. Thus, SynGAP-β already exhibited adult amounts by PND4 in both brain areas (Fig. RI-10D-F).

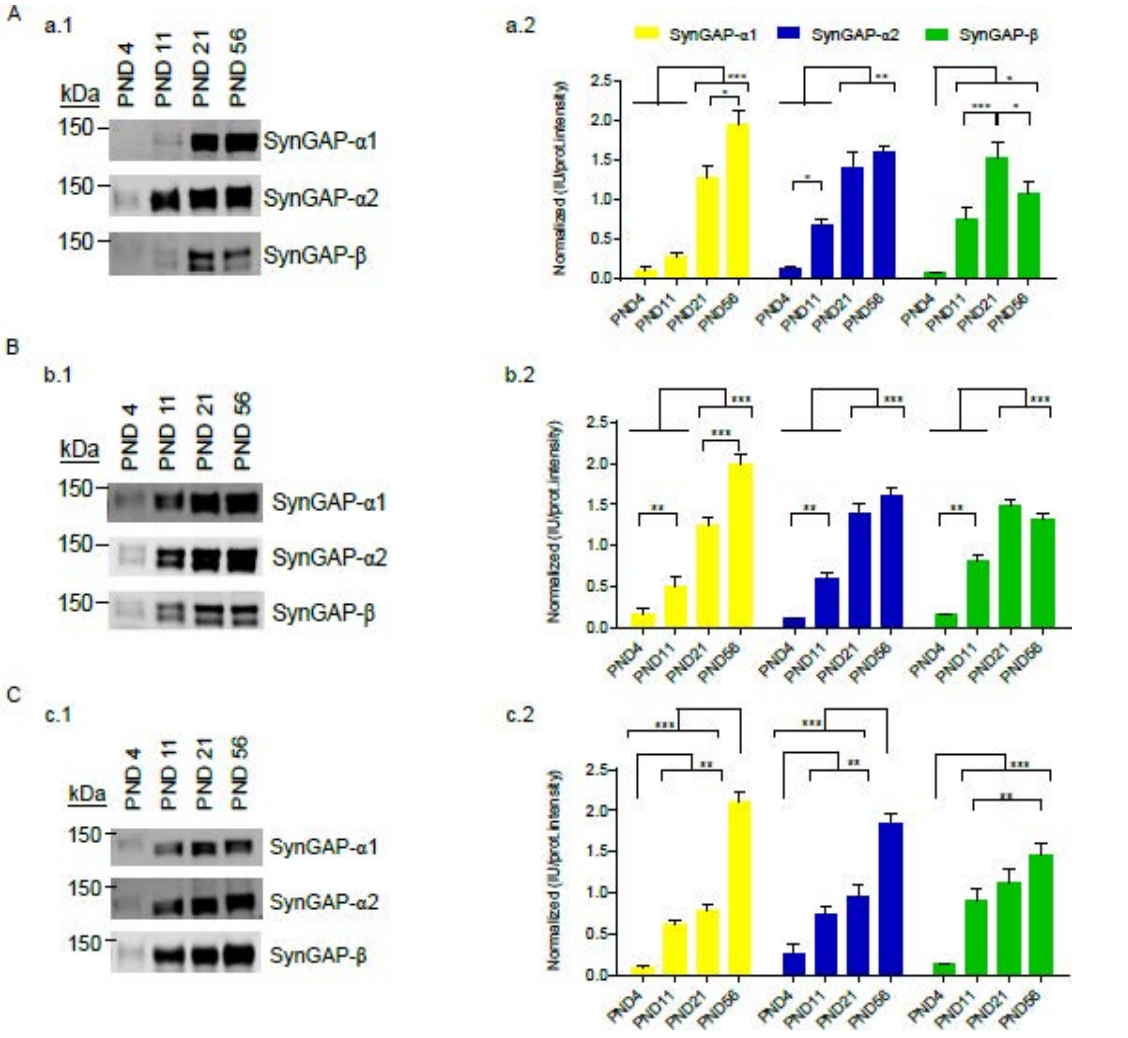

Figure RI-10. SynGAP C-term variants expression throughout development in different mouse brain areas. See complete figure and corresponding footnote overleaf.

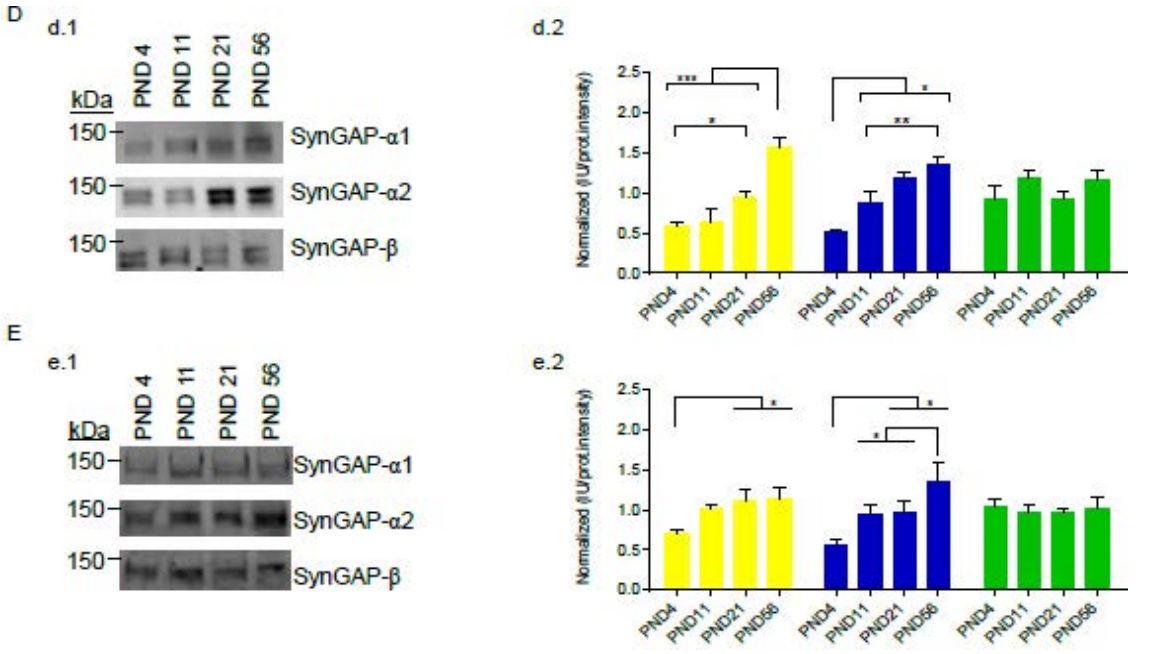

F

	SynGAP-α1 PND56 *vs.*			SynGAP-α2 PND56 *vs.*			SynGAP-β PND56 *vs.*		
Structure	PND4	PND11	PND21	PND4	PND11	PND21	PND4	PND11	PND21
Ctx	16,6	6,6	1,5	11,9	2,3	1,1	13,3	1,4	0,7
Hip	12,7	3,8	1,6	13,6	2,6	1,1	8,2	1,6	0,9
Str	7	2,2	1,7	26,2	3,4	2,7	7,1	2,5	1,9
OB	2,7	2,4	1,7	2,7	1,6	1,1	1,4	1	1,3
Crb	1,6	1,1	1	2,4	1,4	1,4	1	1	1

Figure RI-10. SynGAP C-term variants expression throughout development in different mouse brain areas. (A) Ctx (B) Hip (C) Str (D) OB (E) Crb. (a-e.1) Representative IBs of SynGAP-α1, -α2 and -β abundance at PND 4, 11, 21 and 56 and (a-e.2) bar plots of SynGAP-α1, -α2 and –β summarising IB data. Raw data were first corrected for the amount of protein transferred to the IB membrane and later normalised by the mean intensity of all SynGAP bands. All data followed normal distribution and one-way ANOVA followed by Tukey's post-hoc test was applied. * $p < 0.05$; ** $p < 0.01$ and *** $p < 0.001$. (F) Table showing FC of each SynGAP variant at PND56 relative to a given age in the corresponding brain structure.

The study of SynGAP variant expression between areas showed that at PND4, all SynGAP variants were expressed in similar levels in Ctx, Hip and Str. Furthermore, there were the same levels of SynGAP-α2 and -β in OB but a significant reduced expression in Crb. Contrastingly, SynGAP-α1 was equally expressed in OB and Crb, but significantly less as compared with the other brain regions (Fig. RI-11A). At PND11, the expression pattern slightly changed for SynGAP-α1, as Hip presents higher levels than any other tissue. Also, SynGAP-α1 expression did not differ neither between Ctx and Str nor Crb and OB. Yet, its expression in Crb and OB still was significantly lower than Ctx and Str. For SynGAP-α2 the maximum expression was found at Hip and Str, while the β-containing variants showed its maximum levels at Hip and Ctx. Yet, significant statistical differences in the expression of SynGAP-α2 and SynGAP-β between Ctx and Str were not reached. Furthermore, SynGAP-α2 and SynGAP-β also presented a significant increased expression in OB compared to their one in Crb (Fig. R-11B).

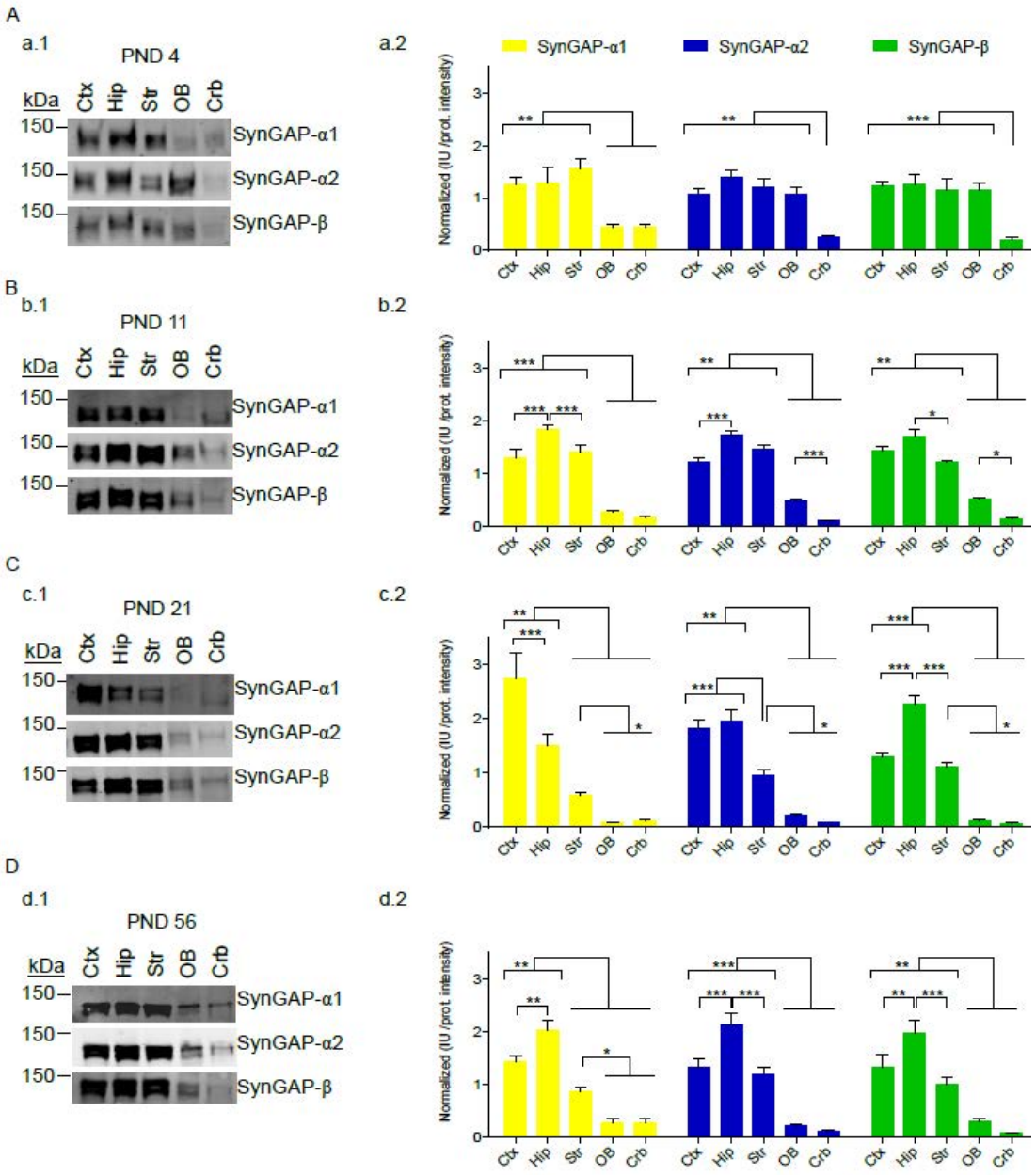

Figure RI-11. SynGAP C-term variants expression in different brain areas throughout mouse development. Inter-structure abundance comparison at (A) PND 4 (B) PND 11 (C) PND 21 (D) PND 56. (a-d.1) Representative IBs of SynGAP-α1, SynGAP-α2 and SynGAP-β in Ctx, Hip, Str, OB and Crb. (a-d.2) Bar plot of SynGAP variants. Raw data were first corrected for the amount of protein transferred to the IB membrane and later normalised by the mean intensity of all SynGAP bands All data followed normal distribution and one-way ANOVA followed by Tukey's post-hoc test was applied. * $p < 0.05$; ** $p < 0.01$ and *** $p < 0.001$.

By the end of the critical period of synaptogenesis, at PND21, all variants showed the same lower abundance in Crb and OB compared to the other brain regions. Moreover, SynGAP-α1 was found significantly more expressed in Ctx, followed by Hip and Str. Contrastingly, SynGAP-β showed a peak expression in Hip at this age, whereas Ctx and Str expressed the same amounts. Interestingly, SynGAP-α2 presented a moderate pattern of expression as compared with SynGAP-α1 and -β since it was expressed equally in Ctx

and Hip and significantly less in Str (Fig. RI-11C). Finally, by PND56 all variants showed similar but more pronounced expression trends among structures as those described at PND11 for Ctx, Hip and Str. Namely, in all cases, Hip was the brain area that expressed the biggest amount of these C-term variants (Fig. RI-11D). It is worth noting that SynGAP-α1 was the only variant that showed a significant different expression between Ctx and Str. Finally, as previously seen in PND21, OB and Crb presented much lower levels when compared with the other tissues assessed. A summary of these developmental expression changes between brain areas and for each variant is also shown in Fig. RI-12.

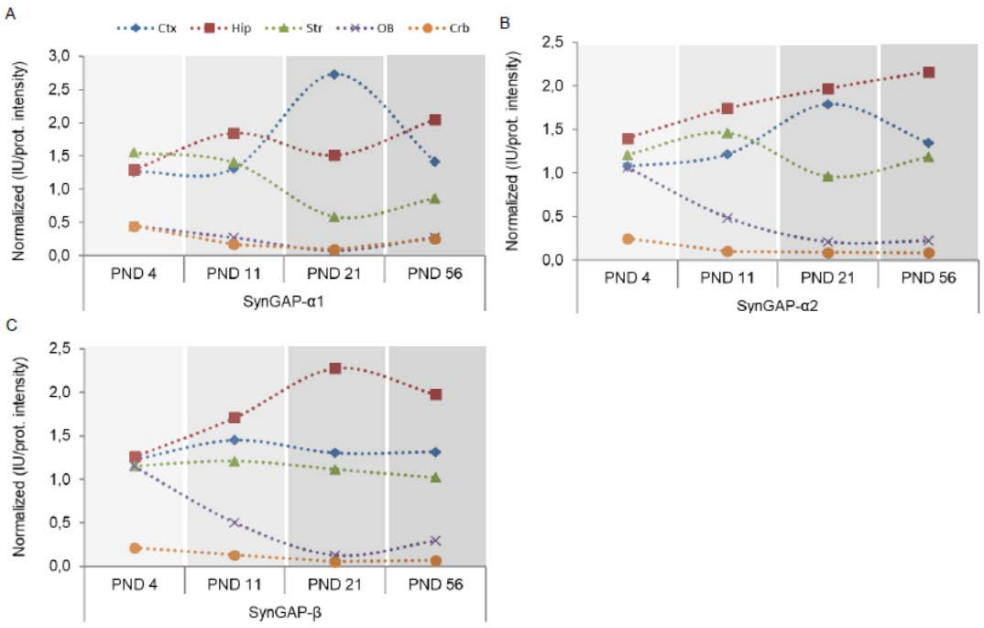

Figure RI-12. Relative inter-structure comparison of SynGAP C-term variants levels. (A) Relative SynGAP-α1 (B) SynGAP-α2 and (C) SynGAP-β levels between structures at a given age assessed (PND4, 11, 21 and 56). Note that relative expression can only be compared within a given age depicted with different greys colours.

2.3 SPATIO-TEMPORAL REGULATION OF PSD-95 AND CAMKII-α

SynGAP-α1 accumulation at the PSD could be done by trimerization through its CC domain and its binding to the PDZ domains of PSD-95 (Zeng et al. 2017). In contrast, SynGAP-β has been proven to interact with the non-phosphorylated form of CAMKII-α (Li et al. 2001). Thus, the expression pattern of these SynGAP interactors was assessed to determine if it resembles the one shown by its corresponding partner. In addition, PSD-95 is a marker of PSD and excitatory synapse maturation in both inhibitory and excitatory neurons, while CAMKII-α is reported to be expressed in both inhibitory and excitatory synapses but mainly from excitatory neurons as previously introduced. Therefore, the precise understanding of their expression pattern could provide indirect information of SynGAP variants preferred localization.

First, the relative intra- and inter-structure abundance comparisons for these two proteins throughout development were carried out. The data relative to PSD-95 expression within a given brain area showed that in general, there was a progressive increase of PSD-95 expression which reached adult levels in Ctx, Str, OB and Crb by PND56 and at PND21 in Hip. Also, all structures excluding Crb, showed a dramatic increase but less important in OB, of the expression of PSD-95 between PND4 and PND11, followed by a second marked increase between PND11 and PND21 (Fig RI-13A). Despite Crb showed a significant up-regulation of PSD-95 expression between PND4 and PND11, presented the same abundance in PND11 and PND21. Of note, the difference in the expression levels of PSD-95 between PND4 and adult was very high, especially in Ctx, but also in Hip and Str, whereas a less pronounced increase could be identified in OB and particularly in Crb.

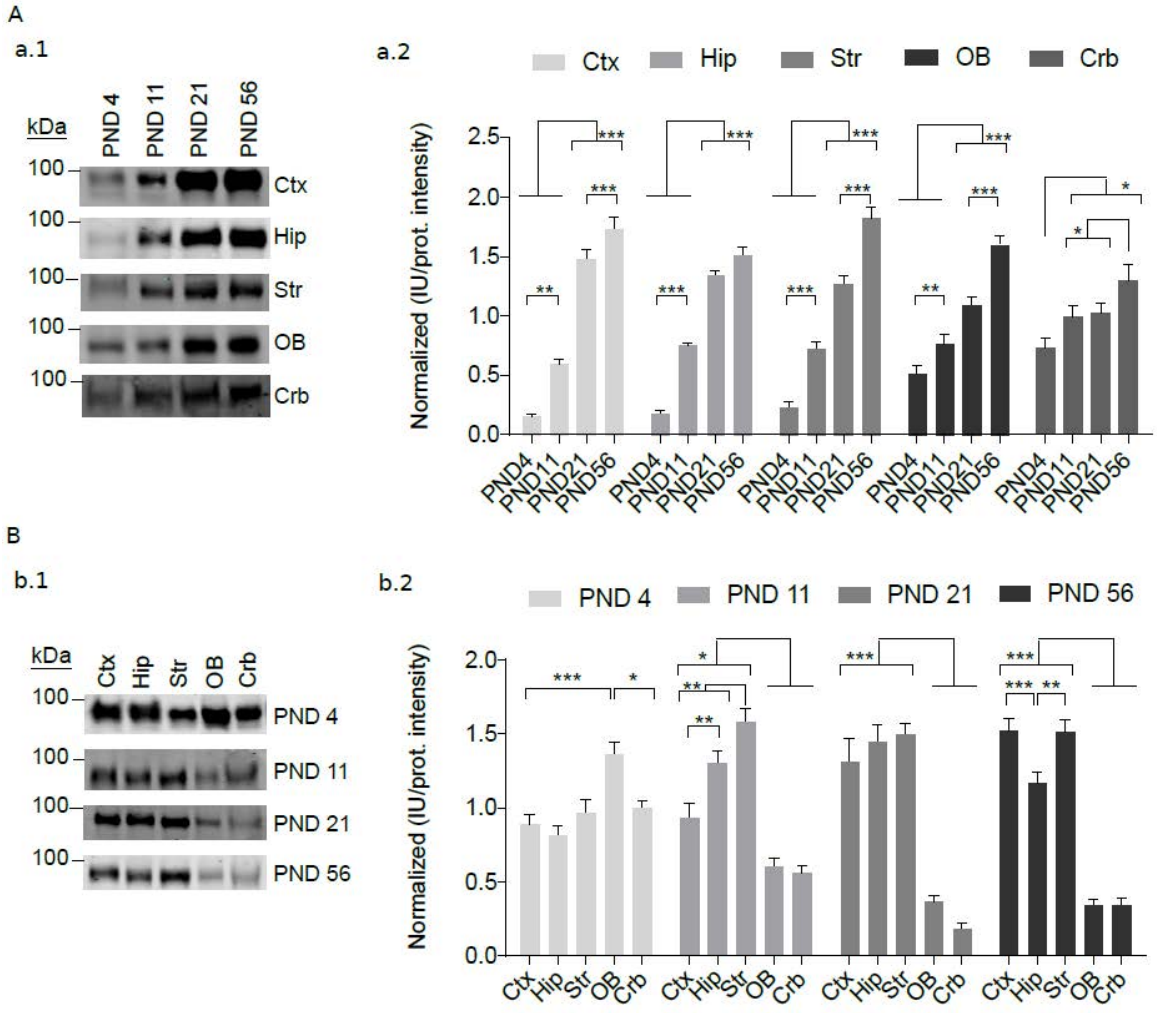

Figure RI-13. PSD-95 expression in different brain areas throughout mouse development. (A) Intra-structure comparison (a.1) Representative IB of PSD-95 (a.2) Bar plot of PSD-95 expression at PND 4, 11, 21 and 56 in Ctx, Hip, Str, OB, and Crb. (B) Inter-structure comparison throughout development. (b.1) IB of relative PSD-95 expression in different brain areas at PND4,11,21 and 56. (b.2) Bar plot of PSD-95 at PND 4; PND 11; PND 21 and PND56. Raw data was normalized by lane protein intensity and ratios between individual band intensity and the mean of corresponding total immunoblot intensity were calculated. All data follow normal distribution and one-way ANOVA followed by Tukey's post-hoc test was applied. * $p < 0.05$; ** $p < 0.01$ and *** $p < 0.001$.

Regarding the inter-structure comparison, at PND4 the maximum levels of PSD-95 were found at OB, whereas at subsequent ages it radically changed to be significantly more abundant in Ctx, Hip and Str. Moreover, at PND11, the maximum abundance of PSD-95 was seen in Str, followed by Hip, which in turn showed a significant higher level of expression than the one found in Ctx. Interestingly, the levels of PSD-95 in Ctx, Hip and Str were equalized by PND21. Yet, this protein still showed a significant lower expression in OB and Crb compared to the other assessed brain areas that remained until PND56. Finally, the expression of PSD-95 at PND56 was more prominent in Ctx and Str than in Hip. Nonetheless, PSD-95 showed a significantly higher expression in Hip than in OB and Crb (Fig. RI-13B).

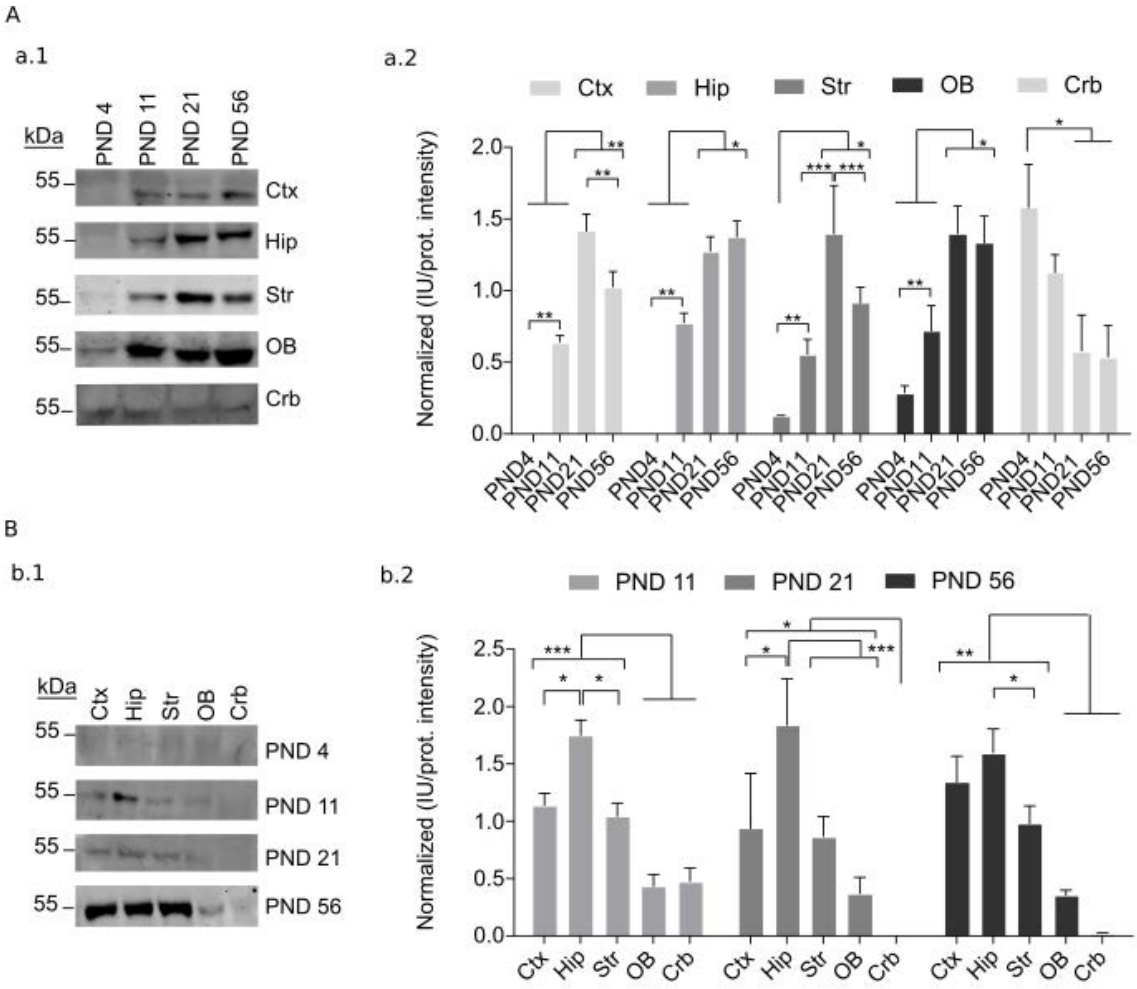

Figure RI-14. CAMKII-α expression in different brain areas throughout mouse development. (A) Intra-structure comparison CAMKII-α expression throughout development. (a.1) Representative IB of CAMKII-α. Note that 120 µg of protein was loaded for Crb samples to detect CAMKII-α expression. (a.2) Bar plot of CAMKII-α expression at PND4, 11, 21 and 56 in Ctx, Hip, Str, BO, and Crb. (B) Inter-structure comparison of CAMKII-α expression throughout development. (b.1) IB of relative CAMKII-α expression in different brain areas at PND4,11,21 and 56. Of note, 30 µg of protein from all structures but Crb were loaded. In the case of Crb, 60 µg of protein was loaded. (b.2) Bar plot of CAMKII-α at PND4, 11, 21 and 56. Raw data was normalized by lane protein intensity and ratios between individual band intensity and the mean of corresponding total IB intensity were calculated Note that the signal for CAMKII-α at PND4 was below the detection limit for almost all cases, so it was not plotted. All data followed normal distribution and one-way ANOVA followed by Tukey's post-hoc test applied. * $p < 0.05$; ** $p < 0.01$ and *** $p < 0.001$.

Related to CAMKII-α expression throughout development, the first important finding was the lack of immunoreactivity at PND4 in both Ctx and Hip even when 30 µg of protein extract were loaded, whereas in Str a weak signal could be barely seen. Instead, it was more expressed at the OB and highly expressed in Crb relative to the other ages. Furthermore, CAMKII-α adult levels were reached at PND21 in Hip and OB, while the other structures showed a distinct pattern. Specifically, in Ctx and Str, the peak expression of CAMKII-α was found at PND21, then its levels were reduced significantly until PND56. However, there was a difference between these two structures in the transition between PND4 and PND11, since the FC increase of CAMKII-α in Str was bigger than the one in Ctx. In stark contrast, Crb showed a higher expression of CAMKII-α at early ages (PND4 and 11) and a significant decrease that stabilized at later ages (Fig. RI-14A).

The assessment of CAMKII-α expression between structures at PND4, demonstrated that this protein could only be detected if very high amounts of protein were used (Fig. RI-14A *vs.* Fig. RI-14B). This fact made unrealistic to compare CAMKII-α expression at PND4 between brain areas, as the number of animals required to obtain enough OB or Hip would be very high. At PND11, CAMKII-α expression at Ctx, Hip and Str was clearly higher than at OB and Crb. Nevertheless, only the comparison between Str and these other areas reached statistical significance (Fig. RI-14B). Interestingly, CAMKII-α was not detected at PND21 and 56 in Crb. Finally, by PND56, CAMKII-α was mostly expressed in Hip, which presented statistically significant higher levels when compared with Str, OB, and as already mentioned, Crb (Fig. RI-14B).

2.4 CORRELATION OF SYNGAP C-TERM VARIANTS AND ITS INTERACTORS EXPRESSION THROUGHOUT DEVELOPMENT IN FIVE BRAIN REGIONS.

As development progressed, SynGAP-α1 and PSD-95 expression pattern correlated significantly in Ctx, Hip and OB (Fig. RI-15). This trend was also observed in Str and Crb, although it did not reach statistical significance. Moreover, α1 and β-containing SynGAP isoforms did not correlate with each other in any structure investigated, suggesting different roles. Interestingly, SynGAP-α1 and CAMKII-α did not significantly correlate in any brain area. Furthermore, SynGAP-β and PSD-95 showed a significant correlation in Hip and Str, whereas SynGAP-β and CAMKII-α correlated only in Ctx and Hip, although they follow a similar expression trend in Str. In contrast, SynGAP-β and CAMKII-α correlated inversely in OB and in Crb (Fig. RI-15D&E). Therefore, these data showed that the expression pattern of SynGAP variants and their reported interactors are regulated similarly in all structures assessed except in Crb and, to a lower degree in Str and OB.

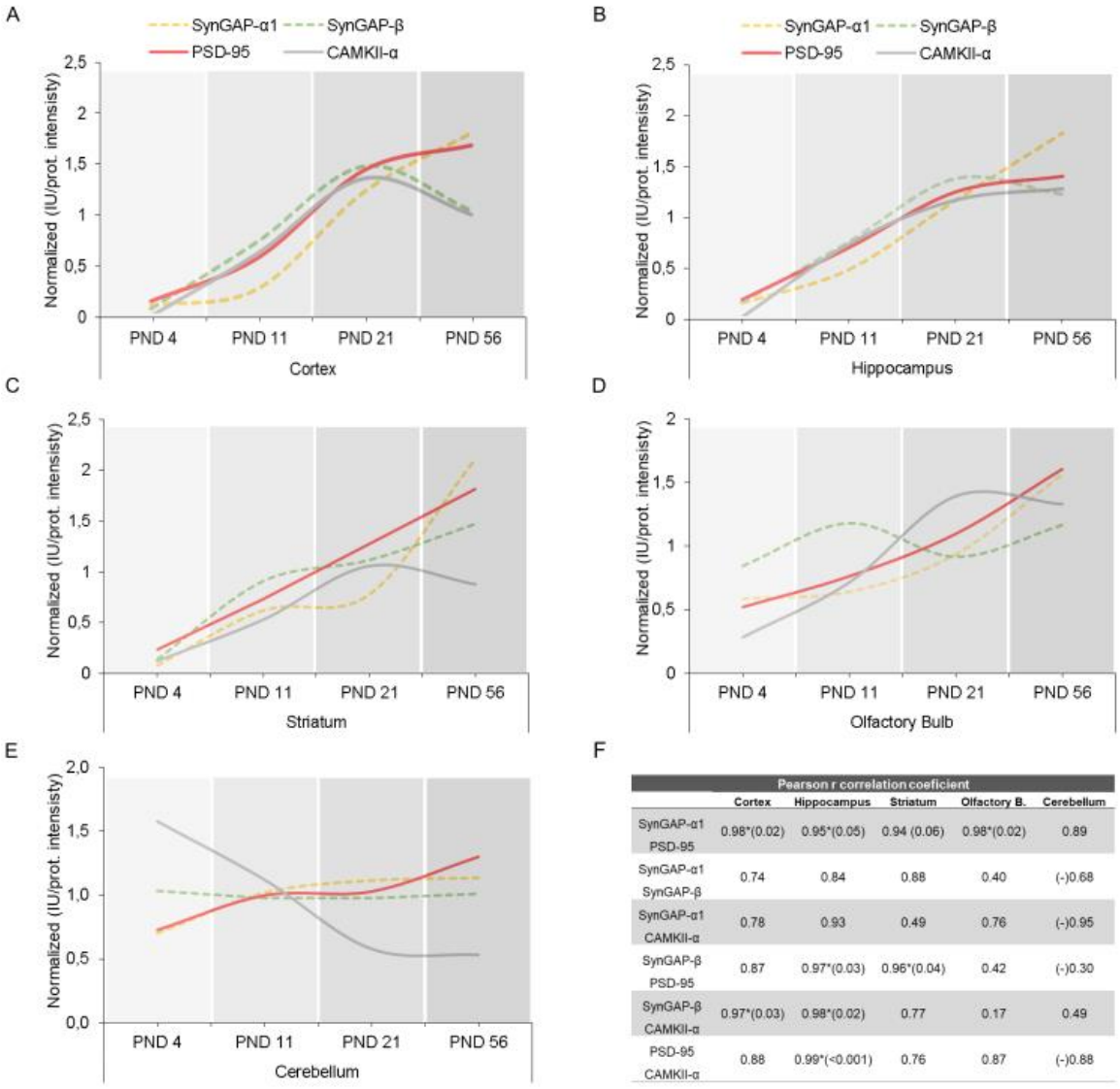

Pearson r correlation coeficient	Cortex	Hippocampus	Striatum	Olfactory B.	Cerebellum
SynGAP-α1 PSD-95	0.98*(0.02)	0.95*(0.05)	0.94 (0.06)	0.98*(0.02)	0.89
SynGAP-α1 SynGAP-β	0.74	0.84	0.88	0.40	(-)0.68
SynGAP-α1 CAMKII-α	0.78	0.93	0.49	0.76	(-)0.95
SynGAP-β PSD-95	0.87	0.97*(0.03)	0.96*(0.04)	0.42	(-)0.30
SynGAP-β CAMKII-α	0.97*(0.03)	0.98*(0.02)	0.77	0.17	0.49
PSD-95 CAMKII-α	0.88	0.99*(<0.001)	0.76	0.87	(-)0.88

Figure RI-15. Correlation assessment of the expression pattern of α1- and β-containing SynGAP isoforms and its reported interactors throughout development in different brain areas. Smooth plot for (A) Ctx, (B) Hip, (C) Str, (D) OB and (E) Crb. (F) Pair-wise comparison in each structure analysed. Data passed Shapiro-Wilk and Kolmogorov-Smirnov normality tests and thus, the Pearson correlation coefficient was computed, and a paired t-test was applied * $p<0.05$.

3. ABSOLUTE QUANTIFICATION OF TOTAL AND SYNGAP C-TERM VARIANTS

The absolute quantification (AQUA) of all reported SynGAP variants in Ctx at different PNDs was determined using a targeted MS approach. This method allowed to identify protein amounts at the femtomole (fmol) scale, overcoming IBs limitations, which only allow comparing the relative expression between variants.

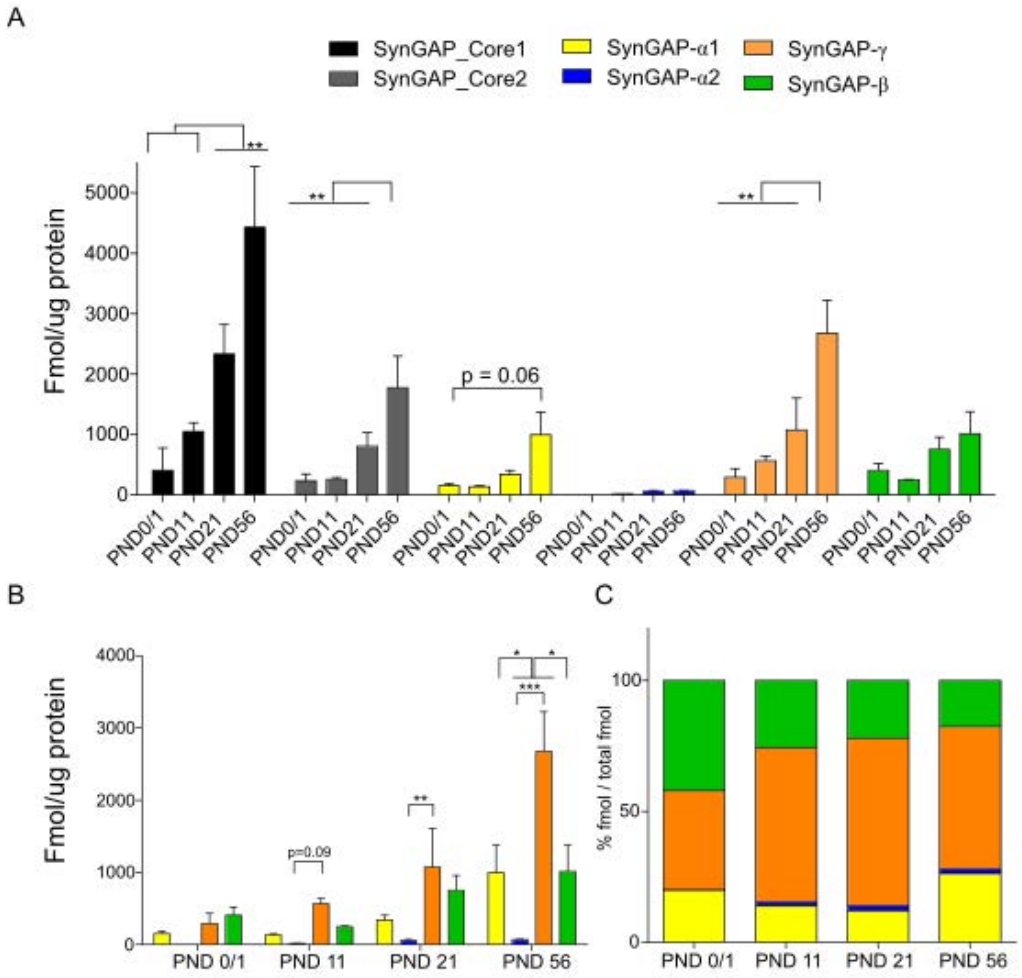

Figure RI-16. Total and SynGAP-α1, -α2, -γ and -β variants AQUA throughout development. Each SynGAP and its C-term variants are expressed in absolute amounts (fmol) per µg of protein. (A) Comparison of the expression of a given protein throughout development. (B) Comparison of the expression between proteins in a given postnatal age. Error bars are plotted as S.E.M. Two-way ANOVA with unmatched repeated measures followed by Tukey's post-hoc test was applied. * $p<0.05$; ** $p<0.01$ and *** $p<0.001$. (C) Comparison of the amounts expressed of each variant assessed (SynGAP-α1, -α2, -γ and -β) in different postnatal ages relative to the total expression of these variants (the sum of all of them). In this case, the amount (Fmol/µg) of each C-term-containing isoform was added in each age to compute the relative proportion of each variant among these total isoforms in percentage. The upper panel shows a legend for SynGAP variant correspondence on both graphs.

Total SynGAP expression was quantified using two peptides from the core region of SynGAP. Their expression profile clearly indicated that total SynGAP expression steadily increased until PND56, age at when it reached its maximum levels (Fig. RI-16).

Nevertheless, the expression differences between PND21 and PND56 did not reach statistical significance when core peptide 1 was used. This is most likely due to the small number of technical replicas that could be performed in this experiment. Specifically, the peak expression and adult levels of SynGAP-α1 and -γ were found at PND56 whereas SynGAP-α2 and -β reached its adult levels by PND21 (Fig. RI-16A). Of note, as previously mentioned, both core peptides for SynGAP followed similar expression patterns, but only one (core peptide 1) reliably quantified the total expression of SynGAP. This assumption relies on the fact that core peptide1 amounts were similar to the sum of the amounts from individual variants. Moreover, SynGAP-β, and specially SynGAP-γ, were more abundant than SynGAP-α1 and -α2 in early stages of development (Fig. 16B-C). In line with this trend, at PND56 SynGAP-α1 and SynGAP-β presented similar expression levels while SynGAP-γ was still the most expressed one.

4. EXPRESSION OF SYNGAP C-TERM VARIANTS AND OTHER SYNAPTIC PROTEINS IN ADULT MOUSE AND HUMAN CORTICES

Subsequently, the expression levels of total and SynGAP-α1, -α2 and –β, PSD-95 and CAMKII-α in young and aged cortical mouse and human samples were analysed. The aims of this study were the assessment of the protein extraction protocol developed for mouse performance in human samples, the comparison of the levels of total and C-term variants, PSD-95 and CAMKII-α in aged as compared with young samples, the evaluation of the SynGAP C-term antibodies immunoreactivity in human samples and the confirmation of the expression of SynGAP-α1, - α2 and -β in human cortices.

Surprisingly, the comparison of SynGAP extraction between the two species using 1% DOC buffer showed that most SynGAP remained in pellets from human samples. Conversely, the major amount of SynGAP in mouse was found in the soluble fraction (Fig. RI-17A). Thus, the expression level of SynGAP, its variants, PSD-95 and CAMKII-α was evaluated using total homogenates (or reconstituted homogenates) from cortical biopsies of two human males (19 and 67 years old) and cortices from mice at equivalent ages (PND56 and 26-months-old mice; Fig.RI-17B).

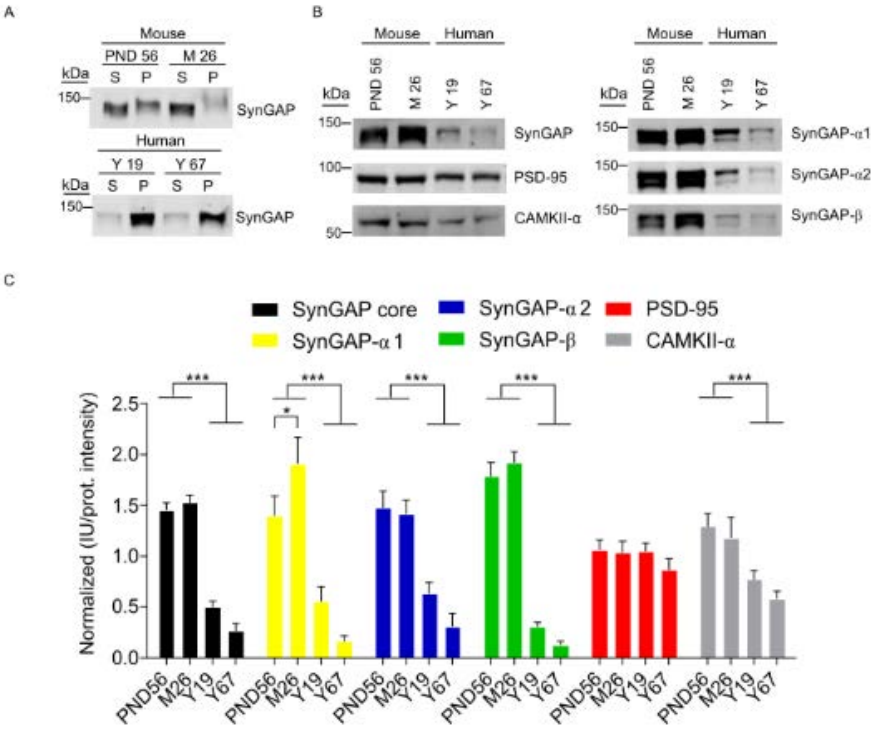

Figure RI-17. Cross-alignment of synaptic proteins between mouse and humans in the mature young and aged brain by IB. (A) Comparison of SynGAP expression in soluble and pellet fractions when mouse and human cortical samples were homogenised with 1% DOC buffer. (B) IBs for SynGAP, SynGAP C-term variants, PSD-95 and CAMKII-α using homogenate or reconstituted homogenate samples from PND56 and 26-month-old mice and 19-year-old (Y 19) and 67-year-old (Y 67) humans. Data followed normal distribution and one-way ANOVA followed by Tukey's multiple comparison post-hoc test was applied. * $p < 0.05$; ** $p < 0.01$ and *** $p < 0.001$.

Studies of the expression of these proteins between mouse samples revealed that there were no major differences in the expression of all these proteins, excluding SynGAP-α1, which was found significantly more expressed in old mice (Fig RI-17B&C). Bearing in mind that the present data came from one human sample per age and could reflect only individual differences, the inter-species comparison showed a reduction of the expression of all proteins but PSD-95 in humans compared to mice. In the case of PSD-95, the same levels of expression between both species were found. Finally, the study of the expression of all these synaptic proteins between young and old humans indicated that as the age progresses there was a trend to reduce the expression of all synaptic proteins investigated in the old Ctx. Yet, this trend did not reach statistical significance (Fig. RI-17C). Importantly, this data demonstrated that all antibodies worked, being especially relevant the SynGAP-β case, since human and mice sequences are not 100% identical and the antibody was developed using the mouse epitope. Therefore, this study corroborates the expression of the SynGAP C-term variants assessed in human cortices and the usefulness of the current developed antibodies for translational studies in humans.

5. SUBCELLULAR LOCALIZATION ANALYSES

The next question that arose was whether SynGAP C-term variants were localized within the same subcellular location and, if so, in which proportion. To unveil this question, a PSD fractionation protocol was applied using mouse cortical samples without the prefrontal part at PND7, PND14, 21 and 56. Also adult hippocampal samples were used.

5.1 TOTAL AND C-TERM SYNGAP VARIANTS SUBCELLULAR LOCALIZATION THROUGHOUT CORTICAL DEVELOPMENT

The different fractions obtained during the PSD purification protocol (see Fig. M-3) were used to assess the yield of each fraction at all ages (Fig. RI-18A). Also, yields from synaptic non-PSD (SNP or alternatively, Triton X-100 soluble) and PSD (Triton X-100 insoluble) fractions were compared with each other, showing how the synthesis of proteins per unit of weight increased as development progresses. Interestingly, at PND14 there was a peak of SNP proteins, whereas at later ages (PND21 and 56), there was a significant decrease in the amount of SNP proteins per unit of tissue paralleled by an increase in corresponding PSD yields (Fig. RI-18B).

A

Protein (ug) / weight (mg)				
	PND 7	PND 14	PND 21	PND 56
H	60,7 +/-3,9	81,5 +/-7,5	83 +/-6,4	86,5 +/-3,4
S1	56,1 +/-4,9	71,8 +/-8,3	72,4 +/-6,4	60,5 +/-4,6
Cytosol	31,5 +/-1,8	32,4 +/-2,6	34,4 +/-6	30 +/-1,7
TM	19 +/-1,3	27,8 +/-4,8	37,3 +/-4,4	17,2 +/-2,2
NSM	2,4 +/-0,8	1,3 +/-0,5	3,3 +/-0,2	1,9 +/-0,2
S-Syn	0,3 +/-0,1	0,5 +/-0,1	2,5 +/-0,6	2,3 +/-0,8
SNP	10,2 +/-0,9	15 +/-2,3	10,2 +/-0,6	7,6 +/-0,4
PSD	1,6 +/-0,5	2,5 +/-0,8	6 +/-0,5	4,5 +/-0,4

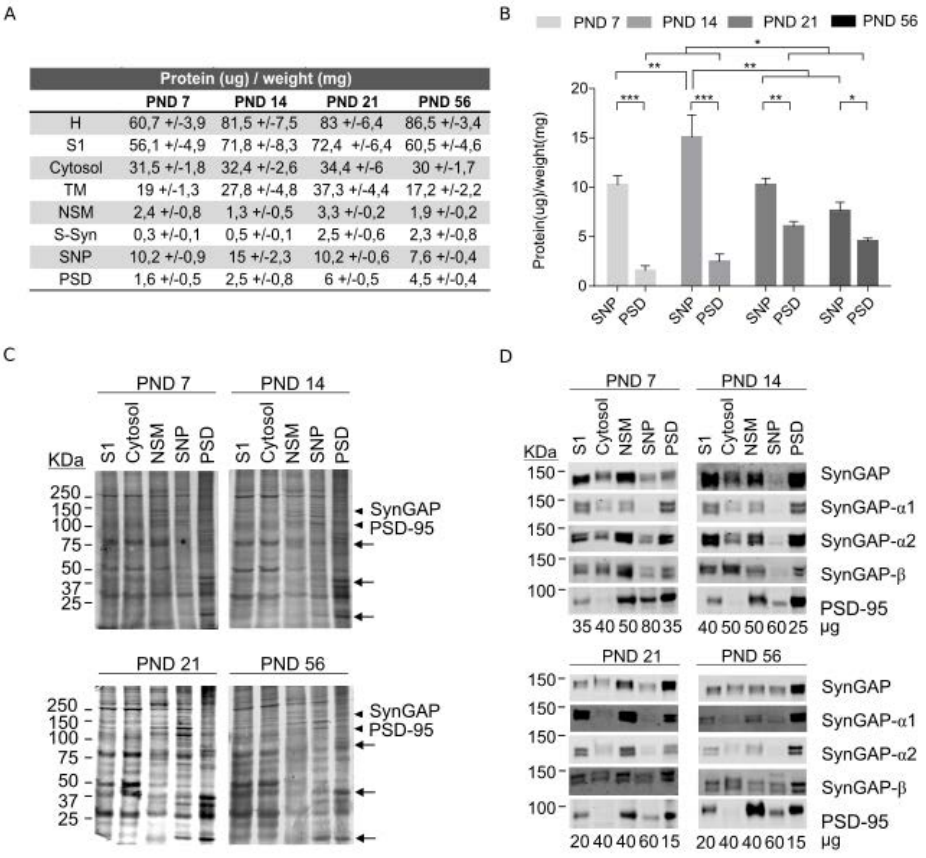

Figure RI-18. Protein yields and SynGAP, SynGAP C-term variants and PSD-95 localization in different subcellular fractions from mouse Ctx without PM/PF region at different developmental ages. See complete figure footnote overleaf.

Figure RI-18 continuation. (A) Yield: µg of protein per mg of weight in homogenate (H), Soluble (S1), Cytosol, total membranes (TM), non-synaptic membranes (NSM); soluble part of synaptosomes (S-Syn), synaptic non-PSD (SNP) and PSD fractions at PND7, 14, 21 and 56. In all cases the error value is preceded by "+/-". (B) Bar plot comparing SNP and PSD yields at each age. Two-way ANOVA followed by Tukey's post-hoc test was applied. * $p < 0.05$; ** $p < 0,01$ and *** $p < 0,001$. (C) Silver stain of SDS-PAGE gels of the fraction assessed by IB. One gel for each of the four developmental stages studied is presented. Arrowheads indicates the approximate location of SynGAP and PSD-95. Arrows show different band pattern between fractions. (D) Representative IBs of the fractionation procedure. The amount of protein loaded (µg) per fraction is shown below the corresponding lane. Note that these figures vary between PNDs.

Of interest, since different fractions presented different protein complexities within one age, SF gels could not be done to correct for protein abundance differences between samples. Instead, silver stains were carried out (Fig. RI-18C, arrows show different protein profiles). Finally, IBs against SynGAP and its C-term variants in S1 (whole extract without nuclei), cytosolic, non-synaptic membranes (NSM), SNP and PSD fractions are shown in Fig.RI-18D. Also, PSD-95 was assessed since it is a marker of synapse and PSD maturation. Thus, it served as a control of protein localization to the PSD.

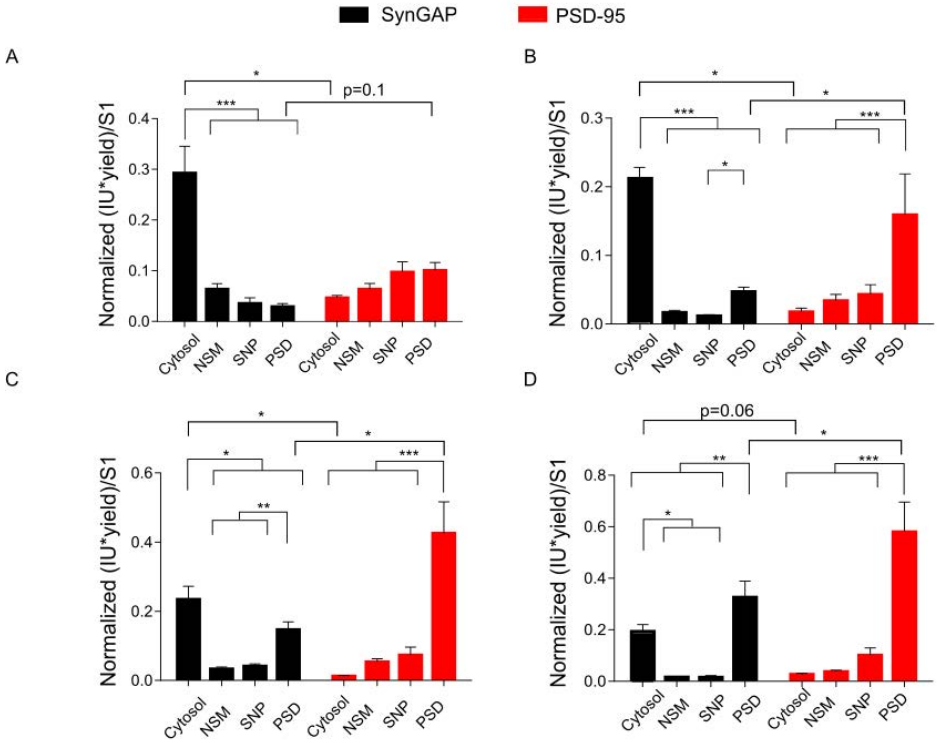

Figure RI-19. SynGAP and PSD-95 subcellular localization during cortical development. Bar plot of SynGAP (black bars) and PSD-95 (red bars) expression at (A) PND 7, (B) PND14, (C) PND21 and (D) PND56 in cytosol, non-synaptic membranes (NSM); synaptic non-PSD (SNP) and PSD. IB data was normalized by the amount of proteins loaded in the corresponding lane before computing the total expression of this protein in a given fraction by using the corresponding yield. Finally, IU*yield of a given fraction were normalized by IU*yield from the matching S1 fraction (see MI-3.3.6). In all cases, data is presented as the mean +/- standard error of the mean" (S.E.M.). All data follow normal distribution and two-way ANOVA was applied followed by Tukey's post-hoc test. * $p < 0.05$; ** $p < 0.01$ and *** $p < 0.001$. In all cases, main effects of fraction and protein were found to be statistically significant as well as the interaction between them them ($p < 0.01$).

At PND7, few PSD-95 containing PSDs could be found, and as the cortex developed, there was an increase in the proportion of PSDs containing PSD-95 (Fig. RI-19A). At the same age, SynGAP was found mainly expressed at the cytosolic fraction, while similarly low

levels were found in NSM, SNP and PSD fractions (Fig.RI-19A). From PND14 onwards, there was a significant increase in PSD numbers (based on protein yields) and a clear enrichment of PSD-95 at the PSD (Fig. RI-19B). Despite a significant amount of synaptic SynGAP was placed at the PSD, the major part remained in the cytosolic fraction. This was confirmed by its difference of expression with PSD-95 abundance in this fraction (Fig.RI-19B). As the postnatal age increased, SynGAP localization changed substantially. Specifically, at PND21 SynGAP was still more present at the cytosolic fraction, but there was a significant increase of its PSD localization when compared with SNP and NSM. Finally, at PND56 SynGAP was significantly more enriched at PSD fractions than in the cytosol.

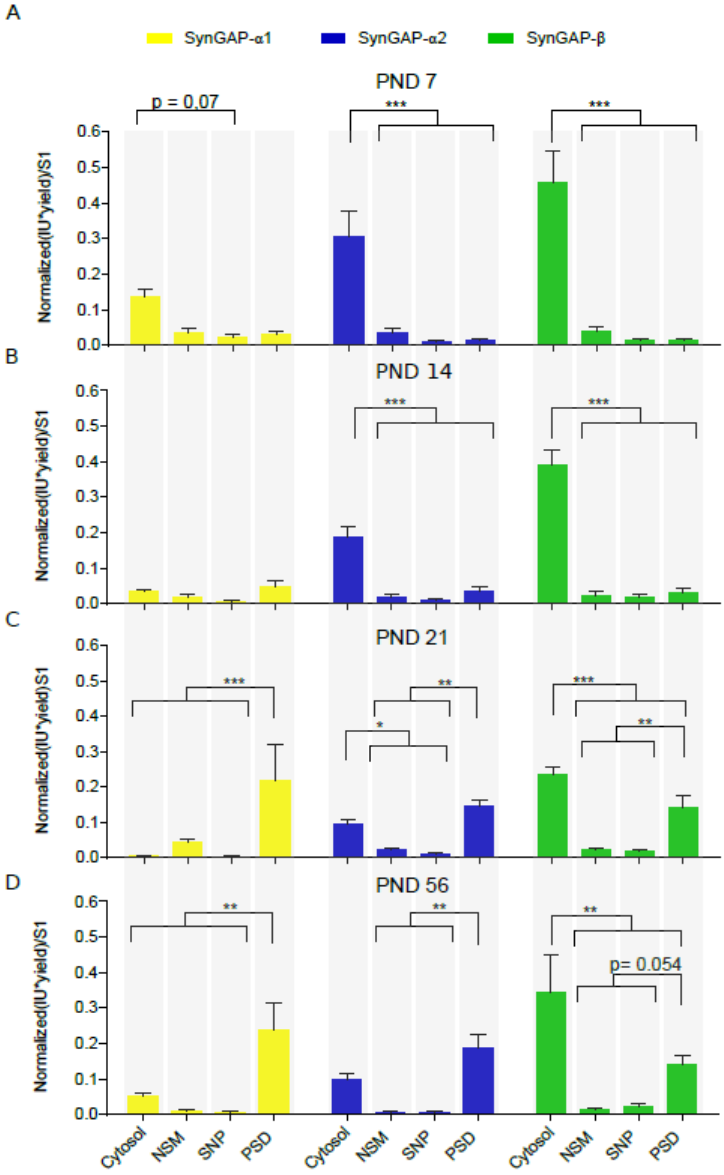

Figure RI-20. SynGAP variants subcellular localization during cortical development. Bar plot of SynGAP-α1, -α2 and β expression at (A) PND 7, (B) PND14, (C) PND21 and (D) PND56 in cytosol; non-synaptic membranes (NSM); synaptic non-PSD (SNP) and PSD from cortex without its prefrontal component. Error bars indicate S.E.M. Vertical grey shadows show longitudinal comparisons. All data follow normal distribution and one-way ANOVA was applied followed by Tukey's post-hoc test. * $p < 0.05$; ** $p < 0.01$ and *** $p < 0.001$.

Additionally, the expression of SynGAP C-term variants in different subcellular fractions was investigated, this was performed along postnatal development. In general, SynGAP-α1, -α2 and -β abundances significantly differed depending on the location as development progressed (Fig. RI-20). Specifically, at early ages (PND7 and 14) SynGAP-α1 was equally expressed in all fractions, although a more cytosolic trend was seen (Fig. RI-20A&B). Interestingly, this expression pattern reached statistical significance for SynGAP-α2 and -β. During PND21 and 56, SynGAP-α1 was highly enriched at the PSD as compared with the other locations, whereas SynGAP-α2 presented the same abundance in cytosol and PSD, being almost undetectable at NSM and SNP (Fig. RI-20C&D). Remarkably, SynGAP-β was still more abundant in the cytosolic fraction as compared with the other fractions, including the PSD. Also, PSD fractions showed much more SynGAP-β than NSM and SNP at these later ages.

The qualitative longitudinal comparison, that is along developmental time (Fig. RI-20; grey columns), for SynGAP variants and PSD-95 expression in cytosol and PSD samples illustrates the increased inclusion of SynGAP variants at the PSD. Furthermore, the relative comparison between the subcellular distribution of SynGAP C-term variants and PSD-95 further supports the previous notions (Fig. RI-21). Despite SynGAP-β followed a similar distribution at the PSD, its expression was still found comparatively higher in the cytosol compared to the abundance of the other variants and PSD-95 in this fraction. Altogether, this data indicated that SynGAP-α1 is highly enriched at the PSD, SynGAP-α2 is placed equally in both locations, whereas SynGAP-β predominates at the cytosol.

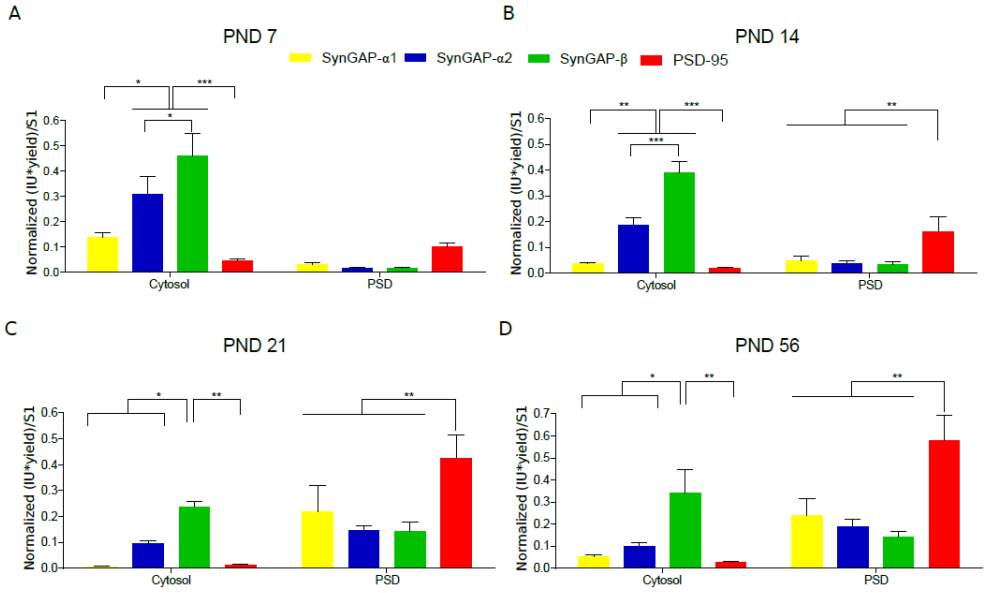

Figure RI-21. Comparison of SynGAP variants and PSD-95 subcellular localization during cortical development. Bar plots compare SynGAP-α1, -α2, -β and PSD-95 expression at (A) PND 7, (B) PND14, (C) PND21 and (D) PND56 in cytosol and PSD fractions from cortex without prefrontal region. Error bars indicate S.E.M. All data follow normal distribution and one-way ANOVA followed by Tukey's post-hoc test was applied. * $p < 0.05$; ** $p < 0.01$ and *** $p < 0.001$.

5.2 SUBCELLULAR LOCALIZATION OF TOTAL AND SYNGAP VARIANTS IN ADULT HIPPOCAMPUS

Next, the localization of SynGAP C-term variants was investigated in adult Hip. In this case, the subcellular fractions investigated were cytosol, SNP and PSD. The yields for S1, cytosol, SNP and PSD fractions were calculated as described in the previous section (Fig. RI-22A). IB data was also normalised as before, thus silver staining of the samples was required (Fig. RI-22B). IB data showed that in adult Hip, SynGAP was found in equal amounts in both cytosol and PSD fractions, whereas PSD-95 was found more enriched in the PSD (Fig. RI-23C&D). Again, SynGAP-α1 and -α2 were significantly enriched in the PSD fraction, whereas SynGAP-β was mainly localised at the cytosol (Fig. RI-22C&E). Therefore, this data confirmed the previous findings.

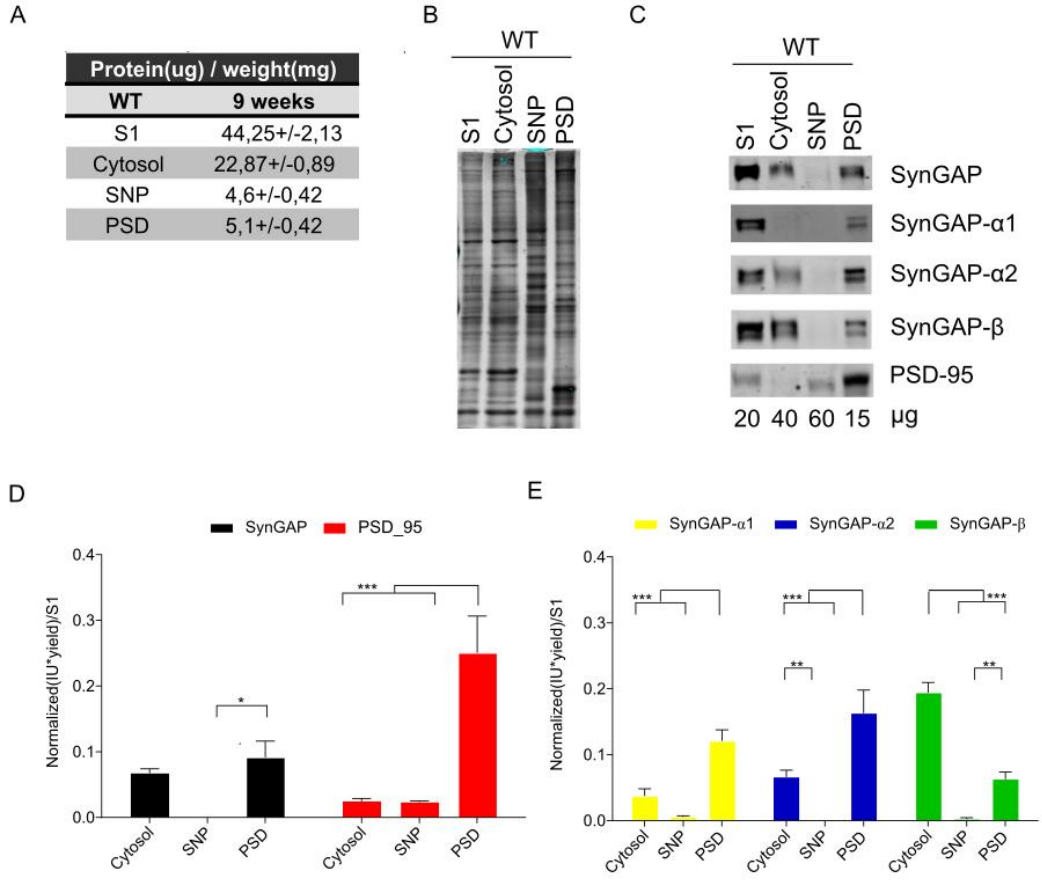

Figure RI-22. Protein yields and subcellular distribution of PSD-95, total and C-term SynGAP variants from adult Hip. (A) µg of protein per mg of tissue weight in total extract (S1), Cytosol, synaptic non-PSD (SNP) and PSD fractions at PND7, 14, 21 and 56. In all cases it is indicated the error (S.E.M) preceded by "+/- ". (B) Silver stain of each fraction. (C) Representative IBs for all proteins tested. Below the lanes the amount of protein loaded is indicated. Bar plots with error bars represent S.E.M for SynGAP and PSD-95 (D) and SynGAP variants (E). All data followed normal distribution. One-way ANOVA followed by Tukey's post-hoc test was applied. * $p < 0.05$; ** $p < 0.01$ and *** $p < 0.001$.

CI-DISCUSSION

1. *IN-SILICO* ANALYSIS OF SYNGAP1/SYNGAP ISOFORMS AND VARIANTS

1.1 *IN-SILICO* ANALYSIS OF *SYNGAP1* TRANSCRIPTS

In mammals, an unexpectedly low number of protein coding genes are expressed (International Human Genome Sequencing, 2004). However, proteome complexity is not only gained by the expression of protein coding genes, but also through alternative splicing (AS). Together with other processes, such as alternative transcription start sites, alternative polyadenylation sites, transcription rates, histone modifications, and chromatin structure, AS enables to increase protein complexity (Kornblihtt et al. 2004, 2013; Lipscombe 2005; Q. Li, Lee, and Black 2007; Luco et al. 2010; Grabowski 2011; Raj and Blencowe 2015).

The *in-silico* analysis of *Syngap1* of both experimentally validated or predicted transcript variants in mouse showed 5 new unreported variants at the 5' region in addition to the previous well studied *Syngap1*-A1, A2, B and C variants (Cheng et al. 1998, Kim et al. 1998, Li et al. 2001; McMahon et al. 2012; Kilinc et al. 2018). Also, at the 3' end, 2 new variants were identified: SynGAP-α3 and -α4. However, since there is a lack of the STOP codon in *Synagp1*-α3 mRNA and different Ensemble releases included it but others not, likely it is an artefactual product of the *in-silico* predictions. It is worth mentioning that there are multiple variations at both 5' and 3' untranslated regions (UTRs) that are not included in the cDNAs or EST derived sequences studied here but in fact, they do play a role in *Syngap1* gene expression regulation and stability (McMahon et al. 2012; Yokoi et al. 2017). Thus, an inclusion of these sequences in the public databases would be helpful for future studies.

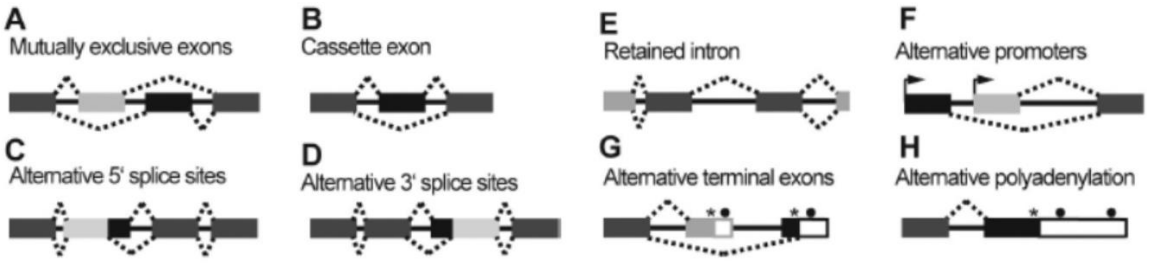

Figure DI-1. Alternative splicing mechanisms. AS results from the use of one or more of the depicted basic modules. Modified from Nilsen and Graveley 2010.

There are several mechanisms of AS involved in SynGAP isoforms production as shown in Fig. D-1. Alternative promoter usage (Fig. DI-1F) is the main mechanism driving A1, A2, B and C N-term SynGAP variants, whereas the variants identified in this thesis, *Syngap1*-A6, A8 or A9 likely arise from several other mechanisms of AS beyond the described

alternative promoter usage. Particularly, exon 4 would be excluded in all variants but in SynGAP-B (Fig. DI-1A). SynGAP-A7 and -α4, are examples of retained intronic sequences (Fig. DI-1E) as well as SynGAP-, which includes a 13 bp insertion from 18-19 intron due to alterative 5' splice sites (Fig. DI-1C). Since *Syngap1*-A5 does not include exons 2 and 3 while SynGAP-B and -γ are the only ones that include exons 4 and 21, it might be reasoned that these variants are generated through a mutually exclusive exon mechanism (Fig. DI-1A). Interestingly, a young boy has been described with a *SYNGAP1*-related disorder caused by the activation of a cryptic 5' acceptor splice site located 9 bp up-stream of exon 17. As a result, 7 bp of intron 16 are included leading to a prematurely truncated product (Brimble et al. 2018). Therefore, these data support the intricate regulation of *Syngap1* and the possible expression of the different discussed AS mechanisms.

Noteworthy, *Syngap1*-γ includes exon 21, which matches with the definition of microexon (Ustianenko, Weyn-Vanhentenryck, and Zhang 2017). Despite inclusion or skipping of microexons represents only approximately 1% of all AS events, they constitute up to 1/3 of all conserved neuronal-regulated AS events between human and mouse (Irimia et al. 2014; Li et al. 2015). Thus, the conservation of *Syngap1*-γ in humans could be expected, although it has not yet been identified. Moreover, our targeted MS data indicated that *Syngap1*-γ is the predominant isoform in adult ages. Thus, taken together, these findings foster the study of the unexplored *Syngap1*-γ, to better understand the neurobiology of SynGAP.

Syngap1-α1 sequence retrieved from Ensembl showed that it arises from an addition of 6bp from exon 21, as also described by Yokoi et al. 2017. However, earlier reports described that the differences between *Syngap1*-α1 and -α2 stem from alternative 3' splice sites, which results in a different ORF, thus yielding a longer C-tail in *Syngap1*-α2 (Kim et al. 1998, Kim et a. 1998; Li et al. 2001; Rumbaugh et al. 2006; McMahon et al. 2012). Since SynGAP-α1 is well-studied and has been sequenced more than once, here is reported the accepted formation mechanism described by the scientific community. Of note, this controversy put at stake the 100% reliability of the sequences retrieved from Ensembl database. Therefore, experimental confirmation of previously unreported sequences and deduced mechanisms of formation is desired.

1.2 *IN-SILICO* ANALYSIS OF SYNGAP ISOFORMS

At least 15 different SynGAP isoforms were identified in the present study, but if all 9 N- and 5 C-term variants could be expressed together, the total number of SynGAP isoforms could rise up to 45. Although this number of SynGAP isoforms might seem high, other

synaptic proteins present much larger numbers of isoforms. As an example, Neurexin genes produce almost 3,000 different isoforms arising from AS (Missler and Südhof 1998; Reble, Dineen, and Barr 2018). Additionally, the presence of multiple clusters of promoters in the *Syngap1* gene (McMahon et al. 2012) and the putative presence of cryptic promoters (Kim et al. 2003), support the expression of more than these 15 reported isoforms. In line with that, genes with alternative promotors, compared with those that only have one, tend to show more AS. In turn, the number of alternative promoters correlates positively with the number of alternative splice events (Epshtein and Nudler 2003; Kornblihtt et al. 2004; Xin, Hu, and Kong 2008). Collectively, these data favours the possibility of a high number of SynGAP isoforms.

To explain the complexity of brain anatomy, development, and function, not only does the brain have a higher number of AS events relative to other tissues (Xu, Modrek, and Lee 2002; Yeo et al. 2004; Pan et al. 2008; Chen and Manley 2009; Barbosa-Morais et al. 2012; Merkin et al. 2012), but also a conservation of the brain-specific AS program is especially prominent through vertebrate evolution suggesting functionality of spliced products (Barbosa-Morais et al. 2012; Merkin et al.2012). Therefore, these high number of SynGAP isoforms could be also expected in humans. In support of that notion, a high transcriptional and protein identity between canonical SynGAP isoforms from rodents and humans has been found like what is reported for the genomic level (McMahon et al. 2012). Moreover, the expression of SynGAP isoforms containing the C-term variants α1, α2 and β in the human Ctx was proven in the present thesis.

In summary, these data illustrate that *Syngap1* is an intricately regulated gene as it is subjected to multiple mechanisms of AS being important also for 5'/N-term generation beyond the alternative promoter usage to yield a putative high number of isoforms. Hence, different SynGAP variant expressions patterns and relative abundance changes throughout development are expected and might have a profound impact on brain function.

1.3 EXPRESSION VALIDATION OF *SYNGAP1* TRANSCRIPTS *IN VIVO*

To further explore the actual presence of these isoforms/variants and how these regulations are exerted throughout development, reverse transcription of the mRNA and PCR of the cDNA obtained at different ages in both Ctx and Hip were carried out. The complete isoforms were unsuccessfully amplified probably due to the high length of the amplicon in addition to the fact that several 5' variants are combined with different 3' variants, thus the coincidence of a pair of forward and reverse primers within the same molecule will be more difficult. As a result, unmatching pairs of primers in the same

Syngap1 cDNA might contribute to the inability to amplify complete isoforms. Also, the lack of unique sequences for all transcripts prevented to test all variants, and thus only some of them could be tested by PCR.

PCR analyses indicated that *Syngap1*-A1/2, -A5, -B, -A7, α1/2, α4 and -γ are expressed in both Ctx and Hip. Yet, SynGAP-α4 was only detected in cortical samples from PND11 and 21. These results agree with previous qPCR studies (McMahon et al. 2012; Li et al. 2001). It is worth noting that in the SynGAP-A1/2 case, there was an 'unexpected' PCR product of ~200 bp that might arose from transcripts containing SynGAP-A5 or, alternatively, from unreported variants or unspecific PCR products. Intriguingly, *Syngap1-α4* was found only expressed in 2 specific ages, PND11 and PND21, and in Ctx, but not in Hip. However, expression of the unreported *Syngap1*-A5 and -A7 variants were confirmed in both Ctx and Hip samples. Surprisingly, these variants were predicted to match with *Syngap1-α4* C-term variant, therefore it is possible that A5 and A7-containing isoforms might be expressed with other C-term variants beyond *Syngap1-α4* in Hip and at Ctx during those ages where *-α4* is not expressed. Although complementary analyses with more sensitive techniques (e.g., qPCR) might help confirming this data, taken together they provide further support to the notion that the *in-silico* predictions might underestimate the real amount of SynGAP isoforms.

1.4 EXPERIMENTAL IDENTIFICATION OF SYNGAP VARIANTS

Proteomic identification of SynGAP variants was only performed with cortical samples. The layered pattern seen in IB from elutes of immunoprecipitated SynGAP already suggests the presence of different isoforms with the predicted molecular weight. Yet, although it cannot be fully excluded that one isoform carrying different PTMs that influence its electrophoretic mobility, could be responsible for this patterned profiled. Accordingly, LC-MS/MS analyses identified several reported variants, including the C-term SynGAP-α1, -α2, -γ and -β and importantly, the previously unreported N-term variant SynGAP-A6. Collectively, these data support the existence of other SynGAP isoforms than the hitherto reported at the protein level.

Despite SynGAP-α4 was identified at the transcript level, none of the LC-MS/MS experiments found unique peptides for this variant. However, a unique peptide of SynGAP-A6 was identified at PND11, while its peptide precursors were identified from PND0 to PND56. Since the only predicted A6-containing isoform was *Syngap1*-A6/α4, it is tempting to speculate that this isoform would be expressed in Ctx and in all ages (including also 14-week-old mice [Data not shown]). In support of this notion, there are examples of cell- or

tissue-specific expression of small GTPases and its regulatory proteins (Coutavas et al. 1994; Tolias et al. 2007), thus it could be possible an exclusive SynGAP-A6/α4 expression in Ctx. Future experiments taking advantage of the targeted approach will be needed to confirm the *in-vivo* expression of SynGAP-α4 variant and this possible tissue-specific expression pattern.

In summary, *in-silico* predictions of *Syngap1* transcript and protein isoforms allowed to identify up to 6 previously unreported *Syngap1* variants of which 4 were validated at the transcript (A5, A7 and α4) or protein (A6) levels in all or specific postnatal ages.

2. STUDY OF PROTEIN DOMAINS AND POSTRANSLATIONAL MODIFICATIONS OF SYNGAP ISOFORMS

A global view of SynGAP domains and putative regions that could be subjected to PTMs in the previously reported and unreported SynGAP isoforms could help elaborating new lines of investigation and ultimately, expand the knowledge of SynGAP neurobiology. Indeed, it is widely accepted that the primary sequence of a protein determines its three-dimensional structure, which in turn, determines its function (Anfinsen 1973). The alignment of protein sequences from each SynGAP variant allowed to find a “modular” pattern that should add different features to each SynGAP isoform. Furthermore, the modular-like assemble of both N- and C-term protein stretches agrees with the idea that modern proteins evolved by fusion and recombination from a more ancient peptide world in which many of the core protein folds observed today may contain homologous building blocks (Söding and Lupas 2003). Therefore, this modular mechanism of SynGAP hypervariable regions might add to the known additional complex functions and regulations beyond Ras small GTPase activity from core regions. Indeed, it has been described that the Rap activity of SynGAP requires the C2 domain (Pena et al. 2008) and the combination of N- and C-term variants influence synaptic strength (McMahon et al. 2012). Moreover, different subcellular localization of GAPs has been reported to be mainly determined by hypervariable domains such as the N- and/or C-term variants in SynGAP (Kooster and Hordjik, 2007; Walkup and Kennedy, 2014). Indeed, subcellular distribution studies of different SynGAP C-term containing isoforms corroborated, at least in part, this assumption.

2.1 N-TERM VARIANTS AND VARIATIONS IN THE PH DOMAIN

The functional properties of some N-term variants have been described in the literature. For instance, the *in vitro* recombinant form of SynGAP-A2/α1, which lacks the first 102 residues (Walkup et al. 2016), prevents its association with membranes. Interestingly, this truncated form of SynGAP showed all its well-characterized PH, C2, and GAP domains preserved (residues 103-725 from SynGAP-A2/α1). Therefore, SynGAP-C, -A6, -A7 and -A9 might be found soluble as all lack these 102 residues, whereas the other N-term containing isoforms would attach to neuronal membranes.

Differences in the SynGAP N-term sequences could also imply different regulation by kinase phosphorylation. For instance, isoforms containing the N-term variants A2, A1 and A8 share a unique sequence that can be subjected to serine/threonine kinase phosphorylation, thus presenting a regulatory region absent from other isoforms. Also,

based on the predictions from different databases conducted, all variants but SynGAP-A6 and -A9 could be subjected to cAMP-dependent kinase phosphorylation, while SynGAP-B showed an additional putative phosphorylation site for this kinase.

Furthermore, depending on the N-term variant, differences in the PH domain length were identified. Sequence differences before or within the PH domain might also influence its role in signal transduction, as this domain mediates PPIs (Musacchio et al. 1993). Examples of proteins carrying a PH domain include β/γ subunits of heterotrimeric G proteins (Wang et al. 1994) or PKC (Yao, Kawakami, and Kawakami 1994). Also, PH domain binding to phosphatidylinositol allow protein recruiting and targeting to different membranes (Hyvönen et al. 1995; Lemmon 2004; Falasca et al. 1998). Therefore, N-term sequences and consequently, SynGAP isoforms might have more different implications in the synaptic physiology than previously reported (McMahon et al. 2012).

2.2 SYNGAP CONSERVED DOMAINS

Beyond N-term and PH domains, the C2 domain might have a role in membrane targeting modulation, as it is capable of Ca^{2+}-dependent membrane binding. C2 domains show a wide range of lipid selectivity for the major components of cell membranes, including phosphatidylserine and phosphatidylcholine (Davletov and Südhof 1993). Interestingly, this lipid selectivity confers different Ca^{2+} sensitivity and subcellular localization (Nalefski and Falke 1996; Lemmon 2004; Cho and Stahelin 2006). Therefore, if SynGAP-A9/α4 is expressed, it might respond differently to Ca^{2+} changes and phospholipid 2nd messengers due to NMDAR activation because is the only isoform that lacks the C2 domain (Kim et al 1998; Yang et al. 2013; Araki et al. 2015; Walkup et al. 2016). Also, this reduced version of SynGAP could affect in its GAP function, as it also lacks a glycine-rich region useful for GAP stabilization, and a smaller number of LC regions. Conversely, the fact that all isoforms but A9, conserved the C2 and GAP domains as well as the SH3 binding motif indicates that these three functional domains play a crucial role in SynGAP activity. Accordingly, the major domains (PH, C2, GAP and CC domains) found in human SynGAP are conserved in the two *Syngap1* ohnologues found in zebrafish (Kozol et al. 2015).

The presence of a proline-rich region in SynGAP, which is a motifs for binding to SH3 domain-containing proteins, would potentially allow its binding proteins such as dynamin, SOS, PI3K or Grb2 (Musacchio et al. 1993; Beneken et al. 2000). Since the SH3-binding motif is located in the core SynGAP region, all its isoforms could potentially bind these proteins. Of note, the present *in-silico* analyses also predict a Proline rich/SH3 binding motif in SynGAP-α2 unique sequence (it is further discussed below). This motif is important

for PPIs and might be relevant for the regulation of several biological pathways by SynGAP. Yet, the interaction of SynGAP with some of the mentioned proteins (i.e., dynamin and SOS) could also take place through their PH domain, as these proteins also present such structural feature (Musacchio et al. 1993). Similarly, all isoforms were found to contain 10 histidine repeats that may be involved in metal chelation binding divalent transition metals, including Zn^{2+} and Cu^{2+}, and therefore, might play a role in the regulation of SynGAP function (Kim et al. 1998).

In-silico predictions also showed that all C-term variants have a CC domain that essentially consists of a long α-helix. These structural elements oligomerise into a bundle of α-helices from different SynGAP polypeptides, allowing trimerisation (Walkup et al. 2016). However, SynGAP-β could be particularly different as a CC with a reduced length was identified. The functional implication of this shorter CC is unclear, but it might hamper oligomerization. Also, SynGAP-β presented a unique sequence after the CC domain, while all other C-term variants had a stretch of 32 common residues. This common region, although it is not strictly part of the CC domain, might contribute to its formation or stabilization. Thus, these findings suggest, at least in part, different functionalities of the CC domain depending on the SynGAP C-term variant. As an example, SynGAP-β could have lower affinity for CC domain from SynGAP-α1 and thus, be less targeted to the PSD, according to the liquid-liquid phase transition model of PSD formation (Zeng et al. 2016).

2.3 C-TERM VARIANTS

As previously introduced, one of the major findings of the present *in-silico* analyses of the domains present in SynGAP isoforms was the identification of a SH3 domain binding motif in the C-term region unique to SynGAP-α2, which might explain several unresolved questions formulated in the literature. For instance, the interaction of this motif with proteins presenting an SH3 domain, including PSD95 or the other MAGUKs, might explain the PSD localization of SynGAP-α2 even when SynGAP-α1 is barely expressed, such as in the first postnatal week of cortical development shown in the present thesis.

Furthermore, SynGAP C-term variants exhibited different composition in terms of their presence of LC regions. As a rule of thumb, centrally-located LC repeats are related to transcription functions, while terminal LC repeats are more relevant to translation and stress response-related functions (Coletta et al. 2010). For instance, SynGAP-α4 was predicted to have two LC regions, SynGAP-α2 and -β only a LC region (in different positions), while SynGAP-α1 and -γ have none. Of note, LC regions-containing proteins tend to have more binding partners across different PPI networks, agreeing with the more

than 100 SynGAP interactors found in adult Ctx (Wilkinson et al. 2017). Accordingly, in the Chapter II is shown the demonstration that LOF of *Syngap1* mutations promote disturbances in the expression of translation related proteins at the PSD.

Regarding the importance of LC regions, they can contribute to the formation of novel coding sequences, facilitating the generation of novel protein functions. Thus, recently emerged proteins tend to contain more LC sequences than older proteins. As a result, LC repeats are considered a hallmark of protein evolution (Toll-Riera et al. 2012). Collectively, these data suggest that SynGAP-α4 followed by -α2 and -β, might be more 'recent' variants as compared with SynGAP-α1 and SynGAP-γ and thus, contribute to more complex brain functions. In support of this idea, in the present work the expression of SynGAP-α1, α2 and β in humans was proven, while in earlier vertebrates, these variants have not been identified (Kozol et al. 2016). Nonetheless, to corroborate this hypothesis, a more comprehensive study of SynGAP isoforms in vertebrate phyla other than mammals will be required.

Finally, regarding the phosphorylation sites in C-term variants, SynGAP-β showed a loss of one putative serine phosphorylation site. As one of the best recognized serine/threonine kinases that modulates SynGAP is CAMKII and its non-phosphorylated α subunit form interact with SynGAP-β (Li et al. 2001), this data implies a possibly more structural role of this isoform than a functional one, which will be further discussed. In contrast, two PKC extra phosphorylation sites in SynGAP-α4 were predicted. Thus, if its expression at the protein level is confirmed, it could participate in PKC-related signalling pathways.

2.4 POST-TRANSLATIONAL MODIFICATIONS

The present study predicted that SynGAP isoforms, not only depending on their N-term, but also its C- term variant, could undergo phosphorylation by kinases that have not been previously shown to phosphorylate SynGAP. These would include Casein Kinase II (CKII), PKC and cAMP-dependent kinases. Phosphorylation by these enzymes might represent a new level of SynGAP regulation in addition to the reported phosphorylation by CAMKII, CDK5 or PLK2 (Chen et al. 1998; Kim et al. 1998; Song et al. 2003&2004; Krapivinsky et al. 2004; Rumbaugh et al. 2006; Lee et al. 2011; Araki et al. 2015; Walkup et al. 2016; Walkup et al. 2018). Bearing in mind that these predictions needs to be experimentally corroborated, these studies indicate that SynGAP-A8 might be subjected to regulation by Plk2, as it has already been described for isoforms containing A2 and A1 (Lee et al. 2011), whereas cAMP-dependent kinases might specifically regulate B-containing SynGAP isoforms.

Finally, it is possible that other PTMs take part in the regulation of SynGAP, such as myristoylation or asparagine glycosylation. For instance, myristoylation facilitates membrane targeting, regulation of signalling pathways by PPIs or protein–lipid interactions and was reported to operate in the regulation of the GEF RasGRP2 and Arf small GTPases (Bos et al. 2007). Interestingly, different number of putative sites for myristoylation in SynGAP isoforms were identified, with SynGAP-A2/β having the highest number of them.

3. SPATIO-TEMPORAL REGULATION OF SYNGAP EXPRESSION

Gene expression studies indicate peak expression of *Syngap1* at PND14 in both Ctx and Hip (Porter et al. 2005; Barnett 2006; McMahon et al. 2012; Clement et al. 2012), whereas protein data presented here show that it might be later (as the expression levels at PND11 and 21, but not at PND14 were assessed). Importantly, these results agree with other reports of SynGAP protein expression throughout development in Ctx, Hip or Crb (Barnett 2006; Yang et al. 2004; Tomoda et al. 2004; Petralia et al. 2005). These discrepancies can be accounted by the operation of post-transcriptional mechanisms such as the non-sense mediated decay and/or translational and post-translational events, like proteasome degradation (Reble et al. 2017). In fact, mRNA transcript stability depends on the length of 3' UTR and associated variants (Yokoi et al. 2017). Therefore, *Syngap1* transcript levels do not reflect the real SynGAP protein amounts and thus, strengthens the importance of the present study at protein expression level despite the well-known regulation of *Syngap1* mRNA or promotor activity along development.

Specifically, IB data from other reports confirm a progressive increase of total SynGAP expression in PSDs from rat Hip and total extracts from mouse Crb and Ctx described in this chapter (Petralia et al. 2005; Tomoda et al. 2005; Barnett et al. 2006). Also, present studies of SynGAP abundance between brain regions indicated that at PND21, a distinctive pattern of regulation could be observed as compared with earlier (PND11) and later (PND56) stages of postnatal development. This pattern was characterised by equivalent levels of SynGAP at Ctx and Hip and a much lower abundance in Str, whereas at PND11 and 56, the Hip presented the highest abundance. These IB data partially overlaps with previous gene expression data relative to different brain areas (Porter et al. 2005). Namely, while gene and protein reports agree on SynGAP levels at PND4, gene expression data fails to identify the pattern of SynGAP expression found at PND21 and PND56. Altogether, these results reinforce the idea that translational and post-translational mechanisms also play a role in regulating SynGAP levels.

If it is assumed that high amounts of SynGAP correlate with a more prominent role for this protein, this would be similar across the brain regions investigated in early development stages. Conversely, as development goes forward, SynGAP roles would be more important in Hip, Ctx and Str than in OB and Crb. Interestingly, SynGAP levels in Crb were found locked in a steady-state expression as compared with the other structures, where SynGAP increased with age. Similarly, total SynGAP expression in early stages (PND4) of OB development showed the same amount of SynGAP as Ctx and Hip, but then from

PND11 onwards it was found expressed at much lower levels. Importantly, these data also agree with previous studies showing high levels of SynGAP expression in adult Ctx and Hip, and low levels in Crb by IB (Kim et al. 1998). Yet, it is in disagreement with previous work, where higher levels of SynGAP in the OB relative to Ctx and Hip were reported (Kim et al. 1998; Porter et al. 2005). These discrepancies could result by the fact that in those previous studies quantitative experiments were not conducted or whole structures were not considered as in the present case, which might lead to misinterpretation of their data.

In summary, these studies showed that SynGAP adult levels are reached differently depending on the brain structure and the amounts expressed are clearly different and constantly rearranged as development progresses. Therefore, there is a regionalized pattern of SynGAP expression throughout development, which is consistent with the idea reported at the gene expression level (Porter et al. 2005).

3.1 SPATIO-TEMPORAL REGULATION OF SYNGAP C-TERM VARIANTS

Bearing in mind the spatio-temporal regulation of total SynGAP, an obvious question is how SynGAP variants can change and influence the overall SynGAP expression pattern. The only SynGAP antibodies developed and tested for specific SynGAP C-term variants are against SynGAP-α1, -α2 and -β (Kim et al. 1998; Chen et al. 1998; Li et al. 2001; Moon et al. 2008), the last one not being commercially available and kindly provided by Dr. Rumbaugh (The Scripps Research Institute, USA) and Dr. Huganir (Johns Hopkins University, USA).

In Ctx, SynGAP isoforms presenting different C-term variants reached their maximum level of expression at different ages. Specifically, SynGAP-α2 and -β achieved their maximum levels of expression at PND21 whereas SynGAP-α1 maximum was not found until PND56. In accordance, α1-containing isoforms were expressed at very low levels during the first postnatal week as shown by subcellular localization studies or by both discovery and targeting MS methods. Furthermore, this reduced expression of SynGAP-α1 also matches with fainter SynGAP-α1 immunoreactive bands observed in early postnatal developmental stages from whole cortical extracts by others (Barnett et al. 2006). Interestingly, SynGAP-β abundance was found to significantly decrease between PND21 and PND56 in Ctx, resulting in the same amounts found at PND11 and 56. This expression pattern was only significantly identified in Ctx, although hippocampal expression of SynGAP-β had a similar trend that fell short of being statistically significant. Noteworthy, this expression progression mirrors that of synaptogenesis, synapse remodelling and synapse density (See Fig. I-16; Flavell et al. 2006; Semple et al. 2013).

In Str, the peak expression of SynGAP-α's was found more pronounced after PND21, whereas SynGAP-β was similarly expressed between PND21 and 56. Conversely, in OB and Crb SynGAP-β adult levels were reached by PND4 while in OB, isoforms bearing SynGAP-α1/2 C-term variants progressively increased their levels. Moreover, SynGAP-α2 were found to reach adult levels at PND21 in OB, whereas in Crb these were delayed until PND56. The different balance on the abundance of these variants might account for different outcomes of SynGAP neurobiology in these structures. Namely, SynGAP-β in Ctx, OB and Crb might have a prominent role in early stages of development in contrast to the isoforms presenting the other C-term assessed variants.

Of note, the expression pattern of SynGAP-α1 and α2 was found to be more similar than that of SynGAP-β in equivalent structures and ages. Probably, α1-2 variants might be subjected to more similar mechanisms of protein turn-over. Still, there were slight differences seen between SynGAP-α1 and -α2 expression that can be explained by other mechanisms like mRNA differential stabilities or the number of LC regions as mentioned before. In support of an mRNA stability role, FUS, ELAVL4 and ELAVL1 control SynGAP mRNA stability in a 3' UTR length-dependent manner, resulting specifically in the stable expression of the alternatively spliced *Syngap1*-α2 (Yokoi et al. 2017). In addition, miRNAs could control the gene expression of *Syngap1* through base pairing between the 3' UTR of mRNA and miRNA "seed" region at the 5' end, thereby inhibiting the translation of the target proteins (Bartel 2009). Importantly, in Ensembl database (Release 91) has been predicted at least one miRNA sequence against the *Syngap1* gene in mouse. This could have a role in differential post-transcriptional regulation since there are miRNAs that recognize the 3'UTR of *Syngap1* mRNAs (Muro et al. 2015).

The inter-structure comparison of C-term variants showed that there is a precise and differential spatio-temporal regulation of SynGAP isoforms, which is characteristic of each terminal sequence. Generally speaking, at PND4 OB and Crb expressed the lowest levels of SynGAP-α1, whereas the other 2 variants showed similar abundances among Ctx, Str, Hip and OB. Consequently, SynGAP-α2 and β only showed an expression pattern similar to that of SynGAP-α1 in Crb. As postnatal development progresses, relative expression of SynGAP isoforms changed according to the variants they present, with SynGAP isoforms containing β being the ones that maintained similar expression levels across the different ages. Also, SynGAP-α1 showed more different rearrangements of its levels between brain areas than SynGAP-α2 from PND4 to PND56.

As just mentioned, at PND4 almost all C-term variants were found similarly regulated in all tissues but Crb since SynGAP-α1 was found at low levels at the OB. At PND11 and

PND56, C-term variants reached maximal expression levels at Hip. Conversely, at PND21 the highest expression of each SynGAP isoform differed depending on the tissue. Particularly, SynGAP-α1 presented its highest levels in Ctx, SynGAP-β in Hip and SynGAP-α2 maximum levels were found in both tissues. Thus, these data suggest that SynGAP C-term variants at PND21 might be subjected to a more intensive differential regulation of their expression depending on the brain area.

This specific regulation found at PND21 would parallel important brain developmental landmarks, such as the peak of synaptogenesis and synapse remodelling (Flavell et al. 2006; Semple et al. 2013) or a critical period for the establishment of sociability and working memory (See Fig. I-16; Semple et al. 2013; Clement et al. 2012; Aceti et al. 2016). Furthermore, during PND21-23 *Syngap1*$^{+/-}$ mice show a reduced FMRP expression in their postsynapses as an attempt to achieve the required SynGAP levels (Paul et al. 2018). Also, the expression of the transcriptional activator MEF2, which regulates gene expression (including that of *Syngap1*) in a neuronal-activity dependent manner, peaks at PND21 (Dietrich et al. 2013). Collectively, these data indicate that PND21 age is important in the neurobiology of SynGAP. Additionally, considering the differential expression pattern at PND4 and PND21 for SynGAP-α1, it is conceivable that this isoform would have different roles as compared with the others during early and critical periods of development.

3.2 HYPOTHETIC MECHANISMS UNDERLYING THE SPATIO-TEMPORAL EXPRESSION REGULATION OF SYNGAP ISOFORMS

The non-overlapping spatio-temporal regulation of SynGAP and, especially, its isoforms could be the result of several factors. Possible explanations, which are not mutually exclusive, are discussed below.

(1) Different expression of SynGAP and its C-term variants correlates with the developmental maturation of each brain area.

Crb is part of the Rhombencephalon (hindbrain) and does not belong to prosencephalon or forebrain as the other structures evaluated, thus it has different embryonic development and markedly different regulation of its maturation (Watson, Paxinos, and Puelles 2012). Specifically, Crb morphogenesis begins at E14 (Goffinet 1983), whereas in forebrain areas it proceeds postnatally (Ingalhalikar et al. 2015). Also, brain circuit formation is regulated developmentally and occurs in a wave-like sequential fashion, from region to region and across interregional layers (Meredith 2015). Indeed, myelination and synaptogenesis occurs in a conserved and region-dependent manner as their maturation progresses from

caudal to rostral (Inder and Huppi 2000) and from ventral to posterior axe (Crair and Malenka 1995; Bender, Rangel, and Feldman 2003; Maravall, Stern, and Svoboda 2004). Thus, this earlier cerebellar maturation would be in line with the rapid acquisition of adult SynGAP levels in this region. On the other hand, the OB, which is located at the other end of the caudo-rostral axis, also presents adult levels of SynGAP early in development (PND4/11). This observation would be in contradiction with a model in which SynGAP expression increases parallel to brain maturation. Yet, its position is more ventral than the other forebrain areas and hence, these results are not completely in disagreement with this hypothesis.

In line with this reasoning, the CAMKII-α promoter activity in the vast majority of excitatory forebrain neurons begins ~1 week after birth (Papadopoulos et al. 2008) which match with the bare detection of CAMKII-α at PND4 seen in Ctx, Hip and Str. As CAMKII-α is more expressed in OB and Crb than the other areas assessed at PND, suggests an earlier maturation of these 2 brain areas. Accordingly, it has been also reported in OB mature neurons by PND 15-30 (Petreanu and Alvarez-Buylla 2002).

Altogether, these data support the idea that an early maturation of a given brain area drives to an early acquisition of adult levels. An attractive way to test this hypothesis will be the study of specific temporal absolute expression of SynGAP C-term variants in each cortical and/or cerebellar layer as they posse different maturation paces (Altman, 1997; Tapias and Wang 2017).

(2) Levels of SynGAP C-term variants correlate with the degree of overall synapse and neuronal plasticity in a given brain area.

Several findings support premature acceleration of dendritic spine maturation, stabilization and plasticity in *Syngap1*$^{-/-}$ neurons and *Syngap1*$^{+/-}$ KO mice (Vazquez et al. 2004; Carlisle et al. 2008; Clement et al. 2012; Aceti et al. 2014; Ozkan et al. 2014). These have been postulated to shorten the critical period of cortical and hippocampal plasticity. Other reports show that a decrease in SynGAP-α2 is directly involved in abnormal spine maturation (Yokoi et al. 2017). As SynGAP C-term variants guide different neuronal and synaptic plasticity states (Tomoda et al. 2004; Rumbaugh et al. 2006; Krapivinsky et al. 2004; McMahon et al. 2012), their precise abundances might be important. If this is the scenario, the earlier increased expression of SynGAP-β deduced from targeted and IB approaches indicates that this variant could guide crucial events early in development, while SynGAP-α variants might be crucial for posterior events.

Accordingly, the mammalian brain maintains few developmental niches where neurogenesis persists into adulthood. One niche is located in the olfactory system since it continuously receives functional interneurons (Mizrahi, 2007). Accordingly, OB has a high degree of plasticity both at the synaptic and cell renewal level, which plays a central role in olfactory learning and memory functions (Laaris et al. 2007; Belluscio and Cummings, 2007; Gribaudo et al. 2009). As in OB and Crb, the SynGAP-β adult-like abundances are reached by PND4, before the other C-term variants assessed which suggests that SynGAP-β levels might correlate with the nascent immature neurons and/or brain areas with high plasticity states. In support of this notion, during binocular deprivation, before the time of eye-opening, spine motility is up-regulated without associated changes in spine density and class distribution during the peak of the visual critical period (PND28). In contrast, the motility is decreased from PND21 to PND28 and remains stable until PND42, so that at this age, observations of lower spine motility correlate with low plasticity of plasticity of mature synapses (Sala et al. 2008; Clement et al. 2012). Interestingly, SynGAP-β and CAMKII-α expression patterns, especially in Ctx, follow this trend, reinforcing the dependence of SynGAP-β expression on the developmental stage and synaptic plasticity state.

Taken together, present data strongly support the assumption that different SynGAP isoform amounts and its precise abundance regulation during development might contribute to different plasticity states both at neuronal and synaptic level in different brain structures. Because OB maintains enhanced neuronal replacement and plastic states that are altered in anosmic mice (Le Pichon et al. 2009), the study of SynGAP C-term variants expression in normal and anosmic mice could provide an evidence of this hypothesis.

(3) Different abundances of SynGAP proteins might correlate with the extend of apoptosis.

In addition to the previous outlined adult neuronal replacement in OB related events, the comparison between Ctx, Hip and Crb shows that significant inter-structure differences are found in the proliferation, differentiation, and apoptotic rates of newly generated or mature cells (Sherstnev et al. 2012). SynGAP levels correlate with the impact of the programmed cell death as *Syngap1*$^{-/-}$ die within the first postnatal week and SynGAP amount correlates negatively with caspase-3 activation and apoptotic rates in Hip (Oh et al. 2003; Knuesel et al. 2005; results chapter II). Furthermore, it has been reported a high neuronal death in an hippocampal adult *Syngap1*$^{+/-}$ KO model (Muhia et al. 2012); a reduction in body weight and brain size (Kim et al. 2003; Vazquez et al. 2004; Barnett et al. 2006) along with an atrophy of Crb in *Syngap1* LOF mutant mice and/or affected

SYNGAP1 LOF patients (Tomoda et al. 2004; Hamdan et al. 2011; Berryer et al. 2013; Mignot et al. 2016; Parker et al. 2015; Redin et al. 2014; Vlaskamp et al. 2019).

In summary, different apoptosis rates depending on the brain area and the developmental stage could explain, at least in part, why both the relative intra- and inter-structure expression of SynGAP and its C-term variants varies.

(4) SynGAP and its C-term variants expression levels might be different depending on the neuron type.

The principal neurons of brain structures are responsible for the maintenance of memory and learning behaviour (Sherstnev et al. 2012). The principal neurons of Crb are inhibitory, whereas OB contains a high number of inhibitory interneurons (Lledo and Lazarini 2007; Gribaudo et al. 2009) such as GABAergic principal periglomerular cells (Sakamoto, Kageyama, and Imayoshi 2014). Indeed, unlike the neocortex, GABAergic inhibitory interneurons in the OB greatly outnumber principal neurons by 50–100:1 (Sakamoto, Kageyama, and Imayoshi 2014). Conversely, the principal neurons of Hip, Ctx and Str are examples of high density spiny excitatory neurons (Sheng and Hoogenraad 2007; Benavides-Piccione et al. 2013; Yuste 2011). Despite SynGAP is expressed in both spiny and non-spiny excitatory (Moon et al. 2008) and inhibitory neurons (Moon et al. 2008; Berryer et al. 2016), probably spiny excitatory neurons might express more SynGAP as there should be more PSD per neuronal unit. Therefore, if it is assumed that inhibitory neurons express less SynGAP, then it would explain the lower expression of SynGAP and certain C-term variants in OB and Crb at PND11 onwards compared to the other brain regions. In support of that, the analysis of the C-term isoforms of SynGAP in cortical layer IV where excitatory synapses are made onto somas of inhibitory interneurons, revealed a preponderance of SynGAP C-term variants different from SynGAP-α1 (Li et al. 2001; Barnett et al. 2006).

Alternatively, based on the type of principal neurons, a predominance of the type of synaptic transmission that classify them could be expected. For instance, as in Crb and OB the principal neurons are inhibitory, is possible to find more inhibitory synapses than other brain areas. Because SynGAP-β did not correlate with the expression of SynGAP-α1 and PSD-95 in any brain area or OB and Crb, respectively it could have other roles beyond those at PSDs such as at inhibitory synapses. Accordingly, early in development the inhibitory neurons and inhibitory synaptic markers (e.g., Neuroligin-2) are expressed before than excitatory ones, suggesting that more inhibitory synapses could be expected to develop prior to the excitatory ones (Wu et al. 2018).

Therefore, a reduced expression of SynGAP-α1 but not the other variants in early developmental ages could be explained by a more prominent regulation of excitatory spine synapses. This hypothesis will be further discussed and supported by other evidences in the following section 6.

(5) Areas related to higher cognitive functions have greater diversity of SynGAP expression patterns.

Areas controlling higher cognitive function contain the greatest synapse diversity (Zhu et al. 2018). Thus, higher expression of SynGAP found in Ctx, Hip, Str vs. Crb and OB could be explained by its capacity to regulate evolved higher cognitive tasks in mammals.

4. EXPRESSION OF C-TERM CONTAINING SYNGAP ISOFORMS IN HUMAN CORTEX

Aged-dependent decrease in the expression of PSD proteins (e.g., NR1, GluR2) and spine density has been reported. These phenomena are likely associated with normal cognitive decline (Hof et al. 2002; Yuste and Bonhoeffer 2004). The evaluation of protein extracts from old human and mouse samples in this thesis offered the opportunity to study changes of neurobiological markers that lead to impaired or preserved memory.

SynGAP, as well as the isoforms containing the C-term variants α1, α2 and β, were found expressed in the human cortex. This is the first time that these isoforms are reported to be expressed in the human cortex at the protein level. Furthermore, the analysis of samples from individuals at very different ages indicated that all these proteins are likely to be expressed throughout human life. Other postsynaptic proteins, PSD-95 and CAMKII-α, were also investigated, and the exact same conclusions were arrived at as for total SynGAP. Parallel analysis of mouse samples, of up to 26 months of age, also suggested that SynGAP, its investigated isoforms and the other two postsynaptic proteins are expressed throughout the whole life, like in humans. Despite there is one residue of difference between human and mouse epitope used to develop SynGAP-β antibody utilized in this work, the human immunoreactivity of SynGAP-β was enough to allow its study by IB. Certainly, the assessment of these three SynGAP C-term variants in humans will help to understand the neurobiology of SynGAP and might be beneficial for the development of therapies for *SYNGAP1* genetic rare variants with a negative impact in humans.

Besides the validation of the immunoreactivity of these antibodies in human samples, biochemical solubilization of proteins with 1% DOC showed that the vast majority of SynGAP remains in the pellets. This finding indicates that the solubilization protocol for human samples, which was developed for rodent samples, needs to be further optimized. Alternatively, the fact that SynGAP in the human brain is associated with more complex structures and/or trapped with insoluble fractions can not be fully discarded. Consequently, crude homogenate or reconstituted homogenate samples were used, although these samples are less suitable to work with as they contain cell debris, nuclei and other molecules that highly increase technical variability.

5. ABSOLUTE QUANTIFICATION OF SYNGAP AND ITS C-TERM VARIANTS

The relatively recent AQUA method developed for targeted proteomics allowed quantifying SynGAP at the fmol scale (fmol/µg of protein; Gerber et al. 2003). Yet, not all unique peptides assessed performed properly as indicated the comparison between two different core peptides. Namely, the core peptide labelled as 1, reproduced better the sum of the SynGAP C-term variants quantified, whereas the SynGAP-Core2 peptide did not. However, statistical analysis of SynGAP-core1 expression indicated that adult levels would be already achieved by PDN21, whereas SynGAP-core2 showed that adult levels would be reached by PND56 matching with our IB results. This discrepancy is likely to be caused by the high variability in the fmols quantified in each biological replica with SynGAP-Core1 peptide at PND56. Therefore, the fact that SynGAP adult levels in Ctx are attained at PND56 was corroborated by two orthogonal methods (IB and MS). In addition, the AQUA of SynGAP-α2 presented very low, almost undetectable, levels. This result is in stark contrast with both the IB data and the discovery proteomics experiments performed in this chapter. As a result, these AQUA values were regarded as a technical mismatch.

Bearing these inconsistencies in mind, SynGAP-α1 expression pattern found by targeted proteomics agrees with IB results, whereas SynGAP-β partially matches with IB data since the peak expression at PND21 was not seen. Nevertheless, the main findings of these experiments were the prominent expression of SynGAP-β and -γ in perinatal ages and that these isoforms were expressed in higher amounts than SynGAP-α1/2. These results are in accordance with reports showing larger SynGAP-β clusters than SynGAP-α1 in adult Hip (Li et al. 2001; Moon et al. 2008). Isoforms containing SynGAP-γ showed a constantly increasing expression trend, although statistically significant abundance differences were only observed between PND56 and all other ages. Thus, SynGAP-γ expression pattern resembled that of SynGAP-α1. In addition, this data showed that, at PND56, isoforms presenting the SynGAP-γ C-term would be significantly more expressed than any other isoforms.

To our knowledge, there is only one report assessing the developmental expression of *Syngap1*-γ by qPCR, which indicate a reduced expression of its mRNA as compared with that of other variants (Li et al. 2001). As previously noted, the expression levels of proteins might not correlate with their transcription level, thus this previous finding does not necessarily invalidate present data. Thus, generation of a SynGAP-γ antibody would yield

new information complementary to MS data, which will be key in the advance the understanding of the functional significance of SynGAP isoforms.

In summary, the AQUA of SynGAP C-term variants supported a prominent expression of SynGAP-β in early stages of cortical development, agreeing with what was found by IB in the present work. These data also showed a developmental regulation of SynGAP-γ in Ctx and an unexpectedly higher expression of the isoforms containing this variant, as compared with the other ones, specially at PND56. Hence, whether isoforms containing SynGAP-γ and -β variants play key roles in early stages of cognitive development requires further investigation. Nonetheless, to fully validate these findings, a reassessment of the absolute amounts of all SynGAP C-term variants would be desirable as well as the investigation of all N-term variants.

6. SUBCELLULAR LOCALIZATION OF SYNGAP AND ITS C-TERM VARIANTS

SynGAP and its isoforms are subjected to different spatio-temporal regulation within different brain structures as previously demonstrated, suggesting distinct roles. Another step towards the comprehension of these distinct functionalities of each SynGAP C-term variant, is the determination of their subcellular localization. Thus, subcellular distribution analyses of total SynGAP and SynGAP-α1, -α2 and -β were performed across several stages of cortical development as well as using adult Hip samples.

6.1 PROTEIN YIELD OF DIFFERENT SUBCELLULAR FRACTIONS

The assessment of the protein yield (µg of proteins/mg of tissue) of the different fractions obtained throughout the PSD enrichment procedure indicated that by PND14, the yield of total protein extracts was found quite similar with that of at later ages. In fact, the yields of S1, cytosolic and total membrane (TM) fractions were found alike in PND14, 21 and 56. Similarly, the synaptosome fraction contained increasing amounts of protein from PND14 onwards. However, the amount of protein found in SNP seemed to be progressively placed into the PSD fraction, as SNP yield decreased towards adult while PSD yield increased. Indeed, yield from PSD samples attained its maximum at PND21 and tended to decrease by PND56, although this difference did not reach statistical significance. Therefore, it is interesting to note that PSD yield progression would run parallel to that of synapse density.

This work showed that total SynGAP mainly localized in the cytosolic fraction until PND21, in contrast to PSD-95, which by PND14 was found significantly enriched at the PSD and localized in the cytosol in very little amounts. By PND56, cortical total SynGAP was significantly more located at the PSD, although a substantial amount remained in the cytosol. Furthermore, in adult hippocampus total SynGAP expression at the PSD was also higher than in the cytosol, yet this difference was not big enough to reach statistical significance.

Few reports have emphasised a cytosolic localization of SynGAP, but its immunoreactivity was seen in the cell soma, growth cones and neurites of granule cells in Crb (Tomoda et al. 2004; Moon et al. 2008), and in other extra-synaptic locations across the brain (Barnett et al. 2006; Moon et al. 2008). As a result, it is widely accepted that SynGAP is predominantly placed to the PSD, like PSD-95, but the present work strengthens the need to update this concept.

6.2 SUBCELLULAR DISTRIBUTION OF SYNGAP ISOFORMS THROUGHOUT DEVELOPMENT

In early ages, where synapses would be still immature and the synapse density would increase progressively, SynGAP isoforms containing -α2 and -β variants, but not those presenting the α1 sequence, were found significantly more expressed at the cytosolic fraction from Ctx without premotor/prefrontal area. As development progresses, all SynGAP isoforms were found increasingly incorporated at the PSD, although at different degrees. Namely, by PND21 α1-containing isoforms were almost completely found at the PSD, whereas α2-containing ones were equally expressed at both cytosolic and PSD fractions. Interestingly, these proportions were maintained even at PND56. However, β-containing isoforms, although they presented an increased PSD location at PND21 and 56, they were still found significantly enriched at the cytosolic fraction. These results were further validated by the analysis of the adult hippocampal subcellular localization of SynGAP isoforms as showed the same subcellular distribution of these variants.

Of note, the subcellular distribution of SynGAP-α1 isoforms in Ctx without premotor/prefrontal area followed an expression pattern similar to that of PSD-95, specifically from PND21 onwards. This finding agrees with the previous correlation studies of their expression in total extracts throughout development. Despite SynGAP-α2 was found to retain some cytosolic localization in adult, both Ctx and Hip subcellular distributions point out to a predominant synaptic role at adult ages, as for SynGAP-α1. Altogether, these findings emphasise the synaptic role of SynGAP-α1/2 previously described by others for total SynGAP (Vazquez et al. 2004; Rumbaugh et al. 2006; Yang et al. 2011;2013; Dosemeci et al. 2015). Importantly, the present data reveal a prominent role of SynGAP-β isoforms in cytosolic compartments, which would be maintained throughout life. This is in stark contrast with the functions of SynGAP-α1/2 isoforms since particularly in adulthood, they would be primarily found at the PSD. In line with this idea, it has been reported that mRNAs with retained introns are transported to and spliced within dendrites (Glanzer et al. 2005). Therefore, this mechanism, could explain, at least in part, the SynGAP-β predominant location in cytosol since the *in-silico* analysis showed that it retains part of an intronic sequence. Finally, these data together with the previous analyses (e.g., *in-silico* studies*,* correlation of SynGAP-α1 and -β expression throughout development…), emphasise again differential regulation of SynGAP-β at both transcript and protein level to that of other SynGAP C-term variants.

6.3 HYPOTHESIS OF THE DIFFERENT SUBCELLULAR DISTRIBUTION OF SYNGAP ISOFORMS PRESENTING DIFFERENT C-TERM VARIANTS.

The differential subcellular distribution of SynGAP isoforms with different C-term variants opens new questions and possible answers to explain its regionalized expression pattern as previously introduced and further discussed here. An attractive hypothesis arising from the present work, is that SynGAP C-term variants could mediate prominent roles in distinct types of synapses. Importantly, most glutamatergic synapses are found in spines, whereas most GABAergic and electric synapses are formed onto dendritic shafts, as well as on the soma and proximal axonal regions (Kaneko and Fujiyama 2002; Keith and El-Husseini 2008; Knott et al. 2006). In addition, owing that shaft and electrical synapses are more prominent in early stages of development (Difiglia, Pasik, and Pasik 1980; Antonopoulos et al. 2002; Knott et al. 2006; Yuste and Bonhoeffer 2004; Pereda et al. 2014), the synaptic components of these synapses could be expected to be found in the cytosol fraction.

6.3.1 ROLE OF ALPHA1-CONTAINING SYNGAP ISOFORMS

PSD-95 is one of the earliest detectable proteins in the PSD (Gomperts 1996) that induces clustering of a number of NT receptors and scaffolding proteins, related to excitatory but not inhibitory synapses (El-Husseini et al. 2002; Kim and Sheng 2004; Zhang et al. 2009). The data reported here about the expression of PSD-95 along development fits well with previous reports, showing increasing expression of PSD-95 with development, in particular, a specific steep increase from PND11 to PND21 and its higher expression in PSDs from forebrain relative to that in Crb (Porter et al. 2005; Cheng et al. 2006; Zhang et al. 2009; Zheng et al. 2012; Henriquez et al. 2013). Also, PSD-95 expression in total extracts correlated with the levels seen in the PSDs, indicating that it mainly localizes to the postsynapse (Petralia et al. 2005). Thus, the positive and significant correlation of PSD-95 and SynGAP-α1 in most brain structures assessed, together with the clear SynGAP-α1 localization in the PSD, supports an almost exclusive expression of α1-containing isoforms in excitatory synapses.

6.3.2 ROLE OF BETA-CONTAINING SYNGAP ISOFORMS

Because expression of SynGAP-β isoforms seem to predominate in early stages of development, their expression patterns do not correlate with SynGAP-α1 and they have a cytosolic localization, a role in inhibitory and electric synapses or a non-synaptic function can be expected.

First, statements in support of SynGAP-β role in inhibitory synapses are: (1) SynGAP interacts with GABA receptor and transporter subunits in developing and adult Ctx (Wilkinson et al. 2017; preliminary data not shown in the present thesis); (2) SynGAP-α1 and -β immunohistochemical labelling showed that SynGAP-β has a prominent localization at inhibitory synapses (co-localized with Gephyrin and GAD), while SynGAP-α1 localizes mainly at excitatory synapses (Moon et al. 2008); (3) CAMKII-α translocates from excitatory to inhibitory synapses under low Ca^{2+} being probably in its non-phosphorylated form, where it interacts with SynGAP-β (Li et al. 2001; Marsden et al. 2010); (4) in Chapter II is shown how different *Syngap1*$^{+/-}$ mouse models present alterations in the abundance of proteins related to inhibitory neurotransmission, and (5) earlier acquisition of SynGAP-β adult levels in OB and Crb, where principal neurons are inhibitory, also supports this hypothesis. Indeed, immunostaining studies in OB indicated a wide location of SynGAP-α1 in the whole OB, excluding new-born regions, from the rostral migratory stream. In contrast, SynGAP-β immunolabelling showed a marked restricted staining in the regions with high density of inhibitory neurons (Moon et al. 2008). Hence, it would be very interesting to further study SynGAP-β and its roles in inhibitory synapses.

Second, supporting evidence regarding a possible role of SynGAP-β in electric synapses are: (1) the revision of the clinical features presented in ASD (see I-5.5) as well as MRD5 patients (See I-5.6.1; Parker et al. 2015; Vlaskamp et al. 2019; personal communications with affected families) such as γ oscillations and sleep disturbances are mainly related to impairments in inhibitory (Bartos, Vida, and Jonas 2007; Berryer et al. 2016) and electrical synapses (Galarreta and Hestrin, 2001; Buhl et al. 2003); (2) electric synapses also show plasticity and the expression of kinases such CAMKII-α, which interacts with SynGAP-β (Li et al. 2001; Pereda et al. 2014); (3) SynGAP interacts with gap junction proteins ZO-1 and ZO-2, specially during the first postnatal week of development while we found alterations in the abundance of gap junction proteins in *Syngap1*$^{+/-}$ mice (see results Chapter II), and finally (4) there is a frequent occurrence of gap junctions between dendrites of GABAergic interneurons of particular types (Fukuda, 2007). Thus, future studies addressed to determine the contribution of SynGAP and specially, SynGAP-β isoforms, in the regulation of gap junction plasticity and synchronous activities of coupled neurons, could help understanding the pathophysiology of MRD5.

Third, a non-synaptic role for SynGAP-β isoforms should not be excluded. Accordingly, (1) these isoforms are expressed more abundantly at PND0-11, when there are fewer synapses, this is directly shown by targeted proteomics and indirectly, by IB data; (2) despite from PND21 onwards a proportion of cortical SynGAP-β was found to be targeted to the PSD, it would be highly located at the cytosol even in adult Ctx and Hip. This data

agrees with larger SynGAP-β clusters observed by immunohistochemistry in hippocampal dendrites as compared with SynGAP-α1 clusters (Moon et al. 2008); (3) SynGAP-β is reported to bind specifically with α-Internexin, an intermediate filament protein that connects dendritic shaft cytoskeleton with spinoskeleton (Benson et al. 1996; Li et al. 2001); (4) SynGAP-β staining without co-localization of excitatory or inhibitory synaptic markers has been shown in neurons from Hip, although this non-synaptic clusters have been suggested to belong to transport vesicles (Vazquez et al. 2004; Knuesel et al. 2005; Moon et al. 2008). However, if this hypothesis is true, it should apply for all SynGAP C-term variants and that is not the case; (5) based on the liquid-liquid transition phase model of PSD formation, SynGAP CC domains are required for trimerisation of SynGAP molecules. *In-silico* analyses showed that this domain in SynGAP-β is reduced and it is directly attached to its unique sequence compared to the other C-term variants as previously mentioned, thus this protein could have less affinity to form trimers and be less targeted to the PSDs (Zeng et al. 2016;2017); (6) a nuclear localization of SynGAP-β has been reported (Moon et al. 2008), and (7) our preliminary discovery MS studies could identify unique peptides from SynGAP-β in total extracts, whereas others failed to identify them in PSD fractions (McMahon et al. 2012). Thus, these data directly or indirectly suggest a predominant abundance of SynGAP-β in non-synaptic fractions.

6.3.3 Role of alpha2-containing SynGAP isoforms

Regarding α2-containing isoforms expression and subcellular localization, they followed an intermediate trend between α1 and β isoforms. Thus, while the role of these isoforms in excitatory synapses is strongly supported by the present thesis and previous research (McMahon et al. 2012, Araki et al. 2015), their possible role in inhibitory synapses has never been suggested. Yet, their expression pattern and subcellular localization resembles that of SynGAP-β, especially early in development. Namely, α2 variants were found mainly expressed in the cytosol during the first two postnatal weeks, such as β ones.

It is for this reason that a role of α2-containing isoforms in inhibitory synapses can be hypothesized. Alternatively, as indicated for SynGAP-β isoforms, they could have an extra-synaptic role, in this case what would exactly be the extra-synaptic functions of α2 or β isoforms in forebrain brain areas, is unknown. Collectively, these data strengthen the need to better study SynGAP isoforms containing the α2 variant. Immunohistochemical analyses of this C-term variant throughout development and in different brain areas, similar to what has been reported for α1 or β variants in Moon and co-workers, could help understanding their subcellular locations beyond excitatory synapses (Moon et al. 2008).

In summary, the present work further corroborates the well-known excitatory synaptic localization of all SynGAP isoforms assessed, but strongly supports a predominant role of α1 isoforms in excitatory synapses, a main role of β-isoforms outside excitatory synapses and a more promiscuous subcellular localization for α2-isoforms. Accordingly, there are examples of synaptic proteins with an exclusive expression in inhibitory or excitatory synapses and examples of proteins that reside in both types. For instance, Neuroligin-1 is mainly found in excitatory synapses (Song et al. 1999; Sumita et al. 2007) in opposition to Neuroligin-2, which is in inhibitory ones (Varoqueaux, Jamain, and Brose 2004). On the other hand, Neuroligin-3 and -4 are found in both type I and II synapses (Chubykin et al. 2007; Tabuchi et al. 2007; van Spronsen and Hoogenraad 2010; Hoon et al. 2011). Other examples are S-SCAM, which is mainly found in inhibitory synapses and PSD-95 which is exclusive of excitatory synapses (Prange et al. 2004; El-Husseini et al. 2002; Keith and El-Husseini 2008). Also, CAM IgSF9b is exclusively expressed in inhibitory synapses, in contrast with a wide range of other CAMs found in excitatory synapses (Woo et al. 2013). Hence, based on these examples, the present hypothesis in which SynGAP isoforms could be found in different types of synapses is plausible.

CHAPTER II

CII-INTRODUCTION

It is believed that overlapping behavioural manifestations of neurological diseases may be related to impaired regulation of synaptic protein abundances (Kelleher and Bear 2008; Zoghbi and Bear 2012). As the possible alterations of the PSD proteome abundances in *Syngap1* KO have not yet been reported, we aimed to relatively quantify by LC-MS/MS the hippocampal PSD proteome in *Syngap1*$^{+/-}$ [HET] mice and compare it that in normal tissue (*Syngap1*$^{+/+}$ [WT]) by using *Syngap1* conditional KO mouse line for genetic rescue studies (Fig. I-21).

Nowadays, the earliest age of *SYNGAP1* LOF diagnosis in humans is after 2-3 years, when cognitive skills such as language can be suspected to be abnormal. Based on several biomarkers, this age is equivalent to PND21 in mice (Semple et al. 2013; Gonzalez-Lozano et al. 2016; Fig. I-16). Also, SynGAP controls synapse maturation during a specific critical period of hippocampal development, which ends at PND21 (Clement et al. 2012; Jeyabalan and Clement, 2012). At this age, SynGAP is already expressed at its adult levels in hippocampus (see results from Chapter I). For these reasons, PND21 was chosen as the age to rescue SynGAP expression (*Syngap1*$^{+/-;Cre+/-}$ [RES]) and assess the dynamics of the hippocampal proteome at young adult mice (PND56; Fig. I-16&21).

In addition, to further understand the roles of SynGAP at the PSD and determine possible other critical periods of SynGAP regulation in dendritic spines, the impact of *Syngap1*$^{+/-}$ haploinsufficiency was evaluated when induced at PND21 by using a conditional *Syngap1*$^{+/-;Cre+/-}$ mice line for KO induction (IND). In this case, we also tested the effects of this heterozygosity induction 4 weeks post-treatment of TMX, i.e., at PND56 (Fig. I-21).

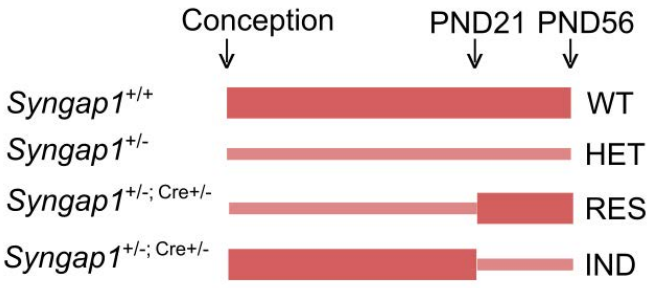

Figure I-22. Scheme of the expected SynGAP expression levels in *Syngap1* conditional KO mouse lines for genetic rescue experiments and KO induction. Thick lines represent normal SynGAP expression levels while slender lines indicate reduced expression of SynGAP by half of normal levels.

CII-MATERIALS AND METHODS

1. BIOLOGICAL MATERIALS AND METHODS

1.1 MOUSE LINES

Two conditional *Syngap1* KO lines were used, these are further described in Clement et al. (2012). These two lines were: 1) a *Syngap1*$^{+/-}$ conditional KO mouse line for genetic rescue experiments and 2) a *Syngap1*$^{+/-}$ conditional mouse line for KO induction. Mice used in this chapter were from F2 and later generations. Both lines were crossed with a Cre$^{+/-}$ transgenic mice line in which the Cre-recombinase is ubiquitously expressed and only activated after TMX administration (Cre-line Jackson's Lab reference: Tg [CAG-cre/Esr1*]5Amc/J).

Specifically, *Syngap1*$^{+/-}$ conditional KO for genetic rescue studies crossed with the Cre-line resulted in *Syngap1*$^{+/-;Cre-/-}$ (HET) offspring with a *Syngap1* floxed allel that contained a loxP-Neo/STOP-loxP construct within a region common to all *Syngap1* isoforms. Cre-mediated recombination of this construct results in the deletion of the loxP-Neo/STOP-loxP cassette, restoring the expression of the *Syngap1* gene in *Syngap1*$^{+/-;Cre+/-}$ (RES) mice. Importantly, in addition to the HET and RES littermates, *Syngap1*$^{+/+-;Cre-/-}$ (WT) control mice were used.

In contrast, the genetic construct from the *Syngap1*$^{+/-;Cre+/-}$ conditional mice line for KO induction (IND mice) presents an insertion of loxP sequences flanking exons 6-7. Therefore, Cre-mediated recombination results in the deletion of exons 6-7 leading to a LOF mutation of *Syngap1* and its haploinsufficiency. In this case, the control mice used was Syngap1$^{+/+;Cre-/-}$ (WT) from this mouse line.

For LTP experiments, IND mice were compared with a *Syngap1* conventional KO mice (described in Table M-1). These experiments were carried by Dr. Sabyasachi Maity from Dr. Gavin Rumbaugh research group at The Scripps Research Institute. Male/ Female aged 9 to 12 weeks were used for all experiments. These animals were housed in the Scripp's animal facility under the guidelines of the TSRI Animal Care and Use Committee.

2. MATERIALS AND METHODS FOR GENOMIC SPECIMENS

2.1 POLYMERASE CHAIN REACTION FOR GENOTYPE DETERMINATION

Mouse genotype was determined by standard PCR. Each of the conditional lines had its specifically designed PCR strategy; PCR reaction mix and thermocycle conditions (Fig. MII-1). Genomic DNA was extracted from mouse tail. General procedures, including sample preparation or electrophoretic conditions are described in section M-2 of general methods.

A

	Primer for *Syngap1* conditional KO mice lines screening		
	Primer name	5'-3' primer	Fragment size (bp)
A	66104sa-RUM2	(F) CACCTATGACTTATTTTTGAGGTCCTGATATGG	No band (WT)
	0070-Neo-16219sa	(R) CCTGCTCTTTACTGAAGGCTCTTTACTATTGC	3,433 (HET)
B	57106flp-RUM1	(F)AGGCCAAGGTGAGCACTGTGGC	431(WT)
	57105flp-RUM1	(R) TCAGATGGTTGGAGGTGGGGT	563(Floxed allel)
C	oIMR1084	(F) GCGGTCTGGCAGTAAAAACTATC	100 bp (Transgene)
	oIMR1085	(R) GTGAAACAGCATTGCTGTCACTT	
	oIMR7338	(F) CTAGGCCACAGAATTGAAAGATCT	324 bp (No transgene)
	oIMR7339	(R) GTAGGTGGAAATTCTAGCATCATCC	

B

	PCR reaction mix final concentrations			
	A (Res Ind)	B (KO Ind)	C (Cre)	µl/rx
Genomic DNA	10	10	>10	ng
Primers	0.75	0.75	0.75	µl each
dNTPs	1.25	1.25	1.25	mM
Buffer	1x buffer buffer 3	1x Taq buffer with Mg2+	1x Taq buffer with Mg2+	vol
DNA polymerase	0.5	0.2	0.5	µl each
Reaction vol	25	25	25	µl

C

	PCR thermocycling conditions			
	Step	Tª (°C)	Duration	Cycles
Syngap1 conditional KO screening	1	94	2 min	1
	2.a	94	30 sec	
	2.b	65	30 sec	35
	2.c	68	2 min	
	3	68	8 min	1
	4	10	Infinity	1
Syngap1 conditional KI screening	1	94	2 min	1
	2.a	94	30 sec	
	2.b	65	30 sec	35
	2.c	68	5 min	
	3	68	8 min	1
	4	4	Infinity	1
Cre transgene screening	1	94	3 min	1
	2.a	94	30 sec	
	2.b	51.7	1 min	35
	2.c	72	1 min	
	3	72	2 min	1
	4	10	Infinity	1

D

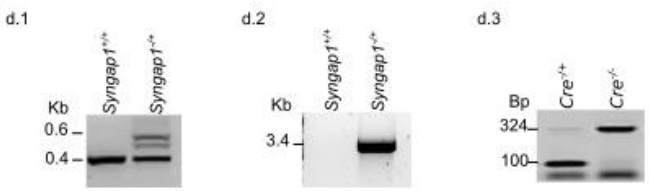

Figure MII-1. PCR conditions for *Syngap1*$^{+/-}$ and Cre$^{+/-}$ screening. (A) Primers used and expected size. (B) Final concentrations of the PCR reaction mix prepared. *Expand long range DNA polymerase or ** Taq DNA polymerase was used. (C) PCR thermocycling conditions (D) Examples of PCR electrophoresis of expected amplicons per each genotype screened. (d.1) Screening for IND. (d.2) Screening for RES. (d.3) Screening of Cre transgene detection. Cre$^{-/-}$ stands for no transgene presence. All but, Cre derived amplicons were run into 1% and 3% agarose gel, respectively.

3. MATERIALS AND METHODS FOR PROTEIN ANALYSIS

3.1 PROTEIN EXTRACTION

Hippocampal PSD enriched samples from all genotypes assessed and both mouse lines were prepared following the same procedures. Each sample arose from the pool of hippocampus (Hip) from 2 mice of the same genotype and gender and a total of 3 biological replicates for each gender were conducted. Thus, a total of 6 biological replicates for each genetic condition were used for both IB and LC-MS/MS analysis. Mouse hippocampal PSD fractions were obtained as previously described (See M-3.1.2) and performed using the same methods, buffers and equipment within the same week and in parallel whenever possible.

3.2 IMMUNOBLOT ANALYSIS

Genotypes were confirmed by SynGAP IBs using PSD fractions of 8-week-old animals (Abcam, see Table M-5). Those samples that better match with the expected SynGAP expression levels in a given genotype were selected for subsequent studies. IBs intended to verify PSD enrichment were done with antibodies against SynGAP and PSD-95 (Table M-5). These were blotted onto the same PVDF membrane (Merck-Millipore). The specific number of replicas for each IB study of this section are indicated in the figure legends. Conventional polyacrylamide using PSD-95 as a loading control or 7.5/12% SF gels were used for sample normalization in addition to the posterior IB normalization steps previously described (see M-3.6). Antibodies and conditions used for validation LC-MS/MS data by IB in RES mice line such as HRas, Dynactin2 or Cofilin-2 are shown in Table M-5.

3.3 SAMPLE PROCESSING FOR LC-MS/MS ANALYSES

Proteomics analysis by LC-MS/MS conducted in this chapter were done in collaboration with the Proteomic Group from the Vall d'Hebron Institut d'Oncologia (VHIO), under Dr. Canals supervision. To this purpose, up to 25 µg of PSD enriched fractions were loaded into conventional 6% polyacrylamide gels. *Coomassie* stained gels were placed onto white-light imaging device and each lane was cut into 6 bands (see Fig. M-4). Gel bands were maintained at -20ºC until processing.

3.3.1 Protein reduction and alkylation

Each gel band was cut into 1x1 mm cubes with a scalpel blade in a previous cleaned glass with EtOH (Merck) in a laminar flow hood and transferred to 1.5 mL tubes for proteomic

analysis (0030 123 328; Eppendorf). 200 µL of 50 mM bicarbonate ammonic (BA) mixed with 50% EtOH was added to each dissected gel band. After a brief vortex, samples were incubated 20 min at RT. The supernatant was removed and then 200 µL of absolute EtOH was added and incubated during 15 min at RT. Once the small gel dices were white, the supernatant was removed and 200 µL of freshly prepared 10mM DTT (dithiothreitol; Merck) in 50mM BA was incubated with the dices 1h at 56 ºC. Afterwards, the supernatant was discarded again and 200 µL of IAA (iodacetamide; Merck) 55 mM in 50 mM BA freshly prepared was dark-incubated during 30 min. Before sample digestion, the supernatants were removed and 200 µL of 25 mM BA was added and dark-incubated for 15 min.

3.3.2 IN-GEL PROTEIN DIGESTION

Supernatant was removed from the tube and 200 µL of 25 mM BA-50% acetonitrile (ACN) was added to each sample and incubated for 15 min. This step was repeated one more time and after discarding the supernatant, 100 µL of 100% ACN were used to dehydrate gel dices and incubated 10 min. Trypsin (Promega) containing solution (the stock concentration: 0.2 µg/µL) was prepared according the estimated volume of 25 mM BA assigned to each gel band (e.g., big gel bands were soaked with 220 µL whereas medium and smaller gel bands with 140 µL and 100 µL, respectively) depending on the dimensions to assure the complete soaking of the gel bands within the solution. Specifically, 0.2 µL of trypsin was added to each 15 µL of 25 mM BA and samples were incubated ON at 30ºC.

3.3.3 PEPTIDE EXTRACTION

Up to 8 µL of 100% ACN was added per each 15 µL of trypsin. Then samples were vortexed (Fisherbrand) and incubated for 15 min at 37ºC. Later, 130 µL of 0.2% trifluoroacetic acid (TFA) was added and incubated for ~30 min at RT. Supernatants were transferred to 0.5 mL tubes (#0030 123 301; Eppendorf) previously washed with ACN to prevent peptide binding to the walls and carefully avoiding touching the gel fragments. The liquid phase was evaporated through SpeedVac (Thermo-Fisher Scientific) and dried peptides were resuspended in 25 µL of 5% ACN and 0.1% formic acid. Afterwards, samples were sonicated 2 min in bath and were vortexed. Samples then were centrifuged for 5 min at RT and maximum speed to check that no pieces of gel remained in the Eppendorf. Once it was assured, samples were stored at -20ºC. 12 µL for bands 1, 2 and 3 or 3 µL for bands 4, 5 and 6 were injected for LC-MS/MS analyses.

3.4 LIQUID CHROMATOGRAPHY COUPLED TO TANDEM MASS SPECTROMETRY ANALYSES

For LC-MS/MS studies tryptic digests were analysed using a linear ion trap Velos-Orbitrap mass spectrometer (Thermo Fisher Scientific, Bremen, Germany). Instrument control was performed using Xcalibur software package, version 2.1.0 (Thermo Fisher Scientific, Bremen, Germany). Peptide mixtures were fractionated by on-line nanoflow liquid chromatography using an EASY-nLC system (Proxeon Biosystems, Thermo Fisher Scientific) with a two-linear-column system. Digests were loaded onto a trapping guard column (EASY-column, 2 cm long, ID 100 µm, packed with Reprosil C18, 5 µm particle size from Proxeon, Thermo Fisher Scientific) at a maximum pressure of 160 Bar. Then, samples were separated on the analytical column (EASY-column, 10 cm long, ID 75 µm, packed with Reprosil, 3 µm particle size from Proxeon, Thermo Fisher Scientific). Elution was achieved by using a mobile phase from 0.1% formic acid and 100% acetonitrile with 0.1% formic acid and applying a linear gradient from 5 to 35% of buffer B for 120 min at a flow rate of 300 nL/min. Ions were generated applying a voltage of 1.9 kV to a stainless steel nano-bore emitter (Proxeon, Thermo Fisher Scientific), connected to the end of the analytical column.

The LTQ Orbitrap Velos mass spectrometer was operated in data-dependent mode. A scan cycle was initiated with a full-scan MS spectrum (from mass to charge [m/z] 300 to 1600) acquired in the Orbitrap with a resolution of 30,000. The 20 most abundant ions were selected for collision-induced dissociation fragmentation in the linear ion trap when their intensity exceeded a minimum threshold of 1000 counts, excluding singly charged ions. Accumulation of ions for both MS and MS/MS scans was performed in the linear ion trap, and the AGC target values were set to 1×10^6 ions for survey MS and 5000 ions for MS/MS experiments. The maximum ion accumulation time was 500 and 200 ms in the MS and MS/MS modes, respectively. The normalized collision energy was set to 35%, and one microscan was acquired per spectrum. Ions subjected to MS/MS with a relative mass window of 10 ppm were excluded from further sequencing for 20 s. For all precursor masses a window of 20 ppm and isolation width of 2 Da was defined. Orbitrap measurements were performed enabling the lock mass option (m/z 445.120024) for survey scans to improve mass accuracy.

LC-MS/MS run associated data was analysed and normalized using Progenesis software (Nonlinear Dynamics, Newcastle, UK). This software allows review of the chromatogram alignments, filtering the data, review peak picking, normalize the data and identify peptides among other features. Specifically, sample ions were automatically aligned to compensate

for drifts in retention time between runs. Yet, they were also reviewed and edited manually. The peak picking limits were automatic, the main ion charge selected was set at 4 and the retention time limits were adjusted according the chromatograms in each sample. Peptide ions were filtered by removing those with a charge of 1 or >4, *m/z* from 300 to 1,600 and the specific retention determined for each case was also set. A normalization step was conducted as it was required to allow comparisons across different sample runs. This normalization was done by assuming that a significant number of peptide ions are unaffected by experimental conditions and the factor by which the sample as a whole varies was used to normalize back to its reference sample in each band from all genotypes analysed.

3.4.1 PROTEIN IDENTIFICATION

Peptides were identified through MS/MS spectra search against the protein database using the search engine MASCOT (Matrix Science, London UK) operated through Proteome Discoverer (Thermo Scientific) to search the SwissProt database (20160108, taxonomy restricted to *Mus musculus*, 16,754 sequences). MS/MS spectra were searched with a precursor mass tolerance of 10 ppm, fragment tolerance of 0.5 Da, trypsin specificity with a maximum of 2 missed cleavages, cysteine carbamidomethylation set as fixed modification and methionine oxidation as variable modification. The quantification method applied to quantify protein abundances was a label-free based approach. MS signal intensities for all non-conflictive peptides (unique peptides) identified from a given protein were integrated to obtain a quantitative value.

The Scaffold software version 4.0.5 (Proteome Software Inc., Portland, OR) was used to validate LC-MS/MS based peptide and protein identifications. Peptide identifications were accepted if were greater than 95,0% probability of an incorrect identification by the Peptide Prophet algorithm (Keller et al. 2002). Protein identifications were accepted if they could be established at greater than 99,0% probability to achieve an FDR less than 1,0% and contained at least 2 identified peptides. Protein probabilities were assigned by the Protein Prophet algorithm (Nesvizhskii et al. 2003), Protein isoforms and members of a protein family would be identified separately only if peptides that enable differentiation of isoforms had been identified based on MS/MS data. Otherwise, Scaffold software would group all isoforms under the same gene name. Thus, different proteins that contained similar peptides and which were not distinguishable based on MS/MS data alone were grouped to satisfy the principles of parsimony.

4. BIOINFORMATIC ANALYSES OF THE PROTEOMIC DATA

4.1 PRE-PROCESSING AND FILTERING OF MASS SPECTROMETRY DATA

Those proteins retrieved from Progenesis software without quantification associated data and/or not identified through Scaffold were removed from the final list. In addition, all missing values were removed as they were automatically assigned a “0” value and all out-layer abundance values were taken out as follows:

1. Absolute standard deviation of the mean for each protein in each condition was calculated without considering gender, therefore male and female values in a given genetic condition were grouped and taken together.
2. The values that were >50% of the standard deviation (SD) of a given genetic condition were removed. The formula used was:

   % of SD change: ([individual value-mean]/mean) *100

3. This criterion was applied when only one value accomplishes these criteria. Thus, if more than one value for a given protein fulfilled these criteria no values were removed. Also, if there was a missing value in a given group, the out-layer value was not removed.

4.2 STATISTICAL ANALYSES

Subsequently, statistical analyses were conducted using IBM SPSS statistic software platform ver.24.0 (see general M-5.1). The normality of the LC-MS/MS data was checked by applying the non-parametric Kolmogorv-Smirov (K-S) test with Lillefors correction. Almost 6-7% of the protein abundances didn’t follow a normal distribution for each genetic condition. For those proteins without a normal distribution, histograms were generated while mean and median were also compared to determine if data distribution in these datasets followed a distribution close to normality. Considering all normality assessments, only 1.6, 1.7 and 2.7% from ~2,478 proteins in WT, HET and RES samples, respectively did not follow a normal distribution. Therefore, the final statistical analysis for MS data was done using tests that assume normal data distribution. Protein abundances from *Syngap1* conditional KO line for genetic rescue were analysed using one-way ANOVA with Tamhane post-hoc mean differences determination. No adjustment was made to the error rate for multiple comparisons. In the case of the *Syngap1* conditional line for KO induction, which only includes two groups of animals, first the Levene's test was used to assess the

equality of variances, and later the corresponding parametric t-test assuming equality or differences in the variances, depending on the case, was used.

For IB data statistical comparisons, two-way ANOVA followed by Bonferroni post-hoc test was applied in both datasets derived from both *Syngap1*$^{+/-}$ conditional KO mouse lines.

4.2.1 Selection criteria for significant altered proteins in MS

Proteins that were statistically different and also presented a fold change (FC) ≥1.15 or ≤ 0.87 were considered up- or down-regulated, respectively.

4.2.2 Histogram and fold change correlation matrix

As not all protein abundance data followed a normal distribution, non-parametric Kendall's tau coefficient was calculated taken all these data that had a significant p-value in at least one of the three compared FCs groups or in the case of HET/WT and HET/RES comparisons, those proteins only found altered at least in one comparison. However, the parametric R of Pearson coefficient was also calculated to be compared with the Kendall's tau coefficient since a low percentage of proteins were following normal distribution as previously indicated. Finally, for matrix correlation assessments data were normalized by using a log10 transformation and R of Pearson coefficient.

4.2.3 Scatter plot

The scatter plot or volcano plot of the FC and corresponding adjusted p-values (also known as volcano plot) per each comparison was performed in R and modified using InkScape ver. 0.92.1 (http://www.inkscape.org).

4.2.4 Venn diagrams

Venn diagrams were built through the venny tool version 2.1 (Oliveros, J.C. 2015) or alternatively, with FunRich free software tool (www.funrich.org; Pathan et al. 2015). This graphical interface enables the representation of proteins overlapped among groups, together with the visualization of differentially expressed proteins in the different groups/fractions.

4.2.5 DATA REDUCTION AND CLUSTER ANALYSES

Only proteins altered in at least one comparison (e.g., HET/WT) were taken for clustering analysis. For clustering analyses the input method was applied whenever required. Namely, those replicas without data were replaced by the mean of its group. Finally, for PCA analysis data was subjected to normalization by log10 transformation, whereas for heatmaps plotting variables were converted into Z-scores. For dendrogram and heatmap plotting the distance measure calculated was Kendall's tau and the clustering method was average linkage in all cases.

Principal component analysis (PCA) was done by an R programming through interphase tools including R-Studio (Racine 2012). To take it as reliable clustering of the data, at least the 2 of the principal components must explained more than 40% of the variability of the dataset. Also, other analysis including hierarchical clustering and heatmaps were done by R programming and R based interphases (Metsalu and Vilo 2015; Babicki et al. 2016) after data normalization. Specific information on the analysis will be indicated in each corresponding section of the present thesis.

4.2.6 GENE ONTOLOGY, PATHWAYS AND PROTEIN DOMAIN ENRICHMENT ANALYSES

Gene ontology (GO) term enrichment analyses against whole *Mus musculus* genome were conducted using FunRich (Pathan et al. 2015), DAVID (Dennis et al. 2003), STRING (Szklarczyk et al. 2017) and BiNGO (Maere et al. 2005) databases. When hippocampal PSD proteome was used, several comparisons were conducted using both DAVID and FunRich databases. Protein domain enrichment analysis was done through DAVID and FunRich databases which retrieve information from InterPro (Finn et al. 2017) and SMART(Letunic et al. 2004), respectively. GO term enrichment analyses against hippocampal PSD reference proteome for Cellular Component (CC), Biological Process (BP) and Molecular Function as well as InterPro protein enrichment studies were conducted through DAVID database.

To search for GO terms associated to specific ID codes, the free tools GOrilla (Eden et al. 2009) and QuickGO database (www.ebi.ac.uk/QuickGO/) were used. Long redundant lists of GO terms were simplified using the REVIGO (Supek et al. 2011) free available tool. For pathways enrichment analyses, Kyoto Encyclopedia of Genes and Genomes KEGG (Aoki and Kanehisa 2005) and Reactome (Croft et al. 201 www.reactome.org/ PathwayBrowser) databases were used.

Finally, the in-depth analyses of different GO terms were conducted using the annotations reported in the AmiGO database (Carbon et al. 2009). Then, proteins identified in AmiGO database were compared with the 2,380 proteins commonly identified in both datasets from both *Syngap1* conditional KO mice lines.

4.2.7 HIPPOCAMPAL PSD REFERENCE PROTEOME

The reference proteome was built by using the list of identified PSD proteins identified in the present study from both *Syngap1* conditional mice lines together with the list of proteins identified in other proteomic studies conducted in mice, one from the laboratory (Reig-Viader et al. in preparation) and the PSD I and II reference proteome from Distler and collaborators (Distler et al. 2014). A total of 5,578 proteins were obtained and used for GO enrichment analyses.

4.2.8 NETWORK ANALYSES

Protein-protein interactions were retrieved from the STRING database ver. 11 (https://string-db.org;Szklarczyk et al. 2017). The settings in all cases unless specified otherwise, were PPI confidence level set at medium confidence (0.4) and the active interaction sources were 'Neighbourhood', 'Gene Fusion', 'Co-expression', 'Database'. The cluster method was K-means set at specific clusters depending on the appearance of the interactome, which is indicated in each corresponding figure footnote. The manual annotation of the GO terms for Molecular Function, BP, CC and KEGG pathways associated to subnetworks, which were derived from STRING, was done with Inkscape (http://www.inkscape.org). Cytoscape ver. 3.6.1 (http://cytoscape.org/; Yeung et al. 2008) and STRING database were used to conduct network analysis. Specifically, the packages implemented for other GO term enrichment studies of clusters and/or selected nodes analyses included BiNGO (Maere, Heymans, and Kuiper 2005) and WordCloud (Oesper et al. 2011). Also, some network studies were conducted through yFiles layout algorithms, ENViz and the DyNet Network importer and analyser (Yeung et al. 2008). Those proteins that were more interconnected than the average edges per node of a given interactome were considered hub proteins.

4.2.8.1 SYNGAP AND PSD-95 INTERACTOME RELATED ANALYSES

PSD-95 interactors from *Mus musculus* reported in the Intact, Mint, Mentha and Imex databases were retrieved and a non-redundant list of proteins from the PSD-95 interactome was created. From this list, the identified proteins common to the two datasets

derived from *Syngap1*$^{+/-}$ mouse lines found altered was used to determine which proteins had a PBM. To this purpose, altered proteins associated to a PBM from the AmiGO, UniProt (Bateman et al. 2017) and PDZbase (Beuming et al. 2005) databases as well as the PBM predictor LMDIPred (Sarkar, Jana, and Saha 2018, 201) were annotated to identify those altered proteins from the PSD-95 interactome annotated with a PBM. Protein sequences were retrieved from UniProt.

The SynGAP interactome was obtained by collapsing the reported SynGAP interactome from prefrontal cortex PSDs (Wilkinson, Li, and Coba 2017), Intact, Biogrid and Mentha databases.

4.2.9 Assessment of sample purities

The mitochondrial proteome was retrieved from MitoCarta 2.0 dataset (Calvo, Clauser, and Mootha 2016), the specific subset of proteins from the mitochondrial respiratory chain complex I or pres-synaptic active zone were obtained from AmiGO database and proteins enriched in synaptic mitochondria *vs.* non-synaptic were retrieved from the study of Graham and co-workers (Graham et al. 2017).

4.2.10 Gene set enrichment analyses

Causal or associated genes and pathways of ID were obtained from the gene Database Project obtained from the University of Denver (Colorado, USA;http://gfuncpathdb.ucdenver.edu/iddrc/iddrc/home.php). The ASD associated genes were retrieved from SFARI database (Banerjee-Basu and Packer 2010); the SCZ associated genes were obtained from SZDB (Wu, Yao, and Luo 2017), while the list of epilepsy genes classified into different categories were kindly provided from Wang and co-workers (Wang et al. 2017). The number of genes annotated in the *Mus musculus* genome (24,408) was retrieved (Bult et al. 2019) and the functional analyses were conducted manually by applying a binomial distribution test. All statistical analyses were conducted with a significance level of $\alpha = 0.05$ ($P < 0.05$). Also, the functional enrichment of phosphatases was conducted manually following the same rationale described here.

4.2.11 Long-lived protein related analyses

The list of 165 synaptic long-lived proteins reported from Heo and collaborators (Heo et al. 2018) was used to identify the amount of long-lived proteins that were found dysregulated in IND mice.

5. MATERIALS AND METHODS FOR ELECTROPHYSIOLOGY

Following cervical dislocation and decapitation, transverse hippocampal slices (350 µm thickness) were collected and transferred to an interface recording chamber (see Ozkan et al. 2014) maintained at 30°C. Slices were continuously perfused (1-2 mL/min) of artificial cerebrospinal fluid (aCSF) composed of (in mM) 124 NaCl, 4.4 KCl, 1.3 MgSO4, 1 NaH2PO4, 26.2 NaHCO3, 2.5 CaCl2, and 10 glucoses, aerated with 95% O2 and 5% CO2. Electrophysiological recording of extracellular field excitatory postsynaptic potentials (fEPSPs) from slices began following a 60 min recovery period after dissection. A glass microelectrode (resistance of 2–3 MΩ) filled with aCSF was positioned in the stratum radiatum of area *Cornus Ammon* 1 (CA1) for fEPSP recording. The hippocampal Schaeffer collateral-commissural pathway was stimulated at two separate sets of inputs (S1 & S2) converging onto the same postsynaptic population of neurons, using two bipolar nickel-chromium electrodes. fEPSPs of 40% of maximal evoked amplitudes (Gelinas and Nguyen, 2005) were obtained by adjusting the stimulus intensity (0.08 ms pulse duration) and these constituted our baseline responses. Subsequent fEPSPs were obtained at the rate of three sweeps per minute at this test stimulation intensity, with S2 stimulation following S1 stimulation by 200 ms. Input-output recordings of neuronal responses from S1 were recorded at increasing stimulus strength. After establishing a 20-min baseline recording, LTP was induced at S1 alone, through application of 5 ‘theta’ bursts, with each burst consisting of four pulses at 100 Hz and the bursts themselves separated by 200 msec (i.e., theta burst stimulation or TBS). The stimulation intensity was not increased during TBS. The control pathway (S2) received baseline stimulation to monitor the health of the slice.

5.1 DATA ANALYSIS OF ELECTROPHYSIOLOGY RECORDINGS

Axon Clampex 10.2 (Molecular Devices) was used for fEPSP analysis. The initial slope of the fEPSP was measured as an index of synaptic strength (Johnston and Wu, 1995). fEPSP slopes were averaged from 20 min of stable baseline recording to obtain a value for each experiment. All subsequent slopes were expressed as percentages of these baseline slopes. To compare LTP levels between 2 groups, we used data points at X min after LTP induction. Data are reported as means ± S.E.M, with n = number of slices.

CII-RESULTS

1. QUANTITATIVE AND QUALITATIVE ANALYSES OF PROTEOMIC DATA

1.1 ASSESSMENT OF THE PSD ENRICHMENT AFTER BIOCHEMICAL FRACTIONATION

To accomplish all the purposes indicated in CII-Introduction section, both the conditional KO mouse lines were crossed with Cre-recombinase transgenic mice as previously described. Briefly, this Cre line expresses a Cre-recombinase fused to a mutated form of the mouse estrogen receptor that only responds to TMX. The estrogen receptor is maintained at the cytoplasm until it binds its ligand, after that, it translocates to the nucleus. Thus, only when TMX binds to the mutated estrogen receptor, it gains access to the nucleus, allowing Cre-recombinase action.

Firstly, the efficiency of PSD fractionation procedure was validated by PSD-95 immunoreactivity assessed by IB. PSD-95 was found enriched in all PSD samples generated, indicating that the protocol was efficiently performed (Fig. RII-1).

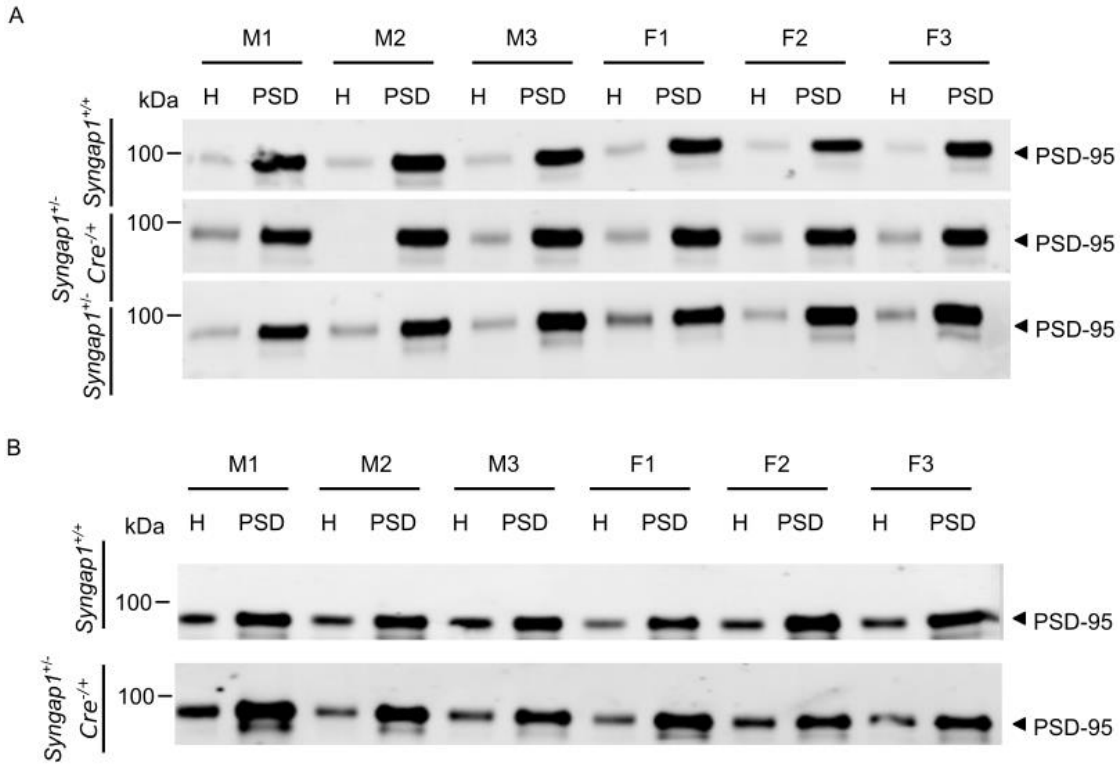

Figure RII-1. Quality control of the hippocampus PSD enriched fractions. IB against PSD-95 in homogenate (H) and PSD enriched fractions in *Syngap1* conditional (A) KO for genetic rescue studies and (B) for KO induction mouse lines. Up to 2.5 µg of protein were loaded in each lane. The samples shown are those used for MS studies.

1.2 GENOTYPE COMPARISON OF SYNGAP LEVELS IN HIPPOCAMPAL PSDS

PSD samples were assessed for total SynGAP levels by IB. The expression levels of SynGAP were expected in each genotype from both *Syngap1*$^{+/-}$ conditional KO mouse lines. Also, no differences between genders were observed (Fig. RII-2).

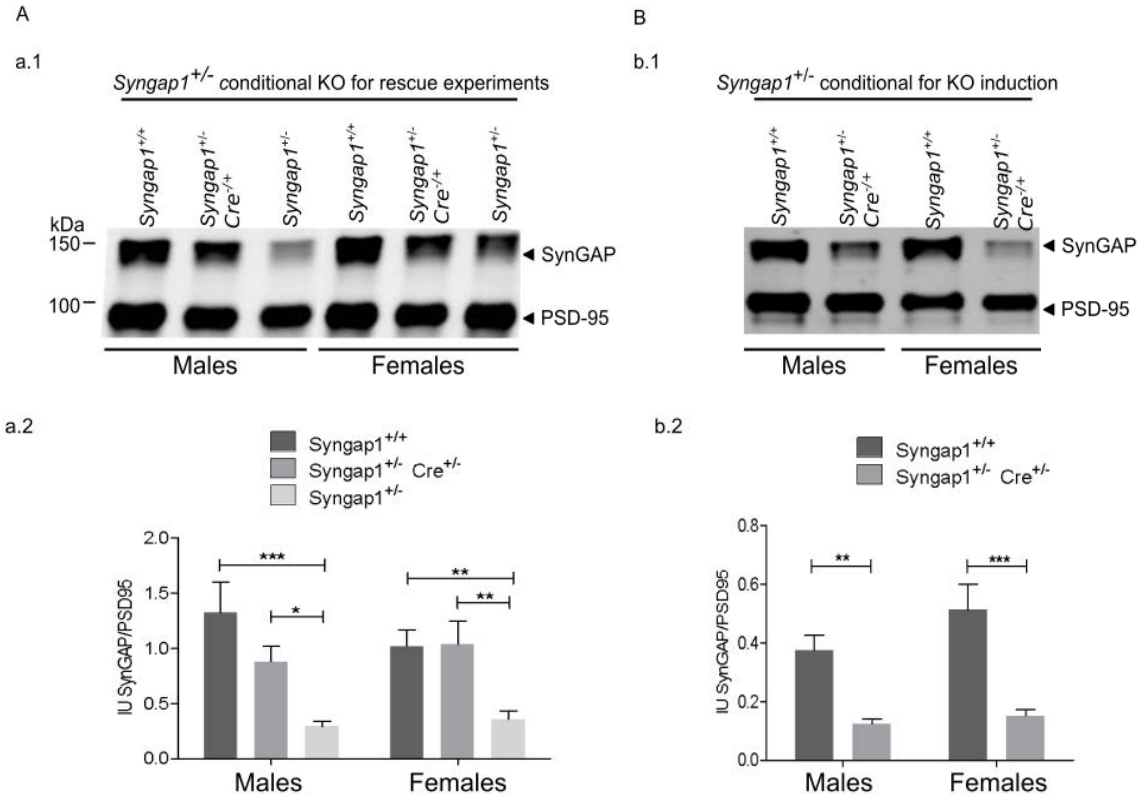

Figure RII-2. SynGAP levels in PSD enriched fraction from *Syngap1* conditional KO mouse lines. (A) Conditional KO mice for genetic rescue experiments (a.1) IBs and (a.2) corresponding bar plots. (B) Conditional mice for KO induction (b.1) IBs and (b.2) bar plots. Three male and three female samples were obtained per genotype and at least two technical replicates for each biological replica were conducted. Thus, considering both biological and technical replicates for each sample the minimum number of replicas was 12. Data normalized by PSD-95 followed normal distribution. Two-way ANOVA followed by Bonferroni post-hoc test was applied. No significant interaction between gender and genotype was found, whereas differences between genotypes were obtained in both mouse lines ($p<0.001$). Differences between groups that are not compared in down-stream analyses are not shown for simplicity. Bar errors indicate S.E.M.

1.3 QUALITATIVE BIOINFORMATIC ANALYSIS OF MS DATA

Using quantitative LC-MS/MS 2,479 proteins were identified in the PSD from *Syngap1* conditional KO mice for genetic rescue experiments, while in the conditional mice for KO induction the number of PSD proteins was slightly higher, 2,582. Importantly, the vast majority of PSD proteins were identified in both mouse lines (>92%). Subsequently, the distribution of protein abundance fold changes (FCs) in each genotype comparison were checked. FC histogram plots (Fig. RII-3) indicate that data followed a normal or a skewed like-normal distribution (Fig. RII-3 a.4). Furthermore, the clear majority of proteins in each comparison were found between the arbitrary range of 0.87 and 1.15. Proteins with FCs that fell within this range were considered unaltered, even if the statistical test applied

subsequently would flag them as having a significantly different expression. On the other hand, proteins outside this range were considered as potentially altered and ultimately, they were classified as altered if the differences reached statistical significance. Interestingly, the FCs distribution showed different amounts of potentially altered proteins, being particularly higher in the IND/WT comparison (Fig. RII-3 a.4). Despite this, similar number of proteins were found altered after statistical testing in HET and IND mice, while the number of altered PSD proteins in RES mice was approximately half.

Additionally, a non-parametric correlation between FCs arising from conditional KO mice for genetic rescue experiments was conducted (Fig. RII-3B). This provided a first insight of the similarity of the protein changes between genotypes. Namely, when proteins showing a statistically different abundance in at least one comparison were used, HET/WT *vs.* HET/RES FCs achieved statistically significant correlations with a coefficient value of 0.62 for Kendall's tau (Fig. RII-3b.1) or ~0.7 for Pearson coefficient (not shown). If this analysis was restricted only to the proteins differentially expressed in HET/WT and HET/RES, the Kendall's tau correlation slightly improved to 0.7. In contrast, the correlation between HET/WT or HET/RES vs. RES/WT, was much lower and did not reach statistical significance.

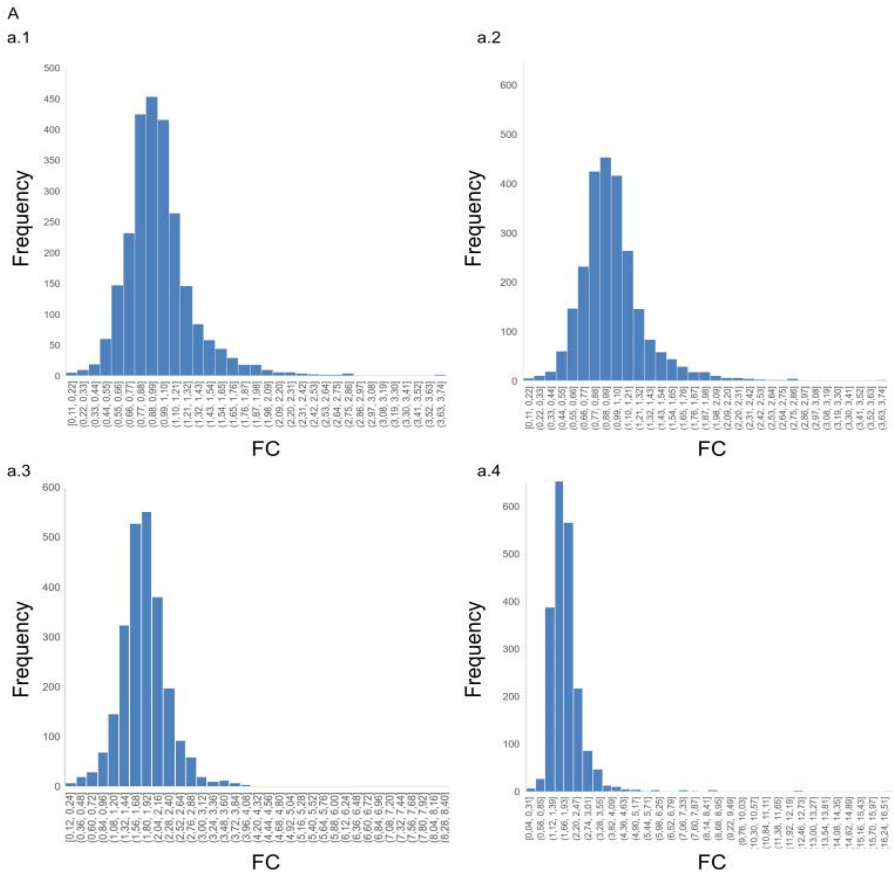

Figure RII-3. Histogram and correlation analyses of protein expression FC. See complete figure and corresponding footnote overleaf.

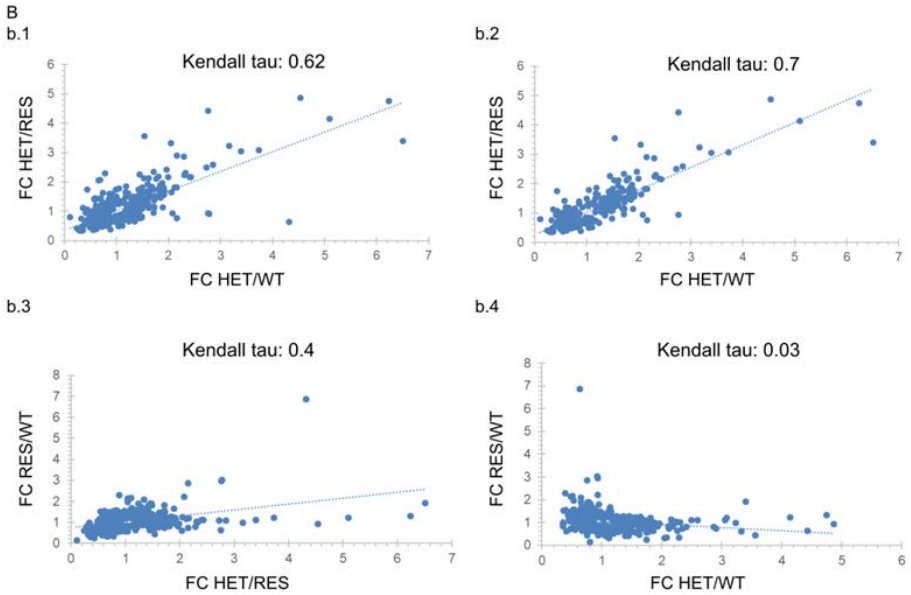

Figure RII-3. Histogram and correlation analyses of protein expression FC. (A) Histogram of protein FC distribution in (a.1) HET/WT comparison, (a.2) HET/RES comparison, (a.3) RES/WT comparison, and (a.4) IND/WT. (B) Kendall's tau correlation coefficient for those proteins whose FC differences passed the statistical test (one-way ANOVA followed by Tamhane post-hoc test without assuming similar variances). (b.1) HET/WT vs. HET/RES, (b.2) HET/WT vs. HET/RES considering only those proteins that had significant p-value and FC outside the range 0.87-1.15 for these two comparisons, (b.3) HET/RES vs. RES/WT and (b.4) HET/WT vs. RES/WT. Data in b.1, b.3 and b.4 include proteins with significantly different expression in all comparisons. In all cases, two-sided p-value tests were applied, and significant differences were obtained for b.1 and b.2 ($p<0.05$).

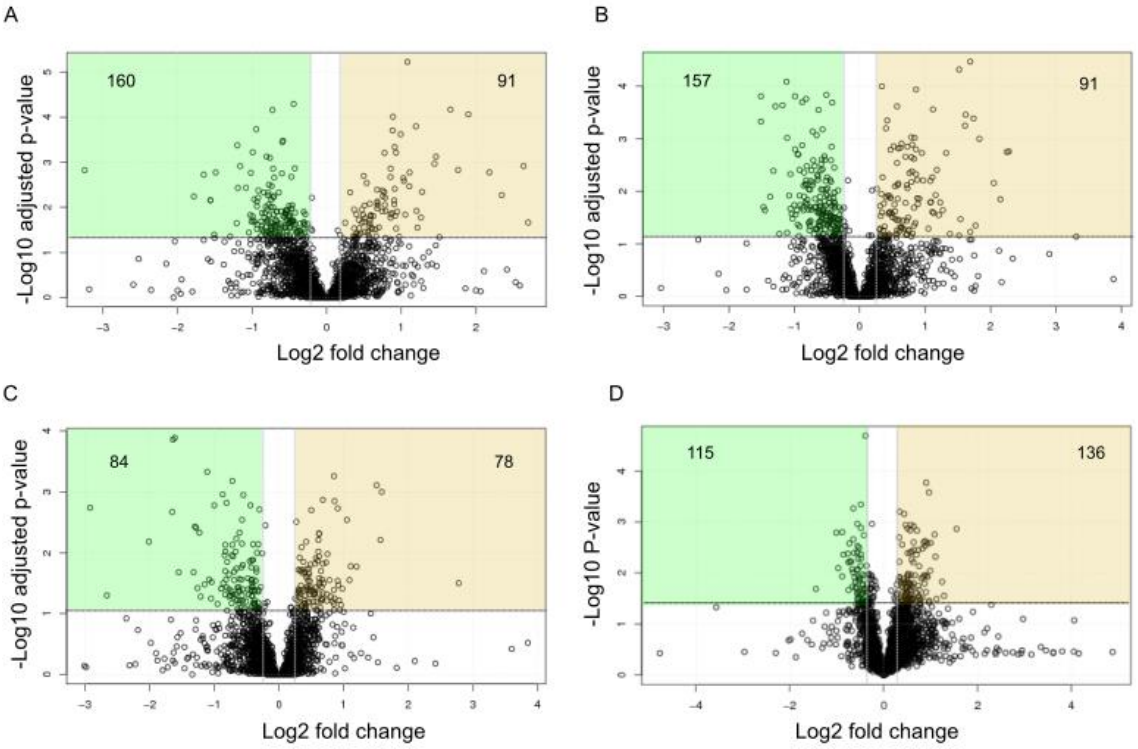

Figure RII-4. Up- and down-regulated significant proteins from both *Syngap1*$^{+/-}$ conditional KO mouse lines. Volcano plots for (A) HET/WT, (B) HET/RES, (C) RES/WT and (D) IND/WT altered proteins. Significantly down-regulated proteins are shadowed in green and up-regulated ones in yellow. The number of up and down-regulated proteins are also provided.

Volcano plots also indicated that similar numbers of proteins were abnormally expressed in HET-related comparisons (251 & 248). Specifically, there were 91 proteins up-regulated in both cases, while 160 and 157 proteins were found down-regulated in HET/WT and HET/RES comparisons, respectively (Fig. RII-4A&B). Furthermore, PSDs from RES mice had 162 proteins that varied significantly. These 162 proteins were symmetrically distributed between up- and down-regulated (78 & 84, respectively). Finally, in the case of the IND mice, 251 proteins were found altered being slightly higher the number of up-regulated proteins (i.e., 115 *vs.* 136; Fig. RII-4). Thus, there is an important number of PSD proteins presenting alterations in their expression even when SynGAP levels are normal until PND21.

1.4 ASSESSMENT OF THE PURITY OF PSD SAMPLES

The expression of presynaptic proteins or complexes typically associated to synaptosomes and presynaptic compartments in PSD-enriched samples was also evaluated. The aim was to assess the purity of the samples and the reliability of the data. These analyses indicated that a 2.1% and ~15% of the 2,682 proteins identified in at least one of the *Syngap1*$^{+/-}$ conditional KO mice belong to pre-synaptic active zone and mitochondria, respectively (Table RII-1). Indeed, proteins from the mitochondrial respiratory chain complex I have been reported to be particularly abundant in synapses (Graham et al. 2017) and ~78% of these proteins were identified (Table RII-1).

Source	Proteome	N proteins	N LC-MS/MS	% ID in LC-MS/MS
MitoCarta	Mitochondria proteome	1158	396	34
Panther GO:0005747	Mitochondrial respiratory chain complex I	51	40	78
Panther GO:0048786	Pre-synaptic active zone	91	57	63
Graham et al., 2016	Non-synaptic mitochondria	540	228	42
Graham et al., 2016	Synaptic-mitochondria	876	428	49
Graham et al., 2016	total	1416	656	46

Table RII-1: Mitochondrial and pre-synaptic active zone proteomes. The source, the number of the proteins published in each proteome (N proteins) as well as the number (N LC-MS/MS) and percentage (% ID in LC-MS/MS) of them identified in the present study for each proteome are shown.

1.5 OVERLAP OF ABNORMALLY EXPRESSED PSD PROTEINS BETWEEN GENOTYPES

The complete list of altered proteins found altered in at least one genetic comparison from the *Syngap1*$^{+/-}$ conditional KO for genetic rescue experiments is shown Table RII-27, whereas the list of altered proteins found in *Syngap1*$^{+/-}$ conditional mouse for KO induction is shown in Table RII-28. Proteins classified as rescued were those found altered in HET/WT but not in RES/WT whereas proteins that were found altered in both HET/WT and HET/RES were included in a confident group of rescued proteins. On the other hand, proteins altered in both HET/WT and RES/WT comparisons were considered un-rescued

proteins. Similarly, the confident group of un-rescued proteins were those altered in HET/WT and RES/WT but not in HET/RES. Finally, proteins found altered in RES/WT but not in HET/WT were considered a mixture of proteins that could be close to be classified as un-rescued proteins or altered collaterally to *Syngap1*$^{+/-}$ rescue from PND21 onwards. For this group, the confident set of proteins altered concomitant to the *Syngap1*$^{+/-}$ reactivation within PND21 and PND56 was defined as those proteins that were altered in RES/WT and HET/RES comparisons.

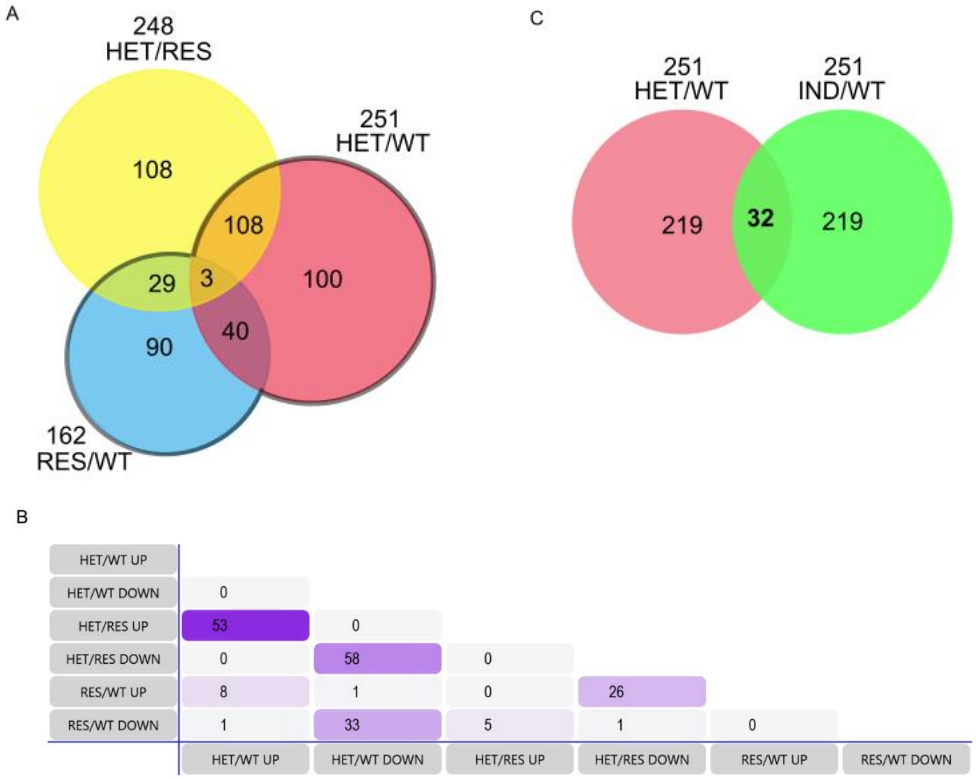

Figure RII-5. Comparison of altered proteins between different genotypes from *Syngap1*$^{+/-}$ conditional mouse lines. Venn diagrams (A-B) comparing (A) the number of common and individual proteins altered in HET/WT, HET/RES and RES/WT comparisons. The size of the spheres illustrates the total number of proteins altered which is also indicated above the corresponding genotype comparison. (B) Table showing the cross-comparison of up and down-regulated proteins in *Syngap1* conditional KO mouse line for genetic rescue studies. The numbers are coloured according the degree of overlapping being the higher overlapping denoted in dark purple and no overlapping in light grey. (C) Venn Diagram showing the overlapping degree of altered proteins found in HET and IND mice.

Interestingly, of the 251 proteins altered in HET mice, 208 were completely rescued while only 43 remained affected. From these 43 proteins, 40 were classified into the confident group of un-rescued proteins just defined above. Thus, these data indicate that by PND56 most proteins recover their normal levels once SynGAP expression at the PSD is recovered from PND21 onwards in RES mice. When evaluated the overlap of proteins found altered in HETs, up to 108 proteins were found altered when HET expression data was compared with either WT or RES data. These proteins constitute the most confident group of rescued proteins (Fig. RII-5A). Moreover, Venn diagrams built with altered

proteins from each genotype comparison, also showed that 119 proteins vary in RES/WT but not in HET/WT comparisons. Hence, these proteins could be potentially classified as altered collaterally due to SynGAP rescued expression or alternatively, as close to match the sorting criteria used for un-rescued proteins. Of these, 29 proteins also present significant differences if HETs were compared with RES and thus, represent the confident group of proteins altered as a consequence of *Syngap1*$^{+/-}$ genetic rescue (Fig.RII-5A). Noteworthy, an extended Venn diagram indicated that from those 108 common proteins dysregulated in HET/WT and HET/RES comparisons, 53 proteins were found up-regulated in both comparisons whereas 58 were found commonly down-regulated (Fig. RII-5B). Also, these analyses showed that the clear majority of un-rescued proteins were down-regulated (i.e., 33 out of 43; Fig. RII-5B).

Finally, a Venn diagram comparing HET/WT and IND/WT altered proteins also showed that although IND and HET mice presented the same number of altered proteins, only 32 were commonly altered (Fig. RII-5C). Indeed, these proteins only represent 12.7% of all altered proteins in IND or HET animals.

1.6 DATA REDUCTION AND CLUSTER ANALYSES

Data reduction methods aim to summarize a large number of variables to a smaller number avoiding the loss of information, whereas cluster analyses allowed the grouping of similar data to form “clusters”. Both methods reflect the quality of the data generated, as replicas within each group should behave similarly.

The principal component analysis (PCA) is a method of data reduction which when comparing HET and RES with WT indicated that 56,4% of the variability can be explained by two components. Importantly, individual HET, WT and RES replicas were more similar between each other than with other groups of replicas (Fig RII-6A). Of note, the first component (PC1), which explains 35,6% of the variability, put RES and WT samples together, whereas HET replicas were found more dissimilar (Fig. RII-6A). The correlation matrix generated from the expression levels of all samples corroborated this result (Fig. RII-6B). Also, the heatmap and associated dendrogram conducted with those proteins that were significantly altered in at least one genotype comparison, grouped together samples from the same genotype while no clusters for gender were found (Fig. RII-6E).

The examination of clusters arising from the heatmap and associated dendrogram, enable to visually identify subgroups of confident up and down-regulated rescued and un-rescued proteins previously defined (Fig. RII-6E). Namely, those proteins that are up-regulated in HET/WT and HET/RES while no significant differences are seen in RES/WT comparisons

were considered confident rescued up-regulated proteins and the other way around. Alternatively, those proteins found altered in HET/WT and RES/WT but not in HET/RES were subgrouped as confidently up- or down-regulated un-rescued proteins (Fig. RII-7A, bottom).

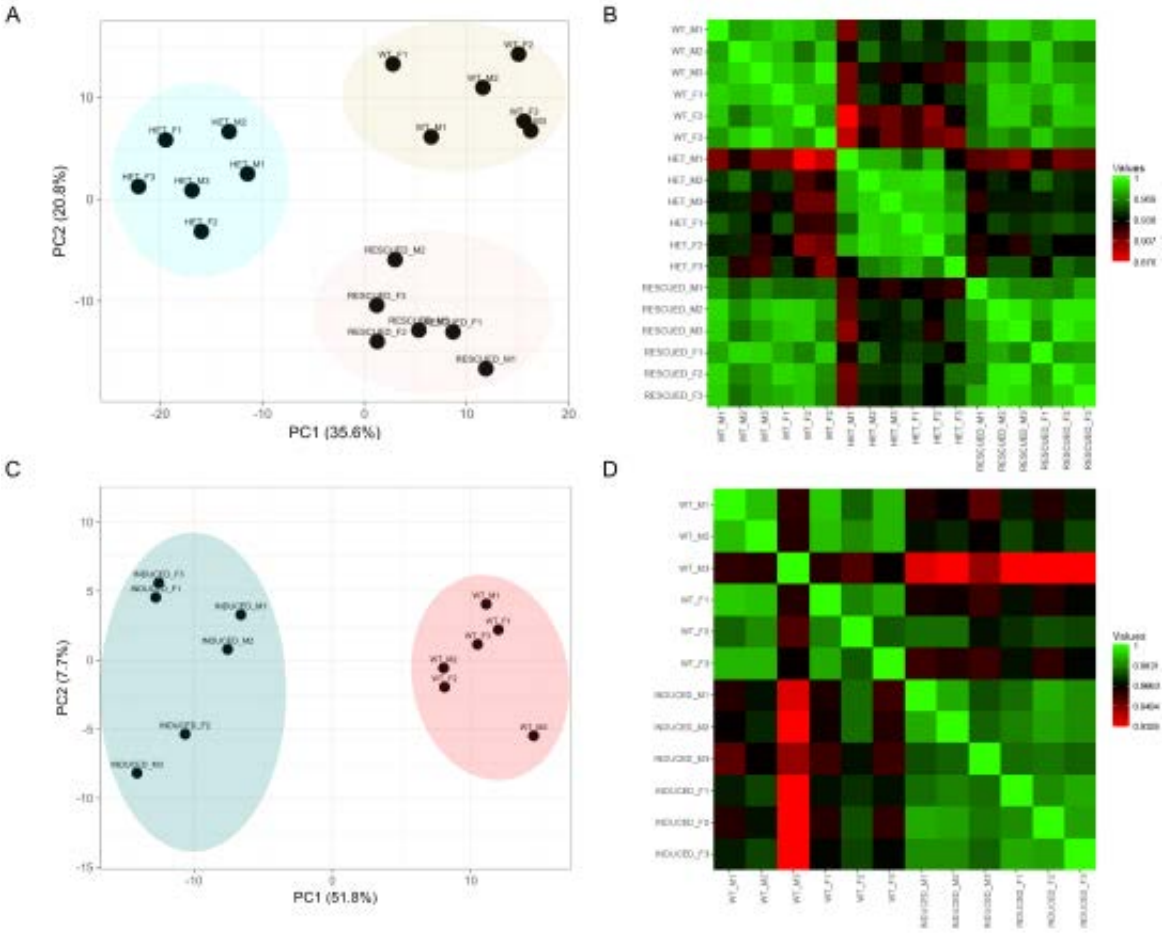

Figure RII-6. Data reduction analyses of altered proteins from both *Syngap1*$^{+/-}$ KO conditional mouse lines. (A) PCA plot showing the most contributing components of variability between samples from *Syngap1*$^{+/-}$ conditional KO for genetic rescue studies mouse line. Coloured ovals indicate the three clusters identified. (B) Correlation matrix of WT, HET and RES protein profiles. (C) PCA analyses of the samples from *Syngap1*$^{+/}$ conditional mouse line for KO induction. Coloured ovals indicate two clusters matching with the two different genotypes assessed. (D) Correlation matrix of WT and IND protein profiles. The right keys in both correlation matrix indicate a maximal correlation in green and the lowest correlation degree in red.

In IND mice, the PCA analysis showed that 58,8% of the variability can be explained by two principal components, with the first being the major contributor (~52%). More importantly, WT and IND replicas perfectly clustered together (Fig. R-6C). In agreement with the previous findings, both the PCA, correlation matrix and heatmap/dendrogram indicated that no differential clustering for gender was found (Fig. RII-6D&7B). Furthermore, PCA and correlation matrix (Fig. RII-6C-D) showed that one sample (WT_M3) presented a lower correlation with the rest of the WT replicas. Yet, as this sample

had a correlation coefficient closer to WT ones than IND samples, this data was also considered for subsequent analyses.

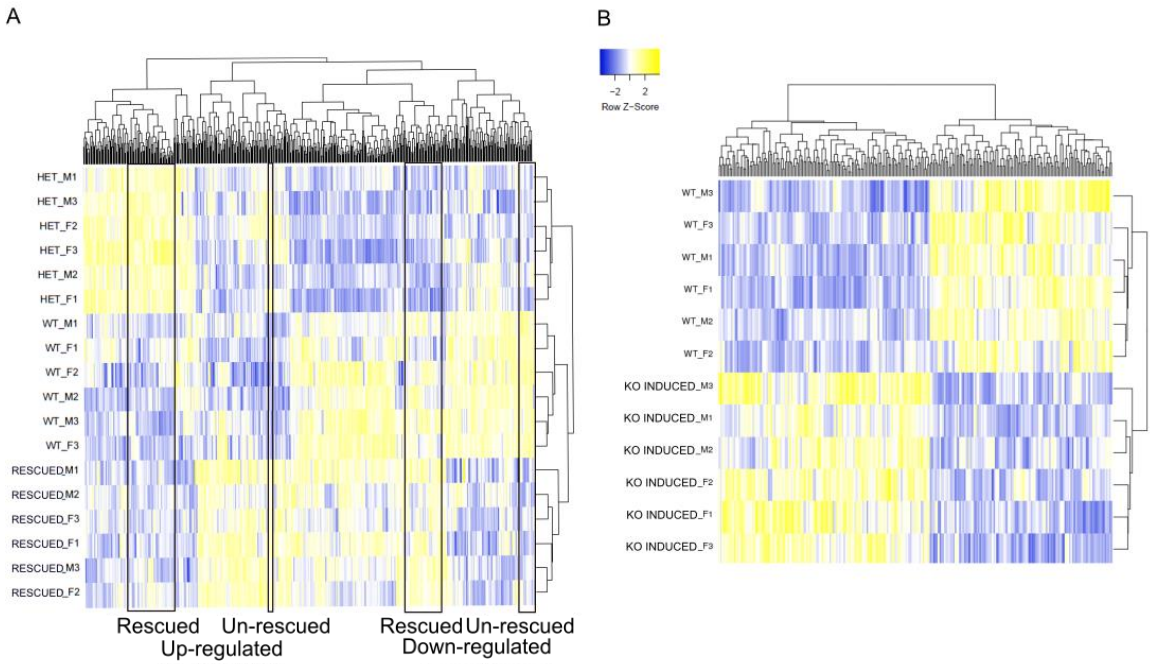

Figure RII-7. Cluster analyses of altered proteins from both *Syngap1*$^{+/-}$ KO conditional mouse lines. (A) Heatmap with associated dendrogram shown for all samples from *Syngap1*$^{+/-}$ conditional KO for genetic rescue studies mouse line (WT, HET and RES). The protein clustering was done by using those proteins that were significantly altered in at least one genotype comparison. Below is shown the clusters related to up- and down-regulated rescued or un-rescued proteins. (B) Heatmap with associated dendrogram for samples from *Syngap1*$^{+/}$ conditional mouse line for KO induction (WT and IND).

2. FUNCTIONAL ENRICHMENT ANALYSES OF ABNORMALLY EXPRESSED PSD PROTEINS

2.1 GO TERM ENRICHMENT ANALYSES AGAINST THE WHOLE MOUSE GENOME

GO term enrichment analyses related to Cellular Component (CC), Molecular Function and Biological Process (BP) against the whole mouse genome were conducted using all dysregulated proteins found in each genotype (Fig. RII-8). The following groups were investigated in these analyses: HET/WT, HET/RES, RES/WT and IND/WT to get an overview of the common or particular GO terms enriched in each genotype comparison. All four groups showed a wide range of common CC terms: neuron projection, membrane, cytoplasm, cytoskeleton, synapse, glutamatergic synapses, postsynapse and PSD. Interestingly, proteins related to the protein neuronal cell body, mitochondrion, perinuclear region of the cytoplasm, synaptic vesicles, myelin shaft and intracellular locations were significantly enriched in all groups but in RES/WT. Other subcellular locations were particularly enriched in HET/WT comparison. These include: proteins from membrane raft, dendritic spines and dendritic shaft. In contrast, only IND mice presented enrichment of terms related to GABAergic synapses, focal adhesion and dendrite locations.

In addition, terms related to CC such as ‘ATP binding’, ‘nucleotide binding’ and ‘protein binding’ were found significantly dysregulated in all groups, whereas protein transport was significantly altered in all cases but in RES mice. Other terms, like ‘GTPase activity’, ‘GTP and GDP binding’, ‘soluble NSF attachment protein activity enzyme’, ‘protein kinase binding’, ‘protein containing complex binding’, ‘structural constituent of the ribosome’, ‘syntaxin binding’ and ‘protein domain specific binding’, were terms commonly enriched in altered proteins from HET/WT and HET/RES comparisons. Other proteins related to Actin and Actin-filament binding proteins were significantly altered in HET and IND *vs.* WT animals. Finally, it is worth noting that ‘NADH deshydrogenase (ubiquinone) activity’, ‘unfolded protein binding’, ‘protein C-term binding’, ‘SH3 domain binding’, and ‘PDZ domain binding’ terms were only found significantly enriched in HET mice when compared with its control littermates.

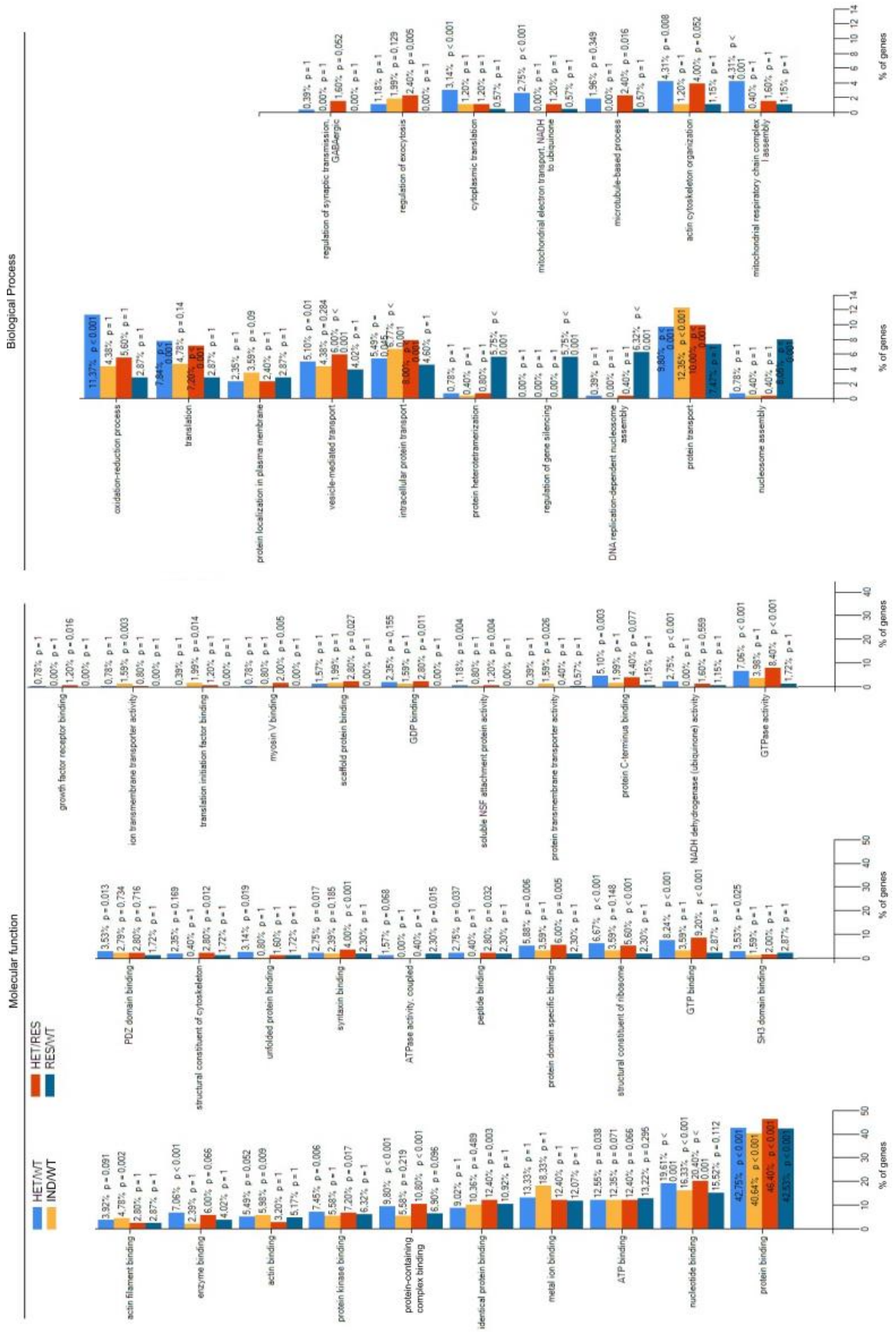

Figure RII-8. GO term enrichment analyses in both *Syngap1*$^{+/-}$ conditional KO mouse lines. Complete figure and corresponding footnote overleaf.

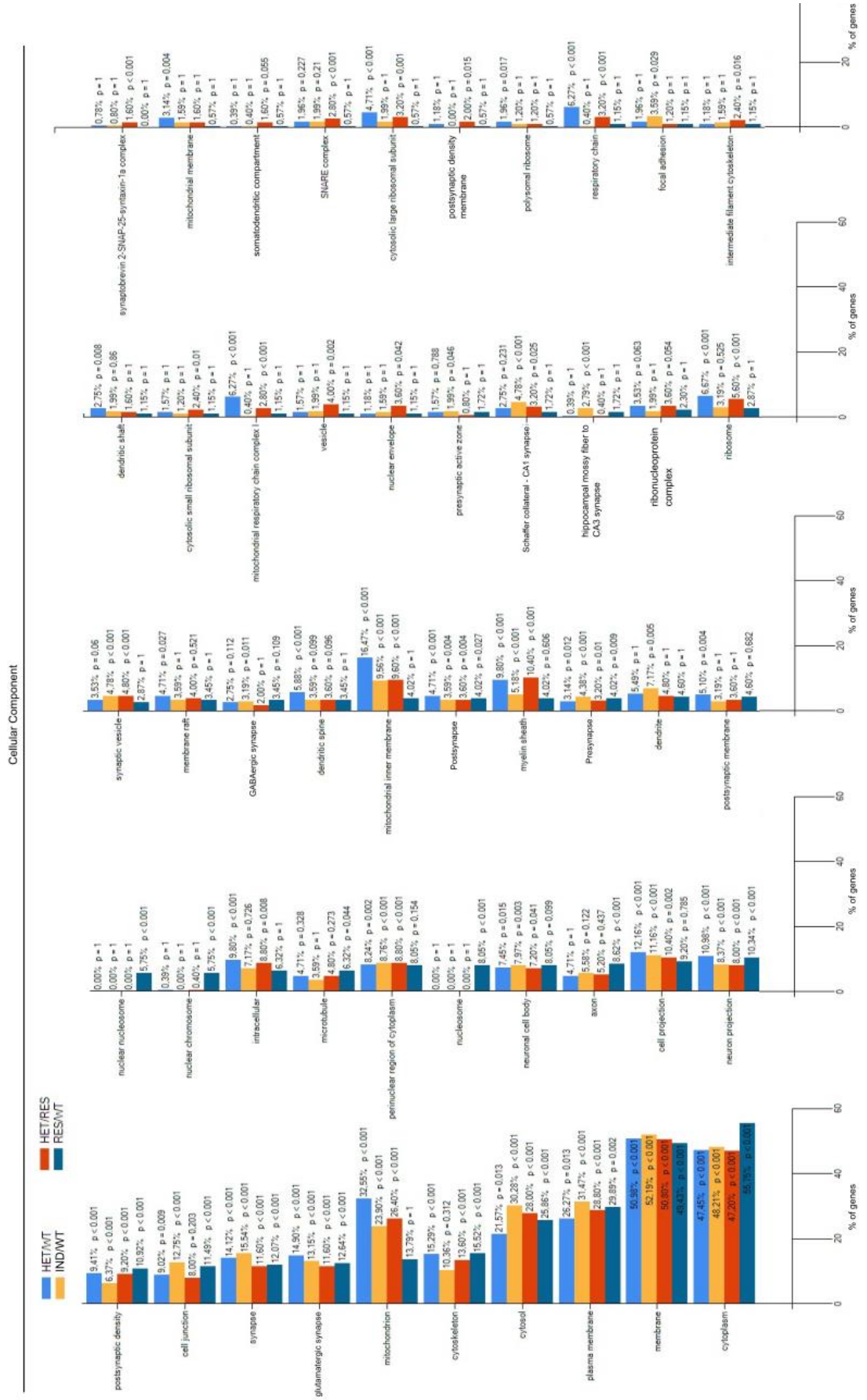

Figure RII-8. GO term enrichment analyses in both *Syngap1*$^{+/-}$ conditional KO mouse lines. Comparison between pair-wise enrichment of GO terms for BP; Molecular Function and CC using the FunRich database.

2.1.1 GO TERMS ALTERED IN UP- AND DOWN-REGULATED PROTEINS FROM *SYNGAP1*$^{+/-}$ MICE

GO term and protein domain enrichment analyses were investigated using the whole list of up- or down-regulated proteins (Table RII-2). On one hand, unique terms related to cytoskeleton organization, metabolic processes and regulation of synaptic plasticity were found up-regulated. On the other hand, BP terms related to translation, small GTPases mediated signalling and mitochondrial related events were found enriched in HET/WT when the group of down-regulated proteins was evaluated. In agreement with these findings, protein domain enrichment studies showed that Ras, Rho and Rab small GTPases were significantly down-regulated in addition to 14-3-3 family of proteins.

GO Biological process specific up-regulated		
ID	Description	FDR
GO:0007010	cytoskeleton organization	1.76e-07
GO:0007399	nervous system development	3.53e-05
GO:0031344	regulation of cell projection organization	9.0e-04
GO:0030030	cell projection organization	2.03e-04
GO:0050803	regulation of synapse structure or activity	5.42e-04
GO:0044712	single-organism catabolic process	0.00199
GO:0048167	regulation of synaptic plasticity	0.00203
GO:1901605	alpha-amino acid metabolic process	0.00271
GO:0010646	regulation of cell communication	0.00571
GO:0065007	biological regulation	0.0121
GO:0048518	positive regulation of biological process	0.0171
GO:0023051	regulation of signaling	0.0186
GO:0009448	gamma-aminobutyric acid metabolic process	0.0186
GO:0007167	enzyme linked receptor protein signaling pathway	0.0206
GO:0050789	regulation of biological process	0.0322
GO:0006796	phosphate-containing compound metabolic process	0.0349
GO:0050896	response to stimulus	0.038
GO:0048519	negative regulation of biological process	0.0392
GO:0051348	negative regulation of transferase activity	0.0395
GO:0044281	small molecule metabolic process	0.0416

	INTERPRO protein domains and features			
	ID	Description	Count in gene set	FDR
UP	IPR002453	Beta tubulin associated domains	4	2.46e-05
DOWN	IPR001806	Small GTPase superfamily	10	7.86e-06
DOWN	IPR005225	Small GTP-binding protein domain	10	2.13e-05
DOWN	IPR003578	Small GTPase superfamily, Rho type	6	2.34e-04
DOWN	IPR020849	Small GTPase superfamily, Ras type	6	5.63e-04
DOWN	IPR003579	Small GTPase superfamily, Rab type	6	0.00639
DOWN	IPR000308	14-3-3 protein	3	0.00565

GO Biological process specific down-regulated		
ID	Description	FDR
GO:0055114	oxidation-reduction process	1.75e-08
GO:0051179	localization	6.71e-08
GO:0006412	translation	2.25e-07
GO:0043603	cellular amide metabolic process	9.81e-07
GO:1901564	organonitrogen compound metabolic process	1.47e-06
GO:0007265	Ras protein signal transduction	1.29e-05
GO:0006886	intracellular protein transport	3.71e-05
GO:0007264	small GTPase mediated signal transduction	6.76e-05
GO:0051641	cellular localization	5.76e-06
GO:0007005	mitochondrion organization	7.66e-05
GO:0061024	membrane organization	9.14e-05
GO:0044710	single-organism metabolic process	1.12e-04
GO:0071840	cellular component organization or biogenesis	1.45e-04
GO:0006120	mitochondrial electron transport, NADH to ubiquinone	4,00E-04
GO:0043624	cellular protein complex disassembly	0.00169
GO:0035556	intracellular signal transduction	0.00179
GO:0060627	regulation of vesicle-mediated transport	0.00638
GO:0044802	single-organism membrane organization	0.00649
GO:0008105	asymmetric protein localization	0.00186
GO:1902600	hydrogen ion transmembrane transport	0.00431
GO:0022411	cellular component disassembly	0.0076
GO:0044267	cellular protein metabolic process	0.0178
GO:0032981	mitochondrial respiratory chain complex I assembly	0.0273
GO:0019538	protein metabolic process	0.0248
GO:1903361	protein localization to basolateral plasma membrane	0.0433
GO:0006793	phosphorus metabolic process	0.0476
GO:0006457	protein folding	0.0148
GO:0065008	regulation of biological quality	0.0450
GO:0050773	regulation of dendrite development	0.0130
GO:0044087	regulation of cellular component biogenesis	0.0110

Table RII-2. Specific GO terms and protein domains found enriched in the up- or down-regulated proteins from HET/WT comparison. GO terms for BP and protein domains enrichment analyses that were specific for each set of proteins are shown. All these studies were done using STRING database.

Biological pathways up and down-regulated arising from HET/RES comparisons were similar than those seen in HET/WT. Yet, new pathways were also identified for both up- and down-regulated proteins. Specifically, up-regulated proteins were enriched in GO terms related to neuronal differentiation processes, whereas down-regulated proteins included terms such as 'SNARE complex disassembly', Golgi vesicle-transport' and 'regulation of MAPK cascade' (Table RII-3).

Finally, the protein domain analysis showed that Septin Tubulin and intermediate filament proteins were enriched in up-regulated proteins from HET animals. Conversely, several types of small GTPases (e.g., Rho, Ras and Rap) were found again significantly down-regulated. Of note, Ran small GTPases, which are associated to nuclear transport, appeared significantly altered in HET/RES comparison. Finally, P-loop containing

hydrolases were found significantly enriched in the subset of down-regulated proteins altered in HET when compared to RES samples.

	GO Biological process specific		
	ID	Description	FDR
UP-REGULATED	GO:0007010	cytoskeleton organization	3.53e-07
	GO:0022607	cellular component assembly	1.01e-05
	GO:0030036	actin cytoskeleton organization	7.97e-04
	GO:0030865	cortical cytoskeleton organization	0.00354
	GO:0006520	cellular amino acid metabolic process	0.00427
	GO:0051258	protein polymerization	0.00592
	GO:0007017	microtubule-based process	0.00819
	GO:0048667	cell morphogenesis involved in neuron differentiation	0.0165
	GO:0010608	posttranscriptional regulation of gene expression	0.0198
	GO:0065007	biological regulation	0.0252
	GO:0030030	cell projection organization	0.0281
	GO:1901605	alpha-amino acid metabolic process	0.0363
	GO:0009448	gamma-aminobutyric acid metabolic process	0.0363
	GO:0007399	nervous system development	0.037
	GO:0060284	regulation of cell development	0.042
DOWN-REGULATED	GO:0006886	intracellular protein transport	5.7e-11
	GO:0061025	Membrane fusion	3.13e-08
	GO:0061024	Membrane organization	1.76e-07
	GO:0007265	Ras protein signal transduction	1.76e-07
	GO:1901566	organonitrogen compound biosynthetic process	4.11e-07
	GO:0006754	ATP biosynthetic process	5.00e-07
	GO:0016192	vesicle-mediated transport	5.18e-07
	GO:0006518	peptide metabolic process	5.18e-07
	GO:0015992	proton transport	1.5e-06
	GO:0006810	transport	1.53e-06
	GO:0043603	cellular amide metabolic process	1.94e-06
	GO:0007264	small GTPase mediated signal transduction	5.44e-06
	GO:0071702	organic substance transport	5.73e-06
	GO:1901564	organonitrogen compound metabolic process	5.94e-06
	GO:0033036	macromolecule localization	6.09e-06
	GO:0048284	organelle fusion	0.000193
	GO:0008152	metabolic process	0.000546
	GO:0055085	transmembrane transport	0.00075
	GO:0050804	modulation of synaptic transmission	0.000778
	GO:0032482	Rab protein signal transduction	0.000892
	GO:0022406	membrane docking	0.00108
	GO:0044087	regulation of cellular component biogenesis	0.00158
	GO:0051049	regulation of transport	0.00163
	GO:0043408	regulation of MAPK cascade	0.00219
	GO:0016050	vesicle organization	0.00235

	GO Biological process specific		
	ID	Description	FDR
DOWN-REGULATED	GO:0016197	endosomal transport	0.00364
	GO:0065008	regulation of biological quality	0.00453
	GO:0007005	mitochondrion organization	0.00495
	GO:0048278	vesicle docking	0.00505
	GO:0007033	vacuole organization	0.00583
	GO:0035494	SNARE complex disassembly	0.00583
	GO:0002262	myeloid cell homeostasis	0.00722
	GO:0006839	mitochondrial transport	0.00756
	GO:0006811	ion transport	0.00832
	GO:0000028	ribosomal small subunit assembly	0.00988
	GO:0048193	Golgi vesicle transport	0.0106
	GO:0006950	response to stress	0.0122
	GO:0035556	intracellular signal transduction	0.0135
	GO:0042274	ribosomal small subunit biogenesis	0.0136
	GO:0051246	regulation of protein metabolic process	0.0155
	GO:0043467	regulation of generation of precursor metabolites and energy	0.0161
	GO:0008105	asymmetric protein localization	0.0217
	GO:0023051	regulation of signaling	0.0247
	GO:0050896	response to stimulus	0.0278
	GO:0090407	organophosphate biosynthetic process	0.0313
	GO:0043457	regulation of cellular respiration	0.0328
	GO:0048872	homeostasis of number of cells	0.0374

	INTERPRO protein domains and features			
	ID	Description	ınt in gene	FDR
UP	IPR000217	Tubulin	4	3.55e-4
	IPR016491	Septin	2	0.0284
	IPR018039	Intermediate filament protein	3	0.0364
DOWN	IPR005225	Small GTP-binding protein domain	13	5.47e-10
	IPR003578	Small GTPase superfamily, Rho type	9	2.12e-09
	IPR020849	Small GTPase superfamily, Ras type	9	2.12e-09
	IPR003579	Small GTPase superfamily, Rab type	9	1.02e-08
	IPR002041	Ran GTPase	6	1.12e-06
	IPR027417	P-loop containing nucleoside triphosphate hydrolase	14	4.67e-4

Table RII-3. Specific GO terms and protein domains found enriched in the up- or down-regulated proteins from HET/RES comparison. GO terms for BP and protein domains enrichment analyses that were specific for each set of proteins are shown. All these studies were done using STRING database.

2.1.2 GO TERMS ALTERED IN UP- AND DOWN-REGULATED PROTEINS FROM RESCUED *SYNGAP1*$^{+/-}$ MICE

Noticeably, very few terms were found enriched for proteins altered in rescued animals when up- and down-regulated molecules are considered separately. Ferric ion transport was a term found enriched in up-regulated proteins while proteins down-regulated were found related to organization of cellular components (Table RII-4).

	GO Biological process specific		
	ID	Description	FDR
UP	GO:0015682	ferric iron transport	0.0415

	GO Biological process specific		
	ID	Description	FDR
DOWN	GO:0016043	cellular component organization	0.0323

Table RII-4. Specific GO terms and protein domains found enriched in the up- or down-regulated proteins from RES/WT comparison. GO terms for BP and protein domains enrichment analyses that were specific for each set of proteins are shown. All these studies were done using STRING database.

In addition, the confident subgroups of up- and down-regulated rescued or un-rescued proteins were analysed through STRING database and terms uniquely found enriched in one of these subgroups are shown in Table RII-5. These studies indicated that there was a higher number of confident pathways rescued than un-rescued. Indeed, a small number of proteins were found in the categories of up- or down-regulated un-rescued proteins. Namely, only one GO term was found enriched in the un-rescued down-regulated group while only the KEGG pathway 'protein processing in ER' could be found significantly enriched when all un-rescued proteins were included in this analysis.

GO enrichment for biological processes

	GO ID	GO term	p-value
RESCUED UP-REGULATED	GO:0007010	cytoskeleton organization	1.71e-05
	GO:0006996	organelle organization	8.56e-05
	GO:0007399	nervous system development	7.67e-04
	GO:0030036	actin cytoskeleton organization	8.47e-04
	GO:1901605	α-amino acid metabolic process	2.59e-03
	GO:0006536	glutamate metabolic process	0.0106
	GO:0009448	GABA metabolic process	0.0131
	GO:0031344	regulation of cell projection organization	0.0171
	GO:0060020	Bergmann glial cell differentiation	0.024
	GO:0070373	negative regulation of ERK1/2 cascade	0.0441
RESCUED DOWN-REGULATED	GO:0006412	translation	9.29e-05
	GO:0007264	small GTPase mediated signal	5.36e-05
	GO:0051179	localization	9.66e-04
	GO:0061024	membrane organization	8.17e-04
	GO:0006886	intracellular protein transport	2.89e-03
	GO:0007265	Ras protein signal transduction	2.98e-03
	GO:0035494	SNARE complex disassembly	5.36e-03
	GO:0048169	regulation of long-term neuronal synapti plasticity	0.02
	GO:0090324	negative regulation of oxidative phosphorylation	0.0343
	GO:0071840	cellular component organization or biogenesis	0.0493

GO enrichment for KEGG pathways

	Pathway ID	Description	p-value
RESCUED DOWN-REGULATED	4916	Melanogenesis	0.0246
	4014	Ras signaling pathway	0.0279
	4722	Neurotrophin signaling pathway	0.0333
	4360	Axon guidance	0.0386
	4530	Tight junction	0.0408
	562	Inositol phosphate metabolism	0.0333
	5206	MicroRNAs in cancer	0.0436
RESCUED UP-REGULATED	4520	Adherens junction	0.00598
	4540	Gap junction	0.00598
	4145	Phagosome	0.0335
UNRESCUED ALL	4141	Protein processing in endoplasmic reticulum (ER)	0.0286

GO enrichment for molecular function

	GO ID	GO TERM	p-value
RESCUED UP-REGULATED	GO:0005525	GTP binding	2.09e-04
	GO:0008092	cytoskeletal protein binding	2.52e-03
	GO:0003924	GTPase activity	0.0123
	GO:0044822	poly(A) RNA binding	0.0129
	GO:0005515	protein binding	0.0129
	GO:0003723	RNA binding	0.0229
	GO:0003824	catalytic activity	0.0113
RESCUED DOWN-REGULATED	GO:0003735	structural constituent of ribosome	2.08e-07
	GO:0005483	soluble NSF attachment protein activity	2.59e-05
	GO:0000149	SNARE binding	1.55e-04
	GO:0019905	syntaxin binding	5.15e-04
	GO:0005525	GTP binding	8.17e-03
	GO:0008137	NADH dehydrogenase (ubiquinone) activity	0.0163
UN-RESCUED DOWN	GO:0051082	Unfolded protein binding	0.05

GO enrichment for KEGG pathways

	Pathway ID	Description	p-value
RESCUED DOWN-REGULATED	5016	Huntington's disease	8.88e-08
	190	Oxidative phosphorylation	1.05e-07
	5012	Parkinson's disease	1.27e-07
	5010	Alzheimer's disease	3.36e-07
	3010	Ribosome	1.0E-06
	1100	Metabolic pathways	1.62E-04
	4720	Long-term potentiation	0.0118
	4721	Synaptic vesicle cycle	0.0118
	4730	Long-term depression	0.0118
	4921	Oxytocin signaling pathway	0.0128
	4062	Chemokine signaling pathway	0.0198
	4540	Gap junction	0.0231
	4912	GnRH signaling pathway	0.0231
	5203	Viral carcinogenesis	0.0236
	4015	Rap1 signaling pathway	0.0246

Table RII-5. GO term for BP and CC categories and KEGG pathway enrichment analyses. The specific confident subsets of up- or down-regulated rescued or un-rescued proteins were subjected to GO term (top panels) as well as KEGG pathways enrichment analyses (bottom panels) enrichment analysis against the whole *Mus musculus* genome through DAVID database. In this analysis the correction for multiple testing was not considered.

Regarding the GO terms found enriched among rescued up-regulated proteins, they mainly belonged to cell processes related to cytoskeleton organization, nervous system

development, protein and NT (Glu and GABA) metabolic processes as well as to the vesicle cycle, glia and cell projection organization (including axon guidance, dendrites, dendritic spines). Also, the negative regulation of ERK1/2 cascade, proteins related to lipid metabolism as well as Gap and adherens junctions were found enriched in this subgroup. Conversely, terms related to translation, protein transport and localization, carcinogenesis, small GTPases (mainly Ras and Rap1), signalling through neurotrophins as well as synaptic plasticity in the form of LTP and LTD were found significantly enriched in the down-regulated rescued proteins. Moreover, when down-regulated rescued proteins were considered for KEGG pathways, a higher number of pathways than for the rescued up-regulated proteins were found (Table RII-5, bottom). These down-regulated rescued down-regulated proteins were significantly associated to neurodegenerative disorders such as Huntington's, Alzheimer's and Parkinson's diseases, which were related to cognitive decline. Also, pathways related to carcinogenesis, ribosome and energy production through oxidative phosphorylation in mitochondria were found enriched.

2.1.3 GO TERMS IN UP- AND DOWN-REGULATED PROTEINS FROM *SYNGAP1*$^{+/-}$ INDUCED KO MICE

When the GO term for BP enrichment analysis was conducted, taking into account those proteins up-regulated in IND mice, several terms were found significantly enriched (Table RII-6). Of note, processes related to chemical synapse neurotransmission, ubiquitin-dependent proteolysis, calcineurin phosphatase signalling, mitochondria, small molecules and lysosomal transport, synaptic vesicle-mediated transport, protein metabolic process and central nervous system development were found significantly enriched among the up-regulated proteins. In contrast, terms associated to translation, lipid metabolism, phosphatases, cytoskeleton related processes, endomembrane system organization synaptic plasticity and protein kinase A signalling were found significantly down-regulated.

Of note, protein domain analyses also showed that protein domains associated to up-regulated proteins did not yield any significant enrichment when used the InterPro database. Conversely, SMART database allowed to find a significant enrichment of Rab small GTPases among up-regulated proteins in IND mice. When the protein domain enrichment analyses were conducted for the down-regulated proteins, several domains were found enriched including C2, PH, Zinc finger (piccolo-type), Clasp, ezrin/radixin/moesin or nebulin repeats. Yet, many of them belong to cytoskeletal proteins or membrane-fusion (Table RII-6, bottom). It is worth noting that no significant enrichment for small GTPases was found in down-regulated proteins from IND mice.

	GO Biological Process specific					
	GO ID	Description	FRD	GO ID	Description	FRD
Up-regulated	GO:0051241	negative regulation of multicellular organismal process	0.00036	GO:0042493	response to drug	0.0230
	GO:0017144	drug metabolic process	0.00037	GO:0007041	lysosomal transport	0.0231
	GO:0007005	mitochondrion organization	0.00088	GO:0060964	regulation of gene silencing by miRNA	0.0244
	GO:0007417	central nervous system development	0.00095	GO:0016032	viral process	0.0248
	GO:0099003	vesicle-mediated transport in synapse	0.0018	GO:0051259	protein oligomerization	0.0251
	GO:0044237	cellular metabolic process	0.0025	GO:0006091	generation of precursor metabolites and energy	0.0300
	GO:0044281	small molecule metabolic process	0.0025	GO:0033173	calcineurin-NFAT signaling cascade	0.0323
	GO:1901135	carbohydrate derivative metabolic process	0.0026	GO:0006807	nitrogen compound metabolic process	0.0367
	GO:0008152	metabolic process	0.0030	GO:0010918	positive regulation of mitochondrial membrane potential	0.0404
	GO:0045665	negative regulation of neuron differentiation	0.0034	GO:0032781	positive regulation of ATPase activity	0.0421
	GO:0051187	cofactor catabolic process	0.0035	GO:0007155	cell adhesion	0.0442
	GO:0051186	cofactor metabolic process	0.0046	GO:0035690	cellular response to drug	0.0442
	GO:0060322	head development	0.0048	GO:0030433	ubiquitin-dependent ERAD pathway	0.0128
	GO:0051093	negative regulation of developmental process	0.0069	GO:0019637	organophosphate metabolic process	1.32e-05
	GO:0099504	synaptic vesicle cycle	0.0091	GO:0017038	protein import	1.94e-05
	GO:0007268	chemical synaptic transmission	0.0142	GO:0055085	transmembrane transport	1.94e-06
	GO:0051453	regulation of intracellular pH	0.0156	GO:0015672	monovalent inorganic cation transport	2.89e-05
	GO:0051130	positive regulation of cellular component organization	0.0156	GO:0009142	nucleoside triphosphate biosynthetic process	3.00e-08
	GO:0019538	protein metabolic process	0.0182	GO:1990542	mitochondrial transmembrane transport	8.75e-06
	GO:0039536	negative regulation of RIG-I signaling	0.0218	GO:0016311	dephosphorylation	0.0048

	GO Biological Process specific					
	GO ID	Description	FRD	GO ID	Description	FRD
Down-regulated	GO:0051129	negative regulation of cellular component organization	0.00018	GO:0048167	regulation of synaptic plasticity	0.0098
	GO:0016358	dendrite development	0.00023	GO:0000278	mitotic cell cycle	0.0107
	GO:0006412	translation	0.00045	GO:1902966	positive regulation of protein localization to early endosome	0.0137
	GO:0007017	microtubule-based process	0.00085	GO:1905050	positive regulation of metallopeptidase activity	0.0137
	GO:0048468	cell development	0.0011	GO:0097435	supramolecular fiber organization	0.0139
	GO:0048284	organelle fusion	0.0016	GO:2000643	positive regulation of early endosome to late endosome transport	0.0157
	GO:0034341	response to interferon-gamma	0.0020	GO:0010033	response to organic substance	0.0165
	GO:0000226	microtubule cytoskeleton organization	0.0022	GO:0010737	protein kinase A signaling	0.0203
	GO:0048519	negative regulation of biological process	0.0025	GO:0007163	establishment or maintenance of cell polarity	0.0240
	GO:0035556	intracellular signal transduction	0.0033	GO:0032535	regulation of cellular component size	0.0274
	GO:0032502	developmental process	0.0037	GO:0060263	regulation of respiratory burst	0.0281
	GO:0007267	cell-cell signaling	0.0044	GO:1903902	positive regulation of viral life cycle	0.0285
	GO:0035418	protein localization to synapse	0.0044	GO:0080134	regulation of response to stress	0.0306
	GO:0030029	actin filament-based process	0.0045	GO:0071214	cellular response to abiotic stimulus	0.0313
	GO:0006635	fatty acid beta-oxidation	0.0046	GO:0016239	positive regulation of macroautophagy	0.0350
	GO:0051716	cellular response to stimulus	0.0047	GO:0006928	movement of cell or subcellular component	0.0389
	GO:0010256	endomembrane system organization	0.0047	GO:0001505	regulation of neurotransmitter levels	0.0410
	GO:0010921	regulation of phosphatase activity	0.0051	GO:0090066	regulation of anatomical structure size	0.0433
	GO:0099526	presynapse to nucleus signaling pathway	0.0057	GO:0043666	regulation of phosphoprotein phosphatase activity	0.0246
	GO:0048790	maintenance of presynaptic active zone structure	0.0057	GO:0034114	regulation of heterotypic cell-cell adhesion	0.0496
	GO:0015931	nucleobase-containing compound transport	0.0088	GO:0044085	cellular component biogenesis	7.12e-05
	GO:0032501	multicellular organismal process	0.0097	GO:0051234	establishment of localization	8.79e-07
	GO:0043603	cellular amide metabolic process	0.0097	GO:0072657	protein localization to membrane	8.89e-07

	Protein domain INTERPRO		
	ID	Description	FDR
Down-regulated	IPR000008	C2 domain	0.0371
	IPR000900	Nebulin repeat	0.0371
	IPR008899	Zinc finger, piccolo-type	0.0371
	IPR008954	Moesin tail domain superfamily	0.0371
	IPR011174	Ezrin/radixin/moesin	0.0371
	IPR011259	Ezrin/radixin/moesin, C-terminal	0.0371
	IPR024395	CLASP N-terminal domain	0.0371
	IPR035892	C2 domain superfamily	0.0371
	IPR011993	PH-like domain superfamily	0.0445
	IPR034085	TOG domain	0.0473
	Protein domain SMART		
	ID	Description	FDR
Up	SM00175	Rab subfamily of small GTPases	0.0455

Table RII-6. Specific GO terms and protein domains found enriched in the up- or down-regulated proteins from IND/WT comparison. GO terms for BP and protein domains enrichment analyses that were specific for each set of proteins are shown. All these studies were done using STRING database. In this case, the analysis of protein domain enrichment using all subgroup of proteins were conducted using InterPro database, yet in the case of up-regulated proteins SMART database was also used since no enrichment was found previously.

2.2 REACTOME PATHWAYS ENRICHMENT ANALYSIS AGAINST THE WHOLE MOUSE GENOME

Reactome pathways common to all groups investigated or unique to some of them are shown in Fig. RII-9. Interestingly, the number of altered pathways in HET/WT and HET/RES comparisons was around 100, while much lower numbers were found for IND/WT (30) and RES/WT (15). Furthermore, over 50% of Reactome pathways enriched in proteins with a differential expression in HET/WTs were also found in the HET/RES comparison. Of the 15 pathways found altered in RES animals, only 2 were also found in HETs. Despite the low overlap of altered proteins found in IND and HET mice, 50% of the pathways found enriched in IND animals were also found in HETs. Thus, these results suggest that some cellular pathways are always affected by SynGAP deficit regardless of the developmental period in which its gene is KO. Finally, only 11 pathways were found uniquely altered either in IND or RES mice.

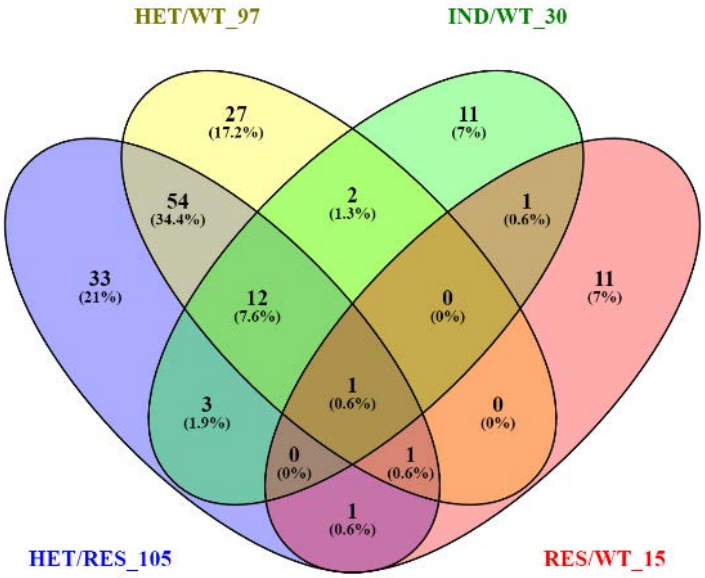

Figure RII-9. Reactome pathways common and unique to genotype comparisons. Numbers close to each genotype comparison indicate the total number of pathways altered. The percentages calculated are relative to the total pathways found enriched in all comparisons.

2.2.1 REACTOME PATHWAYS ALTERED IN *SYNGAP1*$^{+/-}$ MICE

Detailed Reactome pathways found significantly enriched in HET/WT comparison were classified into different categories shown in Table RII-7. Also, the comparison of Reactome pathways found enriched in HET *vs.* RES mice was conducted to further explore possible pathways altered in HET mice. In addition, pathways that for instance, could be found close to significance in HET/WT comparison but were only found significantly altered in HET/RES comparison are shown in Table RII-8.

	Pathway ID	Description	N	Entities	p-value	FDR
Neuronal System	**R-MMU-112316**	Neuronal System	14	499	5.92E-4	2.61E-2
	R-MMU-112315	Transmission across Chemical Synapses	11	293	3.24E-2	2.61E-1
	R-MMU-112310	Neurotransmitter release cycle	5	71	3.89E-3	6.73E-2
	R-MMU-210500	Glutamate Neurotransmitter Release Cycle	2	38	3.55E-2	2.61E-1
	R-MMU-212676	Dopamine Neurotransmitter Release Cycle	3	37	7.63E-3	9.89E-2
	R-MMU-399721	Glutamate binding, activation of AMPA receptors and synaptic plasticity	3	44	3.96E-2	2.61E-1
	R-MMU-6794362	Protein-protein interactions at synapses	3	89	1.12E-7	0
	R-MMU-8849932	Synaptic adhesion-like molecules	1	24	1.23E-9	1.54E-7
	R-MMU-916853	Degradation of GABA	1	2	4.35E-2	2.61E-1
Signal transduction	**R-MMU-171007**	p38MAPK events	2	12	3.45E-2	2.61E-1
	R-MMU-194138	Signaling by VEGF	10	113	2.99E-3	5.99E-2
	R-MMU-194315	Signaling by Rho GTPases	17	571	6.7E-4	2.75E-2
	R-MMU-195258	RHO GTPase Effectors	13	356	2.5E-5	1.95E-3
	R-MMU-195721	Signaling by WNT	5	230	4.62E-2	2.77E-1
	R-MMU-2179392	EGFR Transactivation by Gastrin	2	14	0	2.78E-1
	R-MMU-3769402	Deactivation of the beta-catenin transactivating complex	0	48	2.56E-3	5.12E-2
	R-MMU-399719	Trafficking of AMPA receptors	3	44	3.96E-2	2.61E-1
	R-MMU-4420097	VEGFA-VEGFR2 Pathway	10	104	1.42E-3	3.98E-2
	R-MMU-5610787	Hedgehog 'off' state	5	70	0	2.61E-1
	R-MMU-5625900	RHO GTPases activate CIT	1	14	7.57E-10	1.18E-7
	R-MMU-5625970	RHO GTPases activate KTN1	3	35	4.42E-2	2.65E-1
	R-MMU-5626467	RHO GTPases activate IQGAPs	4	30	6.01E-3	8.65E-2
	R-MMU-5658442	Regulation of RAS by GAPs	3	30	3.27E-2	2.61E-1
	R-MMU-5666185	RHO GTPases Activate Rhotekin and Rhophilins	2	6	1.09E-2	1.31E-1
	R-MMU-5673000	RAF activation	4	36	1.18E-2	1.31E-1
	R-MMU-8848021	Signaling by PTK6	6	67	5.13E-3	8.21E-2
	R-MMU-8849468	PTK6 Regulates Proteins Involved in RNA Processing	1	5	2.13E-2	1.98E-1
	R-MMU-8849471	PTK6 Regulates RHO GTPases, RAS GTPase and MAP kinases	4	19	2.53E-3	5.12E-2
	R-MMU-9006927	Signaling by Non-Receptor Tyrosine Kinases	6	67	5.13E-3	8.21E-2
Programmed cell death	R-MMU-111447	Activation of BAD and translocation to mitochondria	3	12	1.19E-2	1.31E-1
	R-MMU-264870	Caspase-mediated cleavage of cytoskeletal proteins	1	11	1.19E-2	1.31E-1
	R-MMU-114452	Activation of BH3-only proteins	3	20	3.82E-2	2.61E-1
	R-MMU-111465	Apoptotic cleavage of cellular proteins	1	45	4.28E-2	2.61E-1
Cellular respon	**R-MMU-3371497**	HSP90 chaperone cycle for steroid hormone receptors (SHR)	5	60	1.16E-2	1.31E-1
	R-MMU-3371571	HSF1-dependent transactivation	3	33	3.82E-2	2.61E-1
Cell Cycle	**R-MMU-75035**	Chk1/Chk2(Cds1) mediated inactivation of Cyclin B:Cdk1 complex	3	11	2.02E-3	5.04E-2
	R-MMU-380320	Recruitment of NuMA to mitotic centrosomes	7	121	1.97E-2	1.97E-1
	R-MMU-8852276	The role of GTSE1 in G2/M progression after G2 checkpoint	3	26	2.3E-2	2.07E-1
Development biology	**R-MMU-437239**	Recycling pathway of L1	5	43	7.07E-3	9.19E-2
	R-MMU-422475	Axon guidance	14	346	4.6E-2	2.76E-1
	R-MMU-3928663	EPHA-mediated growth cone collapse	4	21	1.35E-3	3.98E-2
	R-MMU-3928662	EPHB-mediated forward signaling	6	52	2.99E-4	1.55E-2
	R-MMU-373760	L1CAM interactions	5	87	4.22E-2	2.61E-1
	R-MMU-2682334	EPH-Ephrin signaling	7	81	1.04E-3	3.98E-2
Immune system	R-MMU-512988	Interleukin-3, Interleukin-5 and GM-CSF signaling	2	56	4.76E-5	3.13E-3
	R-MMU-449147	Signaling by Interleukins	4	290	4.25E-2	2.61E-1
	R-MMU-1169092	Activation of RAS in B cells	2	9	1.75E-2	1.86E-1
	R-MMU-982772	Growth hormone receptor signaling	2	13	0	2.78E-1
	R-MMU-5621575	CD209 (DC-SIGN) signaling	4	33	3.96E-2	2.61E-1

	Pathway ID	Description	N	Entities	p-value	FDR
Metabolism	*R-MMU-77305*	Beta oxidation of palmitoyl-CoA to myristoyl-CoA	1	1	2.2E-2	1.98E-1
	R-MMU-77289	Mitochondrial Fatty Acid Beta-Oxidation	4	45	1.88E-2	1.88E-1
	R-MMU-71032	Propionyl-CoA catabolism	2	5	5.73E-3	8.59E-2
	R-MMU-6799198	Complex I biogenesis	14	60	1.79E-10	3.73E-8
	R-MMU-611105	Respiratory electron transport	15	72	1.8E-10	3.73E-8
	R-MMU-196780	Biotin transport and metabolism	2	11	2.54E-2	2.29E-1
	R-MMU-193775	Synthesis of bile acids and bile salts via 24-hydroxycholesterol	1	2	4.35E-2	2.61E-1
	R-MMU-163200	Respiratory electron transport, ATP synthesis by chemiosmotic coupling	17	94	8.87E-11	3.73E-8
	R-MMU-1428517	The citric acid (TCA) cycle and respiratory electron transport	18	154	2.21E-8	2.3E-6
Metabolism of RNA	R-MMU-927802	Nonsense-Mediated Decay (NMD)	2	13	0	2.78E-1
	R-MMU-975957	Nonsense Mediated Decay (NMD) enhanced by the Exon Junction Complex (EJC)	2	13	0	2.78E-1
	R-MMU-450604	KSRP (KHSRP) binds and destabilizes mRNA	0	14	5.05E-5	3.13E-3
	R-MMU-450531	Regulation of mRNA stability by proteins that bind AU-rich elements	2	42	9.74E-5	5.45E-3
Metabolism of proteins	**R-MMU-948021**	Transport to the Golgi and subsequent modification	11	235	8.24E-3	9.89E-2
	R-MMU-8955332	Carboxyterminal post-translational modifications of tubulin	3	30	3.01E-2	2.61E-1
	R-MMU-72766	Translation	11	181	3.25E-3	6.73E-2
	R-MMU-72737	Cap-dependent Translation Initiation	6	65	4.5E-3	7.66E-2
	R-MMU-72702	Ribosomal scanning and start codon recognition	5	54	7.63E-3	9.89E-2
	R-MMU-72695	Formation of the ternary complex, and subsequently, the 43S complex	4	48	2.32E-2	2.09E-1
	R-MMU-72662	Activation of the mRNA upon binding of the cap-binding complex and eIFs, and subsequent binding to 43S	6	57	2.46E-3	5.12E-2
	R-MMU-72649	Translation initiation complex formation	6	56	1.75E-3	4.55E-2
	R-MMU-72613	Eukaryotic Translation Initiation	7	68	1.19E-3	3.98E-2
	R-MMU-156827	L13a-mediated translational silencing of Ceruloplasmin expression	7	59	4.07E-4	1.95E-2
Metabolism of proteins & vesicle-mediated transport	**R-MMU-8856688**	Golgi-to-ER retrograde transport	10	153	3.33E-3	6.73E-2
	R-MMU-6811434	COPI-dependent Golgi-to-ER retrograde traffic	9	117	1.49E-3	4.02E-2
	R-MMU-6807878	COPI-mediated anterograde transport	9	117	1.4E-3	3.98E-2
	R-MMU-5694530	Cargo concentration in the ER	3	52	3.96E-2	2.61E-1
	R-MMU-204005	COPII-mediated vesicle transport	7	95	6.18E-3	8.65E-2
	R-MMU-199977	ER to Golgi Anterograde Transport	11	200	2.44E-3	5.12E-2
	R-MMU-190872	Transport of connexons to the plasma membrane	3	15	4.79E-3	7.67E-2
	R-MMU-190840	Microtubule-dependent trafficking of connexons from Golgi to the plasma membrane	3	14	3.96E-3	6.73E-2
Vesicle-mediated transport	**R-MMU-6811440**	Retrograde transport at the Trans-Golgi-Network	4	54	3.35E-2	2.61E-1
	R-MMU-6811436	COPI-independent Golgi-to-ER retrograde traffic	4	49	3.35E-2	2.61E-1
	R-MMU-190861	Gap junction assembly	3	30	1.5E-2	1.65E-1
	R-MMU-190828	Gap junction trafficking	4	58	2.11E-2	1.98E-1
	R-MMU-157858	Gap junction trafficking and regulation	4	60	4.64E-2	2.78E-1
	R-MMU-1445148	Translocation of SLC2A4 (GLUT4) to the plasma membrane	3	9	1.14E-3	3.98E-2
Transport of small molecules	R-MMU-1237044	Erythrocytes take up carbon dioxide and release oxygen	2	13	3.45E-2	2.61E-1
	R-MMU-1480926	O2/CO2 exchange in erythrocytes	2	13	3.45E-2	2.61E-1
	R-MMU-8949664	Processing of SMDT1	2	16	0	2.78E-1
Organelle biogenesis & maintenance	**R-MMU-1852241**	Organelle biogenesis and maintenance	12	261	1.86E-2	1.86E-1
	R-MMU-1592230	Mitochondrial biogenesis	3	25	1.89E-2	1.89E-1
	R-MMU-5620924	Intraflagellar transport	4	61	4.86E-2	2.78E-1
Gene expression	R-MMU-8878166	Transcriptional regulation by RUNX2	2	15	0	2.78E-1
	R-MMU-9614399	Regulation of localization of FOXO transcription factors	3	9	6.75E-3	9.19E-2
	R-MMU-9614085	FOXO-mediated transcription	3	25	3.82E-2	2.61E-1
Hemostasis	R-MMU-114604	GPVI-mediated activation cascade	5	35	7.07E-3	9.19E-2
	R-MMU-75892	Platelet Adhesion to exposed collagen	2	14	3.27E-2	2.61E-1

Table RII-7. Reactome pathways altered in HET mice. In bold are shown pathways shared with HET/RES mice, in italics pathways common to RES/WT and pathways found in IND/WT are underlined.

	Pathway ID	Description	N	Entities	p-value	FDR
Neuronal system	R-MMU-888590	GABA synthesis, release, reuptake and degradation	4	38	0.001	0.054
	R-MMU-416993	Trafficking of GluR2-containing AMPA receptors	2	45	0.047	0.285
	R-MMU-264642	Acetylcholine Neurotransmitter Release Cycle	3	9	0.018	0.193
	R-MMU-181430	Norepinephrine Neurotransmitter Release Cycle	3	9	0.018	0.193
Signal transduction	R-MMU-881907	Gastrin-CREB signalling pathway via PKC and MAPK	3	9	0.018	0.193
	R-MMU-5675221	Negative regulation of MAPK pathway	5	71	0.004	0.082
	R-MMU-5674135	MAP2K and MAPK activation	5	71	0.004	0.082
	R-MMU-5610785	GLI3 is processed to GLI3R by the proteasome	2	45	0.047	0.285
	R-MMU-205043	NRIF signals cell death from the nucleus	1	2	0.044	0.285
	R-MMU-187037	Signaling by NTRK1 (TRKA)	5	71	0.004	0.082
	R-MMU-166208	mTORC1-mediated signalling	2	45	0.047	0.285
Immune system	R-MMU-1280215	Cytokine Signaling in Immune system	11	431	0.023	0.212
	R-MMU-2132295	MHC class II antigen presentation	7	25	0.044	0.285
	R-MMU-392517	Rap1 signalling	3	9	0.018	0.193
	R-MMU-622312	Inflammasomes	1	2	0.044	0.285
	R-MMU-844456	The NLRP3 inflammasome	1	2	0.044	0.285
Metabolism	R-MMU-70895	Branched-chain amino acid catabolism	3	9	0.018	0.193
	R-MMU-163210	Formation of ATP by chemiosmotic coupling	6	59	0.002	0.065
	R-MMU-422356	Regulation of insulin secretion	5	71	0.004	0.082
Metabolism proteins	R-MMU-156842	Eukaryotic Translation Elongation	0	1	0.044	0.285
	R-MMU-156902	Peptide chain elongation	0	1	0.044	0.285
	R-MMU-72689	Formation of a pool of free 40S subunits	4	38	0.001	0.054
	R-MMU-8873719	RAB geranylgeranylation	6	59	0.002	0.065
Vesicle-mediated transport	R-MMU-199991	Membrane Trafficking	29	787	0.008	0.120
	R-MMU-199992	trans-Golgi Network Vesicle Budding	6	59	0.002	0.065
	R-MMU-421837	Clathrin derived vesicle budding	6	59	0.002	0.065
	R-MMU-5653656	Vesicle-mediated transport	30	907	0.026	0.218
	R-MMU-6811442	Intra-Golgi and retrograde Golgi-to-ER traffic	13	293	0.003	0.081
Organelle biogenesis	R-MMU-8949613	Cristae formation	6	59	0.002	0.065
Development biology	R-MMU-375165	NCAM signaling for neurite out-growth	4	38	0.001	0.054
Other	R-MMU-373753 (Cell-cell communication)	Nephrin family interactions	2	45	0.047	0.285
	R-MMU-73930 (DNA repair)	Abasic sugar-phosphate removal via the single-nucleotide replacement pathway	1	2	0.044	0.285
	R-MMU-76002 (Hemostasis)	Platelet activation, signaling and aggregation	14	154	0.044	0.285
	R-MMU-5205685 (Mitophagy)	Pink/Parkin Mediated Mitophagy	1	2	0.044	0.285

Table RII-8. Unique Reactome pathways significantly enriched in HET/RES altered proteins. In bold is shown a common altered pathway with RES/WT group of altered proteins.

2.2.2 REACTOME PATHWAYS ALTERED IN *SYNGAP1*$^{+/-}$ RESCUED MICE

Subsequently, the number of pathways that were significantly altered due to the genetic rescue of *Syngap1* were checked. Pathways enriched in RES/WT mice that were common to those found significantly altered in HET/WT mice are shown in Table RII-7 (italics) whereas the eleven unique pathways arising from the RES/WT comparison are shown in Table RII-9. These pathways were related to regulation of apoptosis, signal transduction and immune system. Finally, Reactome pathways found altered in HET/WT and HET/RES represent rescued pathways (Table RII-7, pathways IDs in bold).

	Pathway ID	Description	N	Entities	p-value	FDR
Immune system	R-MMU-936440	Negative regulators of DDX58/IFIH1	2	12	0.022	0.434
	R-MMU-1266695	Interleukin-7 signaling	3	24	0.009	0.434
	R-MMU-202424	Downstream TCR signaling	3	40	0.012	0.434
	R-MMU-388841	Costimulation by the CD28 family	3	76	0.042	0.434
	R-MMU-389356	CD28 co-stimulation	2	33	0.026	0.434
	R-MMU-389357	CD28 dependent PI3K/Akt signaling	2	23	0.044	0.434
	R-MMU-912526	Interleukin receptor SHC signaling	1	29	0.034	0.434
	R-MMU-912631	Regulation of signaling by CBL	1	24	0.040	0.434
Chromatine org.	R-MMU-3214847	HATs acetylate histones	3	42	0.042	0.434
	R-MMU-3214858	RMTs methylate histone arginines	4	76	0.046	0.434
Transport of small molecules	R-MMU-917937	Iron uptake and transport	5	69	0.005	0.434
	R-MMU-917977	Transferrin endocytosis and recycling	3	38	0.019	0.434

Table RII-9. **Reactome pathways uniquely altered in RES/WT mice**.

2.2.3 REACTOME PATHWAYS ALTERED IN *SYNGAP1* INDUCED KO MICE

Overlapping pathways that were found significantly altered in HET and IND mice are shown underlined in Table RII-7, whereas the unique pathways found enriched in IND, like signal transduction, immune system or metabolism, are shown in Table RII-10.

	Pathway ID	Description	N	Entities	p-value	FDR
Cell death	R-MMU-169911	Regulation of Apoptosis	1	2	0.0010	0.569
Signal transduction	R-MMU-170660	Adenylate cyclase activating pathway	2	14	0.0010	0.569
	R-MMU-177504	Retrograde neurotrophin signalling	2	15	0.044	0.569
	R-MMU-195253	Degradation of beta-catenin by the destruction complex	2	43	0.048	0.569
	R-MMU-201681	TCF dependent signaling in response to WNT	1	137	0.045	0.569
	R-MMU-8875656	MET receptor recycling	2	13	0.034	0.569
Immune system	R-MMU-2025928	Calcineurin activates NFAT	2	14	0.039	0.569
	R-MMU-5607763	CLEC7A (Dectin-1) induces NFAT activation	2	14	0.039	0.569
	R-MMU-5607764	CLEC7A (Dectin-1) signaling	4	59	0.034	0.569
	R-MMU-936440	Negative regulators of DDX58/IFIH1 signaling	2	12	0.022	0.434
Metabolism	MU-71336 (Metaboli	Pentose phosphate pathway	2	16	0.001	0.049
	R-MMU-163210	Formation of ATP by chemiosmotic coupling	5	17	4.5E-5	1.02E-2
	R-MMU-8949613	Cristae formation	5	17	4.5E-5	1.02E-2
Other	R-MMU-8873719	RAB geranylgeranylation (metabolism of proteins)	5	77	3.1E-2	5.7E-1
	R-MMU-3371511	HSF1 activation (Cellular response to stimuli)	2	7	0.0009	0.563

Table RII-10. Pathways uniquely altered in IND mice.

2.3 GO TERM, PROTEIN DOMAIN AND KEGG PATHWAYS ENRICHMENT ANALYSES AGAINST HIPPOCAMPAL PSD REFERENCE PROTEOME

The percentage of PSD proteins identified and annotated in a given BP, CC or Molecular Function term was found to be between a range of 17-61% when the whole mouse genome was considered. To perform more focused enrichment analysis, a custom-made hippocampal PSD proteome of 5,578 proteins was generated using different previously generated datasets. The aim of these analyses was to identify specific changes occurring among postsynaptic molecular mechanisms, which could be missed by looking against the entire genome. The GO terms associated with this reference proteome at the Molecular Function and CC levels were evaluated as a measure of quality (Fig. RII-10). Three of the most enriched terms related to Molecular Function were enzyme binding, GTP binding and ion transmembrane transport activity, whereas on the CC domain, cytosolic part, synapse and membrane regions are also predominantly represented.

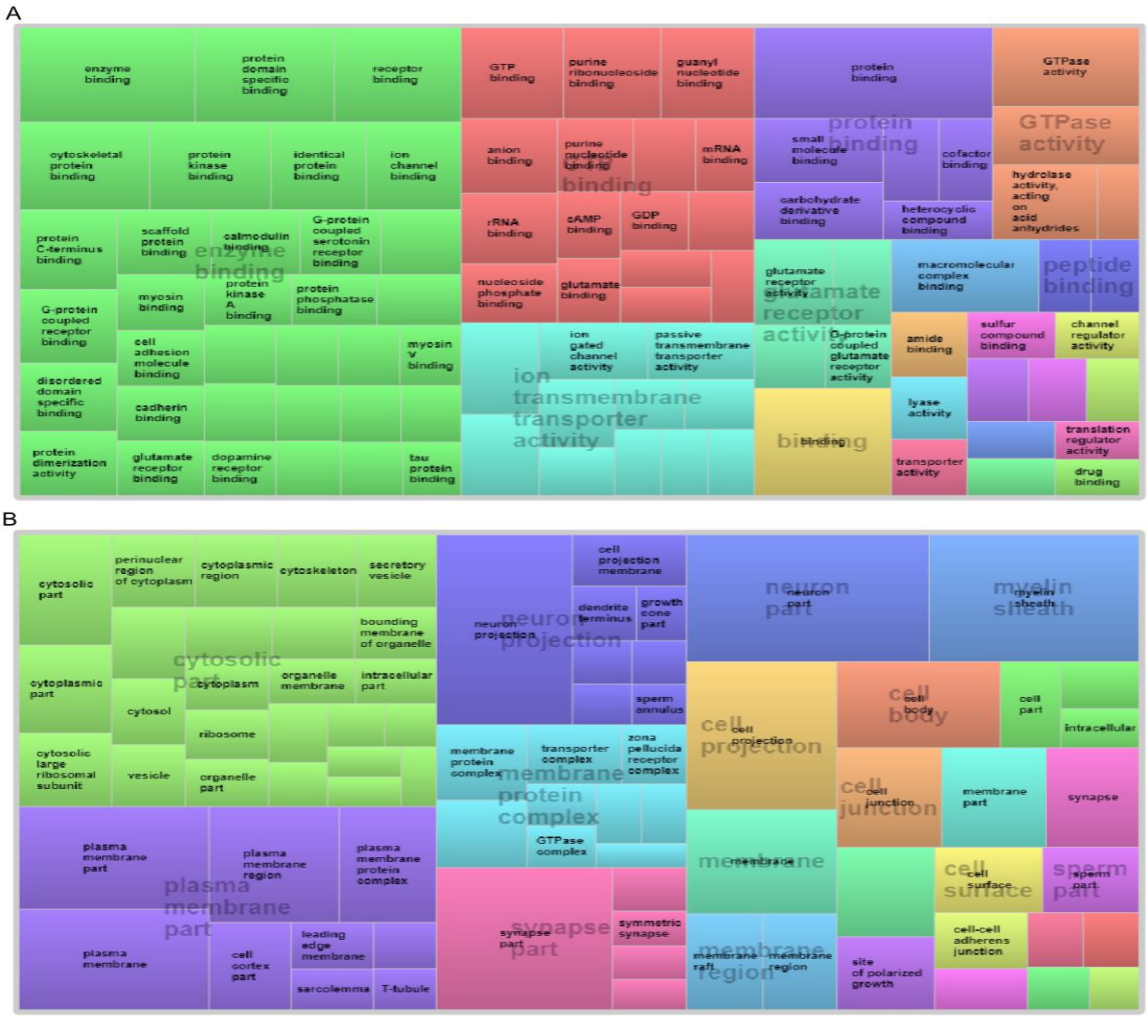

Figure RII-10. GO term for Cellular Component and Molecular Function enrichment analyses in hippocampal PSD reference proteome. The analysis was carried out through DAVID database against the whole mouse genome and redundant GO terms for CC and Molecular Function were removed by semantic similarity measure "SimRel". The size indicates the log10 p-value associated to each term, being higher squares more significant enriched terms.

2.3.1 ENRICHMENT ANALYSIS IN *SYNGAP1*$^{+/-}$ MICE

The outcome of GO term, protein domains and KEGG pathways enrichment analyses is summarized in Table RII-11. Essentially, CC and Molecular Function terms enriched were related to generation of energy/mitochondria, translation/ribosome and transport of proteins or ions. Also, an important role of Actin filament cytoskeleton related pathways and vesicle trafficking (e.g., exosomes) could be identified. Of note, three proteins associated to mTOR cascade were found altered when studied terms when CC terms were examined. When terms related to BP were assessed, up to 50 terms appeared significantly enriched being mainly involved in cell-cell signalling and modulation of synaptic transmission. Specifically, Ras, Erk1/2 and other kinases related to stress signalling are the most widely altered cascades. Moreover, pathways related to nervous system development encompassing glial differentiation and regulation of dendrite development were also found altered.

The analysis of enriched protein domains added new information to the previous analyses. Domains related to small GTPases, NSF attachment protein; the conserved region of 14-3-3 proteins; mitochondrial carriers; beta-Tubulin and Spectrin/α-Actinin were found particularly enriched among abnormally expressed PSD proteins from HETs. Interestingly, these last protein domains are closely related with cytoskeleton events.

Noteworthy, similar to Reactome pathways, there were altered GO terms significantly enriched in HET/RES mice not found in HET/WT, yet some of these terms could arise from those proteins close to reach significance in the HET/WT comparisons (Table RII-11). These include protein ubiquitination and degradation, regulation of GABAergic synaptic transmission, specific vesicle related protein complexes as well as lysosome, vacuole, nuclear matrix and extracellular GO terms for BP and CC, respectively. Regarding protein domain enrichment analysis, the main differences were found in the family of claudin proteins whereas no enrichment for 14-3-3 protein, Spectrin repeat and mitochondrial carrier protein were found in opposition to what was seen in HET/WT related analyses. Yet, some terms are common to both HET/WT and HET/RES analyses such as the term ‘small GTPase superfamily’, which will be later discussed in more detail. Furthermore, the KEGG pathway enrichment analysis identified many terms related to neurodegenerative diseases and cancer. In contrast, components from cholinergic synapse and GAP junctions were identified as uniquely altered in HET compared to RES PSDs (Table RII-12).

GO enrichment against PSD reference proteome							
ID	Description	N	p-value	ID	Description	N	p-value
Biological Process				Biological Process			
GO:0008152	metabolic process	166	0.0117	**GO:0006818**	hydrogen transport	9	0.0031
GO:0006839	mitochondrial transport	17	2.04e-12	**GO:0051179**	localization	136	1.74e-11
GO:0007005	mitochondrion organization	28	0.0042	GO:0017038	protein import	15	0.0039
GO:0010257	NADH dehydrogenase complex assembly	4	0.0296	GO:0071806	protein transmembrane transport	7	0.0095
GO:0097031	mitochondrial respiratory chain complex I biogenesis	4	0.0296	GO:0071822	protein complex subunit organization	44	0.0141
GO:0006793	phosphorus metabolic process	68	0.0096	GO:0022898	regulation of transmembrane transporter activity	12	0.0150
GO:0044710	single-organism metabolic process	81	0.0064	GO:0051647	nucleus localization	5	0.0199
GO:0042273	ribosomal large subunit biogenesis	6	0.0051	GO:0044743	intracellular protein transmembrane import	6	0.0214
GO:0006518	peptide metabolic process	40	1.24e-10	GO:0032409	regulation of transporter activity	12	0.0226
GO:0006091	generation of precursor metabolites and energy	17	0.0060	GO:0035088	establishment or maintenance of apical/basal cell polarity	5	0.0144
GO:0006119	oxidative phosphorylation	10	2.48e-11	GO:0007163	establishment or maintenance of cell polarity	11	0.0243
GO:0055114	oxidation-reduction process	34	7.38e-11	GO:0007267	cell-cell signaling	36	0.0110
GO:0016043	cellular component organization	142	3.30e-12	**GO:0050804**	modulation of synaptic transmission	21	9.74e-11
GO:1901564	organonitrogen compound metabolic process	69	5.62e-09	GO:0050803	regulation of synapse structure or activity	17	0.0071
GO:0043603	cellular amide metabolic process	44	6.93e-09	GO:0030036	actin cytoskeleton organization	26	0.0033
GO:0019538	protein metabolic process	99	0.0123	GO:0030029	actin filament-based process	28	0.0081
GO:0019637	organophosphate metabolic process	31	0.0123	**GO:0061024**	membrane organization	35	0.0074
GO:0044267	cellular protein metabolic process	91	0.0198	GO:0007265	Ras protein signal transduction	14	0.0352
GO:0044089	positive regulation of cellular component biogenesis	19	0.0213	GO:0070371	ERK1 and ERK2 cascade	10	0.0080
GO:0055086	nucleobase-containing small molecule metabolic process	23	0.0230	GO:0043434	response to peptide hormone	12	0.0457
GO:0034641	cellular nitrogen compound metabolic process	95	0.0286	GO:0070304	positive regulation of stress-activated protein kinase signaling cascade	7	0.0224
GO:0032270	positive regulation of cellular protein metabolic process	30	0.0383	GO:0007399	nervous system development	58	0.0459
GO:0044238	primary metabolic process	147	0.0472	GO:0050773	regulation of dendrite development	13	0.0026
GO:0006810	transport	121	4.83e-09	GO:0014009	glial cell proliferation	5	0.0052
GO:0015992	proton transport	9	0.0031	GO:0050792	regulation of viral process	11	0.0128

GO enrichment against PSD reference proteome							
ID	Description	N	p-value	ID	Description	N	p-value
Cellular component				Cellular component			
GO:0097458	neuron part	69	1.21e-12	GO:1902494	catalytic complex	30	0.0101
GO:0005840	ribosome	20	1.31e-12	GO:0032432	actin filament bundle	7	0.0162
GO:0043005	neuron projection	57	1.76e-12	GO:0044425	membrane part	123	0.0171
GO:0005737	cytoplasm	220	1.27e-11	GO:0044424	intracellular part	229	0.0172
GO:0043209	myelin sheath	24	1.82e-11	GO:0043234	protein complex	96	0.0243
GO:0016020	membrane	187	2.52e-11	GO:0005622	intracellular	231	0.0250
GO:0044446	intracellular organelle part	167	5.35e-11	GO:0005576	extracellular region	91	0.0269
GO:0044445	cytosolic part	17	5.47e-11	GO:0043226	organelle	220	0.0290
GO:0005924	cell-substrate adherens junction	32	1.18e-10	GO:0045202	synapse	38	0.0338
GO:0098796	membrane protein complex	54	3.43e-09	GO:0038201	TOR complex	3	0.0381
GO:0031090	organelle membrane	92	2.95e-08	GO:0031982	vesicle	97	0.0434
GO:0044444	cytoplasmic part	187	6.57e-08	GO:0043228	non-membrane-bounded organelle	95	0.0464
GO:1990204	oxidoreductase complex	20	1.21e-07	GO:0043232	intracellular non-membrane-bounded organelle	95	0.0464
GO:0031975	envelope	61	6.20e-07	GO:0042470	melanosome	8	0.0498
GO:0044429	mitochondrial part	60	1.22e-06	GO:0048770	pigment granule	8	0.0498
GO:0070469	respiratory chain	21	1.81e-05				
GO:0005739	mitochondrion	89	6.97e-05	Molecular function			
GO:0044422	organelle part	168	0.0012	GO:0003735	structural constituent of ribosome	11	3.77e-09
GO:0030054	cell junction	59	0.0013	GO:0005198	structural molecule activity	11	8.55e-10
GO:0032991	macromolecular complex	119	0.0024	GO:0005525	GTP binding	24	0.00194
GO:0043229	intracellular organelle	213	0.0028	GO:0016491	oxidoreductase activity	11	1.03e-12
GO:0070062	extracellular exosome	85	0.0030	GO:0042277	peptide binding	11	0.00396
GO:0098794	postsynapse	26	0.0044	GO:0033218	amide binding	12	0.00214
GO:1990904	ribonucleoprotein complex	31	0.0059	GO:0032403	protein complex binding	35	0.00436
GO:0042995	cell projection	70	0.0068	GO:0016655	oxidoreductase activity with different acceptors	31	1.42e-10
GO:0070069	cytochrome complex	5	0.0098	GO:0003924	GTPase activity	22	0.00431

Protein enrichment thorugh domain analysis				KEGG pathways			
IPR002453	Beta tubulin	4	0.004	mmu05016	Huntington's disease	30	26865,4
IPR000744	NSF attachment protein	3	0.005	mmu04932	Non-alcoholic fatty liver disease (NAFLD)	24	3134378
IPR001806	Small GTPase superfamily	10	0.008	mmu05012	Parkinson's disease	26	740553
IPR002017	Spectrin repeat	5	0.009	mmu00190	Oxidative phosphorylation	24	7993995
IPR023395	Mitochondrial carrier domain	6	0.013	mmu05010	Alzheimer's disease	24	2,6E+09
IPR018159	Spectrin/alpha-actinin	5	0.015	mmu03010	Ribosome	17	4E+12
IPR005225	Small GTP-binding protein domain	10	0.027	mmu05203	Viral carcinogenesis	11	0.010
IPR023409	14-3-3 protein, conserved site	3	0.036	mmu01100	Metabolic pathways	44	0.018
IPR002067	Mitochondrial carrier protein	4	0.045				

Table RII-11. **GO terms, protein domains and KEGG pathways enrichment of HET/WT altered proteins when conducted against the hippocampal PSD reference proteome using DAVID database.** In the specific case of GO terms for BP, common enriched terms to HET/RES are shown in bold. The 'N' indicates the number of proteins in the query dataset found altered belonging to the associated term. No adjusted p-values were used.

GO enrichment against PSD reference proteome							
ID	Description	N	p-value	ID	Description	N	p-value
Biological Process				Cellular Component			
GO:0006886	intracellular protein transport	33	0.005	GO:0070044	synaptobrevin 2-SNAP-25-syntaxin-1a complex	4	8.11e-11
GO:0007631	feeding behavior	5	0.028	GO:0044445	cytosolic part	16	0.001
GO:0071840	cellular component organization or biogenesis	139	0.001	GO:0043231	intracellular membrane-bounded organelle	188	0.001
GO:0002262	myeloid cell homeostasis	7	0.037	GO:0043227	membrane-bounded organelle	204	0.001
GO:0043902	positive regulation of multi-organism process	7	0.046	GO:1990204	oxidoreductase complex	11	0.002
GO:0048708	astrocyte differentiation	5	0.044	GO:0005829	cytosol	62	0.002
GO:0010608	posttranscriptional regulation of gene expression	14	0.047	GO:0044464	cell part	237	0.002
GO:0007215	glutamate receptor signaling pathway	7	0.029	GO:0016469	proton-transporting two-sector ATPase complex	7	0.003
GO:0009145	purine nucleoside triphosphate biosynthetic process	7	0.007	GO:0005622	intracellular	226	0.003
GO:0051271	negative regulation of cellular component movement	10	0.018	GO:0042470	melanosome	10	0.004
GO:0022613	ribonucleoprotein complex biogenesis	15	0.028	GO:0012506	vesicle membrane	20	0.004
GO:0010256	endomembrane system organization	21	0.046	GO:0045202	synapse	41	0.004
GO:0044802	single-organism membrane organization	32	0.003	GO:0097458	neuron part	60	0.005
GO:0051641	cellular localization	65	0.021	GO:0048475	coated membrane	9	0.006
GO:0006997	nucleus organization	7	0.049	GO:0005925	focal adhesion	22	0.006
GO:0048284	organelle fusion	10	0.029	GO:0030964	NADH dehydrogenase complex	7	0.011
GO:0032469	endoplasmic reticulum calcium ion homeostasis	4	0.014	GO:0070469	respiratory chain	9	0.011
GO:0016050	vesicle organization	12	0.043	GO:0030140	trans-Golgi network transport vesicle	4	0.017
GO:0042254	ribosome biogenesis	10	0.038	GO:0097708	intracellular vesicle	38	0.017
GO:0043408	regulation of MAPK cascade	19	0.008	GO:0005765	lysosomal membrane	12	0.018
GO:0031098	stress-activated protein kinase signaling cascade	9	0.038	GO:0034399	nuclear periphery	8	0.020
GO:0007264	small GTPase mediated signal transduction	19	0.050	GO:1990904	ribonucleoprotein complex	28	0.020
GO:0044085	cellular component biogenesis	76	0.001	GO:0005773	vacuole	34	0.020
GO:1902589	single-organism organelle organization	57	0.002	GO:0044425	membrane part	118	0.022
GO:0030865	cortical cytoskeleton organization	5	0.031	GO:0044306	neuron projection terminus	12	0.024
GO:0051656	establishment of organelle localization	16	0.037	GO:0030054	cell junction	51	0.025
GO:0016192	vesicle-mediated transport	41	0.021	GO:0001725	stress fiber	6	0.036
GO:0006996	organelle organization	98	66322	GO:0097610	cell surface furrow	5	0.046
GO:0051640	organelle localization	20	0.017	GO:0016363	nuclear matrix	6	0.047
GO:0046129	purine ribonucleoside biosynthetic process	7	0.040	GO:0012505	endomembrane system	80	0.048
GO:0022607	cellular component assembly	70	0.003	GO:0043226	organelle	221	1.16e-12
GO:0051764	actin crosslink formation	3	0.037	GO:0005737	cytoplasm	213	8.42e-08
GO:0051234	establishment of localization	108	0.004	GO:0043229	intracellular organelle	211	9.44e-10
GO:0006626	protein targeting to mitochondrion	9	0.012	GO:0016020	membrane	183	6.06e-09
GO:0070585	protein localization to mitochondrion	9	0.031	GO:0044446	intracellular organelle part	172	1.09e-10
GO:0023014	signal transduction by protein phosphorylation	18	0.033	GO:0032991	macromolecular complex	126	1.03e-11
GO:0008104	protein localization	62	0.045	GO:0031982	vesicle	112	1.41e-11
GO:0000028	ribosomal small subunit assembly	4	0.028	GO:0043234	protein complex	107	4.71e-10
GO:0030336	negative regulation of cell migration	9	0.021	GO:0005576	extracellular region	100	1.69e-11
				GO:0031090	organelle membrane	85	8.74e-07
KEGG pathways				GO:0005739	mitochondrion	70	1.78e-12
mmu05016	Huntington's disease	21	1.04e-11	GO:0098796	membrane protein complex	55	3.67e-08
mmu05010	Alzheimer's disease	20	2.62e-10	GO:0031967	organelle envelope	51	1.15e-11
mmu00190	Oxidative phosphorylation	16	4.03e-10	GO:0098805	whole membrane	51	2.96e-11
mmu05012	Parkinson's disease	16	6.9e-11	GO:0043209	myelin sheath	27	2.26e-09
mmu04721	Synaptic vesicle cycle	9	0.005	GO:0098798	mitochondrial protein complex	22	4.80e-08
mmu03010	Ribosome	14	0.005	GO:0022626	cytosolic ribosome	14	5.48e-11
mmu04540	Gap junction	10	0.006				
mmu05216	Thyroid cancer	4	0.034	Protein enrichment thorugh domain analysis			
mmu04725	Cholinergic synapse	9	0.040	IPR001806	Small GTPase superfamily	13	1.67e-12
				IPR020849	Small GTPase superfamily, Ras type	5	0.007
				IPR002453	Beta tubulin	4	0.004
				IPR000744	NSF attachment protein	3	0.005
				IPR004031	PMP-22/EMP/MP20/Claudin	3	0.036

Table RII-12. **GO term, protein domain and KEGG pathways enrichment of HET/RES significant proteins when conducted against the PSD reference proteome using DAVID database.** The 'N' indicates the number of proteins in the query dataset found altered belonging to the associated term. No adjusted p-values were used.

2.3.2 ENRICHMENT ANALYSIS IN *SYNGAP1*$^{+/-}$ RESCUED MICE

The key aim of the following set of experiments was to assess whether the molecular alterations seen at the PSD level could be reversed after recovering normal SynGAP expression at the PSD. When GO term and pathway enrichment analyses were conducted using the custom-made PSD reference proteome, proteins related to metabolic processes drove by mitochondria and ribosome as well as protein transport, vesicle related processes and components associated with the modulation of synaptic transmission were mainly

rescued together with SynGAP (Fig. RII-11&13). Indeed, the GO enrichment study of the altered PSD proteome of RES animals showed a reduced number of GO terms (20) matching with the lower number of proteins abnormally expressed in this comparison (Fig. RII-13). Still, some pathways were found altered as a result of *Syngap1*$^{+/-}$ rescued expression matching with the group of confident un-rescued proteins or collaterally altered to the genetic manipulation at PND21. These new or un-rescued altered pathways included transport and localization processes related to membrane organization. Additionally, there was a significantly high number of proteins located at the postsynapse, PSD, excitatory synapse, membrane protein complex, and macromolecular protein complexes. Interestingly, only two KEGG pathways were found enriched being one of them the 'protein processing in ER' previously identified in the other analyses against whole mouse genome.

GO enrichment against PSD reference proteome			
ID	**Description**	**N**	**p-value**
Biological pathway			
GO:0051179	localization	85	0.003
GO:1902578	single-organism localization	56	0.003
GO:0033036	macromolecule localization	48	0.017
GO:0051641	cellular localization	47	0.005
GO:0061024	membrane organization	24	0.010
GO:0044802	single-organism membrane organization	22	0.008
GO:0006886	intracellular protein transport	21	0.032
GO:0034622	cellular macromolecular complex assembly	21	0.030
GO:0010256	endomembrane system organization	16	0.024
GO:0044764	multi-organism cellular process	11	0.047
GO:0016567	protein ubiquitination	11	0.026
GO:0034728	nucleosome organization	5	0.046
GO:0001818	negative regulation of cytokine production	5	0.030
GO:0046916	cellular transition metal ion homeostasis	4	0.046
GO:0000086	G2/M transition of mitotic cell cycle	4	0.038
GO:0006826	iron ion transport	4	0.006
GO:0046718	viral entry into host cell	4	0.005
GO:0072512	trivalent inorganic cation transport	3	0.020
GO:0002753	cytoplasmic pattern recognition receptor signaling pathway	3	0.016
GO:0042044	fluid transport	3	0.016

ID	**Description**	**N**	**p-value**
Molecular function			
GO:0005515	protein binding	112	6.58e-10
GO:0042277	peptide binding	8	0.018
GO:0045502	dynein binding	4	0.019
GO:0033218	amide binding	8	0.025
GO:0031491	nucleosome binding	4	0.027
GO:0030246	carbohydrate binding	7	0.028
GO:0032403	protein complex binding	21	0.031
GO:0004842	ubiquitin-protein transferase activity	8	0.036
GO:0019787	ubiquitin-like protein transferase activity	8	0.043
Cellular component			
GO:0043234	protein complex	77	2,1E+10
GO:0030135	coated vesicle	12	2,5E+11
GO:0098796	membrane protein complex	32	5,1E+11
GO:0016020	membrane	120	5,5E+11
GO:0032991	macromolecular complex	82	8,3E+11
GO:0045202	synapse	32	9,4E+11
GO:0060076	excitatory synapse	16	9,7E+11
GO:0030120	vesicle coat	6	9,8E+11
GO:0098794	postsynapse	20	0.001
GO:0030117	membrane coat	8	0.002
GO:0097458	neuron part	44	0.002
GO:0014069	postsynaptic density	14	0.003

Protein enrichment thorugh domain analysis			
IPR000164	Histone H3	3	0.002
IPR016024	Armadillo-type fold	14	0.011
IPR011989	Armadillo-like helical	10	0.018
IPR013126	Heat shock protein 70 family	3	0.038
IPR018181	Heat shock protein 70, conserved site	3	0.038

KEGG pathways			
mmu05162	Measles	5	0.028
mmu04141	Protein processing in ER	8	0.038

Table R-13. **GO term, protein domain and KEGG pathways enrichment of RES/WT significant proteins when conducted against the PSD reference proteome using DAVID database.** The 'N' indicates the number of proteins in the query dataset found altered belonging to the associated term. No adjusted p-values were used.

Finally, the analysis of protein domain enrichment using InterPro database identified several domains characteristic of proteins dysregulated in RES animals. These included: the SPEC domain, found in molecules from the heat shock protein 70 family, the armadillo-

type fold and armadillo-like helical domains, and the Histone H3 domain (Table RII-13). Interestingly, armadillo domains are found in proteins such as Clathrin/coatomer adaptor, Adaptin-like proteins, protein phosphatases or protein kinases. Indeed, specific beta subunits of Clathrin/coatomer adaptor proteins are specifically altered but they cannot explain all the number of proteins found bearing these domains.

2.3.3 Enrichment analysis in *Syngap1*$^{+/-}$ induced KO mice

The analysis of the GO terms for BP, CC, Molecular Function and protein domain enrichment against PSD hippocampal reference proteome of the proteins found altered at PND56 when SynGAP haploinsufficiency is induced at PND21 showed that transport and localization events, mainly vesicle-mediated; purine catabolism related to apoptosis pathways and mitochondrial events, key for ATP synthesis, were found altered (Table RII-14). Of note, only 21 terms for BP were found significantly enriched contrasting with HET mice.

GO enrichment against PSD reference proteome							
ID	Description	N	p-value	ID	Description	N	p-value
Biological pathway				Cellular component			
GO:0044765	single-organism transport	87	1.11e-12	GO:0044444	cytoplasmic part	177	1E+12
GO:0060627	regulation of vesicle-mediated transport	27	1.87e-12	GO:0005743	mitochondrial inner membrane	28	7E+11
GO:1902580	single-organism cellular localization	42	1.88e-12	GO:0031967	organelle envelope	46	7E+11
GO:0006810	transport	116	2.10e-12	GO:0005753	mitochondrial proton-transporting ATP synthase complex	6	7E+11
GO:0009168	purine ribonucleoside monophosphate biosynthetic process	10	3.32e-12	GO:0031975	envelope	46	8E+11
GO:0017157	regulation of exocytosis	16	3.82e-12	GO:0031966	mitochondrial membrane	34	9E+11
GO:1990542	mitochondrial transmembrane transport	9	4.52e-11	GO:0045259	proton-transporting ATP synthase complex	6	1E+12
GO:0051650	establishment of vesicle localization	16	5.02e-11	GO:0016020	membrane	178	0.001
GO:0051234	establishment of localization	116	7.22e-11	GO:0005740	mitochondrial envelope	35	0.001
GO:0008104	protein localization	74	7.37e-11	GO:0097458	neuron part	64	0.001
GO:1902578	single-organism localization	93	5.08e-10	GO:0019866	organelle inner membrane	28	0.001
GO:0051179	localization	140	6.25e-10	GO:0098805	whole membrane	49	0.001
GO:0046129	purine ribonucleoside biosynthetic process	10	0.001	GO:0099503	secretory vesicle	22	0.002
GO:0061025	membrane fusion	14	0.001	GO:0098793	presynapse	22	0.002
GO:0051641	cellular localization	74	0.001	GO:0016023	cytoplasmic, membrane-bounded vesicle	40	0.002
GO:0016192	vesicle-mediated transport	48	0.001	GO:0099568	cytoplasmic region	19	0.002
GO:0033036	macromolecule localization	79	0.001	GO:0031410	cytoplasmic vesicle	42	0.002
GO:0061024	membrane organization	37	0.003	GO:0030141	secretory granule	15	0.003
GO:0015992	proton transport	9	0.003	GO:0097708	intracellular vesicle	42	0.003
GO:0006818	hydrogen transport	9	0.004	GO:0005737	cytoplasm	209	0.003
GO:0099003	vesicle-mediated transport in synapse	10	0.005	GO:0031988	membrane-bounded vesicle	100	0.003
				GO:0098798	mitochondrial protein complex	15	0.003
Molecular function				GO:0098796	membrane protein complex	41	0.003
GO:0044877	macromolecular complex binding	41	0.024	GO:0044455	mitochondrial membrane part	16	0.003
GO:0008092	cytoskeletal protein binding	34	0.027	GO:0016469	proton-transporting two-sector ATPase complex	7	0.003
GO:0005215	transporter activity	34	0.032	GO:0045202	synapse	42	0.003
GO:0032403	protein complex binding	31	0.023	GO:0031090	organelle membrane	72	0.004
GO:0016788	hydrolase activity, acting on ester bonds	21	0.021	GO:0044456	synapse part	36	0.004
GO:0008289	lipid binding	20	0.045	GO:0000276	mitochondrial proton-transporting ATP synthase complex, coupling factor F(o)	4	0.004
GO:0003779	actin binding	18	0.044	GO:0045178	basal part of cell	6	0.004
GO:0022804	active transmembrane transporter activity	15	0.008	GO:0005739	mitochondrion	65	0.004
GO:0042578	phosphoric ester hydrolase activity	13	0.045				
GO:0051015	actin filament binding	10	0.028	Protein enrichment thorugh domain analysis			
GO:0015399	primary active transmembrane transporter activity	9	0.035	IPR001781 PS50023	Zinc finger, LIM-type	4	0.04
GO:0000149	SNARE binding	9	0.048				
GO:0019905	syntaxin binding	9	0.010	KEGG pathway			
GO:0008565	protein transporter activity	8	0.017	mmu00030	Pentose phosphate pathway	4	0.040
GO:1902936	phosphatidylinositol bisphosphate binding	6	0.021				
GO:0005544	calcium-dependent phospholipid binding	5	0.038				
GO:0031369	translation initiation factor binding	5	0.008				
GO:0046933	proton-transporting ATP synthase activity, rotational mechanism	4	0.009				

Table R-14. **GO enrichment of IND/WT significant proteins when compared against the PSD reference proteome using DAVID database.** The 'N' indicates the number of proteins in the query dataset found altered belonging to the associated term. Since specific PSD proteome was used as a background, no adjusted p-values were used.

The compared analysis of GO terms between HET and IND animals indicated that many general terms were shared between them such as translation, cytoskeleton or protein modifications. Nevertheless, more detailed terms within each of these were different (e.g., parent term: translation, filial term in IND: translation initiation factor binding; filial term in HET: ribosome; Tables RII-11&14).

Regarding KEGG pathways enrichment analysis in IND mice, only the metabolic pentose phosphate pathway related to generation of nucleotide precursors was significantly annotated. In the case of the protein domain enrichment analysis, zinc finger motive LIM-type is the only protein domain notably enriched. Altered proteins such as LIM and SH3 protein 1 (Lasp1); Nebulette, Mical3 and Prickle1 carry this domain and possess functions related to Actin binding and/or cytoskeletal organization.

In summary, these data indicate that some pathways remain altered even due to SynGAP reduced expression from PND21 onwards, but most of the pathways related directly to translation and synaptic signalling, apparently are not affected or to a lesser degree compared to a partial developmental lack of *Syngap1*$^{+/-}$ expression.

3. INTERACTOME STUDIES AND FUNCTIONAL ANNOTATION OF ABNORMALLY EXPRESSED PSD PROTEINS

Interactome-based studies can be useful in deciphering the functional associations of genes as they allow to unravel relationship in large datasets and find subnetworks with certain properties (e.g., densely connected proteins related to a given CC or BP), paths between nodes and central nodes in network topology ("hub" genes). These analyses could help to understand the mechanisms whereby different subsets of genes altered in NDDs could drive to the same altered biological pathways and thus, explain the high co- and multimorbidity of this and other diseases.

3.1 ANALYSIS OF *SYNGAP1*$^{+/-}$ MICE INTERACTOME

The interactome arising from altered PSD proteins In HETs included 168 nodes and 712 edges. Based on this data, the average number of edges per node was ~4. This network is organized into three well-defined subnetworks with specialized features (Fig. RII-11). The first one was related to energy production/mitochondrial function, the second to ribosome/translation and the third was the SynGAP-containing subnetwork (Fig. RII-11&12).

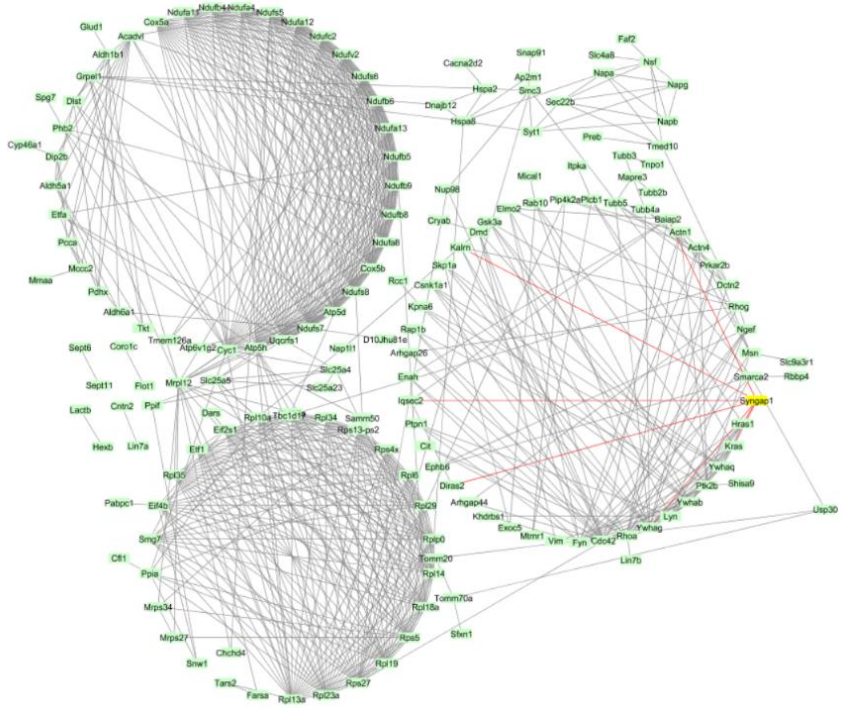

Figure RII-11. Overview of HET/WT arising interactome. Interactions of the abnormally expressed proteins retrieved from STRING database are shown. SynGAP is labelled in yellow and its likely direct interactions are coloured in red. This network includes 168 nodes (proteins) and 712 edges (interactions). The PPI sources used to build the interactome were database, co-expression, neighbourhood and gene fusion, whereas the significant score was set at medium confidence.

Among hub proteins from the SynGAP-related sub-network, there were small GTPases (e.g., Cdc42, RhoA), a GEF (i.e., Ngef), non-receptor tyrosine kinases (e.g., Fyn and Plk2b) and adaptor proteins (e.g., Ywhag). Also, the majority of mitochondrial and ribosomal proteins could be classified as hub proteins as are part or highly interconnected subnetworks. Despite SynGAP was also a hub protein, only 7 proteins from the SynGAP interactome reported in STRING database were found affected in HET mice.

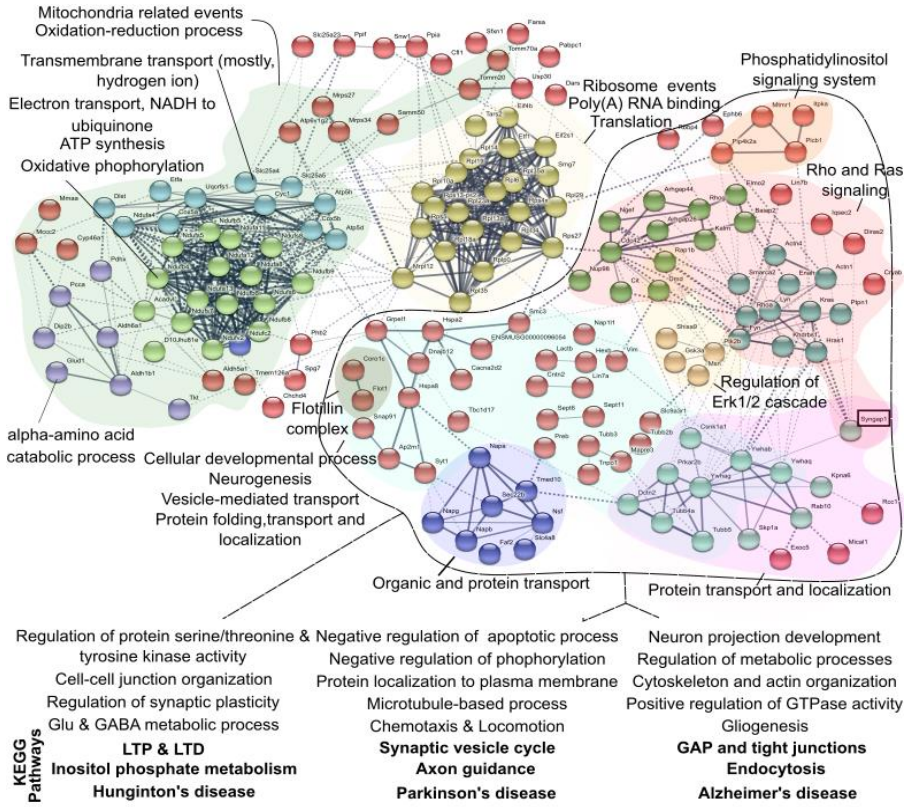

Figure RII-12. **Highly dense networks in HET/WT interactome analysis of abnormal expressed proteins.** Disconnected nodes were removed for simplicity and network edges represent the degree of PPI confidence. Therefore, line thickness correlates with the strength of data support (interaction score). PPIs were obtained from STRING using the following sources: database, co-expression, neighbourhood and gene fusion. The interaction score used was set at medium confidence (0.4). The clustering method implemented was K-means set at 10 clusters. Resulting clusters of more confident interconnected nodes are color-coded. SynGAP location is indicated within a black frame. GO term for BP and KEGG pathways enrichment conducted using indicated clusters or subnetworks of proteins were also calculated with STRING.

The mitochondrial subnetwork (shadowed in green in Fig. RII-12) can be further divided into three functionally related groups. These were defined as: 1) transmembrane transport (mostly hydrogen ions), 2) ATP synthesis and 3) α-aminoacid catabolic process. In this subnetwork, NADH dehydrogenases were hub proteins. Also, ribosome events related to translation both in mitochondria and cytosolic locations form the second densely interconnected subnetwork (shadowed in yellow in Fig. RII-12). Of note, mitochondria and ribosome associated clusters connect to a subnetwork of proteins more obviously related with dendritic spine signalling which is part of the third SynGAP-containing subnetwork.

In this third subnetwork, SynGAP connected Rho and Ras related signalling with sub-clusters formed by proteins related to protein transport or localization. Ras and Rho altered proteins linked to altered pathways like cell adhesion and synaptic plasticity at both the structural (e.g., cytoskeleton and Actin reorganization) and functional (e.g., LTP and LTD) levels. In addition, microtubule-based and chemotaxis processes, protein trafficking to membranes as well as vesicle-mediated and synaptic vesicle cycle events were found altered (shadowed in pink and circled in dot lines in Fig. RII-12).

Next, interactome subnetworks were generated for PSD proteins significantly up- or down-regulated in HET animals (Fig. RII-13). These data showed that there were fewer subnetworks as well as highly enriched inter-connected proteins in the interactome derived from up-regulated proteins compared to the interactome arising from down-regulated proteins. As previously introduced, these studies reinforced the protein tyrosine kinase Fyn as a hub protein within the up-regulated network. Also, some mitochondrial and ribosomal proteins together with SynGAP, Cdc42, Ywhag or Ywhaz (members of the14-3-3 family of proteins) were confirmed as a hub protein of the down-regulated group.

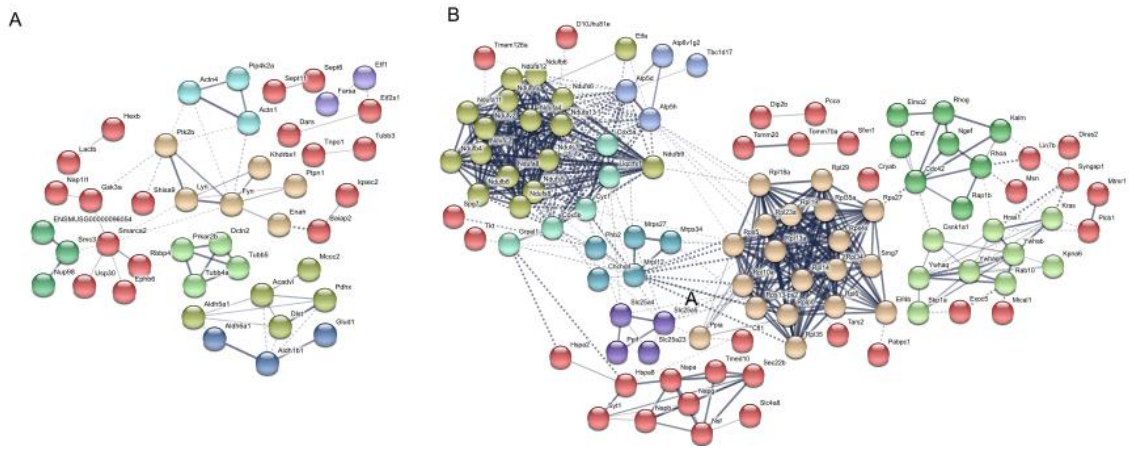

Figure RII-13. Up- and down-regulated networks and GO enrichment analysis in HET/WT interactome analysis of abnormal expressed proteins. (A) Interactome from up-regulated showing 91 nodes and 73 edges. (B) Interactome from down-regulated proteins showing 160 nodes, 456 edges. Disconnected nodes were removed for simplicity and network edges represent the degree of PPI confidence. Therefore, line thickness correlates with the strength of data support. The PPI sources used to build the interactome were database, co-expression, neighbourhood and gene fusion, whereas the interaction score used was set at medium confidence (0.4). The clustering method was K-means set at (A) 7 and (B) 9 clusters for up- and down-regulated subgroups of altered proteins, respectively. Resulting clusters are coloured differently.

The interactome arising from PSD proteins differentially expressed between HET and RES animals supported previous findings, as again three major subnetworks were formed (Fig. RII-14). Importantly, these three subnetworks presented functional characteristics related to mitochondrial function, ribosome/protein translation and SynGAP/dendritic spine signalling, as shown for HET proteins. Of note, despite a similar number of nodes as HETs

were identified (171), a reduced number of interactions (525) were found. Thus, proteins with more than 3 interactions were considered as hub proteins. Interestingly, similar proteins mentioned before such as SynGAP, Fyn or Ywhaz were confirmed as hub proteins in the SynGAP-containing subnetwork that indeed, were rescued in RES mice.

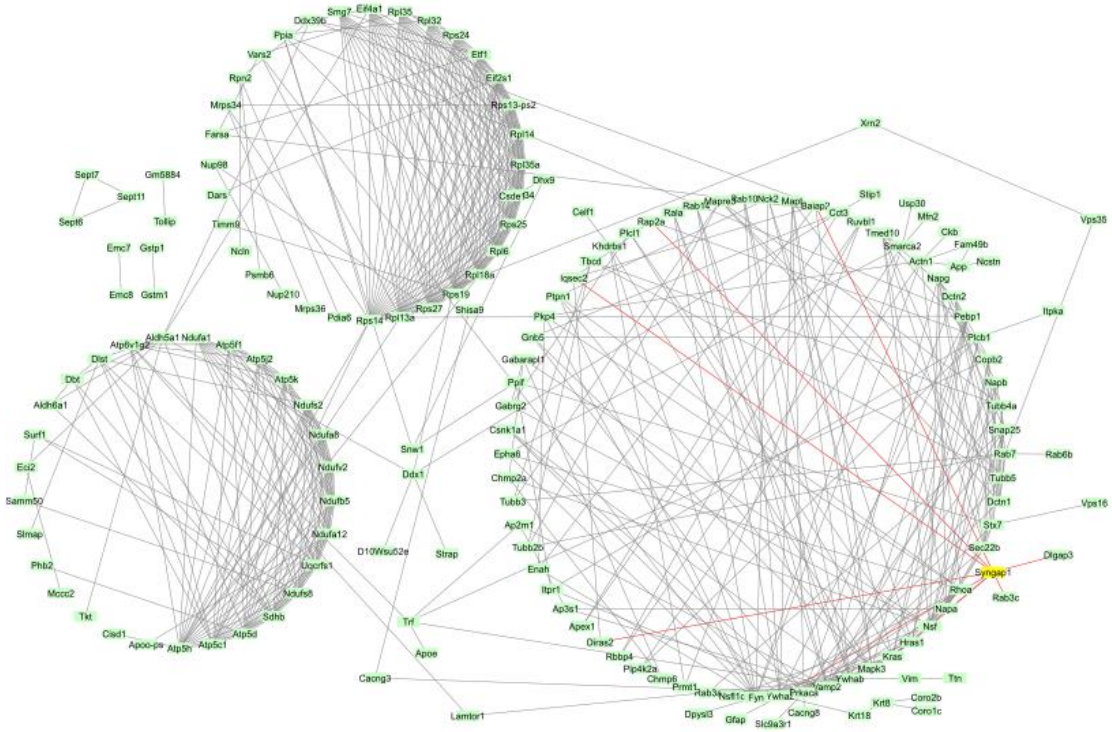

Figure RII-14. Overview of HET/RES arising interactome. Interactions of the abnormally expressed proteins retrieved from STRING database are shown. SynGAP is labelled in yellow and its likely direct interactions are coloured in red. This network includes 171 nodes (proteins) and 525 edges (interactions). The PPI sources used to build the interactome were database, co-expression, neighbourhood and gene fusion, whereas the significant score was set at medium confidence.

Furthermore, the annotation of GO terms in functionally related groups within subnetworks in HET/RES comparisons was also like that observed in the HET/WT interactome (Fig. RII-12&15). However, the SynGAP-containing and mitochondria related subnetworks formed more reduced clusters compared to those found in HET/WT comparison (Fig RII-14&15). Of note, the evaluation of networks that arose from up- and down-regulated proteins confirm Fyn as a hub protein in the up-regulated rescued proteins, whereas mitochondrial, ribosomal, SynGAP or 14-3-3 proteins would be hub proteins for the down-regulated rescued group (Fig. RII-16). Taken all these data together, an incomplete rescue of the normal protein levels was also mirrored by these interactome analyses.

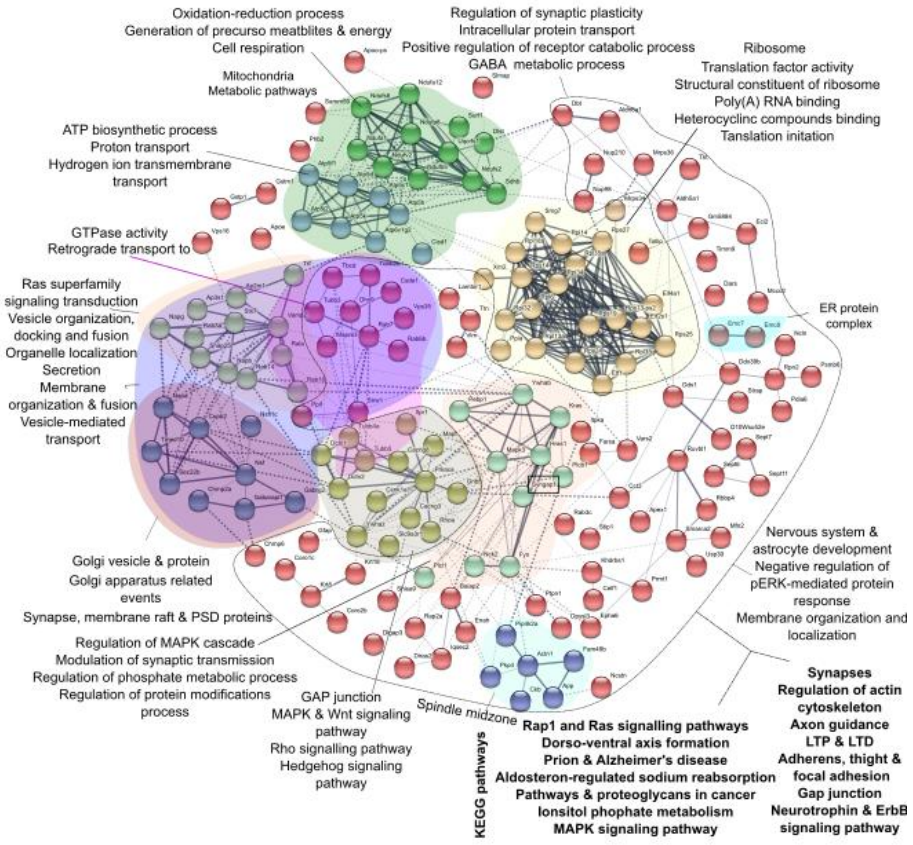

Figure RII-15. **Highly dense networks in HET/RES interactome analysis of abnormal expressed proteins.** The analysis was done using STRING database. Disconnected nodes are removed for simplicity and network edge thickness represent the degree of PPI confidence. The PPI sources used to build the interactome were: database, co-expression, neighbourhood and gene fusion and the interaction score used was set at medium confidence (0.4). The clustering method was K-means set at 10 clusters. GO term for BP and KEGG pathways enrichment conducted using indicated clusters or subnetworks of proteins were also calculated with STRING. Resulting clusters are shown color-coded.

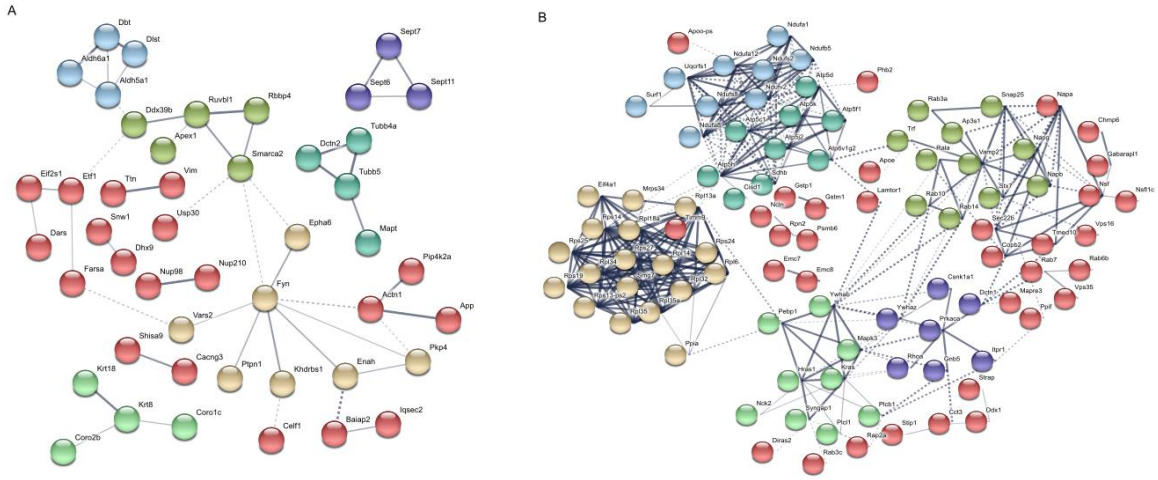

Figure RII-16. Up- and down-regulated networks in HET/RES interactome analysis of abnormally expressed proteins. Interactome from (A) up-regulated showing 91 nodes and 26 edges and (B) down-regulated proteins showing 157 nodes, 256 edges. Disconnected nodes were removed for simplicity and network edge thickness represents the degree of PPI confidence. The PPI sources used to build the interactome were database, co-expression, neighbourhood and gene fusion and the interaction score used was medium confidence (0.4). The clustering method was K-means set at 7 and 7 clusters, respectively. Resulting clusters of nodes are shown coloured differently.

3.2 ANALYSIS OF *SYNGAP1*$^{+/-}$ RESCUED MICE INTERACTOME

The interactome arising from RES/WT showed that there was a reduction of the number of nodes (75/162) which were less densely connected (only 100 edges were found). Thus, ~1.3 edges per node were found, which results in a reduction of ~3 and ~4 edges per node compared to the networks from HET/WT and HET/RES, respectively (Fig. RII-17). This interactome presents one main sub-network as well as a few smaller ones. Nevertheless, the main subnetwork does not present a majority of functionally related proteins. Hence, the major sub-networks identified previously in HET comparisons were not identified in RES/WT interactome, further supporting the high recovery of the PSD proteome.

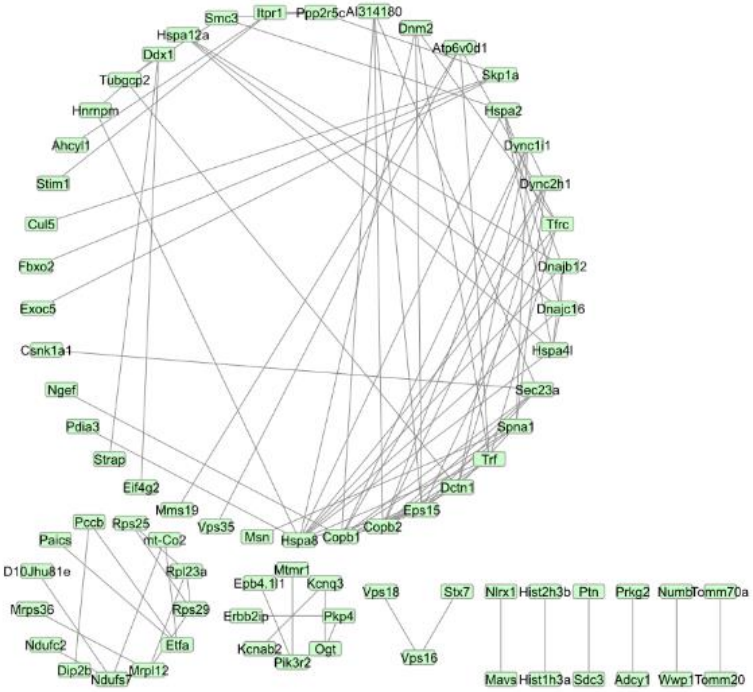

Figure RII-17. Overview of RES/WT interactome. Interactions of the abnormally expressed proteins retrieved from STRING database are shown. This network includes 75 nodes (proteins) and 100 edges (interactions). The PPI sources used to build the interactome were database, co-expression, neighbourhood and gene fusion, whereas the significant score was set at medium confidence.

Structural components of ribosome, intracellular transport and localization define the sub-networks found (Fig. RII-17&18). The annotation of well interconnected groups of proteins (shadowed in different colours in Fig. RII-18) showed that in RES PSDs there were alterations in proteins related to Ca^{2+} channel regulation, pathways related to transport of ferric ions, microtubule-based transport, vesicle-related processes and proteolysis linked to ubiquitin-dependent processes (Fig. RII-18). In addition, Copb and Dctn1 proteins were hub proteins among the up-regulated ones while Mrp12, Skp1a or Hspa8 were hub proteins in the interactome resulting from the down-regulated proteins (Fig. RII-19).

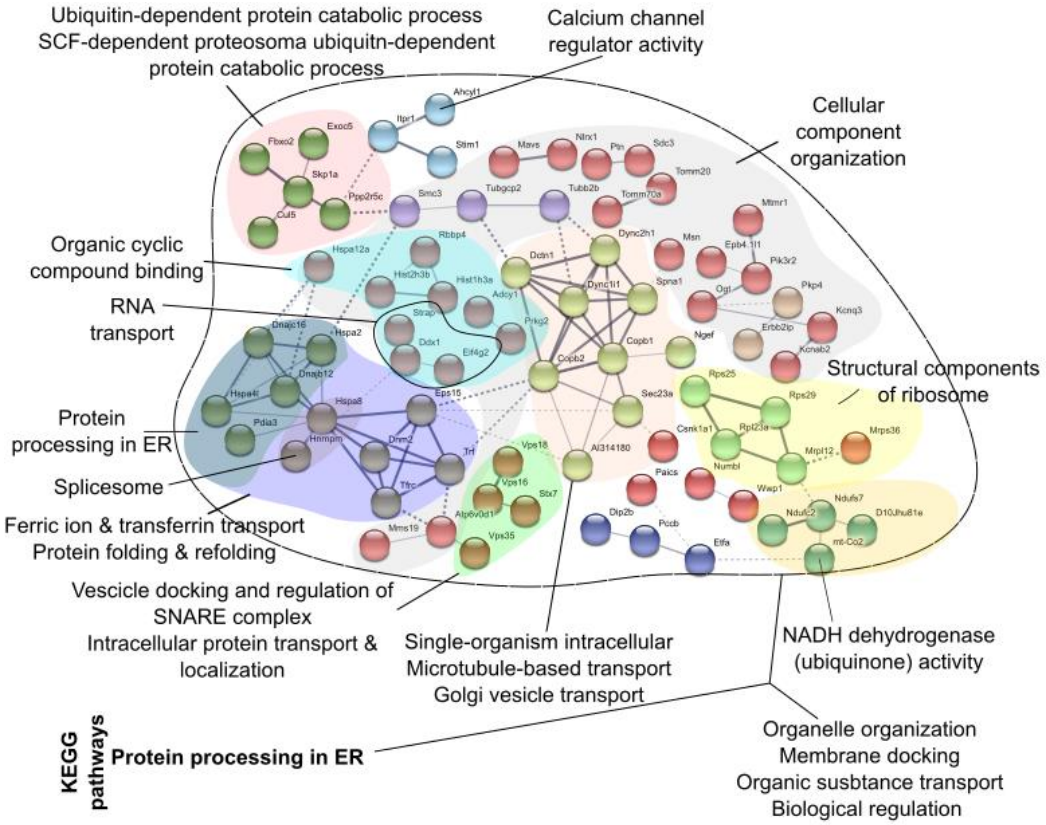

Figure RII-18. **Highly dense networks in RES/WT interactome analysis of abnormal expressed proteins.** Disconnected nodes were removed for simplicity and network edge thickness represents the degree of PPI confidence. The PPI sources used to build the interactome were database, co-expression, neighbourhood and gene fusion and the interaction score used was set at medium confidence (0.4). The clustering method was K-means set at 10 clusters which are shown coloured differently. GO term for BP and KEGG pathways enrichment conducted using indicated clusters or subnetworks of proteins were also calculated with STRING.

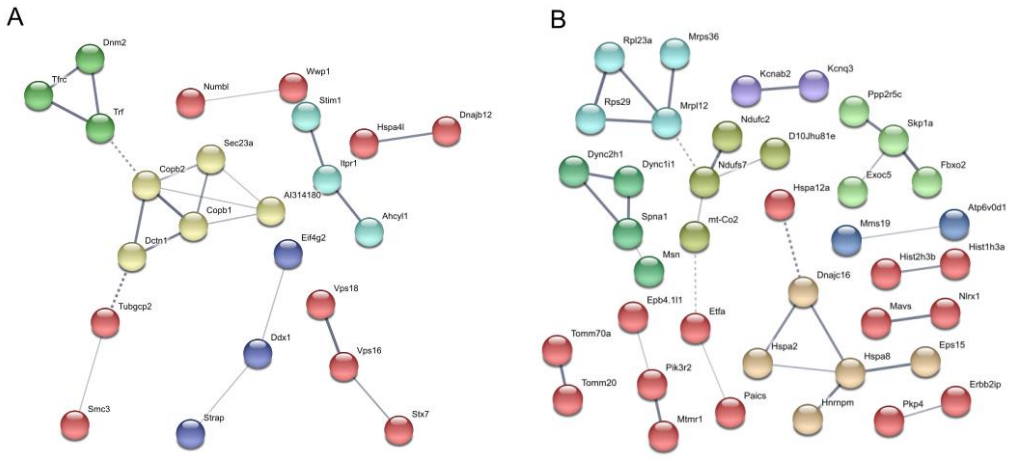

Figure RII-19. Up- and down-regulated networks in RES/WT interactome analysis of abnormally expressed proteins. (A) Interactome from up-regulated proteins with 78 nodes and 9 edges. (B) Interactome from down-regulated proteins with 82 nodes and 14 edges. Disconnected nodes were removed for simplicity and network edge thickness represents the degree of PPI confidence. The PPI sources used to build the interactome were database, co-expression, neighbourhood and gene fusion whereas the interaction score used was set at medium confidence (0.4). The clustering method was K-means set at 5 and 8 clusters, for up- and down-regulated proteins, respectively. Resulting clusters are shown coloured differently.

3.3 COMPARISON OF THE INTERACTOMES OF *SYNGAP1*$^{+/-}$ AND *SYNGAP1*$^{+/-}$ RESCUED MICE

The HET/WT interactome was compared against the RES/WT one (Fig. RII-20). A relatively small number of interacting proteins (15) was found common to both networks, which are indicative of un-rescued processes. Enrichment analysis using the BiNGO database identified terms related to protein folding (GO:0006457), protein metabolic process (GO:0019538) and organelle fission (GO:048285) among GO terms for BP. The analysis of the CC revealed that common altered proteins were mainly from mitochondria (GO:005739), part of protein complexes (GO:0043234) such as ubiquitin ligase complex (GO:0031461; GO:0019005). No terms related to ribosome were found enriched, contrarily to what was found for HETs.

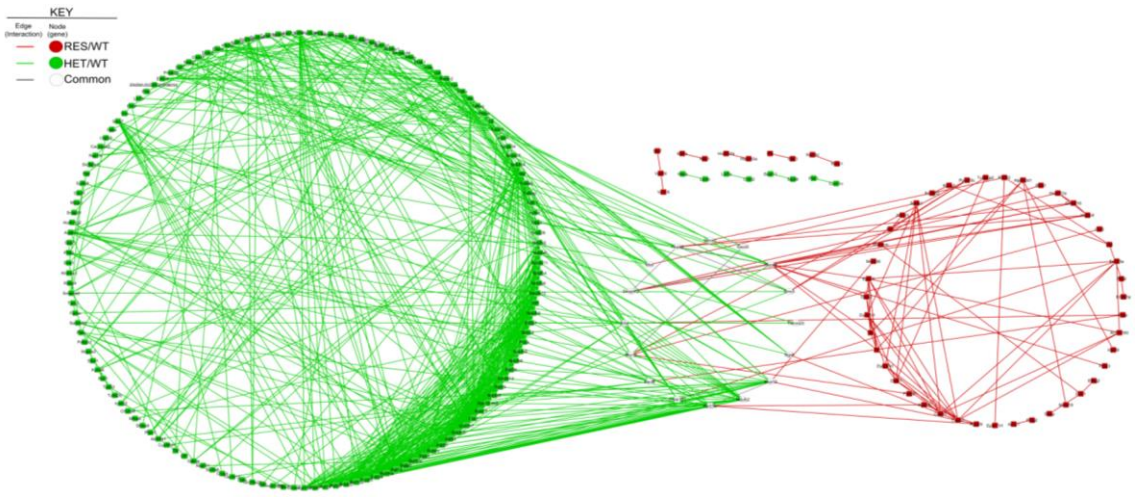

Figure RII-20. Interactome comparison between *Syngap1*$^{+/-}$ conditional KO mice line for genetic rescue studies. Common nodes and the edges between RES/WT (red) and HET/WT (green) interactomes are shown in white and grey, respectively as indicated in the legend.

3.4 ANALYSIS OF *SYNGAP1*$^{+/-}$ INDUCED KO MICE INTERACTOME

The outcome of a reduced expression of SynGAP at the PSD from PND21 onwards at the network level was also assessed. This analysis showed that the large sub-networks seen in the HET interactome were not found in the IND interactome, which only presented one sub-network (Fig. RII-21), although a similar amount of interconnected proteins (150 nodes) was reported. Furthermore, a smaller number of interactions were also found in the IND interactome (249 interactions), as the average interaction per node was ~2 while in the HET case was ~4. Therefore, based on these interactome analysis, the impact of a SynGAP reduction at the PSD level after PND21 is less damaging than an embryonic deficit.

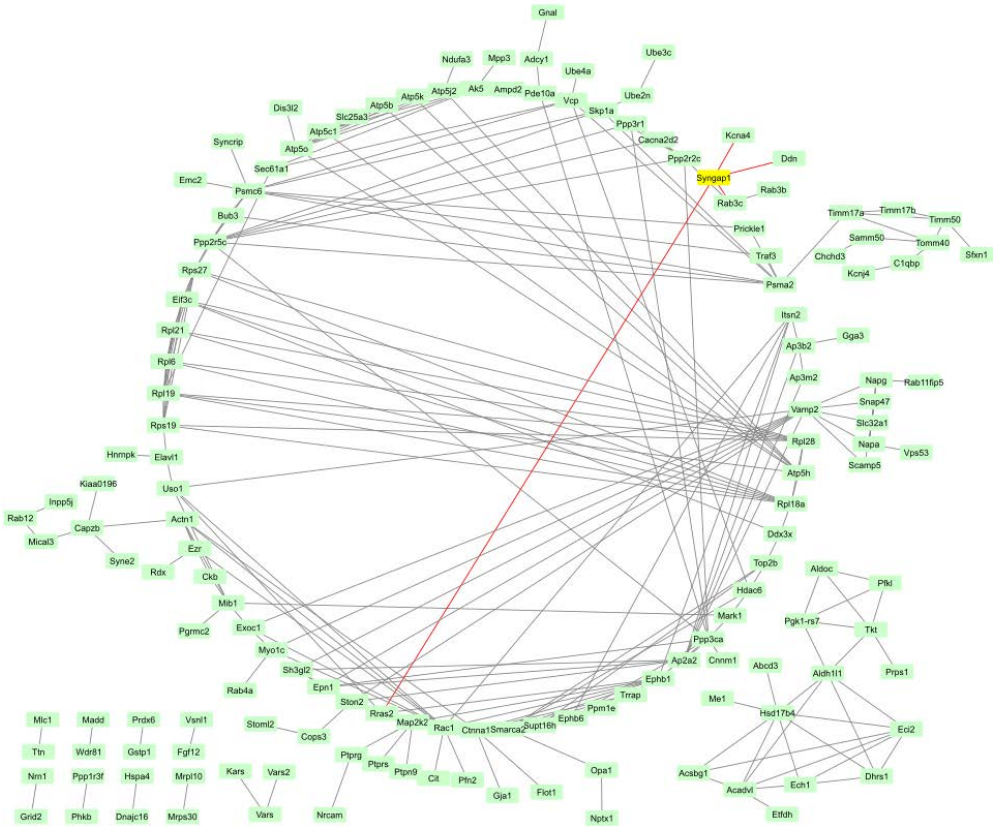

Figure RII-21. Overview of IND/WT interactome. Interactions between abnormally expressed proteins from IND mice retrieved from STRING database are shown. SynGAP is labelled in yellow and its likely direct interactions are coloured in red. This network includes 150 nodes (proteins) and 249 edges (interactions). The PPI sources used to build the interactome were database, co-expression, neighbourhood and gene fusion, whereas the significant score was set at medium confidence.

Within the one subnetwork reported, which considers all proteins regardless of their direction of change, several functional clusters could be identified (Fig. RII-22). Among them, a cluster of proteins associated to Rac1, which presented normal levels in HET animals (Fig. RII-22, shadowed in ochre), another related to ubiquitination and proteasome activity (Fig. RII-22, shadowed in green) or a group of proteins related with protein translation (Fig. RII-22, green nodes) were found. The analysis of hub proteins showed that SynGAP, Rac1, Ephb1, Rpl18a, Atp5h, PsdmC6 and Vamp2 are clear hub proteins in the IND/WT network (Fig. RII-22&23).

Specifically, the interactomes of proteins up- or down-regulated were also computed and showed that Rac1, Actn1 or structural components of the ribosome were hub proteins among up-regulated proteins (Fig. RII-22A), while for the down-regulated set of altered proteins in IND mice Ephb1, Vamp2 or ATP synthases were other hub proteins (Fig. RII-23B).

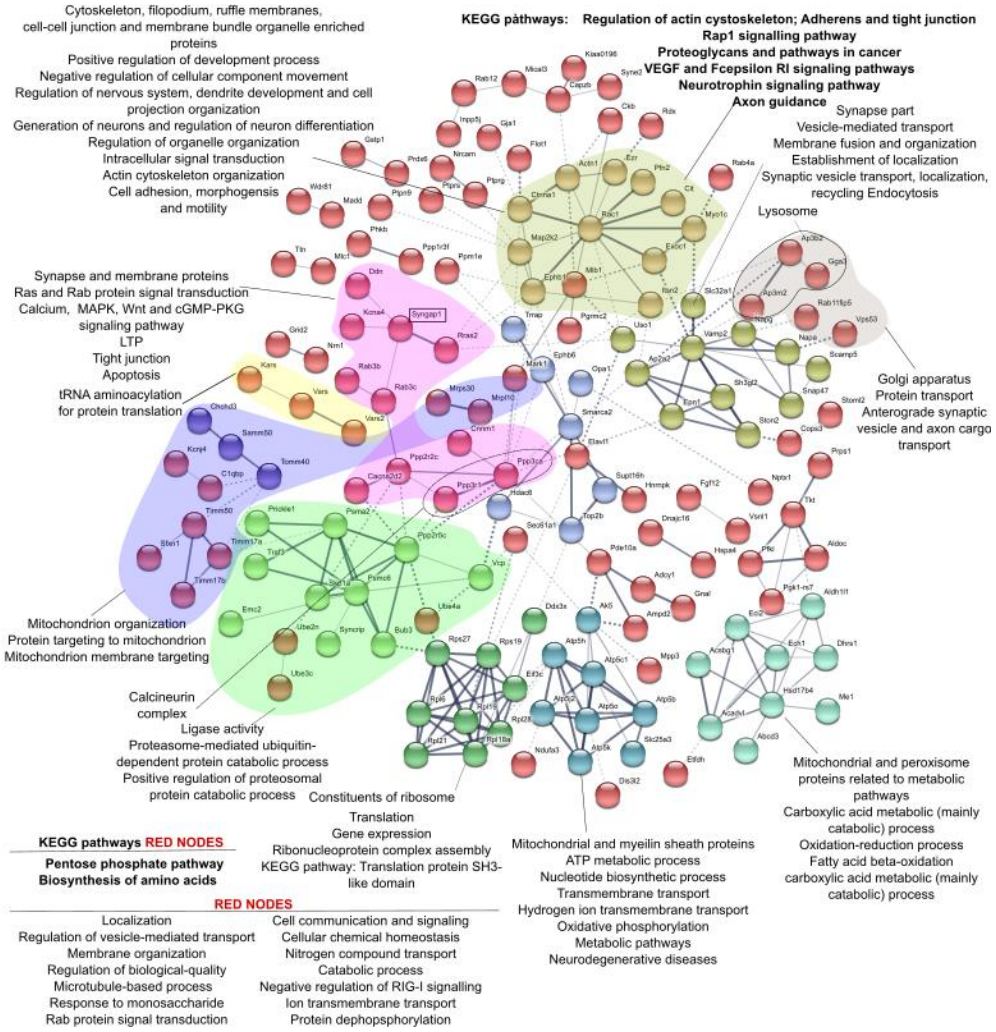

Figure RII-22. **Functional annotation of sub-networks in IND/WT interactome.** Disconnected nodes were removed for simplicity and network edges represent the degree of PPI confidence. Line thickness correlates with the strength of data support. The PPI sources used to build the interactome were database, co-expression, neighbourhood and gene fusion. The interaction score used was medium confidence (0.4). The clustering method was K-means set at 9 clusters which are shown colour-coded differently. GO term for BP and KEGG pathways enrichment conducted using indicated clusters or subnetworks of proteins were also calculated with STRING.

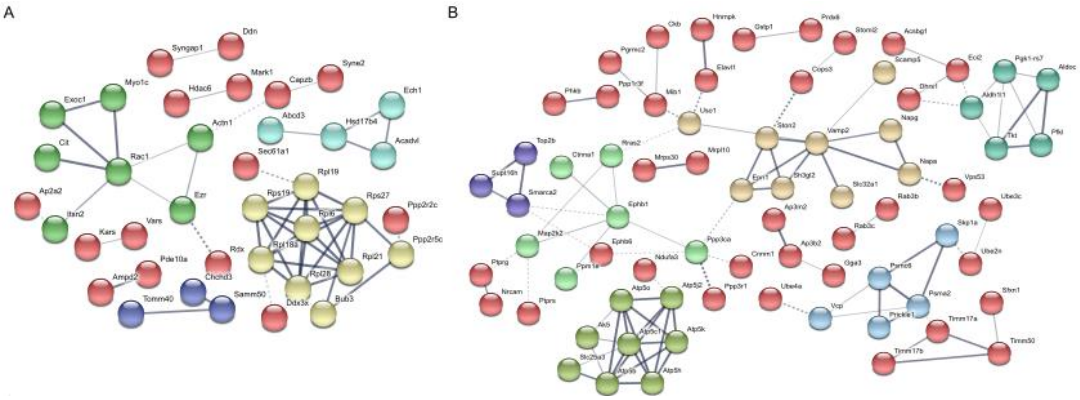

Figure RII-23. Interactomes of up- and down-regulated proteins in IND/WT mice. (A) Interactome of up-regulated proteins, with 134 nodes and 49 edges. (B) Interactome of down-regulated proteins with 114 nodes and 42 edges. Disconnected nodes are removed for simplicity and network edge thickness represents the degree of PPI confidence. The PPI sources used to build the interactome were database, co-expression, neighbourhood and gene fusion. The interaction score used was medium confidence (0.4). The clustering method was K-means set at 5 and 7 clusters for up- and down-regulated proteins, respectively. Resulting clusters are colour-coded differently.

3.5 COMPARISON OF INTERACTOMES OF *SYNGAP1*$^{+/-}$ AND *SYNGAP1*$^{+/-}$ INDUCED MICE

The interactome of proteins altered in HET animals was compared to that generated by proteins dysregulated in IND mice (Fig. RII-24). This comparison allowed to determine if the proteome alterations seen in IND mice were due to the same molecular rearrangements promoted by a germ line deficit of SynGAP.

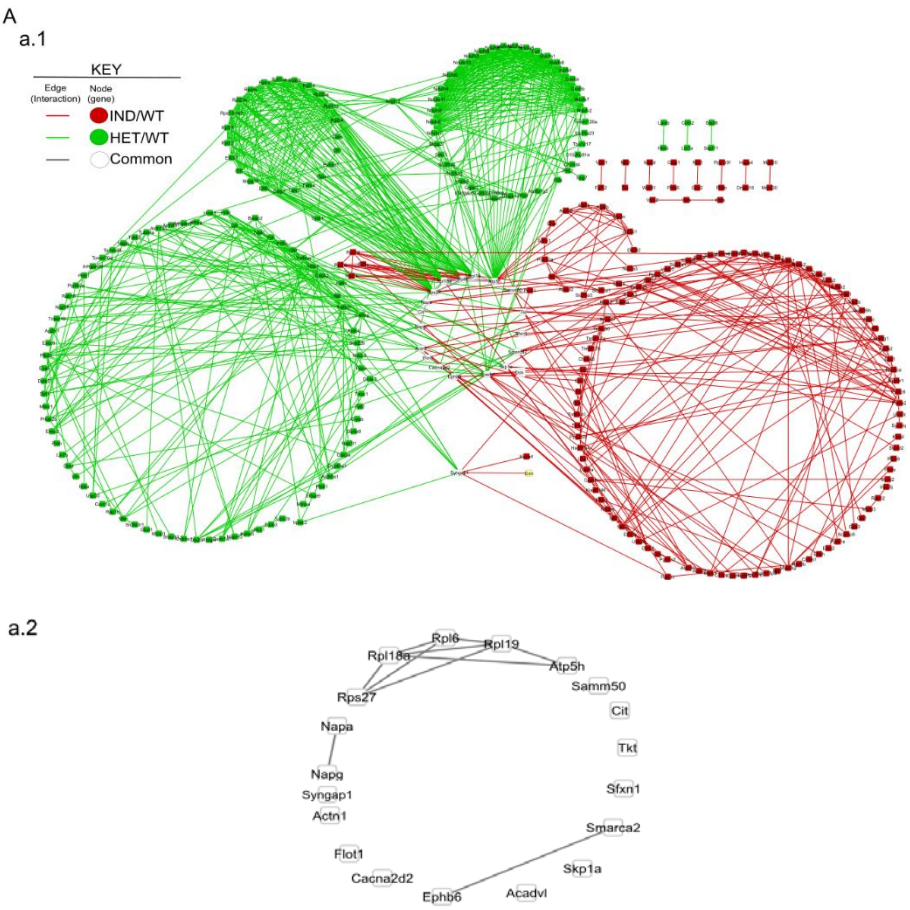

Figure RII-24. Interactome comparison between both *Syngap1* conditional KO mice lines. (a.1) Comparison of the interactomes of altered proteins from HET (green) and IND (red) when compared to their respective control littermates. (a.2) Zoom-in of the common altered proteins to both networks found in a.1 (white).

This analysis indicated that only 19 proteins with interactions to other dysregulated proteins were common to both datasets. As expected, this included SynGAP, but also proteins related to the ribosome, mitochondria, metabolism, Actin cytoskeleton and vesicular transport (Fig. RII-22, a.2). Hence, these 19 proteins are altered irrespectively of the developmental stage at which SynGAP deficiency occurs and could be particularly relevant to the molecular alterations involved in SynGAP haploinsufficiency.

4. IN-DEPTH ANALYSIS OF KEY FUNCTIONAL PROTEIN GROUPS

4.1 TRANSLATION DYSREGULATION IN *SYNGAP1*$^{+/-}$ CONDITIONAL KO MOUSE LINES

Recent reports have shown that *Syngap1* knock-down, using RNA interference methods, in rat cultured cortical neurons and *Syngap1*$^{+/-}$ mice exhibit increased basal protein synthesis (Wang, Held, and Hall 2013; Barnes et al. 2015; Paul et al. 2018). In the present study, GO enrichment terms and interactome analysis indicated that proteins related to translation are generally down-regulated in HET and IND mice, which is in apparent contradiction with the previous literature. Nevertheless, it could be possible that negative regulators of translation were down-regulated. Thus, an extended analysis of the proteins annotated with translation in both *Syngap1*$^{+/-}$ conditional KO mouse lines was conducted (Table RII-15).

UNIPROT ID	Gene Name	HET/WT	HET/RES	RES/WT	IND/WT	UNIPROT ID	Gene Name	HET/WT	HET/RES	RES/WT	IND/WT
Q9CR57	Rpl14	**0,6**	**0,7**	=	=	P62849	Rps24	=	**0,7**	=	=
Q922B2	Dars	**1,4**	**1,6**	=	=	Q9Z1N5	Ddx39b	=	**1,8**	=	=
Q8BWY3	Etf1	**1,8**	**1,9**	=	=	O55033	Nck2	=	**0,7**	=	=
P53026	Rpl10a	**0,8**	=	=	=	P62264	Rps14	=	**0,7**	=	=
P47915	Rpl29	**0,7**	=	=	=	O70133	Dhx9	=	**1,8**	=	=
P62751	Rpl23a	**0,6**	=	**0,6**	=	P60843	Eif4a1	=	**0,5**	=	=
P62717	Rpl18a	**0,6**	**0,6**	=	**0,7**	Q63844	Mapk3	0,76*	**0,7**	=	=
P14869	Rplp0	**0,7**	=	=	=	Q9CZX8	Rps19	=	**0,8**	=	**0,8**
Q9DB15	Mrpl12*	**0,3**	=	**0,4**	=	P12023	App	=	**1,3**	=	=
P84099	Rpl19	**0,7**	=	=	**0,8**	Q3U2A8	Vars2	=	**1,5**	=	**1,2**
Q3UQ84	Tars2	**0,6**	=	**0,5**	=	Q9Z1X4	Ilf3	=	**2,1**	=	=
P62702	Rps4x	**0,8**	=	=	=	P62911	Rpl32	=	**0,7**	=	=
P62301	Rps13	**0,7**	**0,7**	=	=	Q8CI78	Rmnd1*	=	**0,6**	=	=
Q8BGD9	Eif4b	**0,7**	=	=	=	Q62448	Eif4g2	=	=	**1,5**	=
Q9JIK9	Mrps34*	**0,3**	**0,4**	=	=	P62274	Rps29	=	=	**0,6**	=
Q8C0C7	Farsa	**1,7**	**1,7**	=	=	Q61584	**Fxr1**	0,88*	=	**0,6**	=
Q6ZQ58	**Larp1**	**2,1**	=	2,2*	=	P35922	**Fmr1**	1,2*	=	1,3*	**0,7**
P97461	Rps5	**0,7**	=	=	=	Q9Z1Q9	Vars	=	=	=	**0,7**
Q80YE7	**Dapk1**	**0,1**	=	**0,1**	=	Q99MN1	Kars	=	=	=	**0,8**
P19253	**Rpl13a**	**0,7**	**0,7**	=	=	O35658	C1qbp*	=	=	=	**1,6**
O55142	Rpl35a	**0,5**	**0,5**	=	=	Q3TBW2	Mrpl10	=	=	=	**1,4**
P47911	Rpl6	**0,7**	**0,8**	=	**0,8**	Q62167	**Ddx3x**	=	=	=	**0,7**
Q8BK72	Mrps27*	**0,6**	=	=	=	P41105	Rpl28	=	=	=	**0,8**
P20152	Vim	**1,9**	**2,0**	=	=	Q9D0G0	Mrps30	=	=	=	**1,4**
Q6ZWV7	Rpl35	**0,7**	**0,7**	=	=	P70372	Elavl1	=	=	=	**1,6**
Q9QVP9	Ptk2b	**1,7**	=	1,5*	=	Q8R1B4	Eif3c	=	=	=	**1,9**
Q60749	Khdrbs1	**2,4**	**2,2**	=	=	O09167	Rpl21	=	=	=	**0,7**
Q6ZWX6	**Eif2s1**	**2,3**	**2,2**	=	=	Q7TMK9	**Syncrip**	=	=	=	**0,8**

Table RII-15. List of dysregulated PSD proteins annotated with the GO term 'Translation'. In bold are shown proteins annotated as negatively regulating translation whereas positive regulators of translation are underlined. Asterisk (*) indicates mitochondrial translation. The source of GO annotations was AmiGO.

This analysis showed that a high proportion of down-regulated proteins in HET PSDs like those in the Rpl and Rps families are structural components of the ribosome. Yet, almost all proteins annotated with GO terms related to positive regulation of translation were up-regulated, whereas those proteins annotated as negative regulators of the translation were down-regulated (Table RII-15). In addition, four proteins (i.e., Mrpl12, Mrps27; Mrps34 and Rmnd1) are involved in mitochondrial translational. Accordingly, IND mice showed the same trends, although a reduced number of proteins related to translation were identified compared to HET mice. Taken all these results together, the net effect of translation

cannot be deduced since the present study only informs about the abundance of proteins with different effects in the regulation of the basal protein synthesis.

4.2 ASSESSMENT OF PSD PROTEINS WITH PHOSPHATASE ACTIVITY

As the percentage of dysregulated PSD proteins belonging to proteins with kinase and phosphatase activity was very low, in general no significant enrichment of these terms was found (Table RII-16). Only terms related to dephosphorylation and calcineurin signalling were significantly annotated in IND mice through STRING database. For all these reasons, an in-depth study of protein phosphatases was conducted, as these are functional categories important to synaptic biology that encompass a large number of proteins from the mouse genome (Table RII-16).

GO term	Name	N Panther	N LC-MS/MS	% LC-MS/MS
GO:0016301	Kinase activity	1382	241	17
GO:0019901	Protein kinase binding	714	199	28
GO:0016791	Phosphatase activity	432	76	18

Table RII-16. Number of total proteins in *Mus musculus* annotated with GO terms related to kinase or phosphatase activity. The number of proteins annotated in AmiGO with the indicated term (N Panther), identified in both *Syngap1* conditional mice lines (N LC-MS/MS) as well as the corresponding percentage (% LC-MS/MS) are shown.

Interestingly, similar numbers but different protein kinases were found altered in HET and IND mice. Of note, the CAMKII-δ kinase was found significantly up-regulated in HET/WT and HET/RES mice, which indicates that it is recovered in RES mice (see the complete list of altered proteins in Table RII-25). However, the most outstanding finding was that in IND animals, a remarkably higher number of protein phosphatases, including calcineurin (Ppp3Ca), were found as compared with HET animals. Namely, the latter only had 3 abnormally expressed PSD phosphatases while IND mice had 15, being significantly enriched against whole genome (Table RII-17). It is worth noting that RES mice also showed altered expression of 5 phosphatases which were also significantly enriched. In fact, Cdk5rap3 is an un-rescued phosphatase that is also found altered in IND mice that exerts roles in apoptosis, unfolded protein response in ER and ubiquitin-related processes.

	Molecular function proteins *Mus Musculus*					
	UNIPROT ID	Gene Name	HET/WT	HET/RES	RES/WT	IND/WT
Phosphatase activity	P35821	Ptpn1	**3,4**	**3,1**	=	=
	Q99LM2	Cdk5rap3	**2,2**	=	**2,8**	**0,5**
	Q9Z2C4	Mtmr1	**0,7**	=	**0,7**	=
	Q8C8T7	Elfn1	=	**1,4**	=	=
	Q66GT5	Ptpmt1	=	=	**0,4**	=
	Q60996	Ppp2r5c	=	=	**0,8**	**0,8**
	O55023	Impa1	=	=	**1,6**	=
	Q5ND34	Wdr81	=	=	=	**0,8**
	Q8BG02	Ppp2r2c	=	=	=	**0,6**
	Q2M3X8	Phactr1	=	=	=	**0,6**
	Q63810	Ppp3r1	=	=	=	**1,8**
	P63329	Ppp3ca	=	=	=	**1,2**
	Q9D880	Timm50	=	=	=	**1,5**
	B0V2N1	Ptprs	=	=	=	**1,2**
	Q9Y6H1	Chchd3	=	=	=	**1,2**
	Q35239	Ptpn9	=	=	=	**0,6**
	Q80TL0	Ppm1e	=	=	=	**1,3**
	P97434	Mprip	=	=	=	**0,8**
	Q05909	Ptprg	N/A	N/A	N/A	**1,6**

	Molecular function proteins *Mus Musculus*					
	UNIPROT ID	Gene Name	HET/WT	HET/RES	RES/WT	IND/WT
Phosph	P35821	Ptpn1	**3,4**	**3,1**	=	=
	Q99LM2	Cdk5rap3	**2,2**	=	**2,8**	**0,5**
	Q9Z2C4	Mtmr1	**0,7**	=	**0,7**	=
	Q8C8T7	Elfn1	=	**1,4**	=	=
	Q66GT5	Ptpmt1	=	=	**0,4**	=
	Q60996	Ppp2r5c	=	=	**0,8**	**0,8**
	O55023	Impa1	=	=	**1,6**	=
	Q5ND34	Wdr81	=	=	=	**0,8**
	Q8BG02	Ppp2r2c	=	=	=	**0,6**
	Q2M3X8	Phactr1	=	=	=	**0,6**
	Q63810	Ppp3r1	=	=	=	**1,8**
	P63329	Ppp3ca	=	=	=	**1,2**
	Q9Y6H1	Chchd3	=	=	=	**1,2**
	Q9D880	Timm50	=	=	=	**1,5**
	B0V2N1	Ptprs	=	=	=	**1,2**
	Q9Y6H1	Chchd3	=	=	=	**1,2**
	Q35239	Ptpn9	=	=	=	**0,6**
	Q80TL0	Ppm1e	=	=	=	**1,3**
	P97434	Mprip	=	=	=	**0,8**
	Q05909	Ptprg	N/A	N/A	N/A	**1,6**

Table RII-17. List of proteins altered in at least one *Syngap1*$^{+/-}$ genetic condition comparison annotated with phosphatase activity in AmiGO database. Bold text indicates significant FC differences. N/A stands for non-available, thus this protein was not identified in the indicated mouse line. Binomial statistics showed that the enrichment of phosphatases was only significant in two groups: HET/WT p=0.099; HET/RES p=0.23; RES/WT p=7.8E-03 and IND/WT showed a p=2.9E-12.

4.3 ASSESSMENT OF SMALL GTPASES AND ITS REGULATORS EXPRESSION AT THE PSD

Proteins related to small GTPase signalling were found significantly altered and mainly down-regulated in HET mice. Thus, an in-depth analysis of the small GTPases and their regulators in both *Syngap1* conditional KO mice lines was conducted (Table RII-18). This evaluation showed that different members of Ras, Rab, Rho and Ran families of small GTPases were found altered among the different genotype comparisons, as previously found by GO term enrichment analyses (Table RII-3, 3 & 6). The specific members of the Ras family found altered in at least one genotype comparison were p21 Ras (HRas, KRas, RRas2), Rap (Rap1b, Rap2a) and Ral (RalA). In the case of Rho family, Cdc42, Rho (RhoA, RhoG) and Rac (Rac1) were found dysregulated at least in one case. Also, a wide range of different members of the Rab family (i.e., Rab3a, Rab3b, Rab3c, Rab4a, Rab6b, Rab7a, Rab10, Rab12, Rab14 and Rab21) were found altered depending on the genotype comparison (Table RII-18, left panel).

Strikingly, in both HET/WT and HET/RES comparisons the clear majority of the small GTPases were found down-regulated like SynGAP. However, the majority of the small GTPases found altered in IND mice, were found up-regulated and were different from those altered in the *Syngap1* conditional KO line for genetic rescue experiments. For instance, Rabs were found down-regulated in HETS but up-regulated in IND mice, whereas different members of the Ras family (i.e., H/KRas *vs.* RRas2) were abnormally expressed depending on when *Syngap1*$^{+/-}$ haploinsufficiency starts

	Molecular function proteins *Mus Musculus*					
	UNIPROT ID	Gene Name	HET/WT	HET/RES	RES/WT	IND/WT
Small GTPases	P60766	Cdc42	**0,7**	=	=	=
	Q5PR73	Diras2	**0,6**	**0,7**	=	=
	Q61411	Hras	**0,7**	**0,6**	=	=
	P32883	Kras	**0,7**	**0,7**	=	=
	P61027	Rab10	**0,6**	**0,7**	=	=
	P35283	Rab12	=	=	=	**0,6**
	Q91V41	Rab14	=	**0,8**	=	=
	P35282	Rab21	**0,7**	=	=	=
	P63011	Rab3a	=	**0,7**	=	=
	Q9CZT8	Rab3b	=	=	=	**1,4**
	P62823	Rab3c	=	**0,7**	=	**1,7**
	P56371	Rab4a	N/A	N/A	N/A	**1,5**
	P61294	Rab6b	=	**0,5**	=	=
	P51150	Rab7a	=	**0,7**	=	**1,6**
	P63001	Rac1	=	=	=	**0,7**
	P63321	Rala	=	**0,6**	=	=
	Q99JI6	Rap1b	**0,7**	=	=	=
	Q80ZJ1	Rap2a	=	**0,7**	=	=
	Q9QUI0	Rhoa	**0,6**	**0,7**	=	=
	P84096	Rhog	**0,6**	**0,7**	=	=
	P62071	Rras2	=	=	=	**1,3**

	Molecular function proteins *Mus Musculus*					
	UNIPROT ID	Gene Name	HET/WT	HET/RES	RES/WT	IND/WT
GAP	**Q6ZQ82**	**Arhgap26**	**1,3**	=	=	=
	P59281	**Arhgap39**	**1,3**	=	=	=
	Q5SSM3	**Arhgap44**	**1,7**	=	**1,5**	=
	Q9WUM4	Coro1c	**1,8**	**1,8**	=	=
	Q68FH0	Pkp4	=	**1,3**	**0,8**	=
	F6SEU4	**Syngap1**	**0,6**	**0,8**	=	**0,7**
GEF	Q8CHT1	Ngef	**0,6**	=	**0,5**	=
	A2CG49	Kalrn	**0,8**	=	**0,8**	=
	Q8VE37	Rcc1	**3,2**	**3,2**	=	=
	Q9WUQ2	**Preb**	**1,6**	=	=	=
	Q5DU25	**Iqsec2**	**1,2**	**1,4**	=	=
	Q9CQ22	Lamtor1	**=**	**0,4**	**2,3**	=
	Q80U28	**Madd**	**=**	=	=	**1,3**
	Q9Z0R6	Itsn2	**=**	**=**	=	**0,8**
GDI	**Q921I6**	**Sh3bp4**	=	=	**3,0**	**2,9**

Table RII-18. **List of altered small GTPases and its regulators in both *Syngap1*$^{+/-}$ conditional KO mice lines**. Bold numbers stand for the FCs between comparisons. The annotations were retrieved from AmiGO database. UniProt ID and gene names in bold are reported as SynGAP interactors in the custom-made SynGAP interactome.

Regarding the expression of small GTPase regulators, all proteins with GAP activity other than SynGAP are found up-regulated in HET mice (Fig. RII-18, left panel). Of note, several Arhgaps (Rho GTPase-activating proteins) were found altered being one of them clearly un-rescued (Arhgap44). In contrast, two GEFs were found significantly down-regulated in HET mice and un-rescued in RES mice. Conversely, three GEFs including the Preb GEF for SAR1B; Rcc1, a Ran GEF, and the ARF GEF Iqsec2, were found significantly up-regulated. Of these, the last two were rescued. It is worth noting that Lamtor1, which is a GEF for the small GTPase Rag and has a role in regulate protein synthesis among other biological processes, was found specifically altered due to PND21 *Syngap1* rescued expression (Table RII-16). Eventually, in RES/WT and IND/WT comparisons, the GDI (see section 2.5.3.1 from introduction) Sh3bp4 was found significantly up-regulated, which might be an effect derived from changing SynGAP levels from PND21 onwards.

5. SLOT MODEL HYPOTHESIS ASSESSMENT

GO term for Molecular Function enrichment analysis against whole genome showed that in HET mice, there was an enrichment of altered proteins with a motif binding to PDZ and SH3 domains (Fig. RII-8). These proteins were further explored and compared between genotypes to help validate the slot model hypothesis described previously (Walkup et al. 2016). Briefly, SynGAP-α1 isoform binds to all three PDZ domains of PSD-95 and can occupy as many as 15% of these PDZ domains (Walkup et al. 2016). Thus, the slot model hypothesis states that reduced levels of SynGAP-α1 at the PSD would vacate its binding slots to PDZ domains of PSD-95 and other MAGUKs. This would, in turn, allow for other PSD-95 interactors to become more abundant at the PSD. Proteins such as TARPs, Neuroligins or LRRTMs accomplished this model as demonstrated by IB (Walkup et al. 2016).

Interestingly, similar expression levels were found in this study and in the work of Walkup et al. for PSD-95, Nlg-1 and Nlg-2 (Table RII-19). Of these only Nlgn-2 was significantly up-regulated in the HET animals. Instead, LRRTM2, another PSD-95 partner, was found up-regulated by IB but with no expression changes were revealed in this study. Finally, these authors found an increased expression of four TARPs (Cacng2,3,4 and 8) by using an antibody common to all of them. Yet, one of them was not identified in our study (Cacng4). When the expression of these proteins was added, no differences or a tendency to be also up-regulated was found in HET/WT and HET/RES comparisons, respectively. Furthermore, the specific TARPs Cacng3 and Cacng8 were found up-regulated in both HET comparisons, but only in HET/RES these differences reached statistical significance.

Protein	Gene Name	Uniprot ID	Walkup et al., 2016	HET/WT	HET/RES	RES/WT	IND/WT
SynGAP	Syngap1	F6SEU4	Down	**0,6**	**0,8**	=	**0,7**
PSD-95	Dlg4	Q62108	=	=	=	=	=
TARPs-γ-2,3,4 i 8	-	-	Up	=	1,2*	=	=
TARPs-γ-2	Cacng2	O88602	N/A	=	=	=	=
TARPs-γ-3	Cacng3	Q9JJV5	N/A	1,17*	**1,2**	=	=
TARPs-γ-8	Cacng8	Q8VHW2	N/A	1,15*	**1,3**	=	=
LRRTM2	Lrrtm2	Q8BGA3	Up	=	=	=	=
Neuroligin-1	Nlgn1	Q99K10	=	=	=	=	=
Neuroligin-2	Nlgn2	Q69ZK9	Up	**1,4**	1,2*	=	=

Table RII-19. Expression levels of proteins assessed by IB that supported the slot model. Bold FCs are significantly altered whereas * indicates that statistical significance was not achieved (Walkup et al. 2016).

To further assess the slot model hypothesis, the expression levels of proteins annotated with a PBM were assessed. Furthermore, the slot model could also be extended to SH3 binding partners of SynGAP, which has an SH3 binding motif, that could bind to PSD-95 through its SH3 binding domain. To test these hypotheses, the lists of proteins annotated

with GO terms 'PDZ domain binding' and 'SH3 domain binding' were retrieved (Table RII-20) and compared to our list of altered proteins (Table RII-27&28).

GO term	Name	N Panther	N LC-MS/MS	% LC-MS/MS
GO:0030165	PDZ domain binding	117	51	44
GO:0017124	SH3 domain binding	129	56	43

Table RII-20. Number of total proteins in *Mus musculus* annotated in AmiGO with GO terms PDZ and SH3 domain binding. The number of proteins annotated with this term (N Panther), identified in both *Syngap1* conditional mice lines (N LC-MS/MS) as well as the corresponding percentage (% LC-MS/MS) are shown.

These analyses indicated that more than 50% of proteins annotated with a PBM were up-regulated in HET/WT and HET/RES comparisons (Table RII-21, left panel). Of note, another AMPAR associated protein with a PBM not evaluated by Walkup and collaborators, Shisa9, was found two-fold up-regulated. Nonetheless, this is the only protein that remained with an altered abundance after rescuing SynGAP levels. Thus, these results would partially disagree with the slot model, as no differences would be expected between RES and WT expression levels for those proteins subjected to this hypothesis. Moreover, in the case of the IND/WT assessment, an unexpected higher number of PBM-containing proteins were down-regulated than up-regulated (Fig. RII-21, left panel).

	Molecular function proteins *Mus Musculus*					
	UNIPROT ID	Gene Name	HET/WT	HET/RES	RES/WT	IND/WT
PDZ domain binding	Q99MI1	Erc1	**0,7**	=	=	=
	Q3UHD1	Bai1	**1,3**	=	=	=
	O88951	Lin7b	**0,6**	=	=	=
	P49025	Cit	**1,2**	=	=	**0,8**
	P46460	Nsf	**0,6**	**0,8**	=	=
	Q8BKX1	Baiap2	**1,5**	**1,7**	=	=
	P70441	Slc9a3r1	**1,6**	**1,5**	=	=
	Q9CZN4	Shisa9	**2,0**	**3,3**	**0,6**	=
	Q9JJV5	Cacng3	=	**1,2**	=	=
	Q6PH08	Erc2	=	=	**0,8**	=
	O88952	Lin7c	=	=	**0,6**	=
	Q63932	Map2k2	=	=	=	**1,8**
	P52189	Kcnj4	=	=	=	**0,7**
	Q61625	Grid2	=	=	=	**2,0**
	O88910	Mpp3	=	=	=	**0,5**
	P23242	Gja1	=	=	=	**0,8**

	Molecular function proteins *Mus Musculus*					
	UNIPROT ID	Gene Name	HET/WT	HET/RES	RES/WT	IND/WT
SH3 domain binding	Q8VDP3	Mical1	**0,4**	=	=	=
	P25911	Lyn	**2,9**	=	=	=
	F6SEU4	Syngap1	**0,6**	**0,8**	=	**0,7**
	Q60749	Khdrbs1	**2,4**	**2,2**	=	=
	P49025	Cit	**1,2**	=	=	**0,8**
	Q8BHL5	Elmo2	**0,8**	=	**0,7**	=
	P62484	Abi2	**0,7**	=	**0,8**	=
	P0C7L0	Wipf3	**0,6**	=	**0,6**	=
	Q03173	Enah	**1,8**	**1,5**	=	=
	Q62188	Dpysl3	=	**0,7**	=	=
	Q60749	Khdrbs1	=	**2,2**	=	=
	P10637	Mapt	=	**1,5**	=	=
	P42567	Eps15	=	=	**0,8**	=
	P39054	Dnm2	=	=	**1,4**	=
	P59644	Inpp5j	=	=	=	**2,2**
	P23242	Gja1	=	=	=	**0,8**
	Q921I6	Sh3bp4	2.8*	=	**3,0**	**2,9**

Table RII-21. List of altered proteins in both *Syngap1*$^{+/-}$ conditional KO mouse lines annotated as 'PDZ domain binding' and/or 'SH3 domain binding protein'. Bold numbers stand for significant different FCs between comparisons. * indicates that the difference was not statistically significant.

SynGAP isoforms have a SH3 domain binding motif, with SynGAP-α2-containing isoforms expressing also this motif in its C-term as predicted by its sequence (Chapter I). Previously, the high expression of SynGAP-α2 in the PSD has been also demonstrated (see results Chapter I). Despite a direct interaction of SynGAP/SynGAP-α2 and the SH3 domain from PSD-95 has not been reported, the applicability of the slot model for SH3 domain binding motif-containing proteins and SH3 domains from PSD-95 was also assessed.

Up to 6 out of 12 proteins annotated with the term 'SH3 domain binding' were found significantly up-regulated in HET/WT and/or HET/RES (Table RII-19, right panel). Also, almost all altered SH3 domain binding motif-containing proteins in RES/WT were found down-regulated. Yet, the FC of 3 of those 4 up-regulated proteins (i.e., the tyrosine-protein kinase Lyn, Khdrbs1 and the protein enabled homolog [Enah]) have a high FC (ranging from 1.8 to 2.9). In the case of IND mice, only 2 out of 5 SH3 binding motif-containing proteins showed increased expression. Based on these data, an applicability of the slot model to certain SH3 binding motifs containing-proteins couldn't be ruled out.

5.1 ANALYSIS OF PSD-95 DIRECT INTERACTORS

As previously shown, not all proteins annotated with a PBM followed the rationale of the slot model hypothesis. It could be possible that despite some proteins have a PBM, they are not direct interactors of PDZ domains of PSD-95 or, at least, part of the PSD-95 interactome. Hence, mouse PSD-95 interactomes retrieved from several databases were used to generate a PSD-95 interactome of 458 non-redundant direct or indirect interactors. From these 458, 304 proteins were identified in the PSDs from both *Syngap1*$^{+/-}$ KO lines. Next, the group of altered proteins from those identified as a component of the PSD-95 interactome, were subjected to a manual annotation of the PBM by using several approaches including a PBM predictor (see MII-4.2.8.1; Fig. RII-22).

	PSD-95 interactome *Mus Musculus*													
	UNIPROT ID	Gene Name	PBM	HET/WT	HET/RES	RES/WT	IND/WT	UNIPROT ID	Gene Name	PBM	HET/WT	HET/RES	RES/WT	IND/WT
PSD-95 interactome	P70441	Slc9a3r1	YES	**1,6**	**1,5**	=	=	Q91WD5	Ndufs2		=	**0,8**	=	=
	P56564	Slc1a3		**2,3**	**2,9**	=	=	Q11011	Npepps	YES	=	**0,7**	**1,4**	=
	Q5DU25	Iqsec2	YES	**1,2**	**1,4**	=	=	P19157	Gstp1		=	**0,6**	=	**1,5**
	Q6PHZ2	Camk2d		**1,4**	**1,4**	=	=	Q91VR2	Atp5c1		=	**0,6**	=	**1,4**
	Q8BKX1	Baiap2	YES	**1,5**	**1,7**	=	=	Q8K0S0	Phyhip		=	**0,6**	=	**1,6**
	Q8BWF0	Aldh5a1		**1,3**	**1,3**	=	=	Q8K183	Pdxk	YES	=	**0,5**	1,6*	=
	P57780	Actn4		**1,4**	=	=	=	Q9CZY3	Ube2v1		=	**0,5**	=	=
	P31324	Prkar2b		**1,7**	=	=	=	P62264	Rps14		=	**0,7**	=	=
	P26443	Glud1		**1,9**	**1,7**	=	=	P17809	Slc2a1		=	**0,8**	=	=
	Q8C1B7	D5Ertd606e		**2,0**	**2,2**	=	=	Q63844	Mapk3		=	**0,7**	=	=
	Q69ZK9	Nlgn2	YES	**1,4**	=	=	=	P63101	Ywhaz		=	**0,8**	=	=
	P49025	Cit	YES	**1,2**	=	=	**0,8**	P62823	Rab3c	YES	=	**0,7**	=	**1,7**
	P99024	Tubb5	YES	**3,7**	**3,1**	=	=	Q91V41	Rab14		=	**0,8**	=	=
	Q6ZWR6	Syne1	YES	**1,2**	=	=	=	O55023	Impa1		=	=	**1,6**	=
	Q9CWF2	Tubb2b		**6,2**	**4,8**	=	=	P27773	Pdia3		=	=	**1,3**	=
	Q3UHD1	Bai1	YES	**1,3**	=	=	=	Q8K0U4	Hspa12a	YES	=	=	**0,8**	=
	Q80YE7	Dapk1	YES	**0,1**	=	**0,1**	=	P51863	Atp6v0d1		=	=	**0,8**	=
	Q91V61	Sfxn3		**0,5**	**0,6**	=	=	Q8K4G5	Ablim1	YES	=	=	**0,9**	=
	P48962	Slc25a4		**0,6**	=	=	=	P62482	Kcnab2		=	=	**0,8**	=
	P51881	Slc25a5		**0,6**	=	=	=	Q80UW2	Fbxo2		=	=	**0,7**	=
	P28663	Napb		**0,7**	**0,8**	=	=	Q8BIZ1	Anks1b	YES	=	=	**0,8**	**0,6**
	Q9DB05	Napa	YES	**0,7**	**0,6**	=	**1,4**	Q91V14	Slc12a5		=	=	=	**1,3**
	P46460	Nsf	YES	**0,6**	**0,8**	=	=	Q62420	Sh3gl2		=	=	=	**1,5**
	P63017	Hspa8	YES	**0,7**	=	**0,7**	=	Q91V12	Acot7		=	=	=	**1,6**
	P17156	Hspa2		**0,6**	=	**0,6**	=	P63328	Ppp3ca		=	=	=	**1,2**
	O35129	Phb2		**0,5**	**0,6**	=	=	P09411	Pgk1	YES	=	=	=	**1,4**
	P40142	Tkt	YES	**0,6**	**0,6**	=	**1,3**	P61089	Ube2n		=	=	=	**1,8**
	P46096	Syt1		**0,8**	=	=	=	Q99JY8	Plpp3		=	=	=	**1,4**
	Q3UXZ6	Fam81a		**0,7**	=	=	=	P56480	Atp5b	YES	=	=	=	**1,7**
	P18760	Cfl1		**0,8**	=	=	=	Q9DB20	Atp5o		=	=	=	**2,0**
	A2CG49	Kalrn		**0,8**	=	**0,8**	=	P05063	Aldoc		=	=	=	**1,4**
	Q8K377	Lrrtm1	YES	**0,4**	=	**0,4**	=	Q61423	Kcna4	YES	=	=	=	**1,2**
	P61982	Ywhag		**0,8**	=	=	=	Q9CZT8	Rab3b	YES	=	=	=	**1,4**
	F6SEU4	Syngap1	YES	**0,6**	**0,8**	=	**0,7**	Q810U4	Nrcam		=	=	=	**1,4**
	P83510	Tnik		**0,8**	=	=	**0,8**	P46660	Ina		=	=	=	**0,7**
	Q9CQV8	Ywhab		**0,7**	**0,7**	=	=	P16330	Cnp		=	=	=	**0,7**
	P61027	Rab10		**0,6**	**0,7**	=	=	P52189	Kcnj4	YES	=	=	=	**0,7**
	P17742	Ppia		**0,6**	**0,6**	=	=	P63001	Rac1		=	=	=	**0,7**
	Q3UH60	Dip2b		**0,6**	=	**0,6**	=	P35922	Fmr1		=	=	=	**0,7**
	Q6PFD5	Dlgap3	YES	=	**1,3**	=	=	Q6ZWQ0	Syne2	YES	=	=	=	**0,6**
	P12023	App		=	**1,3**	=	=	Q60803	Traf3		=	=	=	**0,8**
	Q60864	Stip1		=	**0,7**	=	=	P24369	Ppib		=	=	=	**0,7**
	P60879	Snap25		=	**0,8**	=	=	P04370	Mbp		=	=	=	**0,7**
	Q9CZN4	Shisa9	YES	**2,0**	**3,3**	**0,6**	=							

Table RII-22. List of altered proteins from the PSD-95 interactome. A PSD-95 interactor list was built by using data reported for *Mus musculus* from Mint, Mentha, Interact and Imex databases (September 2018). This table showed the list of proteins altered in at least one *Syngap1* genetic condition comparison of proteins found in the PSD-95 interactome. Bold numbers stand for the FCs between comparisons.

Up to 15 proteins from the PSD-95 interactome that were found altered in HET/WT mice had a PBM (excluding SynGAP; Table RII-20). According to the slot model, 60% of the altered proteins in HET/WT comparisons that are likely direct interactors of the PSD-95 through its PBM were found up-regulated. When assessed those proteins found in the group of confidently rescued (i.e., altered in both HET/WT and HET/RES comparisons) ~62% were found significantly up-regulated, further supporting the slot model. In the case of RES/WT comparison, only 1 out of 7 altered proteins from the PSD-95 interactome with a PBM was found up-regulated. Finally, in the case of IND mice, 12 altered proteins that belong to the PSD-95 complex presented a PBM. From these, ~58% were found up-regulated (Table RII-22). Altogether, this data supports the slot model hypothesis for more than half of the altered proteins belonging to the PSD-95 interactome and with a PBM.

6. ANALYSIS OF A PROTEIN SCAFFOLDING ROLE FOR SYNGAP

The proposed role of SynGAP as a PSD scaffolding protein (Sheng and Kim, 2011) suggests that its interactors should be down-regulated in HET mice. In addition, based on this hypothesis, other scaffolding or adaptor proteins could take over this role of SynGAP and thus become up-regulated.

UNIPROT ID	Gene Name	Source	HET/WT	HET/RES	RES/WT	IND/WT
P56564	Slc1a3	Wilkinson et al., 2015; I-B-M	**2,3**	**2,9**	=	=
P61027	Rab10	Wilkinson et al., 2015; I-B-M	**0,6**	**0,7**	=	=
P61982	Ywhag	Wilkinson et al., 2015;I-B-M	**0,8**	=	=	=
Q8BKX1	Baiap2	Wilkinson et al., 2015; I-B-M	**1,5**	**1,7**	=	=
Q8R071	Itpka	Wilkinson et al., 2015; I-B-M	**1,7**	**1,8**	=	=
Q5DU25	Iqsec2	Wilkinson et al., 2015; I-B-M	**1,2**	**1,4**	=	=
Q9QVP9	Ptk2b	Wilkinson et al., 2015; I-B-M	**1,7**	**=**	=	=
P59281	Arhgap39	Wilkinson et al., 2015; I-B-M	**1,3**	=	=	=
Q3UXZ6	Fam81a	Wilkinson et al., 2015; I-B-M	**0,7**	**0,9**	=	=
A2CG49	Kalrn	Wilkinson et al., 2015; I-B-M	**0,8**	=	**0,8**	=
F6SEU4	Syngap1	Intact, Biogrid and Mentha	**0,6**	**0,8**	=	**0,8**
P83510	Tnik	Intact, Biogrid and Mentha	**0,8**	=	=	**0,9**
Q61411	Hras	Intact, Biogrid and Mentha	**0,7**	**0,6**	=	=
Q5PR73	Diras2	Intact, Biogrid and Mentha	**0,6**	**0,7**	=	=
Q80TS7	Ddn	Intact, Biogrid and Mentha	**1,3**	=	=	=
Q99JI6	Rap1b	Intact, Biogrid and Mentha	**0,7**	=	=	=
P32883	Kras	Intact, Biogrid and Mentha	**0,7**	**0,7**	=	=
Q6PFD5	Dlgap3	Wilkinson et al., 2015; I-B-M	**=**	**1,3**	=	=
Q80ZJ1	Rap2a	Intact, Biogrid and Mentha	**=**	**0,7**	=	=
Q3USB7	Plcl1	Wilkinson et al., 2015; I-B-M	**=**	**0,5**	=	=
P63011	Rab3a	Wilkinson et al., 2015; I-B-M	**=**	**0,7**	=	=
P63101	Ywhaz	Wilkinson et al., 2015; I-B-M	**=**	**0,8**	=	=
Q60864	Stip1	Wilkinson et al., 2015; I-B-M	**=**	**0,7**	=	=
P62823	Rab3c	Wilkinson et al., 2015; I-B-M	**=**	**0,7**	=	**1,7**
Q63844	Mapk3	Wilkinson et al., 2015; I-B-M	**=**	**0,7**	=	=
P62482	Kcnab2	Wilkinson et al., 2015; I-B-M	**=**	=	**0,8**	=
Q8K4G5	Ablim1	Wilkinson et al., 2015; I-B-M	**=**	**=**	**0,9**	=
Q80UW2	Fbxo2	Wilkinson et al., 2015; I-B-M	**=**	=	**0,7**	=
Q8BIZ1	Anks1b	Wilkinson et al., 2015;I-B-M	**=**	**=**	**0,8**	**0,6**
P58281	Opa1	Wilkinson et al., 2015;I-B-M	**=**	**=**	=	**0,9**
Q80TS7	Ddn	Wilkinson et al., 2015;I-B-M	**=**	**=**	=	**0,7**
Q61423	Kcna4	Wilkinson et al., 2015;I-B-M	**=**	=	=	**1,2**
P35922	Fmr1	Intact, Biogrid and Mentha	**=**	**=**	=	**0,7**
P62071	RRas2	Intact, Biogrid and Mentha	**=**	=	=	**1,3**

Table RII-23. List of SynGAP interactors altered in at least one *Syngap1*$^{+/-}$ genetic condition. Bold numbers stand for the significant FCs between comparisons. I-B-M stands for IntAct, BioGRID and Mentha databases.

To unveil these questions, the expression level of reported SynGAP interactors was assessed more deeply. It is worthwhile noting that by the time of this analysis, the STRING database didn't include the last update of the SynGAP interactome reported by Wilkinson and colleagues (Wilkinson et al. 2017). Therefore, an in-house SynGAP interactome was built. A final list of 258 interactors was obtained, of these, around 124 (68%) proteins were identified in the hippocampal PSD dataset generated in this study. From these 124

interactors, only 38 showed abnormal expression levels at the PSD when all genotype comparisons were considered (Table RII-23). Interestingly, ~56% of these likely interactors were found down-regulated like SynGAP. Noteworthy, a number of these 38 proteins were also altered in more than one comparison, although generally low overlapping degrees were observed between genotypes, with the exception of the comparison between HET/WT and HET/RES. Although not all these reported proteins are known to be direct SynGAP interactors, they could be part of SynGAP-containing complexes as shown by interactome analyses and by the significant enrichment of the term "scaffold protein binding" in the HET/RES comparison (GO:0097110; Fig. RII-8).

Subsequently, proteins annotated with a signalling adaptor activity in the AmiGO database were retrieved to evaluate if other proteins could compensate the lack of the scaffold provided by SynGAP (Table RII-24). Up to 12 proteins belonging to this GO term were identified in the different PSD datasets from this study (Table RII-24, top panel), being 4 of them abnormally expressed in at least one genetic comparison (Table RII-24, bottom panel). Of note, Khdrbs1 and Baiap2 were found in the confident group of rescued up-regulated proteins with high FCs but were not found altered in IND mice. Therefore, these proteins could accomplish the role of SynGAP as scaffolding protein when *Syngap1*$^{+/-}$ haploinsufficiency had an embryonic origin. However, this effect could be related to other circumstances. Finally, this effect was not observed for other scaffolding proteins when as IND mice didn't show alterations in the expression levels of any signalling adaptor protein.

GO term	Name	N Panther	N LC-MS/MS	% LC-MS/MS
GO:0035591	signalling adaptor activity	51	12	24

	Molecular function proteins *Mus Musculus*						
	UNIPROT ID	Gene Name	Source	HET/WT	HET/RES	RES/WT	IND/WT
Adaptor	Q60749	Khdrbs1	AmiGO	**2,4**	**2,2**	=	=
	Q8BKX1	Baiap2	AmiGO	**1,5**	**1,7**	=	=
	Q8VCF0	Mavs	AmiGO	**0,5**	=	**0,67**	=
	O55033	Nck2	AmiGO	=	**0,7**	=	=

Table RII-24. Analysis of proteins with an adaptor/scaffolding activity. (Top) Number of total proteins in *Mus musculus* annotated with the GO term 'signalling adaptor activity'. The number of proteins annotated with this term (N Panther), identified in both *Syngap1* conditional mice lines (N LC-MS/MS) as well as the corresponding percentage (% LC-MS/MS) are shown. (Bottom) Signalling adaptor proteins found altered in at least one genotype comparison.

7. ORTHOGONAL METHODS USED TO VALIDATE LC-MS/MS DATA

Alternative methods to LC-MS/MS analysis were conducted to corroborate the results found. Thus, in addition to SynGAP expression and PSD-95 assessment by IB shown before, other proteins were investigated using this method. Also, hippocampal LTP induction, expression and maintenance in conventional KO and IND mice was evaluated.

7.1 IMMUNOBLOT ANALYSIS OF PROTEIN LEVELS IN *SYNGAP1*$^{+/-}$ AND *SYNGAP1*$^{+/-}$ RESCUED MICE

IB analyses indicates that the expression of the small GTPase HRas is down-regulated in HET animals, as determined by quantitative proteomics. Nevertheless, the difference observed did not reach statistical significance (Fig. RII-25A). On the other hand, no up-regulation was observed for Dynactin2, which was clearly up-regulated by LC-MS/MS (Fig. RII-25B). Cofilin-1 was found down-regulated in the HET mice PSDs and IB data suggests a similar trend. Yet, this protein was found insufficiently expressed in the PSD to be reliably detectable by IB as demonstrated through subcellular localization analyses (Fig. RII-25C).

Since several hypothesized technical issues (Fig. RII-25D) were faced to reliably quantify by IB proteins found significantly altered through LC-MS/MS studies, qualitative subcellular localization analyses were conducted for those proteins that could not be detected by IB in the PSD (Fig. RII-25E). This analysis indicated that some proteins such as Cofilin-1, HRas and Mrps34 were enriched in other fractions than the PSD, contrasting with PSD-95. Reason why they were difficult to study in this sub-synaptic fraction by IB.

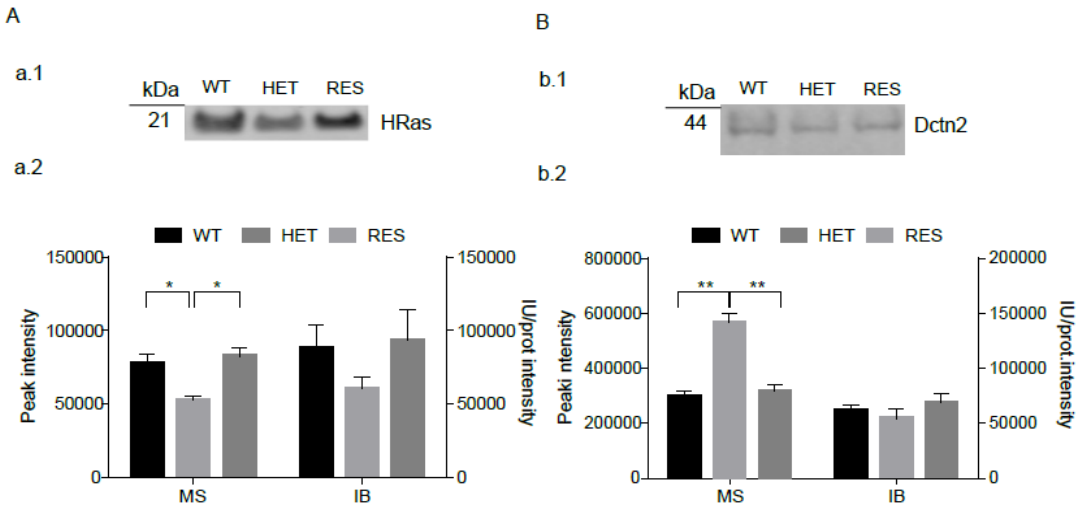

Figure RII-25. Immunoblot assessment of altered proteins in *Syngap1*$^{+/-}$ conditional KO mice for genetic rescue experiments. See complete figure and corresponding footnote overleaf.

C

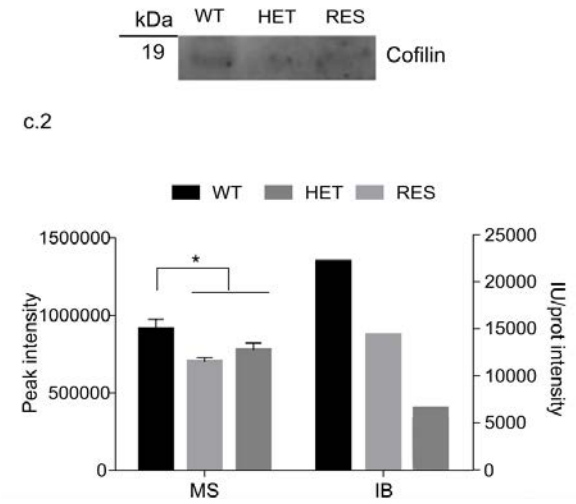

D

	Proven antibodies			
	Gene Name	Test	Success	Possible reason
Rescued up-regulated	PTPN1	Yes	Yes	Multiple bands
	DCTN2	Yes	Yes	
	NDRG2	Yes	No	Multiple bands found at unexpected Mw
Rescued down-regulated	RHOA	Yes	No	Likely enriched in SNP
	HRAS	Yes	Yes	Enriched in SNP
	Mrps34	Yes	No	Enriched in SNP
Unrescued Up-regulated	FAK2	Yes	No	Multiples bands
	CK5P3	Yes	No	No band
	LYN	Yes	No	No band
Unrescued Down-regulated	DAPK	No	-	
	COF-1	Yes	Yes*	Enriched in cytosol and SNP fractions

E

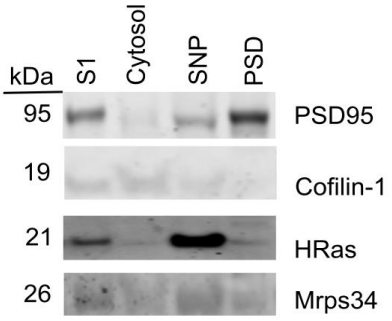

Figure RII-25. Immunoblot assessment of altered proteins in *Syngap1*$^{+/-}$ conditional KO mice for genetic rescue experiments. (A) HRas, n= 15 trios composed by the three genotypes studied (WT; HET and RES). (B) Dynactin 2 n= 5 trios, (C) Cofilin-1 n= 5 trios. (D) List of all proteins assessed by IB and possible explanation of IB issues. (E) Qualitative assessment of the expression of Cofilin (n=6/fraction), HRas (n=6/fraction) or Mrps34 (n=3/fraction). In all cases PSD-95 was used as a control of proper PSD enrichment during the fractionation procedure. S1 stands for total protein extracts and SNP for synaptic non-PSD.

7.2 ANALYSIS OF LONG-TERM POTENTIATION IN *SYNGAP1*$^{+/-}$ INDUCED KO MICE

An assessment of LTP induction in hippocampal CA1 neurons from IND mice and *Synagp1*$^{+/-}$ conventional KO mice was conducted. This electrophysiology experiments showed that expression and maintenance of excitatory postsynaptic potentials (EPSPs) from conventional HET animals was impaired (Fig. RII-26A) while EPSP in animals which *Syngap1*$^{+/-}$ haploinsufficiency was induced at PND21 followed the same pattern as in control animals (Fig. RII-26B). Consequently, LTP was not abnormally expressed and maintained in these mice. Therefore, these data suggest a less damaging effect in cognitive functioning due to a PND21 haploinsufficiency compared to an embryonic *Syngap1* haploinsufficiency.

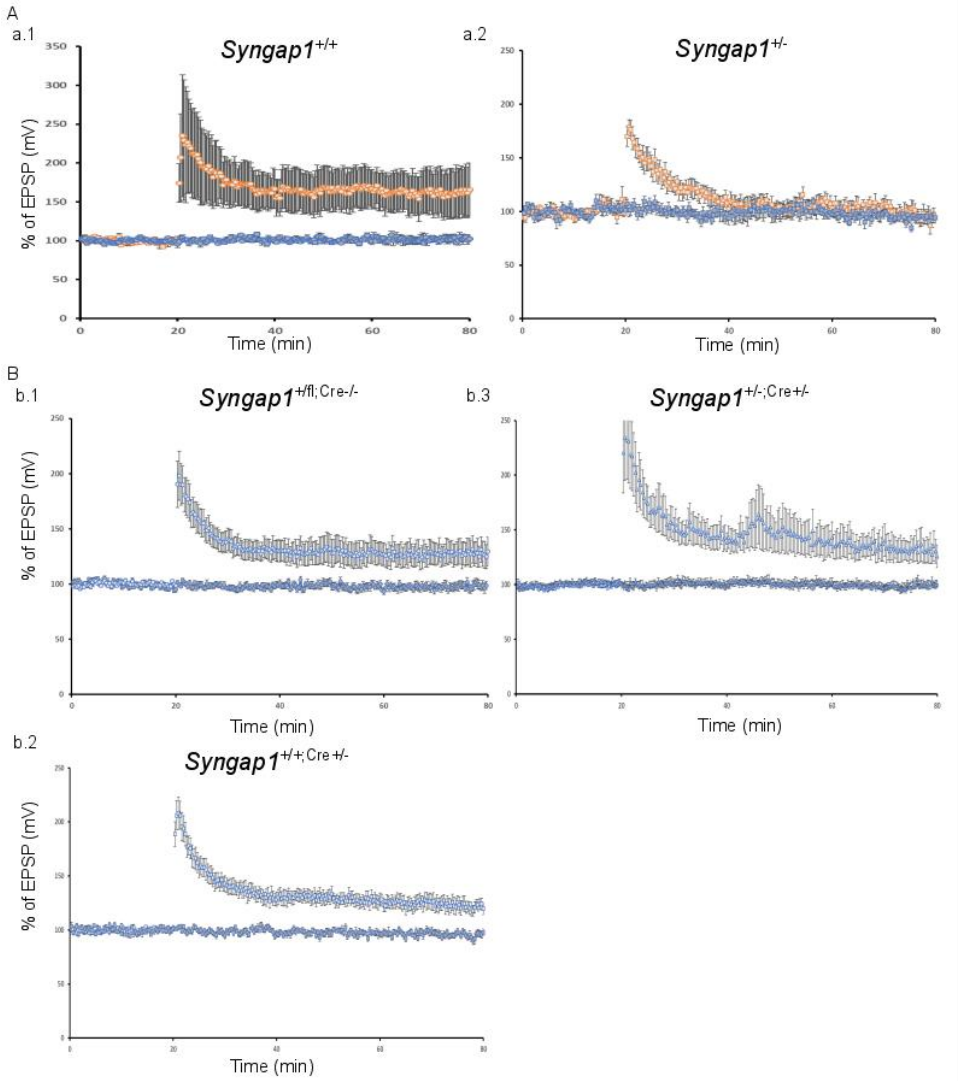

Figure RII-26. Electrophysiology recordings in *Syngap1*$^{+/-}$ conditional and conventional KO mice. (A) LTP induction and maintenance in *Syngap1*$^{+/-}$ conventional KO. Excitatory postsynaptic potentials (EPSP) recordings from (a.1) WT (n=4) and (a.2) HET (n=6) mice are shown. (B) *Syngap1*$^{+/-}$ conditional mice for KO induction mice line. In (b.1) is shown the EPSP from WT controls with a floxed allele (n=11); in (b.2) WT carrying the Cre transgene used also as a control (n=9) and in (b.3) EPSP from IND (n=10) mice recorded at PND>60.

7.2.1 POTENTIAL IMPACT OF LONG-LIVED SYNAPTIC PROTEINS IN THE LTP PHENOTYPE

The absence of a significant impairment of LTP in IND mice could be the result of a high stability of LTP due to synaptic long-lived proteins such as HRas (Bliss T. V. P. et al. 2003; Gonzales Lozano et al. 2016; Heo et al. 2018). The list of long-lived synaptic proteins retrieved from Heo and co-workers were defined as synaptic stable proteins with half-lives of 7 weeks or longer periods using high-resolution MS. Therefore, up to 165 long-lived synaptic proteins reported by them were compared to our list of identified proteins in both *Syngap1*$^{+/-}$ conditional mice lines to test this hypothesis (Heo et al. 2018).

Long-lived proteins								
Uniprot ID	Gene Name	FC	Uniprot ID	Gene Name	FC	Uniprot ID	Gene Name	FC
Q8BGH2	Samm50	0,8	Q9DB20	Atp5o	2,0	Q9CXJ4	Abcb8	0,8
Q7TPR4	Actn1	0,7	Q60803	Traf3	0,8	Q7TSJ2	Map6	0,7
Q9DCX2	Atp5h	1,8	Q9CRB9	Chchd3	0,7	P16330	Cnp	0,7
Q99JR1	Sfxn1	1,5	O35658	C1qbp	1,6	P62071	Rras2	1,3
Q91VR2	Atp5c1	1,4	P56480	Atp5b	1,7	P97427	Crmp1	1,4
P04370	Mbp	0,7	Q8CFV4	Nrn1	0,8			

Table RII-25. Synaptic long-lived proteins with an altered PSD expression found in IND mice. Long-lived proteins reported in Heo et al. 2018 with significant altered fold changes (FCs) in IND mice are shown.

Up to 128 long-lived proteins were identified in the *Syngap1* conditional mice for KO induction, however only 17 of them were significantly altered in IND mice (Table RII-23). Of special interest, were those long-lived proteins that were down-regulated after inducing *Syngap1* KO. This would be indicative of an important change in their turnover rate due to SynGAP deficiency at the PSD. From these 17 significantly altered proteins, 9 (~53%) were significantly down-regulated. Therefore, despite electrophysiology experiments indicated that germline insufficiency of SynGAP before PND21 does most of the damage to the LTP machinery, an effect of long-lived proteins in this unaltered LTP phenotype found in IND mice can not be ruled out.

8. ENRICHMENT OF PROTEINS RELATED TO NDDS AMONG ABNORMALLY EXPRESSED PSD PROTEINS

The current "Spine dysfunction theory of cognitive disorders" states that diverse genetic causes of ID and ASD converge on common cellular pathways (Penzes et al. 2011). Importantly, a comparison of hippocampal pathophysiology in *Syngap1*$^{+/-}$ and *Fmr1*$^{-/y}$ mice supported this hypothesis (Barnes et al. 2016). *SYNGAP1* causal variants are enriched in individuals with ID, ASD, severe epilepsy and SCZ (Guo et al. 2009; Aceti et al. 2015; Kilinc et al. 2018; Table I-1). Therefore, the percentage of altered proteins whose coding genes are linked to ID, ASD, epilepsy or SCZ has been evaluated.

Interestingly, 7% of the altered proteins in HET PSDs were found to be encoded by ID causative genes, whereas 34% of the altered proteins interact with a protein-protein interacting (PPI) gene from the ID gene project database (University of Denver, Colorado). Also, the analysis with the same database showed that 63% of the altered proteins found altered in HET were a component of ID reported pathways. These results were similar in HET/RES but contrasted with RES/WT and IND/WT altered proteins, which showed a lower percentage in each category (Table RII-26, top panel). Of note, the application of binomial statistics showed that the enrichment in altered proteins related to ID was significantly higher in HET mice compared to WT or RES, whereas in RES and IND mice ID genes were not found significantly enriched when compared with its corresponding WT mice.

Regarding the enrichment analysis of those genes linked to ASD, high percentages of proteins produced by these genes in each genetic comparison were found (Table RII-26, top panel). Intriguingly, the relative proportion of all proteins altered was maximum in RES and IND mice relative to WT mice. Nonetheless, in all cases the enrichment was significant, thus it could be expected autistic traits not only in HET but also in RES and IND mice. In contrast, the assessment of SCZ genes, for which *SYNGAP1* is also a risk gene, showed a significant enrichment of altered SCZ associated genes in HET and RES mice but not in IND mice.

Finally, genes related to epilepsy were assessed using a recent review (Wang et al. 2017), which classified epilepsy-related genes into several categories shown in Table RII-26 (bottom panel). These categories were built by grouping genes based on the manifestation of epilepsy in the phenotype, i.e., whether epilepsy is the exclusive outcome of the mutation or part of a group of unrelated symptoms. Namely, 'epilepsy genes' include those whose mutations cause pure or relatively pure epilepsies, or syndromes with epilepsy as

the core symptom. The class 'NDD-associated epilepsy genes' include mutations in genes that produce gross neurodevelopmental malformations and epilepsy, which may vary in severity. The list of 'epilepsy-related genes' included those genes associated with diseases presenting gross physical, or other systemic abnormalities that could be accompanied by epilepsy or seizures. Of note, this category included *SYNGAP1*. Finally, these genes that were reported to be potentially associated with epilepsy, but they were not present in the OMIM database and warranted further verification in most of the cases, were sorted into the 'potential-epilepsy related genes' category.

	ID genes				ID ppi gene			ID pathway			ASD genes				SCZ ge	
	N	% vs. Altered	% vs. total identified	p-value	N	% vs. Altered	% vs. total identified	N	% vs. Altered	% vs. total identified	N	% vs. Altered	% vs. total identified	p-value	N	% from altered
HET/WT	18	7	0,7	0,000	86	34	3,5	158	63	6,4	23	9	0,9	0,000	40	16
HET/RES	12	5	0,5	0,003	84	34	3,4	151	61	6,1	18	7	0,7	0,011	37	15
RES/WT	5	3	0,2	0,116	49	30	2,0	84	52	3,4	20	12	0,8	0,003	26	16
IND/WT	6	2	0,2	0,147	84	33	3,3	119	47	4,6	25	10	1,0	0,000	32	13

ene		ID pathway		ID genes				ID ppi gene			ID pathway			ASD genes				
% vs. total identified	N	% vs. Altered		N	% vs. Altered	% vs. total identified	p-value	N	% vs. Altered	% vs. total identified	N	% vs. Altered	% vs. total identified	N	% vs. Altered	% vs. total identified	p-value	N
3,5	158	63	HET/WT	18	7	0,7	0,000	86	34	3,5	158	63	6,4	23	9	0,9	0,000	40
3,4	151	61	HET/RES	12	5	0,5	0,003	84	34	3,4	151	61	6,1	18	7	0,7	0,011	37
2,0	84	52	RES/WT	5	3	0,2	0,116	49	30	2,0	84	52	3,4	20	12	0,8	0,003	26
3,3	119	47	IND/WT	6	2	0,2	0,147	84	33	3,3	119	47	4,6	25	10	1,0	0,000	32

			All Epilepsy genes categories				Epilepsy genes				Neurodevelopment-associated epilepsy genes				Epilepsy-related g	
			N	% vs. Altered	% vs. total ID	p-value	N	% vs. Altered	% vs. total ID	p-value	N	% vs. Altered	% vs. total ID	p-value	N	% vs. Altered
0,12	0,05	4	HET/WT	26	10	1,0	0,000	3	1	0,12	0,05	4	2	0,2	0,01	16	6
0,12	0,03	2	HET/RES	29	12	1,2	0,000	3	1	0,12	0,03	2	1	0,1	0,13	18	7
0,12	0,22	1	RES/WT	12	5	0,5	0,095	3	2	0,12	0,22	1	1	0,0	0,30	3	2
0,12	0,23	2	IND/WT	25	10	1,0	0,000	3	1	0,12	0,23	2	1	0,1	0,13	13	5

Neurodevelopment-associated e genes				All Epilepsy genes categories				Epilepsy genes				Potential-epilepsy associated genes							
N	% vs. Altered	% vs. total ID		N	% vs. Altered	% vs. total ID	p-value	N	% vs. Altered	% vs. total ID	p-value	N	% vs. Altered	% vs. total ID	p-value				
4	2	0,2	HET/WT	26	10	1,0	0,000	3	1	0,12	0,05	31	10,5	1,2	0,016	4	2	0,2	0,01	16	6
2	1	0,1	HET/RES	29	12	1,2	0,000	3	1	0,12	0,03	32	11,0	1,2	0,023	2	1	0,1	0,13	18	7
1	1	0,0	RES/WT	12	5	0,5	0,095	3	2	0,12	0,22	33	21,9	1,2	0,221	1	1	0,0	0,30	3	2
2	1	0,1	IND/WT	25	10	1,0	0,000	3	1	0,12	0,23	33	11,1	1,2	0,233	2	1	0,1	0,13	13	5

Table RII-26. Genes associated or causative of NDDs reported in different databases. The database for ID genes, PPI ID gene and pathways was retrieved from The University of Denver ID Gene Database Project. For ASD genes, the SFARI database was used. In the case of epilepsy-related genes Wang et al. 2017 report was used and the SZC genes were obtained from the SZDB (Wu et al. 2017). The percentage of genes identified compared to the number of altered genes found in a given genotype is shown as '% vs. altered' whereas the proportion of genes altered compared to all genes altered or not in a given genetic category are shown as '% vs. total ID identified genes'. Binomial statistic was used to calculate the p-values for enrichment analysis. A p≤ 0.05 was considered significant.

When considering all epilepsy genes together, IND mice have a similar proportion of epilepsy genes among its altered proteins as HETs. Furthermore, more than 50% of altered epilepsy genes found in any of the categories analysed were recovered to normal levels in RES mice, matching with a lack of significant enrichment of all epilepsy genes in these animals. Genes known to cause epilepsy as a core feature and neurodevelopment-associated genes were only found altered in HET, whereas epilepsy-related genes, which included genes that were associated but unlikely causal, were found altered in both HET

and IND mice. Interestingly, proteins matching with the potential-epilepsy related genes, for which there is less confidence on their role in disease, were not found significantly enriched in any genotype comparison.

The data collected here suggested that an embryonic deficit would be more damaging, as no significant enrichment in ID, SCZ, epilepsy and NDD-associated epilepsy genes is found in IND animals. In contrast, all these genes, in addition to ASD genes, were significantly found enriched in HET mice. Finally, based on these analyses, some ASD and schizophrenic traits but not epileptic or severe ID features could be predicted to occur in RES mice. Taken all these data together, *Syngap1*$^{+/-}$ deficiency would have a different impact on synaptic physiology depending on its developmental origin.

9. COMPLETE LIST OF ALTERED PROTEINS FROM BOTH *SYNGAP1*$^{+/-}$ CONDITIONAL KO MOUSE LINES

Gene Name	UNIPROT ID	HET/WT FC	p-value	HET/RES FC	p-value	RES/WT FC	p-value	Gene Name	UNIPROT ID	HET/WT FC	p-value	HET/RES FC	p-value	RES/WT FC	p-value
Rbbp4	Q60972	**6,51**	2,2E-02	**3,40**	5E-02	**1,91**	9E-02	Cacna2d2	Q6PHS9	**1,28**	4,3E-02	**1,03**	1E+00	**1,24**	1E-01
Tubb2b	Q9CWF2	**6,24**	1,2E-03	**4,75**	2E-03	**1,31**	6E-02	Iqsec2	Q5DU25	**1,24**	4,6E-03	**1,39**	2E-03	**0,90**	4E-01
Tom1	O88746	**5,09**	5,3E-03	**4,14**	7E-03	**1,23**	4E-01	Syne1	Q6ZWR6	**1,19**	2,2E-02	**1,19**	2E-01	**1,00**	1E+00
Ndrg2	Q9QYG0	**4,53**	1,7E-03	**4,87**	2E-03	**0,93**	9E-01	Cit	P49025	**1,17**	5,0E-02	**1,03**	1E+00	**1,14**	3E-01
Tubb5	P99024	**3,73**	8,6E-05	**3,08**	3E-04	**1,21**	4E-01	Flot1	O08917	**0,86**	3,0E-02	**0,98**	1E+00	**0,88**	6E-02
Ptpn1	P35821	**3,39**	1,5E-03	**3,05**	6E-04	**1,11**	1E+00	Kalrn	A2CG49	**0,84**	2,3E-02	**1,01**	1E+00	**0,83**	1E-02
Rcc1	Q8VE37	**3,16**	6,7E-05	**3,23**	3E-05	**0,98**	1E+00	Mlec	Q6ZQI3	**0,83**	4,6E-02	**0,60**	4E-03	**1,39**	3E-02
Lyn	P25911	**2,85**	4,6E-02	**2,59**	6E-02	**1,10**	1E+00	Rpn2	Q9DBG6	**0,82**	1,4E-02	**0,82**	2E-02	**0,99**	1E+00
Dnajb12	Q9QYI4	**2,76**	7,5E-04	**0,93**	1E+00	**2,96**	6E-03	Hsdl1	Q8BTX9	**0,82**	3,5E-02	**0,90**	5E-01	**0,91**	5E-01
Kctd16	Q5DTY9	**2,72**	1,1E-03	**2,49**	2E-03	**1,09**	4E-01	Nwd2	Q6P5U7	**0,82**	2,4E-02	**0,81**	2E-02	**1,01**	1E+00
Aldh6a1	Q9EQ20	**2,43**	4,5E-03	**2,16**	5E-03	**1,12**	8E-01	Caskin1	Q6P9K8	**0,81**	2,1E-02	**0,82**	2E-01	**0,99**	1E+00
Khdrbs1	Q60749	**2,40**	1,7E-02	**2,16**	2E-02	**1,11**	9E-01	Snap91	Q61548	**0,81**	3,1E-02	**0,94**	8E-01	**0,86**	7E-02
Nup98	Q6PFD9	**2,33**	2,8E-02	**2,31**	3E-02	**1,01**	1E+00	Rps4x	P62702	**0,81**	2,2E-02	**0,81**	3E-01	**1,00**	1E+00
Eif2s1	Q6ZWX6	**2,30**	1,2E-02	**2,24**	1E-02	**1,03**	1E+00	Plcb1	Q9Z1B3	**0,81**	1,3E-02	**0,74**	1E-03	**1,09**	3E-01
Slc1a3	P56564	**2,29**	1,6E-04	**2,87**	5E-05	**0,80**	5E-01	Tnik	P83510	**0,79**	3,9E-02	**0,90**	6E-01	**0,88**	4E-01
Endod1	Q8C522	**2,16**	1,7E-03	**1,82**	5E-03	**1,19**	6E-01	Syt1	P46096	**0,78**	4,3E-02	**0,87**	3E-01	**0,90**	5E-01
Cdk5rap3	Q99LM2	**2,16**	3,4E-03	**0,76**	1E-01	**2,85**	8E-04	Rpl10a	P53026	**0,78**	2,3E-02	**0,72**	2E-01	**1,09**	9E-01
Negr1	Q80Z24	**2,12**	5,9E-06	**1,81**	1E-04	**1,17**	5E-01	Ywhag	P61982	**0,78**	3,3E-02	**0,89**	3E-01	**0,87**	3E-01
Larp1	Q6ZQ58	**2,08**	1,5E-02	**0,93**	1E+00	**2,22**	2E-01	C1qb	P14106	**0,78**	3,5E-02	**0,74**	9E-02	**1,05**	1E+00
Pip4k2a	O70172	**2,05**	2,6E-03	**1,64**	8E-03	**1,25**	5E-01	Elmo2	Q8BHL5	**0,78**	3,3E-02	**1,15**	3E-01	**0,67**	3E-03
Shisa9	Q9CZN4	**2,04**	2,3E-03	**3,33**	4E-04	**0,61**	1E-02	Cfl1	P18760	**0,77**	4,7E-02	**0,90**	5E-01	**0,85**	3E-01
D5Ertd606e	Q8C1B7	**1,99**	2,4E-04	**2,17**	3E-04	**0,92**	8E-01	Mmaa	Q8C7H1	**0,76**	4,5E-02	**0,85**	5E-01	**0,90**	7E-01
Mccc2	Q3ULD5	**1,96**	4,5E-02	**2,41**	2E-02	**0,81**	3E-01	Slc25a23	Q6GQS1	**0,76**	3,7E-02	**0,81**	1E-01	**0,94**	9E-01
Synpo	Q8CC35	**1,92**	1,2E-02	**1,67**	3E-02	**1,15**	6E-01	Gdap1	O88741	**0,76**	3,3E-02	**0,82**	2E-01	**0,93**	8E-01
Top1	Q04750	**1,91**	3,0E-02	**1,56**	5E-02	**1,22**	8E-01	Acot9	Q9R0X4	**0,75**	3,6E-02	**1,01**	1E+00	**0,75**	5E-02
Dctn2	Q99KJ8	**1,91**	6,1E-04	**1,79**	9E-04	**1,07**	9E-01	Kras	P32883	**0,75**	1,3E-02	**0,75**	2E-04	**1,00**	1E+00
Smc3	Q9CW03	**1,89**	1,5E-02	**1,14**	7E-01	**1,66**	1E-02	Agk	Q9ESW4	**0,74**	1,4E-03	**0,66**	4E-02	**1,13**	6E-01
Glud1	P26443	**1,88**	4,6E-04	**1,74**	1E-03	**1,08**	8E-01	Atp6ap2	Q9CYN9	**0,74**	2,4E-02	**0,92**	7E-01	**0,81**	2E-01
Tubb3	Q9ERD7	**1,88**	3,9E-03	**1,73**	7E-03	**1,09**	9E-01	Dmd	P11531	**0,74**	2,9E-02	**0,89**	3E-01	**0,84**	1E-01
Kiaa0128	Q9R1T4	**1,87**	8,5E-03	**1,84**	1E-02	**1,02**	1E+00	Fam81a	Q3UXZ6	**0,74**	2,0E-02	**0,93**	8E-01	**0,79**	9E-02
Vim	P20152	**1,87**	7,0E-03	**1,96**	6E-03	**0,96**	1E+00	Rpl6	P47911	**0,74**	5,1E-05	**0,79**	1E-02	**0,93**	4E-01
Fyn	P39688	**1,85**	9,7E-05	**1,53**	1E-03	**1,21**	3E-01	Adgrl1	Q80TR1	**0,73**	1,9E-02	**0,92**	8E-01	**0,80**	8E-02
Usp30	Q3UN04	**1,85**	2,0E-04	**1,46**	8E-03	**1,27**	2E-01	Rps5	P97461	**0,73**	2,1E-02	**0,82**	4E-01	**0,89**	7E-01
Etf1	Q8BWY3	**1,84**	1,3E-02	**1,88**	1E-02	**0,98**	1E+00	Ywhab	Q9CQV8	**0,73**	9,0E-03	**0,74**	3E-03	**0,98**	1E+00
Ddx6	P54823	**1,82**	1,4E-02	**1,49**	6E-02	**1,22**	8E-02	Ca4	Q64444	**0,72**	2,0E-02	**0,89**	5E-01	**0,81**	9E-02
Enah	Q03173	**1,81**	1,7E-02	**1,54**	5E-02	**1,18**	7E-01	Rplp0	P14869	**0,72**	1,0E-02	**0,85**	5E-01	**0,85**	4E-01
Dlst	Q9D2G2	**1,81**	1,4E-03	**1,73**	2E-03	**1,05**	9E-01	Mapre3	Q6PER3	**0,72**	2,1E-03	**0,79**	3E-02	**0,91**	4E-01
Coro1c	Q9WUM4	**1,81**	2,1E-03	**1,78**	2E-03	**1,02**	1E+00	Cep120	Q7TSG1	**0,72**	2,7E-02	**0,77**	2E-01	**0,93**	9E-01
Tubb4a	Q9D6F9	**1,73**	1,2E-02	**1,51**	3E-02	**1,14**	7E-01	Rpl13a	P19253	**0,72**	2,0E-02	**0,70**	1E-02	**1,02**	1E+00
Prkar2b	P31324	**1,73**	4,7E-02	**1,37**	2E-01	**1,26**	1E-01	Ndufb4	Q9CQC7	**0,71**	4,9E-02	**0,81**	5E-01	**0,88**	6E-01
Ptk2b	Q9QVP9	**1,72**	6,1E-03	**1,15**	7E-01	**1,50**	1E-01	Lin7a	Q8JZS0	**0,71**	2,2E-02	**0,75**	2E-01	**0,95**	1E+00
Arhgap44	Q5SSM3	**1,72**	8,8E-03	**1,12**	7E-01	**1,53**	5E-03	Rpl35	Q6ZWV7	**0,71**	1,6E-02	**0,70**	9E-03	**1,02**	1E+00
Abhd16a	Q9Z1Q2	**1,71**	6,2E-04	**0,95**	9E-01	**1,80**	5E-04	Rpl19	P84099	**0,71**	4,2E-02	**0,85**	2E-01	**0,84**	4E-01
Farsa	Q8C0C7	**1,71**	4,6E-03	**1,74**	4E-03	**0,98**	1E+00	Msn	P26041	**0,71**	2,2E-02	**1,04**	1E+00	**0,68**	1E-03
Cntn2	Q61330	**1,69**	5,6E-03	**1,15**	4E-01	**1,46**	5E-02	Rap1b	Q99JI6	**0,71**	2,2E-02	**0,75**	2E-01	**0,94**	9E-01
Samm50	Q8BGH2	**1,68**	4,2E-03	**1,50**	1E-02	**1,12**	6E-01	Pabpc1	P29341	**0,71**	2,9E-02	**0,74**	1E-01	**0,95**	1E+00
Itpka	Q8R071	**1,68**	1,2E-02	**1,84**	6E-03	**0,91**	9E-01	Abi2	P62484	**0,71**	1,5E-02	**0,94**	8E-01	**0,75**	3E-02
Iglon5	Q8HW98	**1,63**	2,8E-02	**1,57**	4E-02	**1,03**	1E+00	Erc1	Q99MI1	**0,70**	9,3E-03	**0,86**	6E-01	**0,82**	4E-01
Slc9a3r1	P70441	**1,61**	9,0E-03	**1,46**	2E-02	**1,10**	7E-01	Sec22b	O08547	**0,70**	2,2E-02	**0,62**	3E-03	**1,12**	6E-01
Smarca2	Q6DIC0	**1,60**	8,1E-03	**1,93**	2E-03	**0,83**	4E-01	Napg	Q9CWZ7	**0,70**	1,6E-02	**0,64**	3E-04	**1,08**	7E-01
Coro2b	Q8BH44	**1,60**	7,4E-03	**1,69**	4E-03	**0,95**	9E-01	Qdpr	Q8BVI4	**0,70**	1,1E-02	**0,69**	1E-01	**1,01**	1E+00
Hexb	P20060	**1,60**	1,1E-02	**1,27**	1E-01	**1,26**	2E-01	D10Jhu81e	Q9D172	**0,69**	1,1E-02	**0,92**	8E-01	**0,75**	3E-02
Faf2	Q3TDN2	**1,60**	4,1E-03	**1,30**	7E-02	**1,23**	3E-01	Slc25a29	Q8BL03	**0,69**	3,5E-02	**0,86**	7E-01	**0,80**	4E-01
Rtcb	Q99LF4	**1,58**	4,4E-02	**1,65**	4E-02	**0,96**	9E-01	Cyb5b	Q9CQX2	**0,69**	2,0E-02	**0,78**	1E-01	**0,89**	6E-01
Preb	Q9WUQ2	**1,58**	3,1E-02	**1,25**	3E-01	**1,27**	1E-01	Rpl29	P47915	**0,69**	4,1E-02	**0,88**	6E-01	**0,79**	2E-01
Actn1	Q7TPR4	**1,54**	1,6E-02	**1,44**	1E-03	**1,07**	9E-01	Napa	Q9DB05	**0,69**	1,2E-02	**0,61**	7E-04	**1,13**	4E-01
Snw1	Q9CSN1	**1,53**	3,1E-02	**2,12**	6E-03	**0,72**	3E-01	Rpl34	Q9D1R9	**0,68**	1,2E-02	**0,59**	5E-02	**1,16**	7E-01
Baiap2	Q8BKX1	**1,52**	2,8E-02	**1,65**	9E-03	**0,92**	9E-01	Cdc42	P60766	**0,68**	1,4E-02	**0,85**	4E-01	**0,81**	2E-01
Gsk3a	Q2NL51	**1,51**	1,6E-02	**1,25**	2E-01	**1,20**	4E-01	Hras	Q61411	**0,68**	2,8E-02	**0,64**	5E-03	**1,07**	9E-01
Ephb6	O08644	**1,51**	1,5E-02	**1,16**	9E-01	**1,30**	7E-01	Eif4b	Q8BGD9	**0,68**	1,3E-02	**0,87**	7E-01	**0,78**	2E-01
Tnpo1	Q8BFY9	**1,50**	1,9E-02	**1,09**	9E-01	**1,37**	2E-01	Napb	P28663	**0,68**	1,7E-02	**0,76**	4E-03	**0,89**	5E-01
Cyp46a1	Q9WVK8	**1,49**	2,2E-02	**1,63**	2E-03	**0,92**	9E-01	Arpc5l	Q9D898	**0,67**	2,7E-02	**0,94**	1E+00	**0,72**	1E-01
Atl1	Q8BH66	**1,49**	8,3E-03	**1,81**	2E-03	**0,82**	5E-01	Cox5b	P19536	**0,67**	4,8E-02	**0,87**	6E-01	**0,77**	2E-01
Tsg101	Q61187	**1,49**	4,8E-02	**1,19**	5E-01	**1,25**	5E-01	Ndufb9	Q9CQJ8	**0,67**	1,6E-02	**0,79**	3E-01	**0,85**	4E-01
Klc2	O88448	**1,48**	2,6E-02	**0,81**	2E-01	**1,82**	1E-03	Hspa8	P63017	**0,67**	3,3E-04	**0,90**	5E-01	**0,74**	2E-03
Nfs1	Q9Z1J3	**1,48**	4,1E-02	**1,21**	4E-01	**1,22**	4E-01	Trim2	Q9ESN6	**0,66**	3,6E-04	**0,84**	7E-02	**0,79**	1E-02
Acadvl	P50544	**1,46**	3,6E-02	**1,07**	9E-01	**1,37**	2E-01	Mtmr1	Q9Z2C4	**0,66**	4,3E-02	**1,01**	1E+00	**0,66**	3E-02
Nlgn2	Q69ZK9	**1,45**	2,9E-03	**1,15**	1E-01	**1,26**	9E-02	Rps13	P62301	**0,66**	1,8E-03	**0,66**	4E-02	**1,00**	1E+00
Dars	Q922B2	**1,43**	1,7E-02	**1,55**	1E-03	**0,92**	9E-01	Uqcrfs1	Q9CR68	**0,66**	2,7E-02	**0,76**	1E-02	**0,87**	5E-01
Nptx1	Q62443	**1,43**	3,5E-02	**1,32**	2E-01	**1,08**	9E-01	Rab21	P35282	**0,65**	1,2E-02	**0,84**	3E-01	**0,77**	7E-02
Gfap	P03995	**1,42**	2,1E-02	**1,73**	9E-04	**0,82**	3E-01	Tomm20	Q9DCC8	**0,65**	2,3E-02	**1,17**	8E-01	**0,56**	1E-02
Actn4	P57780	**1,42**	9,1E-03	**1,19**	9E-02	**1,20**	3E-01	Wbscr17	Q7TT15	**0,65**	3,1E-02	**1,16**	8E-01	**0,56**	7E-03
Ap2m1	P84091	**1,41**	2,0E-03	**1,49**	2E-04	**0,95**	9E-01	Ndufa11	Q9D8B4	**0,65**	4,4E-02	**0,79**	1E-01	**0,82**	4E-01
Pde10a	Q8CA95	**1,40**	1,5E-02	**1,19**	3E-01	**1,18**	4E-01	Nsf	P46460	**0,64**	3,6E-02	**0,81**	3E-02	**0,80**	2E-01
Scn1b	P97952	**1,39**	2,2E-02	**1,11**	2E-01	**1,25**	1E-01	Synpr	Q8BGN8	**0,64**	4,7E-02	**0,67**	9E-03	**0,95**	1E+00
Lactb	Q9EP89	**1,39**	1,1E-02	**1,50**	2E-03	**0,92**	8E-01	Rpl18a	P62717	**0,64**	4,7E-03	**0,61**	7E-03	**1,05**	9E-01
Camk2d	Q6PHZ2	**1,37**	3,8E-02	**1,42**	3E-02	**0,97**	1E+00	Mrps27	Q8BK72	**0,64**	4,1E-02	**0,84**	9E-01	**0,76**	4E-01
Efr3b	Q6ZQ18	**1,35**	2,9E-02	**0,95**	9E-01	**1,42**	2E-03	Rps27	Q6ZWU9	**0,63**	4,7E-02	**0,74**	2E-02	**0,85**	6E-01
Nap1l1	P28656	**1,35**	1,9E-02	**0,92**	9E-01	**1,46**	2E-01	Ndufb5	Q9CQH3	**0,63**	2,1E-02	**0,72**	4E-02	**0,88**	6E-01
Pdhx	Q8BKZ9	**1,35**	4,1E-02	**1,29**	5E-02	**1,05**	9E-01	Prdx6	O08709	**0,63**	1,2E-02	**1,02**	1E+00	**0,62**	5E-02
Aldh5a1	Q8BWF0	**1,32**	3,9E-02	**1,30**	5E-02	**1,02**	1E+00	**Syngap1**	F6SEU4	**0,63**	1,3E-02	**0,78**	4E-02	**0,81**	2E-01
Arhgap39	P59281	**1,32**	4,8E-02	**1,01**	1E+00	**1,31**	2E-01	Slc25a4	P48962	**0,63**	2,6E-02	**0,70**	9E-02	**0,89**	8E-01
Bai1	Q3UHD1	**1,32**	1,4E-02	**1,16**	3E-01	**1,13**	6E-01	Slc25a11	Q9CR62	**0,63**	1,9E-02	**0,83**	4E-01	**0,76**	1E-01
Arhgap26	Q6ZQ82	**1,30**	4,4E-02	**1,17**	4E-01	**1,11**	8E-01	Tpm3	P21107	**0,62**	1,9E-02	**0,68**	2E-02	**0,91**	8E-01
Rbm14	Q8C2Q3	**1,29**	5,0E-02	**1,18**	2E-01	**1,10**	6E-01	Snrk	Q8VDU5	**0,62**	3,7E-02	**0,77**	1E-01	**0,81**	4E-01
Aldh1b1	Q9CZS1	**1,29**	1,1E-02	**1,23**	8E-02	**1,05**	9E-01	Slc25a5	P51881	**0,62**	2,8E-02	**0,71**	1E-01	**0,87**	7E-01
Spon1	Q8VCC9	**1,29**	2,9E-02	**1,18**	1E-01	**1,09**	6E-01	Slc4a8	Q8JZR6	**0,62**	2,7E-02	**0,91**	8E-01	**0,68**	6E-02

Table RII-27. List of altered proteins in *Syngap1*$^{+/-}$ conditional KO mouse line for genetic rescue studies. The remaining parts of the table are shown in next pages. The figure footnote is shown in leaf 241.

Gene Name	UNIPROT ID	HET/WT FC	p-value	HET/RES FC	p-value	RES/WT FC	p-value	Gene Name	UNIPROT ID	HET/WT FC	p-value	HET/RES FC	p-value	RES/WT FC	p-value
Tmed10	Q9D1D4	**0,61**	2,2E-03	**0,50**	2E-02	**1,23**	4E-01	Ptxnc1	Q9QZC2	**1,13**	2,9E-01	**1,35**	1E-02	**0,84**	2E-01
Ppia	P17742	**0,61**	2,5E-02	**0,61**	3E-03	**1,00**	1E+00	Elfn1	Q8C8T7	**1,12**	5,1E-01	**1,36**	3E-02	**0,83**	2E-01
Skp1	Q9WTX5	**0,61**	5,6E-03	**0,86**	4E-01	**0,72**	4E-02	Sacs	Q9JLC8	**1,28**	1,2E-01	**1,37**	3E-02	**0,94**	9E-01
Slc25a20	Q9Z2Z6	**0,61**	1,4E-02	**0,64**	6E-03	**0,95**	1E+00	Fbxo41	Q6NS60	**1,36**	7,4E-02	**1,37**	2E-02	**0,99**	1E+00
Ndufa8	Q9DCJ5	**0,61**	6,0E-03	**0,75**	3E-02	**0,82**	2E-01	Gk	Q64516	**1,30**	1,9E-01	**1,37**	1E-02	**0,95**	1E+00
Smg7	Q5RJH6	**0,61**	9,9E-03	**0,55**	8E-03	**1,10**	8E-01	Krt18	P05784	**1,52**	2,0E-01	**1,39**	1E-02	**1,09**	1E+00
Rpl14	Q9CR57	**0,61**	1,4E-03	**0,66**	5E-02	**0,93**	9E-01	Gabrg2	P22723	**0,85**	2,6E-01	**1,40**	3E-02	**0,61**	7E-04
Grpel1	Q99LP6	**0,61**	3,9E-02	**0,70**	3E-01	**0,87**	8E-01	Lpcat4	Q6NVG1	**1,54**	7,5E-02	**1,45**	2E-02	**1,06**	1E+00
Rhoa	Q9QUI0	**0,61**	4,3E-02	**0,69**	2E-03	**0,88**	7E-01	Dbt	P53395	**1,29**	1,9E-01	**1,45**	3E-02	**0,89**	9E-01
Spg7	Q3ULF4	**0,60**	6,9E-05	**0,82**	3E-01	**0,74**	4E-02	Vars2	Q3U2A8	**1,17**	5,7E-01	**1,49**	3E-03	**0,79**	3E-01
Ngef	Q8CHT1	**0,60**	3,4E-03	**1,09**	6E-01	**0,55**	1E-03	Mapt	P10637	**1,41**	7,4E-02	**1,49**	4E-02	**0,95**	9E-01
Ndufs8	Q8K3J1	**0,60**	2,6E-02	**0,73**	4E-02	**0,82**	4E-01	Cntrob	Q8CB62	**0,99**	1,0E+00	**1,50**	8E-03	**0,66**	9E-02
Tars2	Q3UQ84	**0,60**	6,7E-03	**1,20**	2E-01	**0,50**	2E-03	Homer3	Q99JP6	**1,33**	1,3E-01	**1,51**	7E-03	**0,88**	8E-01
Ywhaq	P68254	**0,60**	3,9E-02	**0,74**	3E-01	**0,81**	6E-01	Xrn2	Q9DBR1	**1,22**	4,6E-01	**1,62**	2E-02	**0,75**	4E-01
Ociad1	Q9CRD0	**0,60**	3,0E-02	**0,64**	5E-03	**0,93**	9E-01	Epha6	Q62413	**1,18**	6,5E-01	**1,66**	1E-03	**0,71**	3E-01
Lin7b	O88951	**0,60**	3,3E-02	**0,64**	8E-02	**0,93**	1E+00	Ddx39b	Q9Z1N5	**1,68**	1,4E-01	**1,78**	4E-02	**0,94**	1E+00
Tmem126a	Q9D8Y1	**0,59**	9,8E-03	**0,79**	3E-01	**0,75**	9E-02	Krt8	P11679	**1,04**	9,9E-01	**1,78**	2E-02	**0,59**	5E-02
Ndufa13	Q9ERS2	**0,59**	2,2E-02	**0,75**	7E-02	**0,80**	3E-01	Dhx9	O70133	**1,67**	1,0E-01	**1,80**	4E-02	**0,93**	1E+00
Rhog	P84096	**0,59**	3,9E-02	**0,70**	6E-03	**0,85**	6E-01	Cldn11	Q60771	**1,18**	6,0E-01	**1,86**	2E-02	**0,64**	6E-02
Rab10	P61027	**0,59**	4,0E-02	**0,71**	5E-03	**0,84**	5E-01	Ilf3	Q9Z1X4	**1,76**	6,9E-02	**2,11**	2E-02	**0,84**	9E-01
Extl2	Q9ES89	**0,59**	7,9E-04	**0,58**	4E-02	**1,01**	1E+00	Nup210	Q9QY81	**1,61**	7,6E-02	**2,12**	2E-02	**0,76**	6E-01
Diras2	Q5PR73	**0,59**	1,5E-02	**0,68**	3E-02	**0,87**	6E-01	Pdia6	Q922R8	**1,81**	5,7E-02	**2,18**	3E-02	**0,83**	7E-01
Hspa2	P17156	**0,58**	3,1E-03	**0,93**	9E-01	**0,63**	6E-03	Apex1	P28352	**1,45**	3,4E-01	**2,26**	4E-03	**0,64**	5E-01
Ndufa12	Q7TMF3	**0,58**	3,4E-02	**0,71**	4E-02	**0,83**	5E-01	Celf1	P28659	**1,71**	7,9E-02	**2,34**	2E-02	**0,73**	5E-01
Ndufs5	Q99LY9	**0,58**	8,7E-03	**0,74**	1E-01	**0,79**	2E-01	Ruvbl1	P60122	**2,15**	7,3E-02	**2,90**	3E-02	**0,74**	5E-01
Csnk1a1	Q8BK63	**0,58**	4,7E-03	**0,86**	5E-02	**0,68**	2E-02	Lemd3	Q9WU40	**1,54**	3,4E-01	**3,56**	1E-03	**0,43**	3E-01
Exd2	Q8VEG4	**0,58**	1,9E-02	**0,89**	8E-01	**0,65**	4E-02	Chmp2a	Q9DB34	**2,76**	7,0E-02	**4,43**	1E-02	**0,62**	9E-01
Rpl23a	P62751	**0,58**	4,5E-02	**1,02**	1E+00	**0,57**	4E-02	Timm17a	Q9Z0V8	**0,55**	1,3E-01	**0,36**	2E-02	**1,51**	3E-01
Ndufb8	Q9D6J5	**0,58**	5,4E-03	**0,70**	1E-01	**0,83**	3E-01	Lamtor1	Q9CQ22	**0,89**	7,7E-01	**0,39**	1E-02	**2,29**	2E-02
Ndufb6	Q3UIU2	**0,58**	2,1E-02	**0,84**	3E-01	**0,69**	8E-02	Nsfl1c	Q9CZ44	**0,61**	2,9E-01	**0,40**	4E-03	**1,53**	2E-01
Cyc1	Q9D0M3	**0,58**	1,1E-02	**0,74**	1E-01	**0,78**	2E-01	Atp5i	Q06185	**0,24**	5,7E-02	**0,41**	2E-04	**0,60**	3E-01
Tomm70	Q9CZW5	**0,57**	2,0E-02	**1,02**	1E+00	**0,56**	2E-02	Cltb	Q6IRU5	**0,58**	2,4E-01	**0,44**	2E-04	**1,33**	4E-01
Atp6v1g2	Q9WTT4	**0,57**	7,5E-04	**0,53**	4E-03	**1,08**	9E-01	Sugt1	Q9CX34	**0,71**	8,6E-01	**0,48**	5E-03	**1,48**	6E-01
Rictor	Q6QI06	**0,57**	3,4E-02	**1,43**	7E-01	**0,40**	2E-02	Phyhipl	Q8BGT8	**0,61**	1,2E-01	**0,48**	2E-02	**1,27**	3E-01
Pcca	Q91ZA3	**0,57**	4,2E-02	**0,87**	5E-01	**0,65**	1E-01	Hectd3	Q3U487	**1,04**	1,0E+00	**0,49**	3E-02	**2,13**	3E-02
Dip2b	Q3UH60	**0,57**	2,7E-02	**1,01**	1E+00	**0,56**	1E-02	Psmb6	Q60692	**0,70**	6,6E-01	**0,49**	3E-02	**1,42**	5E-01
Ndufs7	Q9DC70	**0,57**	9,7E-03	**0,92**	9E-01	**0,62**	2E-02	Gstm1	P10649	**0,70**	8,8E-02	**0,50**	2E-03	**1,39**	5E-02
Tmem38a	Q3TMP8	**0,57**	3,9E-02	**0,90**	1E+00	**0,63**	4E-01	Chmp6	P0C0A3	**0,69**	5,1E-02	**0,50**	2E-04	**1,37**	2E-02
Ndufc2	Q9CQ54	**0,56**	1,4E-02	**0,87**	6E-01	**0,64**	4E-02	Rab6b	P61294	**0,75**	7,9E-01	**0,51**	3E-02	**1,47**	5E-01
Tkt	P40142	**0,56**	1,7E-02	**0,57**	3E-03	**0,98**	1E+00	Strap	Q9Z1Z2	**1,11**	7,4E-01	**0,51**	2E-02	**2,15**	2E-02
Wipf3	P0C7L0	**0,56**	4,7E-03	**0,88**	8E-01	**0,63**	2E-02	Ube2v1	Q9CZY3	**0,80**	3,4E-01	**0,52**	2E-03	**1,54**	5E-03
Cox5a	P12787	**0,56**	3,5E-02	**0,80**	6E-01	**0,70**	2E-01	Tbcd	Q8BYA0	**0,57**	1,7E-01	**0,52**	4E-02	**1,10**	1E+00
Cox7a2l	Q61387	**0,55**	1,3E-02	**0,69**	1E-01	**0,79**	4E-01	Eif4a1	P60843	**0,81**	7,9E-01	**0,52**	2E-03	**1,56**	1E-01
Plgrkt	Q9D3P8	**0,55**	2,6E-02	**0,59**	4E-02	**0,92**	9E-01	Tf	Q921I1	**1,04**	1,0E+00	**0,53**	1E-02	**1,97**	4E-02
Cyb5r1	Q9DB73	**0,55**	3,0E-02	**0,72**	1E-01	**0,75**	3E-01	Ncstn	P57716	**0,73**	6,8E-01	**0,53**	5E-02	**1,38**	5E-01
Ndufs6	P52503	**0,54**	2,1E-02	**0,76**	2E-01	**0,72**	1E-01	Pdxk	Q8K183	**0,84**	3,2E-01	**0,53**	2E-02	**1,58**	6E-02
Etfa	Q99LC5	**0,54**	4,2E-02	**1,01**	1E+00	**0,54**	4E-02	Pebp1	P70296	**0,72**	3,0E-01	**0,54**	1E-03	**1,33**	2E-01
Clta	O08585	**0,53**	4,2E-03	**0,46**	8E-05	**1,16**	4E-01	Plcl1	Q3USB7	**0,61**	1,2E-01	**0,55**	2E-02	**1,11**	9E-01
Ndufv2	Q9D6J6	**0,53**	6,1E-03	**0,60**	2E-02	**0,88**	8E-01	Usp46	P62069	**0,78**	6,3E-01	**0,55**	2E-02	**1,42**	2E-01
Phb2	O35129	**0,52**	2,4E-02	**0,58**	9E-03	**0,90**	9E-01	Apoo	Q9DCZ4	**0,54**	1,1E-01	**0,55**	4E-03	**0,98**	1E+00
Ndufa4	Q62425	**0,52**	3,0E-02	**0,81**	3E-01	**0,64**	9E-02	Sdhb	Q9CQA3	**0,39**	5,8E-02	**0,56**	7E-03	**0,69**	4E-01
Tbc1d17	Q8BYH7	**0,52**	9,4E-03	**0,66**	5E-02	**0,80**	3E-01	Phyhip	Q8K0S0	**0,63**	5,9E-02	**0,56**	2E-02	**1,13**	8E-01
Sfxn1	Q99JR1	**0,52**	7,5E-03	**0,63**	2E-02	**0,83**	5E-01	Prmt1	Q9JIF0	**0,72**	1,3E-01	**0,57**	8E-03	**1,27**	8E-03
Fat3	Q8BNA6	**0,52**	1,9E-04	**0,46**	7E-01	**1,13**	1E+00	Gstp1	P19157	**0,60**	5,9E-02	**0,57**	6E-03	**1,05**	1E+00
Emc7	Q9EP72	**0,51**	2,1E-02	**0,59**	2E-02	**0,86**	7E-01	Rps25	P62852	**0,80**	3,8E-01	**0,57**	2E-04	**1,40**	4E-02
Rab23	P35288	**0,51**	6,7E-03	**0,77**	6E-01	**0,66**	1E-01	Tollip	Q9QZ06	**0,87**	7,2E-01	**0,58**	1E-02	**1,50**	6E-02
Anxa6	P14824	**0,51**	2,0E-02	**0,57**	2E-02	**0,88**	8E-01	Atp5f1	Q9CQQ7	**0,44**	6,2E-02	**0,58**	2E-02	**0,76**	6E-01
Mavs	Q8VCF0	**0,50**	6,0E-04	**0,75**	3E-01	**0,67**	2E-02	Atp5j2	P56135	**0,48**	1,3E-01	**0,59**	4E-02	**0,82**	8E-01
Sfxn3	Q91V61	**0,50**	1,6E-02	**0,56**	1E-02	**0,90**	9E-01	Atp5c1	Q91VR2	**0,53**	5,0E-02	**0,59**	9E-03	**0,90**	9E-01
Mtfp1	Q9CRB8	**0,50**	2,1E-02	**0,64**	5E-02	**0,77**	4E-01	Cisd1	Q91WS0	**0,54**	1,1E-01	**0,59**	6E-03	**0,91**	9E-01
Cryab	P23927	**0,49**	1,7E-03	**0,46**	6E-02	**1,07**	1E+00	Tspan2	Q922J6	**0,71**	4,3E-01	**0,61**	8E-03	**1,16**	8E-01
Ppif	Q99KR7	**0,49**	1,5E-02	**0,46**	9E-04	**1,06**	9E-01	Necab2	Q91ZP9	**0,84**	5,0E-01	**0,62**	2E-02	**1,35**	1E-01
Rpl35a	O55142	**0,49**	3,6E-02	**0,54**	2E-04	**0,90**	9E-01	Ap3s1	Q9DCR2	**0,67**	9,5E-02	**0,62**	1E-02	**1,08**	9E-01
Atrn	Q9WU60	**0,47**	3,7E-03	**0,98**	1E+00	**0,48**	6E-02	Fam49b	Q921M7	**0,79**	3,4E-01	**0,63**	9E-04	**1,25**	2E-01
Tmem14c	Q9CQN6	**0,45**	1,2E-03	**0,74**	3E-01	**0,61**	7E-03	Clcn6	O35454	**0,98**	1,0E+00	**0,64**	2E-02	**1,55**	3E-02
Lrrtm1	Q8K377	**0,44**	3,7E-03	**1,06**	9E-01	**0,41**	4E-03	Rala	P63321	**0,75**	1,1E-01	**0,65**	4E-02	**1,16**	6E-01
Exoc5	Q3TPX4	**0,44**	4,2E-04	**0,94**	6E-01	**0,46**	5E-04	Rmnd1	Q8CI78	**0,63**	5,3E-02	**0,65**	2E-02	**0,97**	1E+00
Pex6	Q99LC9	**0,43**	2,2E-02	**1,75**	8E-01	**0,25**	7E-03	Epn2	Q8CHU3	**0,94**	9,1E-01	**0,65**	2E-02	**1,45**	4E-02
Cpne4	Q8BLR2	**0,41**	4,5E-02	**0,94**	1E+00	**0,43**	5E-02	Uchl1	Q9R0P9	**0,66**	6,5E-02	**0,65**	3E-02	**1,00**	1E+00
Kpna6	O35345	**0,36**	1,7E-03	**1,12**	8E-01	**0,32**	2E-03	Esyt1	Q3U7R1	**0,79**	4,0E-01	**0,65**	2E-02	**1,21**	4E-01
Mical1	Q8VDP3	**0,35**	4,8E-02	**0,48**	1E-01	**0,73**	6E-01	Prrc2a	Q7TSC1	**0,80**	1,4E-01	**0,66**	2E-02	**1,23**	2E-01
Atp5d	Q9D3D9	**0,35**	4,0E-02	**0,37**	2E-02	**0,96**	1E+00	Wdr91	Q7TMQ7	**1,24**	2,4E-01	**0,66**	1E-02	**1,88**	2E-03
Chchd4	Q8VEA4	**0,34**	6,9E-03	**0,35**	5E-04	**0,97**	1E+00	Emc8	O70378	**0,71**	5,4E-02	**0,66**	4E-02	**1,09**	9E-01
Atp5h	Q9DCX2	**0,34**	7,0E-03	**0,47**	1E-02	**0,71**	2E-01	Phf24	Q80TL4	**0,82**	3,2E-01	**0,66**	4E-03	**1,24**	8E-02
Mrpl12	Q9DB15	**0,32**	1,9E-03	**0,75**	7E-01	**0,42**	5E-03	Ndufa1	O35683	**0,73**	1,3E-01	**0,66**	3E-03	**1,10**	8E-01
Mrps34	Q9JIK9	**0,29**	5,7E-03	**0,35**	2E-04	**0,83**	6E-01	Rps14	P62264	**0,79**	2,5E-01	**0,66**	9E-03	**1,19**	4E-01
Dapk1	Q80YE7	**0,11**	1,5E-03	**0,80**	9E-01	**0,13**	2E-03	Timm9	Q9WV98	**0,52**	1,7E-01	**0,67**	2E-03	**0,79**	7E-01
Map7d1	A2AJI0	**1,03**	9,8E-01	**1,24**	2E-02	**0,83**	3E-01	Pcmt1	P23506	**0,42**	9,4E-02	**0,67**	3E-02	**0,63**	3E-01
Cacng3	Q9JJV5	**1,17**	3,6E-01	**1,25**	3E-02	**0,94**	9E-01	Csrp1	P97315	**0,83**	4,1E-01	**0,67**	3E-02	**1,24**	3E-01
Ttn	A2ASS6	**1,27**	8,1E-02	**1,26**	1E-02	**1,01**	1E+00	Gabarapl1	Q8R3R8	**0,65**	7,9E-02	**0,67**	7E-04	**0,96**	1E+00
Pkp4	Q68FH0	**1,01**	9,9E-01	**1,27**	1E-04	**0,80**	4E-02	Apoe	P08226	**0,74**	1,8E-01	**0,68**	4E-03	**1,10**	8E-01
Epb41l1	Q9Z2H5	**1,04**	9,2E-01	**1,27**	3E-02	**0,82**	4E-02	Stip1	Q60864	**0,83**	6,9E-01	**0,68**	3E-02	**1,24**	4E-01
Cacng8	Q8VHW2	**1,15**	3,7E-01	**1,28**	5E-03	**0,90**	6E-01	Nck2	O55033	**0,80**	2,6E-01	**0,68**	2E-02	**1,17**	5E-01
App	P12023	**1,15**	5,1E-01	**1,29**	2E-02	**0,89**	7E-01	Eci2	Q9WUR2	**0,85**	2,7E-01	**0,68**	4E-02	**1,24**	3E-01
Mrps36	Q9CQX8	**0,85**	4,9E-01	**1,32**	1E-02	**0,65**	4E-02	Crip2	Q9DCT8	**0,79**	9,2E-02	**0,68**	2E-02	**1,16**	3E-01
Sept7	O55131	**1,03**	9,8E-01	**1,32**	6E-04	**0,78**	2E-01	Rpl32	P62911	**0,73**	2,2E-01	**0,69**	2E-02	**1,06**	1E+00
Dlgap3	Q6PFD5	**1,10**	4,0E-01	**1,34**	4E-04	**0,82**	8E-02	Surf1	P09925	**0,72**	1,8E-01	**0,69**	2E-03	**1,05**	1E+00

Table RII-27. List of altered proteins in *Syngap1*$^{+/-}$ conditional KO mouse line for genetic rescue studies. The remaining part of the table and figure footnote are shown overleaf.

me	UNIPROT ID	HET/WT FC	p-value	HET/RES FC	p-value	RES/WT FC	p-value	Gene Name	UNIPROT ID	HET/WT FC	p-value	HET/RES FC	p-value	RES/WT FC	p-value
	Q9QZC2	**1,13**	2,9E-01	**1,35**	1E-02	**0,84**	2E-01	Rps24	P62849	**0,82**	4,2E-01	**0,70**	2E-02	**1,18**	4E-01
	Q8C8T7	**1,12**	5,1E-01	**1,36**	3E-02	**0,83**	2E-01	Zc2hc1a	Q8BJH1	**0,85**	5,1E-01	**0,70**	3E-02	**1,21**	4E-01
	Q9JLC8	**1,28**	1,2E-01	**1,37**	3E-02	**0,94**	9E-01	Stx7	O70439	**1,06**	8,7E-01	**0,70**	3E-02	**1,52**	1E-02
1	Q6NS60	**1,36**	7,4E-02	**1,37**	2E-02	**0,99**	1E+00	Copb2	O55029	**1,03**	9,9E-01	**0,70**	4E-02	**1,47**	4E-02
	Q64516	**1,30**	1,9E-01	**1,37**	1E-02	**0,95**	1E+00	Rap2a	Q80ZJ1	**0,70**	2,7E-01	**0,70**	1E-04	**1,00**	1E+00
	P05784	**1,52**	2,0E-01	**1,39**	1E-02	**1,09**	1E+00	Cd81	P35762	**0,74**	1,4E-01	**0,71**	1E-02	**1,05**	1E+00
2	P22723	**0,85**	2,6E-01	**1,40**	3E-02	**0,61**	7E-04	Npepps	Q11011	**0,96**	9,8E-01	**0,71**	9E-03	**1,35**	4E-02
4	Q6NVG1	**1,54**	7,5E-02	**1,45**	2E-02	**1,06**	1E+00	Ckb	Q04447	**0,75**	6,0E-02	**0,72**	3E-02	**1,04**	1E+00
	P53395	**1,29**	1,9E-01	**1,45**	3E-02	**0,89**	9E-01	Ndrg3	Q9QYF9	**1,15**	8,6E-01	**0,72**	4E-02	**1,60**	5E-02
	Q3U2A8	**1,17**	5,7E-01	**1,49**	3E-03	**0,79**	3E-01	Rab3c	P62823	**0,81**	6,6E-02	**0,72**	2E-02	**1,12**	5E-01
	P10637	**1,41**	7,4E-02	**1,49**	4E-02	**0,95**	9E-01	Rab3a	P63011	**0,62**	1,2E-01	**0,73**	1E-02	**0,86**	8E-01
b	Q8CB62	**0,99**	1,0E+00	**1,50**	8E-03	**0,66**	9E-02	Vps16	Q920Q4	**1,12**	7,0E-01	**0,73**	3E-02	**1,53**	1E-02
3	Q99JP6	**1,33**	1,3E-01	**1,51**	7E-03	**0,88**	8E-01	Mapk3	Q63844	**0,76**	4,5E-01	**0,73**	6E-03	**1,03**	1E+00
	Q9DBR1	**1,22**	4,6E-01	**1,62**	2E-02	**0,75**	4E-01	Rab7a	P51150	**0,83**	7,2E-01	**0,73**	5E-02	**1,13**	9E-01
	Q62413	**1,18**	6,5E-01	**1,66**	1E-03	**0,71**	3E-01	Csde1	Q91W50	**1,00**	1,0E+00	**0,73**	3E-02	**1,37**	3E-02
b	Q9Z1N5	**1,68**	1,4E-01	**1,78**	4E-02	**0,94**	1E+00	Dpysl3	Q62188	**0,87**	5,7E-01	**0,74**	3E-02	**1,19**	4E-01
	P11679	**1,04**	9,9E-01	**1,78**	2E-02	**0,59**	5E-02	Armc6	Q8BNU0	**1,18**	3,8E-01	**0,74**	3E-02	**1,60**	1E-03
	O70133	**1,67**	1,0E-01	**1,80**	4E-02	**0,93**	1E+00	Gnb5	P62881	**0,86**	1,7E-01	**0,74**	7E-03	**1,17**	1E-01
1	Q60771	**1,18**	6,0E-01	**1,86**	2E-02	**0,64**	6E-02	Slc25a46	Q9CQS4	**0,87**	4,8E-01	**0,74**	3E-02	**1,18**	1E-01
	Q9Z1X4	**1,76**	6,9E-02	**2,11**	2E-02	**0,84**	9E-01	Cct3	P80318	**0,80**	8,2E-02	**0,75**	4E-02	**1,07**	8E-01
0	Q9QY81	**1,61**	7,6E-02	**2,12**	2E-02	**0,76**	6E-01	Itpr1	P11881	**0,93**	6,3E-01	**0,76**	1E-02	**1,24**	4E-02
	Q922R8	**1,81**	5,7E-02	**2,18**	3E-02	**0,83**	7E-01	Fis1	Q9CQ92	**0,68**	1,2E-01	**0,76**	5E-02	**0,90**	8E-01
	P28352	**1,45**	3,4E-01	**2,26**	4E-03	**0,64**	5E-01	Ppp1r7	Q3UM45	**0,81**	8,3E-01	**0,76**	3E-02	**1,06**	1E+00
	P28659	**1,71**	7,9E-02	**2,34**	2E-02	**0,73**	5E-01	Syngr3	Q8R191	**0,76**	1,2E-01	**0,76**	2E-02	**1,00**	1E+00
	P60122	**2,15**	7,3E-02	**2,90**	3E-02	**0,74**	5E-01	Vamp2	P63044	**0,76**	2,2E-01	**0,76**	3E-02	**1,00**	1E+00
3	Q9WU40	**1,54**	3,4E-01	**3,56**	1E-03	**0,43**	3E-01	Mfn2	Q80U63	**0,98**	9,9E-01	**0,76**	2E-02	**1,28**	2E-02
a	Q9DB34	**2,76**	7,0E-02	**4,43**	1E-02	**0,62**	9E-01	Vps35	Q9EQH3	**1,03**	9,9E-01	**0,76**	1E-02	**1,35**	2E-02
a	Q9Z0V8	**0,55**	1,3E-01	**0,36**	2E-02	**1,51**	3E-01	Ndufs2	Q91WD5	**0,64**	8,4E-02	**0,77**	3E-02	**0,83**	5E-01
1	Q9CQ22	**0,89**	7,7E-01	**0,39**	1E-02	**2,29**	2E-02	Ncln	Q8VCM8	**1,03**	9,9E-01	**0,77**	2E-02	**1,34**	7E-03
	Q9CZ44	**0,61**	2,9E-01	**0,40**	4E-03	**1,53**	2E-01	Rps19	Q9CZX8	**0,79**	1,1E-01	**0,77**	2E-02	**1,04**	1E+00
	Q06185	**0,24**	5,7E-02	**0,41**	2E-04	**0,60**	3E-01	Rab14	Q91V41	**0,77**	8,6E-02	**0,79**	4E-02	**0,98**	1E+00
	Q6IRU5	**0,58**	2,4E-01	**0,44**	2E-04	**1,33**	4E-01	Slmap	Q3URD3	**0,63**	8,5E-01	**0,79**	3E-02	**0,80**	1E+00
	Q9CX34	**0,71**	8,6E-01	**0,48**	5E-03	**1,48**	6E-01	Snap25	P60879	**0,78**	9,2E-02	**0,79**	4E-02	**0,98**	1E+00
l	Q8BGT8	**0,61**	1,2E-01	**0,48**	2E-02	**1,27**	3E-01	Ywhaz	P63101	**0,78**	1,1E-01	**0,80**	3E-02	**0,98**	1E+00
3	Q3U487	**1,04**	1,0E+00	**0,49**	3E-02	**2,13**	3E-02	Prkaca	P05132	**0,87**	5,3E-01	**0,81**	4E-02	**1,08**	8E-01
6	Q60692	**0,70**	6,6E-01	**0,49**	3E-02	**1,42**	5E-01	Ddx1	Q91VR5	**1,09**	7,4E-01	**0,82**	3E-02	**1,34**	4E-02
	P10649	**0,70**	8,8E-02	**0,50**	2E-03	**1,39**	5E-02	Purg	Q8R4E6	**0,97**	9,9E-01	**0,84**	2E-02	**1,15**	3E-01
6	P0C0A3	**0,69**	5,1E-02	**0,50**	2E-04	**1,37**	2E-02	Slc2a1	P17809	**0,83**	1,1E-01	**0,85**	5E-02	**0,98**	1E+00
	P61294	**0,75**	7,9E-01	**0,51**	3E-02	**1,47**	5E-01	Dctn1	O08788	**1,03**	9,6E-01	**0,85**	4E-02	**1,21**	3E-03
	Q9Z1Z2	**1,11**	7,4E-01	**0,51**	2E-02	**2,15**	2E-02	Trim46	Q7TNM2	**1,09**	6,5E-01	**0,89**	2E-01	**1,22**	5E-02
1	Q9CZY3	**0,80**	3,4E-01	**0,52**	2E-03	**1,54**	5E-03	Pccb	Q99MN9	**0,94**	9,4E-01	**0,76**	1E-01	**1,23**	4E-02
	Q8BYA0	**0,57**	1,7E-01	**0,52**	4E-02	**1,10**	1E+00	Hspa4l	P48722	**1,12**	3,1E-01	**0,91**	4E-01	**1,23**	2E-02
	P60843	**0,81**	7,9E-01	**0,52**	2E-03	**1,56**	1E-01	Slc27a4	Q91VE0	**1,14**	4,6E-01	**0,92**	7E-01	**1,24**	4E-02
	Q921I1	**1,04**	1,0E+00	**0,53**	1E-02	**1,97**	4E-02	Sec23a	Q01405	**1,31**	5,3E-02	**1,05**	9E-01	**1,25**	1E-02
	P57716	**0,73**	6,8E-01	**0,53**	5E-02	**1,38**	5E-01	Adcy1	O88444	**1,17**	2,2E-01	**0,93**	4E-01	**1,25**	5E-02
	Q8K183	**0,84**	3,2E-01	**0,53**	2E-02	**1,58**	6E-02	Pdia3	P27773	**1,23**	1,9E-01	**0,98**	1E+00	**1,26**	4E-02
	P70296	**0,72**	3,0E-01	**0,54**	1E-03	**1,33**	2E-01	Xkr4	Q5GH67	**1,05**	7,1E-01	**0,83**	5E-02	**1,26**	2E-02
	Q3USB7	**0,61**	1,2E-01	**0,55**	2E-02	**1,11**	9E-01	Soga3	Q6NZL0	**1,01**	1,0E+00	**0,80**	7E-02	**1,26**	3E-02
	P62069	**0,78**	6,3E-01	**0,55**	2E-02	**1,42**	2E-01	Arid1a	A2BH40	**1,12**	7,2E-01	**0,88**	5E-01	**1,28**	2E-02
	Q9DCZ4	**0,54**	1,1E-01	**0,55**	4E-03	**0,98**	1E+00	Mlf2	Q99KX1	**1,22**	1,1E-01	**0,93**	8E-01	**1,31**	1E-02
	Q9CQA3	**0,39**	5,8E-02	**0,56**	7E-03	**0,69**	4E-01	Efr3a	Q8BG67	**1,27**	8,4E-02	**0,96**	1E+00	**1,32**	2E-02
b	Q8K0S0	**0,63**	5,9E-02	**0,56**	2E-02	**1,13**	8E-01	Rnf214	Q8BFU3	**1,10**	2,4E-01	**0,82**	1E-01	**1,34**	3E-02
	Q9JIF0	**0,72**	1,3E-01	**0,57**	8E-03	**1,27**	8E-03	Dnm2	P39054	**1,34**	6,9E-02	**0,99**	1E+00	**1,35**	4E-02
	P19157	**0,60**	5,9E-02	**0,57**	6E-03	**1,05**	1E+00	Sdc3	Q64519	**1,31**	9,8E-02	**0,96**	9E-01	**1,37**	2E-02
	P62852	**0,80**	3,8E-01	**0,57**	2E-04	**1,40**	4E-02	C2cd2l	Q80X80	**1,22**	1,1E-01	**0,89**	6E-01	**1,37**	2E-02
	Q9QZ06	**0,87**	7,2E-01	**0,58**	1E-02	**1,50**	6E-02	Brsk1	Q5RJI5	**1,20**	2,1E-01	**0,87**	2E-01	**1,38**	2E-02
	Q9CQQ7	**0,44**	6,2E-02	**0,58**	2E-02	**0,76**	6E-01	Numbl	O08919	**1,16**	5,0E-01	**0,84**	1E-01	**1,38**	4E-02
	P56135	**0,48**	1,3E-01	**0,59**	4E-02	**0,82**	8E-01	Ahcyl1	Q80SW1	**1,30**	1,9E-01	**0,93**	9E-01	**1,40**	4E-02
l	Q91VR2	**0,53**	5,0E-02	**0,59**	9E-03	**0,90**	9E-01	Tubgcp2	Q921G8	**1,31**	7,2E-02	**0,93**	7E-01	**1,41**	2E-02
	Q91WS0	**0,54**	1,1E-01	**0,59**	6E-03	**0,91**	9E-01	Rell2	Q8BRJ3	**1,62**	6,6E-02	**1,12**	8E-01	**1,45**	5E-02
2	Q922J6	**0,71**	4,3E-01	**0,61**	8E-03	**1,16**	8E-01	Pag1	Q3U1F9	**1,43**	1,6E-01	**0,98**	1E+00	**1,46**	5E-02
2	Q91ZP9	**0,84**	5,0E-01	**0,62**	2E-02	**1,35**	1E-01	Nectin1	Q9JKF6	**1,24**	2,3E-01	**0,84**	9E-02	**1,48**	2E-02
	Q9DCR2	**0,67**	9,5E-02	**0,62**	1E-02	**1,08**	9E-01	Copb1	Q9JIF7	**1,15**	6,0E-01	**0,78**	2E-01	**1,48**	4E-02
b	Q921M7	**0,79**	3,4E-01	**0,63**	9E-04	**1,25**	2E-01	Vcpip1	Q8CDG3	**1,16**	7,8E-01	**0,78**	2E-01	**1,49**	1E-02
	O35454	**0,98**	1,0E+00	**0,64**	2E-02	**1,55**	3E-02	Eif4g2	Q62448	**1,23**	2,1E-01	**0,81**	9E-02	**1,52**	6E-03
	P63321	**0,75**	1,1E-01	**0,65**	4E-02	**1,16**	6E-01	Marcks	P26645	**1,20**	5,3E-01	**0,79**	1E-01	**1,53**	1E-02
l	Q8CI78	**0,63**	5,3E-02	**0,65**	2E-02	**0,97**	1E+00	Birc6	O88738	**1,28**	3,7E-01	**0,83**	3E-01	**1,54**	3E-02
	Q8CHU3	**0,94**	9,1E-01	**0,65**	2E-02	**1,45**	4E-02	Vps18	Q8R307	**1,32**	4,0E-01	**0,86**	7E-01	**1,54**	5E-02
	Q9R0P9	**0,66**	6,5E-02	**0,65**	3E-02	**1,00**	1E+00	Wwp1	Q8BZZ3	**1,34**	2,7E-01	**0,87**	7E-01	**1,54**	3E-02
	Q3U7R1	**0,79**	4,0E-01	**0,65**	2E-02	**1,21**	4E-01	Rgs12	Q8CGE9	**1,22**	3,9E-01	**0,78**	2E-01	**1,56**	2E-02
a	Q7TSC1	**0,80**	1,4E-01	**0,66**	2E-02	**1,23**	2E-01	Impa1	O55023	**1,14**	9,0E-01	**0,72**	2E-01	**1,58**	4E-02
	Q7TMQ7	**1,24**	2,4E-01	**0,66**	1E-02	**1,88**	2E-03	Slitrk3	Q810B9	**1,17**	7,6E-01	**0,73**	2E-01	**1,59**	3E-02
	O70378	**0,71**	5,4E-02	**0,66**	4E-02	**1,09**	9E-01	Cul5	Q9D5V5	**1,42**	2,4E-01	**0,88**	8E-01	**1,61**	2E-02
	Q80TL4	**0,82**	3,2E-01	**0,66**	4E-03	**1,24**	8E-02	Nomo1	Q6GQT9	**1,10**	9,2E-01	**0,68**	1E-01	**1,62**	3E-02
l	O35683	**0,73**	1,3E-01	**0,66**	3E-03	**1,10**	8E-01	Srprb	P47758	**1,11**	9,0E-01	**0,66**	1E-01	**1,68**	5E-02
	P62264	**0,79**	2,5E-01	**0,66**	9E-03	**1,19**	4E-01	Tfrc	Q62351	**1,40**	1,1E-01	**0,83**	1E-01	**1,69**	1E-02
	Q9WV98	**0,52**	1,7E-01	**0,67**	2E-03	**0,79**	7E-01	H1f0	P10922	**1,29**	7,6E-01	**0,75**	5E-01	**1,72**	3E-02
	P23506	**0,42**	9,4E-02	**0,67**	3E-02	**0,63**	3E-01	Stim1	P70302	**1,42**	3,7E-01	**0,79**	2E-01	**1,80**	4E-02
	P97315	**0,83**	4,1E-01	**0,67**	3E-02	**1,24**	3E-01	Cp	Q61147	**1,48**	4,3E-01	**0,79**	6E-01	**1,88**	3E-02
l1	Q8R3R8	**0,65**	7,9E-02	**0,67**	7E-04	**0,96**	1E+00	Ogt	Q8CGY8	**1,45**	8,3E-02	**0,77**	3E-01	**1,89**	3E-02
	P08226	**0,74**	1,8E-01	**0,68**	4E-03	**1,10**	8E-01	Nisch	Q80TM9	**1,34**	7,7E-01	**0,65**	3E-01	**2,08**	3E-03
	Q60864	**0,83**	6,9E-01	**0,68**	3E-02	**1,24**	4E-01	Sh3bp4	Q921I6	**2,78**	2,0E-01	**0,92**	1E+00	**3,02**	1E-03
	O55033	**0,80**	2,6E-01	**0,68**	2E-02	**1,17**	5E-01	Ecm29	Q6PDI5	**4,32**	2,6E-01	**0,63**	6E-01	**6,86**	3E-02
	Q9WUR2	**0,85**	2,7E-01	**0,68**	4E-02	**1,24**	3E-01	Hspa12a	Q8K0U4	**0,86**	6,7E-02	**1,05**	8E-01	**0,81**	2E-03
	Q9DCT8	**0,79**	9,2E-02	**0,68**	2E-02	**1,16**	3E-01	Ablim1	Q8K4G5	**0,94**	6,1E-01	**1,08**	5E-01	**0,87**	4E-03
	P62911	**0,73**	2,2E-01	**0,69**	2E-02	**1,06**	1E+00								
	P09925	**0,72**	1,8E-01	**0,69**	1E-02	**1,04**	1E+00								

Table RI-27. List of altered proteins in *Syngap1*$^{+/-}$ conditional KO mouse line for genetic rescue studies. Gene names and UniProt ID codes are provided. Abundance alterations expressed in fold change (FC) arising from relative quantitation obtained from LC-MS/MS analysis are shown in bold. One-way ANOVA was applied followed by post-hoc test Tamhane.

GENE NAME	UNIPROT ID	IND/KO FC	T-test	GENE NAME	UNIPROT ID	IND/KO FC	T-test	GENE NAME	UNIPROT ID	IND/KO FC	T-test	GENE NAME	UNIPROT ID	IND/KO FC	T-test
Acot7	Q91V12	**1,59**	5,0E-02	Mrps30	Q9D0G0	**1,44**	3,5E-02	Uso1	Q9Z1Z0	**1,23**	3,7E-02	Kctd16	Q5DTY9	**0,75**	3,9E-02
Acsbg1	Q99PU5	**1,44**	3,8E-02	Mtfp1	Q9CRB8	**1,37**	2,8E-02	Usp15	Q8R5H1	**1,47**	3,5E-02	Lasp1	Q61792	**0,67**	4,1E-02
Adcy1	O88444	**1,26**	1,2E-02	Naa25	Q8BWZ3	**1,28**	4,9E-02	Usp19	Q3UJD6	**1,38**	2,1E-02	Lgi3	Q8K406	**0,59**	4,2E-03
Ak5	Q920P5	**1,39**	2,5E-02	Napa	Q9DB05	**1,45**	1,6E-02	Vamp2	P63044	**1,46**	2,1E-02	Map6	Q7TSJ2	**0,72**	3,1E-02
Aldh1l1	Q8R0Y6	**1,41**	2,5E-02	Napg	Q9CWZ7	**1,52**	3,1E-02	Vars2	Q3U2A8	**1,25**	1,4E-02	Map7d1	A2AJI0	**0,81**	4,9E-02
Aldoc	P05063	**1,40**	3,5E-02	Ndufa3	Q9CQ91	**1,68**	2,8E-02	Vcp	Q01853	**1,42**	1,5E-02	Mark1	Q8VHJ5	**0,73**	1,1E-02
Anxa7	Q07076	**1,62**	4,4E-03	Nlgn4l	B0F2B4	**1,32**	4,2E-02	Vps18	Q8R307	**1,38**	3,6E-02	Mast3	Q3U214	**0,54**	1,6E-03
Ap3b2	Q9JME5	**1,51**	5,5E-03	Nlrx1	Q3TL44	**1,33**	4,6E-02	Vps53	Q8CCB4	**1,43**	1,0E-02	Mbp	P04370	**0,75**	4,3E-02
Ap3m2	Q8R2R9	**1,42**	2,8E-02	Nptx1	Q62443	**1,32**	1,8E-02	Xpo7	Q9EPK7	**1,36**	4,4E-02	Mpp3	O88910	**0,51**	8,0E-03
Aqp4	P55088	**1,48**	3,9E-02	Nrcam	Q810U4	**1,39**	1,9E-02	Zhx1	P70121	**4,90**	4,2E-02	Mprip	P97434	**0,83**	1,1E-02
Atp5b	P56480	**1,71**	3,3E-02	Osbpl6	Q8BXR9	**1,64**	4,5E-02	Abcb8	Q9CXJ4	**0,81**	3,1E-02	Myo1c	Q9WTI7	**0,54**	1,2E-02
Atp5c1	Q91VR2	**1,40**	4,8E-02	P2ry12	Q9CPV9	**1,42**	1,3E-03	Abcd3	P55096	**0,80**	1,0E-02	Nebl	Q9DC07	**0,71**	4,3E-03
Atp5h	Q9DCX2	**1,80**	2,5E-03	Pfkl	P12382	**1,33**	4,5E-02	Acadvl	P50544	**0,81**	4,3E-02	Nrn1	Q8CFV4	**0,76**	3,6E-02
Atp5i	Q06185	**2,04**	4,6E-02	Pfn2	Q9JJV2	**1,48**	4,0E-03	Acan	Q61282	**0,70**	1,3E-02	Nup155	Q99P88	**0,70**	1,3E-02
Atp5j2	P56135	**2,37**	1,5E-02	Pgk1	P09411	**1,37**	5,0E-02	Actn1	Q7TPR4	**0,65**	1,2E-02	Opa1	P58281	**0,86**	2,9E-02
Atp5o	Q9DB20	**1,95**	2,6E-04	Pgrmc2	Q80UU9	**1,73**	4,1E-02	Adck1	Q9D0L4	**0,84**	1,7E-02	Pag1	Q3U1F9	**0,70**	2,2E-02
C1qbp	O35658	**1,64**	1,5E-03	Phkb	Q7TSH2	**1,25**	2,2E-02	Ampd2	Q9DBT5	**0,73**	3,9E-02	Palm2	Q8BR92	**0,86**	3,2E-02
Cacna2d2	Q8PHS9	**1,41**	2,3E-02	Phyhip	Q8K0S0	**1,55**	6,2E-03	Anks1b	Q8BIZ1	**0,64**	2,2E-03	Pclo	Q9QYX7	**0,77**	2,8E-02
Cadps	Q80TJ1	**1,51**	2,2E-02	Plpp3	Q99JY8	**1,41**	1,1E-02	Anxa4	P97429	**0,68**	8,4E-03	Pde10a	Q8CA95	**0,68**	2,5E-02
Cd38	P56528	**1,55**	1,2E-03	Ppm1e	Q80TL0	**1,26**	2,0E-03	Ap2a2	P17427	**0,84**	1,1E-03	Phactr1	Q2M3X8	**0,61**	5,9E-03
Chchd4	Q8VEA4	**2,12**	1,8E-03	Ppp1r3f	Q9JIG4	**1,71**	4,0E-02	Appl1	Q8K3H0	**0,67**	2,0E-02	Ppib	P24369	**0,75**	2,0E-02
Ckb	Q04447	**1,31**	3,5E-02	Ppp3ca	P63328	**1,21**	1,7E-02	Atad3	Q925I1	**0,73**	2,5E-02	Ppp2r2c	Q8BG02	**0,62**	6,0E-03
Cnnm1	Q0GA42	**1,69**	3,9E-02	Ppp3r1	Q63810	**1,80**	1,2E-02	Atp6v1h	Q8BVE3	**0,84**	3,0E-02	Ppp2r5c	Q60996	**0,83**	1,3E-02
Cops3	O88543	**1,40**	4,9E-02	Prdx6	O08709	**1,55**	1,6E-02	Bcas1	Q80YN3	**0,84**	1,2E-02	Prmt8	Q6PAK3	**0,78**	3,6E-02
Crmp1	P97427	**1,41**	4,1E-02	Prickle1	Q3U5C7	**1,56**	2,5E-03	Bsn	O88737	**0,81**	2,6E-02	Prps1	Q9D7G0	**0,71**	7,3E-03
Ctnna1	P26231	**1,42**	4,2E-02	Psma2	P49722	**1,85**	2,4E-03	Bub3	Q9WVA3	**0,76**	2,1E-02	Ptpn9	O35239	**0,55**	4,4E-03
Dhrs1	Q99L04	**1,50**	1,7E-02	Psmc6	P62334	**2,44**	2,8E-02	Capzb	P47757	**0,78**	2,0E-02	Purg	Q8R4E6	**0,80**	1,1E-02
Dtna	Q9D2N4	**1,23**	4,9E-02	Ptprg	Q05909	**1,56**	3,5E-03	Cdk5rap3	Q99LM2	**0,50**	1,6E-03	Qdpr	Q8BVI4	**0,74**	3,8E-02
Eci2	Q9WUR2	**1,42**	4,0E-03	Ptprs	B0V2N1	**1,19**	3,5E-02	Cep131	Q62036	**0,69**	2,4E-02	Rab11fip5	Q8R361	**0,72**	3,9E-02
Eif3c	Q8R1B4	**1,91**	2,6E-03	Pydc3	Q3V3Q4	**1,28**	4,7E-02	Chchd3	Q9CRB9	**0,68**	4,0E-03	Rab12	P35283	**0,65**	4,0E-03
Elavl1	P70372	**1,59**	1,1E-02	Rab3b	Q9CZT8	**1,37**	2,7E-02	Cit	P49025	**0,84**	2,0E-02	Rac1	P63001	**0,71**	1,3E-03
Ephb1	Q8CBF3	**1,56**	3,2E-02	Rab3c	P62823	**1,74**	1,3E-02	Clasp1	Q80TV8	**0,76**	1,1E-02	Rdx	P26043	**0,74**	4,2E-02
Ephb6	O08644	**1,35**	1,6E-02	Rab4a	P56371	**1,47**	2,9E-02	Clasp2	Q8BRT1	**0,78**	1,6E-02	Rph3a	P47708	**0,75**	1,8E-03
Epn1	Q80VP1	**2,15**	4,8E-03	Rab7a	P51150	**1,62**	4,6E-02	Cnp	P16330	**0,71**	4,5E-04	Rpl18a	P62717	**0,72**	5,2E-03
Eppk1	Q8R0W0	**1,70**	3,0E-02	Rras2	P62071	**1,32**	4,6E-02	Cryab	P23927	**0,66**	1,5E-02	Rpl19	P84099	**0,82**	1,9E-02
Ermp1	Q3UVK0	**1,50**	2,7E-02	Rtn1	Q8K0T0	**1,69**	7,3E-03	Ctage5	Q8R311	**0,79**	4,8E-02	Rpl21	O09167	**0,74**	1,7E-02
Etfdh	Q921G7	**1,29**	3,0E-02	Scamp5	Q9JKD3	**1,87**	2,4E-02	Ddah2	Q99LD8	**0,66**	1,9E-02	Rpl28	P41105	**0,78**	2,4E-02
Fermt2	Q8CIB5	**1,88**	1,1E-02	Sfxn1	Q99JR1	**1,50**	1,1E-02	Ddn	Q80TS7	**0,70**	4,3E-02	Rpl6	P47911	**0,80**	3,4E-02
Fgf12	P61329	**1,29**	3,3E-02	Sfxn5	Q925N0	**1,48**	1,5E-03	Ddx3x	Q62167	**0,72**	4,0E-02	Rps19	Q9CZX8	**0,78**	7,2E-03
Fibp	Q9JI19	**1,63**	2,4E-02	Sh3bp4	Q921I6	**2,93**	1,4E-03	Dgcr8	Q9EQM6	**0,73**	3,7E-02	Rps27	Q6ZWU9	**0,69**	1,2E-02
Gdpd1	Q9CRY7	**1,32**	3,4E-02	Sh3gl2	Q62420	**1,47**	1,6E-02	Dis3l2	Q8CI75	**0,70**	4,2E-02	Samm50	Q8BGH2	**0,81**	2,1E-02
Gga3	Q8BMI3	**1,69**	2,2E-02	Skp1	Q9WTX5	**1,37**	1,5E-02	Dnajc16	Q80TN4	**0,87**	2,3E-02	Sec61a1	P61620	**0,77**	2,8E-02
Ghitm	Q91VC9	**1,46**	4,5E-02	Slc12a5	Q91V14	**1,31**	2,8E-03	Ech1	O35459	**0,63**	8,4E-03	Slc25a51	Q5HZI9	**0,73**	1,7E-02
Gpr37l1	Q99JG2	**1,26**	6,0E-03	Slc20a2	Q80UP8	**1,95**	3,8E-02	Emc2	Q9CRD2	**0,77**	3,6E-02	Slmap	Q3URD3	**0,69**	4,1E-02
Grid2	Q61625	**2,00**	2,6E-03	Slc25a3	Q8VEM8	**1,87**	1,7E-04	Exd2	Q8VEG4	**0,67**	8,8E-03	Snap47	Q8R570	**0,78**	3,6E-02
Gstp1	P19157	**1,52**	3,3E-02	Slc32a1	O35633	**1,44**	1,1E-02	Exoc1	Q8R3S6	**0,68**	3,1E-02	Snph	Q80U23	**0,80**	3,8E-02
Hnrnpdl	Q9Z130	**1,53**	1,9E-02	Slc4a10	Q5DTL9	**1,23**	4,8E-02	Ezr	P26040	**0,74**	4,1E-02	Spata2l	Q8BNN1	**0,68**	1,1E-03
Hnrnpk	P61979	**1,35**	7,0E-04	Slc6a17	Q8BJI1	**1,96**	3,5E-02	Flot1	O08917	**0,83**	3,8E-02	Syncrip	Q7TMK9	**0,77**	4,4E-02
Hspa4	Q61316	**1,42**	1,4E-02	Smarca2	Q6DIC0	**1,67**	1,8E-02	Fmr1	P35922	**0,71**	2,6E-02	Syne2	Q6ZWQ0	**0,64**	9,7E-03
Iba57	Q8CAK1	**1,40**	4,6E-02	Spg7	Q3ULF4	**1,43**	3,3E-02	G3bp2	P97379	**0,73**	4,3E-02	**Syngap1**	F6SEU4	**0,68**	3,0E-03
Icam5	Q60625	**1,67**	3,5E-03	Spon1	Q8VCC9	**1,30**	1,6E-02	Gabra5	Q8BHJ7	**0,63**	1,9E-02	Syt7	Q9R0N7	**0,76**	2,1E-05
Inpp5j	P59644	**2,18**	3,2E-02	Stoml2	Q99JB2	**1,49**	1,1E-03	Gja1	P23242	**0,76**	4,3E-02	Tbl2	Q9R099	**0,76**	3,0E-02
Kcna4	Q61423	**1,20**	2,7E-02	Ston2	Q8BZ60	**1,52**	3,5E-02	Gnal	Q8CGK7	**0,37**	2,0E-02	Tmem214	Q8BM55	**0,59**	6,2E-03
Kiaa0196	Q8C2E7	**1,52**	3,1E-02	Supt16h	Q920B9	**1,84**	2,9E-03	Gprasp1	Q5U4C1	**0,60**	2,2E-02	Tnik	P83510	**0,82**	3,8E-02
Madd	Q80U28	**1,26**	6,3E-04	Timm17a	Q9Z0V8	**1,99**	9,0E-03	Hdac6	Q9Z2V5	**0,70**	3,0E-02	Tomm40	Q9QYA2	**0,79**	3,4E-02
Map1s	Q8C052	**1,29**	4,1E-02	Timm17b	Q9Z0V7	**1,23**	4,8E-02	Hsd17b4	P51660	**0,78**	4,1E-02	Traf3	Q60803	**0,84**	4,2E-02
Map2k2	Q63932	**1,83**	1,6E-02	Timm29	Q8BGX2	**1,42**	3,2E-02	Ildr2	B5TVM2	**0,80**	3,6E-02	Trrap	Q80YV3	**0,08**	4,7E-02
Me1	P06801	**1,91**	1,2E-02	Timm50	Q9D880	**1,51**	3,8E-03	Ina	P46660	**0,70**	1,5E-02	Ttn	A2ASS6	**0,85**	1,4E-02
Mib1	Q80SY4	**1,39**	1,1E-03	Tkt	P40142	**1,34**	1,3E-02	Irgm1	Q60766	**0,75**	3,9E-02	Vars	Q9Z1Q9	**0,70**	3,2E-03
Mical3	Q8CJ19	**1,17**	3,1E-02	Top2b	Q64511	**1,46**	3,1E-02	Itsn2	Q9Z0R6	**0,78**	2,1E-02	Vsnl1	P62761	**0,60**	2,6E-03
Mios	Q8VE19	**1,27**	1,3E-02	Ube2n	P61089	**1,77**	3,1E-02	Jph4	Q80WT0	**0,69**	5,3E-03	Wdr81	Q5ND34	**0,76**	4,2E-02
Mlc1	Q8VHK5	**1,23**	2,5E-02	Ube3c	Q80U95	**1,82**	1,1E-02	Kars	Q99MN1	**0,79**	4,0E-02	Znf365	Q8BG89	**0,64**	5,4E-04
Mrpl10	Q3TBW2	**1,41**	1,9E-02	Ube4a	E9Q735	**1,77**	3,3E-03	Kcnj4	P52189	**0,69**	3,3E-02				

Table RII-28. List of altered proteins in *Syngap1*$^{+/-}$ conditional mouse line for KO induction. Gene names and UniProt ID codes are provided. Fold changes (FC) arising from relative quantitation obtained from LC-MS/MS analysis are shown in bold. Unpaired t-test was applied, and the significance level was set at $\alpha = 0.05$ ($p \leq 0.05$).

CII-DISCUSSION

To improve our understanding of ID and ASD through the establishment of common altered pathways in NDDs, it is essential to investigate specific cases first (Kaufman, Ayub, and Vincent 2010). The present study evaluated at PND56 (adult mice) the effects of *Syngap1* haploinsufficiency from conception as well as of its re-expression at PND21. In addition, the effects of conditional *Syngap1* KO mutation induction from PND21 were also examined. This experimental design sought to identify: (1) the alterations of the hippocampal PSD proteome due to a lack of SynGAP contributing to MRD5, (2) the degree of reversibility of the defects in the PSD by a lack of SynGAP, (3) the therapeutical relevance of recovering endogenous protein expression levels at PND21 and (4) key information about the development of a pharmacological strategy for humans affected by a *SYNGAP1* LOF mutation. For these reasons, this study represents the most comprehensive analysis of the effect of SynGAP deficiency and rescue in the hippocampal PSD proteome.

1. RELIABILITY OF THE DATA

The enrichment of proteins specific to the PSD compared to total homogenate indicated that the biochemical procedure to isolate PSDs was conducted properly. In addition, the data obtained from SynGAP IBs matched with the MS data, showing reduced levels of SynGAP but not of PSD-95 in HET and IND PSDs compared to the WT or RES littermates. Thus, no differences due to technical issues accounted for the alterations in the PSD proteomes found in each genotype.

Data reduction (PCA) and cluster analyses (expression correlation matrix and heatmap with dendrogram) in both KO mice lines, also confirmed the reliability of the data as replicates from the same sample grouped together. Interestingly, replicates from the same sample but from different genders segregated together. These results agree with the fact that an unbalanced sex ratio of affected individuals with a *SYNGAP1* LOF has not been reported, which is expected given its autosomal location (see Table I-X; Mignot et al. 2016; Bimble et al. 2018; Weldon et al, 2018; Kilinc et al. 2018). Therefore, male and female replicates were taken together for subsequent analyses.

Firstly, the correlation of protein expression FCs between genotypes was investigated. The fact that FCs from HET/WT *vs.* HET/RES correlated with a higher degree than RES/WT *vs.* HET/RES implicates that HET protein abundances were more similar in RES

and WT than in HET samples. In addition, the HET/WT and RES/WT comparison had a very poor correlation score (0.03), suggesting that protein abundances in HET and RES groups of mice were dissimilar and that the alterations in their PSD proteome were not the same. Indeed, the low correlation of HET/WT vs. RES/WT was supported by the other down-stream analyses such as volcano plots, cluster, GO term enrichment, pathways and interactome analyses as the number of proteins, biological processes, KEGG and Reactome pathways as well as proteins forming subnetworks in RES/WT were significantly lower than in HET comparisons.

1.1 LIMITATIONS OF THE PRESENT STUDY

To try to avoid misleading conclusions that do not represent the outcomes of an haploinsufficiency of *Syngap1*$^{+/-}$ at the PSD, some of the limitations of the present study have to be taken into consideration: 1) only expression levels of proteins from PSD enriched fractions were assessed, thus the terms 'up-regulation' and 'down-regulation' refer to protein expression levels, not gene expression; 2) protein activity levels were not taken into consideration, for instance we did not assess the changes at the level of the phosphoproteome or enzymatic activity; 3) we cannot distinguish between specific changes in subsets of synapses or cell types. As a result, the provided information is a static picture of the mean alterations from all hippocampal synapses and associated PSDs; 4) there were technical limitations in the proteins that can be identified in a quantitative manner. Consequently, there could be missing proteins that are relevant to the haploinsufficiency of *SYNGAP1*, and finally 5) Cre induction at PND21 could have a collateral role in the proteome composition. However, it is worth noting that these possible collateral effects were not observed at the behavioural and electrophysiological levels when used the same *Syngap1*$^{+/-}$ conditional mouse lines (Clement et al. 2012; Ozkan et al. 2014; Aceti et al. 2015).

1.2 PURITY OF THE PSD FRACTIONS ISOLATED

The purity of the final PSD preparation is determined by several factors. For instance, if presynaptic elements are especially abundant in the starting synaptosome preparation (Jhou and Tai, 2017), the PSD can contain a larger fraction of presynaptic active zone or mitochondria. On the other hand, the protocol used in this thesis to isolate PSDs does not include a second sucrose gradient, which results in purer PSDs (Cohen et al. 1977; Carlin et al. 1980; Suzuki et al. 2011). This is because this second sucrose gradient requires larger amounts of tissue than those available for this study (~50 mg of tissue). Furthermore, highly-abundant brain proteins, such as myelin basic protein or glial fibrillary

acidic protein (GFAP), are often found as PSD contaminants (Walikonis et al. 2000; Li et al. 2003; Peng et al. 2004; Dosemeci et al. 2006). Finally, as Triton X-100 (a non-ionic detergent) was used to isolate PSDs from synaptosomes, all proteins from synaptosome, beyond those in the PSD, insoluble to this detergent will co-precipitate in our PSD preparations. In support of that, GO term enrichment and interactome analyses identified subnetworks of proteins that could form high mass molecular complexes in other subcellular locations than PSDs, such as mitochondria, nucleosome or presynaptic active-zone.

CC-related GO term enrichment analyses indicated that neuron projection, membrane, cytoplasm, cytoskeleton, synapse, glutamatergic synapses, postsynapses and PSD terms were significantly associated with altered proteins from all comparisons, as expected from purer PSD samples. However, proteins associated with other compartments such as gap junctions, mitochondria, presynaptic active zone, membrane rafts, nuclear proteins, axon, myelin sheath or microtubule among others were identified and altered in certain genotypes. If these changes account for differences that represent the *in vivo* ongoing processes or are just another limitation of the subcellular fractionation process remains to be clarified as many PSD proteins have diverse locations and pleiotropic roles (Jordan et al. 2004; Collins et al. 2006; Racz and weinberg 2006). Hence, the identification of the previously mentioned proteins that are not generally associated to the PSD does not necessarily reflect a contamination from other subcellular compartments (Jordan et al. 2004; Delint-Ramirez et al. 2010; Asaki et al. 2003).

2. ALTERATIONS IN POSTSYNAPTIC DENSITY PROTEIN ABUNDANCES AND RELATED PATHWAYS IN *SYNGAP1*$^{+/-}$ MICE

Up to 251 proteins altered in PSD enriched samples from haploinsufficient *Syngap1*$^{+/-}$ mice (HET) compared to WT littermates were identified in the present thesis. GO term enrichment analyses through DAVID, STRING, FunRich and BinGO databases, pathway enrichment analysis through KEGG and Reactome as well as protein domain enrichment studies using InterPro, allow to get a picture of the functional characteristics of the alterations of the hippocampal PSD proteome of *Syngap1*$^{+/-}$ mice.

Of note, GO term analyses of HET/WT altered proteins using DAVID and a PSD reference proteome resulted in up to 50 main GO BP and 97 Reactome pathways related to neuronal system, development biology, signal transduction, energetic metabolism, RNA and protein metabolism, transport of small molecules, vesicle-mediated transport, cellular responses to external stimuli; cell cycle and programmed cell death, organelle biogenesis and maintenance, gene expression and haemostasis. An in-depth analysis of each pathway altered in HET mice is shown below.

2.1. NEUROTRANSMISSION

Proteomics data indicated that *Syngap1*$^{+/-}$ mice should present impairments in both neurotransmission across glutamatergic and GABAergic chemical synapses matching with reported abnormalities in both L2/3 Somatosensory Ctx GABAergic and glutamatergic cellular populations from *Syngap1*$^{+/-}$ mice when evoked its activation (Michaelson et al. 2018). As expected, proteins mainly associated to glutamatergic synapses were found significantly altered. Namely, processes like glutamate binding, the transport and activation of AMPARs, related signalling cascades such as Erk1/2 and synaptic plasticity were found abnormally expressed at the PSD agreeing with current knowledge of *Syngap1* KO effects at the synapse (Jeyabalan and Clement 2016; Kilinc et al. 2018; Kopanitsa et al. 2018). Together, these data agree with a previous report showing the main contribution of glutamatergic pyramidal neurons of Ctx in a cell-specific *Syngap1*$^{+/-}$ conditional KO to several aberrant *Syngap1*$^{+/-}$ mice phenotypes (Ozkan et al. 2014).

Conversely, although to a weaker degree, possible alterations in GABAergic neurotransmission in *Syngap1*$^{+/-}$ HIP were also identified, matching with a reduced level of GABAergic connectivity onto somatosensory Ctx pyramidal cells (Berryer et al. 2015). However, the present experimental design did not properly assessed the inhibitory postsynaptic compartment proteome as PSD fractions are expected to be mainly

composed of excitatory asymmetric PSDs (Carlin et al. 1980; Jhou and Tai 2017). Since the E/I balance is key for proper functioning (Lee et al. 2017; Zhou and Yu 2018), there could be expected a compensatory mechanism of GABAergic neurotransmission to the hyperexcitability of glutamatergic HET neurons (Clement et al. 2012; Ozkan et al. 2014). Yet, others report a reduced synaptic connectivity in somatosensory Ctx from HET mice which would not be accompanied by a compensatory inhibitory neurotransmission increase. These findings together with the ones from Chapter I, support a cell- and region-specific effect of *Syngap1* pathogenicity (Michaelson et al. 2018). Thus, an analysis of the proteome of GABAergic synapses in HIP of HET mice could provide complementary knowledge.

In addition to chemical synapses, pathways and GO enrichment analyses indicated that there are defects in the trafficking, assembly and regulation of Gap junctions, suggesting an impairment of electric coupling in hippocampal neurons from HET mice. Despite these proteins might be contaminants or just part of the link between junctional complexes like Claudins and Actin cytoskeleton, these differences could also reflect defects of this type of cell-cell communication in *Syngap1*$^{+/-}$ mice. In support of this notion, alterations in electrical coupling along with inhibitory control might contribute to the defects in oscillatory rhythms and sleep disturbances seen in ASD, SCZ or MRD5 patients (Garcia-Rill et al. 2008; Williams and Boksa 2010; Maxwell et al. 2015; Michaelson et al. 2018; Vlaskamp et al. 2019; personal communications with parents of affected individuals) as well as in mouse models of neuropsychiatric disorders like GABAergic cell-specific *Syngap1*$^{+/-}$ mice (Berryer et al. 2016). Therefore, electrical synapses, in addition to chemical ones, could also play a role in the oscillatory defects promoted by reduced SynGAP expression.

2.2 SIGNALLING TRANSDUCTION

Assessed *Synagap1*$^{+/-}$ mice exhibited several alterations in postsynaptic signalling. Of note, abnormal expression levels of proteins related to small GTPases, GAPs and GEFs mediated signal transduction including MAPK cascades, such as Ras/Raf/Erk1/2/MAPK3, Rap/p38MAPK or Rho/LIMK/Cofilin, were identified in this study. In addition, neurotrophic factors signalling through receptor tyrosine kinases (e.g., Ephb6), non-receptor tyrosine kinases (e.g., Ptpn1 or PTK6 signaling), Wnt/β-catenin, mTOR, hedgehog (Hdg) transduction cascades and pathways related to peptide hormone response through growth hormone and interleukin receptors have also been found significantly enriched in HET mice.

2.2.1 SMALL GTPASE SIGNALLING

Reduced levels of SynGAP at the PSD core would release its brake onto small GTPases, which in turn would become hyperactivated. As many small GTPases were found down-regulated in *Syngap1*$^{+/-}$, is possible that overactive Small GTPases in HET PSDs undergo compensatory reductions of their abundances. In support of this hypothesis, Ras GTPase and Rho GTPase ubiquitylations have been reported as an alternative mode of GTPase (in)activation and an important means to control signalling output (Nethe and Hordijk 2010) agreeing with the alteration of 17 and 20 proteins related to protein turnover in HET and IND mice, respectively.

Dysregulations in small GTPases encompassed distinct families of the Ras superfamily, including, Ras, Rab and Rho, as were shown by GO Biological Process terms and InterPro protein domain enrichment analyses. Considering all genotype comparisons of *Synagap1*$^{+/-}$ mice, the specific small GTPases found altered were p21 Ras (HRas, KRas, RRas2); Rap (Rap1b, Rap2a); Diras2; RalA (RalA); Rho (RhoA, RhoG); Cdc42; Rac1 and several Rab subgroups. All these small GTPases could be linked with the reported direct bifunctional Ras/Rap GAP activity of SynGAP or indirect repression of Rac1 and Rab5 by SynGAP (Tomoda et al. 2004; Krapivinsky et al. 2004; Pena et al. 2008; Carlisle et al. 2008). Together, these data extend the number and type of potential small GTPases that are directly or indirectly regulated by SynGAP. Also, the present findings predict defects in functional and structural synaptic plasticity, as Ras, Rac1, Cdc42, and RhoA and their regulators as they are essential modulators of synaptic strength and structure (Ye and Carew 2010; Araki et al. 2015 and references therein).

Functional synaptic plasticity through Ras and Erk signalling

Syngap1$^{+/-}$ mice have enhanced synaptic transmission and Erk activity while their LTP is impaired (Komiyama et al. 2002; Ji et al. 2003; Yang et al. 2011; Araki et al. 2015; Kopanitsa et al. 2018). Bearing in mind that the active state is not known based on the present data, this study demonstrated no differences in Erk1/2 expression between HET and WT mice. Accordingly, previous reports also have indicated that total Erk levels are unchanged in hippocampal slices (Komiyama et al. 2002; Kopanitsa et al. 2018). In contrast, HRas was found to be significantly down-regulated by LC-MS/MS, despite this difference did not reach statistical significance using data from IBs. This partial disagreement can be explained by several studies showing that protein quantification via MS can be more robust, reproducible and achieve lower limits of detection than IBs (Aebersold, Burlingame, and Bradshaw 2013). Correspondingly, subcellular localization studies of HRas showed that the major part remains on the SNP fraction, which also

agrees with the reported enrichment of Ras proteins in synaptosome but not in PSD fractions (Yang et al. 2011). In forebrain total extracts, an increased proportion of active Ras and Rac (Komiyama et al. 2004; Carlisle et al. 2008) has been reported in *Syngap1*$^{+/-}$ mice, but to our knowledge there are no previous reports describing an altered expression of small GTPase levels in PSDs. Owing that in IND mice the same expression pattern has not been observed, a comparative immunohistochemical study of small GTPase levels in HET and WT mice could provide further evidence to fully clarify these results.

In general terms, LTP required recruitment of AMPARs to the membrane attached to the PSD, whereas LTD promotes their removal mediated both by Ras small GTPases (Kim et al. 2003; Vazquez et al. 2004; Rumbaugh et a. 2006; Kaprivinsky et al. 2004; Yang et al. 2011; Lee et al. 2011; Jeyabaln and Clement 2012; McMahon et al. 2012). In line with this assumption, GO, Reactome pathways and protein domain enrichment analyses in HET mice also showed significant alterations in proteins involved in synaptic plasticity terms such as LTP/LTD, glutamate binding, the activation of AMPARs or down-regulation of Ras small GTPases. Despite changes in the expression of AMPAR subunits are known, like GluR1 in HET mice (Kim et al. 2003), and the specific Reactome pathways: 'Trafficking of AMPAR subunits' in HET/WT and 'Trafficking of GluR2-containing AMPARs' in HET/RES-derived analyses were significantly enriched, differences in the protein abundances of specific AMPAR subunits were not found in HET mice.

Several hypothesis can account for this discrepancy: 1) a fraction of synaptic AMPARs, likely those more loosely attached to the PSD, are known to be soluble to Triton X-100 (Leonard et al. 1998), thus not all synaptic AMPARs would be quantified by MS in HET mice; 2) due to the role of SynGAP in non-Hebbian plasticity to scale-down abnormal increased synaptic strengths to compensate for the enhanced network excitability in HET mice (Wang et al. 2013; Barnes et al. 2015), is possible that an homeostatic compensatory change explains the lack of differences in the abundances of AMPAR subunits reported here. In support of that explanation, it has been reported that a cooperation of GEFs and GAPs down-regulates excitatory synapses, dendritic spines, and surface AMPARs following chronic overexcitation (Lee et al. 2011); 3) in *Syngap1*$^{+/-}$ animals the overactivity of Ras results in an increase of AMPARs exocytosis to the postsynaptic membrane (Komiyama et al. 2002; Vazquez et al. 2004; Rumbaugh et al. 2006; Kennedy 2005, McMahon et al. 2012) while Rap1 activity increases endocytosis of AMPARs (Zhu et al. 2002; Kennedy 2005; McMahon et al. 2012;).

In line with this opposite effect, both members of Ras and Rap small GTPase families were found down-regulated. Therefore, is possible that the absence of differences seen in the

AMPARs expression arises from opposite effects carried out by Ras and Rap due to the analysis of the averaged changes in a given hippocampal PSD, and finally 4) changes in extrasynaptic GluN1 and GluA1 expression at hippocampus of *Syngap1*$^{+/-}$ have been described (Muhia et al. 2012). Thus, possibly in the present study, these extrasynaptic proteins were not isolated in the PSD fraction resulting in no detection of direct expression changes. Taken together all these data, the lack of alterations in AMPAR levels seen in an average hippocampal PSD does not contradict current knowledge of AMPARs dynamics in neuronal *Syngap1*$^{+/-}$ models.

Structural plasticity through Rho small GTPases

GO terms such as cytoskeleton organization or more specifically, Actin cytoskeleton and regulation of cell projection organization, among others, refer to PSD components that were identified in the confident group of up-regulated proteins. When all altered proteins were considered, additional terms such as synapse structure and activity, Actin filament-based process and cortical cytoskeleton organization appeared enriched too. These results agree with the fact that SynGAP regulates dendritic spine morphology by limiting its volume, thus *Syngap1* haploinsufficiency promotes premature enlargement of spine head volume and length (Vazquez et al. 2004; Carlisle et a., 2008; Lee et al. 2011). Also, a biased distribution towards mushroom-type spines has been reported in *Syngap1*$^{+/-}$ mice (Carlisle et al. 2008; Clement et al. 2012; Aceti et al. 2015). In addition, both Rac1-PAK and RhoA-ROCK pathways are essential for the induction and maintenance of spine enlargement (Araki et al. 2015), whereas Ral proteins exert roles related to spine remodelling through Rho/Rac/Cdc42 mediation (Polzin et al. 2002; Ye and Carew 2010; Teodoro et al. 2013).

Noteworthy, when considering alterations in GAPs and GEFs, most of them were found related to Rho Small GTPases. Namely, the Rho GEFs Kalirin or Ephexin-1 (Ngef) and 3 Arhgaps (Rho GAPs) were found altered in HET mice. Autoantibodies against Arhgap21 have been linked to cerebellar ataxia as well as psychotic, affective, and cognitive symptoms. Noteworthy, only a subset of hippocampal neurons express Arhgap21 (Doss et al. 2014, 21; Jarius et al. 2015, 26; Bartels, Prüss, and Finke 2018). Arhgap39 is critically required for neurodevelopment, learning and memory, and highly expressed in hippocampus throughout life (Nowak, 2018), whereas Arhgap44 has a BAR (Bin/Amphiphysin/Rvs) domain, key for membrane curvature regulation, and its expression increases during neuronal development concurrent with a decrease in the rate of filopodia formation (Galic et al. 2014). Importantly, our data emphasises for the first time,

the role of Arghaps in *Syngap1*$^{+/-}$ mice and could suggest molecular basis for motor problems seen in patients with *SYNGAP1* mutation.

Also, dysregulations in small GTPase effectors including the Rho-interacting kinase Citron were found. Interestingly, defective neurogenesis has been described in Citron KO mice due to altered cytokinesis and massive apoptosis (Di Cunto et al. 2000). Moreover, scaffolding proteins linking Cdc42 and Rac1 with Arp2/3 and WASF signalling (i.e., Baiap2 and Enah), 18 ABPs and Synaptopodin were found to be significantly altered (Hahn et al. 2009; Ahmed, Goh, and Bu 2010). Indeed, Synaptopodin, an Actin-associated protein essential for the modulation of spine shape and the formation of the spine apparatus (Deller et al. 2003), was found significantly up-regulated in both HET genotype comparisons, matching with the presence of spine apparatuses in potentiated enlarged dendritic spines (Harris and Weinberg 2012; Maiti et al. 2015; Petralia et al. 2016). Furthermore, proteins related to filopodia and prematurely motile spines, such as Cdc42, RhoA and Rac1 (Govek, Newey and Aelst 2012), were found down-regulated while proteins that reduce the number of filopodia (e.g., Arghaps or Synaptopodin) or sever Actin filaments in an active state (i.e., Cofilin), were up- and down-regulated in HET PSDs, respectively. Collectively, these data not only strength the previously reported reduced structural synaptic plasticity in dendritic spines from *Syngap1*$^{+/-}$ mice (Clement et al. 2012; Aceti et al. 2016) and suggest indirect regulation of Rho Small GTPases by SynGAP (Tam et al. 2015; Araki et al. 2015; Jeyabalan and Clement, 2016), but also provide molecular basis of this processes in terms of synaptic protein abundances.

Forebrain extracts from *Syngap1*$^{+/-}$ mice exhibit alterations in the Cofilin phosphorylation state but not its total levels, producing a net increase in actin polymerization over time and a shift toward larger spine heads as Actin filaments cannot be severed (Carlisle and Kennedy 2005; Carlisle et al. 2008). In contrast, LC-MS/MS data indicated a significant reduction of Cofilin-1 expression in HET and RES mice. Unfortunately, the subsequent IB analyses conducted failed to validate the LC-MS/MS data as the detection of Cofilin-1 by the corresponding antibody was compromised due to its low affinity and the intrinsic low Cofilin expression at the PSD demonstrated by subcellular localization studies. Yet, when high PSD protein amounts were loaded for IB analyses, only WT samples showed a clear faint band, thus supporting LC-MS/MS data. The discrepancies between previous reports and present studies could arise because Carlisle and collaborators analysed together the expression of two Cofilin (i.e., Cofilin-1 and 2) paralogues (with a pan-Cofilin antibody) and not the expression of Coflilin-1 as in our case. Also, they used forebrains extracts from mature adult mice and not hippocampal PSDs samples as in this case.

Translation and mTOR signaling through Rheb

It has been reported that SynGAP represses protein synthesis (Wang, Held, and Hall 2013; Barnes et al. 2015). In one proposed mechanism, SynGAP stimulates the Ras/Erk pathway, which in turn promotes the dissociation of the Tsc1/2 complex, activating the small GTPase Rheb and ultimately, mTOR (Garami et al. 2003; Laplante and Sabatini 2012; Wang, Held, and Hall 2013). In agreement with that, GO terms related to mTOR complex and alterations in the proteins forming this complex have been identified in HET mice. Yet, Rheb and several reported up- or down-stream mTOR activated kinases (e.g., Akt, p70S6 kinase) and effectors including elongation factors (e.g., 4E-BP1/eIF4E) were not identified in the present proteomics study (Lapante and Sabatini, 2012). This agrees with a previous report showing a restricted expression of elongation factors in lipid rafts instead of PSD fractions, while regulatory kinases could be found in PSD or lipid rafts (Asaki et al. 2003).

Among the proteins related to mTOR signalling, Tsc1 and Tsc2 were found down-regulated in HET mice to half of their normal protein levels, although this change did not reach statistical significance. Hence, if Tsc1/2 expression is down-regulated in these animals, this would result in an overactivity of mTOR signalling and could provide the molecular base of the previously referred enhanced protein synthesis in HET and $Fmr1^{-/y}$ HIPs (Barnett et al. 2015). Accordingly, abnormal expression levels of the scaffold protein for mTORC2 complex Rictor and members of mTORC1 signalling complex: Lamtor1 and Larp1 were also identified. In addition, up-stream kinases that could regulate mTOR signalling appeared to be dysregulated (Hoeffer and Klann 2010). For instance, Dapk1, a Ca^{2+}/calmodulin-dependent serine/threonine that phosphorylates Tsc2 in response of growth factor signalling, was found profoundly down-regulated (FC= 0.11) while GSK3α kinase, the non-receptor Fyn and the receptor tyrosine Eph6B kinases were significantly up-regulated and identified as hub proteins (Nakamoto 2000; Stevens et al. 2009).

Protein transport mediated by Rab and Arf Small GTPases

Defects relevant to synaptic vesicle cycle (e.g., transport, endocytosis or exocytosis) seen in the present study can be partially caused by the abnormal expression levels of several small GTPases from the Rab family. Namely, 4 out of 9 abnormally expressed Rab proteins in HET PSDs belong to Golgi membrane budding, whereas Rab3a was the only altered Rab that was found annotated with a direct synaptic location (Stenmark and Olkkonen 2001; Wennerberg 2005). Mutation of Rab proteins and/or their effectors underlie human diseases such as cancer (Rab25, Rab5 and Rab7), neuronal dysfunction (Rab1 and Rab7), retinal degeneration (Rab8) and immune and pigmentation disorders

(Rab27 and Rab3; Schwartz et al. 2007; Vilariño-Güell et al. 2011). Accordingly, GO terms such as melanogenesis were found enriched among dysregulated PSD proteins from HET mice.

The Arf–coat-protein complex facilitates cargo sorting and vesicle formation and release. Particularly, the Arf GEF Iqsec2 regulates the formation of vesicle coats at different steps in the exocytic and endocytic pathways and interacts with different effectors including vesicle coat proteins. Of note, mutations in *IQSEC2* cause non-syndromic ID (Shoubridge et al. 2010; Madrigal et al. 2016). Because Iqsec2 is found among the confident group of up-regulated proteins in HET mice, it is plausible that its increased expression could compensate the cognitive and behavioural abnormalities previously described in HET mice or contrarily, contribute to their pathophysiology.

2.2.2 EPHRIN RECEPTOR MEDIATED SIGNALLING

Ephrin type-B receptor 6 (Ephb6) and Ephrine type-A receptor 6 (Epha6) were found significantly up-regulated in HET mice compared with WT or RES mice and in IND/WT Ephb6 and Ephb1 were found also significantly up-regulated. Conversely, in RES/WT none of these Ephrin receptors appeared abnormally expressed. These data suggested that changes in SynGAP abundance at the PSD, irrespective of the developmental time of this change, correlates negatively with alterations in EphRs levels. Interestingly, Eph receptors and its ligands play important roles in many developmental processes, including neuronal network formation, the patterning of the neural tube or guidance of cell migration (Nakamoto 2000). Thus, they possibly exert a compensatory role to overcome reduced connected networks due to increased neuronal death in hippocampus of HET mice (Knuesel et al. 2005; Muhia et al. 2012). In line with this assumption, despite circuit hyperexcitability has been associated to brain structures more linked to reduced synaptic connectivity, a circuit hypoconnectivity in upper-lamina somatosensory cortex and disrupted tactile-related processing in *SYNGAP1* haploinsufficient humans has recently been reported (Michaelson et al. 2018).

Moreover, it has been reported that members of the CaMKII family induce postsynaptic secretion of the trophic factors BDNF and NT-3 in hippocampal neurons as a response to excitotoxic damage (Kolarow, Brigadski, and Lessmann 2007), yet only CAMKII-δ was found significantly up-regulated in HET *vs.* WT and RES. Thus, it could be speculated that CAMKII-δ exerts a neuroprotective role due to the lack of SynGAP by increasing Ephrine receptors expression. However, the small GTPase RalA, which regulates growth factor receptor endocytosis was found down-regulated in HET/RES matching with increased

expression of these receptors but questioning its neuroprotective role as LOF mutations in RalA have been linked to ID and developmental delay (Teodoro et al. 2013; Hiatt et al. 2018).

2.3 CELL-CELL ADHESION

Proteins related to cell-substrate adherens junctions and focal adhesion that connect the pre- and postsynaptic compartments were found significantly altered in the GO enrichment analyses. Also, alterations in pathways involving synaptic adhesion-like molecules were enriched according to Reactome pathways studies. As an example, the cell adhesion proteins Spondin-1 (Spon1) or Neuroligin-2 (Nlg2) were found significantly up-regulated but Neuroligin-1 was not. Of note, the differences in the expression of Neuroligin-1 and 2 matches with previously reported IB data (Walkup et al. 2016). Interestingly, the plasminogen receptor (Plgrkt), which is required for structural plasticity through synaptic cleft remodelling by activating matrix metalloproteinases (e.g., MMP9), and the engulfment and cell motility protein (Elmo2), were both significantly down-regulated in HET mice (Lighvani et al. 2011; Kreutz and Sala, 2012). The alterations in all these proteins together with those related to Rho Small GTPase signalling could be related to the accelerated maturation of dendritic spines as well as the increased proportion of less motile spines (mushroom and subby) reported in HET mice (Clement et al. 2012; 2013; Aceti et al. 2015).

Finally, alterations such as the EGFR transactivation pathway through Gastrin, found enriched through Reactome analysis, suggest that cell-cell adhesion molecules could organize presynaptic changes as a consequence of postsynaptic alterations by trans-synaptic signalling (Yu and Goda 2009). As an example, Lin7A, Spondin-1, Latrophilin-1 or Ephrine receptors, which could mediate these events, were found altered in HET mice.

2.4 DEVELOPMENTAL BIOLOGY

Pathways related to nervous system development, important for synapse specification, organization and formation were also identified. Specifically, pathways related to L1CAM interactions and recycling pathways, both important for axon guidance, as well as receptor tyrosine kinases, which are crucial for migration, repulsion and adhesion during neuronal development, were found altered based on Reactome analyses. Furthermore, proteins involved in the establishment or maintenance of apical/basal cell polarity, glial cell proliferation, regulation of dendrite development and cell projection organization appear dysregulated in *Syngap1*$^{+/-}$ mice when conducted GO term enrichment studies.

It is possible that terms related to glia might resulted from random contaminations of the PSD enrichment preparations, but the role of SynGAP in neuronal development events is further supported by the dysregulation of important signalling cascades such as Hdg and Wnt-related ones, as both molecules are important morphogens during development. Also, Cofilins, required for neural tube morphogenesis and neural crest cell migration (Gurniak, Perlas, and Witke 2005), were found dysregulated in HET mice. Finally, SynGAP has a Rab GTPase activity *in vitro,* while provides a scaffolding complex that regulates the endocytic membrane organization during axon formation (Tomoda et al. 2004; Kilinc et al. 2018). Therefore, alterations in the abundance of several Rabs in HET mice could also account for abnormalities in synapse development and brain circuit formation exhibited by *Syngap1*$^{+/-}$ mice (Michaelson et al. 2018).

Interestingly, the significant enrichment of proteins related to dendrite development agrees with a reduction of the spatial volume occupied by the dendritic trees of individual dentate gyrus neurons found in *Syngap1*$^{+/-}$ mice (Clement et al. 2012) and the ability of some small GTPases to regulate neuronal development and cell projections through cytoskeleton like Rho small GTPases and their regulators (Govek, Newey, and Aelst 2005; Hall and Lalli 2010).

2.5 RNA AND PROTEIN METABOLISM

It is widely accepted that *Syngap1*$^{+/-}$ models present an increased level of basal and local translation at dendritic spines (Wang, Held, and Hall 2013; Barnes et al. 2015; Yokoi et al. 2017; Paul et al. 2018) as well as an impaired translation-dependent homeostatic synaptic plasticity mechanisms (Lee et al. 2011; Wang, Held, and Hall 2013). Noteworthy, ribosomal proteins could be part of PSD fractions as ribosomes localize in close proximity to or are attached to PSDs and cytoskeleton (Hesketh et al. 1999; Asaki et al. 2003). As expected, the present work revealed defects in processes related to translation, including pathways involved in mRNA stability shown through the enrichment of Reactome pathway 'nonsense-mediated mRNA decay enhanced by the exon junction complex (EJC)'. In addition, terms related to formation of the translation ternary complex, translation initiation, ribosome proteins and protein PTMs have been shown significantly enriched in Reactome and GO term enrichment analyses. Therefore, alterations in the translation rates are supported by terms related to RNA and protein metabolism.

All this previous data indicated that proteomic changes occurring at the PSD should be in the direction of increased protein expression. Nevertheless, this study identified a higher proportion of down-regulated than up-regulated proteins (160 vs. 91). Also, in HET mice,

terms related to translation appeared enriched among the group of down-regulated proteins, due to a prominent reduction of ribosome constituents, as shown by GO term and network analyses. Consequently, these data suggested opposite effects in translation rates than those reported in the aforementioned references. Despite this apparent controversy, the in-depth analysis of proteins related to translation, showed that proteins promoting translation were mainly up-regulated, whereas proteins that negatively regulate translation were found down-regulated. Also, mTOR signalling was predicted to be overactive as previously described and thus, would also support an increase in protein synthesis. Finally, if the number of mitochondrial proteins and ribosome constituents were removed from the list of altered proteins in HET mice, as happens in IND/WT comparison, there would be a higher number of up-regulated than down-regulated proteins. Therefore, this would agree with an increased basal translation in HET mice. Taken all these data together, the net effect of translation could not be assured but points towards an increased protein synthesis that could be compensated by reducing the number of ribosomes ready for local translation in the synaptic spine.

2.6 METABOLISM REGULATION

Mitochondria are responsible for essential functions such as producing 90-95% of cellular energy using the electron transport chain and oxidative phosphorylation (Ly and Verstreken 2006), buffering intracellular Ca^{2+} (Duchen, Verkhratsky, and Muallem 2008), regulating apoptosis (de Pablo et al. 1999) or modulating synaptic activity, stability and morphology (Somerville et al. 2011; Graham et al. 2017). Hence, it is not surprising that mutations in mitochondrial genes have been found responsible of neurologic diseases like neurodegenerative disorders, stroke and psychiatric disorders, including ASD, SCZ or ID (Mattson, Gleichmann, and Cheng 2008; Sheng and Cai 2012; Valenti et al. 2014; Gómez de Salazar et al. 2018).

Neuronal mitochondria are transported to 3 specific neuronal locations: the presynaptic terminal, the axon and the dendrite (Sheng and Cai 2012; Santuy et al. 2018; Rangaraju, Lauterbach, and Schuman 2019). Despite defects of mitochondrial metabolism have been mainly associated to the presynaptic compartment, a high energy demand of postsynaptic events has been demonstrated, matching with mitochondrial translocation into dendritic spines upon postsynaptic stimulation. Moreover, mitochondria could be found in dendritic filopodia of humans and/or mice and thorny excrescences in CA3 of rat hippocampus (Cameron, Kaliszewski, and Greer 1991; Popov et al. 2005; MacAskill, Atkin, and Kittler 2010; Pickett et al. 2018; Cameron et al. 1991; Li et al. 2004; Popov et al. 2005; Sung et al. 2006; McAskill et al. 2010; Sheng and Cai, 2012; Pickett et al. 2018; Rangaraju et al.

2019). As the assessment by EM or other techniques of the components of the PSD fractions generated here (without a second sucrose gradient) remains elusive, it is unclear if mitochondria alterations are product of a random contamination or if they are *bona fide* PSD constituents. Alternatively, mitochondria proteins could reflect synaptic mitochondria that are contaminating the PSD fractions obtained with the described method in the present thesis. This possible contamination is supported by the fact that modifications of the present used protocol, allowed to identify mitochondria alterations in hippocampal extrasynaptic fractions rather than in the PSD ones (Gómez de Salazar et al. 2018).

To shed light on this matter, the number of proteins identified from the reported mitochondrion proteome in MitoCarta was analysed. Up to 396 mitochondrial proteins (34%) were identified in the PSD proteomes from both *Syngap1* conditional mice lines. In addition, mitochondrial proteins enriched in synaptic *vs.* non-synaptic mitochondria has been published (Graham et al. 2017). Despite almost 50% of these mitochondrial proteins were identified in the PSDs in this study, GO term and network analyses showed that proteins enriched in synaptic-mitochondria were a significant part of the altered subgroup of PSD proteins. These formed clusters of functionally related proteins, such as those from the mitochondrial respiratory chain complex I. Specifically, 78% of the proteins forming this complex I were identified in the PSD fraction, with 40% of these being significantly down-regulated in HET mice. In contrast, only 2.5% and 5% of the proteins from this mitochondrial complex had significantly different abundances in the PSD of RES and IND animals, respectively. In summary, since this complex is a specialized feature of synaptic mitochondria (Graham et al. 2017) and its defects play a role in synaptopathies (Heng Du et al. 2010; Rubeis and Bauxman; 2014; Jhou and Tai, 2017; Pickett 2018), abnormalities in synaptic mitochondria and metabolism could underlie part of the *Syngap1*$^{+/-}$ phenotype.

An in-depth study of the mitochondrial impairments by network assessment of the most interconnected altered mitochondrial proteins as well as Reactome pathways and GO term enrichment analyses indicated that oxidative phosphorylation mediated by mitochondrial complex I might be significantly dysregulated in HET mice. Furthermore, proteins related to the metabolism of lipids and generation of energy through other catabolic pathways, including β-oxidation were also abnormally expressed in HET animals. Noteworthy, there were up to 3 proteins with differences in abundance that represented the pathway involved in the translocation of SLC2A4 (glucose transporter 4) to the plasma membrane. This pathway is related to glycolysis and ATP production.

In summary, the present data indicated for the first time that *Syngap1*$^{+/-}$ mice have defects in synaptic energy production. Hence, decreased availability of energy may be a

mechanism of homeostatic reduction of synaptic overexcitability and up-regulated translation described in these animals (Clement et al. 2012, 2013; Ozkan et al. 2014; Wang, Held, and Hall 2013; Barnes et al. 2015; Paul et al. 2018; Michaelson et al. 2018).

2.7 ORGANELLE BIOGENESIS & MAINTENANCE

According to dysregulations in mitochondria, polyribosomes, ER and Golgi proteins, terms related to organelle and vesicle-mediated transport were found significantly enriched in KEGG pathways, protein domains, GO terms enrichment and network analysis among proteins differentially expressed in HET mice. Proteins such as Dynamin-2, Tubulin or Tau that mediate the transport of organelles in and out the dendritic spines, could account for the down-regulation of structural components of mitochondrial and ribosomal proteins found in HET mice. For the specific case of Tau, its expression was up-regulated in HETs, although this difference did not reach statistical significance (FC >1.4; p=0.07). In accordance, overexpression of Tau inhibits anterograde mitochondrial transport and disrupts mitochondrial distribution in neurites, resulting in perinuclear clumping in the soma (Pickett et al. 2018). Moreover, the spine apparatus facilitates the movement of mitochondria into the neck and head of granule cell spines in the absence of microtubules (Cameron et al. 1991) and one of the main components of this organelle, Synaptopodin, is increased in HET PSDs with a FC of ~2, as it has previously been noted. Therefore, in addition to the reported defects in small GTPases with a role in cytoskeleton rearrangement and motor proteins, spine apparatus-related proteins may also contribute to the protein transport defects and synaptic mitochondrial localization in HET mice.

2.8 VESICLE-MEDIATED TRANSPORT

Several proteins that promote vesicle-mediated transport were found altered in HET mice. Up to 63% of proteins annotated in the term presynaptic active-zone (GO: 048789) form complexes related to vesicle trafficking (e.g., SNARE complex or Rabs) that are found altered in HET PSD enriched fractions. However, these vesicle trafficking proteins might have a pleiotropic role and thus, could represent abnormalities in postsynaptic EZs vesicle fusion processes mediated by specialized SNAREs (Newpher and Ehlers 2008; Z.-H. Sheng and Cai 2012; Jurado et al. 2013; Colgan and Yasuda 2014). In addition, members of the COPI and COPII complexes, which are involved in anterograde/retrograde transport between ER and Golgi were found abnormally expressed in HET mice, thus contributing to this dysregulated vesicle-mediated transport. It is possible that alterations in these proteins arise from extra-synaptic contaminating Golgi or ER, yet their true postsynaptic nature cannot be fully ruled out as the ER is a well-known postsynaptic organelle, going

even into dendritic spines (Spacek and Harris 1997; Toresson and Grant 2005; Dieterich and Kreutz 2016).

2.9 TRANSPORT OF SMALL MOLECULES, HAEMOSTASIS AND IMMUNE SYSTEM

Alterations in protein abundances from pathways related to transport of small molecules and haemostasis were found in the threshold of significance (p= 0.05). In line with that, the FDR associated values were far from being significant and only Reactome showed alterations in pathways related to angiogenesis. This enrichment might be produced by alterations of proteins with alternative roles depending on the cellular context. For instance, neurotrophic factors or small GTPases were associated to angiogenesis and haemostasis (Bluff et al. 2008; Walsh et al. 2019). Therefore, the identification of haemostasis herein, which was only found in Reactome pathways analysis, could be taken as a false positive-result. In contrast, alterations in the ion transport could suggest channel deficiencies matching with the reported epileptic deficits in MRD5 patients (Table I-1, Weldon et al. 2018). Furthermore, immune system alterations found in HET mice, including cascades mediated by interleukins or growth factor signalling (e.g., EGFR and growth hormone), could be related to the well-known association between epilepsy or acute neurological diseases with seizures and dysfunction of genes related to the immune system (Lascano, Korff, and Picard 2016; Wang et al. 2017).

In line with the hitherto unreported contribution of the immune system in *Syngap1* HET endophenotypes, neurons are known to express cytokines and associations of the immune system such as microglia and pruning defects in NDDs including ASD and SCZ (Ashwood, Wills, and Water 2006; Giovanoli et al. 2016; Visan 2017). Moreover, SynGAP levels in hippocampus of pubescent rats (PND35) are reduced due to early-life insults (Giovanoli et al. 2015), while an acceleration of synaptogenesis and synaptic pruning has been described in HETs (Aceti et al. 2016). Therefore, alterations of proteins related to immune pathways identified here could be linked to premature pruning events in *Syngap1*$^{+/-}$ mice.

2.10 CELL CYCLE, PROGRAMMED CELL DEATH AND GENE EXPRESSION

A role of SynGAP in programmed cell death has been already demonstrated since homozygous (HOMO) *Syngap1*$^{-/-}$ mice die during the first days of postnatal development (Kim et al. 2003; Komiyama et al. 2004; Vazquez et al. 2004), whereas no apoptosis has been detected in P1 and adult mice expressing only a half of normal SYNGAP1 amount (Knuesel et al. 2005). Hence, the level of neuronal apoptosis and the survival rates of these animals depend on the extent of SynGAP reduction. Yet, reduction of calbindin-

positive interneurons in the adult CA1/CA3 hippocampal sub-fields due to apoptosis of newly differentiating cells and a reduced integration in the DG network has been described in HET mice (Muhia et al. 2010). Considering this data, the fact that 3 pathways related to cell cycle were found enriched in Reactome pathways analysis is not surprising. However, other pathways not classified within this category could provide further information regarding the specific mechanisms whereby SynGAP regulates cell cycle and apoptosis. For instance, Ras signalling cascades could be modulators of multiple effects of neurotrophic factors, including neuronal differentiation, proliferation and survival (Muhia et al. 2010). Thus, the previously mentioned neurotrophic, Wnt and Hdg signalling pathways could also have a role in cell cycle and apoptosis in HET animals.

Synapse-to-nucleus signalling molecules in PSD samples that control gene expression were described (Jordan and Kreutz 2009), whereas altered patterns of gene expression and abnormalities in cell differentiation during cancer were also linked (Jones and Baylin 2007). Accordingly, one of the proteins up-regulated belonging to the group of cell differentiation was the tumour susceptibility gene 101 (Tsq101). The alteration of this protein matches with other GO terms found enriched in HETs, such as carcinogenesis or viral carcinogenesis. As the overactivity of the RAS pathway defines RASopathies (San Martín and Pagani 2014), abnormalities in cell differentiation, gene expression and tumorigenesis can be expected in a *Syngap1* KO animals. Nonetheless, brain carcinogenesis has not yet been reported in humans with *SYNGAP1* mutations, neither major changes in the cortical or hippocampal transcriptome have been demonstrated in *Syngap1*$^{+/-}$ neurons (unpublished data, personal communications with G. Rumbaugh and SG. Grant).

2.10 ENRICHMENT OF PROTEINS RELATED TO NDDS IN *SYNGAP1*$^{+/-}$ MICE

The study of the proteins found altered in HET mice that are associated or causative of the three main core features (ID, epilepsy and ASD) of the *SYNGAP1* LOF syndrome (Parker et al. 2015) along with the association of certain *SYNGAP1* variants with SCZ (Guo et al. 2009; Aceti et al. 2015), could help understand the neurobiology of MRD5 and the other NDDs.

Equivalent to the impairments reported herein, previous genetics studies have described multiple high-risk genes for autism that play roles in synaptic connectivity and function, dendritic and axonal growth, trafficking, transcription and translation among others (Gilbert and Man 2017). Accordingly, a similar proportion of genes related to ASD, ID, epilepsy and SZC genes were found significantly enriched among PSD proteins dysregulated in

HET mice. In addition, high numbers of ID pathways and proteins interacting with gene products altered in ID were also identified using the ID database from University of Denver (Colorado, USA). Noteworthy, genes related to neurodevelopment-associated epilepsy were only found enriched in HET mice, matching with what is known about MRD5 and *Syngap1*$^{+/-}$ models (See Table I-1; Weldon et al. 2018; Kilinc et al. 2018).

Interestingly, the proportion of altered epilepsy genes was even higher than that of ID genes in HET mice. The fact that *SYNGAP1* was found classified in the epilepsy-related genes category but not in the neurodevelopment-associated epilepsy genes seems inconsistent. However, developmental and epileptic encephalopathy has recently been associated with a cohort of 57 *SYNGAP1* patients presenting mild (8%) to severe (88%) ID with a mean of 2 years of onset (Vlaskamp et al. 2019), whereas other affected individuals express epilepsy or seizures with a late onset (personal communication with parents of affected children in Spain). In support of the reliability of these classifications, HET mice did not show a significant enrichment of potential-epilepsy associated genes.

Finally, it is worth also mentioning that functional enrichment analyses conducted with PSD and non-PSD Kalirin, Agap2 and SynGAP interactomes, showed that all these GEF and GAPs complexes are similar and significantly enriched in ASD and ID associated gene products, whereas only PSD Agap2 and both PSD and non-PSD SynGAP interactomes were significantly enriched in SCZ risk factors (Wilkinson et al. 2017). Collectively, all these data illustrate the crucial role of PSD, small GTPases and SynGAP leading to ID, ASD, SCZ and epilepsy when are abnormally expressed.

3. RESCUE OF THE PSD PROTEOME IN PND21 *SYNGAP1*$^{+/-}$

Although historically NDDs such as ID and ASD were considered to be caused by irreversible changes during development, today it has been demonstrated the reversibility of a wide array of NDDs endophenotypes by pharmacological or genetic rescue in adulthood (San Martín and Pagani 2014; Sztainberg and Zoghbi 2016). Some examples are found in Down syndrome (Fernandez et al. 2007); Fragile X syndrome (FXS; Dölen et al. 2007; Meredith 2015); MECP2 duplication syndrome (MDS; Sztainberg et al. 2015); Tuberous Sclerosis Complex (TSC; Ehninger et al. 2008; Santini and Klann 2014); Angelman syndrome (Meng et al. 2015); Rett syndrome model (Mecp2; Weng et al. 2011; Zoghbi and Bear 2012); *Shank3* KO model of Phelan-McDermid syndrome (Monteiro and Feng 2017) and a drosophila model of Kleefstra syndrome (EHMT; Kramer et al. 2011; van Bokhoven 2011). However, corresponding with a neurodevelopmental component, in most of the cases some cognitive deficits remained.

Consistent with this partial rescue, adult *Shank3*$^{-/-}$ conditional KO mice after its genetic rescue continued to display hypoactivity, avoided risk, and had abnormal motor coordination and exploratory behaviour. In contrast, *Shank3*$^{-/-}$ reactivation in young mice (PND20–21) led to even more behavioural improvements while a germline rescue restored all behavioural phenotypes (Mei et al. 2016). Also, in a Rett syndrome model, a genetic reversal induced at PND14-21 significantly prolonged the lifespan of mutant animals and delayed the onset of neurologic symptoms (Giacometti et al. 2007). Another example is found in the early pharmacological rescue performed in a Fragile X syndrome model, as Fmr1$^{-/y}$ KO mouse pups (PND0) was more efficient in correcting spine morphology abnormalities than in juvenile mice (PND42; Su et al.2011). Bearing in mind the convergence of hippocampal phenotype in Fmr1$^{-/y}$ and *Syngap1*$^{+/-}$ mice (Barnes et al. 2015), the genetic rescue at PND21 of *Syngap1*$^{+/-}$ resulted in a restoration of ~83% of the alterations detected in HET mice. In other words, abundances of 43 proteins altered in HET animals remained abnormally expressed after recovering normal SynGAP levels at the PSD. Thus, this result recapitulates at the molecular level what had been shown for the spine phenotype in Fmr1$^{-/y}$ KO mice.

Noteworthy, a total of 162 proteins with abnormal expression levels were identified in RES mice. Thus, in addition of the un-rescued proteins, 119 were found altered in these animals but not in HETs. Of this group, 29 resulted altered collaterally to SynGAP rescue at PND21, since their expression in RES was found significantly different when compared with both HETs and WTs. Finally, from the remaining 90 proteins, approximately half of them were

close to be classified in the confident group of altered proteins because of the SynGAP rescue at PND21 and the other half followed a trend that would match with the confident group of un-rescued proteins.

3.1 RESCUED PROTEINS AND PATHWAYS

Enrichment analyses conducted with HET/WT and HET/RES altered proteins retrieved a similar number of GO terms for BPs and pathways when different bioinformatic resources were used: FunRich (9 *vs.* 6), Reactome (97 *vs.* 105), STRING (20 *vs.* 15 in up-regulated proteins and 30 *vs.* 47 in down-regulated), KEGG (8 *vs.* 9) and David (50 *vs.* 51). In addition, the overlap in altered GO terms and pathways between HET/WT and HET/RES was above 50% and interactome analyses showed similar subnetworks, which were not found in the RES/WT comparison. Indeed, only few terms were found altered in RES mice. Namely, 2 GO terms for Biological Processes were found altered using FunRich or STRING, and 20 using DAVID. Analyses through Reactome retrieved 15 statistically enriched pathways. Moreover, the degree of interaction between altered proteins of HET *vs.* WT and HET *vs.* RES was found similar, as the first presented an average number of connections per node of ~4 and the later of ~3. This result contrasts with the lower number of interactions per node (~1) found in the RES/WT comparison. Hence, data from down-stream analyses paralleled what was found when comparing numbers of altered proteins between genotypes. Consequently, all these data agree with a significant recovery of the altered proteome and pathways associated.

The comparison of Reactome pathways found enriched in HET/WT and HET/RES but not in RES/WT showed all pathways previously described in HET mice, excluding transport of small molecules and pathways were taken as false positives (e.g., haemostasis). In addition, other downstream analyses, including KEGG pathways and DAVID GO enrichment studies, performed using confident groups of up- and down-regulated rescued proteins (i.e., 52 and 56 proteins, respectively), demonstrated again that BPs related to cytoskeleton, neurotransmission, development, synaptic plasticity, translation, small GTPases mediating signalling, vesicular-traffic processes mediated by SNARE complex and energy production associated to mitochondria were rescued to proper levels. Of note, proteins related to negative regulation of the Erk1/2 cascade were classified in the up-regulated group of rescued proteins, which agrees with an overactivity of Ras signalling due to the lack of SynGAP and a possible compensatory increase of other negative regulators than SynGAP. Also, some Reactome pathways that were significantly enriched when considering the FDR p-value, included p38MAK events or Rho GTPases effectors. Thus, these results match with adult rescue of hippocampal plasticity in terms of LTP and

Erk signalling defects assessed using the same HET mice (Ozkan et al. 2014) and with the recovery of normal translation rates found abnormal in CA1 HIP pyramidal neurons from other conventional *Syngap*$^{+/-}$ mice when treated with drugs (Barnes et al. 12015). Namely, lovastatin and U0126, which selectively target and downregulate mGlu5 receptors and Ras-Erk1/2 signalling, respectively, rescued normal basal protein synthesis in these mice by downregulating ERK1/2 activity (Barnes et al. 2015).

Noteworthy, from those proteins found altered only in the HET/RES comparison a subset represents proteins that potentially could be rescued as were found in the limit of significance in HET/WT comparisons. Similarly, other proteins related to neuronal system, signal transduction and metabolism pathways were likely to be also rescued since were found close to the limit of statistical significance to be classified as confidently rescued proteins.

3.2 UN-RESCUED PROTEINS AND PATHWAYS

The identification of un-rescued proteins might help designing complementary therapies to overcome the limitations of genetic rescue strategies or other therapies such as inhibition of the Erk pathway (Kopanitsa et al. 2018). Up to 43 proteins were identified as un-rescued while some of the 90 proteins that were only altered in RES/WT can be found in the limit of classification as un-rescued as noted before. That is, when the FCs from HET/WT matched with RES/WT ones but did not reach statistical significance in HET/WTs. Analyses of GO term enrichment and KEGG pathways from the confident groups of up- and down-regulated un-rescued proteins only returned data for the latter, which showed defects in the unfolded protein binding pathway, whereas when considered all confident un-rescued proteins the enriched BP term was ‘protein processing in ER’. Also, network comparison between HET/WT and RES/WT interactomes identified that out of the 43 un-rescued proteins only 15 were interconnected, reducing the support for confidently un-rescued proteins. Yet, the GO enrichment analyses for BPs conducted with these 15 proteins showed again the association of these proteins with processing in ER events. This observation matched with alterations in the ubiquitin ligase complex and the unfolded protein binding pathways previously mentioned. Also, it is worth noting that some residual alterations in the expression of mitochondrial but not ribosomal proteins were found within the group of un-rescued proteins connected with at least one node in each HET/WT and RES/WT interactomes.

Finally, proteins close to be classified as un-rescued proteins and thus, found only altered in RES/WT could provide further information regarding the irreversible molecular defects.

When considered up- and down-regulated RES/WT proteins, only two pathways were found altered: 'ferric ion transport' and 'cellular component organization regulation'. Moreover, Reactome pathways related to chromatin organization and transport of small molecules were found enriched when considered all proteins in RES/WT comparison. Accordingly, GO term for Biological Pathways: 'gene silencing' and 'nucleosome assembly' were found significantly enriched through FunRich. Nevertheless, bearing in mind that PSD samples were examined, differences in proteins like histones that are associated to gene functioning and regulation, could arise from a combination of contaminations during the removing of DNA during the first centrifugation step of the PSD preparation protocol (Fig. M-3). Alternatively, these possible changes in gene activity could be concomitant to the genetic rescue at PND21 as further discussed below.

3.3 PROTEINS COLLATERALLY ALTERED DUE TO SYNGAP RE-EXPRESSION AT PND21

Those 162 proteins that were found altered in RES/WT and HET/RES encompassed a group of proteins specifically altered because of the genetic rescue (29). Also, a subset of proteins among the 90 unique proteins altered in RES/WT and not in the other genetic comparisons could be added to these group of 29 confident proteins altered collaterally to the rescued expression of *Syngap1*$^{+/-}$. The main Reactome pathways mediated by these 29 proteins that were equally expressed in WT and HETs but altered in RES mice are likely relate to proteostasis (e.g., Lamtor1, Rps25 or Ube2v1); endocytosis and other vesicle-mediated processes (e.g., Dctn1, Stx7 or Wdr91) as well as mitophagy.

When considered all 119 proteins from RES/WT regardless the fact that some of them were potentially un-rescued proteins, pathways enriched were related to the immune system, being of interest PI3K/Akt mediated signalling. Also, as previously noted, GO term BPs related to transport of small molecules and protein ubiquitination were found enriched. These pathways matched with other enriched GO terms related to endocytosis and vesicle-mediated processes seen before, as the 29 confident altered proteins due to the genetic rescue were included in this analysis. In support of alterations in these pathways concomitant to *Syngap1*$^{+/-}$ reactivation at PND21, IND mice, whose floxed *Syngap1* allele was subjected to genetic modifications at the same age, showed also alterations in ubiquitin-dependent catabolic and transport of small molecules processes. Collectively, these results were consistent with a possible reorganization of the proteome by the recovery of normal levels of SynGAP at the PSD, the slot model hypothesis (Opazo, Sainlos, and Choquet 2012; Walkup et al. 2016) and the role of SynGAP as a scaffolding protein (Sheng and Kim 2011).

Finally, subsets of proteins that were found altered only in HET/RES could also be potentially classified as collaterally altered due to SynGAP$^{+/-}$ rescue at PND21, as a confident rescued protein or as a contaminant protein that gave random alterations. Therefore, it is likely that cell-cell communication or mitophagy pathways found enriched only in HET/RES comparison arose from proteins that could be close to be classified as rescued while terms like platelet activation, signalling and aggregation pathways were perhaps found altered as a consequence of the *Syngap1*$^{+/-}$ genetic reactivation at PND21, due to impurities in the PSD samples or because of proteins with different roles in other regions than synapses.

3.4 ENRICHMENT OF PROTEINS RELATED TO NDDS FOUND ALTERED IN *SYNGAP1*$^{+/-}$ RESCUED MICE

Based on the spine dysfunction theory of cognitive disorders, ID and ASD outcomes could converge to common molecular substrates (Penzes et al. 2011). Yet, each NDD shows distinctive features, thus specific cognitive and behavioural defects could be dissociated. Therefore, as the number of ID and epileptic genes were not found significantly enriched in RES mice concomitant to a reduced number of pathways and proteins interacting with ID proteins, these findings agree with an attenuation of ID and epilepsy. Yet, proteins altered in RES mice were significantly enriched in ASD- and SZC-associated gene products, which could indicate that some ASD and SCZ endophenotypes might remain affected even after genetic rescue of *SYNGAP1*. Accordingly, when *Syngap1*$^{+/-}$ was reactivated at PND21 using the same conditional KO mice for genetic rescue studies used in this chapter and some behavioural paradigms were tested, HET mice exhibited irreversibility of anxiety and risk-taking behaviours, a partial rescue of brain dysfunctions (e.g., the performance in the open arena field test) and complete rescue of some forms of long-term memory such as contextual memory (Aceti et a. 2015). It is likely that these reported and predicted herein remaining traits arise due to a lack of SynGAP during the 3 weeks of development, coincident with the critical period of synapse formation (Clement et al. 2012) or due to alterations at other levels such as permanent abnormalities at the brain circuit level. Hence, to make progress on MRD5 treatment it is necessary to investigate how these un-rescued or partially rescued endophenotypes could be reversed or, at least, ameliorated. For instance, an evaluation of the rescue ability of PSD proteome and cognitive deficiencies when mice are rescued at PND14 instead of PND21 would be desirable.

4. PSD ABNORMALITIES AFTER *SYNGAP1*$^{+/-}$ KO INDUCTION IN PND21 MICE

The reduced levels of SynGAP from PND21 onwards altered the expression of 251 out of 2,583 PSD proteins. Despite being the same number of proteins altered in the embryonic haploinsufficient mice, there was only an overlap of 6,8% between these two protein sets. In addition, a lower number of significantly enriched GO terms and pathways was generally identified when comparing those obtained from IND and HET mice. Namely, FunRich (2 vs. 6), Reactome (30 vs. 97), DAVID (21 vs. 50) and KEGG (1 vs. 8). These analyses showed a significant number of proteins but fewer pathways related to: glutamatergic and GABAergic neurotransmission, protein trafficking, cell-cell adhesion, synaptic signalling including small GTPases, neurotrophin, Wnt/β-catenin and interleukin cascades, energy production, metabolism of RNA through regulation of its stability, events related to proteostasis (e.g., translation), apoptosis and neurogenesis. Consistent with these findings, certain hippocampal GABAergic interneurons showed higher apoptotic rates in adult *Syngap1*$^{+/-}$ mice (Muhia et al. 2010), which could be linked to alterations in Wnt signalling, since Wnt is involved in cell fate specification and adult hippocampal neurogenesis (Codocedo, Montecinos-Oliva, and Inestrosa 2015). Also, several of these pathways that were found altered in IND mice have been associated to several diseases including autism, SCZ and Alzheimer (Muro et al. 2015). Trafficking and expression of AMPARs subunits to the membrane bound to the PSD are altered in adult-specific hippocampal *Syngap1*$^{+/-}$ KO induced mice (Muhia et al. 2012), while a link between small GTPases and protein-ubiquitination pathways have also been reported (Lee et al 2011).

Of note, this study also showed possible alterations in IND animals that were not shared with HET mice, including dysregulation of the adenylate cyclase activating pathway, alterations of proteins with phosphatase activity, ubiquitin-catabolic processes, Rabs lipidation, GABA related processes through Gabrg2 channel, as well as hippocampal mossy fiber-CA3 (MF-CA3) and the Schaffer collateral-CA1 (SC-CA1) synapses. Accordingly, when *Syngap1*$^{+/-}$ haploinsufficiency was induced in adulthood using the same mouse line as in the present study, minimal impact in spine synapses but intrinsic excitability of dentate gyrus neurons has been reported. In contrast, conventional KO and neonatal induced haploinsufficient *Syngap1*$^{+/-}$ KO mice present alterations in all these phenotypes (Clement et al. 2012). Altogether, these data suggest that there are critical periods of SynGAP development encompassing PND21-young adulthood that could be disrupted by *Syngap1* KO induction at PND21 and thus, are independent of the previous developmental stages.

4.1 ALTERATIONS IN MF-CA3 AND SC-CA1 SYNAPSES

The hippocampal formation consists of three types of principal neurons which form the so-called trisynaptic circuit: granule cells in the dentate gyrus connect to CA3 pyramidal cells through mossy fibers, which in turn synapse with CA1 pyramidal neurons through Schaffer collaterals (Bischofberger et al. 2006). Interestingly, there are reports linking these particular types of synapses in Hebbian and non-Hebbian forms of synaptic plasticity (Gruart, Muñoz, and Delgado-García 2006; Deeg 2009; Berberich et al. 2017). Consistent with the crucial role of SynGAP in these two types of synaptic plasticity, GO enrichment analyses using FundRich showed a significant number of altered proteins belonging to SC-CA1 synapses in both HET and IND mice, whereas a significant number of proteins from MF-CA3 synapses were found only enriched in IND/WT mice. Hence, these data suggest impairments in the trysinaptic circuit of hippocampus mainly due to dysfunction of pyramidal neurons as others have already demonstrated (Ozkan et al. 2014).

4.2 DEFECTS IN SYNAPTIC FUNCTIONAL PLASTICITY

GO term BP enrichment analyses of up- and down-regulated proteins using STRING showed that the terms ‘regulation of protein phosphatase activity’ and ‘dephosphorylation’ were significantly enriched in IND/WT mice. Accordingly, an in-depth analysis of proteins with phosphatase activity found altered in HET and IND mice using AmiGO database, also showed that a significant high number of phosphatases were found exclusively abnormally expressed at the PSD of IND mice. In addition, both analyses suggest that the number of up- and down-regulated phosphatases were roughly the same (i.e., 8 *vs.* 7). These data indicated that the PND21 reduction of SynGAP at the PSD promotes changes in the activity of its proteome. Therefore, the impairments in the PSD from IND mice might arise not only due to an abundance defect of its proteome but also by an enzymatic activity dysregulation. Analyses on the phospho-proteome with these animals could benefit from understanding the *Syngap1* physiopathology.

Despite the term ‘small GTPases’ was not found significantly enriched as in HETs, terms related to protein domains of Rab or Rab small GTPases PTMs were identified by at least two different databases. Interestingly, depending on the time of *Syngap1*$^{+/-}$ haploinsufficiency induction, different small GTPases (e.g., H/KRas *vs.* RRas2 or RhoA/G vs. Rac1) from a given family were altered. Indeed, an in-depth analysis of the small GTPases and their regulators indicated that 2 out of 5 altered Rabs in IND mice belong to the Rab3 subclass, which were specific to presynaptic compartments (Binotti, Jahn, and Chua 2016). The up-regulation of these presynaptic Rabs could be linked with a higher excitatory neurotransmission as the only small GTPase from the Ras family found altered

in IND mice (RRas2) was found up-regulated. In turn, the expected overexcitability might be balanced by an increased GABAergic neurotransmission through Gabrg2. Moreover, the increased expression of Rab3 and the other up-regulated Rabs seemed to mirror alterations in processes related to exocytosis and vesicle mediated trafficking as these were terms and proteins (e.g., the GDI Sh3bp4) found only altered in IND and RES mice compared to their controls. Thus, it is possible that events related to vesicle mediate processes and protein trafficking are especially sensible to abnormal SynGAP levels from PND21 to PND56 at the PSD.

4.2.1 LONG-TERM POTENTIATION EXPRESSION IN *SYNGAP1*$^{+/-}$ INDUCED KO MICE

Concomitantly to a reduced number of proteins, GO terms and pathways that were enriched in IND mice, interactome analysis also showed that the abnormally expressed proteins had a low degree of interaction. Specifically, ~2 edges per node were found agreeing with a reduced number of likely direct SynGAP interactors (4), as reported in STRING. Again, these results contrasted with a higher number of interactions and SynGAP interactors identified in the embryonic *Syngap1*$^{+/-}$ (4 edges per node and 7 likely direct interactors). In support of these notions, LTP induction and maintenance through electrophysiology recordings in IND adult mice (>PND60) showed no impairments, whereas the *Syngap1*$^{+/-}$ conventional mice had defects in LTP expression and maintenance, as previously demonstrated by others (Komiyama et al. 2002; Kim et al. 2003; Kopanitsa et al. 2018). Thus, these data agree with less altered levels of small GTPases found in IND compared to HET mice.

Still, it is striking not to find an LTP impairment in IND mice, as this is found completely recovered by adult rescue of SynGAP levels (Ozkan et al. 2014), together with Ras and Erk activity. Consequently, this finding suggests a correlation of signalling pathways linked to LTP and the levels of SynGAP independent of its levels in development. In agreement with that, induction of *Syngap1* heterozygosity in adult hippocampus results in an impairment of several features related to reversal learning and spatial memory-dependent processes (Muhia et al. 2012). Therefore, the lack of LTP impairments in IND mice after 4 weeks could be due to the fact that certain forms of synaptic plasticity, including LTP, could be maintained for many months to years (Bliss et al. 2003).

The molecular basis of this lasting LTP may related to proteins with a low turnover rate, the so-called long-live proteins, which show half-lives of several weeks, months or longer in mice (Gonzalez-Lozano et al. 2016; Heo et al. 2018). As an example, HRas is a long-lived protein that was found not altered in IND mice. To discard a possible masking effect

of LTP impairments in IND animals due to long-lived proteins, the number of identified long-lived proteins reported in Heo et al. were computed. While ~78% of them were identified, only ~13% showed abnormal expression with approximately half of them being down-regulated. As a result, it can not be discarded the possibility that the lack of LTP impairments arose from a long-lasting effect of SynGAP stability and specially of long-lived proteins. Thus, future experiments should be addressed to perform the same assessments in IND mice but after longer periods (i.e., more than 4 weeks).

Finally, it is worth mentioning that the only Ras small GTPase found altered in IND was RRas2, which indeed was expressed ~1,3 times more than in that of WT counterparts. Presumably, this result is inconsistent with HET-related data as all Ras proteins were found down-regulated. However, UniProt describes that RRas2 might exerts its effect through an effector shared with the Ras proteins but in an antagonistic fashion. In addition, RRas2 also might transduce growth inhibitory signals across the cell membrane matching with alterations in EphRs (i.e., Ephb1 and Ephb6) expression. Hence, this opposite effect of Ras protein subtypes could explain these differential expressions among these Ras members in both *Syngap1*$^{+/-}$ conditional KO mice lines used in the present study.

4.3 DEFECTS IN SYNAPTIC STRUCTURAL PLASTICITY

Like HET mice, the term related to translation was significantly enriched based on GO term enrichment analyses in IND mice. When significant enriched terms unique to up- and down-regulated proteins were evaluated, also the term ‘translation’ was found significantly enriched in down-regulated proteins, in agreement with a more discrete number of ribosome constituents found dysregulated (5 in front of ~18 identified in HET comparisons). Again, an in-depth analysis of proteins annotated under the translation term revealed that negative regulators of translation (e.g., Fmr1, DDx3x or Rpl13a) were found down-regulated while only one protein (Elavl1) clearly associated with an enhancement of protein synthesis was also found up-regulated. Despite the net effect in the translation rates cannot be interpreted based on this data, these findings support again a clear disturbance in proteins required for translation in IND mice. Furthermore, it is tentative to speculate that in IND mice basal protein synthesis might be also up-regulated as in HET mice from the present study and other previously referred ones (see 2.5). In support of that, the higher number of proteins found up-regulated than down-regulated also support an increased translation in these mice. Again, the reduction of ribosomal subunits could be attributed to a compensatory mechanism in IND mice, as described for HET animals.

Interestingly, *Syngap1*$^{+/-}$ mice showed a developmental down-regulation of FMRP expression in hippocampal lysates during PND21-23 but not at earlier or later ages, which is hypothesized to compensate the required peak expression of SynGAP levels at PND21 (results from chapter I; Paul et al. 2018). Of note, FMRP, which represses *Syngap1* translation (Barnes et al. 2015), was found down-regulated in PND56 IND mice but not in PND56 HETs from the present study. Conversely, in RES mice other regulators of mRNA translation (e.g., Fxr1 or Eif4g2) were found altered while there was a non-significant tendency of FMRP expression to be increased due to *Syngap1*$^{+/-}$ genetic rescue. As happens for LTP, is possible that the alterations related to translation in IND mice last longer than in RES mice and thus, account for non-significant up-regulation of FMRP expression reported in the latter group of mice. Altogether, these data support the idea that the induction of *Syngap1*$^{+/-}$ haploinsufficiency in mice at PND21 may promote the reduction of FMRP expression to compensate for the lack of SynGAP while in RES mice, FMRP would be up-regulated to reduce overlay increased translation of *Syngap1* mRNA.

In addition to a dysregulated protein synthesis, proteins related to the proteasome and ATP production through mitochondria were found abnormally expressed in IND mice. In fact, more proteins related to the ubiquitin-dependent protein catabolic process and lysosome transport have been found up-regulated than in HET mice, while RES mice present also alterations in protein degradation via proteasome. Also, in line with these expected structural alterations, the unique Rho Small GTPase found altered in IND mice was Rac1. The down-regulation of Rac1 expression may account for abnormalities seen in the expression of the hub Rho/Rac effector Citron, 20 ABPs and 14 additional cytoskeletal binding proteins to ultimately promote alterations in structural synaptic plasticity of these mice. In summary, because PSD proteome remodelling is sustained by increased rates of translation, protein degradation and energy supply (Louros and Osterweil 2016; Rangaraju, Lauterbach, and Schuman 2019), the present study agree with an alteration of PSD structural plasticity due to an aberrant proteostasis in PND21-induced *Syngap1*$^{+/-}$ KO mice.

4.4 ENRICHMENT OF PROTEINS RELATED TO NDDS IN INDUCED *SYNGAP1*$^{+/-}$ KO MICE

Gene-set enrichment analyses showed that altered proteins whose related genes were reported in the ID database from The University of Denver (Colorado) or in the SCZ database (Wu, Yao, and Luo 2017) were not significantly enriched in IND mice, as opposed to what was observed in HET mice. In line with that, the number of proteins involved in an ID pathway was also lower (4.6 vs. 6.4%). In contrast, ASD and epilepsy

related genes were found significantly enriched among the altered proteome of IND mice. Indeed, a higher percentage of altered proteins associated with ASD were identified as compared with HET mice (10 vs. 9%). Therefore, these results could be linked to different critical period for ID and SCZ (e.g., before or up to PND21), whereas the critical period of ASD and epilepsy might encompass different periods. Consistent with these suggestions, other authors reported that there is no single *Syngap1* critical period for behavioural modalities (Aceti et al. 2015) and a less damaging effect of an adult *Syngap1*$^{+/-}$ haploinsufficiency induction in cognitive and non-cognitive domains (Muhia et al. 2012; Clement et al. 2012; Ozkan et al. 2014).

Noteworthy, there was no significant enrichment in genes classified into the category of neurodevelopment-associated genes. Rather, an E/I imbalance, regardless of the age might account for the propensity in both humans as well as *Syngap1* mice models to epileptic seizures (Jeyabalan and Clement, 2016, Weldon et al., 2018; Kilinc et al. 2018). Indeed, an abnormal elevated excitation is sufficient to disrupt cognition and sociability (Yizhar et al. 2011). Thus, the E/I imbalance causing epilepsy and associated-epilepsy proteins could favour and explain, at least in part, the comorbidity with the ASD phenotype and for extension, the multimorbidity with these two endophenotypes and possible “mild” ID defects predicted in IND mice.

Taken all these data together, the damaging defects of a reduction of SynGAP at PND21 could be less damaging than embryonic haploinsufficiency but might promote more deleterious effects than induction at later, adulthood developmental stages.

5. ASSESSMENT OF THE SLOT MODEL HYPOTHESIS

SynGAP-α1, which has a PBM known to bind PDZ domains from MAGUKs including SAP102 and PSD-95, is mainly located to the PSD (PDZbase, Kim et al. 1998; results from chapter I). Thus, given the high amount of SynGAP and PSD-95 molecules found at the PSD, it was proposed that the alterations of its composition in *Syngap1*$^{+/-}$ mice might arise from reduced binding competition of SynGAP-α1 to PDZ domains from PSD-95 (Walkup et al. 2016).

The comparison of the expression levels of these proteins that validate the model by IB and the present LC-MS/MS data indicated that the vast majority of the compared proteins followed the same expression pattern. Yet, abundance differences for LRRTM2 or other members of the same belonging family were not found. This disagreement could be due to the fact that they used PSD forebrain extracts and not hippocampal ones used here. Alternatively, the use of different *Syngap1*$^{+/-}$ mouse lines might explain these slight differences. Also, in the case of Cacng/TARPs, only differences for 2 out of 3 of them were found in HET/RES comparisons. The fact that an antibody against all four Cacng proteins (i.e., 2, 3, 4 and 8) was used for IB analyses, with Cacng4 being not being identified in the present study, likely explains the trend seen in HET/WT and the significant enrichment found in the case of Cacng3 and 8 in HET/RES comparison. Despite these slight differences, in addition to the IB analyses of proteins such as HRas, the accordance between the results of this and the study by Walkup and co-workers further validates our data. Of note, no differences in the expression of these and the other reported proteins in IND mice were found. In summary, in light of these studies, the expression of TARPs and Neuroligins but not LRRTMs corroborates the slot model hypothesis in HET mice but not in IND mice.

Interestingly, as more than 2,000 proteins were identified in this study, it was possible to conduct a reassessment of this hypothesis considering other proteins with a PBM in HET mice. Of the 51 proteins identified with a PBM by AmiGO (GO term ‘PDZ domain binding’), only 9 had altered expression. Of these, 6 were up-regulated in HET/WT or HET/RES comparisons. In addition, 4 of them were classified within the confident group of rescued proteins and of these, 75% followed the expected increased expression at the PSD due to “free” slots. HET mice present a ratio of up- to down-regulated proteins of 1:2 while the number of up-regulated proteins with a PBM was 2:1, thus the overall ratio of up- to down-regulated proteins appeared to be inverted in HETs. Strikingly, in IND mice this contrast was not seen. Namely, only 2 out of 6 proteins with a PBM were found up-regulated.

Not all proteins with a PBM necessarily bind PSD-95. Thus, to further validate the slot model hypothesis, a list of PSD proteins that were also components of the PSD-95 complex and have a PBM among altered proteins was prepared. On this occasion, a manual search was conducted and added to PBM annotations from AmiGO. This returned a total of 16 proteins (excluding SynGAP1-α1) from the PSD-95 complex with a PBM that were found altered, with 10 (~63%) being up-regulated. Therefore, these results would support, at least in part, the slot model hypothesis. On the other hand, after rescuing SynGAP expression, only 4 proteins from PSD-95 interactome and with a PBM were altered. This difference found between HET and RES mice in the number of altered proteins with a PBM, further supports the slot model. Finally, among the altered proteins found in the PSD-95 interactome from IND mice, 12 had a PBM, of which 7 (58%) were found up-regulated and thus, this would also be supportive of the slot model. However, the present model would not be valid for all proteins. Indeed, recent reports reject the classic model of NMDAR-MAGUK assembly mediated by PDZ domain slots (Frank and Grant, 2017).

Alternatively, those proteins that did not behave as predicted by the model might have preferred partners other than PSD-95 or were indeed not direct PSD-95 interactors despite having a PBM. To illustrate this idea, the interaction between PSD-95 and GAP junction α-1 protein (Gja1) is unlikely since Gja1, despite being down-regulated and harbouring a PBM, is expressed in electrical synapses, where the presence of PSD-95 was not been reported. On the other hand, the regulator of AMPAR activity Shisa9 was found up-regulated and, by similarity with Shisa6, it could interact with PSD-95 through its PBM (Karataeva et al. 2014; Klaassen et al. 2016). Therefore, the present data validates and extends the applicability of the slot model to other proteins such as Shisa9 or Baiap2.

The discrepancies of the slot model between HET and IND mice could arise due to the rescue approach as it is possible that it quickly recovers normal SynGAP levels while the KO induction effects requires more time to be effective as SynGAP has a medium-high stability at the PSD and the are long-lived proteins in the PSD, as previously discussed. Alternatively, a sensible period for suitable PSD composition may exist before or until ~PND21, which fits well with a high recovery expression levels of proteins with a PBM and from PSD-95 interactome in RES/WT. In favour of this hypothesis, a critical period of three postnatal weeks (PND21) where this protein plays a key role in determining the rate of dendritic spine synapse development and a need of higher levels of SynGAP in *Syngap1* heterozygous hippocampus at PND21-23 has been described (Clement et al. 2012; Aceti et al. 2016; Paul et al. 2018; results from Chapter I). Also, the formation of synaptic supramolecular complexes would be dictated by genetic rules predicating the development

timing of PSD supercomplexes formation (Frank et al. 2016, 2017). Therefore, the acute recovery of SynGAP levels could modulate the PSD composition within the critical period of synaptogenesis, whereas the reduction of SynGAP in IND animals will be effective beyond this critical period and thus, could explain the reduced supporting evidences of the slot model in these mice.

5.1 AN EXTENSION OF THE SLOT MODEL HYPOTHESIS FOR SH3 BINDING MOTIVES

The present thesis also suggested an intriguing new model of PSD composition regulation mediated by SynGAP interactions as altered proteins carrying a SH3 domain binding motif were found significantly enriched in HET mice through FunRich analysis. Since SynGAP has a SH3 domain binding motif and PSD-95 has an SH3 domain it is possible that these two proteins could interact via SH3 domain despite this interaction, to our knowledge, has not been proved. In addition, not all altered proteins from the PSD-95 complex annotated with this motif also have a PBM, thus their altered expression could be due to an interaction through the SH3 domain from PSD95. Indeed, SynGAP-α2 showed a SH3 binding motif but not a PBM in its C-term unique sequence and was also found enriched in the PSD fraction of hippocampal synapses (see results Chapter I). Therefore, the same rationale applied for PBM of SynGAP-α1 and PDZ domain from PSD-95 could be extended to the SH3 domain binding motif of SynGAP-α2 and/or all SynGAP isoforms and SH3 domains from PSD-95. Additionally, as SynGAP is a protein with a high molecular mass, the binding of SynGAP-α1 to the third PDZ domain of PSD-95, which is found in proximity with the SH3 domain, could limit the binding of SH3 domain binding motif-containing proteins with SH3 domain from PSD-95.

When the applicability of the slot model hypothesis for the SynGAP-α2 or all SynGAPs was evaluated, only 4 out of 9 proteins with an SH3 domain binding motif that were dysregulated in HETs, were found up-regulated in the PSD. Also, out of 6 proteins with a SH3 binding motif classified in the confident group, only 2 were up-regulated. In addition, those proteins containing SH3 binding motif but not the PBM, which were found up-regulated in HET mice, such as Slc1a3, Lyn or Khdrbs1 were not reported as PSD-95 interactors. Altogether, these data question the applicability of the slot model to SH3 domains of PSD-95 even if the association of SynGAP/SynGAP-α2 with PSD-95 via SH3 domain will be confirmed.

6. ROLE OF SYNGAP AS A SCAFFOLDING PROTEIN

As previously noted in the introduction, SynGAP is a protein with a high molecular weight and expression at the PSD (Kim et al. 1998; Chen et al. 1998; Sheng and Kim, 2011), thus a role as scaffold has been postulated for SynGAP. Accordingly, FunRich analyses showed a significant enrichment of the term 'scaffold protein binding' in the HET/RES altered proteome. Therefore, the study of the role of SynGAP as a scaffold for PSD proteins could provide further knowledge about the neurobiology of SynGAP and the mechanisms by which the PSD composition is determined.

First, the number of proteins from a custom-made SynGAP interactome was elaborated to further increase the number of interactions reported by the STRING database. These analyses showed that up to 26 proteins from this SynGAP interactome were significantly altered when HET/WT and HET/RES comparisons were taken together. From these 26 proteins, ~65% (17) are down-regulated in HETs while in IND mice, ~42% (5) of 11 proteins were found significantly down-regulated. Hence, these results agree with a loss of proteins due to the loss of SynGAP as scaffold.

In line with that, from the down-regulated proteins found in HETs, 1/3 were found interacting with at least 3 proteins that were also down-regulated (e.g., Kalirin), leading to an increased number of proteins that interact directly or indirectly to SynGAP and thus, form complexes that could be subjected to be depleted from the PSD. As an example, protein domain enrichment through InterPro and interactome analyses have shown that members of the family of 14-3-3 proteins (i.e., Ywhab, Ywhag and Ywhaz) were forming a complex with SynGAP that was significantly down-regulated. This hypothesis would be supported by the liquid-liquid phase transition model as states that part of the organization of PSD mega-assemblies is driven by the SynGAP/PSD-95 complex and its associated proteins, which is concentration-dependent of SynGAP/PSD-95 components (Zeng et al. 2016). Also, the view of a multifarious soup of proteins forming the PSD, has been replaced by a model in which complexes, supercomplexes and nanodomains are building blocks of the synapse (Frank and Grant, 2017). Therefore, it is possible that the half expression of SynGAP at the PSD, reduces the ability to cluster and hold proteins that normally were targeted together to the PSD.

Whether the absence of SynGAP and thus, its role as scaffolding, might be then accomplished by other adaptor proteins as a compensatory mechanism were also explored. The analysis of the adaptor proteins annotated by AmiGO showed that two of them, Khdrbs1 and Baiap2, were significantly up-regulated by more than 1.5 FC in HET

mice and then returned to normal levels in RES mice. Furthermore, Khdrbs1 has an SH3 domain binding motif that is likely to mediate the interaction with the SH3 domains of the hub non-receptor tyrosine kinases Fyn and Lyn, as suggested by network studies of up-regulated proteins in HET/WT and HET/RES. In addition, despite NHERF1/EBP50 protein (Slc9a3r1) was not found annotated as an adaptor or scaffold protein in AmiGO database, a scaffolding role has been described for this protein (Vaquero et al. 2017), which is also significantly up-regulated. Finally, CAMKIIs have been suggested to accomplish an scaffold role due to its high abundance at the PSD, like SynGAP (Sheng and Kim 2011). Accordingly, CAMKII-δ was found in the group of confident rescued up-regulated proteins. Yet, in IND mice there were no significant changes in the expression of any of these adaptor proteins matching with the previous suggested critical period for PSD composition.

Collectively, these data suggest that other scaffolding proteins expressed in the PSD of HET mice with similar properties as SynGAP (e.g., an adaptor activity and presence of a SH3 binding motif) may take over of the SynGAP role as a scaffold in a developmentally regulated fashion and could explain the significant enrichment of proteins annotated with the term ‘SH3 domain binding’ in HET mice.

CONCLUSIONS

1. *In-silico* studies have revealed 6 previously unreported *Syngap1/*SynGAP *5'/*N- or 3'/C-term variants. Of these, three have been validated at the transcript and one at the protein level in mouse brain. Also, the expression in human cortex of the well-known α1, α2 and β-containing SynGAP isoforms has been proven.

2. Total SynGAP and its α1-, α2- and β-containing isoforms show different expression patterns in the spatial and temporal axes. Importantly, SynGAP-β and -γ could have a prominent role at early stages of brain development.

3. At PND21, just after the critical period in *Syngap1*$^{+/-}$ animals closes, SynGAP isoforms exhibit maximal variability of spatial expression compared to PND4, 11 and 56.

4. In mouse cortex without premotor/prefrontal area, total SynGAP is mainly cytosolic during the first three weeks of postnatal development, while at PND56, it is significantly more expressed at the PSD. Yet, at this age, both cortex and hippocampus, still show 1/3 of total SynGAP remaining in the cytosol.

5. In the developing cortex and adult hippocampus, SynGAP-α1 isoforms are essentially located at the PSD, while SynGAP-β ones are principally cytosolic. Isoforms bearing the α2 C-terminus show an intermediate trend in their subcellular localization.

6. The hippocampal PSD of adult *Syngap1*$^{+/-}$ mice exhibit alterations in ~10% of its proteome. Remarkably, a significant number of small GTPases as well as proteins related to ID, ASD, SCZ and epilepsy have altered expression.

7. *Syngap1*$^{+/-}$ mice exhibit major proteomic dysfunctions related to signalling pathways involved in structural and functional synaptic plasticity, translation, energy production, apoptosis and protein transport.

8. Restoring PSD protein levels of SynGAP after PND21 results in the recovery of around 83% of its altered proteome, including small GTPases and proteins involved in translation and energy production.

9. The alterations that persist or newly emerge in *Syngap1*$^{+/-}$ rescued mice are mainly associated with protein processing at the ER, transport of small molecules and proteasomal degradation. The proportion of altered proteins in rescued mice that are related to ID and epilepsy is much reduced.

10. The induction of *Syngap1*$^{+/-}$ haploinsufficiency at PND21 results in the dysregulation of a similar number of PSD proteins when compared with embryonic heterozygous *Syngap1*$^{+/-}$ mice. Yet, proteins found abnormally expressed in each KO condition are very different, indicating a developmental role in the molecular alterations observed in latter mice.

11. The most remarkable abnormalities found in *Syngap1*$^{+/-}$ induced KO mice are alterations in the amount of Rab small GTPases, phosphatases and proteins related to translation or protein turnover. Accordingly, gen set enrichment analyses show a significant number of altered proteins associated to epilepsy and ASD but not ID.

12. Based on the present analyses, the composition of the PSD is likely developmentally regulated by the slot model mechanism in conjunction with the role of SynGAP as scaffolding protein.

ANNEX

A-INTRODUCTION

Individuals with mutations in the genes encoding SHANK (also known as ProSAP) family scaffolding synaptic proteins account for ~1% of all patients with ASD (Leblond et al. 2014). Indeed, mutations in this family of genes have been linked to syndromic and idiopathic ASD as well as to other NDDs, including ID and SCZ (Monteiro and Feng 2017). Because of the strong genetic association between *SHANK3* mutations and ASD, many mice models and neurobiology studies have focused on this particular gene, whereas *SHANK2* mutations have been less reported and only two *Shank2* conventional KO mouse models have been developed up to date (Won et al. 2012; Schmeisser et al. 2012; Monteiro and Feng 2017). Despite several biochemical and phenotypic analyses have been described (Monteiro and Feng 2017), the exact molecular mechanisms underlying *Shank2* haploinsufficiency remains to be explored. Hence, the goal of this section was to establish *a Shank2*$^{+/-}$ conditional KO that would also allow genetic rescue studies. To accomplish this purpose, a gene targeting strategy to modify the *Shank2* gene in mice was designed. The engineered mutation would abolish the expression of all known *Shank2* transcripts by the introduction of a STOP cassette between exons 16 and 17. In addition, to enable the genetic rescue, these exons would be flanked by two loxP sites, one at each end, that will remove the STOP cassette upon the action of an active Cre-recombinase.

A-MATERIALS AND METHODS

1. BIOLOGICAL MATERIALS AND METHODS

1.1 MOUSE LINES

Beyond C57BL/6J mice, described in the general methods section, C57BL/6 albino mice (or B6 pure albino mice; Charles River) or FlpO$^{+/-}$ transgenic mice (CAGGs-Flpo-IRES-puro; IRB mouse mutant core facility inner colony provided by Dr. Forrow) were used to breed *Shank2* chimeric mice. *Shank2* conditional KO mice for genetic rescue studies without NeoR *cassette* (Shank2$^{+/-;NeoR-/-}$), were also crossed with Cre$^{+/-}$ transgenic mice (see general M-1.2) to obtain final *Shank2*$^{+/-;Cre+/-}$ for *in-vivo* genetic rescue studies.

1.1.1 EMBRYONIC STEM CELLS MICROINJECTION FOR CHIMERIC MICE OBTENTION

Selected positive embryonic stem cell (ESC) clones 2F6; 2H4 and 3B12 at passage 6; 4A5, 4A7 and 5E10 at passage 7; 8D7 and 9D4 (unknown passage) could have been subjected to microinjection into pure albino B6 blastocysts. Finally, microinjections were only performed with clones 5E10, 8D7 and 9D4. Then, blastocysts were transferred to a pure albino B6 foster mother. In the first round, only 4 new-born mice with low chimerism were obtained, two females and two males. Females had to be discarded for the establishment of the mouse line, thus only two males with low degree of chimerism (30 and 60%) were bred. Nevertheless, these crosses did not produce mice carrying the genetic modification in *Shank2*. For this reason, a second round of ESC transformation, expansion, validation by LR-PCR and microinjection was conducted with the same ESC clones. This second round of microinjections yielded 80-90% chimeric mice which were breed with B6 pure albino or, alternatively, FlpO transgenic mice with C57BL/6 background.

1.1.2 *SHANK2*$^{+/-}$ CONDITIONAL KO MOUSE LINE ESTABLISHMENT

The breeding of 3 chimeric mice with FlpO transgenic animals resulted in mice with 3 possible fur colours: white (when coming from pure albino blastocyst) and thus without the *Shank2* modification, agouti or black (from JM8A1.N3 ESC [strain C57BL/6N-A^{tm1Brd}; UC DAVIS KOMP repository]) with the transgenic modification. To maintain heterozygosity, targeted animals were crossed with C57BL/6 mice, and to obtain homozygous mice,

heterozygous mice were bred together. The chimerism degree from 8D7 derived mice was 90%, whereas for the other mice were < 80%. However, only mice coming from the 8D7 clone were successfully obtained based on PCR genotyping. The second mouse line (from clone 9D4) unexpectedly gave birth to white mice at generation F3-4 that matched with a WT genotype in all cases. Finally, the third mouse line (i.e., from 5E10 ESC clone) was sterile, and animals were obese from the very beginning. Consequently, only the *Shank2*$^{+/-}$ mouse line coming from the clone 8D7 were used for subsequent analyses.

1.2 BACTERIA AND VECTORS

Escherichia coli (*E. coli*) strains used were DH10B (Addgene), Stbl3, TOP10 (both from Life technologies), 294-Cre and 294-Flp (Buchholz, Angrand, and Stewart 1996) and both provided by Dr. Forrow (IRB, Barcelona).

1.2.1 PLOXPNEORFLRT PLASMID

The plasmid ploxpNeorflrt is 4,899 bp in length and carries an ampicillin resistance (AmpR), a lactose operon interrupted by a simian virus (SV) 40 promoter-poly(A) signal and a neomycin/kanamycin resistances (NeoR) driven by a PGK/EM7 promoter flanked by two Flp recombination target (FRT) sequences equally orientated as well as other sequences such as ColE1 and F1 origin. This plasmid was kindly provided by Prof. Grant (Edinburgh University).

1.2.2 PLOXSTOPLOX PLASMID

It is a 9,267 bp long vector that carries zeocin/kanamycin and puromycin (PuroR) antibiotic resistances as well as four repetitions of SV40 late poly(A) sequence. It was transformed and maintained in electrocompetent Stbl3 cells (Invitrogen, Life technologies) and purchased from Addgene.

1.2.3 PR3R4CCDB_ASISI PLASMID

The pR3R4ccdB_AsiSI has a length of 4,743 bp and has a ColeE1 replication origin, an AmpR and chloramphenicol resistance as well as some other sequences for cloning approaches. It was used to amplify AmpR by PCR. It was acquired from UC Davis KOM repositories.

1.2.4 pTARGETER PLASMID

A 4,673 bp plasmid that carried a tetracycline resistance (TetR) gene, a p15A origin and a negative diphtheria (DTA) selector cassette was used for homologous recombination strategies (as a negative selector in ESCs). pTargeter was transformed into chemically competent TOP10 cells and grown with LB and 3 µg/mL tetracycline as it is a low copy and slow replication plasmid. It is worth mentioning that pTargeter and its subsequent intermediate modified versions were unsuccessfully transformed into electrocompetent Stbl3 cells. This plasmid was kindly provided by Prof. Seth Grant (Edinburgh University).

1.2.5 PCR-BLUNT STUI DIG PLASMID

The PCR-Blunt StuI digested vector (from Zero blunt PCR cloning kit, Thermo Fisher Scientific) is a 3,519 bp plasmid which has a neomycin resistance (NeoR). This plasmid is linearized by StuI restriction enzyme. It carries a negative selector for those plasmids which wouldn't incorporate the insert and an AmpR for positive selection. It was transformed and maintained in electrocompetent TOP10 cells.

1.2.6 PRED/ET PLASMID

The pRED/ER vector is 2,682 bp long and carries a TetR gene. This plasmid expresses Red, Gam and RecA proteins required for recombination of homologous DNA sequences. pRed/ET recombination allows the engineering of DNA in *E. coli* using homologous recombination between bacteria artificial chromosomes (BACs) and episomal plasmids. It is convenient to remove it after recombination induction. This removal can be achieved when cells are grown at 37ºC. This plasmid was transformed into DH10B cells and was provided by the mouse mutant core facility (IRB, Barcelona).

1.2.7 BACTERIAL ARTIFICIAL CHROMOSOME

The *Shank2* intron 16-17 was selected for targeting. Therefore, the BAC clone carrying this sequence was bMQ87K10 (Source Bioscience, Nottingham, UK). It was maintained on *E. coli* competent DH10B cells (Invitrogen, Thermo Fisher Scientific). This BAC was 117,929 bp long, it carried a chloramphenicol resistance gene and encompassed intron 16-17 (108,696 bp) from *Shank2* (Shank-003; Ensembl database).

1.3 BACTERIAL CULTURE

The free webpage http://www.sciencegateway.org/tools/bacteria.htm was used to calculate bacterial growth rate. LB broth medium (tryptone 10g/L; yeast extract 5 g/L; NaCl10g/L; 1L H_2O; all from Sigma-Aldrich) and LB agar dishes (tryptone 10 g/L, yeast extract 5 g, NaCl 10 g, NaOH 1N 12,5 mL, agar 1.5%, H_2O 1 L) were autoclaved. In the case of LB agar plates, the required antibiotic was added before solidification. Briefly, in the first place a strike of glycerinates containing the desired cells was grown onto LB agar plates. The cells were further spread with a curved glass pipette and incubated ON at 37ºC (or their optimal temperature). Individual colonies from the LB plate were inoculated in 3 mL of LB with the appropriate antibiotic in falcons of 15 mL (VWR). Larger liquid cultures were made with 1 L Erlenmeyer flasks containing 150 mL of LB medium, incubated ON at 37ºC or 30ºC during recombineering steps. Thus, ~10-25% of the Erlenmeyer was let free so that there was enough oxygen for the culture to grow. These liquid cultures allow different plasmid DNA preparations depending on the volume (see section MIII-2.1). The usual culture conditions including final antibiotic concentrations are shown in Table MIII-1.

List of antibiotics			
Vector	T (ºC)	Antibiotic used	Final [] µg/mL
ploxPneoflrt	37	Ampicillin	50
ploxSTOPlox	37	Zeocin	20
Final ploxSTOPlox	37	Zeocin	20
		Kanamycin	25-50
pTargeter	37	Tetracyclin	3 or 5
Final pTargeter	37	Ampicillin	50
		Kanamycin	15
BAC bMQ87K10	37/30	Cloramphenicol	12.5
PCR-Blunt StuI DIG	37	Ampicillin	50
pR3R4ccdB_AsiSI	37	Ampicillin	50
pRED/ET	30	Tetracyclin	3

Table MIII-1. Antibiotic concentrations used unless specifically indicated.

1.3.1 GLYCEROL STOCKS

Selected cell colonies grown in liquid LB cultures and tested by enzymatic restriction and/or PCR were used for glycerol stocks (500 µL 80% glycerol and v:v of culture). These were stored at -80ºC until use.

1.4 TRANSFORMATION OF BACTERIA

1.4.1 INDUCTION OF ELECTROCOMPETENCY

Electrocompetent *E. coli* generally have a higher transformation efficiency than chemically competent cells (Expected > 5x 10^6 cells/µg DNA). For electrocompetency induction, a

desired colony was inoculated into 2 mL LB media with the appropriate antibiotic if required and incubated ON at the optimal temperature, usually 37ºC unless indicated otherwise. Before starting the protocol, all buffers were placed on ice. Approximately 1 mL of inoculated LB was stored for reference. Then 1 mL of inoculated LB grown ON was added into ~100-150 mL of LB plus antibiotic if required and let grow at the appropriate temperature in constant agitation at 300 rpm. The OD_{600} was measured in a spectrophotometer (Shimadzu 1240 Uvmini) every hour and at more frequent intervals as the OD_{600} became closer to the required range (0.4-0.6). Usually, after 2.5 h an OD_{600} of 0.533 was obtained. A new 500 mL cell culture flask (Corning, Thermo Fisher Scientifc) was labelled and placed on ice for subsequent steps. Then, 75 mL of double distilled H_2O (ddH_2O) was placed into clean and chilled sterile 50 mL falcons (VWR). Once the correct OD_{600} was achieved the culture was placed on ice for 15 min and was transferred to a pre-chilled Erlenmeyer flask (Corning, Thermo Fisher Scientific).

Subsequently, the cells were centrifuged in an ultra-centrifuge (IJ-25, Beckman Coulter, CA, USA) during 10 min at 4,000 rpm at 2ºC. The supernatant was discarded by placing it into a beaker with bleach or virkon (Antec Int., Sudbury, Suffolk, UK). Then, the pellets were resuspended (without pipetting or moving out the flask from the ice more than a few seconds) in a small volume of chilled ddH_2O, and when cells were completely resuspended, the appropriate final volume of ddH_2O was added. Usually, 3 mL was used. Afterwards, cells were centrifuged at 4,000 rpm during 10 min at 2ºC and the resulting pellet was resuspended as before. Two more washes were conducted, and the final pellet was resuspended in a pre-chilled 10% glycerol solution (Sigma-Aldrich; for every 100 mL of culture, 4 mL of 10% glycerol was added) using a filter tip (VWR). The mixture was centrifuged at 6,000 rpm during 10 min at 2 ºC. The newly generated pellets were resuspended with pre-chilled 10% glycerol and 50 µL aliquots were made using pre-chilled 1.5 mL tubes (Eppendorf). Noteworthy, a bore tip was used and all aliquots were quickly frozen in a -80ºC fridge. The efficiency control was conducted by Puc19 plasmid (from Dr. Forrow's lab, IRB, Barcelona) transformation into the electrocompetent cells and computed as follows:

nº colonies/ µg Puc19 DNA * µL of volume/µL plated

Ideally, 10^9-10^{10} colonies/µg of DNA transformed was expected.

1.4.2 TRANSFORMATION OF ELECTROCOMPETENT CELLS

For this purpose, cuvettes for electroporation (#Z706094-50EA 0.4cm; SIGMA) were cooled down in ice during 5-10 min while frozen cells for transformation by electroporation were also placed in ice. SOC medium (SOB medium containing 20 mM-glucose; Sigma-Aldrich) was pre-warmed at 37ºC. Cells placed into the cuvettes were gently resuspended and 1-5 µL of the ligation reaction, depending on the case, was used. More than 50% of ligation reaction mix would inhibit the electrocompetency induction. Before the addition of the cells, cuvettes were pre-cleaned to assure the correct electric current pass between the walls of the 1 mm gap. The settings of the electroporation machine (XCell Electroporator; Bio-Rad) were programmed for *E. coli* transformation at 1,750 V, 25 µF; 200 Ώ and 1 mm cuvette gap with an exponential transition program. 1 mL filter tips were prepared with 500 µL of pre-warmed SOC medium before electroporation, to quickly add SOC medium after the electroporation. Electroporated cells were removed from the cuvette and placed into a 1.5 mL tube (Eppendorf). Cells were incubated 1h at 37 ºC in a rocking platform (Stuart) with constant shake set at 500 rpm. Finally, cells were plated onto a LB agar plate with the corresponding antibiotic, if required.

1.4.3 TRANSFORMATION OF CHEMICALLY COMPETENT CELLS

Up to 50 µL of commercially available chemically competent cells (e.g., one shot TOP10) and 1 µL of the ligation reaction were placed in a 1.5 mL tube and incubated for 10 min in ice, following 45 sec at 42 ºC in a thermoblock (VWR) and 2 min in ice. Then, 0.5 mL of LB was added to the cells, which were then incubated at 37ºC during 1 h. Transformed cells were centrifuged 1 min at 13,000 rpm (5415R, Eppendorf), and pellets were spread using glass spheres in LB agar dishes with the corresponding antibiotic.

1.5 EMBRYONIC STEM CELLS TRANSFORMATION

Expanded ESCs were transformed to introduce the linearized targeting vector following the steps previously shown by bacteria transformation but with slight modifications indicated in this section. The final pTargeter vector (200 and 80 µg) was linearized using SwaI. The resulting digested fragment sizes were assessed by electrophoresis in 0.6% agarose gel and an EtOH precipitation was conducted. Specifically, the ESC JM8A1.N3 (strain C57BL/6N-A^{tm1Brd}; UC DAVIS KOMP repository) were transformed with 20 µg of linearized final pTargeter vector by electroporation to allow homologous recombination with the endogenous *Shank2* locus. The electroporation conditions for ESCs placed in 4mm cuvettes were 800V; 10 µF and infinite resistance conducted with XCell

Electroporator (Bio-rad). Then, 20 mL of warm ESC medium was used to recover cells from cuvettes. Those cells that homologously recombined the *Shank2* modification, were grown in 200 µg/mL of G418 antibiotic (Gibco) onto 10 cm plates (Nunc, Denmark) with drug resistant feeder cells (DR4 MEF feeder dishes) during 24 h after electroporation.

1.6 HOMOLOGOUS RECOMBINATION IN BACTERIA

Once the final ploxSTOPlox and the pre-final pTargeter (pTargeter+AmpR+A+B) vectors were obtained (see Fig. RIII-3). The next step was the recombination of the linearized genetic construct into the *Shank2* BAC bMQ87K10. This recombination event occurred through X and Y homology arms. Subsequently, the modified BAC was captured by a linearized pre-final pTargeter. In this case the capturing took place through the recombination between A and B homology arms. The reaction had to be carried out in *E. coli* strains specially engineered for such purpose (e.g., SW102 or SW106) or, alternatively, in cells transfected with a pRED/ET vector. The pRED/ET choice was conducted.

1.6.1 RECOMBINANT COMPETENCY INDUCTION IN BAC CONTAINING DH10B CELLS

DH10B cells containing the bM87K10 BAC were made competent for recombination by transforming them with the pRED/ET vector. To this purpose, 1 mL of DH10B cells cultured ON with chloramphenicol was diluted 1:4 times with the same medium and incubated again ON at 37ºC. The electrocompetency of DH10B cells was induced in the exponential phase of growth (2-3 h at 37ºC) when the adequate OD_{600} (~0.3) was achieved. Cells were centrifuged at 11,000 rpm (5415R, Eppendorf centrifuge) during 30 sec at 2ºC. Supernatants were discarded, and cells were resuspended in 1 mL ice-cold medium by pipetting up and down. Centrifugation and suspension steps were repeated twice. About 50-100 µL of the resulting supernatant was left in the tube with the pellet and cells were resuspended by gently flicking the tube whilst keeping it in ice. Then ~50 ng of pRED/ET vector was added and the transformation into electrocompetent induced cells was conducted as described in MIII-1.4.2, but with modifying the post-electroporation incubation to 30ºC during 70 min with constant shaking in a rocking platform. Then, cells were centrifuged at 4,000 rpm for 5 min and 50 µL of pelleted cells was spread onto LB plates with 12,5 µg/mL chloramphenicol and 3 µg/mL tetracycline and incubated ON at 30ºC to allow growth of cells containing the bMQ87K10 BAC and pRED/ET vector. These conditions allow to grow the cells without the induction of the recombineering machinery. Minipreps of BAC and pRED/ET were conducted to assure the presence of plasmid DNA.

1.6.2 INDUCTION OF RECOMBINATION IN BACTERIA

For the induction of recombination by the pRED/ET vector, cells were incubated with 10% L-arabinose (Sigma-Aldrich) for 90 min at 37ºC to activate the promoter of the genes encoding for the recombineering machinery. Those samples that had no L-arabinose constituted a negative control, since cells would not express proteins needed for recombination.

1.6.2.1 RECOMBINATION BETWEEN GENETIC LSNXY CONSTRUCT AND BAC BMQ87K10

Recombinant and competent DH10B cells were grown ON at 30ºC in LB broth with 12.5 µg/µL chloramphenicol and 3µg/µL tetracycline. The following day a new culture was started by diluting the ON culture 1:50 in two 1.5 mL tubes, being one of them a negative control of the procedure. The diluted cultures from 1.5 tubes were incubated 2.5 h at 30ºC (to achieve exponential bacterial growth phase). Then, the expression of the recombination machinery was induced by addition of 50 µL of L-arabinose (Sigma-Aldrich), in all tubes but negative controls, and incubation for 45 min at 37ºC. Then, cells were prepared for electrocompetent transformation by centrifuging 1 min at 11,000 rpms at 2ºC, resuspending the pellet in 1 mL of Milli-Q H_2O and discarding the supernatant. This was repeated three more times. The final resuspension was done with 100 µL of H_2O Milli-Q.

The genetic construct “loxSTOPNeoRlox with X and Y fragments”, also referred to as LSNXY, which is derived from the final ploxSTOPlox plasmid was precipitated in EtOH and resuspended to obtain a concentration of ~900 ng/µL as previously described (see MIII-2.2.1). The same electroporation procedure (see MIIII-1.4.2) was conducted with ~450 ng of this genetic construct. Cells recovered with 500 µL of SOC were induced for recombination (see MIII-1.6.2) to allow the substitution of this fragment in the BAC and thus, *Shank2* modification by homologous recombination induction. Next, cells were centrifuged for 1 min at 13,000 rpms and cells were plated in LB agar with 12.5 µg/µL chloramphenicol, 3 µg/µL tetracycline and 30 µg/mL kanamycin. Importantly, cells were grown at 30ºC for 48 h to allow the selection of positive clones.

1.6.2.2 CAPTURE OF SHANK2 MODIFICATION FROM BAC BY PRE-FINAL PTARGETER THROUGHOUT HOMOLOGOUS RECOMBINATION

The properly modified BAC bMQ87K10 clones that were checked by cell-PCR and conventional PCR were grown ON at 30ºC in LB broth with 12.5 µg/mL chloramphenicol, 3 µg/mL tetracycline and 30 µg/mL kanamycin permit grow of modified BAC clones only. Then, the same procedure conducted previously was carried out but with the following

modifications: ~500 ng of pre-final pTargeter (instead of the genetic construct fragment) was introduced by electroporation to capture the modification placed in the BAC. Next, the expression of the recombination machinery was induced in these cells (see MIII-1.6.2). Afterwards, these cells were plated in LB agar with 50 µg/mL ampicillin and 15 µg/mL kanamycin at 37ºC to remove the pRED/ET vector. Finally, cell-PCRs and/or PCR with GoTaq DNA polymerase as well as enzymatic restrictions were conducted again to be sure that the gene-targeting vector (final pTargeter) carried the expected genetic construct with the sequences in the proper direction and without any mutation that could compromise the functionality of the construct.

1.6.3 FUNCTIONALITY OF CRE AND FLP RECOMBINATION TARGETS

The 294-Cre and 294-Flp *E. coli* strains (see MIII-1.2) were used to test the functionalities of the recombinases Cre and Flp. In both strains, the recombinases are under the control of the lPR-promoter, which is inactive above 23ºC, so that no Flp, and little Cre recombination is observed in cultures grown at >30ºC. To accomplish this goal, up to ~200 ng of the final pTargeter vector was transformed into these cells by electroporation (MIII-1.4.2) and incubated 1.5 h at 30ºC. Then cells were spread onto LB agar plates with 50 µg/mL of ampicillin and incubated ON at 37ºC. Next, positive colonies were grown in LB broth and 50 µg/mL of ampicillin ON at 37ºC to conduct minipreps and analyse the functionality of the Flp and Cre recombinases. Therefore, since loxP as well as FRT sequences were placed in the same direction, we expected to remove all DNA flanked by loxPs or FRTs, depending on the recombinase expressed. Then the resulting recombined final pTargeters from both cell strains were analysed by restriction enzyme digestion.

1.7 EMBRYONIC STEM CELL CLONE SELECTION AND EXPANSION

The specific gene targeting experiment was conducted by the mouse mutant core facility team (IRB, Parc Científic Barcelona). Briefly, electroporated ESC were plated onto 10cm plates (Plasticware plates, Nunc) with ESC selection medium (DMEM, 15% FBS, 2 mM L-glutamine, Non-essential amino acids, 0.1 mM mercaptoethanol, 1,000 u/mL LIF and Gentamycin) plus 200 µg/mL of G418 (Fig. MIII-1). This medium was replaced every 24h. For this gene targeting experiment, more than 4x 10^7 cells were required. After 6 or more days of selection, resistant colonies should appear, and 48 colonies were picked. Trypsinized colonies were plated into 96-well mouse embryonic fibroblasts (MEF) feeder plates with DMEM, 10% FBS, 2 mM L-glutamine and Gentamycin prepared the day before. Plates were grown until almost confluent (usually it took 2-3 days). Cells were checked

and fed every day to avoid cell overgrowth. Splits were conducted with 0.05% trypsin and using 1:1 to 1:6 ratio. The last split of the cells was conducted the day before electroporation. Once cells were transformed, resistant clones were plated onto 20 x 10 cm drug resistant MEF feeder plates and 75% of almost confluent cells were frozen and the rest used for subsequent LR-PCR analysis (Fig. MIII-1). Cells were counted using a haemocytometer. Positive colonies were expanded for further analyses, such as a second test by LR-PCR, Southern blot, karyotype and manipulations like microinjection into blastocysts.

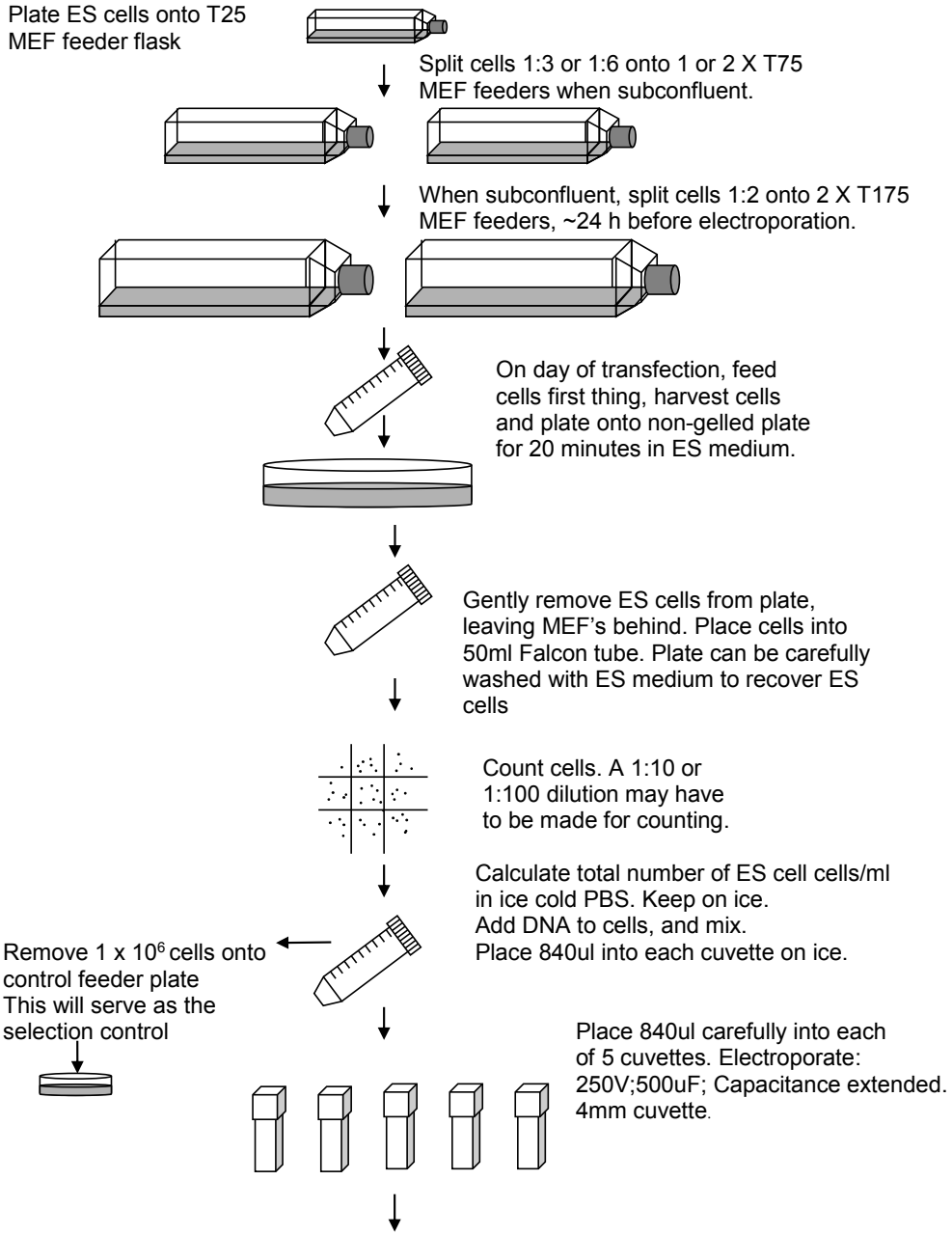

Figure MIII-1. Overview of ESC clones selection and expansion. See complete figure overleaf.

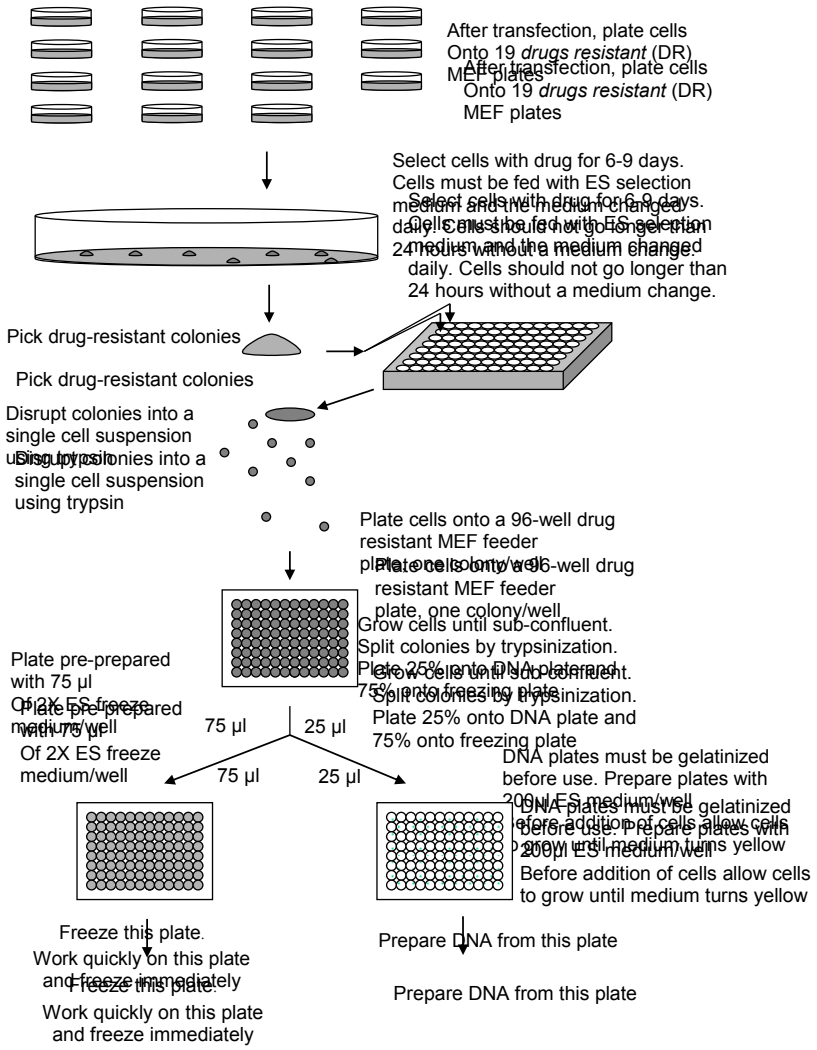

Figure MIII-1. Overview of ESC clones selection and expansion.

2. MATERIALS AND METHODS FOR GENOMIC SPECIMENS

2.1 PLASMID DNA PURIFICATION FROM BACTERIAL CULTURES

GeneJET Plasmid Miniprep Kit (Thermo Fisher Scientific) was used to assess protocol performance, such as in ligation reactions. GeneJET Plasmid Midiprep Kit (Thermo Fisher Scientific) was conducted for colonies validated from miniprep cultures and when higher amounts of DNA were needed. Maxipreps (Endotoxin-Free Maxi, Qiagen) were conducted when the modified final ploxSTOPlox, pre-final pTargeter (pTargeter+AmpR+ A+B) as well as final pTargeter vectors (See Fig. RIII-3) had to be isolated in very large amounts. In any case, a bacterial restriction and/or PCR were always conducted after DNA isolation to assure that the expected vector was purified. Plasmid DNA from minipreps was usually resuspended with 20 µL of TE solution. Whereas for midi and maxipreps 75 µL and 250 µL were used respectively. These dilutions yielded DNA at a concentration of < 10 µg/µL.

2.2 PRECIPITATION OF DNA

2.2.1 ETHANOL PRECIPITATION

Up to 50 µL of the purified DNA was mixed with 5 µL (10%) of 3M sodium acetate at pH 5.2 and 150 µL (3 volumes) of 100% EtOH. The mixture was incubated 30 min at 4 ºC and centrifuged at maximum speed. The pellet was washed with 0.5 mL of 70% EtOH and air-dried during 10 min.

2.2.2 ISOPROPANOL PRECIPITATION

DNA precipitation with isopropanol was conducted as described in general methods but with the modification: after precipitation DNA was resuspended with 75 µL of 1x TE buffer (10 mM Tris, pH 8.0 and 1 mM EDTA). DNA was then quantified with Qubit (Invitrogen Qubit 2.0 Fluorometer; Life technologies, Thermo Fisher Scientific).

2.3 ENZYMATIC RESTRICTION

Restriction enzymes were used according the manufacturer's instructions. In general terms 15 µg of DNA; 1x restriction buffer; 1x BSA (if required); 2 µL of restriction enzyme and Milli-Q H_2O were used to a final volume of 50 µL. For those restrictions used only to validate the resulting products of subcloning steps a final volume of 20 µL was used, whereas when fragments had to be cut and purified from agarose gels (e.g., southern

probes) up to ~150 ng and 50 µL were used. The reaction mix was incubated ON at 37 ºC followed by heat inactivation during ~20 min at 80 ºC unless indicated otherwise by the manufacturer's instructions. Whenever possible high-fidelity enzymes were used (Thermo Fisher Scientific). EcoRI was from NEB (Izasa). The list of restriction enzymes used is shown in Table MIII-2.

	List of restriction enzymes			
	Plasmid	**Insert/process**	**RE**	**ER to test the ligation product**
Shank2 modification	ploxSTOPlox	NeoR	BsrGI+AflII	KpnI+SpeI; HindIII; BssHII
	ploxSTOPlox+NeoR	X	PacI+AscI	BssHII; EcoRI; NdeI+EcoRV
	ploxSTOPlox+NeoR +X	Y	Eco47III+BsrGI	BssHII; NdeI+EcoRV; PacI+BsrGI
	final ploxSTOPlox	1st recombineering	PacI+BsrGI	ApaI+AatII+HindIII; BamHI
	pTargeter	AmpR	XbaI+SpeI	XmnI; XbaI+PstI
	pTargeter+AmpR	A	NdeI+BssHI	BsrGI+BstBI; XmnI
	pTargeter+AmpR+A	B	SalI+EcoRV	NdeI+EcoRI; XbaI; PmeI+SphI
	Final pTargeter	2nd recombineering	PmeI+SphI	EcoRV; NdeI; SacI; XbaI
	Final pTargeter	Flp recimbinase	SwaI; BamHI; ApaI+HindIII+AatII	
	Final pTargeter	Cre recombinase	BamHI; ApaI+HindIII+AatII	
	PCR-Blunt StuI DIG	A	NdeI+BssHI	
	PCR-Blunt StuI DIG	B	SalI+EcoRV	
	PCR-Blunt StuI DIG	X	PacI+AscI	
	PCR-Blunt StuI DIG	Y	Eco47III+BsrGI	
	PCR-Blunt StuI DIG	NeoR	BsrGI +AflII	Sfi I
	PCR-Blunt StuI DIG	AmpR	XbaI+SpeI	AatII
Southern Blot	PCR-Blunt StuI DIG	5.1 probe	SmaI+HindIII; BfuAI	
	PCR-Blunt StuI DIG	5.2 probe	SmaI+KpnII; BfuAI	
	PCR-Blunt StuI DIG	3.1 probe	BsaI+XcmI+SmaI; BfuAI	
	PCR-Blunt StuI DIG	3.2 probe	NdeI+XcmI; PvuII; BfuAI	
	PCR-Blunt StuI DIG	Neo probe	SmaI+XcmI+ PstI; BfuAI	

Table MIII-2. Enzymatic restrictions conducted to generate the gene-targeting vector.

2.4 ENZYMATIC DNA LIGATION

To enzymatically ligate DNA fragments into linearized vectors, T4 DNA ligase (New England Biolabs [NEB]-IZASA, Barcelona) was used. The amount of insert added was determined visually by the electrophoretic gel appearance. As a rule of thumb, the insert needed to be at least twice times in excess as compared with the targeting vector. Typically, 0.5 µL (20-50 ng) of vector was mixed with 1 µL (~100-200 ng) of the insert or 7.4 µL for AmpR fragment in the pTargeter ligation; with ligation buffer 1x and 1 µL of T4 DNA ligase (both from New England Biolabs [NEB]-IZASA, Barcelona) and Milli-Q H_2O up

to a final volume of 10 µL. Negative controls were prepared without the addition of the insert. Finally, the reaction was incubated at 16ºC during 2.5-6 h.

2.5 PCR AND ELECTROPHORESIS IN AGAROSE GELS

Electrophoresis was usually run at 120V during 30 min. The loading sample buffer, samples, agarose gels and TAE 1x buffer were prepared as described in the general methods section. However, the ladders used were from a different provider (Thermo Fisher Scientific). SYBER Green (Sigma-Aldrich) stain was used for DNA visualization in agarose gels. Also, when the Fast digest buffer (Thermo Fisher Scientific) was used for bacterial restrictions, it was directly loaded in the gel without need of previous sample preparation.

2.5.1 CONVENTIONAL PCR

All those inserts that needed to be cloned into the PCR-Blunt StuI DIG vector were amplified with KOD-Hot Start DNA polymerase (Novagen, Merck-Millipore). For AmpR and NeoR amplifications, pR3R4ccdB_AsiSI and ploxpNeoFlrt were used respectively. In the case of amplified BAC fragments, the primer-BLAST tool (Ye et al. 2012) was used to select the four best ≈500 bp sequences (A, B, X and Y) from intron 16-17. DNA from BAC positive clones was checked through PCR amplifications with High fidelity expand DNA polymerase (Roche diagnostics, Mannheim, Germany).

A

	PCR thermocycling conditions			
	Step	Tª (ºC)	Duration	Cycles
AmpR amplification	1	95	5 min	1
	2.a	95	30 sec	
	2.b	55	30 sec	35
	2.c	70	1 min	
	3	70	5 min	1
	4	18	Infinity	1
NeoR amplification	1	95	5 min	1
	2.a	95	30 sec	
	2.b	60	30 sec	35
	2.c	70	1 min	
	3	70	5 min	1
	4	18	Infinity	1
A,B,X & Y fragments amplification & Shank2 test	1	95	5 min	1
	2.a	95	30 sec	
	2.b	59	30 sec	35
	2.c	70	1 min	
	3	70	5 min	1
	4	18	Infinity	1
Other tests conducted with GoTaq DNA polymerase	1	94	5 min	1
	2.a	94	30 sec	
	2.b	60	30 sec	30
	2.c	72	3 min*/30 sec**	
	3	72	5 min	1
	4	12	Infinity	1

B

PCR reaction mix final concentrations		
KOD-HS DNA polymerase Kit		
		Units
Vector DNA	10	ng
Primers	15	pmol each
dNTPs	0.5	mM
Buffer	1x buffer KOD-HS	vol
$MgCl_2$	2.5	mM
DNA polymerase	2.5	U
Reaction vol	25	µl
GOTaq DNA polymerase Kit		
		Units
Vector DNA	10	ng
Primers	0.5	µM each
dNTPs	0.2	mM each dNTP
Buffer	1x buffer GOtaq	vol
$MgCl_2$	2.5	mM
DNA polymerase	1.25	U
Reaction vol	25	µl

Table MIII-3. Conventional PCR for subcloning steps. PCR conditions for (A) cycling conditions. * when amplicons were > 500 bp and ** when amplicons where < 500 bp. (B) Reaction mix final concentrations for each DNA polymerase kit used.

PCRs for testing ligations were conducted using KOD-Hot Start DNA polymerase (Novagen, Merck-Millipore) or, alternatively, with GoTaq DNA polymerase (Promega Biotech Ibérica, Madrid, Spain) as indicated in each case (Table MIII-3). The PCR cycling conditions and final concentrations of the PCR reaction mix used in each case was different (Fig. MIII-3). Designed primers for BAC and subcloning steps tests and its associated sequences are shown in Table MIII-4. In addition, agouti and black new-born mice obtained from chimeric B6 x FlpO mice (all with BC57BL/6 background) and subsequent breeding were subjected to genotyping using High fidelity DNA polymerase (see Fig. M-2 for HF Span DNA Polymerase PCR mix). Specific thermocycling conditions are shown in Table MIII-5.

	List of primers				
Goal	Primer name	5'-3' Sequence Goal		Primer name	Sequence
To test Shank2	Test Shank2_1F	TGGTCCCCAAGGTCTGTTAG	X frag.	X_F	GTTAATTAAATTAAGGCAAAGGGCATGTG
	Test Shank2_1R	TTGACCATGGGTCCTTTCTC		X-R	AAGGCGCGCCAGTACTGAAGCAAGTGGAAC TGCTC
	Test Shank2_2F	CAGGCTGTTTCACCATAGCA	Y frag.	Y_F	CTACTAAGCGCTACACCTGCCTAAACCATTC C
	Test Shank2_2R	GGGACAGCAAGAGAGACCAG		Y_R	CTGTACACACTGCCACCACAAAATCAC
To check pTargeter.DTA	pTarg F_Test_AmpR	AGAGATTACGCGCAGACCAA	A frag.	A_F	GTCCATATGATTTAAATTGGTCCCCAAGGTC GTTAG
	pTarg_ R_Test_AmpR	CCACTAGAGTCGAGGGATGC		A_R	ACTGAAGCGCGCGCGTACCCATGCTTCGTC AGT
	AmpR_Test_F	ACTTTCACCAGCGTTTCTGGG	B frag.	B_F	GACGTCGACATTCCACCCCCACTCTGACT
	AmpR_Test_R	TGGGTCTCGCGGTATCATTG		B_R	GCCTCAGATATCCACAGCATGTGTGTGTTTT CAGT
	A_Test_F	CTTACATCGGCGTGTGCTTC	To test recombinations	F_Test_shank2_XYNeo	AGCCCTTAAGCCAACTCACC
	B_Test_F	GCACATGAGGATCACAGGGT		ploxSTOP_Test_XR	CCATGGCTTGAGTAAGTCTGC
	pTarg_ R_Test_AmpRAB	CCACTAGAGTCGAGGGATGC		PGKNeoR_Test_F	GTGGATGTGGAATGTGTGCG
To check ploxSTOPlox	ploxSTOP_Test_NeoRY_R	TGCACCACCGGGTAAAGTTC		F_Test_Shank2g_XY	AGCCCTTAAGCCAACTCACC
	PGKNeoR_Test_F	GTGGATGTGGAATGTGTGCG		R_Test_Shank2g_XY	ACAGGGTGGTGAATGCTCAG
	ploxSTOP_Test_NeoR_F	TGGTGATAGGTGGCAAGTGG		DTA_F	CAGGCACCTATACTCACCCA
	NeoR_Test_R	GACATAGCGTTGGCTACCCG		DTA_R	GTAGCCTGAACAGGAGGGACA
	ploxSTOP_Test_XF	ACAGCTATGACCATGATTACGC		Shank2 GF3	TGTCAGGGCAATCTGACCG
	X_Test_R	GTCACCAGCAACAGGTACGA	Southern blot probes	Shank2 5probe F1	TGGCTAGCATGACGTGTGTT
	ploxSTOP_Test_XR	CCATGGCTTGAGTAAGTCTGC		Shank2 5robe R1	CCCAATTGGCTGGGTGAGAT
To check genomic region	F_Test_Shank2g_XY	AGCCCTTAAGCCAACTCACC		Shank2 5probe F2	GGATACCCTAGCCTGTCCCA
	R_Test_Shank2g_XY	ACAGGGTGGTGAATGCTCAG		Shank2 5probe R2	AAAAGTGTCACCCCAAGGCA
	Shank2 GF1	GGGATGTCCTGCATACCACC		Shank2 3probe F1	TCCCAGCACCACTGTTCATT
	Shank2 GF2	GTAGATGGATGCACACCCCC		Shank2 3probe R1	TAGAGGATGGCACTGGGTGT
	Shank2 GR1	ATGGCAGTGTACCATGCTGA		Shank2 3probe F2	GGCAACTTTTGGGAGTTGCTT
	Shank2 GR2	CCCACTGGGTACAGGGACTT		Shank2 3probe R2	CCTGAAGGCTCCACAGTACC
	Shank2 GF3	AGTCTCCTGTCTCTGCTAGGG		Neo probe F1	GGTTCTTTTTGTCAAGACCG
	Shank2 GR3	TGTCAGGGCAATCTGACCG		Neo probe R1	GCTCTTCAGCAATATCACGG
NeoR	NeoF	GTTTTCCCAGTCACGACGTT			
	NeorR	TGTGGAATTGTGAGCGGATA			
AmpR	AmpF2	CAGCGTTCTAGAAGGTATGTAGGC GTGCTAC			
	AmpR	AGCCTCACTAGTTAGACGTCAGGT GCACTTT			

Table MIII-4. **Primer list and sequences used for *Shank2* modification generation and test.**

PCR thermocycling conditions			
Step	Ta (ºC)	Duration	Cycles
1	94	2 min	1
2.a	94	30 sec	34
2.b	60	30 sec	
2.c	68	7 min	
3	68	8 min	1
4	4	Infinity	1

Table MIII-5. Conventional PCR for *Shank2* and FlpO transgenic mice genotyping.

2.5.2 LONG RANGE-POLYMERASE CHAIN REACTION

LR-PCR was conducted using SequalPrep™ Long PCR kit (Life Technologies; Thermo Fisher Scientific) to select for positive ESC clones (carrying *Shank2* modifications). Out of 48 ESC clones genetically screened, 13 were found positive (2F6; 2H4; 3B12; 4A5; 4A7; 5E10; 8A3; 8D1, 8D7; 8E8; 9D4; 9G10 and 9H3). Then, these clones were further expanded and were re-assessed by PCR with 4 different pairs of primers (See Table MIII-6 for primer sequences). Then, LR-PCR was conducted to those previous positive clones to reconfirm the results using genomic precipitated DNA (gDNA) with isopropanol (see MIII-2.2.2).

	List of primers	
Goal	**Primer name**	**5'-3' Sequence**
Screening by PCR of ESC clones	Shank 2 GF1	GGGATGTCCTGCATACCACC
	Shank 2 GF2	GTAGATGGATGCACACCCCC
	F_Test_Shank2g_XY	AGCCCTTAAGCCAACTCACC
	ploxSTOP_Test_XR	CCATGGCTTGAGTAAGTCTGC
	ploxSTOP R1	GTCTGCAGGTCGAGGGACCTA
	PGK prom F2	GCCAGAGGCCACTTGTGTAG
	PGK FrtF	GGTAGAATTCCTGCAGCCCG
	R_Test_Shank2g_XY	ACAGGGTGGTGAATGCTCAG
	Shank2 GR4	AGGTGTGATGGCAGTGTACC
	Shank2 GR5	AGGCACCTTGATGTGGTCAG

Table MIII-6. Primer sequences for transfected ESC clones with final targeting vectors genetic screening.

2.5.3 QUANTITATIVE REAL-TIME PCR

In the present work, quantitative real-time PCR was conducted to validate *Shank2* modified animals. For qPCR analyses, 6-7 biological replicas, depending on the genotype (WT, HET and HOMO), were performed. Each replica consisted of the forebrain from one animal (strain derived from ESC clone 8D7). Both male and female animals were used. Samples of all genotypes were divided into 2 groups, and RNA extractions were conducted in different days. RNA isolation and cDNA synthesis were done as previously described (see M-2.1, 2.3 & 2.4). RIN measures were conducted as previously indicated (see M-2.1.2) to be sure that similar RINs were obtained for all samples. In general, good RINs were attained, ranging from 8.5 to 9.60. For the evaluation of *Shank2* expression in Crb, RNA extraction and cDNA synthesis were conducted using 3 WT and HOMO samples, respectively. RINs from Crb samples had slightly lower values: 7.7 to 9.5. A final

concentration of 125 ng/µL of brain and 240 ng/µL of Crb cDNA was used for qPCR analysis.

Specifically, qPCR reactions included 1 µL of cDNA, 3.5 µL of sterile water type II (Milli-Q water; Merck-Millipore), 5 µL Taqman Master Mix (Applied Biosystems, Foster City, CA) and 0.5 µL of specific mouse TaqMAN™ probes (Applied Biosystems). The probes used for *Shank2* quantification were Mm00683065_m1 and Mm01163737_m1_FAM, whereas reference genes *Actb* (Mm00607939_s1), *Gapdh* (Mm05724508_g1) and *18S* (Mm03928990_g1) were used in mouse tissue gene expression analyses. *Shank2* probes Mm00683065_m1 and Mm01163737_m1_FAM targeted *Shank2a* exons boundaries 8-9 and 10-11, respectively. Thus, they anneal after the introduced genetic modification as it is placed at exon boundaries 7-8 of *Shank2-002* or *Shank2a.* Samples were loaded with automatic pipettes and optical-quality sealing films (Corning, Merck-Millipore) were used to cover the top of the 96-well plates. These plates were then centrifuged with a custom-made system to concentrate the sample in the bottom and assure no droplets remained in the walls of the wells. All air bubbles were carefully removed with a plastic device to avoid fingerprints onto the optical sealing cover which could alter the fluorescence recording. All qRT-PCR reactions were run in duplicate in 2 independent experiments and mean Ct values (the point at which the fluorescence curve intersects the threshold line) for each reaction were taken. The negative controls used to check for reagent contamination were prepared with a) a complete reaction mixture in which the RNA sample was replaced by RNase-free water and b) no enzyme was added in the other negative controls to assess the background spontaneous fluorescence release. Reactions were run on a CFX96TM Real-Time System (Bio-Rad, Hercules, CA) according to the manufacturer's instructions and thermocycling conditions indicated in Table MIII-7. A minimum of 2 technical replicas per sample were done.

PCR thermocycling conditions			
Step	**T^{a} (ºC)**	**Duration**	**Cycles**
1	95	10 min	1
2	95	15 sec	39
3	60	1 min	
4	4	Infinity	

Table MIII-7. Quantitative real-time PCR thermocycling conditions.

2.5.3.1 CALCULATION OF $_M$RNA EXPRESSION LEVELS

Relative mRNA expression levels were calculated using the ΔCt method. Specifically, Ct mean values from a given sample and specific housekeeping gene were subtracted from Ct mean values of the Taqman probe:

$$\Delta\Delta Ct = \text{Mean Ct (Reference gene)} - \text{Mean Ct (}\textit{Shank2}\text{ probe)}$$

Gapdh, 18S and *β-Actin* (*Actb*) genes were used as a reference. Yet, the *Actb* probe was the only one used in all experiments. Next, ΔΔCt normalized to each reference gene was calculated as $2^{-\Delta\Delta Ct}$. Then, the sample $2^{-\Delta\Delta Ct}$/mean of all $2^{-\Delta\Delta Ct}$ of the control group (e.g., WT) was obtained (i.e., $2^{-\Delta\Delta Ct}/2^{-\Delta\Delta Ct}$ mean of WT samples). This calculation indicates the FC of each genotype relative to its control. Finally, the mean of the individual arbitrary units (AU) values and the S.E.M of the group was used to see the general trend of expression.

2.6 SOUTHERN BLOT OF POSITIVE EMBRYONIC STEM CELL CLONES

Those positive ESC clones tested by LR-PCR were then evaluated by Southern blot. This technique was conducted under the direction of Dr. Franco Lucchini (Centro Ricerche Biotecnologiche and Istituto di Microbiologia, Cremona, Italy) or, depending on the case, by the mouse mutant facility core (IRB, Parc Científic Barcelona). Collected genomic DNA (gDNA) samples were dissolved in TE 1x at a concentration of 1-2 μg/μL. Southern blot probes against 5' and 3' regions were amplified by a conventional PCR using KOD start DNA polymerase and subcloned into PCR-Blunt StuI DIG vectors. Primers designed for such a purpose are shown in Table MIII-4. Each probe was subcloned into PCR Blunt StuI Dig vector and the 5' probe was retrieved and purified by digestion with BfuAI and SmaI and HindIII for 3' and Neo probes. These probes were labelled by incorporating fluorescent dyes. Specifically, the dNTPs used in a standard mix were replaced by the following reagents: dATP 1mM, dCTP 1mM, dGTP 1mM, dTTP 0,6 mM and DIG-11-dUTP 0,4 mM. The stock solution of DIG-11-dUTP nucleotide (ROCHE) was provided with Alkali-labile (Roche).

At least 45 μg of gDNA from positive ESC clones were digested ON at the right temperature with BamHI or XbaI for detection of the 5' probe, whereas HindII and XhoI were used for detection of 3' and Neo probes. Digested samples and markers (1 kBa Dig lambda/HindIII; loading dye buffer; water) were analysed by electrophoresis in agarose gels run with TAE buffer at 8-25V/cm^2 ON. Specifically, up to 15μg of restricted DNA was loaded. Gels were prepared with 0.8% agarose. Then separated samples were transferred using long sheets of Whatman 3 mm filter paper soaked in the buffer, then three sheets of 3 mm paper with the dimension of the gel; one piece of N+ Nylon membrane (Merck-

Millipore) and 0.4 N NaOH into the plexiglass support and tray. Both neutral and alkaline transfer solutions were used to transfer the DNA from the gel onto the membrane during 6 h. The membrane was prehybridized by placing the filter in the roller bottle with 10 mL of warm hybridization solution during 1h at 42ºC. Then, to hybridize the membrane, the probes were warmed up at 68ºC for 10 min, whereas the previous hybridization solution was removed and replaced by a solution containing the probe into the roller bottle. This was incubated ON at 42ºC. Two washes of the probe were done by using sterile 2x SSC (Stock 20x SSC: 3M NaCl, 300 mM trisodium citrate dihydrate, pH at 7 with NaOH and water up to 1 L) and 0.1% SDS buffer for 5 min. Then, 2 more washes of 0.1X SSC, 01% SDS buffer during 15 min at 68ºC using a pre-warmed hoover. Finally, two washes of 15 min with 0.1M Tris HCl pH 9.5; 0.1M NaCl adjusted up to 100 mL with water. The labelled hybridized probes then were detected using and anti-DIG antibody (1:20,000; Roche) and blocking solution (150 mL DIG Buff [0.1 M Maleic Acid; 0.15 M NaCl; 1600 mL H2O adjusted at 7.5 with NaOH pellet; and water until 2L]; 1.5g of blocking reagent [1% w/v; Roche]). After hybridization, excess probe was washed from the membrane using last washing buffer and the pattern of hybridization was visualized. The gDNA from WT JM8A1.N3 was the negative control.

2.7 KARYOTYPE OF POSITIVE EMBRYONIC STEM CELL CLONES

Subconfluent ESC used for karyotype assessment, were split the day before the analysis of metaphases on mouse embryonic fibroblast (MEF) with the correct medium of growing and transferred to T25 flasks. The karyotype was conducted by the mouse mutant facility core (IRB, Parc Cientific Barcelona). Briefly, Colcemid solution (10 µg/mL Colcemid KaryoMAX; Gibco); fixative solution (Methanol with glacial acetic acid at 3:1 [v:v]) were prepared. Then, Colcemid solution was added at 0.1 µg/mL for 2 h at 37ºC to prefeed cells 1h before the start of the protocol. The medium was collected in one falcon tube of 15 mL while cells were washed with PBS before trypsinization. Trypsinized cells were then collected in the same tube and centrifuged for 5 min at 1,000 rpm. The supernatant was thrown away and several microliters of medium was left to flick the cell pellet in it. ESCs were resuspended by pipetting them during 6 min. Next, KCl was added 1 mL by 1 mL until a final volume of 5 mL. The mixture was centrifuged at 1,500 rpm's at RT for 10 min, and KCl was removed gradually. Then, a total of 6 mL of fixative solution was added and cells were quickly mixed by pipetting. The ESCs were centrifuged at 1,500 rpm during 10 min and supernatant was removed. The remaining fixative solution was used to resuspend ESC pellets. ESC spreads were done into slides with evaporated ethanol using 50 µL of cell-containing solution and were left wet during night. Next, DAPI staining was conducted

by placing two drops of DAPI (Vectashield; Vector Laboratories) and covering the slide. Then, the staining was proceeded ON at -20 ºC. Finally, metaphases were identified at 40x magnifications into an optic microscope and chromosomes were counted by using immersion oil at 100x magnifications. Those ESC clones with correct karyotypes were selected for establishment of *Shank2* conditional KO for genetic rescue experiments mouse lines (Fig. MIII-2)

Figure MIII-2. Metaphasic chromosomes from a positive ESC clone. DAPI staining was conducted to determine the karyotypes of analysed cells.

3. MATERIALS AND METHODS FOR PROTEIN ANALYSES

3.1 PROTEIN EXTRACTIONS

In addition to total extracts from brain areas, obtained as described in general methods, protein heart extracts were obtained to generate negative controls for *Shank2* IBs. The homogenization buffer prepared for heart samples was composed of 2% SDS (Merck-Millipore), 50 mM Tris-HCl pH 7,4 (Sigma-Aldrich), 50 mM NaF (Merck-Millipore), 20 mM ZnCl2 (Sigma-Aldrich), 1 mM ortho-vanadate (Sigma-Aldrich), 1:2.500 PMSF (Sigma-Aldrich), 2 µg/mL aprotinin (Merck-Millipore), 2 µg/mL leupeptin (Sigma-Aldrich) and 1 mM β-glycerophosphate (Sigma-Aldrich). Then, the same mechanical and biochemical procedures described for 1% DOC solubilization of brain tissue were applied (See M-3.1.1; Fig. M-2).

3.2 IMMUNOBLOT ANALYSES

Shank2 expression assessment by IB was conducted using 7.5% SF acrylamide gels as described in the general methods section. For PSD-enriched fractions, up to 3 adult animals per genotype (WT, HET, HOMO) were used, whereas for assessment in homogenate samples a minimum of 6 biological replicates were analysed and more than 2 technical replicas were conducted. The same amounts for PSD-enriched samples as used for adult mice in the subcellular localization studies from chapter I were loaded. For pErk1/2 (Cat. No. 4370, Cell Signaling, Beverly, MA, USA) and PSD-95 (see Table M-5 from general methods), only 2 technical replicas from a given sample were conducted.

4. BIOINFORMATIC ANALYSES OF THE DATA

4.1 CONCEPTUALIZATION OF THE GENE TARGETING STRATEGY

The specific genetic construct design was built with SnapGene software (GSL Biotech; available at www.snapgene.com) and the primer-BLAST tool previously referred (https://www.ncbi.nlm.nih.gov/tools/primer-blast/). Ensemble databases and Ape software previously indicated were also used.

4.2 STATISTICAL ANALYSIS OF MENDELIAN TRANSMISSION

A contingency table was created using expected and observed number of genotypes from HET x HET breeding and the Pearson's chi-square test was applied to assess the significance of the observed frequencies of genotypes in relation to the expected values. These analyses allowed to determine whether the observed cases fit the expected distribution (Montoliu 2012).

4.3 STATISTICAL ANALYSIS FOR GENE EXPRESSION

For qPCR analysis, as data did not follow a normal distribution, the non-parametric Kruskal-Wallis test was applied using Graph Pad Prism (see M-4.3 for further detail).

A-RESULTS

1. GENETIC STRATEGY FOR *SHANK2* MODIFICATION

1.1 MOUSE *SHANK2* REPORTED TRANSCRIPTS

The *Shank2* gene from *Mus musculus* is located at chromosome 7 (144,001,928-144,424,494 forward strand) and has 24 exons based on Ensembl database (release 93 of July 2018). The *Shank2* gene yields at least 3 protein isoforms (Fig. RIII-1). Ensemble also reports an unprocessed transcript that would not produce a protein (Shank2-004, not depicted). Importantly, intron 16-17 is the longest intron common to all variants.

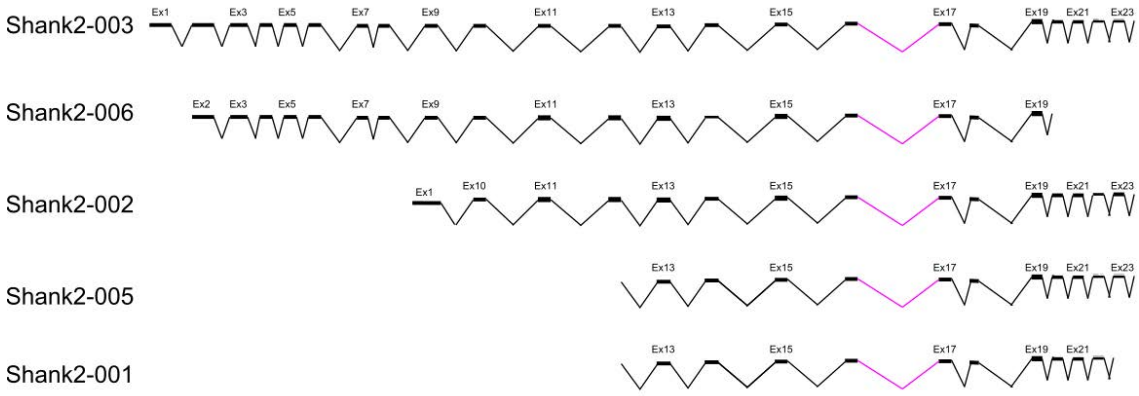

Figure RIII-1. *Shank2* transcript variants. These data are based on the last update of Ensemble release 93 in July 2018 (accessed 10/04/2018). The longest common intronic sequence, between exons 16 and 17, is shown in pink.

1.2 EXPERIMENTAL DESIGN

To obtain a *Shank2* conditional KO mice line for genetic rescue studies, a premature STOP was introduced in intron 16-17. This genetic construct (i.e., LoxPNeoR/STOPloxP) included two loxP sequences positioned in the same direction, three SV-40 late poly(A) signals (STOP sequences) and two FRT sequences flanking a Kanamycin/Neomycin resistance *cassette* (NeoR) controlled by the PGK/EM7 promoter with its own SV-40 polyA sequence, all in reverse direction (Fig. RIII-2). Thus, the modified *Shank2* allele was expected to yield truncated mRNAs, which should be degraded by the machinery responsible for non-sense mediated mRNA decay, and thus no protein would be produced. The breeding of these *Shank2* conditional KO mice with a Flp transgenic mice would allow to remove the NeoR, which is required for ESC clone selection. Finally, mice with the floxed allele (but without the NeoR) could be breed with Cre driver mice lines such as the

used in this study (Cg-Tg[CAG-cre/Esr1]5Amc/J). Then, the activation of the Cre recombinase by TMX would promote the deletion of the STOP construct and thus, rescue

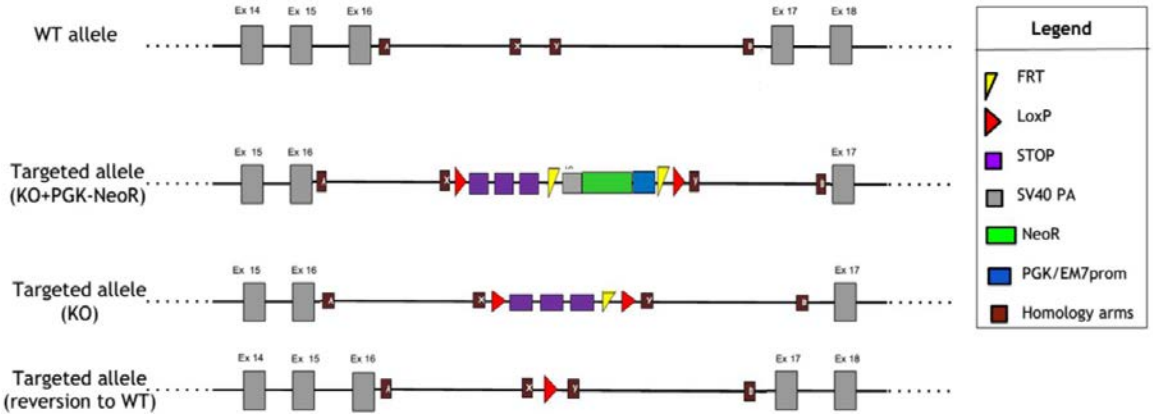

normal *Shank2* expression (Fig. RIII-2, bottom).

Figure RIII-2. Genetic strategy for *Shank2* modification. Intron 16-17 was selected to introduce the STOP genetic construct floxed by loxP sites. The action of Flp recombinase would enable to remove of the NeoR *cassette* while the Cre-recombinase action would result in the excision of the STOP cassette, as shown in the bottom drawing.

1.3 OVERVIEW OF THE ASSEMBLY OF THE FINAL GENE-TARGETING VECTOR

To achieve a *Shank2*$^{+/-}$ conditional KO mice line for genetic rescue studies, a final targeting vector was assembled into pTargeter plasmid (Fig. RIII-3E). This final targeting vector carried the *Shank2* modification to replace one allele of the JM8A1.N3 ESCs. The obtention of this final targeting vector included several steps. First, the plasmid backbone ploxSTOPlox was used to assembly the genetic construct LoxPNeoR/STOPloxP with X and Y homology arms (LNSXY; Fig. RIII-3B). The NeoR *cassette* subcloned in the ploxSTOPlox was obtained from ploxPneoflrt vector (Fig.RIII-3A). Then, LNSXY was homologously recombined by the BAC clone bMQ87K10 (Fig. RIII-3B&C) that carries the selected target sequence desired to modify from the *Shank2* intron 16-17. Subsequently, the modified genomic *Shank2* sequence containing the LNSXY from the BAC, was homologous recombined with the linearized modified pre-final pTargeter plasmid. Namely, original pTargeter was subcloned with two homology arms and the TetR was replaced by an AmpR for subsequent bacterial clone selection (Fig. RIII-3D). Therefore, the pre-final pTargeter vector was “gap-repaired” by “retrieving” the appropriate sequence from the BAC. Then, the final pTargeter or gene-targeting vector containing the modified *Shank2* genomic DNA was obtained (Fig. RIII-3E).

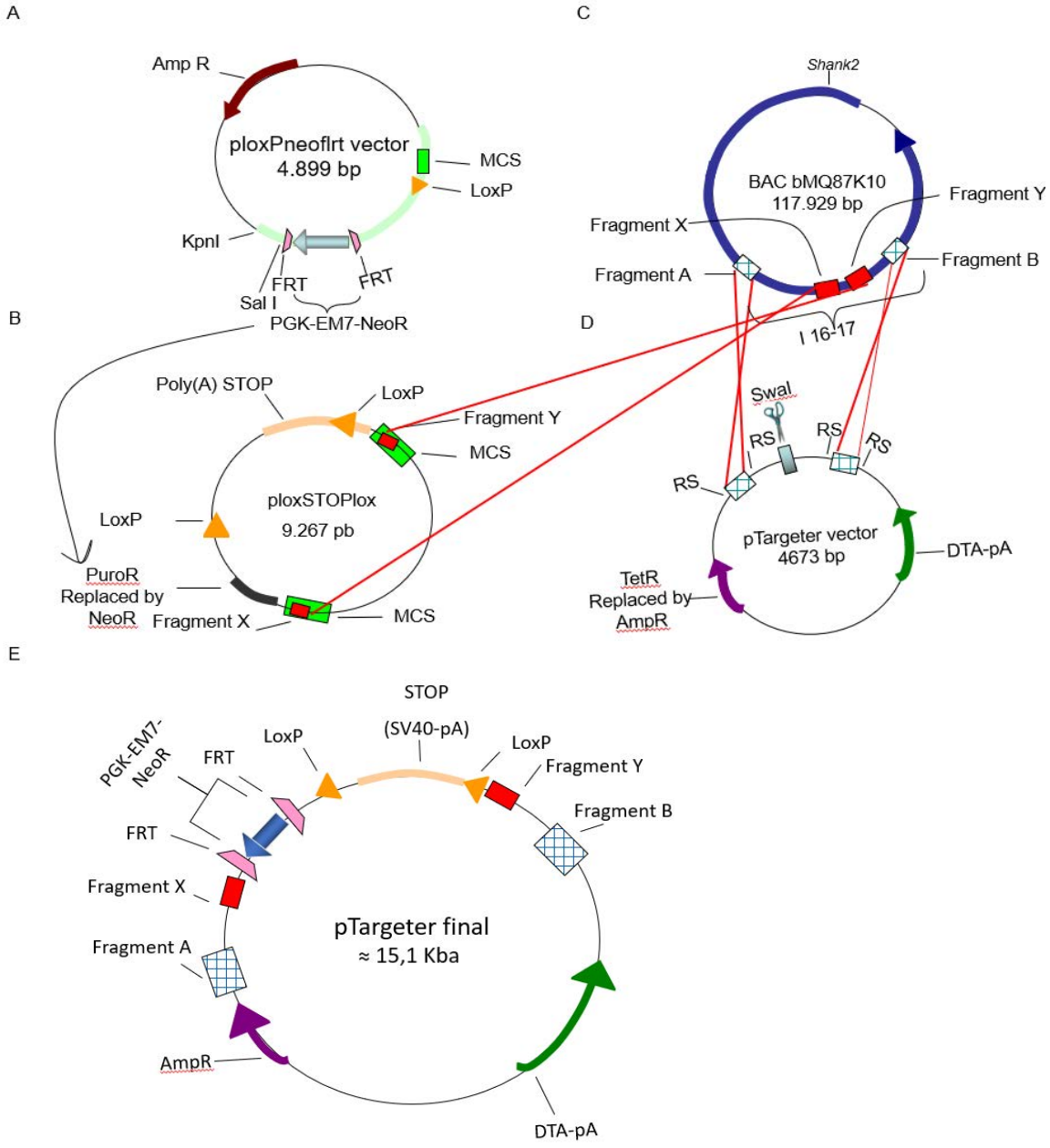

Figure RIII-3. Overview of the strategy conducted for the final targeting vector generation. (A) ploxPneoflrt vector was used to amplify by PCR the neomycin resistance (NeoR). (B) ploxSTOPlox vector was the backbone to ensemble the genetic construct as Puromycin resistance (PurR) was replaced by NeoR, and two *Shank2* fragments (X and Y) amplified from BAC bMQ87K10 were subcloned as the homology arms to generate the final ploxSTOPlox+NeoR+X+Y (LNSXY)-containing vector. (C) The genetic construct LNSXY from the final ploxSTOPlox plasmid was captured by the BAC bMQ87K10 through the homologous recombination of X and Y fragments. (D) The modified *Shank2* region from the BAC was captured by the SwaI-linearized pre-final pTargeter (a pTargeter with replaced TetR by AmpR, and A and B subcloned *Shank2* homology arms). (E) Scheme of the final targeting vector obtained (final pTargeter). MCS stands for multicloning sites and RS for restriction site. Red lines indicate homology recombination.

2. CONSTRUCTION OF *SHANK2* GENE-TARGETING VECTOR

2.1 FINAL PLOXSTOPLOX AND PRE-FINAL PTARGETER VECTOR CONSTRUCTION

2.1.1 AMPLIFICATION OF FRAGMENTS FOR GENETIC CONSTRUCT ASSEMBLY BY CONVENTIONAL PCR

To generate the ploxSTOPlox and pTargeter vectors, several DNA fragments were amplified by conventional PCR: FRT-NeoR cassette, and four BAC fragments named X, Y, A and B (Fig. RIII4-E). The NeoR was required for selection of ESC clones, whereas the AmpR was needed for selection of recombinant plasmids in *E. coli*. On the other hand, X and Y amplified fragments from *Shank2* intron 16-17 were prepared for subcloning into ploxSTOPlox, whereas A and B fragments were prepared for AmpR-containing pTargeter vector subcloning (Fig. MIII-4).

A

NAME	TEMPLATE	PRIMERS	FRAGMENT SIZE
NeoR	ploxNeoFRT	NeoF+NeorR	2 Kba
AmpR	PR3R4AsiSI	AmpF2+AmpR	1 Kba
C1-4 X	BAC bMQ87K10	X_F+X_R	500 bp
C1-4 Y	BAC bMQ87K10	Y_F+Y_R	400 bp
C1-4 A	BAC bMQ87K10	A_F+A_R	500 bp
C1-4 B	BAC bMQ87K10	B_F+B_R	500 bp

B

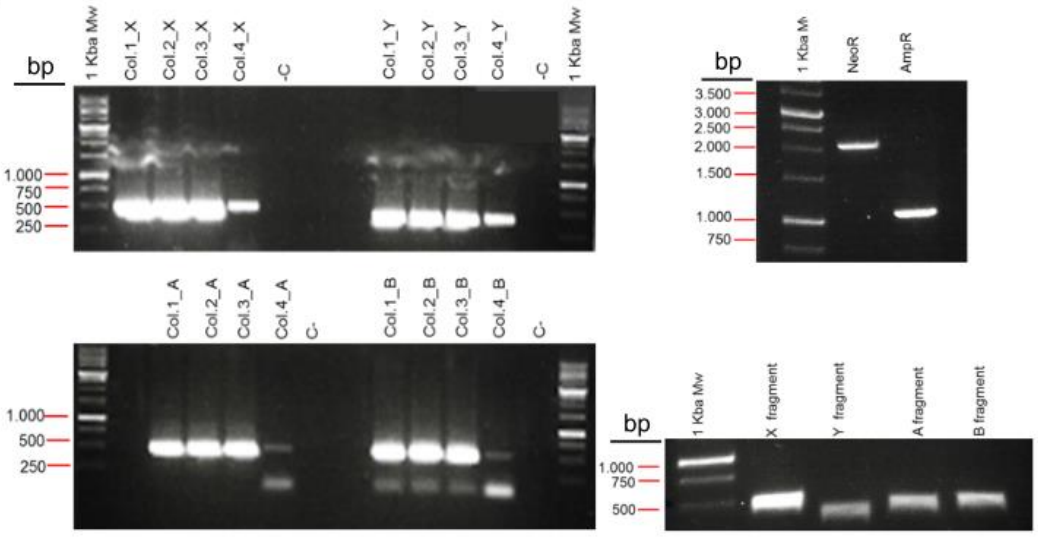

Figure RIII-4. Amplicons for genetic construct assembly. (A) Names, DNA template, primers used and expected sizes of the PCR products. Col. stands for colony. (B) PCR of the fragments amplified. In the bottom right image is shown the appearance of post-purified PCR products. -C stands for negative control.

2.1.2 SUBCLONING OF AMPLIFIED FRAGMENTS INTO PCR-BLUNT PLASMID

Amplified PCR fragments were synthesized with a DNA polymerase that generates blunt ends and primers designed with sequences for required restriction enzymes when needed. First, these fragments were subcloned into the PCR-Blunt plasmid and later isolated by enzymatic restriction (see Fig. RIII-5 for examples of these procedures). Second, these fragments were subcloned into ploxSTOPlox or pTargeter as required, using appropriate restriction enzymes.

A

NAME	TEMPLATE	RESTRICTION ENZYME	EXPECTED FRAGMENT SIZE
NeoR Col1-3	PCR Blunt+NeoR	Sfi I	(F) 3.000 bp 2.600 bp (R) 3.600 bp 2.000 bp
NeoR Col1-3	PCR Blunt+NeoR	BsrGI+AflII	(F&R): 3.200 bp 2.000 bp 300 bp
AmpR Col1-3	PCR Blunt+AmpR	XbaI+SpeI	(F&R): 3.430 bp 1.027 bp 60 bp 40 bp
AmpR Col1-3	PCR Blunt+AmpR	AatII	(F): 2.598 bp 1.959 bp (R): 3.500 bp 1.057 bp

B

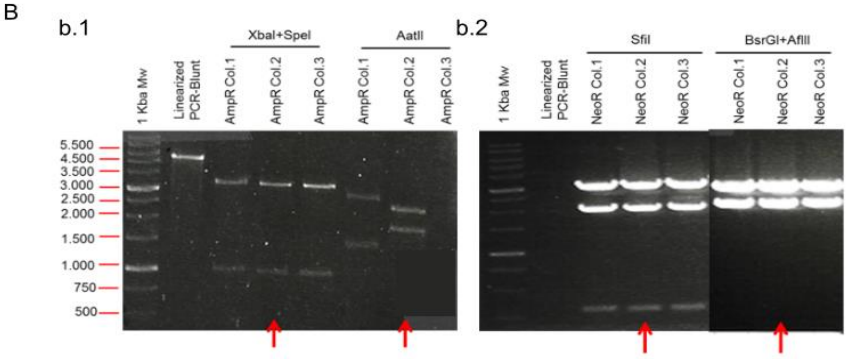

C

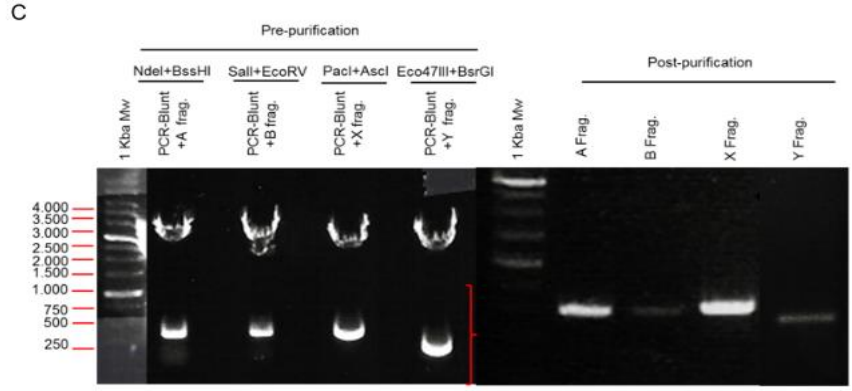

Figure RIII-5. Enzymatic restriction of 'PCR-Blunt StuI Digested Vector'. (A) Restriction pattern expected for a given restriction enzyme, or combination of them, assuming forward (F) or reverse (R) insertion of the AmpR and NeoR. (B) Restriction pattern for (b.1) AmpR and (b.2) NeoR. Red arrows indicate the colonies selected for glycerinate stocks and subsequent subcloning steps. (C) A, B, X and Y restricted fragments from PCR-Blunt StuI DIG and purified fragments shown at right. All fragments were ~500 bp.

2.1.3 REPLACEMENT OF ANTIBIOTIC RESISTANCE IN PLOXSTOPLOX AND PTARGETER

The original ploxSTOPlox vector carried a PuroR *cassette*, which had to be replaced by NeoR, this was first amplified by PCR as previously shown. This replacement was achieved by ligation of the amplified and purified from PCR-blunt vectors NeoR *cassette* into a ploxSTOPlox vector that was previously enzymatically restricted to remove the PuroR *cassette* (Fig. MIII-6A&B). The replaced vector was checked by a second restriction (Fig. MIII-6D&E). The same procedure was conducted to exchange the original TetR with the previously amplified and purified AmpR in pTargeter (Fig. RIII-6).

A

NAME	TEMPLATE	RESTRICTION ENZYMES	EXPECTED FRAGMENTS
ploxSTOP	ploxSTOP	BsrGI+AflII	4.900 bp 4.300 bp
pTargeter	pTargeter	XbaI+SpeI	3.400 bp 1.250 bp

B

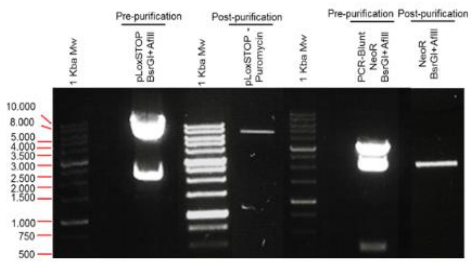

C

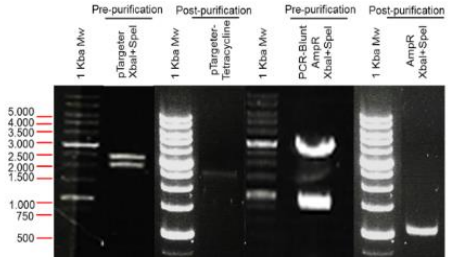

D

NAME	TEMPLATE	RESTRICTION ENZYMES	EXPECTED FRAGMENTS
ploxSTOP	ploxSTOP	KpnI+SpeI	4.900 bp 4.300 bp
ploxSTOP+NeoR	ploxSTOP+NeoR	KpnI+SpeI	5.400 bp 3.200 bp 360 bp
ploxSTOP	ploxSTOP	HindIII	4.600 bp
ploxSTOP+NeoR	ploxSTOP+NeoR	HindIII	5.200 bp 3.800 bp
pTargeter	pTargeter	XbaI+PstI	3.490 bp 1.200 bp
pTargeter+AmpR	pTargeter+AmpR	XbaI+PstI	2.050 bp 1.200 bp 350 bp
pTargeter	pTargeter	XmnI	3.400 bp 1.250 bp
pTargeter+AmpR	pTargeter+AmpR	XmnI	1.500 bp 1.300 bp 840 bp

E

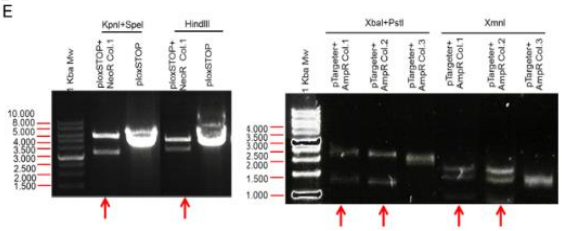

Figure RIII-6. Antibiotic replacement into ploxSTOPlox and pTargeter vectors. (A&D) The name, template, restriction enzymes (ER) and expected fragment sizes used for the correct identification of ploxSTOPlox and pTargeter plasmids. (B-C) Purifications of digested vectors and ligated inserts in ploxSTOPlox and pTargeter plasmids, respectively. (E) ploxSTOPlox with NeoR and pTargeter with AmpR restriction pattern and selected colonies (red arrows) for subsequent steps.

2.1.4 SUBCLONING OF HOMOLOGY ARMS INTO PLOXSTOPLOX

Fragment X was subcloned into the ploxSTOPlox vector containing the NeoR *cassette* to generate the 'LSNX' construct (ploxpSTOPlox+X). This was checked by enzymatic restriction (Fig. MIII-7A) and PCR (Fig. RIII-7B). Then, fragment Y was subcloned into pLSNX to generate the final ploxSTOPlox vector (pLSNXY, Fig. RIII-8).

A

a.1

NAME	TEMPLATE	RESTRICTION ENZYMES	EXPECTED FRAGMENTS
ploxSTOP	ploxSTOP	EcoRI	9.270 bp
ploxSTOP+NeoR	ploxSTOP+NeoR	EcoRI	5.500 bp 3.440 bp
ploxSTOP+NeoR+X	ploxSTOP+NeoR+X	EcoRI	5.500 bp 3.460 bp 490 bp

a.2

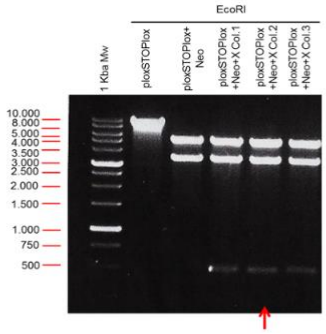

B

b.1

NAME	TEMPLATE	PRIMERS	EXPECTED FRAMENT SIZE
pLSNX	A ploxSTOP+NeoR+X	ploxSTOP_Test_XR ploxSTOP_Test_XY	713 bp
-C	H2O	ploxSTOP_Test_XR ploxSTOP_Test_XY	-
pLSNX	B ploxSTOP+NeoR+X	ploxSTOP_Test_NeroR_F ploxSTOP_Test_NeoRY_R	353 bp
-C	H2O	ploxSTOP_Test_NeroR_F ploxSTOP_Test_NeoRY_R	-

b.2

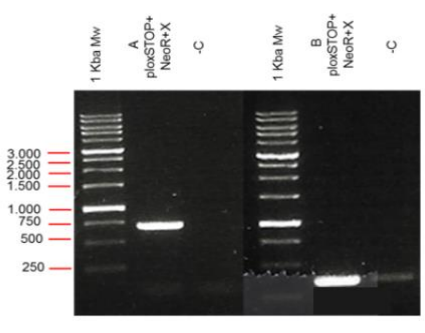

Figure RIII-7. Test of ploxSTOPlox-derived vectors. (A) Restriction pattern checking (a.1) with the name, template, enzymes used and expected fragments from enzymatic restriction and (b.1) PCR. Corresponding electrophoresed digested DNA with EcoRI (a.1) and PCR amplicons (a.2). Red arrows indicate the colonies selected for glycerinate stocks and subsequent subcloning steps.

A

NAME	TEMPLATE	RESTRICTION ENZYMES	EXPECTED FRAGMENT SIZE
ploxSTOP	ploxSTOP	BssHII	5.070 bp 2.600 bp 1.600 bp
ploxSTOP+NeoR	ploxSTOP+NeoR	BssHII	4.500 bp 2.900 bp 1.600 bp
ploxSTOP+NeoR+X	ploxSTOP+NeoR+X	BssHII	4.500 bp 2.800 bp 2.050 bp

NAME	TEMPLATE	RESTRICTION ENZYMES	EXPECTED FRAGMENT SIZE
ploxSTOP+NeoR+X+Y	ploxSTOP+NeoR+X+Y	BssHII	4.500 bp 3.300 bp 2.050 bp
ploxSTOP	ploxSTOP	NdeI+EcoRV	9.040 bp 230 bp
ploxSTOP+NeoR	ploxSTOP+NeoR	NdeI+EcoRV	8.950 bp
ploxSTOP+NeoR+X	ploxSTOP+NeoR+X	NdeI+EcoRV	9.440 bp
ploxSTOP+NeoR+X+Y	ploxSTOP+NeoR+X+Y	NdeI+EcoRV	7.800 bp 2.000 bp

B

C

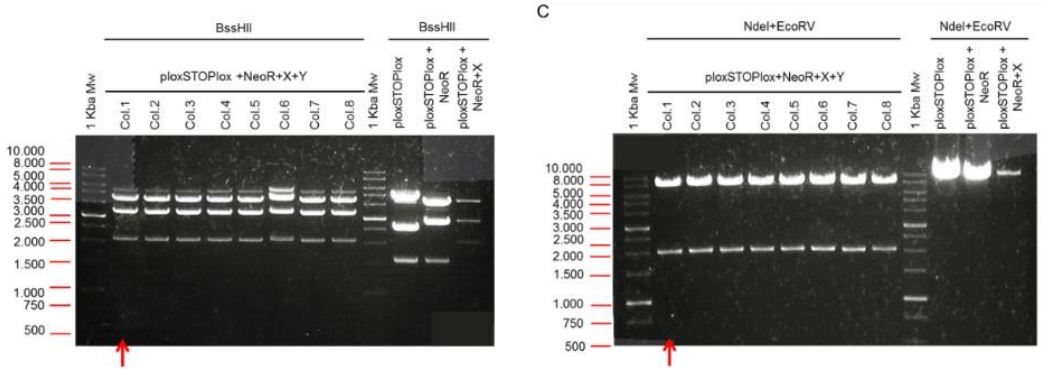

Figure RIII-8. Final ploxSTOPlox vector evaluation. (A) The name, template, restriction enzymes (ER) and expected fragment sizes used for the correct identification of final ploxSTOPlox vector. (B) Electrophoresis of the digested vector by BssHII, and (C) NdeI and EcoRV showing the expected fragments and the colony (Col.) selected for further experiments is indicated by a red arrow.

2.1.5 HOMOLOGY ARMS SUB-CLONING INTO PTARGETER

Fragment A was subcloned into AmpR-containing pTargeter, and pTargeter+AmpR+A was ligated with B fragment to obtain pTargeter+AmpR+A+B vector (pre-final pTargeter). Enzymatic restrictions (Fig. MIII-9) and PCR (Fig. MIII-10) tests were conducted.

A

NAME	TEMPLATE	RESTRICTION ENZYMES	EXPECTED FRAGMENT SIZE
pTargeter	pTargeter	BsrGI+BstBI	3.400 bp
pTargeter+AmpR	pTargeter+AmpR	BsrGI+BstBI	2.600 bp
			980 bp
pTargeter+AmpR+A	pTargeter+AmpR+A	BsrGI+BstBI	1.800 bp
			1.200 bp
			980 bp
pTargeter	pTargeter	XmnI	
pTargeter+AmpR	pTargeter+AmpR	XmnI	1.500 bp
			1.300 bp
			840 bp
pTargeter+AmpR+A	pTargeter+AmpR+A	XmnI	1.500 bp
			1.290 bp
			1.250 bp

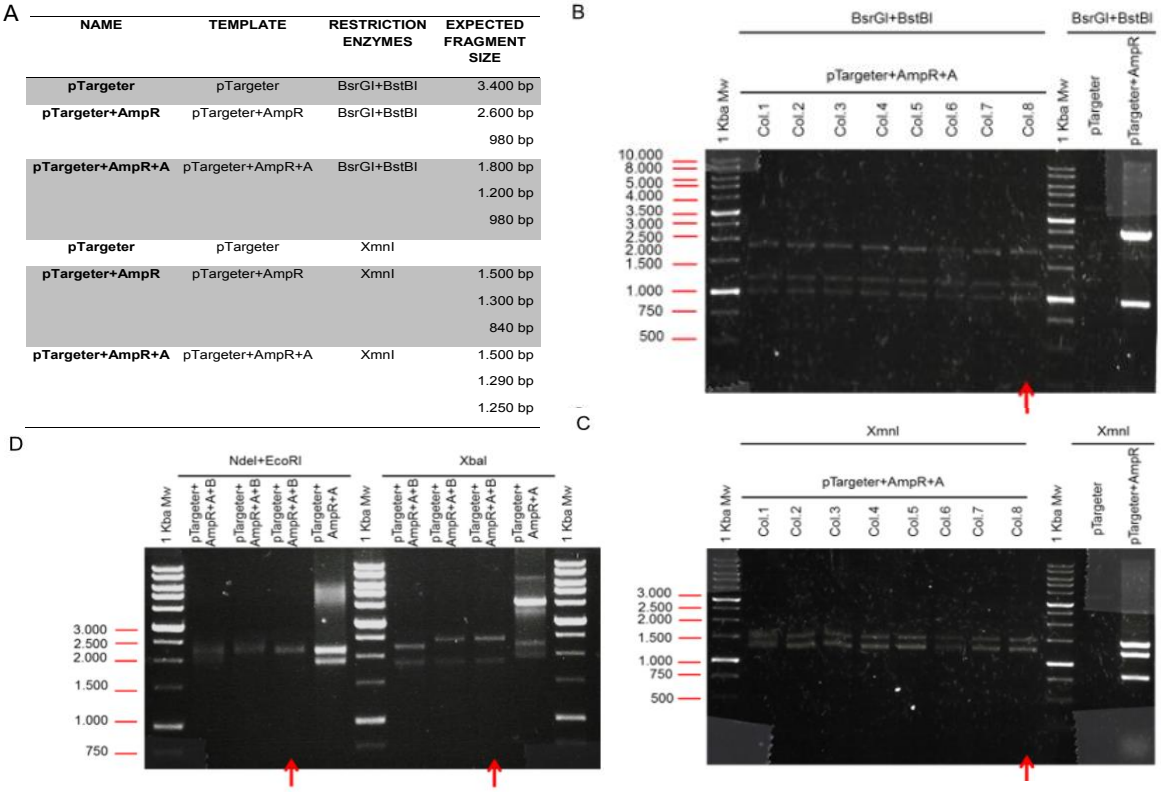

Figure RIII-9. Evaluation of pTargeter-derived vectors by enzymatic restriction. (A) The name, template, restriction enzymes (ER) and expected fragment sizes used for the correct identification of pTargeter+AmpR+A and pTargeter+AmpR+A+B vectors are provided. Corresponding electrophoresed digested pTargeter+AmpR+A and control vectors with (B) BsrGI and BstBI (C) XmnI; and (D) pTargeter+AmpR+A+B digested with (left) NdeI and EcoRI (right) XbaI. Col stands for colony and red arrows indicate the colonies selected for glycerinate stocks and subsequent subcloning steps.

A

NAME	TEMPLATE	PRIMERS	FRAGMENT SIZE
pTargeter 1st set of primers	pTargeter	pTarg_F_test_AmpR pTarg_R_test_AmpR	2.770 bp
pTargeter+AmpR 1st set of primers	pTargeter+AmpR	pTarg_F_test_AmpR pTarg_R_test_AmpR	1.670 bp
pTargeter+AmpR+A 1st set of primers	pTargeter+AmpR+A	pTarg_F_test_AmpR pTarg_R_test_AmpR	2.210 bp
pTargeter+AmpR+A+B 1st set of primers	pTargeter+AmpR+B	pTarg_F_test_AmpR pTarg_R_test_AmpR	2.350 bp
pTargeter 2nd set of primers	pTargeter	AmpR_Test_F1 AmpR_Test_R	-
pTargeter+AmpR 2nd set of primers	pTargeter+AmpR	AmpR_Test_F1 AmpR_Test_R	2.960 bp
pTargeter+AmpR+A 2nd set of primers	pTargeter+AmpR+A	AmpR_Test_F1 AmpR_Test_R	3.400 bp
pTargeter+AmpR+A+B 2nd set of primers	pTargeter+AmpR+B	AmpR_Test_F1 AmpR_Test_R	3.630 bp
pTargeter 3rd set of primers	pTargeter	A_Test_F pTargeter_R_Test_AmpRAB	-
pTargeter+AmpR 3rd set of primers	pTargeter+AmpR	A_Test_F pTargeter_R_Test_AmpRAB	-
pTargeter+AmpR+A 3rd set of primers	pTargeter+AmpR+A	A_Test_F pTargeter_R_Test_AmpRAB	704 bp
pTargeter+AmpR+A+B 3rd set of primers	pTargeter+AmpR+A+B	A_Test_F pTargeter_R_Test_AmpRAB	923 bp
pTargeter 4th set of primers	pTargeter	B_Test_F pTargeter_R_Test_AmpRAB	-
pTargeter+AmpR 4th set of primers	pTargeter+AmpR	B_Test_F pTargeter_R_Test_AmpRAB	-
pTargeter+AmpR+A 4th set of primers	pTargeter+AmpR+A	B_Test_F pTargeter_R_Test_AmpRAB	-
pTargeter+AmpR+A+B 4th set of primers	pTargeter+AmpR+A+B	B_Test_F pTargeter_R_Test_AmpRAB	540 bp

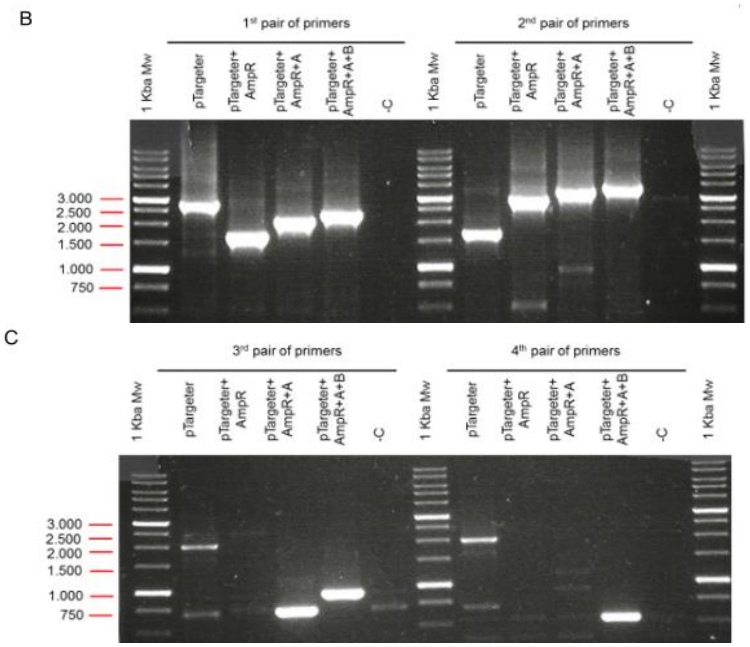

Figure RIII-10. Evaluation of pTargeter-derived vectors by PCR. (A) The name, template, primer pairs and expected fragment sizes used for the evaluation of all pTargeter vectors are shown. (B&C) Corresponding electrophoresis of the amplicons obtained from each pair of primers.

2.2 FINAL TARGETING VECTOR GENERATION

2.2.1 CAPTURE OF LSNXY FRAGMENT INTO BAC DNA BY HOMOLOGOUS RECOMBINATION

The tests of BAC, final ploxSTOPlox and pre-final pTargeter needed for final pTargeter generation before electroporation and recombination induction are shown in Fig. MIII-11.

A

NAME	TEMPLATE	RESTRICTION ENZYMES	EXPECTED FRAGMENT SIZE
finalploxSTOP	ploxSTOP+NeoR+X+Y	PacI+BsrGI	6.657 bp 3.183 bp
pTargeter+AmpR+A+B	pTargeter+AmpR+A+B	PmeI+SphI	4.232 bp

NAME	TEMPLATE	PRIMERS	EXPECTED FRAGMENT SIZE
BAC Shank2 1st set of primers	bMQ87K10	Test Shank2_F1 Test Shank2_R1	5.284 bp
BAC Shank2 2nd set of primers	bMQ87K10	Test Shank2_F2 Test Shank2_R2	5.528 bp

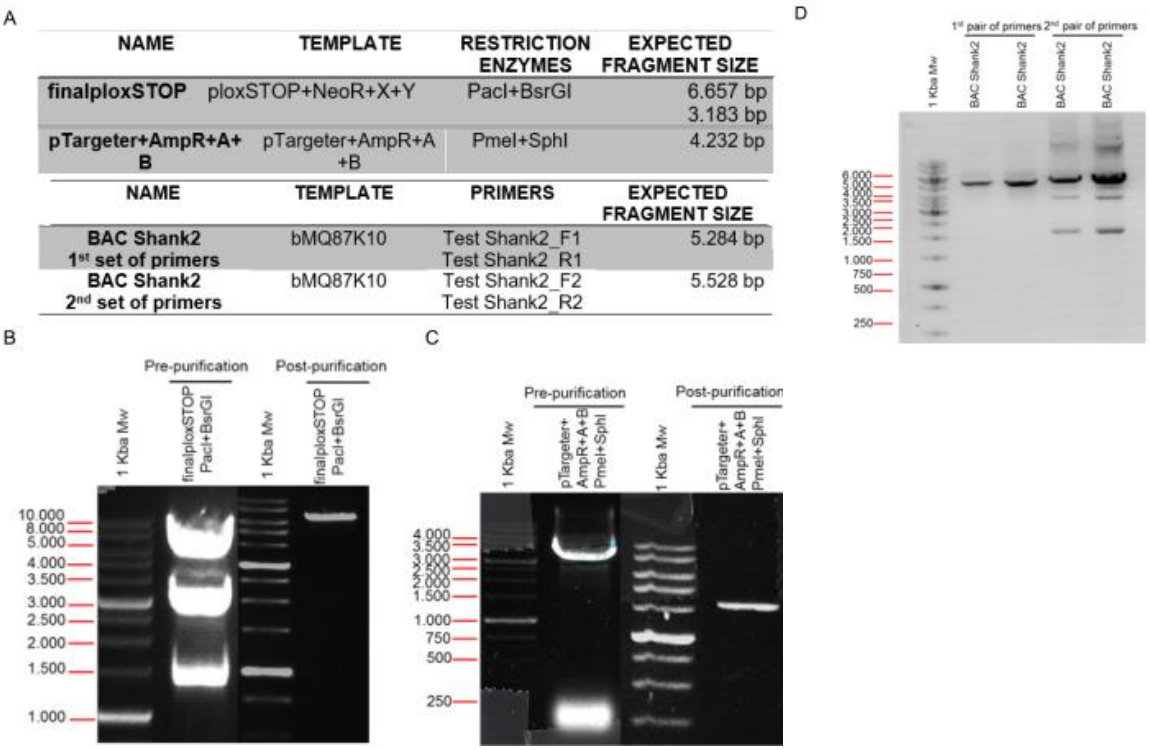

Figure RIII-11. Test of BAC, final ploxSTOPlox and pre-final pTargeter vectors for subsequent recombination events. (A) Information regarding the restriction enzymes used to retrieve the genetic construct from ploxSTOPlox and linearize the pTargeter+AmpR+A+B vector. Also, information about the PCR to test the integrity of the intron 16-17 from the BAC bMQ87K10 is shown on the bottom part of the table. (B-C) Electrophoresis of the fragments obtained by the restriction enzymes and aspect of the purified bands for both plasmids. (D) The first pair of primers gave an amplicon that covered the first 2,284 bps and the second pair encompasses the following 4,528 bps of the intronic sequence subjected to modification. Yet, total amplicon sizes were 5,284 and 5,528, respectively.

The genetic construct from the ploxSTOPlox vector was captured by the BAC bMQ87K10 via homologous recombination of fragments X and Y (Fig. RIII-12).

A

NAME	TEMPLATE	PRIMERS	EXPECTED FRAGMENT SIZE
BAC Shank2 Col.1-8 **1st recombination** **1st set of primers**	bMQ87K10	F_Test_shank2_XYNeo ploxSTOP_Test_XR	-
BAC Shank2 Col.1-8 **1st recombination** **1st set of primers**	bMQ87K10+LNXY	F_Test_shank2_XYNeo ploxSTOP_Test_XR	951 bp
BAC Shank2 Col.1-8 **1st recombination** **2nd set of primers**	bMQ87K10	PGKNeoR_Test_F R_Test_Shank2g_XY	-
BAC Shank2 Col.1-8 **1st recombination** **2nd set of primers**	bMQ87K10+LNXY	PGKNeoR_Test_F R_Test_Shank2g_XY	798 bp
BAC Shank2 Col.1-8 **1st recombination** **3rd set of primers**	bMQ87K10	F_Test_shank2_XY R_Test_shank2_XY	1.900 bp
BAC Shank2 Col.1-8 **1st recombination** **3rd set of primers**	bMQ87K10+LNXY	F_Test_shank2_XY R_Test_shank2_XY	7.050 bp

B

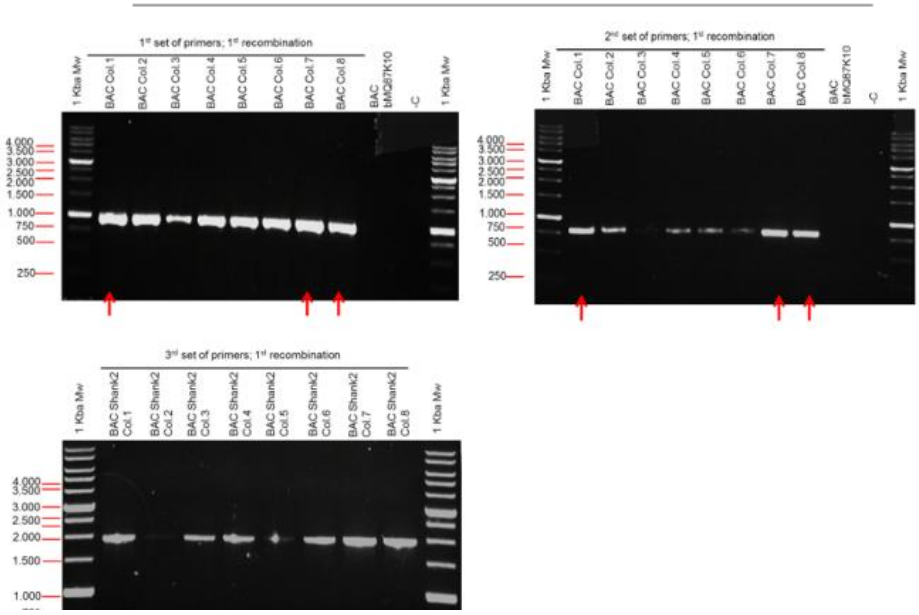

Figure RIII-12. PCR to test the *Shank2* modification by homologous recombination. (A) The name, template, primer pairs and expected fragment sizes used for the evaluation the first recombination between the fragment loxSTOPNeoRlox from final ploxSTOPlox vector and the BAC bMQ87K10. (B) Corresponding electrophoresis of the amplicons obtained from each pair of primers and the size obtained. Red arrows indicated the colony (col.) selected for glycerol stocks and next analysis.

2.2.2 HOMOLOGOUS RECOMBINATION FOR FINAL PTARGETER GENERATION

The second recombineering step included the homologous recombination between the modified BAC and linearized pTargeter with SwaI (Fig. RIII-13).

A

NAME	TEMPLATE	PRIMERS	EXPECTED FRAGMENT SIZE
Final pTargeter Col.1-10 2nd recombination 1st set of primers	Final pTargeter	DTA_F DTA_R	1.400 bp
pTargeter+AmpR+A+B 2nd recombination 1st set of primers	pTargeter+AmpR+ A+B	DTA_F DTA_R	1.400 bp
BAC Shank2+LNXY 2nd recombination 1st set of primers	bMQ87K10+LNXY	DTA_F DTA_R	-
Final pTargeter Col.1-10 2nd recombination 2nd set of primers	Final pTargeter	Shank2 GF3 DTA_R	2.200 bp
pTargeter+AmpR+A+B 2nd recombination 2nd set of primers	pTargeter+AmpR+ A+B	Shank2 GF3 DTA_R	-
BAC Shank2+LNXY 2nd recombination 2nd set of primers	bMQ87K10+LNXY	Shank2 GF3 DTA_R	-
Final pTargeter Col.1-10 2nd recombination 3rd set of primers	Final pTargeter	Shank2 GF3 DTA_R	970 bp
pTargeter+AmpR+A+B 2nd recombination 3rd set of primers	pTargeter+AmpR+ A+B	Shank2 GF3 DTA_R	-
BAC Shank2+LNXY 2nd recombination 3rd set of primers	bMQ87K10+LNXY	Shank2 GF3 DTA_R	-

B

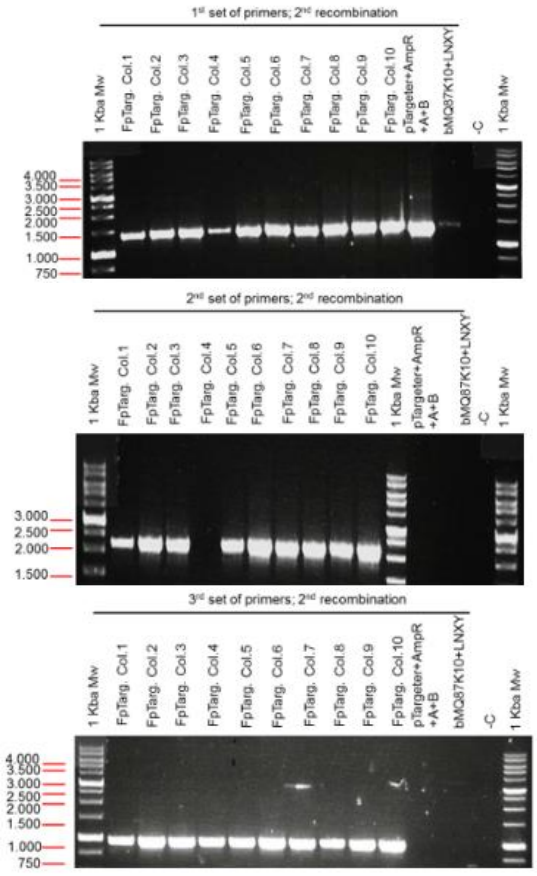

Figure RIII-13. Final pTargeter test by PCR. (A) The name, template, primer pairs and expected fragment sizes used for the evaluation of the second homologous recombination between the *Shank2* modification from the BAC and the pTargeter to obtain final targeting vector. (B) Electrophoresis of the amplicons obtained from each pair of primers.

To be sure that the *Shank2* modification was assembled properly in the final pTargeter vector, PCRs (Fig. RIII-13&14) and enzymatic restrictions (Fig. RIII-15) were conducted. Almost all PCRs produced the expected amplicons and thus, validated the final pTargeter. Then, final pTargeter was linearized using SwaI restriction enzyme.

A

NAME	TEMPLATE	PRIMERS	FRAGMENT SIZE
Final pTargeter 1st set of primers	Final pTargeter	AmpR_Test_F Shank2g_GR3	972 bp
BAC Shank2 1st set of primers	BAC bMQ87K10	AmpR_Test_F Shank2g_GR3	-
ploxSTOP+NeoR+X+Y 1st set of primers	Final ploxSTOPlox	AmpR_Test_F Shank2g_GR3	-
pTargeter 1st set of primers	Original pTargeter	AmpR_Test_F Shank2g_GR3	-
Final pTargeter 2nd set of primers	Final pTargeter	Shank2g GF3 pTargeter_R_Test_AmpRAB	1,118 bp
BAC Shank2 2nd set of primers	BAC bMQ87K10	Shank2g GF3 pTargeter_R_Test_AmpRAB	-
ploxSTOP+NeoR+X+Y 2nd set of primers	Final ploxSTOPlox	Shank2g GF3 pTargeter_R-Test_AmpRAB	-
pTargeter 2nd set of primers	Original pTargeter	Shank2g GF3 pTargeter_R_Test_AmpRAB	-
Final pTargeter 3rd set of primers	Final pTargeter	DTA_R Shank2g_GF3	951 bp
BAC Shank2 3rd set of primers	BAC bMQ87K10	DTA_R Shank2g_GF3	-
ploxSTOP+NeoR+X+Y 3rd set of primers	Final ploxSTOPlox	DTA_R Shank2g_GF3	-
pTargeter 3rd set of primers	Original pTargeter	DTA_R Shank2g_GF3	-
Final pTargeter 4th set of primers	Final pTargeter	Test Shank2g_XY_F ploxSTOP_Test_XR	2.200 bp
BAC Shank2 4th set of primers	BAC bMQ87K10	Test Shank2g_XY_F ploxSTOP_Test_XR	-
ploxSTOP+NeoR+X+Y 4th set of primers	Final ploxSTOPlox	Test Shank2g_XY_F ploxSTOP_Test_XR	-
pTargeter 4th set of primers	Original pTargeter	Test Shank2g_XY_F ploxSTOP_Test_XR	-
Final pTargeter 5th set of primers	Final pTargeter	PGKNeoR_Test_F R_Test_Shank2g_XY	798 bp
BAC Shank2 5th set of primers	BAC bMQ87K10	PGKNeoR_Test_F R_Test_Shank2g_XY	-
ploxSTOP+NeoR+X+Y 5th set of primers	Final ploxSTOPlox	PGKNeoR_Test_F R_Test_Shank2g_XY	-
pTargeter 5th set of primers	Original pTargeter	PGKNeoR_Test_F R_Test_Shank2g_XY	-
Final pTargeter 6th set of primers	Final pTargeter	X_F X_R	519 bp
BAC Shank2 6th set of primers	BAC bMQ87K10	X_F X_R	518 bp
ploxSTOP+NeoR+X+Y 6th set of primers	Final ploxSTOPlox	X_F X_R	-
pTargeter 6th set of primers	Original pTargeter	X_F X_R	-
Final pTargeter 7th set of primers	Final pTargeter	F_Test_Shank2g_XY R_Test_Shank2g_XY	6.300 bp
BAC Shank2 7th set of primers	BAC bMQ87K10	F_Test_Shank2g_XY R_Test_Shank2g_XY	7.050 bp 1.900 bp
ploxSTOP+NeoR+X+Y 7th set of primers	Final ploxSTOPlox	F_Test_Shank2g_XY R_Test_Shank2g_XY	-
pTargeter 7th set of primers	Original pTargeter	F_Test_Shank2g_XY R_Test_Shank2g_XY	-

Figure RIII-14. PCRs to test the final pTargeter from minipreps. Complete figure and figure footnote overleaf.

B

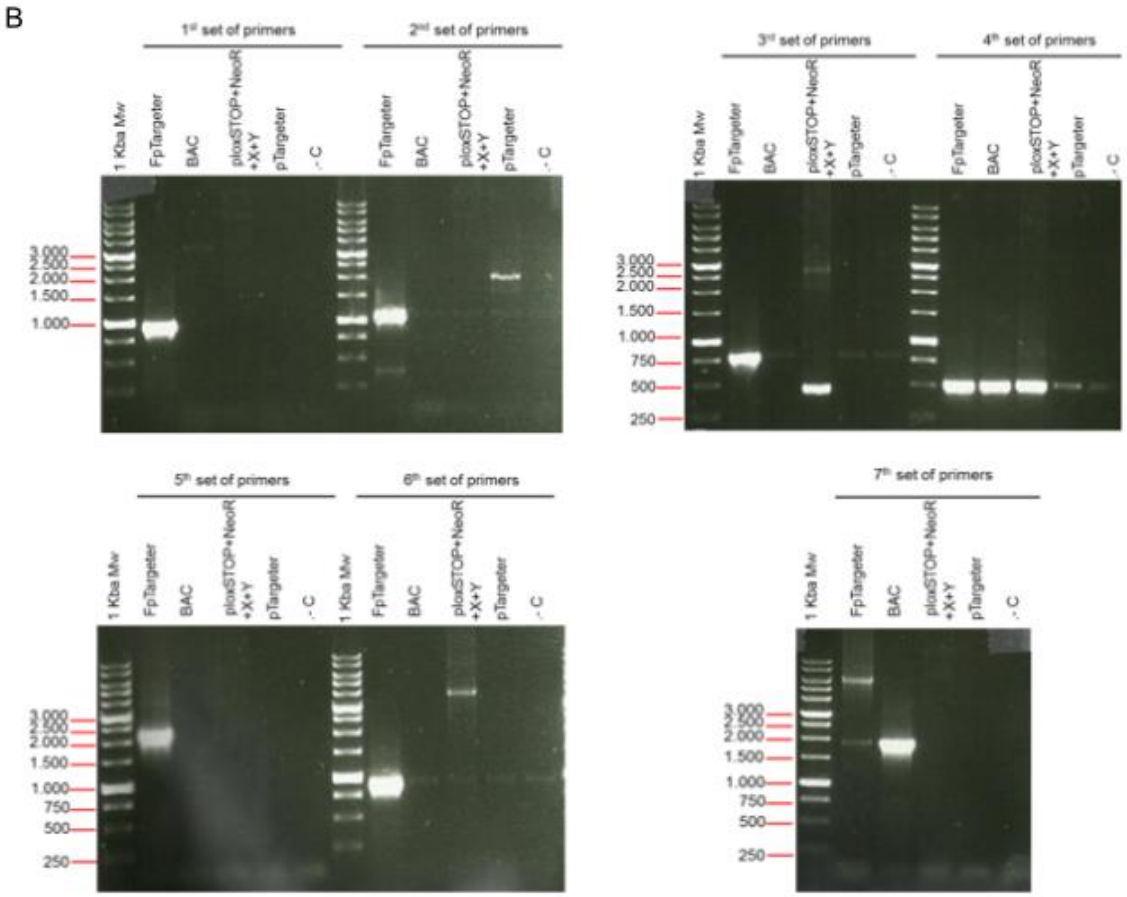

Figure RIII-14. PCRs to test the final pTargeter from minipreps. (A) The name, template, primer pairs and expected fragment sizes used for the evaluation the second homologous recombination between the *Shank2* modification from the BAC and the pTargeter. (B) Corresponding electrophoresis of the amplicons obtained from each pair of primers.

A

NAME	TEMPLATE	RESTRICTION ENZYMES	EXPECTED FRAGMENT SIZE
pTargeter	pTargeter	ApaI+AatII+HindIII	3.740 bp 410 bp 93 bp
Final pTargeter Col.1-3	pTargeter+AmpR+A+B+LNXY	ApaI+AatII+HindIII	6.400 bp 4.300 bp 3.700 bp 2.600 bp 400 bp
pTargeter	pTargeter	ApaI+AatII+HindIII	4.250 bp
Final pTargeter Col.1-3	pTargeter+AmpR+A+B+LNXY	BamHI	6.500 bp 5.200 bp 3.700 bp 2.000 bp
Final pTargeter	Final pTargeter	EcoRI	4.600 bp 4.500 bp 4.100 bp 1.400 bp 490 bp 114 bp
Final pTargeter	Final pTargeter	EcoRV	9.200 bp 2.900 bp 4.500 bp
Final pTargeter	Final pTargeter	NdeI	8.100 bp 5.900 bp 2.100 bp 475 bp
Final pTargeter	Final pTargeter	SacI	8.200 bp 7.000 bp 1.400 bp
Final pTargeter	Final pTargeter Cre plasmid	XbaI	6.900 bp 2.400 bp 1.900 bp 1.800 bp 1.400 bp 1.300 bp 400 bp

B

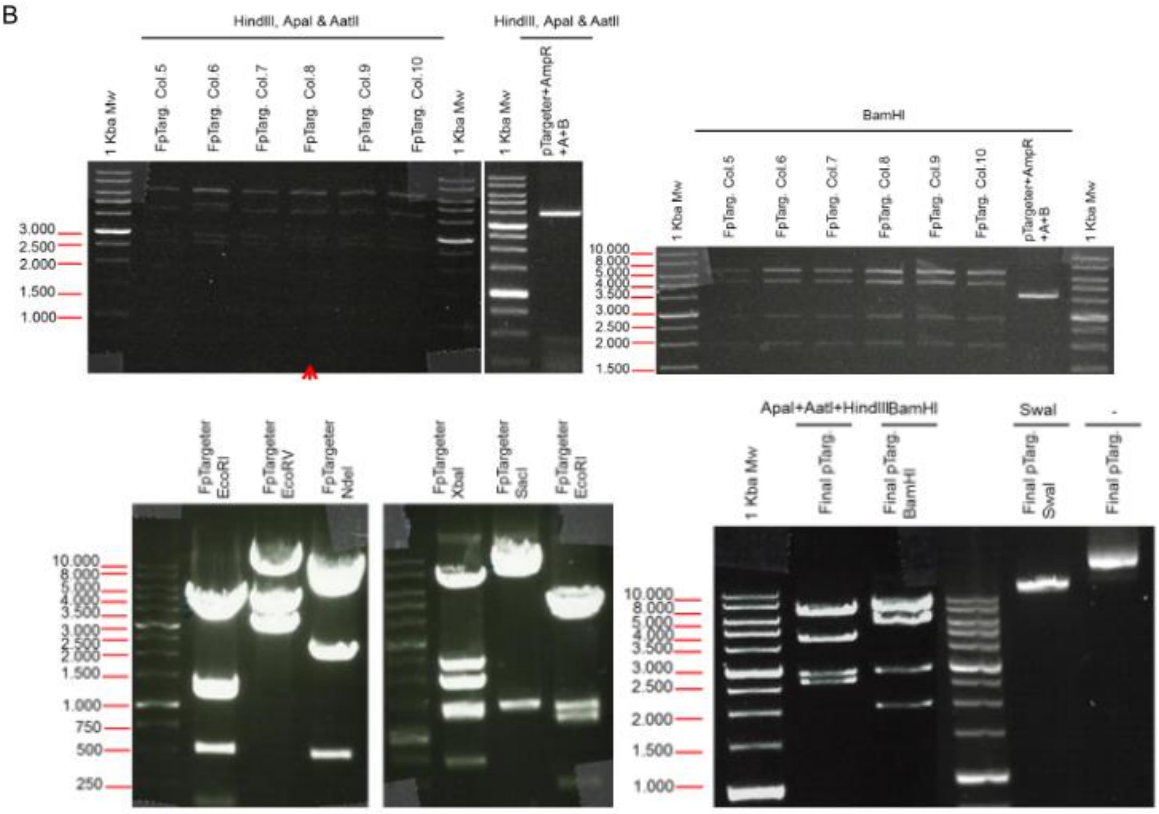

Figure RIII-15. Final pTargeter test by enzymatic restriction. (A) The name, template, restriction enzymes (ER) and expected fragment sizes used to test final pTargeter vector. (B) Electrophoresis of the digested final pTargeter fragments. Col. stands for colony and red arrowhead indicates the colonies selected for glycerol stocks and subsequent experiments.

3. DETERMINATION OF LOXP AND FRT RECOMBINATION SITES FUNCTIONALITY

To be sure that the final gene-targeting (final pTargeter) vector carried non-mutated loxP and FRT sites in the proper direction, their functionality was tested. Thus, *E. coli* cells expressing Cre and Flp recombinases (see MIII-1.6.3) were transformed with the final targeting vector. Then, FRT/FLP and LoxP/Cre functionality tests were conducted and showed that both recombination systems worked properly in 100% of the recombined clones assessed by enzymatic restriction (Fig. RIII-16).

A

NAME	TEMPLATE	RESTRICTION ENZYMES	EXPECTED FRAGMENT SIZE
Final pTargeter Col.1-8 Flp recombinase	Final pTargeter Flp plasmid	SwaI	14.500 bp
Final pTargeter Col.1-8 Flp recombinase	Final pTargeter Flp plasmid	BamHI	6.500 bp 5.200 bp 2.800 bp
Final pTargeter Col.1-8 Flp recombinase	Final pTargeter Flp plasmid	ApaI+HindIII+AatII	4.500 bp 4.300 bp 2.900 bp 2.600 bp 400 bp
Final pTargeter Col.1-8 Cre recombinase	Final pTargeter Cre plasmid	BamHI	6.500 bp 5.200 bp
Final pTargeter Col.1-8 Cre recombinase	Final pTargeter Creplasmid	ApaI+HindIII+AatII	4.500 bp 4.300 bp 2.600 bp 400 bp

B

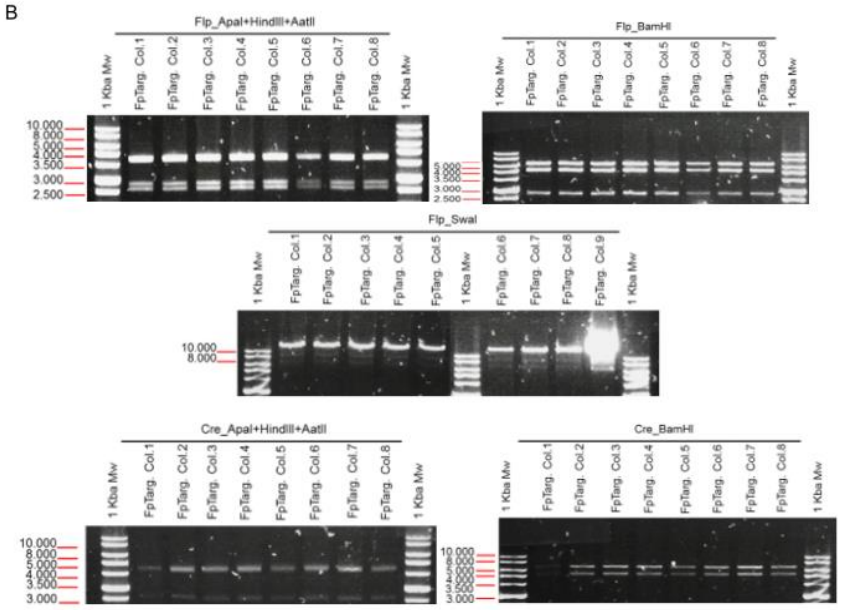

Figure RIII-16. Functionality test of Flp/FRT and Cre/loxP recombinase systems. (A) The name, template, restriction enzymes (ER) and expected fragment sizes used for the correct identification of recombined final pTargeter vector with Flp/FRT and Cre/loxP systems. (B) Corresponding electrophoresis of digested final pTargeter vector and other control vectors. The 400 bp bands are not shown as needed higher UV light exposition to be visualized.

4. GENERATION OF *SHANK2* CONDITIONAL KO MOUSE FOR GENETIC RESCUE EXPERIMENTS

The final targeting vector was transformed in JM8A1.N3 ESC (Fig. RIII-17A), and those that underwent appropriate homologous recombination were selected by the antibiotic G418 (Neomycin). Next, the positive ESCs were assessed by LR-PCR (Fig. RIII-17A&B) and Southern blot (Fig. RIII-17C). These tests were important to check that the genome was modified at the exact position that was planned.

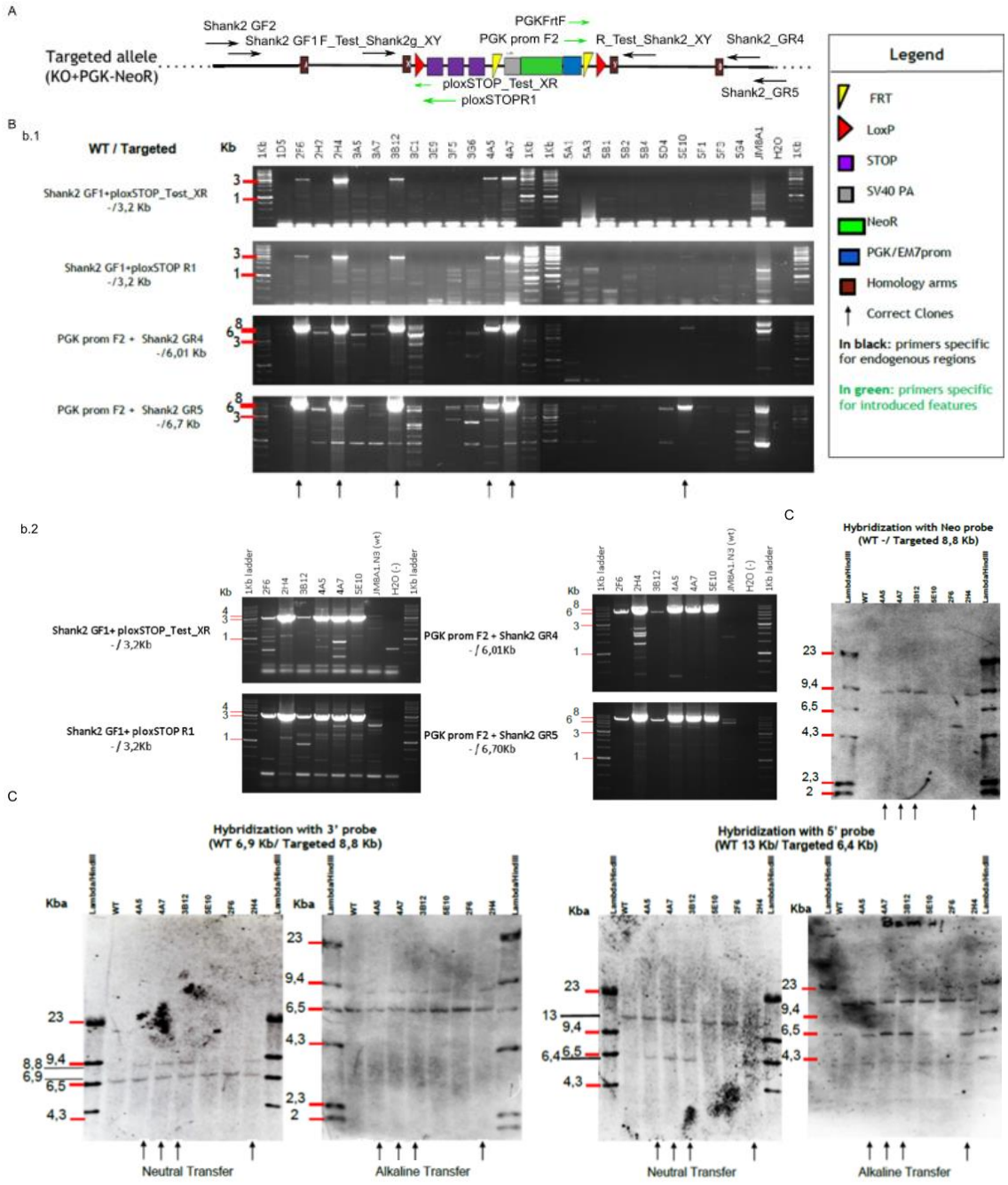

Figure RIII-17. Validation of gene targeting procedure in ESCs. (A) Arrows indicate the exact location of primer hybridization. See complete figure footnote overleaf.

Figure RIII-17 continuation. (B) LR-PCR of neomycin resistant expanded clones. Black arrows show positive and reliable ESC clones. (b.1) First PCR (b.2) re-assessment of positive clones from b.1. (C) Southern blot conducted with 5', 3' and Neo probes with neutral or alkaline transfer buffer. In the case of the Neo probe transference only worked in alkaline conditions. Expected sizes for each genotype are indicated on the top of each membrane. ESC clone code is shown at the top of each lane. Black arrows indicate positive confirmed clones. Of note, the actual ESC used to generate *Shank2*$^{+/-}$ conditional KO mice came from a second set of experiments, these images are just shown as an example.

4.1 ASSESSMENT OF FECUNDITY AND PROOF OF MENDELIAN GERMLINE TRANSMISSION

Positive ESC clones with the expected karyotype were microinjected into mouse blastocysts, which were then placed into a foster mother to generate chimeric mice. Male mice with high percentage of recombinant cells (> 80%), were then selected for the establishment of three mouse colonies derived from three different ESC clones (8D7, 9D4 and 5E10). Three pairs of primers were established to identify the modified alleles; one pair to detect Flp transgene and two pairs to check for NeoR-FRT deletion (Fig. R-18A&C). The specific PCR established to genotype the litter from chimeric mice crossed with FlpO transgenic allowed to select those mice that carried the *Shank2* modification without NeoR (Fig. RIII-18A-C).

A

	List of primers and expected amplicons from gDNA		
Goal	Primer name	5'-3' Sequence	Fragment size
Shank2 mutation	Shank 2 GF1	GGGATGTCCTGCATACCACC	3,200 (Het & Homo)
	ploxSTOP R1	GTCTGCAGGTCGAGGGACCTA	
Deletion of FRT-NeoR-FRT screening	R_Test_Shank2g_XY	ACAGGGTGGTGAATGCTCAG	0.936 (Het & Homo)
	ploxSTOP R1	GTCTGCAGGTCGAGGGACCTA	
	Shank2 F1	AGGTTCCTTCACAAAGATCCCT	2,566 (with NeoR)
	Shank2 YR1	TCTCTGTTCTGAGTCAAGCATGT	0.687 (NeoR deleted)
	Shank2 F2	ATGGCTGAACTGAGCGAACA	2,273 (with NeoR)
	Shank2 R2	ACACGCTACCAATGAGGTGG	0,394 (NeoR deleted)
FlpO screening	FlpO 1:5	GCTATCGAATTCCACCATGGCTCC AAGAAGAA	1,300 (Tg) - (WT)
	FlpO 2:5	CAATGCGATGAATTCTCAGATCCGC CTCTTGATGTA	

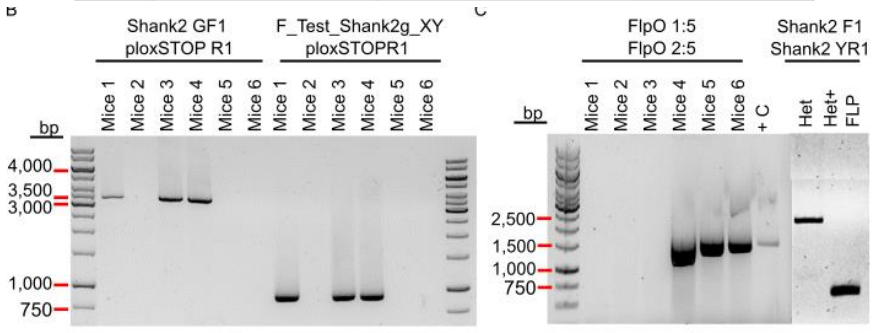

D

Mendelian assessment *Shank2* Het x Het				
	WT	HET	HOMO	TOTAL
Expected	31.75	63.5	31.75	127
Observed	36	78	13	127
Freq. Expected (%)	25	50	25	100
Freq. Observed (%)	28.35	61.42	10.24	100

E

Figure RIII-18. Genotyping of conditional *Shank2*$^{+/-}$ KO colonies of mice and Mendelian transmission assessment. (A) Primer pairs sequences and expected amplicon length. (B) Illustrative PCR to genotype *Shank2* mutation with two different pair of primers. (C) Representative electrophoretic gel showing FLP transgene detection, and the deletion of FRT-NEO-FRT screening by PCR. (D) Table showing the expected and observed genotypes and its frequency for assessment of the modification of the genetic transmission ($p=0.001$; $\chi^2=14.953$ with two degrees of freedom). (E) Chimeric mice with ~80% recombinant cells in right mouse.

As previously detailed in A-Materials and Methods, 2 out of 3 mice colonies could not be maintained. In one case, the progeny turned out to be sterile (that of clone 5E10) and in the other, there was no genetic transmission of the modification (mouse line from clone 9D4). Finally, the third mouse colony derived from high recombinant chimeric mice (8D7; Fig. RIII-18E) was fertile and neither gross morphology alterations were observed, nor the fur colour was the unexpected. Thus, the established mouse line for subsequent analysis derived from ES clone 8D7. Finally, analyses of genotype proportions from litters of mice born from HET x HET mattings (127 typed; Fig. RIII-18D) indicated that there was a non-mendelian transmission of generated *Shank2*$^{+/-}$ conditional mouse line for genetic rescue studies derived from clone 8D7. Indeed, these mice showed a reduced embryonic and postnatal rate of survival of HOMO mice ($p=0.001$; $\chi^2=14.953$).

5.VALIDATION OF THE *SHANK2* KO MOUSE MODEL

The following experiments were conceptualized to validate the developed *Shank2*$^{+/-}$ conditional KO for genetic rescue studies both at the gene and protein expression levels.

5.1 *SHANK2*$^{+/-}$ GENE EXPRESSION ANALYSIS

The expression levels of *Shank2* transcripts were assessed by qPCR. For this purpose, cDNA obtained from whole brain and 2 TaqMan probes for *Shank2* at different positions after the genetic modification were used (Fig. RIII-19A&B). Several housekeeping genes (*Actb, 18S* and *Gapdh)* were tested, with *Actb* being the one selected for normalization of the data. For instance, *18S* housekeeping gene was checked but presented lower Ct values than those achieved by *Shank2* probes, thus it was unsuitable for normalization of *Shank2* data. Also, the efficiency tests in Crb indicated that *Gapdh* was not reliable, since its calibration presented a reduced linearity (R^2=0.78, Fig. RIII-19F). Thus, the efficiency values went out of the desirable range (90 – 110%) for an accurate quantification of gene expression. These assays indicated that the expression levels of *Shank2* from HOMO mice, when normalized with *Actb,* were significantly reduced ($p<0.05$) as compared with WTs (Fig. RIII-19A). This was observed using any of the *Shank2* probes. Finally, although 18S Ct values were low*,* if they were used to normalize *Shank2* expression data obtained with probe Mm00683065_m1 (Fig. RIII-19B), they also reported a significantly reduced *Shank2* expression.

Furthermore, *Shank2* expression was also evaluated in the Crb as the longest protein isoform is found highly expressed in this brain structure (Schmeisser et al. 2012). For this analysis, cDNA from WTs and HOMOs Crbs was used. However, expression levels were not significantly different (data not shown). Nevertheless, unspecific electrophoretic bands were observed from qPCR reactions (Fig. RIII-19D) which did not allow to take these results into account.

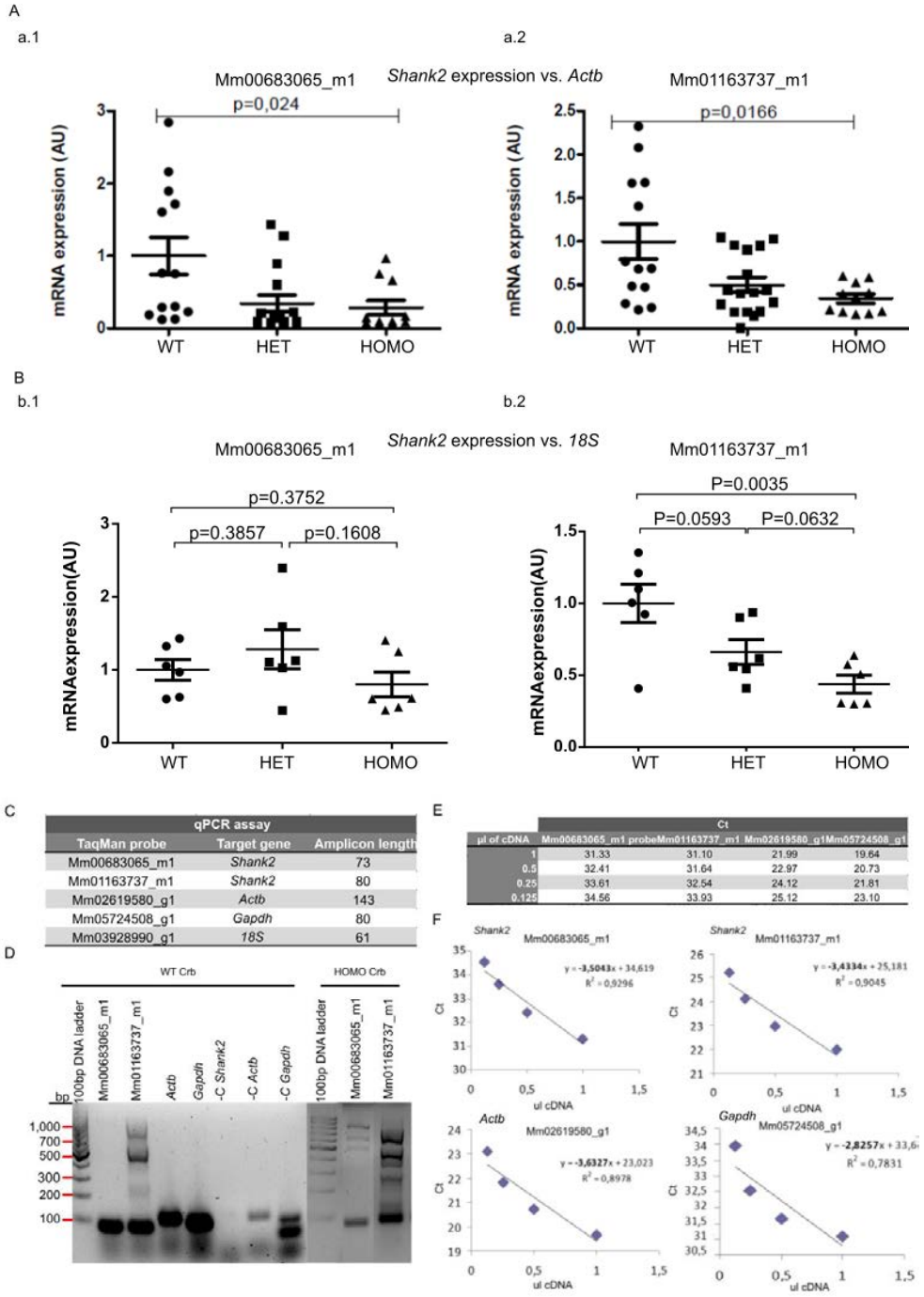

Figure RIII-19. qPCR analysis in Shank2 mice. Forebrain *Shank2* expression normalised by (A) *Actb* (WT n=7; HET n=9; HOMO n=6 biological and at least two technical replicas each) and (B) *18S* RNA (three biological replicas and two technical replicas for each genotype). qPCR with *Shank2* TaqMan probe (a.1) Mm00683065_m1 and (a.2) Mm01163737_m1. Since data didn't follow a normal distribution the Kruskal-Wallis test was applied. Bars indicate S.E.M. (C) Expected amplicon sizes for each TaqMan probe used in qPCR assays. (D) 1% agarose gel showing the unspecific amplicons obtained in the qPCR with cerebellar cDNA. (E) qPCR efficiency evaluation for *Shank2, Actb* and *Gapdh* TaqMan probes used. (F) Pearson correlation calculations. In bold is indicated the "m" of the equation, which show the efficiency of the qPCR.

5.2 VALIDATION OF THE MOUSE MODEL THROUGH SHANK2 IMMUNOBLOTS

As qPCR results could not be completely validated with 2 reference genes, IBs against Shank2 were performed. For these experiments, both PSD fractions and total protein

extracts obtained by 1% DOC solubilization procedure in the latter case, were analysed (Fig. RIII-20). These analyses showed that two different antibodies, sold as specific for Shank2 by differential commercial brands, showed immunoreactivity in all genotypes assessed (HOMO, HET and WTs). Therefore, these data suggest that the expression of Shank2, and that the genetic modification performed failed to achieve its goal. Nonetheless, beyond Shank2 protein there are other proteins (Shank1 and Shank3) making up the Shank family of scaffold proteins. Of note, Shank1 yields at least two isoforms and up to 10 isoforms for Shank3 have been reported (Monteiro and Feng 2017). All these isoforms show high conservation with Shank2 ones. (Lim et al. 1999). Thus, is possible that the antibodies were not specific despite the vendor's report.

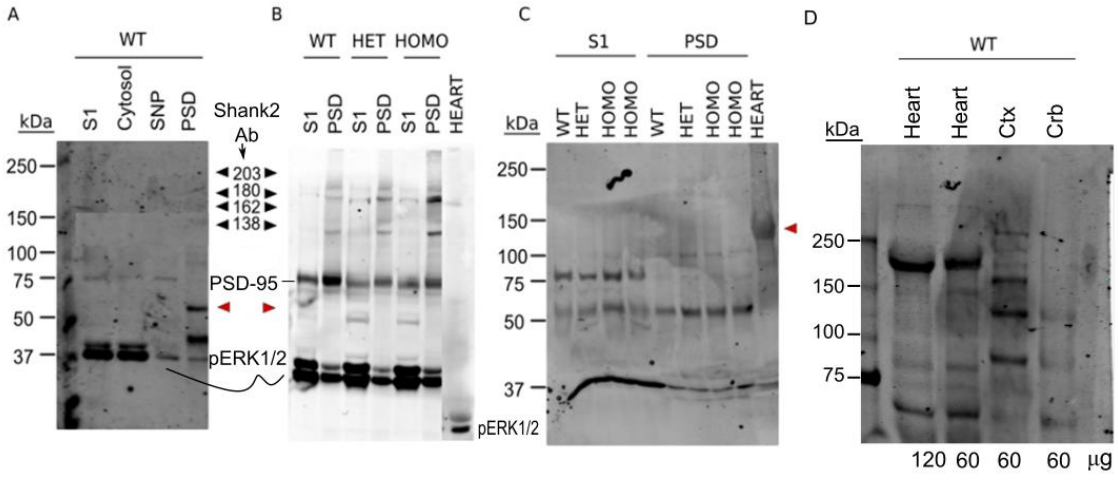

E

	S1			PSD Ctx			PSD Hip	
Protein	WT	HET	HOMO	WT	HET	HOMO	WT	HET
Upper band Shank2	100%	145%	189%	100%	159%	215%	100%	93%
Lower band Shank2	-	-	-	100%	107%	109%	100%	85%
PSD95	100%	78%	73%	100%	82%	57%	100%	56%
pERK1	100%	269%	295%	100%	43%	89%	100%	44%
pERK2	100%	205%	249%	100%	42%	102%	100%	41%

Figure RIII-20. **Immunoblot of Shank2 in total protein extracts and subcellular fractions.** IB of (A) S1, cytosol, SNP and PSD fractions from Hip and (B) genotype comparison of PSD enriched samples from Ctx and corresponding total extracts without nuclei (S1) using USBI041698 antibody. (C) IBs of PSD enriched samples using SC-30192 antibody, and heart sample as a negative control. Black arrowheads indicated expected bands based on Ensembl and NCBI databases whereas red arrowhead shows identified protein bands at unexpected mass weights. PSD-95 and pERK1/2 reblotting are also indicated. (D) Total protein extracts from Ctx and Crb solubilized with 1% DOC are compared with different amounts of negative controls indicated in the bottom of the image using the antibody SC-30192. Red arrowhead strength the antibody unspecific binding in the negative control. (E) Relative amounts of protein bands when USBI041698 antibody was used in S1 and PSD samples from PSD enrichment protocol as well as PSD95; pERK1 and pERK2. As the number of technical replicas were only 2, no statistical analyses were applied, and this data could be only taken as preliminary.

To verify the specificity of the antibodies, other experiments were conducted. Since *Shank1* mRNA is exclusively expressed in brain; *Shank2* mRNA is strongly expressed in brain and at lower levels in liver and kidney, whereas *Shank3* mRNA is expressed

abundantly in heart and moderately in brain and spleen (Lim et al. 1999), protein extracts from heart were prepared and used as a negative control. Surprisingly, one of these two antibodies (SC-30192) turned out to be unspecific for Shank2, as heart samples showed a prominent band, indicative of Shank3 immunoreactivity (Fig. RIII-20D). In contrast, the alignment of the reported epitope used for the second antibody tested (USBI041698) indicated specificity for Shank2. Based on public databases, this antibody should label the following bands: ~250, ~159, ~135 kDa. Yet, as shown in Fig. RIII-20A-B, the immunoreactive bands present in WT samples did not match this pattern. Indeed, IBs showed a faint band of ~180 kDa and another unexpected band below PSD-95 (Fig. R-20B, red arrowhead). These unexpected bands were also observed when HET or HOMO samples were used. In conclusion, these results question the quality of these data and thus, were inconclusive.

To further explore the validity of this mouse model, the expression of other proteins that were reported as altered when Shank2 levels were reduced in haploinsufficient *Shank2* KO mice (Schmessier et al. 2012) or by specific long-lasting *Shank2* silencing through shRNA were assessed (Grabrucker et al. 2011). Among the described altered proteins, pErk levels and PSD-95 were also checked in the present study. These IB data suggested that PSD95 expression at the PSD tended to be reduced in both HET and HOMO samples, whereas pErk1/2 levels tend to be increased in homogenate samples but reduced in PSD fractions. However, these data were taken as preliminary since not enough replicates could be performed (Fig. RIII-20A, B&E).

5.3 GENETICALLY MODIFIED *SHANK2* MOUSE LINE VALIDATION BY GENETIC RESCUE EXPERIMENTS

To assess the loxP functionality and recombinase system *in-vivo*, mice from the *Shank2*$^{+/-}$ conditional KO mouse line was bred with the Cre-line Cg-Tg (CAG-cre/Esr1)54mc/J and the progeny were subjected to genetic rescue experiments. All new-born mice from 2 litters (n=9 pups in total) were treated with TMX. Unfortunately, only one mouse carried the modifications and the Cre transgene (*Shank2*$^{+/-;Cre+/-}$). The PCR assessments before and after TMX administration indicated that the loxP/Cre recombinase system worked, although further analysis will be required to assure this assumption.

A-DISCUSSION

Mutations in *SHANK* family genes have been linked to syndromic and idiopathic ASD as well as other neuropsychiatric and NDDs including SCZ and mild to moderate ID (Gauthier et al. 2009; Sato et al. 2012; Leblond et al. 2014; Sala and Verpelli 2016; Monteiro and Feng 2017). Despite considerable progress has been made in the study of these synaptopathies, it is still required to delineate physiological mechanisms of ASD, and the other NDDs, with the potential for therapeutic application (Monteiro and Feng 2017).

The family of ProSAPs/Shanks includes three paralogs (*Shank1-3*), which build large homo- and heteromeric protein complexes at excitatory synapses and organize the complex protein machinery of the PSD in a laminar fashion (Sheng and Kim 2000; Baron et al. 2006; Grabrucker et al. 2011). Furthermore, depletion of synaptic Shanks causes rapid disassembly of PSDs and the reduction of several postsynaptic molecules including Homer1, PSD-95 and NMDARs (Grabrucker et al. 2011). Different *Shank2*$^{+/-}$ conventional KO models exhibit ASD-like behaviours, including reduced social interaction and social communication by ultrasonic vocalizations, repetitive jumping or anxiety-like phenotypes (Won et al. 2012; Monteiro and Feng, 2012). In addition, these KO mice also show abnormalities in NMDAR activity linked to social dysfunctions, fewer dendritic spines (Won et al. 2012; Schmeissier et al. 2012) and spatial memory deficits (Lim et al. 2017). Although a key synaptic role of Shanks is supported by these studies, the dynamics of the synaptic proteome due to *Shank2*$^{+/-}$ haploinsufficiency still remains to be clarified. Hence, the state of the art for Shank2 and NDDs drove us to conceptualize and develop a conditional *Shank2* KO mouse model for genetic rescue experiments.

1. COMPARISON BETWEEN MOUSE MODELS

Both conventional *Shank2* KO mouse models that have been reported were generated by removing exons 16-17 or exon 17, respectively (Schmeissier et al. 2012; Won et al. 2012; Monteiro and Feng, 2017), whereas in this study, is introuced a genetic construct was introduced into intron 16-17 to allow rescue experiments. Additionally, 129 SvJ or 129 SvR1 ESC were used in both cases despite C57BL/6 is one of the best characterized inbred strains of mice and is the reference strain for the mouse genome sequence (Mouse Genome Sequencing Consortium, 2002). Since the reliance on 129 ES cells is not ideal, particularly for genetic studies of immunology, neurobiology and physiology (Pettitt et al.

2009), we sought to develop a KO mouse with a C57BL/6 background, better suited for the large-scale phenotyping efforts that will follow.

Beyond the fact that the development of a *Shank2*$^{+/-}$ conditional KO mice for genetic rescue experiments would serve to study both the synaptic and behavioural roles of *Shank2* in C57BL/6 genetic background, it would also be the first mice model reported up to date to evaluate the ability to recover such specific *Shank2*$^{+/-}$-related dysfunctions by its rescued expression. The resulting phenotype assessments will provide valuable information not only on the mechanism operated by Shank2 and in general Shank family of proteins, but also by other molecular entities associated to synaptopathies. Hence, it will represent a step forward on the understanding of mechanisms by which ASD and other related NDDs arise.

2. VALIDITIES OF *SHANK2*$^{+/-}$ CONDITIONAL KO FOR GENETIC RESCUE STUDIES

The mouse line developed accomplishes a set of the following 5 major criteria: homological validity which group species validity and strain validity; pathogenic or construct validity; mechanistic validity; face validity (including ethological and biomarker validity) and predictive validity (Belzung and Lemoine 2011; Greene-Schloesser et al. 2011). Particularly, Belzung and Lemoine (2011) defined: 1) homological validity as the need of an adequate selection of specie and strain to model a given disorder. In the subcategory of the species validity, primates will be considered to have a higher score than drosophila, whereas when considering strain validity, strains that have a wide repertoire of pup care, scores higher than strains that in normal conditions are more limited to show such behaviours; 2) pathological validity corresponds to the fact that, in order to shape pathological characteristics, the organism has been manipulated both during the developmental period and/or during adulthood depending on the model. For instance, to test if there is a correlation between ASD and vaccines it should be administered the compounds in equivalent human ages; 3) mechanistic or construct validity is defined by the fact that the cognitive (e.g., cognitive bias) or biological mechanisms (e.g., dysfunction of social behaviour) underlying the disorder are identical in both humans and animals; 4) face validity corresponds to the observable behavioural (ethological validity) or biological outcomes (biomarker validity). For example, ultrasonic vocalization and pup retrieval behaviour (ethological validity) or reduced Shank2 expression (biomarker validity). Finally, 5) predictive validity matches to the identity of the relationship between the triggering factor and the outcome which is particularly referred as induction validity. Also, the similarities on the effects of a treatment between the model and humans fall into this category.

Regarding the homological validity, the strain used should score better than previous KO lines, since it has been developed in JM8A1.N3 ES cells coming from mouse strain C57BL/6N-A^{tm1Brd,} which is much more studied and better characterised for neuroscience research. Also, construct validity is accomplished by this model, because *Shank2* was modified so that animals become haploinsufficient, as it occurs with pathological human mutations (Leblond et al. 2012). Yet, this mouse line is not reproducing exact SHANK2 pathogenic mutations. Conversely, face predictive and mechanistic validities remain to be determined. Notwithstanding, predictive validity will likely be accomplished as mice were designed to conduct genetic rescue therapies to assess PSD proteome alterations and behavioural rescue abilities, similar to the experiments conducted in chapter II for *Syngap1*. Also, because the PSDs proteomes between mice and humans show a high

degree of conservation, it is expected a high score in the predictive validity (Bayés et al. 2012).

2.1 ASSESSMENT OF THE CONSTRUCT VALIDITY

Our gene-targeting strategy and mice obtained meet the expected outcomes (Pettitt et al. 2009). Namely, these cells possess a normal male (XY) karyotype. Also, injections of early-passage ESC into albino C57BL/6-*Tyr*$^{c\text{-}Brd}$ blastocysts produced chimeras with high coat colour chimerism (> 79%) and a sex distortion in favour of males and a high proportion of chimeras with a high contribution to both somatic and germline tissues were accomplished. Indeed, >50% of the chimeras were male, indicating that sex-conversion of female host blastocysts had occurred in a high proportion of cases, which is a good indicative of the procedure (Pettitt et al. 2009; Fielder et al. 2012). Furthermore, if the targeted ESC clone contributes to the development of the foetus, the pups produced will be chimeras, exhibiting patches of coat colour from the host embryo and patches from the injected ES clone. Particularly, JM8A1.N3 ESCs were modified to correct the black mutation on the agouti allele, thus chimeric mice derived from these cells are expected to have patches of agouti coat colour spread within white colour derived from pure albino blastocyst cells. These expected “colour code” chimeras were always obtained.

Moreover, as most targeted ESCs were heterozygous for the modification, it could be expected about half of the coat-colour germline pups to test positive, this was indeed the case. To determine if the ESCs could contribute to the germline of the chimera and produce offspring with *Shank2* modification without NeoR *cassette*, chimeric mice were crossed with FlpO C57BL/6 transgenic mice. In the case of the mouse line coming from the 5E10 clone, all resulting mice were obese and sterile and whenever a litter with the expected colour coat was obtained, the ESC modification was not transmitted to the progeny. In contrast, litters from chimeric mice derived from 8D7 and 9D4 ESC clones crossed with Flp transgenic mice were not sterile. Nevertheless, only 8D4 ESC-derived mice with NeoR deletion gave birth to pups with the expected genotype and colour coat in all generations (Fig. DIII-1), since 9D4 ESC-derived mice from the second generation (F2) gave birth to unexpected white pups. This could be explained by a mutagenesis phenomenon related to genes of colour coat or likely to another complex genetic mechanism. It is difficult to hypothesize which genetic mechanism operated to explain this phenomenon, as our unexpected white mice arose from the breeding of agouti or black *Shank2*$^{+/-;NeoR-/-}$ with black (aa) C57BL/6. Therefore, only black or agouti mice were expected (Fig. DIII-1).

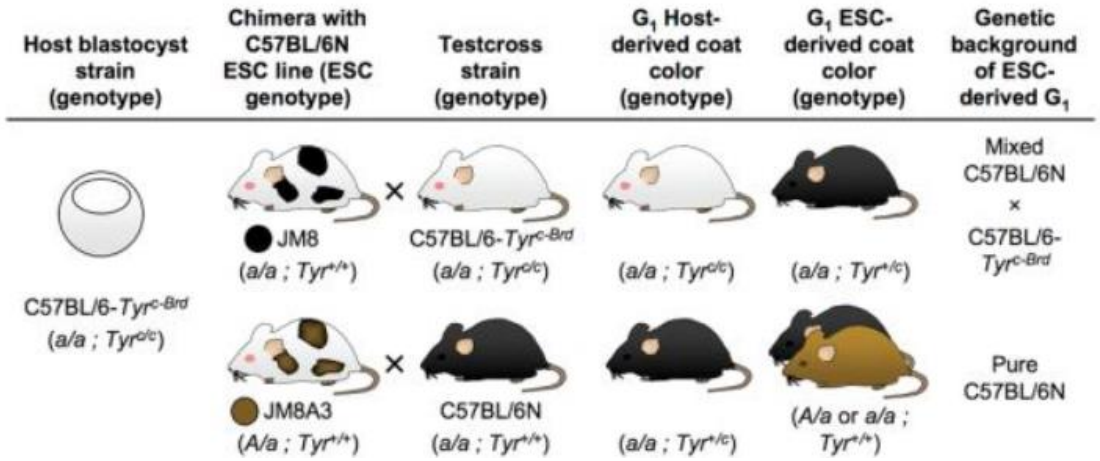

Figure DIII-1. Expected genotypes derived from agouti ESCs grown in albino blastocysts. This figure is obtained from Pettitt et al. 2009.

2.2 MENDELIAN TRANSMISSION ASSESSMENT

Based on the previous information, the only final *Shank2* conditional mice colony reliable that was further maintained for subsequent analysis came from pure C57BL/6N mice derived from clone 8D7 whose *Shank2*$^{+/-;NeoR-/-}$ genotype matched with NeoR deletion. Subsequently, we further assessed the validity of this mouse model by assessing whether the genetic modification followed Mendelian transmission from HET x HET inbreed breeding. This assessment was done considering the genotype of PND21, or older mice, and showed that there was non-Mendelian transmission, as the number of HOMOs was lower than expected. These results agree with the lower survival reported for a *Shank2*$^{-/-}$ conventional KO mice (Schmessier et al. 2012) and mirror what has been reported for other KO mouse models of postsynaptic proteins such as *Syngap1* which, in homozygosity, is lethal (Vazquez et al. 2004; Porter et al. 2005). In addition, Schmeissier and co-workers, reported also that *Shank2* mutants displayed normal appearance and overall brain morphology was not abnormal. In line with their findings, the *Shank2*$^{+/-}$ conditional KO mice developed here also presented no gross abnormalities in the brain morphology of HOMO and HET mice.

2.3 ASSESSMENT OF THE FACE AND MECHANISTIC VALIDITY

Shank2 expression in forebrain was evaluated by qPCR and the expression in HETs and HOMOs matched with the one reported by Won et al. 2012. However, this could only be observed for one of the two selected reference genes (*Actb*). This result could be the consequence of the unsuitability of *18S* reference gene since it showed a Ct quite different than average Ct for *Shank2* expression. Furthermore, cDNA from Crb was obtained to further assess *Shank2* expression as the longest Shank2 isoform (Shank2E) has been reported to be abundantly expressed in mouse Crb (Leblond et al. 2012; Schmeissier et

al. 2012). Yet, no significant expression differences between WT and HOMO samples were found. This contradictory result could be related to the fact that both *Shank2* TaqMan probes appear not to be specific in Crb as some unspecific bands were identified when qPCR products were run in agarose gels. In addition, a lower number of samples (n=3) than for whole brain (n≥6 with several technical replicas) was used to compare the expression levels, which could hamper statistical analysis. Finally, the Ct values were quite high (Ct=~31-32) meaning that its expression in Crb must be low, matching with the reported specific expression of *Shank2* in Purkinje cells (Monteiro and Feng, 2017) and a low abundance of the expression of synaptic proteins in Crb compared to forebrain (Cheng et al. 2006). Hence, an enrichment of Purkinje cells prior to RNA extraction and a repetition of the qPCR using a better suitable housekeeping gene for Crb, could provide reliable data that match with the *Shank2* expression results from whole brain.

At the protein level, Shank2 analyses did not clarify this previous controversial result. First, the specificity of one of the assessed antibodies (SC-30192) was questioned. Despite Shank2 has not been reported to be expressed in heart, a prominent immunoreactivity for this antibody in heart extracts was seen matching with the prominent expression of Shank3 in this tissue (Lim et al. 1999; Monteiro and Feng, 2017). Conversely, the other antibody used did not show immunoreactivity in heart samples. Accordingly, its epitope alignment with the reported Shank1, 2, and 3 isoforms showed specificity for Shank2 proteins. However, despite it would be more specific, IBs from hippocampal PSD did not show immunoreactivity at the expected high mass weights. Also, genotype comparison of S1 and PSD enriched fractions from Ctx indicated that PSDs were enriched in bands from ~135-180 kDa. Strikingly, the band intensity of Shank2 in HOMO HET and WT samples decrease progressively between these genotypes, respectively. In addition, there was unexpected staining in low mass weights.

This unexpected higher intensities in HOMO and HET compared to WT samples suggest two hypotheses: 1) the antibody also recognized other Shank paralogues. Since a compensatory mechanism by Shank3 in *Shank2*$^{-/-}$ mice has been reported, it could explain that the highest intensity of Shank2 antibody immunoreactivity was found in the HOMO band. Yet, no bands in heart samples were found but it is possible that not all 10 Shank3 isoforms are expressed in heart like in different brain regions/cell types (Monteiro and Feng, 2017); or 2) it is possible that *Shank2* modification is not working as expected. For instance, the modification introduced foster more promotor activity and expression of *Shank2* gene instead. Thus, it could explain this qualitative increased level seen in independent IBs. Whatsoever the reason of these disagreements, the face and mechanistic validities of the model remained to be confirmed.

In an attempt to found indirect evidences to prove these validities, the expression of PSD-95, pErk1 and pErk2 proteins were also assessed because they were found altered in one of the *Shank2*$^{+/-}$ reported KO models (Grabrucker et al. 2011; Schmeissier et al. 2012). Although these analyses were preliminary as only two technical replicas could be conducted, PSD-95 levels were reduced due to *Shank2* haploinsufficiency in both S1 and PSDs. Accordingly, PSD-95 levels in rat PSDs from hippocampal primary cultures were reduced after *Shank2* knock-down (Grabrucker et al. 2011), but disagree with the unaltered PSD-95 levels found in whole brain homogenates from *Shank2* conventional KO mice (Won et al. 2012). Moreover, pErk1/2 levels in whole brain homogenates were reported to be significantly reduced in HOMO *vs.* WT mice (Won et al. 2012). On one hand, the present data indicates the opposite, as an increased level of pERK1/2 in S1 fraction was seen. On the other hand, agree with the reduced levels of pErks trend seen at the PSD of Ctx and Hip from HET mice. Collectively, these data suggest differences in the expression or phosphorylation degree of other synaptic proteins in *Shank2*$^{+/-}$ conditional KO mice line for genetic rescue experiment. Yet, these assumptions need to be further confirmed.

3. FUTURE DIRECTIONS

The studies from this annex showed that the developed *Shank2*$^{+/-}$ conditional KO mice model for genetic rescue experiments follow a non-Mendelian transmission of the modification with a reduced *Shank2* expression in the brain of HET and HOMO mice. Also, possible changes in synaptic proteins due to *Shank2* modification could be expected. Finally, Cre/TMX system worked only in one mouse when *Shank2*$^{+/-}$ reactivation was tested *in-vivo*. Collectively, this data support somehow that the present mouse model derived from 8D7 ESC clone, could be valid for future studies. However, further analyses will be required to corroborate this assumption. To this purpose, an on-going Shank2 relative quantification by LC-MS/MS analysis using WT, HET and HOMO PSD samples from whole brain, Ctx and Hip would shed light on the usefulness of this *Shank2*$^{+/-}$ mouse model.

COLLABORATIONS

1. Bars-Cortina, David, Antoni Riera-Escamilla, **Gemma Gou**, Carme Piñol-Felis, and María-José Motilva. 2019. 'Design, Optimization and Validation of Genes Commonly Used in Expression Studies on DMH/AOM Rat Colon Carcinogenesis Model'. PeerJ 7: e6372. PubMed PMID: 30713822.

2. Ramos-Vicente, David, Jie Ji, Esther Gratacòs-Batlle, **Gemma Gou**, Rita Reig-Viader, Javier Luís, Demian Burguera, et al. 2018. 'Metazoan Evolution of Glutamate Receptors Reveals Unreported Phylogenetic Groups and Divergent Lineage-Specific Events'. ELife 7. PubMed PMID: 30465522.

3. Kopanitsa, Maksym V., **Gemma Gou**, Nurudeen O. Afinowi, Àlex Bayés, Seth G. N. Grant, and Noboru H. Komiyama. 2018 'Chronic treatment with a MEK inhibitor reverses enhanced excitatory field potentials in *Syngap1*$^{+/-}$ mice'. Pharmacol Rep.;70(4):777-783. PubMed PMID: 29940508.

4. Bayés, Àlex, Mark O. Collins, Rita Reig-Viader, **Gemma Gou**, David Goulding, Abril Izquierdo, Jyoti S. Choudhary, Richard D. Emes, and Seth G. N. Grant. 2017 'Evolution of complexity in the zebrafish synapse proteome'. Nat Commun. Mar 2; 8:14613. PubMed Central PMCID: PMC5337974.

5. Bayés, Àlex, Mark O. Collins, Clare M. Galtrey, Clémence Simonnet, Marcia Roy, Mike D. R. Croning, **Gemma Gou**, et al. 2014 'Human post-mortem synapse proteome integrity screening for proteomic studies of postsynaptic complexes'. Mol Brain.; 7:88. PubMed Central PMCID: PMC4271336.

BIBLIOGRAPHY

Aarts, Michelle, Yitao Liu, Lidong Liu, Shintaro Besshoh, Mark Arundine, James W. Gurd, Yu-Tian Wang, Michael W. Salter, and Michael Tymianski. 2002. 'Treatment of Ischemic Brain Damage by Perturbing NMDA Receptor- PSD-95 Protein Interactions'. Science 298 (5594): 846–50. https://doi.org/10.1126/science.1072873.

Abbott, L F, and Sacha B Nelson. 2000. 'Synaptic Plasticity: Taming the Beast' 3: 6.

Aceti, Massimiliano, Thomas K. Creson, Thomas Vaissiere, Camilo Rojas, Wen-Chin Huang, Ya-Xian Wang, Ronald S. Petralia, Damon T. Page, Courtney A. Miller, and Gavin Rumbaugh. 2015. 'Syngap1 Haploinsufficiency Damages a Postnatal Critical Period of Pyramidal Cell Structural Maturation Linked to Cortical Circuit Assembly'. Biological Psychiatry 77 (9): 805–15. https://doi.org/10.1016/j.biopsych.2014.08.001.

Adrian, Max, Remy Kusters, Corette J. Wierenga, Cornelis Storm, Casper C. Hoogenraad, and Lukas C. Kapitein. 2014. 'Barriers in the Brain: Resolving Dendritic Spine Morphology and Compartmentalization'. Frontiers in Neuroanatomy 8 (December). https://doi.org/10.3389/fnana.2014.00142.

Aebersold, Ruedi, Alma L. Burlingame, and Ralph A. Bradshaw. 2013. 'Western Blots versus Selected Reaction Monitoring Assays: Time to Turn the Tables?' *Molecular & Cellular Proteomics : MCP* 12 (9): 2381–82. https://doi.org/10.1074/mcp.E113.031658.

Afroze, Bushra, and Bushra Chaudhry. 2013. 'Genetics of Non-Syndromic Autosomal Recessive Mental Retardation'. JPMA. The Journal of the Pakistan Medical Association 63 (1): 106–10.

Ahmari, Susanne E., Victoria B. Risbrough, Mark A. Geyer, and H. Blair Simpson. 2012. 'Impaired Sensorimotor Gating in Unmedicated Adults with Obsessive–Compulsive Disorder'. *Neuropsychopharmacology* 37 (5): 1216–23. https://doi.org/10.1038/npp.2011.308.

Ahmed, Sohail, Wah Ing Goh, and Wenyu Bu. 2010. 'I-BAR Domains, IRSp53 and Filopodium Formation'. *Seminars in Cell & Developmental Biology*, Membrane Curvature, 21 (4): 350–56. https://doi.org/10.1016/j.semcdb.2009.11.008.

Airaksinen, Eila M., Riitta Matilainen, Tarja Mononen, Kirsi Mustonen, Juhani Partanen, Veikko Jokela, and Pirjo Halonen. 2000. 'A Population-Based Study on Epilepsy in Mentally Retarded Children'. Epilepsia 41 (9): 1214–20. https://doi.org/10.1111/j.1528-1157.2000.tb00328.x.

Alfieri, Paolo, Giorgia Piccini, Cristina Caciolo, Francesca Perrino, Maria Luigia Gambardella, Maria Mallardi, Laura Cesarini, et al. 2014. 'Behavioral Profile in RASopathies'. American Journal of Medical Genetics. Part A 164A (4): 934–42. https://doi.org/10.1002/ajmg.a.36374.

Allely, C. S. 2013. 'Pain Sensitivity and Observer Perception of Pain in Individuals with Autistic Spectrum Disorder'. Research article. The Scientific World Journal. 2013. https://doi.org/10.1155/2013/916178.

Allen, John A., Robyn A. Halverson-Tamboli, and Mark M. Rasenick. 2007. 'Lipid Raft Microdomains and Neurotransmitter Signalling'. Nature Reviews Neuroscience 8 (2): 128–40. https://doi.org/10.1038/nrn2059.

Altman, Joseph. n.d. 'Postnatal Development of the Cerebellar Cortex in the Rat. II. Phases in the Maturation of Purkinje Cells and of the Molecular Layer'. Journal of Comparative Neurology 145 (4): 399–463. https://doi.org/10.1002/cne.901450402.

American Psychiatric Association. Diagnostic and Statistical Manual of Mental Disorders. 4. Washington, DC: American Psychiatric Publishing; 2000. Text Revision (DSM-IVTR)

Amir, R. E., I. B. Van den Veyver, M. Wan, C. Q. Tran, U. Francke, and H. Y. Zoghbi. 1999. 'Rett Syndrome Is Caused by Mutations in X-Linked MECP2, Encoding Methyl-CpG-Binding Protein 2'. Nature Genetics 23 (2): 185–88. https://doi.org/10.1038/13810.

Andersen, Susan L. 2003. 'Trajectories of Brain Development: Point of Vulnerability or Window of Opportunity?' Neuroscience & Biobehavioral Reviews, Brain Development, Sex Differences and Stress: Implications for Psychopathology, 27 (1): 3–18. https://doi.org/10.1016/S0149-7634(03)00005-8.

Anfinsen, Christian B. 1973. 'Principles That Govern the Folding of Protein Chains'. *Science* 181 (4096): 223–30.

Antonopoulos, J., I. Dori, A. Dinopoulos, M. Chiotelli, and J. G. Parnavelas. 2002. 'Postnatal Development of the Dopaminergic System of the Striatum in the Rat'. *Neuroscience* 110 (2): 245–56. https://doi.org/10.1016/S0306-4522(01)00575-9.

Aoki, Kiyoko F., and Minoru Kanehisa. 2005. 'Using the KEGG Database Resource'. *Current Protocols in Bioinformatics* 11 (1): 1.12.1-1.12.54. https://doi.org/10.1002/0471250953.bi0112s11.

Aoki, Yoko, Tetsuya Niihori, Shin-ichi Inoue, and Yoichi Matsubara. 2016. 'Recent Advances in RASopathies'. Journal of Human Genetics 61 (1): 33–39. https://doi.org/10.1038/jhg.2015.114.

Araki, Yoichi, Menglong Zeng, Mingjie Zhang, and Richard L. Huganir. 2015. 'Rapid Dispersion of SynGAP from Synaptic Spines Triggers AMPA Receptor Insertion and Spine Enlargement during LTP'. Neuron 85 (1): 173–89. https://doi.org/10.1016/j.neuron.2014.12.023.

Arellano, Jon I., Ruth Benavides-Piccione, Javier DeFelipe, and Rafael Yuste. 2007. 'Ultrastructure of Dendritic Spines: Correlation between Synaptic and Spine Morphologies'. Frontiers in Neuroscience 1. https://doi.org/10.3389/neuro.01.1.1.010.2007.

Artigas-Pallares, Josep, and Isabel Paula. 2012. 'El Autismo 70 Años Después de Leo Kanner y Hans Asperger'. Revista de La Asociación Española de Neuropsiquiatría 32 (115): 567–87. https://doi.org/10.4321/S0211-57352012000300008.

Artola, Alain, Josefien C. von Frijtag, Patrick C. J. Fermont, Willem Hendrik Gispen, Loes H. Schrama, Amer Kamal, and Berry M. Spruijt. 2006. 'Long-Lasting Modulation of the Induction of LTD and LTP in Rat Hippocampal CA1 by Behavioural Stress and Environmental Enrichment'. The European Journal of Neuroscience 23 (1): 261–72. https://doi.org/10.1111/j.1460-9568.2005.04552.x.

Asaki, Chie, Nobuteru Usuda, Ayami Nakazawa, Kiyokazu Kametani, and Tatsuo Suzuki. 2003. 'Localization of Translational Components at the Ultramicroscopic Level at Postsynaptic Sites of the Rat Brain'. *Brain Research* 972 (1): 168–76. https://doi.org/10.1016/S0006-8993(03)02523-X.

Ashby, Michael C., Susie R. Maier, Atsushi Nishimune, and Jeremy M. Henley. 2006. 'Lateral Diffusion Drives Constitutive Exchange of AMPA Receptors at Dendritic Spines and Is Regulated by Spine Morphology'. The Journal of Neuroscience: The Official Journal of the Society for Neuroscience 26 (26): 7046–55. https://doi.org/10.1523/JNEUROSCI.1235-06.2006.

Ashwood, Paul, Sharifia Wills, and Judy Van de Water. 2006. 'The Immune Response in Autism: A New Frontier for Autism Research'. *Journal of Leukocyte Biology* 80 (1): 1–15. https://doi.org/10.1189/jlb.1205707.

Avery, Adam W., Claudia Figueroa, and Anne B. Vojtek. 2007. 'UNC-51-like Kinase Regulation of Fibroblast Growth Factor Receptor Substrate 2/3'. Cellular Signalling 19 (1): 177–84. https://doi.org/10.1016/j.cellsig.2006.06.003.

Babicki, Sasha, David Arndt, Ana Marcu, Yongjie Liang, Jason R. Grant, Adam Maciejewski, and David S. Wishart. 2016. 'Heatmapper: Web-Enabled Heat Mapping for All'. *Nucleic Acids Research* 44 (W1): W147-153. https://doi.org/10.1093/nar/gkw419.

Bale, Tracy L., Tallie Z. Baram, Alan S. Brown, Jill M. Goldstein, Thomas R. Insel, Margaret M. McCarthy, Charles B. Nemeroff, et al. 2010. 'Early Life Programming and Neurodevelopmental Disorders'. Biological Psychiatry 68 (4): 314–19. https://doi.org/10.1016/j.biopsych.2010.05.028.

Baloch, Sajjad, Ragini Verma, Hao Huang, Parmeshwar Khurd, Sarah Clark, Paul Yarowsky, Ted Abel, Susumu Mori, and Christos Davatzikos. 2009. 'Quantification of Brain Maturation and Growth Patterns in C57BL/6J Mice via Computational Neuroanatomy of Diffusion Tensor Images'. Cerebral Cortex (New York, N.Y.: 1991) 19 (3): 675–87. https://doi.org/10.1093/cercor/bhn112.

Banke, T. G., D. Bowie, H.-K. Lee, R. L. Huganir, A. Schousboe, and S. F. Traynelis. 2000. 'Control of GluR1 AMPA Receptor Function by CAMP-Dependent Protein Kinase'. Journal of Neuroscience 20 (1): 89–102. https://doi.org/10.1523/JNEUROSCI.20-01-00089.2000.

Baranek, Grace T., Fabian J. David, Michele D. Poe, Wendy L. Stone, and Linda R. Watson. 2006. 'Sensory Experiences Questionnaire: Discriminating Sensory Features in Young Children with Autism, Developmental Delays, and Typical Development'. Journal of Child Psychology and Psychiatry, and Allied Disciplines 47 (6): 591–601. https://doi.org/10.1111/j.1469-7610.2005.01546.x.

Barbosa-Morais, Nuno L., Manuel Irimia, Qun Pan, Hui Y. Xiong, Serge Gueroussov, Leo J. Lee, Valentina Slobodeniuc, et al. 2012. 'The Evolutionary Landscape of Alternative Splicing in Vertebrate Species'. *Science (New York, N.Y.)* 338 (6114): 1587–93. https://doi.org/10.1126/science.1230612.

Bardoni, Barbara, and Sabiha Abekhoukh. 2014. 'CYFIP Family Proteins between Autism and Intellectual Disability: Links with Fragile X Syndrome'. Frontiers in Cellular Neuroscience 8. https://doi.org/10.3389/fncel.2014.00081.

Barker, Alison J., and Erik M. Ullian. 2010. 'Astrocytes and Synaptic Plasticity'. The Neuroscientist: A Review Journal Bringing Neurobiology, Neurology and Psychiatry 16 (1): 40–50. https://doi.org/10.1177/1073858409339215.

Barnes, Stephanie A., Lasani S. Wijetunge, Adam D. Jackson, Danai Katsanevaki, Emily K. Osterweil, Noboru H. Komiyama, Seth G.N. Grant, et al. 2015. 'Convergence of Hippocampal Pathophysiology in Syngap+/− and Fmr1−/y Mice'. The Journal of Neuroscience 35 (45): 15073–81. https://doi.org/10.1523/JNEUROSCI.1087-15.2015.

Barnes, Stephanie A., Lasani S. Wijetunge, Adam D. Jackson, Danai Katsanevaki, Emily K. Osterweil, Noboru H. Komiyama, Seth G.N. Grant, et al. 2015. 'Convergence of Hippocampal Pathophysiology in Syngap+/− and Fmr1−/y Mice'. *The Journal of Neuroscience* 35 (45): 15073–81. https://doi.org/10.1523/JNEUROSCI.1087-15.2015.

Barnett, M. W. 2006. 'Synaptic Ras GTPase Activating Protein Regulates Pattern Formation in the Trigeminal System of Mice'. Journal of Neuroscience 26 (5): 1355–65. https://doi.org/10.1523/JNEUROSCI.3164-05.2006.

Barnett, M. W. 2006. 'Synaptic Ras GTPase Activating Protein Regulates Pattern Formation in the Trigeminal System of Mice'. *Journal of Neuroscience* 26 (5): 1355–65. https://doi.org/10.1523/JNEUROSCI.3164-05.2006.

Baron, Marisa K., Tobias M. Boeckers, Bianca Vaida, Salem Faham, Mari Gingery, Michael R. Sawaya, Danielle Salyer, Eckart D. Gundelfinger, and James U. Bowie. 2006. 'An Architectural Framework That May Lie at the Core of the Postsynaptic Density'. *Science* 311 (5760): 531–35. https://doi.org/10.1126/science.1118995.

Barria, Andres, and Roberto Malinow. 2005. 'NMDA Receptor Subunit Composition Controls Synaptic Plasticity by Regulating Binding to CaMKII'. Neuron 48 (2): 289–301. https://doi.org/10.1016/j.neuron.2005.08.034.

Bartel, David P. 2009. 'MicroRNAs: Target Recognition and Regulatory Functions'. *Cell* 136 (2): 215–33. https://doi.org/10.1016/j.cell.2009.01.002.

Bartels, Frederik, Harald Prüss, and Carsten Finke. 2018. 'Anti-ARHGAP26 Autoantibodies Are Associated With Isolated Cognitive Impairment'. *Frontiers in Neurology* 9. https://doi.org/10.3389/fneur.2018.00656.

Bartos, Marlene, Imre Vida, and Peter Jonas. 2007. 'Synaptic Mechanisms of Synchronized Gamma Oscillations in Inhibitory Interneuron Networks'. *Nature Reviews Neuroscience* 8 (1): 45–56. https://doi.org/10.1038/nrn2044.

Bassani, Silvia, Alessandra Folci, Jonathan Zapata, and Maria Passafaro. 2013. 'AMPAR Trafficking in Synapse Maturation and Plasticity'. Cellular and Molecular Life Sciences 70 (23): 4411–30. https://doi.org/10.1007/s00018-013-1309-1.

Bateman, Alex, Maria Jesus Martin, Claire O'Donovan, Michele Magrane, Emanuele Alpi, Ricardo Antunes, Benoit Bely, et al. 2017. 'UniProt: The Universal Protein Knowledgebase'. *Nucleic Acids Research* 45 (D1): D158–69. https://doi.org/10.1093/nar/gkw1099.

Bayer, K. Ulrich, and Howard Schulman. 2001. 'Regulation of Signal Transduction by Protein Targeting: The Case for CaMKII'. Biochemical and Biophysical Research Communications 289 (5): 917–23. https://doi.org/10.1006/bbrc.2001.6063.

Bayés, Alex, and Seth G. N. Grant. 2009. 'Neuroproteomics: Understanding the Molecular Organization and Complexity of the Brain'. Nature Reviews. Neuroscience 10 (9): 635–46. https://doi.org/10.1038/nrn2701.

Bayés, Àlex, and Seth G. N. Grant. 2016. 'Chapter 6 - Synapse Proteomes and Disease: The MASC Paradigm'. In Neuronal and Synaptic Dysfunction in Autism Spectrum Disorder and Intellectual Disability, edited by Carlo Sala and Chiara Verpelli, 85–99. San Diego: Academic Press. https://doi.org/10.1016/B978-0-12-800109-7.00006-6.

Bayés, Alex, Mark O. Collins, Mike D. R. Croning, Louie N. van de Lagemaat, Jyoti S. Choudhary, and Seth G. N. Grant. 2012. 'Comparative Study of Human and Mouse Postsynaptic Proteomes Finds High Compositional Conservation and Abundance Differences for Key Synaptic Proteins'. PloS One 7 (10): e46683. https://doi.org/10.1371/journal.pone.0046683.

Bayés, Àlex, Mark O. Collins, Rita Reig-Viader, Gemma Gou, David Goulding, Abril Izquierdo, Jyoti S. Choudhary, Richard D. Emes, and Seth G. N. Grant. 2017. 'Evolution of Complexity in the Zebrafish Synapse Proteome'. Nature Communications 8 (March). https://doi.org/10.1038/ncomms14613.

Bear, M. F., and A. Kirkwood. 1993. 'Neocortical Long-Term Potentiation'. Current Opinion in Neurobiology 3 (2): 197–202.

Belluscio, Leonardo, and Diana M. Cummings. 2008. 'Charting Plasticity in the Regenerating Maps of the Mammalian Olfactory Bulb'. *The Neuroscientist* 14 (3): 251–63. https://doi.org/10.1177/1073858408315026.

Belov, Artur A., and Moosa Mohammadi. 2013. 'Molecular Mechanisms of Fibroblast Growth Factor Signaling in Physiology and Pathology'. Cold Spring Harbor Perspectives in Biology 5 (6). https://doi.org/10.1101/cshperspect.a015958.

Belzung, Catherine, and Maël Lemoine. 2011. 'Criteria of Validity for Animal Models of Psychiatric Disorders: Focus on Anxiety Disorders and Depression'. *Biology of Mood & Anxiety Disorders* 1 (1): 9. https://doi.org/10.1186/2045-5380-1-9.

Ben-Ari, Yehezkel, Ilgam Khalilov, Kristopher T. Kahle, and Enrico Cherubini. 2012. 'The GABA Excitatory/Inhibitory Shift in Brain Maturation and Neurological Disorders'. The Neuroscientist 18 (5): 467–86. https://doi.org/10.1177/1073858412438697.

Ben-Ari, Yehezkel. 2002. 'Excitatory Actions of Gaba during Development: The Nature of the Nurture'. Nature Reviews. Neuroscience 3 (9): 728–39. https://doi.org/10.1038/nrn920.

Benavides-Piccione, Ruth, Isabel Fernaud-Espinosa, Victor Robles, Rafael Yuste, and Javier DeFelipe. 2013. 'Age-Based Comparison of Human Dendritic Spine Structure Using Complete Three-Dimensional Reconstructions'. Cerebral Cortex (New York, N.Y.: 1991) 23 (8): 1798–1810. https://doi.org/10.1093/cercor/bhs154.

Bender, Kevin J., Juliana Rangel, and Daniel E. Feldman. 2003. 'Development of Columnar Topography in the Excitatory Layer 4 to Layer 2/3 Projection in Rat Barrel Cortex'. *The Journal of Neuroscience: The Official Journal of the Society for Neuroscience* 23 (25): 8759–70.

Beneken, Jutta, Jian Cheng Tu, Bo Xiao, Mutsuo Nuriya, Joseph P. Yuan, Paul F. Worley, and Daniel J. Leahy. 2000. 'Structure of the Homer EVH1 Domain-Peptide Complex Reveals a New Twist in Polyproline Recognition'. *Neuron* 26 (1): 143–54. https://doi.org/10.1016/S0896-6273(00)81145-9.

Beneyto, Monica, Lars V. Kristiansen, Akinwunmi Oni-Orisan, Robert E. McCullumsmith, and James H. Meador-Woodruff. 2007. 'Abnormal Glutamate Receptor Expression in the Medial Temporal Lobe in Schizophrenia and Mood Disorders'. Neuropsychopharmacology: Official Publication of the American College of Neuropsychopharmacology 32 (9): 1888–1902. https://doi.org/10.1038/sj.npp.1301312.

Bennett, Michael V. L, and R. Suzanne Zukin. 2004. 'Electrical Coupling and Neuronal Synchronization in the Mammalian Brain'. Neuron 41 (4): 495–511. https://doi.org/10.1016/S0896-6273(04)00043-1.

Benson, Deanna L., and George W. Huntley. 2012. 'Building and Remodeling Synapses'. Hippocampus 22 (5): 954–68. https://doi.org/10.1002/hipo.20872.

Benson, Deannal L., James W. Mandell, Gerry Shaw, and Gary Banker. 1996. 'Compartmentation of Alpha-Internexin and Neurofilament Triplet Proteins in Cultured Hippocampal Neurons'. *Journal of Neurocytology* 25 (1): 181–96. https://doi.org/10.1007/BF02284795.

Benvenuto, Arianna, Romina Moavero, Riccardo Alessandrelli, Barbara Manzi, and Paolo Curatolo. 2009. 'Syndromic Autism: Causes and Pathogenetic Pathways'. World Journal of Pediatrics 5 (3): 169–76. https://doi.org/10.1007/s12519-009-0033-2.

Berberich, Sven, Jörg Pohle, Marie Pollard, Janet Barroso-Flores, and Georg Köhr. 2017. 'Interplay between Global and Pathway-Specific Synaptic Plasticity in CA1 Pyramidal Cells'. *Scientific Reports* 7 (1): 17040. https://doi.org/10.1038/s41598-017-17161-z.

Berkel, Simone, Christian R. Marshall, Birgit Weiss, Jennifer Howe, Ralph Roeth, Ute Moog, Volker Endris, et al. 2010. 'Mutations in the SHANK2 Synaptic Scaffolding Gene in Autism Spectrum Disorder and Mental Retardation'. Nature Genetics 42 (6): 489–91. https://doi.org/10.1038/ng.589.

Bernardinelli, Yann, Irina Nikonenko, and Dominique Muller. 2014. 'Structural Plasticity: Mechanisms and Contribution to Developmental Psychiatric Disorders'. Frontiers in Neuroanatomy 8 (November). https://doi.org/10.3389/fnana.2014.00123.

Bernards, Andre, and Jeffrey Settleman. 2004. 'GAP Control: Regulating the Regulators of Small GTPases'. Trends in Cell Biology 14 (7): 377–85. https://doi.org/10.1016/j.tcb.2004.05.003.

Bernards, André. 2003. 'GAPs Galore! A Survey of Putative Ras Superfamily GTPase Activating Proteins in Man and Drosophila'. Biochimica Et Biophysica Acta 1603 (2): 47–82.

Berryer, Martin H., Bidisha Chattopadhyaya, Paul Xing, Ilse Riebe, Ciprian Bosoi, Nathalie Sanon, Judith Antoine-Bertrand, et al. 2016. 'Decrease of SYNGAP1 in GABAergic Cells Impairs Inhibitory Synapse

Connectivity, Synaptic Inhibition and Cognitive Function'. Nature Communications 7 (November). https://doi.org/10.1038/ncomms13340.

Berryer, Martin H., Bidisha Chattopadhyaya, Paul Xing, Ilse Riebe, Ciprian Bosoi, Nathalie Sanon, Judith Antoine-Bertrand, et al. 2016. 'Decrease of SYNGAP1 in GABAergic Cells Impairs Inhibitory Synapse Connectivity, Synaptic Inhibition and Cognitive Function'. *Nature Communications* 7 (November). https://doi.org/10.1038/ncomms13340.

Berryer, Martin H., Bidisha Chattopadhyaya, Paul Xing, Ilse Riebe, Ciprian Bosoi, Nathalie Sanon, Judith Antoine-Bertrand, et al. 2016. 'Decrease of SYNGAP1 in GABAergic Cells Impairs Inhibitory Synapse Connectivity, Synaptic Inhibition and Cognitive Function'. *Nature Communications* 7 (November). https://doi.org/10.1038/ncomms13340.

Berryer, Martin H., Fadi F. Hamdan, Laura L. Klitten, Rikke S. Møller, Lionel Carmant, Jeremy Schwartzentruber, Lysanne Patry, et al. 2013. 'Mutations in SYNGAP1 Cause Intellectual Disability, Autism, and a Specific Form of Epilepsy by Inducing Haploinsufficiency'. Human Mutation 34 (2): 385–94. https://doi.org/10.1002/humu.22248.

Bilimoria, Parizad M., and Beth Stevens. 2015. 'Microglia Function during Brain Development: New Insights from Animal Models'. Brain Research 1617 (August): 7–17. https://doi.org/10.1016/j.brainres.2014.11.032.

Binotti, Beyenech, Reinhard Jahn, and John Jia En Chua. 2016. 'Functions of Rab Proteins at Presynaptic Sites'. *Cells* 5 (1). https://doi.org/10.3390/cells5010007.

Bischofberger, Josef, Dominique Engel, Michael Frotscher, and Peter Jonas. 2006. 'Timing and Efficacy of Transmitter Release at Mossy Fiber Synapses in the Hippocampal Network'. *Pflügers Archiv* 453 (3): 361–72. https://doi.org/10.1007/s00424-006-0093-2.

Blanpied, Thomas A., Justin M. Kerr, and Michael D. Ehlers. 2008. 'Structural Plasticity with Preserved Topology in the Postsynaptic Protein Network'. Proceedings of the National Academy of Sciences of the United States of America 105 (34): 12587–92. https://doi.org/10.1073/pnas.0711669105.

Bliss T. V. P., Collingridge G. L., Morris R. G. M., and Abraham Wickliffe C. 2003. 'How Long Will Long-Term Potentiation Last?' *Philosophical Transactions of the Royal Society of London. Series B: Biological Sciences* 358 (1432): 735–44. https://doi.org/10.1098/rstb.2002.1222.

Bluff, Joanne E, Nicola J Brown, Malcolm WR Reed, and Carolyn A Staton. 2008. 'Tissue Factor, Angiogenesis and Tumour Progression'. *Breast Cancer Research : BCR* 10 (2): 204. https://doi.org/10.1186/bcr1871.

Bockstaele, Elisabeth J. Van, and Virginia M. Pickel. n.d. 'Ultrastructure of Serotonin-Immunoreactive Terminals in the Core and Shell of the Rat Nucleus Accumbens: Cellular Substrates for Interactions with Catecholamine Afferents'. Journal of Comparative Neurology 334 (4): 603–17. https://doi.org/10.1002/cne.903340408.

Bokhoven, Hans van. 2011. 'Genetic and Epigenetic Networks in Intellectual Disabilities'. Annual Review of Genetics 45: 81–104. https://doi.org/10.1146/annurev-genet-110410-132512.

Bonhoeffer, Tobias, and Rafael Yuste. 2002. 'Spine Motility: Phenomenology, Mechanisms, and Function'. Neuron 35 (6): 1019–27. https://doi.org/10.1016/S0896-6273(02)00906-6.

Bos, Johannes L., Holger Rehmann, and Alfred Wittinghofer. 2007. 'GEFs and GAPs: Critical Elements in the Control of Small G Proteins'. Cell 129 (5): 865–77. https://doi.org/10.1016/j.cell.2007.05.018.

Bourgeron, Thomas. 2016. 'Current Knowledge on the Genetics of Autism and Propositions for Future Research'. Comptes Rendus Biologies 339 (7–8): 300–307. https://doi.org/10.1016/j.crvi.2016.05.004.

Bozzi, Yuri, Simona Casarosa, and Matteo Caleo. 2012. 'Epilepsy as a Neurodevelopmental Disorder'. Frontiers in Psychiatry 3. https://doi.org/10.3389/fpsyt.2012.00019.

Bradley, P., and M. Berry. 1976. 'The Effects of Reduced Climbing and Parallel Fibre Input on Purkinje Cell Dendritic Growth'. Brain Research 109 (1): 133–51.

Braga, Raphael J., Georgios Petrides, and Ivan Figueira. 2004. 'Anxiety Disorders in Schizophrenia'. Comprehensive Psychiatry 45 (6): 460–68. https://doi.org/10.1016/j.comppsych.2004.07.009.

Brimble, Elise, Christopher Lee-Messer, Peter L. Nagy, Jennifer Propst, and Maura R. Z. Ruzhnikov. 2018. 'Clinical Transcriptome Sequencing Confirms Activation of a Cryptic Splice Site in Suspected

SYNGAP1-Related Disorder'. *Molecular Syndromology* 9 (6): 295–99. https://doi.org/10.1159/000492706.

Bromley, R. L., G. E. Mawer, M. Briggs, C. Cheyne, J. Clayton-Smith, M. Garcia-Finana, R. Kneen, et al. 2013. 'The Prevalence of Neurodevelopmental Disorders in Children Prenatally Exposed to Antiepileptic Drugs'. Journal of Neurology, Neurosurgery & Psychiatry 84 (6): 637–43. https://doi.org/10.1136/jnnp-2012-304270.

Brose, Nils, Vincent O'Connor, and Paul Skehel. 2010. 'Synaptopathy: Dysfunction of Synaptic Function?' Biochemical Society Transactions 38 (2): 443–44. https://doi.org/10.1042/BST0380443.

Brown, Julie F., Milton Z. Brown, and Paige Dibiasio. 2013. 'Treating Individuals With Intellectual Disabilities and Challenging Behaviors With Adapted Dialectical Behavior Therapy'. Journal of Mental Health Research in Intellectual Disabilities 6 (4): 280–303. https://doi.org/10.1080/19315864.2012.700684.

Brown, Tyler C., Irwin C. Tran, Donald S. Backos, and José A. Esteban. 2005. 'NMDA Receptor-Dependent Activation of the Small GTPase Rab5 Drives the Removal of Synaptic AMPA Receptors during Hippocampal LTD'. Neuron 45 (1): 81–94. https://doi.org/10.1016/j.neuron.2004.12.023.

Buchholz, Frank, Pierre-Olivier Angrand, and A. Francis Stewart. 1996. 'A Simple Assay to Determine the Functionality of Cre or FLP Recombination Targets in Genomic Manipulation Constructs'. Nucleic Acids Research 24 (15): 3118–19. https://doi.org/10.1093/nar/24.15.3118.

Buhl, Derek L., Kenneth D. Harris, Sheriar G. Hormuzdi, Hanna Monyer, and György Buzsáki. 2003. 'Selective Impairment of Hippocampal Gamma Oscillations in Connexin-36 Knock-out Mouse in Vivo'. *The Journal of Neuroscience: The Official Journal of the Society for Neuroscience* 23 (3): 1013–18.

Burch, Amelia, Jung-Hwa Tao-Cheng, and Ayse Dosemeci. 2017. 'A Novel Synaptic Junction Preparation for the Identification and Characterization of Cleft Proteins'. PLoS ONE 12 (3). https://doi.org/10.1371/journal.pone.0174895.

Butler, M. G., M. J. Dasouki, X.-P. Zhou, Z. Talebizadeh, M. Brown, T. N. Takahashi, J. H. Miles, et al. 2005. 'Subset of Individuals with Autism Spectrum Disorders and Extreme Macrocephaly Associated with Germline PTEN Tumour Suppressor Gene Mutations'. Journal of Medical Genetics 42 (4): 318–21. https://doi.org/10.1136/jmg.2004.024646.

Butler, M. P, J. J O'Connor, and P. N Moynagh. 2004. 'Dissection of Tumor-Necrosis Factor-α Inhibition of Long-Term Potentiation (LTP) Reveals a P38 Mitogen-Activated Protein Kinase-Dependent Mechanism Which Maps to Early—but Not Late—Phase LTP'. Neuroscience 124 (2): 319–26. https://doi.org/10.1016/j.neuroscience.2003.11.040.

Cameron, H. A., C. K. Kaliszewski, and C. A. Greer. 1991. 'Organization of Mitochondria in Olfactory Bulb Granule Cell Dendritic Spines'. Synapse (New York, N.Y.) 8 (2): 107–18. https://doi.org/10.1002/syn.890080205.

Carbon, Seth, Amelia Ireland, Christopher J. Mungall, ShengQiang Shu, Brad Marshall, and Suzanna Lewis. 2009. 'AmiGO: Online Access to Ontology and Annotation Data'. Bioinformatics 25 (2): 288–89. https://doi.org/10.1093/bioinformatics/btn615.

Carlin, R. K., D. J. Grab, R. S. Cohen, and P. Siekevitz. 1980. 'Isolation and Characterization of Postsynaptic Densities from Various Brain Regions: Enrichment of Different Types of Postsynaptic Densities.' The Journal of Cell Biology 86 (3): 831–45. https://doi.org/10.1083/jcb.86.3.831.

Carlisle, Holly J., and Mary B. Kennedy. 2005. 'Spine Architecture and Synaptic Plasticity'. *Trends in Neurosciences* 28 (4): 182–87. https://doi.org/10.1016/j.tins.2005.01.008.

Carlisle, Holly J., and Mary B. Kennedy. 2005. 'Spine Architecture and Synaptic Plasticity'. Trends in Neurosciences 28 (4): 182–87. https://doi.org/10.1016/j.tins.2005.01.008.

Carlisle, Holly J., and Mary B. Kennedy. 2005. 'Spine Architecture and Synaptic Plasticity'. Trends in Neurosciences 28 (4): 182–87. https://doi.org/10.1016/j.tins.2005.01.008.

Carlisle, Holly J., Pasquale Manzerra, Edoardo Marcora, and Mary B. Kennedy. 2008. 'SynGAP Regulates Steady State and Activity-Dependent Phosphorylation of Cofilin'. The Journal of Neuroscience : The Official Journal of the Society for Neuroscience 28 (50): 13673–83. https://doi.org/10.1523/JNEUROSCI.4695-08.2008.

Carlisle, Holly J., Pasquale Manzerra, Edoardo Marcora, and Mary B. Kennedy. 2008. 'SynGAP Regulates Steady State and Activity-Dependent Phosphorylation of Cofilin'. The Journal of Neuroscience : The Official Journal of the Society for Neuroscience 28 (50): 13673–83. https://doi.org/10.1523/JNEUROSCI.4695-08.2008.

Carter, C. J. 2006. 'Schizophrenia Susceptibility Genes Converge on Interlinked Pathways Related to Glutamatergic Transmission and Long-Term Potentiation, Oxidative Stress and Oligodendrocyte Viability'. Schizophrenia Research 86 (1): 1–14. https://doi.org/10.1016/j.schres.2006.05.023.

Carulli, Daniela, Kate E. Rhodes, and James W. Fawcett. 2007. 'Upregulation of Aggrecan, Link Protein 1, and Hyaluronan Synthases during Formation of Perineuronal Nets in the Rat Cerebellum'. The Journal of Comparative Neurology 501 (1): 83–94. https://doi.org/10.1002/cne.21231.

Carvill, Gemma L., Sinéad B. Heavin, Simone C. Yendle, Jacinta M. McMahon, Brian J. O'Roak, Joseph Cook, Adiba Khan, et al. 2013. 'Targeted Resequencing in Epileptic Encephalopathies Identifies de Novo Mutations in CHD2 and SYNGAP1'. Nature Genetics 45 (7): 825–30. https://doi.org/10.1038/ng.2646.

Casanova, Emily L., and Manuel F. Casanova. 2014. 'Genetics Studies Indicate That Neural Induction and Early Neuronal Maturation Are Disturbed in Autism'. Frontiers in Cellular Neuroscience 8: 397. https://doi.org/10.3389/fncel.2014.00397.

Castro, Edouard de, Christian J. A. Sigrist, Alexandre Gattiker, Virginie Bulliard, Petra S. Langendijk-Genevaux, Elisabeth Gasteiger, Amos Bairoch, and Nicolas Hulo. 2006. 'ScanProsite: Detection of PROSITE Signature Matches and ProRule-Associated Functional and Structural Residues in Proteins'. Nucleic Acids Research 34 (suppl_2): W362–65. https://doi.org/10.1093/nar/gkl124.

Celio, Marco R, Roberto Spreafico, Silvia De Biasi, and Laura Vitellaro-Zuccarello. 1998. 'Perineuronal Nets: Past and Present'. Trends in Neurosciences 21 (12): 510–15. https://doi.org/10.1016/S0166-2236(98)01298-3.

Cellot, Giada, and Enrico Cherubini. 2014. 'GABAergic Signaling as Therapeutic Target for Autism Spectrum Disorders'. Frontiers in Pediatrics 2 (July). https://doi.org/10.3389/fped.2014.00070.

Chahrour, Maria, Sung Yun Jung, Chad Shaw, Xiaobo Zhou, Stephen T. C. Wong, Jun Qin, and Huda Y. Zoghbi. 2008. 'MeCP2, a Key Contributor to Neurological Disease, Activates and Represses Transcription'. Science (New York, N.Y.) 320 (5880): 1224–29. https://doi.org/10.1126/science.1153252.

Chater, Thomas E., and Yukiko Goda. 2014. 'The Role of AMPA Receptors in Postsynaptic Mechanisms of Synaptic Plasticity'. Frontiers in Cellular Neuroscience 8. https://doi.org/10.3389/fncel.2014.00401.

Chen, Hong-Jung, Michelle Rojas-Soto, Asako Oguni, and Mary B. Kennedy. 1998. 'A Synaptic Ras-GTPase Activating Protein (P135 SynGAP) Inhibited by CaM Kinase II'. Neuron 20 (5): 895–904. https://doi.org/10.1016/S0896-6273(00)80471-7.

Chen, Jerry L., Katherine L. Villa, Jae Won Cha, Peter T. C. So, Yoshiyuki Kubota, and Elly Nedivi. 2012. 'Clustered Dynamics of Inhibitory Synapses and Dendritic Spines in the Adult Neocortex'. Neuron 74 (2): 361–73. https://doi.org/10.1016/j.neuron.2012.02.030.

Chen, Mo, and James L. Manley. 2009. 'Mechanisms of Alternative Splicing Regulation: Insights from Molecular and Genomics Approaches'. Nature Reviews. Molecular Cell Biology 10 (11): 741–54. https://doi.org/10.1038/nrm2777.

Chen, Xiaobing, Christine Winters, Rita Azzam, Xiang Li, James A. Galbraith, Richard D. Leapman, and Thomas S. Reese. 2008. 'Organization of the Core Structure of the Postsynaptic Density'. Proceedings of the National Academy of Sciences of the United States of America 105 (11): 4453–58. https://doi.org/10.1073/pnas.0800897105.

Chen, Xiaobing, Lucia Vinade, Richard D. Leapman, Jennifer D. Petersen, Terunaga Nakagawa, Terry M. Phillips, Morgan Sheng, and Thomas S. Reese. 2005. 'Mass of the Postsynaptic Density and Enumeration of Three Key Molecules'. Proceedings of the National Academy of Sciences 102 (32): 11551–56. https://doi.org/10.1073/pnas.0505359102.

Cheng, Dongmei, Casper C. Hoogenraad, John Rush, Elizabeth Ramm, Max A. Schlager, Duc M. Duong, Ping Xu, et al. 2006. 'Relative and Absolute Quantification of Postsynaptic Density Proteome Isolated from Rat Forebrain and Cerebellum'. Molecular & Cellular Proteomics 5 (6): 1158–70. https://doi.org/10.1074/mcp.D500009-MCP200.

Cherfils, Jacqueline, and Mahel Zeghouf. 2013. 'Regulation of Small GTPases by GEFs, GAPs, and GDIs'. Physiological Reviews 93 (1): 269–309. https://doi.org/10.1152/physrev.00003.2012.

Chiu, Chiayu Q., Gyorgy Lur, Thomas M. Morse, Nicholas T. Carnevale, Graham C. R. Ellis-Davies, and Michael J. Higley. 2013. 'Compartmentalization of GABAergic Inhibition by Dendritic Spines'. Science (New York, N.Y.) 340 (6133): 759–62. https://doi.org/10.1126/science.1234274.

Chklovskii, D. B., B. W. Mel, and K. Svoboda. 2004. 'Cortical Rewiring and Information Storage'. Special Features. Nature. 13 October 2004. https://doi.org/10.1038/nature03012.

Cho, Wonhwa, and Robert V. Stahelin. 2006. 'Membrane Binding and Subcellular Targeting of C2 Domains'. Biochimica et Biophysica Acta (BBA) - Molecular and Cell Biology of Lipids, Lipid-Binding Domains, 1761 (8): 838–49. https://doi.org/10.1016/j.bbalip.2006.06.014.

Choquet, Daniel, and Antoine Triller. 2003. 'The Role of Receptor Diffusion in the Organization of the Postsynaptic Membrane'. Nature Reviews Neuroscience 4 (4): 251–65. https://doi.org/10.1038/nrn1077.

Christensen, Deborah L., Deborah A. Bilder, Walter Zahorodny, Sydney Pettygrove, Maureen S. Durkin, Robert T. Fitzgerald, Catherine Rice, Margaret Kurzius-Spencer, Jon Baio, and Marshalyn Yeargin-Allsopp. 2016. 'Prevalence and Characteristics of Autism Spectrum Disorder Among 4-Year-Old Children in the Autism and Developmental Disabilities Monitoring Network'. Journal of Developmental and Behavioral Pediatrics: JDBP 37 (1): 1–8. https://doi.org/10.1097/DBP.0000000000000235.

Christopherson, Karen S., Erik M. Ullian, Caleb C. A. Stokes, Christine E. Mullowney, Johannes W. Hell, Azin Agah, Jack Lawler, Deane F. Mosher, Paul Bornstein, and Ben A. Barres. 2005. 'Thrombospondins Are Astrocyte-Secreted Proteins That Promote CNS Synaptogenesis'. Cell 120 (3): 421–33. https://doi.org/10.1016/j.cell.2004.12.020.

Chubykin, Alexander A., Deniz Atasoy, Mark R. Etherton, Nils Brose, Ege T. Kavalali, Jay R. Gibson, and Thomas C. Südhof. 2007. 'Activity-Dependent Validation of Excitatory versus Inhibitory Synapses by Neuroligin-1 versus Neuroligin-2'. Neuron 54 (6): 919–31. https://doi.org/10.1016/j.neuron.2007.05.029.

Chubykin, Alexander A., Deniz Atasoy, Mark R. Etherton, Nils Brose, Ege T. Kavalali, Jay R. Gibson, and Thomas C. Südhof. 2007. 'Activity-Dependent Validation of Excitatory versus Inhibitory Synapses by Neuroligin-1 versus Neuroligin-2'. Neuron 54 (6): 919–31. https://doi.org/10.1016/j.neuron.2007.05.029.

Chung, Hee Jung, Jordan P. Steinberg, Richard L. Huganir, and David J. Linden. 2003. 'Requirement of AMPA Receptor GluR2 Phosphorylation for Cerebellar Long-Term Depression'. Science 300 (5626): 1751–55. https://doi.org/10.1126/science.1082915.

Clancy, Barbara, Barbara L. Finlay, Richard B. Darlington, and K. J. S. Anand. 2007. 'Extrapolating Brain Development from Experimental Species to Humans'. Neurotoxicology 28 (5): 931–37. https://doi.org/10.1016/j.neuro.2007.01.014.

Clarke, Dave F., Wendy Roberts, Mina Daraksan, Annie Dupuis, Jane McCabe, Halyey Wood, O. Carter Snead, and Shelly K. Weiss. 2005. 'The Prevalence of Autistic Spectrum Disorder in Children Surveyed in a Tertiary Care Epilepsy Clinic'. Epilepsia 46 (12): 1970–77. https://doi.org/10.1111/j.1528-1167.2005.00343.x.

Clarke, Dave F., Wendy Roberts, Mina Daraksan, Annie Dupuis, Jane McCabe, Halyey Wood, O. Carter Snead, and Shelly K. Weiss. 2005. 'The Prevalence of Autistic Spectrum Disorder in Children Surveyed in a Tertiary Care Epilepsy Clinic'. Epilepsia 46 (12): 1970–77. https://doi.org/10.1111/j.1528-1167.2005.00343.x..

Clement, J.P., Aceti, M., Creson, T.K., Ozkan, E.D., Shi, Y., Reish, N.J., Almonte, A.G., Miller, B.H., Wiltgen, B.J., Miller, C.A., et al. (2012). Pathogenic SYNGAP1 mutations impair cognitive development by disrupting maturation of dendritic spine synapses. Cell 151, 709–723.

Clement, J.P., Ozkan, E.D., Aceti, M., Miller, C.A., and Rumbaugh, G. (2013). SYNGAP1 Links the Maturation Rate of Excitatory Synapses to the Duration of Critical-Period Synaptic Plasticity. J. Neurosci. 33, 10447–10452.

Clement, James P., Emin D. Ozkan, Massimiliano Aceti, Courtney A. Miller, and Gavin Rumbaugh. 2013. 'SYNGAP1 Links the Maturation Rate of Excitatory Synapses to the Duration of Critical-Period Synaptic Plasticity'. The Journal of Neuroscience 33 (25): 10447–52. https://doi.org/10.1523/JNEUROSCI.0765-13.2013.

Clement, James P., Emin D. Ozkan, Massimiliano Aceti, Courtney A. Miller, and Gavin Rumbaugh. 2013. 'SYNGAP1 Links the Maturation Rate of Excitatory Synapses to the Duration of Critical-Period Synaptic Plasticity'. The Journal of Neuroscience 33 (25): 10447–52. https://doi.org/10.1523/JNEUROSCI.0765-13.2013.

Clement, James P., Massimiliano Aceti, Thomas K. Creson, Emin D. Ozkan, Yulin Shi, Nicholas J. Reish, Antoine G. Almonte, et al. 2012. 'Pathogenic SYNGAP1 Mutations Impair Cognitive Development by

Disrupting Maturation of Dendritic Spine Synapses'. Cell 151 (4): 709–23. https://doi.org/10.1016/j.cell.2012.08.045.

Codocedo, Juan F., Carla Montecinos-Oliva, and Nibaldo C. Inestrosa. 2015. 'Wnt-Related SynGAP1 Is a Neuroprotective Factor of Glutamatergic Synapses against Aβ Oligomers'. Frontiers in Cellular Neuroscience 9 (June). https://doi.org/10.3389/fncel.2015.00227.

Codocedo, Juan F., Carla Montecinos-Oliva, and Nibaldo C. Inestrosa. 2015. 'Wnt-Related SynGAP1 Is a Neuroprotective Factor of Glutamatergic Synapses against Aβ Oligomers'. Frontiers in Cellular Neuroscience 9 (June). https://doi.org/10.3389/fncel.2015.00227.

Coletta, Alain, John W. Pinney, David Y. Weiss Solís, James Marsh, Steve R. Pettifer, and Teresa K. Attwood. 2010. 'Low-Complexity Regions within Protein Sequences Have Position-Dependent Roles'. BMC Systems Biology 4 (April): 43. https://doi.org/10.1186/1752-0509-4-43.

Colgan, Lesley A., and Ryohei Yasuda. 2014. 'Plasticity of Dendritic Spines: Subcompartmentalization of Signaling'. Annual Review of Physiology 76: 365–85. https://doi.org/10.1146/annurev-physiol-021113-170400.

Colonnier, Marc. 1968. 'Synaptic Patterns on Different Cell Types in the Different Laminae of the Cat Visual Cortex. An Electron Microscope Study'. Brain Research 9 (2): 268–87. https://doi.org/10.1016/0006-8993(68)90234-5.

Colón-Ramos, Daniel A. 2009. 'Chapter 2 Synapse Formation in Developing Neural Circuits'. In Current Topics in Developmental Biology, 87:53–79. Elsevier. https://doi.org/10.1016/S0070-2153(09)01202-2.

Corbeil, Denis, Jana Karbanová, Christine A. Fargeas, and József Jászai. 2013. 'Prominin-1 (CD133): Molecular and Cellular Features Across Species'. In Prominin-1 (CD133): New Insights on Stem & Cancer Stem Cell Biology, edited by Denis Corbeil, 3–24. Advances in Experimental Medicine and Biology. New York, NY: Springer New York. https://doi.org/10.1007/978-1-4614-5894-4_1.

Corrêa, Sônia A. L., and Katherine L. Eales. 2012. 'The Role of P38 MAPK and Its Substrates in Neuronal Plasticity and Neurodegenerative Disease'. Research article. Journal of Signal Transduction. 2012. https://doi.org/10.1155/2012/649079.

Coss, R. G., and D. H. Perkel. 1985. 'The Function of Dendritic Spines: A Review of Theoretical Issues'. Behavioral and Neural Biology 44 (2): 151–85.

Coutavas, E. E., C. M. Hsieh, M. Ren, G. T. Drivas, M. G. Rush, and P. D'Eustachio. 1994. 'Tissue-Specific Expression of Ran Isoforms in the Mouse'. Mammalian Genome 5 (10): 623–28. https://doi.org/10.1007/BF00411457.

Crair, M. C., and R. C. Malenka. 1995. 'A Critical Period for Long-Term Potentiation at Thalamocortical Synapses'. Nature 375 (6529): 325–28. https://doi.org/10.1038/375325a0.

Croft, David, Gavin O'Kelly, Guanming Wu, Robin Haw, Marc Gillespie, Lisa Matthews, Michael Caudy, et al. 2011. 'Reactome: A Database of Reactions, Pathways and Biological Processes'. Nucleic Acids Research 39 (Database issue): D691-697. https://doi.org/10.1093/nar/gkq1018

Cromm, Philipp M., Jochen Spiegel, Tom N. Grossmann, and Herbert Waldmann. 2015. 'Direct Modulation of Small GTPase Activity and Function'. Angewandte Chemie International Edition 54 (46): 13516–37. https://doi.org/10.1002/anie.201504357.

Crozier, Robert A., Yun Wang, Cheng-Hang Liu, and Mark F. Bear. 2007. 'Deprivation-Induced Synaptic Depression by Distinct Mechanisms in Different Layers of Mouse Visual Cortex'. Proceedings of the National Academy of Sciences 104 (4): 1383–88. https://doi.org/10.1073/pnas.0609596104.

Cruz-Martín, Alberto, Michelle Crespo, and Carlos Portera-Cailliau. 2010. 'Delayed Stabilization of Dendritic Spines in Fragile X Mice'. Journal of Neuroscience 30 (23): 7793–7803. https://doi.org/10.1523/JNEUROSCI.0577-10.2010.

Dailey, M. E., and S. J. Smith. 1996. 'The Dynamics of Dendritic Structure in Developing Hippocampal Slices'. The Journal of Neuroscience: The Official Journal of the Society for Neuroscience 16 (9): 2983–94.

Dani, Adish, Bo Huang, Joseph Bergan, Catherine Dulac, and Xiaowei Zhuang. 2010. 'Superresolution Imaging of Chemical Synapses in the Brain'. Neuron 68 (5): 843–56. https://doi.org/10.1016/j.neuron.2010.11.021.

Davletov, B. A., and T. C. Südhof. 1993. 'A Single C2 Domain from Synaptotagmin I Is Sufficient for High Affinity Ca2+/Phospholipid Binding'. The Journal of Biological Chemistry 268 (35): 26386–90.

Deb, S., M. Thomas, and C. Bright. 2001. 'Mental Disorder in Adults with Intellectual Disability. 1: Prevalence of Functional Psychiatric Illness among a Community-Based Population Aged between 16 and 64 Years'. Journal of Intellectual Disability Research: JIDR 45 (Pt 6): 495–505.

Deeg, Katherine E. 2009. 'Synapse-Specific Homeostatic Mechanisms in the Hippocampus'. Journal of Neurophysiology 101 (2): 503–6. https://doi.org/10.1152/jn.91115.2008.

Deister, C., and C. E. Schmidt. 2006. 'Optimizing Neurotrophic Factor Combinations for Neurite Outgrowth'. Journal of Neural Engineering 3 (2): 172. https://doi.org/10.1088/1741-2560/3/2/011.

Delint-Ramirez, Ilse, Esperanza Fernández, Alex Bayés, Emese Kicsi, Noboru H. Komiyama, and Seth G. N. Grant. 2010. 'In Vivo Composition of NMDA Receptor Signaling Complexes Differs between Membrane Subdomains and Is Modulated by PSD-95 and PSD-93'. The Journal of Neuroscience: The Official Journal of the Society for Neuroscience 30 (24): 8162–70. https://doi.org/10.1523/JNEUROSCI.1792-10.2010.

Delint-Ramirez, Ilse, Esperanza Fernández, Alex Bayés, Emese Kicsi, Noboru H. Komiyama, and Seth G. N. Grant. 2010. 'In Vivo Composition of NMDA Receptor Signaling Complexes Differs between Membrane Subdomains and Is Modulated by PSD-95 and PSD-93'. The Journal of Neuroscience: The Official Journal of the Society for Neuroscience 30 (24): 8162–70. https://doi.org/10.1523/JNEUROSCI.1792-10.2010.

Deller, Thomas, Martin Korte, Sophie Chabanis, Alexander Drakew, Herbert Schwegler, Giulia Good Stefani, Aimee Zuniga, et al. 2003. 'Synaptopodin-Deficient Mice Lack a Spine Apparatus and Show Deficits in Synaptic Plasticity'. Proceedings of the National Academy of Sciences of the United States of America 100 (18): 10494–99. https://doi.org/10.1073/pnas.1832384100.

Dennis, Glynn, Brad T. Sherman, Douglas A. Hosack, Jun Yang, Wei Gao, H. Clifford Lane, and Richard A. Lempicki. 2003. 'DAVID: Database for Annotation, Visualization, and Integrated Discovery'. Genome Biology 4 (5): P3.

Derkach, Victor A., Michael C. Oh, Eric S. Guire, and Thomas R. Soderling. 2007. 'Regulatory Mechanisms of AMPA Receptors in Synaptic Plasticity'. Nature Reviews. Neuroscience 8 (2): 101–13. https://doi.org/10.1038/nrn2055.

Di Cunto, Ferdinando, Sara Imarisio, Emilio Hirsch, Vania Broccoli, Alessandro Bulfone, Antonio Migheli, Cristiana Atzori, et al. 2000. 'Defective Neurogenesis in Citron Kinase Knockout Mice by Altered Cytokinesis and Massive Apoptosis'. Neuron 28 (1): 115–27. https://doi.org/10.1016/S0896-6273(00)00090-8.

Dickson, Barry J. 2001. 'Rho GTPases in Growth Cone Guidance'. Current Opinion in Neurobiology 11 (1): 103–10. https://doi.org/10.1016/S0959-4388(00)00180-X.

Dieterich, Daniela C., and Michael R. Kreutz. 2016. 'Proteomics of the Synapse – A Quantitative Approach to Neuronal Plasticity'. Molecular & Cellular Proteomics 15 (2): 368. https://doi.org/10.1074/mcp.R115.051482.

Dietrich, Jean-Bernard. 2013. 'The MEF2 Family and the Brain: From Molecules to Memory'. Cell and Tissue Research 352 (2): 179–90. https://doi.org/10.1007/s00441-013-1565-2.

Difiglia, Marian, Pedro Pasik, and Tauba Pasik. 1980. 'Early Postnatal Development of the Monkey Neostriatum: A Golgi and Ultrastructural Study'. Journal of Comparative Neurology 190 (2): 303–31. https://doi.org/10.1002/cne.901900207.

Dillon, Christian, and Yukiko Goda. 2005. 'THE ACTIN CYTOSKELETON: Integrating Form and Function at the Synapse'. Annual Review of Neuroscience 28 (1): 25–55. https://doi.org/10.1146/annurev.neuro.28.061604.135757.

Distler, Ute, Michael J. Schmeisser, Assunta Pelosi, Dominik Reim, Jörg Kuharev, Roland Weiczner, Jan Baumgart, et al. 2014. 'In-Depth Protein Profiling of the Postsynaptic Density from Mouse Hippocampus Using Data-Independent Acquisition Proteomics'. PROTEOMICS 14 (21–22): 2607–13. https://doi.org/10.1002/pmic.201300520.

Dityatev, Alexander, and Dmitri A Rusakov. 2011. 'Molecular Signals of Plasticity at the Tetrapartite Synapse'. Current Opinion in Neurobiology, Synaptic function and regulation, 21 (2): 353–59. https://doi.org/10.1016/j.conb.2010.12.006.

Dobbing, John, and Jean Sands. 1978. 'Head Circumference, Biparietal Diameter and Brain Growth in Fetal and Postnatal Life'. Early Human Development 2 (1): 81–87. https://doi.org/10.1016/0378-3782(78)90054-3.

Dölen, Gül, Emily Osterweil, B. S. Shankaranarayana Rao, Gordon B. Smith, Benjamin D. Auerbach, Sumantra Chattarji, and Mark F. Bear. 2007. 'Correction of Fragile X Syndrome in Mice'. Neuron 56 (6): 955–62. https://doi.org/10.1016/j.neuron.2007.12.001.

Domon, Bruno, and Ruedi Aebersold. 2006. 'Mass Spectrometry and Protein Analysis'. Science 312 (5771): 212–17. https://doi.org/10.1126/science.1124619.

Dosemeci, Ayse, Dana Toy, Thomas S. Reese, and Jung-Hwa Tao-Cheng. 2015. 'AIDA-1 Moves out of the Postsynaptic Density Core under Excitatory Conditions'. PLoS ONE 10 (9). https://doi.org/10.1371/journal.pone.0137216.

Dosemeci, Ayse, Richard J. Weinberg, Thomas S. Reese, and Jung-Hwa Tao-Cheng. 2016. 'The Postsynaptic Density: There Is More than Meets the Eye'. Frontiers in Synaptic Neuroscience 8. https://doi.org/10.3389/fnsyn.2016.00023.

Doss, Sarah, Astrid Nümann, Annerose Ziegler, Eberhard Siebert, Kathrin Borowski, Winfried Stöcker, Harald Prüss, Brigitte Wildemann, Matthias Endres, and Sven Jarius. 2014. 'Anti-Ca/Anti-ARHGAP26 Antibodies Associated with Cerebellar Atrophy and Cognitive Decline'. Journal of Neuroimmunology 267 (1): 102–4. https://doi.org/10.1016/j.jneuroim.2013.10.010.

Dresbach, Thomas, Anne Hempelmann, Christina Spilker, Susanne tom Dieck, Wilko D Altrock, Werner Zuschratter, Craig C Garner, and Eckart D Gundelfinger. 2003. 'Functional Regions of the Presynaptic Cytomatrix Protein Bassoon: Significance for Synaptic Targeting and Cytomatrix Anchoring'. Molecular and Cellular Neuroscience 23 (2): 279–91. https://doi.org/10.1016/S1044-7431(03)00015-0.

Dubos, Aline, Gaelle Combeau, Yann Bernardinelli, Jean-Vianney Barnier, Oliver Hartley, Hubert Gaertner, Bernadett Boda, and Dominique Muller. 2012. 'Alteration of Synaptic Network Dynamics by the Intellectual Disability Protein PAK3'. The Journal of Neuroscience: The Official Journal of the Society for Neuroscience 32 (2): 519–27. https://doi.org/10.1523/JNEUROSCI.3252-11.2012.

Duchan, Erin, and Dilip R. Patel. 2012. 'Epidemiology of Autism Spectrum Disorders'. Pediatric Clinics of North America 59 (1): 27–43, ix–x. https://doi.org/10.1016/j.pcl.2011.10.003.

Duchen, Michael R., Alexei Verkhratsky, and Shmuel Muallem. 2008. 'Mitochondria and Calcium in Health and Disease'. Cell Calcium 44 (1): 1–5. https://doi.org/10.1016/j.ceca.2008.02.001.

Dudek, S. M., and M. F. Bear. 1992. 'Homosynaptic Long-Term Depression in Area CA1 of Hippocampus and Effects of N-Methyl-D-Aspartate Receptor Blockade'. Proceedings of the National Academy of Sciences of the United States of America 89 (10): 4363–67.

Dulac, Olivier, Barbara Plecko, Svetlana Gataullina, and Nicole I. Wolf. 2014. 'Occasional Seizures, Epilepsy, and Inborn Errors of Metabolism'. The Lancet Neurology 13 (7): 727–39. https://doi.org/10.1016/S1474-4422(14)70110-3.

Dun, Xin-peng, and John K. Chilton. 2010. 'Control of Cell Shape and Plasticity during Development and Disease by the Actin-Binding Protein Drebrin'. Histology and Histopathology 25 (4): 533–40. https://doi.org/10.14670/HH-25.533.

Dutta, Sulagna, and Pallav Sengupta. 2016. 'Men and Mice: Relating Their Ages'. Life Sciences 152 (May): 244–48. https://doi.org/10.1016/j.lfs.2015.10.025.

Ebert, Daniel H., and Michael E. Greenberg. 2013. 'Activity-Dependent Neuronal Signalling and Autism Spectrum Disorder'. Nature 493 (7432): 327–37. https://doi.org/10.1038/nature11860.

Eccles, J C. 1982. 'The Synapse: From Electrical to Chemical Transmission'. Annual Review of Neuroscience 5 (1): 325–39. https://doi.org/10.1146/annurev.ne.05.030182.001545.

Eden, Eran, Roy Navon, Israel Steinfeld, Doron Lipson, and Zohar Yakhini. 2009. 'GOrilla: A Tool for Discovery and Visualization of Enriched GO Terms in Ranked Gene Lists'. BMC Bioinformatics 10 (February): 48. https://doi.org/10.1186/1471-2105-10-48.

Ehninger, Dan, Weidong Li, Kevin Fox, Michael P. Stryker, and Alcino J. Silva. 2008. 'Reversing Neurodevelopmental Disorders in Adults'. Neuron 60 (6): 950–60. https://doi.org/10.1016/j.neuron.2008.12.007.

Ehrlich, Ingrid, Matthew Klein, Simon Rumpel, and Roberto Malinow. 2007. 'PSD-95 Is Required for Activity-Driven Synapse Stabilization'. Proceedings of the National Academy of Sciences 104 (10): 4176. https://doi.org/10.1073/pnas.0609307104.

El-Husseini, Alaa El-Din, Eric Schnell, Srikanth Dakoji, Neal Sweeney, Qiang Zhou, Oliver Prange, Catherine Gauthier-Campbell, Andrea Aguilera-Moreno, Roger A. Nicoll, and David S. Bredt. 2002. 'Synaptic Strength Regulated by Palmitate Cycling on PSD-95'. Cell 108 (6): 849–63. https://doi.org/10.1016/S0092-8674(02)00683-9.

Elias, Guillermo M., Lars Funke, Valentin Stein, Seth G. Grant, David S. Bredt, and Roger A. Nicoll. 2006. 'Synapse-Specific and Developmentally Regulated Targeting of AMPA Receptors by a Family of MAGUK Scaffolding Proteins'. Neuron 52 (2): 307–20. https://doi.org/10.1016/j.neuron.2006.09.012.

Elschenbroich, Sarah, and Thomas Kislinger. 2011. 'Targeted Proteomics by Selected Reaction Monitoring Mass Spectrometry: Applications to Systems Biology and Biomarker Discovery'. Molecular BioSystems 7 (2): 292–303. https://doi.org/10.1039/C0MB00159G.

Elston, Guy N., Ruth Benavides-Piccione, Alejandra Elston, Paul R. Manger, and Javier Defelipe. 2011. 'Pyramidal Cells in Prefrontal Cortex of Primates: Marked Differences in Neuronal Structure among Species'. Frontiers in Neuroanatomy 5: 2. https://doi.org/10.3389/fnana.2011.00002.

Emes, Richard D, Andrew J Pocklington, Christopher N G Anderson, Alex Bayes, Mark O Collins, Catherine A Vickers, Mike D R Croning, et al. 2008. 'Evolutionary Expansion and Anatomical Specialization of Synapse Proteome Complexity'. Nature Neuroscience 11 (7): 799–806. https://doi.org/10.1038/nn.2135.

Emes, Richard D., and Seth G. N. Grant. 2012. 'Evolution of Synapse Complexity and Diversity'. Annual Review of Neuroscience 35 (1): 111–31. https://doi.org/10.1146/annurev-neuro-062111-150433.

Engel, Jerome. 2006. 'ILAE Classification of Epilepsy Syndromes'. Epilepsy Research, Epileptic Syndromes in Infancy and Early Childhood, 70 (August): 5–10. https://doi.org/10.1016/j.eplepsyres.2005.11.014.

Epshtein, Vitaly, and Evgeny Nudler. 2003. 'Cooperation between RNA Polymerase Molecules in Transcription Elongation'. Science (New York, N.Y.) 300 (5620): 801–5. https://doi.org/10.1126/science.1083219.

Falasca, M., S. K. Logan, V. P. Lehto, G. Baccante, M. A. Lemmon, and J. Schlessinger. 1998. 'Activation of Phospholipase Cγ by PI 3-kinase-induced PH Domain-mediated Membrane Targeting'. The EMBO Journal 17 (2): 414–22. https://doi.org/10.1093/emboj/17.2.414.

Fauth, Michael, and Christian Tetzlaff. 2016. 'Opposing Effects of Neuronal Activity on Structural Plasticity'. Frontiers in Neuroanatomy 10 (June). https://doi.org/10.3389/fnana.2016.00075.

Feldman, Daniel E. 2012. 'The Spike-Timing Dependence of Plasticity'. Neuron 75 (4): 556–71. https://doi.org/10.1016/j.neuron.2012.08.001.

Fernandez, Fabian, Wade Morishita, Elizabeth Zuniga, James Nguyen, Martina Blank, Robert C. Malenka, and Craig C. Garner. 2007. 'Pharmacotherapy for Cognitive Impairment in a Mouse Model of Down Syndrome'. Nature Neuroscience 10 (4): 411–13. https://doi.org/10.1038/nn1860.

Feyder, Michael, Rose-Marie Karlsson, Poonam Mathur, Matthew Lyman, Roland Bock, Reza Momenan, Jeeva Munasinghe, et al. 2010. 'Association of Mouse Dlg4 (PSD-95) Gene Deletion and Human DLG4 Gene Variation with Phenotypes Relevant to Autism Spectrum Disorders and Williams' Syndrome'. The American Journal of Psychiatry 167 (12): 1508–17. https://doi.org/10.1176/appi.ajp.2010.10040484.

Fiala, J. C., M. Feinberg, V. Popov, and K. M. Harris. 1998. 'Synaptogenesis via Dendritic Filopodia in Developing Hippocampal Area CA1'. The Journal of Neuroscience: The Official Journal of the Society for Neuroscience 18 (21): 8900–8911.

Fielder, Thomas J., Charles S. Yi, Juliet Masumi, Katrina G. Waymire, Hsiao-Wen Chen, Shuling Wang, Kai-Xuan Shi, Douglas C. Wallace, and Grant R. MacGregor. 2012. 'Comparison of Male Chimeric Mice Generated from Microinjection of JM8.N4 Embryonic Stem Cells into C57BL/6J and C57BL/6NTac Blastocysts'. Transgenic Research 21 (6): 1149–58. https://doi.org/10.1007/s11248-012-9605-3.

Finn, Robert D., Teresa K. Attwood, Patricia C. Babbitt, Alex Bateman, Peer Bork, Alan J. Bridge, Hsin-Yu Chang, et al. 2017. 'InterPro in 2017-beyond Protein Family and Domain Annotations'. Nucleic Acids Research 45 (D1): D190–99. https://doi.org/10.1093/nar/gkw1107.

Fischer, M., S. Kaech, U. Wagner, H. Brinkhaus, and A. Matus. 2000. 'Glutamate Receptors Regulate Actin-Based Plasticity in Dendritic Spines'. Nature Neuroscience 3 (9): 887–94. https://doi.org/10.1038/78791.

Flavell, Steven W., Christopher W. Cowan, Tae-Kyung Kim, Paul L. Greer, Yingxi Lin, Suzanne Paradis, Eric C. Griffith, Linda S. Hu, Chinfei Chen, and Michael E. Greenberg. 2006. 'Activity-Dependent

Regulation of MEF2 Transcription Factors Suppresses Excitatory Synapse Number'. Science 311 (5763): 1008–12. https://doi.org/10.1126/science.1122511.

Fombonne, Eric. 2003. 'Epidemiological Surveys of Autism and Other Pervasive Developmental Disorders: An Update'. Journal of Autism and Developmental Disorders 33 (4): 365–82. https://doi.org/10.1023/A:1025054610557.

Forrest, Marc P., Euan Parnell, and Peter Penzes. 2018. 'Dendritic Structural Plasticity and Neuropsychiatric Disease'. Nature Reviews Neuroscience 19 (4): 215–34. https://doi.org/10.1038/nrn.2018.16.

Foster, Michael, Charles Scott Sherrington, and London Library Services University College. 1897. A Textbook of Physiology. With C.S. Sherrington. Part 3. The Central Nervous System [Electronic Resource]. London : Macmillan. http://archive.org/details/b21271458.

Fox, K., S. Glazewski, and S. Schulze. 2000. 'Plasticity and Stability of Somatosensory Maps in Thalamus and Cortex'. Current Opinion in Neurobiology 10 (4): 494–97.

Frank, René A. W., Noboru H. Komiyama, Tomás J. Ryan, Fei Zhu, Thomas J. O'Dell, and Seth G. N. Grant. 2016. 'NMDA Receptors Are Selectively Partitioned into Complexes and Supercomplexes during Synapse Maturation'. *Nature Communications* 7 (April): 11264. https://doi.org/10.1038/ncomms11264.

Frank, René A. W., Fei Zhu, Noboru H. Komiyama, and Seth G. N. Grant. 2017. 'Hierarchical Organization and Genetically Separable Subfamilies of PSD95 Postsynaptic Supercomplexes'. *Journal of Neurochemistry* 142 (4): 504–11. https://doi.org/10.1111/jnc.14056.

Frank, René AW, and Seth GN Grant. 2017. 'Supramolecular Organization of NMDA Receptors and the Postsynaptic Density'. *Current Opinion in Neurobiology* 45 (August): 139–47. https://doi.org/10.1016/j.conb.2017.05.019.

Fryer, A. E., J. P. Osborne, R. Tan, and D. C. Siggers. 1987. 'Tuberous Sclerosis: A Large Family with No History of Seizures or Mental Retardation'. Journal of Medical Genetics 24 (9): 547–48.

Fu, Zhanyan, Sang Hyoung Lee, Alyson Simonetta, Jonathan Hansen, Morgan Sheng, and Daniel T. S. Pak. 2007. 'Differential Roles of Rap1 and Rap2 Small GTPases in Neurite Retraction and Synapse Elimination in Hippocampal Spiny Neurons'. Journal of Neurochemistry 100 (1): 118–31. https://doi.org/10.1111/j.1471-4159.2006.04195.x.

Fukaya, Masahiro, Mika Tsujita, Maya Yamazaki, Etsuko Kushiya, Manabu Abe, Kaori Akashi, Rie Natsume, et al. 2006. 'Abundant Distribution of TARP γ-8 in Synaptic and Extrasynaptic Surface of Hippocampal Neurons and Its Major Role in AMPA Receptor Expression on Spines and Dendrites'. European Journal of Neuroscience 24 (8): 2177–90. https://doi.org/10.1111/j.1460-9568.2006.05081.x.

Fukuda, Takaichi, and Toshio Kosaka. 2000. 'The Dual Network of GABAergic Interneurons Linked by Both Chemical and Electrical Synapses: A Possible Infrastructure of the Cerebral Cortex'. Neuroscience Research 38 (2): 123–30. https://doi.org/10.1016/S0168-0102(00)00163-2.

Fukuda, Takaichi. 2007. 'Structural Organization of the Gap Junction Network in the Cerebral Cortex'. The Neuroscientist: A Review Journal Bringing Neurobiology, Neurology and Psychiatry 13 (3): 199–207. https://doi.org/10.1177/1073858406296760.

Funk, Adam J., Robert E. McCullumsmith, Vahram Haroutunian, and James H. Meador-Woodruff. 2012. 'Abnormal Activity of the MAPK- and CAMP-Associated Signaling Pathways in Frontal Cortical Areas in Postmortem Brain in Schizophrenia'. Neuropsychopharmacology 37 (4): 896–905. https://doi.org/10.1038/npp.2011.267.

Gaertner, Tara R., Steven J. Kolodziej, Dan Wang, Ryuji Kobayashi, John M. Koomen, James K. Stoops, and M. Neal Waxham. 2004. 'Comparative Analyses of the Three-Dimensional Structures and Enzymatic Properties of α, β, γ, and δ Isoforms of Ca2+-Calmodulin-Dependent Protein Kinase II'. Journal of Biological Chemistry 279 (13): 12484–94. https://doi.org/10.1074/jbc.M313597200.

Galarreta, Mario, and Shaul Hestrin. 2001. 'Electrical Synapses between Gaba-Releasing Interneurons'. Nature Reviews Neuroscience 2 (6): 425–33. https://doi.org/10.1038/35077566.

Galizia, C. Giovanni, Dorothea Eisenhardt, and Martin Giurfa. 2011. Honeybee Neurobiology and Behavior: A Tribute to Randolf Menzel. Springer Science & Business Media.

Gall, Christine M., and Gary Lynch. 2004. 'Integrins, Synaptic Plasticity and Epileptogenesis'. In Recent Advances in Epilepsy Research, edited by Devin K. Binder and Helen E. Scharfman, 12–33. Advances in Experimental Medicine and Biology. Boston, MA: Springer US. https://doi.org/10.1007/978-1-4757-6376-8_2.

Garami, Attila, Fried J. T Zwartkruis, Takahiro Nobukuni, Manel Joaquin, Marta Roccio, Hugo Stocker, Sara C Kozma, Ernst Hafen, Johannes L Bos, and George Thomas. 2003. 'Insulin Activation of Rheb, a Mediator of MTOR/S6K/4E-BP Signaling, Is Inhibited by TSC1 and 2'. Molecular Cell 11 (6): 1457–66. https://doi.org/10.1016/S1097-2765(03)00220-X.

Garcia-Rill, Edgar, Amanda Charlesworth, David Heister, Meijun Ye, and Abdallah Hayar. 2008. 'The Developmental Decrease in REM Sleep: The Role of Transmitters and Electrical Coupling'. Sleep 31 (5): 673–90. https://doi.org/10.1093/sleep/31.5.673.

Gatto, Cheryl L., and Kendal Broadie. 2010. 'Genetic Controls Balancing Excitatory and Inhibitory Synaptogenesis in Neurodevelopmental Disorder Models'. Frontiers in Synaptic Neuroscience 2. https://doi.org/10.3389/fnsyn.2010.00004.

Gauthier, Julie, Dan Spiegelman, Amélie Piton, Ronald G. Lafrenière, Sandra Laurent, Judith St-Onge, Line Lapointe, et al. 2009. 'Novel de Novo SHANK3 Mutation in Autistic Patients'. American Journal of Medical Genetics Part B: Neuropsychiatric Genetics 150B (3): 421–24. https://doi.org/10.1002/ajmg.b.30822.

Geiss-Friedlander, Ruth, and Frauke Melchior. 2007. 'Concepts in Sumoylation: A Decade On'. Nature Reviews. Molecular Cell Biology 8 (12): 947–56. https://doi.org/10.1038/nrm2293.

Geiss-Friedlander, Ruth, and Frauke Melchior. 2007. 'Concepts in Sumoylation: A Decade On'. Nature Reviews. Molecular Cell Biology 8 (12): 947–56. https://doi.org/10.1038/nrm2293.

Gerber, Scott A., John Rush, Olaf Stemman, Marc W. Kirschner, and Steven P. Gygi. 2003. 'Absolute Quantification of Proteins and Phosphoproteins from Cell Lysates by Tandem MS'. Proceedings of the National Academy of Sciences 100 (12): 6940–45. https://doi.org/10.1073/pnas.0832254100.

Gerits, Nancy, Sergiy Kostenko, Alexey Shiryaev, Mona Johannessen, and Ugo Moens. 2008. 'Relations between the Mitogen-Activated Protein Kinase and the CAMP-Dependent Protein Kinase Pathways: Comradeship and Hostility'. Cellular Signalling 20 (9): 1592–1607. https://doi.org/10.1016/j.cellsig.2008.02.022.

Gerrow, Kimberly, and Alaa El-Husseini. 2006. 'Cell Adhesion Molecules at the Synapse'. Frontiers in Bioscience: A Journal and Virtual Library 11 (September): 2400–2419.

Giacometti, Emanuela, Sandra Luikenhuis, Caroline Beard, and Rudolf Jaenisch. 2007. 'Partial Rescue of MeCP2 Deficiency by Postnatal Activation of MeCP2'. Proceedings of the National Academy of Sciences 104 (6): 1931–36. https://doi.org/10.1073/pnas.0610593104.

Gilbert, James, and Heng-Ye Man. 2017. 'Fundamental Elements in Autism: From Neurogenesis and Neurite Growth to Synaptic Plasticity'. Frontiers in Cellular Neuroscience 11: 359. https://doi.org/10.3389/fncel.2017.00359.

Giovanoli, Sandra, Ulrike Weber-Stadlbauer, Manfred Schedlowski, Urs Meyer, and Harald Engler. 2016. 'Prenatal Immune Activation Causes Hippocampal Synaptic Deficits in the Absence of Overt Microglia Anomalies'. Brain, Behavior, and Immunity 55: 25–38. https://doi.org/10.1016/j.bbi.2015.09.015.

Glanzer, J., K. Y. Miyashiro, J.-Y. Sul, L. Barrett, B. Belt, P. Haydon, and J. Eberwine. 2005. 'RNA Splicing Capability of Live Neuronal Dendrites'. Proceedings of the National Academy of Sciences 102 (46): 16859–64. https://doi.org/10.1073/pnas.0503783102.

Goel, Anubhuti, Linda W. Xu, Kevin P. Snyder, Lihua Song, Yamila Goenaga-Vazquez, Andrea Megill, Kogo Takamiya, Richard L. Huganir, and Hey-Kyoung Lee. 2011. 'Phosphorylation of AMPA Receptors Is Required for Sensory Deprivation-Induced Homeostatic Synaptic Plasticity'. PLOS ONE 6 (3): e18264. https://doi.org/10.1371/journal.pone.0018264.

Goffinet, A. M. 1983. 'The Embryonic Development of the Cerebellum in Normal and Reeler Mutant Mice'. Anatomy and Embryology 168 (1): 73–86.

Gómez de Salazar, Macarena, Cristina Grau, Francisco Ciruela, and Xavier Altafaj. 2018. 'Phosphoproteomic Alterations of Ionotropic Glutamate Receptors in the Hippocampus of the Ts65Dn Mouse Model of Down Syndrome'. Frontiers in Molecular Neuroscience 11. https://doi.org/10.3389/fnmol.2018.00226.

Gomperts, Stephen N. 1996. 'Clustering Membrane Proteins: It's All Coming Together with the PSD-95/SAP90 Protein Family'. Cell 84 (5): 659–62. https://doi.org/10.1016/S0092-8674(00)81043-0.

Gonzalez-Lozano, Miguel A., Patricia Klemmer, Titia Gebuis, Chopie Hassan, Pim van Nierop, Ronald E. van Kesteren, August B. Smit, and Ka Wan Li. 2016. 'Dynamics of the Mouse Brain Cortical Synaptic Proteome during Postnatal Brain Development'. Scientific Reports 6 (October): 35456. https://doi.org/10.1038/srep35456.

Good, Matthew C., Jesse G. Zalatan, and Wendell A. Lim. 2011. 'Scaffold Proteins: Hubs for Controlling the Flow of Cellular Information'. Science (New York, N.Y.) 332 (6030): 680–86. https://doi.org/10.1126/science.1198701.

Govek, Eve-Ellen, Sarah E. Newey, and Linda Van Aelst. 2005. 'The Role of the Rho GTPases in Neuronal Development'. Genes & Development 19 (1): 1–49. https://doi.org/10.1101/gad.1256405.

Grabowski, Paula. 2011. 'Alternative Splicing Takes Shape during Neuronal Development'. Current Opinion in Genetics & Development 21 (4): 388–94. https://doi.org/10.1016/j.gde.2011.03.005.

Grabrucker, Andreas M., Mary J. Knight, Christian Proepper, Juergen Bockmann, Marisa Joubert, Magali Rowan, G. Ulrich Nienhaus, et al. 2011. 'Concerted Action of Zinc and ProSAP/Shank in Synaptogenesis and Synapse Maturation'. The EMBO Journal 30 (3): 569–81. https://doi.org/10.1038/emboj.2010.336.

Graf, Ethan R., XueZhao Zhang, Shan-Xue Jin, Michael W. Linhoff, and Ann Marie Craig. 2004. 'Neurexins Induce Differentiation of GABA and Glutamate Postsynaptic Specializations via Neuroligins'. Cell 119 (7): 1013–26. https://doi.org/10.1016/j.cell.2004.11.035.

Graham, Laura C., Samantha L. Eaton, Paula J. Brunton, Abdelmadjid Atrih, Colin Smith, Douglas J. Lamont, Thomas H. Gillingwater, Giuseppa Pennetta, Paul Skehel, and Thomas M. Wishart. 2017. 'Proteomic Profiling of Neuronal Mitochondria Reveals Modulators of Synaptic Architecture'. Molecular Neurodegeneration 12 (October). https://doi.org/10.1186/s13024-017-0221-9.

Grant, Seth G. N. 2003. 'Synapse Signalling Complexes and Networks: Machines Underlying Cognition'. BioEssays: News and Reviews in Molecular, Cellular and Developmental Biology 25 (12): 1229–35. https://doi.org/10.1002/bies.10381.

Grant, Seth G. N. 2007. 'Toward a Molecular Catalogue of Synapses'. Brain Research Reviews 55 (2): 445–49. https://doi.org/10.1016/j.brainresrev.2007.05.003.

Grant, Seth G. N. 2019. 'The Synaptomic Theory of Behavior and Brain Disease'. *Cold Spring Harbor Symposia on Quantitative Biology*, March, 037887. https://doi.org/10.1101/sqb.2018.83.037887.

Grant, Seth G. N., Claudia Bagni, and Thomas J. O'Dell. 2016. 'Synaptopathy--From Biology to Therapy'. Neuropharmacology 100 (January): 1. https://doi.org/10.1016/j.neuropharm.2015.08.022.

Grant, Seth G. N., Michael C. Marshall, Keri-Lee Page, Mark A. Cumiskey, and J. Douglas Armstrong. 2005. 'Synapse Proteomics of Multiprotein Complexes: En Route from Genes to Nervous System Diseases'. Human Molecular Genetics 14 Spec No. 2 (October): R225-234. https://doi.org/10.1093/hmg/ddi330.

Grant, Seth G. N., Michael C. Marshall, Keri-Lee Page, Mark A. Cumiskey, and J. Douglas Armstrong. 2005. 'Synapse Proteomics of Multiprotein Complexes: En Route from Genes to Nervous System Diseases'. Human Molecular Genetics 14 Spec No. 2 (October): R225-234. https://doi.org/10.1093/hmg/ddi330.

Grant, Seth G.N. 2012. 'Synaptopathies: Diseases of the Synaptome'. Current Opinion in Neurobiology 22 (3): 522–29. https://doi.org/10.1016/j.conb.2012.02.002.

Grantham-McGregor, Sally, Yin Bun Cheung, Santiago Cueto, Paul Glewwe, Linda Richter, Barbara Strupp, and International Child Development Steering Group. 2007. 'Developmental Potential in the First 5 Years for Children in Developing Countries'. Lancet (London, England) 369 (9555): 60–70. https://doi.org/10.1016/S0140-6736(07)60032-4.

Gray, E. G. 1959. 'Electron Microscopy of Synaptic Contacts on Dendrite Spines of the Cerebral Cortex'. Nature 183 (4675): 1592–93.

Greene-Schloesser, D. M., E. A. Van der Zee, D. K. Sheppard, M. R. Castillo, K. A. Gregg, T. Burrow, H. Foltz, M. Slater, and A. Bult-Ito. 2011. 'Predictive Validity of a Non-Induced Mouse Model of Compulsive-like Behavior'. Behavioural Brain Research 221 (1): 55–62. https://doi.org/10.1016/j.bbr.2011.02.010.

Greger, Ingo H, Latika Khatri, Xiangpeng Kong, and Edward B Ziff. 2003. 'AMPA Receptor Tetramerization Is Mediated by Q/R Editing'. Neuron 40 (4): 763–74. https://doi.org/10.1016/S0896-6273(03)00668-8.

Greger, Ingo H., Edward B. Ziff, and Andrew C. Penn. 2007. 'Molecular Determinants of AMPA Receptor Subunit Assembly'. Trends in Neurosciences 30 (8): 407–16. https://doi.org/10.1016/j.tins.2007.06.005.

Gribaudo, S., S. Bovetti, D. Garzotto, A. Fasolo, and S. De Marchis. 2009. 'Expression and Localization of the Calmodulin-binding Protein Neurogranin in the Adult Mouse Olfactory Bulb'. Journal of Comparative Neurology 517 (5): 683–94. https://doi.org/10.1002/cne.22177.

Grice, Dorothy E., and Joseph D. Buxbaum. 2006. 'The Genetics of Autism Spectrum Disorders'. Neuromolecular Medicine 8 (4): 451–60. https://doi.org/10.1385/NMM:8:4:451.

Grinspan, Zachary M., Niu Tian, Elissa G. Yozawitz, Patricia E. McGoldrick, Steven M. Wolf, Tiffani L. McDonough, Aaron Nelson, Baria Hafeez, Stephen B. Johnson, and Dale C. Hesdorffer. 2018. 'Common Terms for Rare Epilepsies: Synonyms, Associated Terms, and Links to Structured Vocabularies'. Epilepsia Open 3 (1): 91–97. https://doi.org/10.1002/epi4.12095.

Gruart, Agnès, María Dolores Muñoz, and José M. Delgado-García. 2006. 'Involvement of the CA3–CA1 Synapse in the Acquisition of Associative Learning in Behaving Mice'. Journal of Neuroscience 26 (4): 1077–87. https://doi.org/10.1523/JNEUROSCI.2834-05.2006.

Grunditz, Asa, Niklaus Holbro, Lei Tian, Yi Zuo, and Thomas G. Oertner. 2008. 'Spine Neck Plasticity Controls Postsynaptic Calcium Signals through Electrical Compartmentalization'. The Journal of Neuroscience: The Official Journal of the Society for Neuroscience 28 (50): 13457–66. https://doi.org/10.1523/JNEUROSCI.2702-08.2008.

Grutzendler, Jaime, Narayanan Kasthuri, and Wen-Biao Gan. 2002. 'Long-Term Dendritic Spine Stability in the Adult Cortex'. Nature 420 (6917): 812–16. https://doi.org/10.1038/nature01276.

Gulledge, Allan T., Nicholas T. Carnevale, and Greg J. Stuart. 2012. 'Electrical Advantages of Dendritic Spines'. PLoS ONE 7 (4). https://doi.org/10.1371/journal.pone.0036007.

Guo, Xiaochuan, Peter Hamilton, Nicholas J. Reish, J. David Sweatt, Courtney A. Miller, and Gavin Rumbaugh. 2009. 'Reduced Expression of the NMDA Receptor-Interacting Protein SynGAP Causes Behavioral Abnormalities That Model Symptoms of Schizophrenia'. Neuropsychopharmacology : Official Publication of the American College of Neuropsychopharmacology 34 (7): 1659–72. https://doi.org/10.1038/npp.2008.223.

Gurniak, Christine B., Emerald Perlas, and Walter Witke. 2005. 'The Actin Depolymerizing Factor N-Cofilin Is Essential for Neural Tube Morphogenesis and Neural Crest Cell Migration'. Developmental Biology 278 (1): 231–41. https://doi.org/10.1016/j.ydbio.2004.11.010.

Hafner, Christian, and Leopold Groesser. 2013. 'Mosaic RASopathies'. Cell Cycle (Georgetown, Tex.) 12 (1): 43–50. https://doi.org/10.4161/cc.23108.

Hahn, Won-Ho, Jin-Soon Suh, Byoung-Soo Cho, and Sung-Do Kim. 2009. 'The Enabled Homolog Gene Polymorphisms Are Associated with Susceptibility and Progression of Childhood IgA Nephropathy'. Experimental & Molecular Medicine 41 (11): 793–801. https://doi.org/10.3858/emm.2009.41.11.085.

Halassa, Michael M., Tommaso Fellin, and Philip G. Haydon. 2007. 'The Tripartite Synapse: Roles for Gliotransmission in Health and Disease'. Trends in Molecular Medicine 13 (2): 54–63. https://doi.org/10.1016/j.molmed.2006.12.005.

Hall, A. 1990. 'Ras and GAP--Who's Controlling Whom?' Cell 61 (6): 921–23.

Hall, Alan, and Giovanna Lalli. 2010. 'Rho and Ras GTPases in Axon Growth, Guidance, and Branching'. Cold Spring Harbor Perspectives in Biology 2 (2): a001818. https://doi.org/10.1101/cshperspect.a001818.

Hallmayer, Joachim, Sue Cleveland, Andrea Torres, Jennifer Phillips, Brianne Cohen, Tiffany Torigoe, Janet Miller, et al. 2011. 'Genetic Heritability and Shared Environmental Factors among Twin Pairs with Autism'. Archives of General Psychiatry 68 (11): 1095–1102. https://doi.org/10.1001/archgenpsychiatry.2011.76.

Hamdan, Fadi F., Hussein Daoud, Amélie Piton, Julie Gauthier, Sylvia Dobrzeniecka, Marie-Odile Krebs, Ridha Joober, et al. 2011. 'De Novo SYNGAP1 Mutations in Nonsyndromic Intellectual Disability and Autism'. Biological Psychiatry 69 (9): 898–901. https://doi.org/10.1016/j.biopsych.2010.11.015.

Hamdan, Fadi F., Julie Gauthier, Dan Spiegelman, Anne Noreau, Yan Yang, Stéphanie Pellerin, Sylvia Dobrzeniecka, et al. 2009. 'Mutations in SYNGAP1 in Autosomal Nonsyndromic Mental Retardation'. The New England Journal of Medicine 360 (6): 599–605. https://doi.org/10.1056/NEJMoa0805392.

Hamdan, Fadi F., Julie Gauthier, Yoichi Araki, Da-Ting Lin, Yuhki Yoshizawa, Kyohei Higashi, A-Reum Park, et al. 2011. 'Excess of De Novo Deleterious Mutations in Genes Associated with Glutamatergic Systems in Nonsyndromic Intellectual Disability'. American Journal of Human Genetics 88 (3): 306–16. https://doi.org/10.1016/j.ajhg.2011.02.001.

Hamdan, Fadi F., Julie Gauthier, Yoichi Araki, Da-Ting Lin, Yuhki Yoshizawa, Kyohei Higashi, A-Reum Park, et al. 2011. 'Excess of De Novo Deleterious Mutations in Genes Associated with Glutamatergic Systems in Nonsyndromic Intellectual Disability'. American Journal of Human Genetics 88 (3): 306–16. https://doi.org/10.1016/j.ajhg.2011.02.001.

Hanse, Eric, Henrik Seth, and Ilse Riebe. 2013. 'AMPA-Silent Synapses in Brain Development and Pathology'. Nature Reviews Neuroscience 14 (12): 839–50. https://doi.org/10.1038/nrn3642.

Harnett, Mark T., Judit K. Makara, Nelson Spruston, William L. Kath, and Jeffrey C. Magee. 2012. 'Synaptic Amplification by Dendritic Spines Enhances Input Cooperativity'. Nature 491 (7425): 599–602. https://doi.org/10.1038/nature11554.

Harris, K M, and S B Kater. 1994. 'Dendritic Spines: Cellular Specializations Imparting Both Stability and Flexibility to Synaptic Function'. Annual Review of Neuroscience 17 (1): 341–71. https://doi.org/10.1146/annurev.ne.17.030194.002013.

Harris, Kristen M., and Richard J. Weinberg. 2012. 'Ultrastructure of Synapses in the Mammalian Brain'. Cold Spring Harbor Perspectives in Biology 4 (5). https://doi.org/10.1101/cshperspect.a005587.

Harvey, Christopher D., and Karel Svoboda. 2007. 'Locally Dynamic Synaptic Learning Rules in Pyramidal Neuron Dendrites'. Nature 450 (7173): 1195–1200. https://doi.org/10.1038/nature06416.

Hayashi, Mariko Kato, Chunyan Tang, Chiara Verpelli, Radhakrishnan Narayanan, Marissa H. Stearns, Rui-Ming Xu, Huilin Li, Carlo Sala, and Yasunori Hayashi. 2009. 'The Postsynaptic Density Proteins Homer and Shank Form a Polymeric Network Structure'. Cell 137 (1): 159–71. https://doi.org/10.1016/j.cell.2009.01.050.

Hebb DO. 1949. The organization of behavior: a neuropsychological theory. New York: Wiley;

Heidelberger, Ruth, Harel Shouval, Robert S. Zucker, and John H. Byrne. 2014. 'Synaptic Plasticity'. In From Molecules to Networks, 533–61. Elsevier. https://doi.org/10.1016/B978-0-12-397179-1.00018-X.

Hell, Johannes W. 2014. 'CaMKII: Claiming Center Stage in Postsynaptic Function and Organization'. Neuron 81 (2): 249–65. https://doi.org/10.1016/j.neuron.2013.12.024.

Henriquez, Berta, Fernando J. Bustos, Rodrigo Aguilar, Alvaro Becerra, Felipe Simon, Martin Montecino, and Brigitte van Zundert. 2013. 'Ezh1 and Ezh2 Differentially Regulate PSD-95 Gene Transcription in Developing Hippocampal Neurons'. Molecular and Cellular Neuroscience 57 (November): 130–43. https://doi.org/10.1016/j.mcn.2013.07.012.

Hensch, Takao K. 2004. 'Critical Period Regulation'. Annual Review of Neuroscience 27 (1): 549–79. https://doi.org/10.1146/annurev.neuro.27.070203.144327.

Hensch, Takao K. 2005. 'Critical Period Plasticity in Local Cortical Circuits'. Nature Reviews. Neuroscience 6 (11): 877–88. https://doi.org/10.1038/nrn1787.

Hensch, Takao K., and Michela Fagiolini. 2005. 'Excitatory-Inhibitory Balance and Critical Period Plasticity in Developing Visual Cortex'. Progress in Brain Research 147: 115–24. https://doi.org/10.1016/S0079-6123(04)47009-5.

Heo, Seok, Graham H. Diering, Chan Hyun Na, Raja Sekhar Nirujogi, Julia L. Bachman, Akhilesh Pandey, and Richard L. Huganir. 2018. 'Identification of Long-Lived Synaptic Proteins by Proteomic Analysis of Synaptosome Protein Turnover'. Proceedings of the National Academy of Sciences of the United States of America 115 (16): E3827–36. https://doi.org/10.1073/pnas.1720956115.

Herculano-Houzel, Suzana. 2012. 'The Remarkable, yet Not Extraordinary, Human Brain as a Scaled-up Primate Brain and Its Associated Cost'. Proceedings of the National Academy of Sciences of the United States of America 109 (Suppl 1): 10661–68. https://doi.org/10.1073/pnas.1201895109.

Hering, Heike, and Morgan Sheng. 2001. 'Dentritic Spines : Structure, Dynamics and Regulation'. Nature Reviews Neuroscience 2 (December): 880.

Hering, Heike, Chih-Chun Lin, and Morgan Sheng. 2003. 'Lipid Rafts in the Maintenance of Synapses, Dendritic Spines, and Surface AMPA Receptor Stability'. Journal of Neuroscience 23 (8): 3262–71. https://doi.org/10.1523/JNEUROSCI.23-08-03262.2003.

Hiatt, Susan M., Matthew B. Neu, Ryne C. Ramaker, Andrew A. Hardigan, Jeremy W. Prokop, Miroslava Hancarova, Darina Prchalova, et al. 2018. 'De Novo Mutations in the GTP/GDP-Binding Region of RALA, a RAS-like Small GTPase, Cause Intellectual Disability and Developmental Delay'. PLOS Genetics 14 (11): e1007671. https://doi.org/10.1371/journal.pgen.1007671.

Hill, W. D., G. Davies, D. C. Liewald, A. Payton, C. J. McNeil, L. J. Whalley, M. Horan, et al. 2016. 'Examining Non-Syndromic Autosomal Recessive Intellectual Disability (NS-ARID) Genes for an Enriched Association with Intelligence Differences'. Intelligence 54 (January): 80–89. https://doi.org/10.1016/j.intell.2015.11.005.

Hirosawa, Makoto, Masaki Hoshida, Masato Ishikawa, and Tomoyuki Toya. 1993. 'MASCOT: Multiple Alignment System for Protein Sequences Based on Three-Way Dynamic Programming'. Bioinformatics 9 (2): 161–67. https://doi.org/10.1093/bioinformatics/9.2.161.

Hoeffer, Charles A., and Eric Klann. 2010. 'MTOR Signaling: At the Crossroads of Plasticity, Memory and Disease'. Trends in Neurosciences 33 (2): 67–75. https://doi.org/10.1016/j.tins.2009.11.003.

Hof, Patrick R., Huiling Duan, Tanya L. Page, Michael Einstein, Bridget Wicinski, Yong He, Joseph M. Erwin, and John H. Morrison. 2002. 'Age-Related Changes in GluR2 and NMDAR1 Glutamate Receptor Subunit Protein Immunoreactivity in Corticocortically Projecting Neurons in Macaque and Patas Monkeys'. Brain Research 928 (1): 175–86. https://doi.org/10.1016/S0006-8993(01)03345-5.

Hollmann, Michael, and Stephen Heinemann. 1994. 'Cloned Glutamate Receptors'. Annual Review of Neuroscience 17 (1): 31–108. https://doi.org/10.1146/annurev.ne.17.030194.000335.

Hoon, Mrinalini, Tolga Soykan, Björn Falkenburger, Matthieu Hammer, Annarita Patrizi, Karl-Friedrich Schmidt, Marco Sassoè-Pognetto, et al. 2011. 'Neuroligin-4 Is Localized to Glycinergic Postsynapses and Regulates Inhibition in the Retina'. Proceedings of the National Academy of Sciences, January, 201006946. https://doi.org/10.1073/pnas.1006946108.

Hormuzdi, Sheriar G., Isabel Pais, Fiona E. N. LeBeau, Stephen K. Towers, Andrei Rozov, Eberhard H. Buhl, Miles A. Whittington, and Hannah Monyer. 2001. 'Impaired Electrical Signaling Disrupts Gamma Frequency Oscillations in Connexin 36-Deficient Mice'. Neuron 31 (3): 487–95. https://doi.org/10.1016/S0896-6273(01)00387-7.

Horne, Eric A., and Mark L. Dell'Acqua. 2007. 'Phospholipase C Is Required for Changes in Postsynaptic Structure and Function Associated with NMDA Receptor-Dependent Long-Term Depression'. The Journal of Neuroscience: The Official Journal of the Society for Neuroscience 27 (13): 3523–34. https://doi.org/10.1523/JNEUROSCI.4340-06.2007.

Hotulainen, Pirta, and Casper C. Hoogenraad. 2010. 'Actin in Dendritic Spines: Connecting Dynamics to Function'. The Journal of Cell Biology 189 (4): 619–29. https://doi.org/10.1083/jcb.201003008.

Hsiao, Elaine Y., Sara W. McBride, Sophia Hsien, Gil Sharon, Embriette R. Hyde, Tyler McCue, Julian A. Codelli, et al. 2013. 'Microbiota Modulate Behavioral and Physiological Abnormalities Associated with Neurodevelopmental Disorders'. Cell 155 (7): 1451–63. https://doi.org/10.1016/j.cell.2013.11.024.

Hu, Bing-Ren, Minkyu Park, Maryann E. Martone, Wolfgang H. Fischer, Mark H. Ellisman, and Justin A. Zivin. 1998. 'Assembly of Proteins to Postsynaptic Densities after Transient Cerebral Ischemia'. Journal of Neuroscience 18 (2): 625–33. https://doi.org/10.1523/JNEUROSCI.18-02-00625.1998.

Huang, Chiung-Chun, Jia-Lin You, Mei-Ying Wu, and Kuei-Sen Hsu. 2004. 'Rap1-Induced P38 Mitogen-Activated Protein Kinase Activation Facilitates AMPA Receptor Trafficking via the GDI.Rab5 Complex. Potential Role in (S)-3,5-Dihydroxyphenylglycene-Induced Long Term Depression'. The Journal of Biological Chemistry 279 (13): 12286–92. https://doi.org/10.1074/jbc.M312868200.

Huber, Andrea B., Alex L. Kolodkin, David D. Ginty, and Jean-François Cloutier. 2003. 'SIGNALING AT THE GROWTH CONE: Ligand-Receptor Complexes and the Control of Axon Growth and Guidance'. Annual Review of Neuroscience 26 (1): 509–63. https://doi.org/10.1146/annurev.neuro.26.010302.081139.

Huganir, Richard L., and Roger A. Nicoll. 2013. 'AMPARs and Synaptic Plasticity: The Last 25 Years'. Neuron 80 (3): 704–17. https://doi.org/10.1016/j.neuron.2013.10.025.

Husi, Holger, Malcolm A. Ward, Jyoti S. Choudhary, Walter P. Blackstock, and Seth G. N. Grant. 2000. 'Proteomic Analysis of NMDA Receptor–Adhesion Protein Signaling Complexes'. Nature Neuroscience 3 (7): 661–69. https://doi.org/10.1038/76615.

Hyvönen, M., M. J. Macias, M. Nilges, H. Oschkinat, M. Saraste, and M. Wilmanns. 1995. 'Structure of the Binding Site for Inositol Phosphates in a PH Domain'. The EMBO Journal 14 (19): 4676–85.

Ibata, Keiji, Qian Sun, and Gina G. Turrigiano. 2008. 'Rapid Synaptic Scaling Induced by Changes in Postsynaptic Firing'. Neuron 57 (6): 819–26. https://doi.org/10.1016/j.neuron.2008.02.031.

Ikeda, Kaori, and John M. Bekkers. 2006. 'Autapses'. Current Biology 9 (16): R308. https://doi.org/10.1016/j.cub.2006.03.085.

Inder, T. E., and P. S. Huppi. 2000. 'In Vivo Studies of Brain Development by Magnetic Resonance Techniques'. Mental Retardation and Developmental Disabilities Research Reviews 6 (1): 59–67. https://doi.org/10.1002/(SICI)1098-2779(2000)6:1<59::AID-MRDD8>3.0.CO;2-E.

Ingalhalikar, Madhura, Drew Parker, Yasser Ghanbari, Alex Smith, Kegang Hua, Susumu Mori, Ted Abel, Christos Davatzikos, and Ragini Verma. 2015. 'Connectome and Maturation Profiles of the Developing Mouse Brain Using Diffusion Tensor Imaging'. Cerebral Cortex 25 (9): 2696–2706. https://doi.org/10.1093/cercor/bhu068.

International Human Genome Sequencing Consortium. 2004. 'Finishing the Euchromatic Sequence of the Human Genome'. Nature 431 (7011): 931–45. https://doi.org/10.1038/nature03001.

Iossifov, Ivan, Brian J. O'Roak, Stephan J. Sanders, Michael Ronemus, Niklas Krumm, Dan Levy, Holly A. Stessman, et al. 2014. 'The Contribution of de Novo Coding Mutations to Autism Spectrum Disorder'. Nature 515 (7526): 216–21. https://doi.org/10.1038/nature13908.

Irimia, Manuel, Robert J. Weatheritt, Jonathan D. Ellis, Neelroop N. Parikshak, Thomas Gonatopoulos-Pournatzis, Mariana Babor, Mathieu Quesnel-Vallières, et al. 2014. 'A Highly Conserved Program of Neuronal Microexons Is Misregulated in Autistic Brains'. Cell 159 (7): 1511–23. https://doi.org/10.1016/j.cell.2014.11.035.

Isaac, John T. R., Michael C. Ashby, and Chris J. McBain. 2007. 'The Role of the GluR2 Subunit in AMPA Receptor Function and Synaptic Plasticity'. Neuron 54 (6): 859–71. https://doi.org/10.1016/j.neuron.2007.06.001.

Ivanov, Hristo Y., Vili K. Stoyanova, Nikolay T. Popov, and Tihomir I. Vachev. 2015. 'Autism Spectrum Disorder - A Complex Genetic Disorder'. Folia Medica 57 (1). https://doi.org/10.1515/folmed-2015-0015.

Jacobs, Bob, Matthew Schall, Melissa Prather, Elisa Kapler, Lori Driscoll, Serapio Baca, Jesse Jacobs, Kevin Ford, Marcy Wainwright, and Melinda Treml. 2001. 'Regional Dendritic and Spine Variation in Human Cerebral Cortex: A Quantitative Golgi Study'. Cerebral Cortex 11 (6): 558–71. https://doi.org/10.1093/cercor/11.6.558.

Jaffer, Sajjida, Vasily Vorobyov, Peter C. Kind, and Frank Sengpiel. 2012. 'Experience-Dependent Regulation of Functional Maps and Synaptic Protein Expression in the Cat Visual Cortex'. The European Journal of Neuroscience 35 (8): 1281–94. https://doi.org/10.1111/j.1460-9568.2012.08044.x.

Jarius, S., B. Wildemann, W. Stöcker, A. Moser, and K. P. Wandinger. 2015. 'Psychotic Syndrome Associated with Anti-Ca/ARHGAP26 and Voltage-Gated Potassium Channel Antibodies'. Journal of Neuroimmunology 286 (September): 79–82. https://doi.org/10.1016/j.jneuroim.2015.07.009.

Jeyabalan, Nallathambi, and James P. Clement. 2016. 'SYNGAP1: Mind the Gap'. Frontiers in Cellular Neuroscience 10 (February). https://doi.org/10.3389/fncel.2016.00032.

Jhou, Jia-Fong, and Hwan-Ching Tai. 2017. 'The Study of Postmortem Human Synaptosomes for Understanding Alzheimer's Disease and Other Neurological Disorders: A Review'. Neurology and Therapy 6 (Suppl 1): 57–68. https://doi.org/10.1007/s40120-017-0070-z.

Ji, Ru-Rong, Tatsuro Kohno, Kimberly A. Moore, and Clifford J. Woolf. 2003. 'Central Sensitization and LTP: Do Pain and Memory Share Similar Mechanisms?' Trends in Neurosciences 26 (12): 696–705. https://doi.org/10.1016/j.tins.2003.09.017.

Johansson, Barbro B. 2000. 'Brain Plasticity and Stroke Rehabilitation: The Willis Lecture'. Stroke 31 (1): 223–30. https://doi.org/10.1161/01.STR.31.1.223.

Johnson, Mark H. 2005. 'Sensitive Periods in Functional Brain Development: Problems and Prospects'. Developmental Psychobiology 46 (3): 287–92. https://doi.org/10.1002/dev.20057.

Jones, EG, GW Huntley, and DL Benson. 1994. 'Alpha Calcium/Calmodulin-Dependent Protein Kinase II Selectively Expressed in a Subpopulation of Excitatory Neurons in Monkey Sensory- Motor Cortex: Comparison with GAD-67 Expression'. The Journal of Neuroscience 14 (2): 611. https://doi.org/10.1523/JNEUROSCI.14-02-00611.1994.

Jones, Peter A., and Stephen B. Baylin. 2007. 'The Epigenomics of Cancer'. Cell 128 (4): 683–92. https://doi.org/10.1016/j.cell.2007.01.029.

Jordan, Bryen A., and Michael R. Kreutz. 2009. 'Nucleocytoplasmic Protein Shuttling: The Direct Route in Synapse-to-Nucleus Signaling'. Trends in Neurosciences 32 (7): 392–401. https://doi.org/10.1016/j.tins.2009.04.001.

Jordan, Bryen A., Brian D. Fernholz, Muriel Boussac, Chongfeng Xu, Gabriela Grigorean, Edward B. Ziff, and Thomas A. Neubert. 2004. 'Identification and Verification of Novel Rodent Postsynaptic Density Proteins'. Molecular & Cellular Proteomics 3 (9): 857–71. https://doi.org/10.1074/mcp.M400045-MCP200.

Jurado, Sandra, Debanjan Goswami, Yingsha Zhang, Alfredo J. Miñano Molina, Thomas C. Südhof, and Robert C. Malenka. 2013. 'LTP Requires a Unique Postsynaptic SNARE Fusion Machinery'. Neuron 77 (3): 542–58. https://doi.org/10.1016/j.neuron.2012.11.029.

Jurado, Sandra, Marion Benoist, Argentina Lario, Shira Knafo, Cortney N. Petrok, and José A. Esteban. 2010. 'PTEN Is Recruited to the Postsynaptic Terminal for NMDA Receptor-Dependent Long-Term Depression'. The EMBO Journal 29 (16): 2827–40. https://doi.org/10.1038/emboj.2010.160.

Kamiguchi, H., and V. Lemmon. 2000. 'Recycling of the Cell Adhesion Molecule L1 in Axonal Growth Cones'. The Journal of Neuroscience: The Official Journal of the Society for Neuroscience 20 (10): 3676–86.

Kandt, R. S., J. L. Haines, M. Smith, H. Northrup, R. J. Gardner, M. P. Short, K. Dumars, E. S. Roach, S. Steingold, and S. Wall. 1992. 'Linkage of an Important Gene Locus for Tuberous Sclerosis to a Chromosome 16 Marker for Polycystic Kidney Disease'. Nature Genetics 2 (1): 37–41. https://doi.org/10.1038/ng0992-37.

Kaneko, Takeshi, and Fumino Fujiyama. 2002. 'Complementary Distribution of Vesicular Glutamate Transporters in the Central Nervous System'. Neuroscience Research 42 (4): 243–50. https://doi.org/10.1016/S0168-0102(02)00009-3.

Kappel, David, Stefan Habenschuss, Robert Legenstein, and Wolfgang Maass. 2015. 'Network Plasticity as Bayesian Inference'. PLoS Computational Biology 11 (11): e1004485. https://doi.org/10.1371/journal.pcbi.1004485.

Kasai, Haruo, Masahiro Fukuda, Satoshi Watanabe, Akiko Hayashi-Takagi, and Jun Noguchi. 2010. 'Structural Dynamics of Dendritic Spines in Memory and Cognition'. Trends in Neurosciences 33 (3): 121–29. https://doi.org/10.1016/j.tins.2010.01.001.

Kasai, Haruo, Masanori Matsuzaki, Jun Noguchi, Nobuaki Yasumatsu, and Hiroyuki Nakahara. 2003. 'Structure–Stability–Function Relationships of Dendritic Spines'. Trends in Neurosciences 26 (7): 360–68. https://doi.org/10.1016/S0166-2236(03)00162-0.

Kaufman, Liana, Muhammad Ayub, and John B. Vincent. 2010. 'The Genetic Basis of Non-Syndromic Intellectual Disability: A Review'. Journal of Neurodevelopmental Disorders 2 (4): 182. https://doi.org/10.1007/s11689-010-9055-2.

Kaushik, R., K. M. Grochowska, I. Butnaru, and M. R. Kreutz. 2014. 'Protein Trafficking from Synapse to Nucleus in Control of Activity-Dependent Gene Expression'. Neuroscience 280 (November): 340–50. https://doi.org/10.1016/j.neuroscience.2014.09.011.

Kazmin, Dmitri, Robert A. Edwards, Raymond J. Turner, Eric Larson, and Jean Starkey. 2002. 'Visualization of Proteins in Acrylamide Gels Using Ultraviolet Illumination'. Analytical Biochemistry 301 (1): 91–96. https://doi.org/10.1006/abio.2001.5488.

Keith, Dove J., and Alaa El-Husseini. 2008. 'Excitation Control: Balancing PSD-95 Function at the Synapse'. Frontiers in Molecular Neuroscience 1. https://doi.org/10.3389/neuro.02.004.2008.

Kelleher, Raymond J., and Mark F. Bear. 2008. 'The Autistic Neuron: Troubled Translation?' Cell 135 (3): 401–6. https://doi.org/10.1016/j.cell.2008.10.017.

Kelly, Paul T., and Paula Vernon. 1985. 'Changes in the Subcellular Distribution of Calmodulin-Kinase II during Brain Development'. Developmental Brain Research 18 (1): 211–24. https://doi.org/10.1016/0165-3806(85)90265-2.

Kennedy, Mary B. 1993. 'The Postsynaptic Density'. Current Opinion in Neurobiology 3 (5): 732–37. https://doi.org/10.1016/0959-4388(93)90145-O.

Kennedy, Mary B. 2000. 'Signal-Processing Machines at the Postsynaptic Density'. Science 290 (5492): 750–54. https://doi.org/10.1126/science.290.5492.750.

Kennedy, Mary B. 2016. 'Synaptic Signaling in Learning and Memory'. Cold Spring Harbor Perspectives in Biology 8 (2): a016824. https://doi.org/10.1101/cshperspect.a016824.

Kennedy, Mary B., Holly C. Beale, Holly J. Carlisle, and Lorraine R. Washburn. 2005. 'Integration of Biochemical Signalling in Spines'. Nature Reviews Neuroscience 6 (6): 423. https://doi.org/10.1038/nrn1685.

Kerr, Justin M., and Thomas A. Blanpied. 2012. 'Subsynaptic AMPA Receptor Distribution Is Acutely Regulated by Actin-Driven Reorganization of the Postsynaptic Density'. The Journal of Neuroscience 32 (2): 658. https://doi.org/10.1523/JNEUROSCI.2927-11.2012.

Kielland, Anders, Genrieta Bochorishvili, James Corson, Lei Zhang, Diane L. Rosin, Paul Heggelund, and J. Julius Zhu. 2009. 'Activity Patterns Govern Synapse-Specific AMPA Receptor Trafficking between Deliverable and Synaptic Pools'. Neuron 62 (1): 84–101. https://doi.org/10.1016/j.neuron.2009.03.001.

Kilinc, Murat, Thomas Creson, Camilo Rojas, Massimiliano Aceti, Jacob Ellegood, Thomas Vaissiere, Jason P. Lerch, and Gavin Rumbaugh. 2018. 'Species-Conserved SYNGAP1 Phenotypes Associated with Neurodevelopmental Disorders'. Molecular and Cellular Neuroscience, March. https://doi.org/10.1016/j.mcn.2018.03.008.

Kim, Eunjoon, and Morgan Sheng. 2004. 'PDZ Domain Proteins of Synapses'. Nature Reviews. Neuroscience 5 (10): 771–81. https://doi.org/10.1038/nrn1517.

Kim, Eunjoon, Scott Naisbitt, Yi-Ping Hsueh, Anuradha Rao, Adam Rothschild, Ann Marie Craig, and Morgan Sheng. 1997. 'GKAP, a Novel Synaptic Protein That Interacts with the Guanylate Kinase-like Domain of the PSD-95/SAP90 Family of Channel Clustering Molecules'. The Journal of Cell Biology 136 (3): 669–78. https://doi.org/10.1083/jcb.136.3.669.

Kim, J.H., Lee, H.-K., Takamiya, K., and Huganir, R.L. (2003). The Role of Synaptic GTPase-Activating Protein in Neuronal Development and Synaptic Plasticity. J. Neurosci. 23, 1119–1124.

Kim, Jae-Ick, Hye-Ryeon Lee, Su-eon Sim, Jinhee Baek, Nam-Kyung Yu, Jun-Hyeok Choi, Hyoung-Gon Ko, et al. 2011. 'PI3Kγ Is Required for NMDA Receptor-Dependent Long-Term Depression and Behavioral Flexibility'. Nature Neuroscience 14 (11): 1447–54. https://doi.org/10.1038/nn.2937.

Kim, Jee Hae, Dezhi Liao, Lit-Fui Lau, and Richard L. Huganir. 1998. 'SynGAP: A Synaptic RasGAP That Associates with the PSD-95/SAP90 Protein Family'. Neuron 20 (4): 683–91. https://doi.org/10.1016/S0896-6273(00)81008-9.

Kim, Jee Hae, Hey-Kyoung Lee, Kogo Takamiya, and Richard L. Huganir. 2003. 'The Role of Synaptic GTPase-Activating Protein in Neuronal Development and Synaptic Plasticity'. Journal of Neuroscience 23 (4): 1119–24.

Kim, Myung Jong, Anthone W. Dunah, Yu Tian Wang, and Morgan Sheng. 2005. 'Differential Roles of NR2A- and NR2B-Containing NMDA Receptors in Ras-ERK Signaling and AMPA Receptor Trafficking'. Neuron 46 (5): 745–60. https://doi.org/10.1016/j.neuron.2005.04.031.

Kim, Myung Jong, Kensuke Futai, Jihoon Jo, Yasunori Hayashi, Kwangwook Cho, and Morgan Sheng. 2007. 'Synaptic Accumulation of PSD-95 and Synaptic Function Regulated by Phosphorylation of Serine-295 of PSD-95'. Neuron 56 (3): 488–502. https://doi.org/10.1016/j.neuron.2007.09.007.

Kim, Seho, Alain Burette, Hye Sun Chung, Seok-Kyu Kwon, Jooyeon Woo, Hyun Woo Lee, Karam Kim, Hyun Kim, Richard J. Weinberg, and Eunjoon Kim. 2006. 'NGL Family PSD-95–Interacting Adhesion Molecules Regulate Excitatory Synapse Formation'. Nature Neuroscience 9 (10): 1294–1301. https://doi.org/10.1038/nn1763.

Kimura, Ryuichi, Kaichi Yoshizaki, and Noriko Osumi. 2018. 'Risk of Neurodevelopmental Disease by Paternal Aging: A Possible Influence of Epigenetic Alteration in Sperm'. In Developmental Origins of Health and Disease (DOHaD) : From Biological Basis to Clinical Significance, edited by Takeo Kubota and Hideoki Fukuoka, 75–81. Advances in Experimental Medicine and Biology. Singapore: Springer Singapore. https://doi.org/10.1007/978-981-10-5526-3_8.

Kimura, Yuichi, Moe Akahira-Azuma, Noriaki Harada, Yumi Enomoto, Yoshinori Tsurusaki, and Kenji Kurosawa. 2018. 'Novel SYNGAP1 Variant in a Patient with Intellectual Disability and Distinctive Dysmorphisms'. Congenital Anomalies, January. https://doi.org/10.1111/cga.12273.

King, Philip D., Beth A. Lubeck, and Philip E. Lapinski. 2013. 'Nonredundant Functions for Ras GTPase-Activating Proteins in Tissue Homeostasis'. Science Signaling 6 (264): re1. https://doi.org/10.1126/scisignal.2003669.

Klemann, Cornelius J. H. M., and Eric W. Roubos. 2011. 'The Gray Area between Synapse Structure and Function-Gray's Synapse Types I and II Revisited'. Synapse (New York, N.Y.) 65 (11): 1222–30. https://doi.org/10.1002/syn.20962.

Klitten, Laura L., Rikke S. Møller, Marina Nikanorova, Asli Silahtaroglu, Helle Hjalgrim, and Niels Tommerup. 2011. 'A Balanced Translocation Disrupts SYNGAP1 in a Patient with Intellectual Disability, Speech Impairment, and Epilepsy with Myoclonic Absences (EMA)'. Epilepsia 52 (12): e190–93. https://doi.org/10.1111/j.1528-1167.2011.03304.x.

Klooster, Jean Paul ten, and Peter L. Hordijk. 2007. 'Targeting and Localized Signalling by Small GTPases'. Biology of the Cell 99 (1): 1–12. https://doi.org/10.1042/BC20060071.

Knott, Graham W., Anthony Holtmaat, Linda Wilbrecht, Egbert Welker, and Karel Svoboda. 2006. 'Spine Growth Precedes Synapse Formation in the Adult Neocortex in Vivo'. Nature Neuroscience 9 (9): 1117–24. https://doi.org/10.1038/nn1747.

Knuesel, I., Elliott, A., Chen, H.-J., Mansuy, I.M., and Kennedy, M.B. (2005). A role for synGAP in regulating neuronal apoptosis. Eur. J. Neurosci. 21, 611–621.

Knuesel, Irene, Abigail Elliott, Hong-Jung Chen, Isabelle M. Mansuy, and Mary B. Kennedy. 2005. 'A Role for SynGAP in Regulating Neuronal Apoptosis'. European Journal of Neuroscience 21 (3): 611–21. https://doi.org/10.1111/j.1460-9568.2005.03908.x.

Koeberle, Solveigh Cornelia, Shinji Tanaka, Toshihiko Kuriu, Hirohide Iwasaki, Andreas Koeberle, Alexander Schulz, Dario-Lucas Helbing, Yoko Yamagata, Helen Morrison, and Shigeo Okabe. 2017. 'Developmental Stage-Dependent Regulation of Spine Formation by Calcium-Calmodulin-Dependent Protein Kinase IIα and Rap1'. Scientific Reports 7 (1): 13409. https://doi.org/10.1038/s41598-017-13728-y.

Kohane, Isaac S., Andrew McMurry, Griffin Weber, Douglas MacFadden, Leonard Rappaport, Louis Kunkel, Jonathan Bickel, et al. 2012. 'The Co-Morbidity Burden of Children and Young Adults with Autism Spectrum Disorders'. PloS One 7 (4): e33224. https://doi.org/10.1371/journal.pone.0033224.

Kolarow, Richard, Tanja Brigadski, and Volkmar Lessmann. 2007. 'Postsynaptic Secretion of BDNF and NT-3 from Hippocampal Neurons Depends on Calcium–Calmodulin Kinase II Signaling and Proceeds via Delayed Fusion Pore Opening'. Journal of Neuroscience 27 (39): 10350–64. https://doi.org/10.1523/JNEUROSCI.0692-07.2007.

Koleske, Anthony J. 2013. 'Molecular Mechanisms of Dendrite Stability'. Nature Reviews Neuroscience 14 (July): 536.

Komiyama, N.H., Watabe, A.M., Carlisle, H.J., Porter, K., Charlesworth, P., Monti, J., Strathdee, D.J.C., O'Carroll, C.M., Martin, S.J., Morris, R.G.M., et al. (2002). SynGAP Regulates ERK/MAPK Signaling, Synaptic Plasticity, and Learning in the Complex with Postsynaptic Density 95 and NMDA Receptor. J. Neurosci. 22, 9721.

Komiyama, Noboru H., Ayako M. Watabe, Holly J. Carlisle, Karen Porter, Paul Charlesworth, Jennifer Monti, Douglas J. C. Strathdee, et al. 2002. 'SynGAP Regulates ERK/MAPK Signaling, Synaptic Plasticity, and Learning in the Complex with Postsynaptic Density 95 and NMDA Receptor'. The Journal of Neuroscience 22 (22): 9721. https://doi.org/10.1523/JNEUROSCI.22-22-09721.2002.

Kopanitsa, Maksym V., Gemma Gou, Nurudeen O. Afinowi, Àlex Bayés, Seth G. N. Grant, and Noboru H. Komiyama. 2018. 'Chronic Treatment with a MEK Inhibitor Reverses Enhanced Excitatory Field Potentials in Syngap1+/− Mice'. Pharmacological Reports 70 (4): 777–83. https://doi.org/10.1016/j.pharep.2018.02.021.

Kornblihtt, Alberto R., Ignacio E. Schor, Mariano Alló, Gwendal Dujardin, Ezequiel Petrillo, and Manuel J. Muñoz. 2013. 'Alternative Splicing: A Pivotal Step between Eukaryotic Transcription and Translation'. Nature Reviews. Molecular Cell Biology 14 (3): 153–65. https://doi.org/10.1038/nrm3525.

Kornblihtt, Alberto R., Manuel de la Mata, Juan Pablo Fededa, Manuel J. Munoz, and Guadalupe Nogues. 2004. 'Multiple Links between Transcription and Splicing'. RNA (New York, N.Y.) 10 (10): 1489–98. https://doi.org/10.1261/rna.7100104.

Kozol, Robert A., Holly N. Cukier, Bing Zou, Vera Mayo, Silvia De Rubeis, Guiqing Cai, Anthony J. Griswold, et al. 2015. 'Two Knockdown Models of the Autism Genes SYNGAP1 and SHANK3 in Zebrafish Produce Similar Behavioral Phenotypes Associated with Embryonic Disruptions of Brain Morphogenesis'. Human Molecular Genetics 24 (14): 4006–23. https://doi.org/10.1093/hmg/ddv138.

Kramár, Enikö A., Bin Lin, Christopher S. Rex, Christine M. Gall, and Gary Lynch. 2006. 'Integrin-Driven Actin Polymerization Consolidates Long-Term Potentiation'. Proceedings of the National Academy of Sciences 103 (14): 5579–84. https://doi.org/10.1073/pnas.0601354103.

Kramer, Jamie M., Korinna Kochinke, Merel A. W. Oortveld, Hendrik Marks, Daniela Kramer, Eiko K. de Jong, Zoltan Asztalos, et al. 2011. 'Epigenetic Regulation of Learning and Memory by Drosophila EHMT/G9a'. PLOS Biology 9 (1): e1000569. https://doi.org/10.1371/journal.pbio.1000569.

Krapivinsky, Grigory, Igor Medina, Luba Krapivinsky, Svetlana Gapon, and David E. Clapham. 2004. 'SynGAP-MUPP1-CaMKII Synaptic Complexes Regulate P38 MAP Kinase Activity and NMDA Receptor-Dependent Synaptic AMPA Receptor Potentiation'. Neuron 43 (4): 563–74. https://doi.org/10.1016/j.neuron.2004.08.003.

Krepischi, Ana Cristina V., Carla Rosenberg, Silvia S. Costa, John A. Crolla, Shuwen Huang, and Angela M. Vianna-Morgante. 2010. 'A Novel de Novo Microdeletion Spanning the SYNGAP1 Gene on the Short Arm of Chromosome 6 Associated with Mental Retardation'. American Journal of Medical Genetics Part A 152A (9): 2376–78. https://doi.org/10.1002/ajmg.a.33554.

Kreutz, Michael R., and Carlo Sala. 2012. Synaptic Plasticity: Dynamics, Development and Disease. Springer Science & Business Media.

Kumar, Vikas, Ming-Xiang Zhang, Michael W. Swank, Jeannette Kunz, and Gang-Yi Wu. 2005. 'Regulation of Dendritic Morphogenesis by Ras–PI3K–Akt–MTOR and Ras–MAPK Signaling Pathways'. Journal of Neuroscience 25 (49): 11288–99. https://doi.org/10.1523/JNEUROSCI.2284-05.2005.

Kuriu, Toshihiko, Akihiro Inoue, Haruhiko Bito, Kenji Sobue, and Shigeo Okabe. 2006. 'Differential Control of Postsynaptic Density Scaffolds via Actin-Dependent and -Independent Mechanisms'. The Journal of Neuroscience 26 (29): 7693. https://doi.org/10.1523/JNEUROSCI.0522-06.2006.

Kwon, Taekyung, Masayuki Sakamoto, Darcy S. Peterka, and Rafael Yuste. 2017. 'Attenuation of Synaptic Potentials in Dendritic Spines'. Cell Reports 20 (5): 1100–1110. https://doi.org/10.1016/j.celrep.2017.07.012.

Laaris, Nora, Adam Puche, and Matthew Ennis. 2007. 'Complementary Postsynaptic Activity Patterns Elicited in Olfactory Bulb by Stimulation of Mitral/Tufted and Centrifugal Fiber Inputs to Granule Cells'. Journal of Neurophysiology 97 (1): 296–306. https://doi.org/10.1152/jn.00823.2006.

Lambert, John M., Que T. Lambert, Gary W. Reuther, Angeliki Malliri, David P. Siderovski, John Sondek, John G. Collard, and Channing J. Der. 2002. 'Tiam1 Mediates Ras Activation of Rac by a PI(3)K-Independent Mechanism'. Nature Cell Biology 4 (8): 621–25. https://doi.org/10.1038/ncb833.

Laplante, Mathieu, and David M. Sabatini. 2012. 'MTOR Signaling in Growth Control and Disease'. Cell 149 (2): 274–93. https://doi.org/10.1016/j.cell.2012.03.017.

Larsen, Rylan S., Deepti Rao, Paul B. Manis, and Benjamin D. Philpot. 2010. 'STDP in the Developing Sensory Neocortex'. Frontiers in Synaptic Neuroscience 2. https://doi.org/10.3389/fnsyn.2010.00009.

Lascano, Agustina M., Christian M. Korff, and Fabienne Picard. 2016. 'Seizures and Epilepsies Due to Channelopathies and Neurotransmitter Receptor Dysfunction: A Parallel between Genetic and Immune Aspects'. Molecular Syndromology 7 (4): 197–209. https://doi.org/10.1159/000447707.

Lau, Lit-Fui, Andrew Mammen, Michael D. Ehlers, Stefan Kindler, Wook Joon Chung, Craig C. Garner, and Richard L. Huganir. 1996. 'Interaction of the N-Methyl—Aspartate Receptor Complex with a Novel Synapse-Associated Protein, SAP102'. Journal of Biological Chemistry 271 (35): 21622–28. https://doi.org/10.1074/jbc.271.35.21622.

Laumonnier, Frédéric, Peter C. Cuthbert, and Seth G. N. Grant. 2007. 'The Role of Neuronal Complexes in Human X-Linked Brain Diseases'. The American Journal of Human Genetics 80 (2): 205–20. https://doi.org/10.1086/511441.

Lautz, Jonathan D., Emily A. Brown, Alison A. Williams VanSchoiack, and Stephen E. P. Smith. 2018. 'Synaptic Activity Induces Input-Specific Rearrangements in a Targeted Synaptic Protein Interaction Network'. Journal of Neurochemistry 146 (5): 540–59. https://doi.org/10.1111/jnc.14466.

Laver, Christopher R. J., and Joanne A. Matsubara. 2017. 'Structural Divergence of Essential Triad Ribbon Synapse Proteins among Placental Mammals - Implications for Preclinical Trials in Photoreceptor Transplantation Therapy'. Experimental Eye Research 159: 156–67. https://doi.org/10.1016/j.exer.2017.03.005.

Le Pichon, Claire E., Matthew T. Valley, Magdalini Polymenidou, Alexander T. Chesler, Botir T. Sagdullaev, Adriano Aguzzi, and Stuart Firestein. 2009. 'Olfactory Behavior and Physiology Are Disrupted in Prion Protein Knockout Mice'. Nature Neuroscience 12 (1): 60–69. https://doi.org/10.1038/nn.2238.

Leblond, Claire S., Caroline Nava, Anne Polge, Julie Gauthier, Guillaume Huguet, Serge Lumbroso, Fabienne Giuliano, et al. 2014. 'Meta-Analysis of SHANK Mutations in Autism Spectrum Disorders: A Gradient

of Severity in Cognitive Impairments'. PLoS Genetics 10 (9): e1004580. https://doi.org/10.1371/journal.pgen.1004580.

Lee, Eunee, Jiseok Lee, and Eunjoon Kim. 2017. 'Excitation/Inhibition Imbalance in Animal Models of Autism Spectrum Disorders'. Biological Psychiatry 81 (10): 838–47. https://doi.org/10.1016/j.biopsych.2016.05.011.

Lee, Kea Joo, Hyang-Sook Hoe, and Daniel T. S. Pak. 2011. 'Plk2 Raps up Ras to Subdue Synapses'. Small GTPases 2 (3): 162–66. https://doi.org/10.4161/sgtp.2.3.16454.

Lee, Kea Joo, Yeunkum Lee, Aaron Rozeboom, Ji-Yun Lee, Noriko Udagawa, Hyang-Sook Hoe, and Daniel T.S. Pak. 2011. 'Requirement for Plk2 in Orchestrated Ras and Rap Signaling, Homeostatic Structural Plasticity, and Memory'. Neuron 69 (5): 957–73. https://doi.org/10.1016/j.neuron.2011.02.004.

Leisman, Gerry, Raed Mualem, and Safa Khayat Mughrabi. 2015. 'The neurological development of the child with the educational enrichment in mind'. Psicología Educativa - Educational Psychology 21 (2): 79–96. https://doi.org/10.1016/j.pse.2015.08.006.

Lemmon, M. A. 2004. 'Pleckstrin Homology Domains: Not Just for Phosphoinositides'. Biochemical Society Transactions 32 (5): 707–11. https://doi.org/10.1042/BST0320707.

Lepeta, Katarzyna, Mychael V. Lourenco, Barbara C. Schweitzer, Pamela V. Martino Adami, Priyanjalee Banerjee, Silvina Catuara-Solarz, Mario de La Fuente Revenga, et al. 2016. 'Synaptopathies: Synaptic Dysfunction in Neurological Disorders – A Review from Students to Students'. Journal of Neurochemistry 138 (6): 785–805. https://doi.org/10.1111/jnc.13713.

Lepeta, Katarzyna, Mychael V. Lourenco, Barbara C. Schweitzer, Pamela V. Martino Adami, Priyanjalee Banerjee, Silvina Catuara-Solarz, Mario de La Fuente Revenga, et al. 2016. 'Synaptopathies: Synaptic Dysfunction in Neurological Disorders – A Review from Students to Students'. Journal of Neurochemistry 138 (6): 785–805. https://doi.org/10.1111/jnc.13713.

Letunic, Ivica, Richard R. Copley, Steffen Schmidt, Francesca D. Ciccarelli, Tobias Doerks, Jörg Schultz, Chris P. Ponting, and Peer Bork. 2004. 'SMART 4.0: Towards Genomic Data Integration'. Nucleic Acids Research 32 (suppl_1): D142–44. https://doi.org/10.1093/nar/gkh088.

Leucht, S., T. Burkard, J. Henderson, M. Maj, and N. Sartorius. 2007. 'Physical Illness and Schizophrenia: A Review of the Literature'. Acta Psychiatrica Scandinavica 116 (5): 317–33. https://doi.org/10.1111/j.1600-0447.2007.01095.x.

Lewis, David A., and Pat Levitt. 2002. 'Schizophrenia as a Disorder of Neurodevelopment'. Annual Review of Neuroscience 25 (1): 409–32. https://doi.org/10.1146/annurev.neuro.25.112701.142754.

Li, Ka Wan, Martin P. Hornshaw, Roel C. Van der Schors, Rod Watson, Stephen Tate, Bruno Casetta, Connie R. Jimenez, et al. 2004. 'Proteomics Analysis of Rat Brain Postsynaptic Density IMPLICATIONS OF THE DIVERSE PROTEIN FUNCTIONAL GROUPS FOR THE INTEGRATION OF SYNAPTIC PHYSIOLOGY'. Journal of Biological Chemistry 279 (2): 987–1002. https://doi.org/10.1074/jbc.M303116200.

Li, Qin, Ji-Ann Lee, and Douglas L. Black. 2007. 'Neuronal Regulation of Alternative Pre-MRNA Splicing'. Nature Reviews. Neuroscience 8 (11): 819–31. https://doi.org/10.1038/nrn2237.

Li, Weidong. 2001. 'Characterization of a Novel SynGAP Isoform, SynGAP-β'. 15 January 2001. http://www.jbc.org/content/276/24/21417.long.

Li, Yang I., Luis Sanchez-Pulido, Wilfried Haerty, and Chris P. Ponting. 2015. 'RBFOX and PTBP1 Proteins Regulate the Alternative Splicing of Micro-Exons in Human Brain Transcripts'. Genome Research 25 (1): 1–13. https://doi.org/10.1101/gr.181990.114.

Li, Zheng, Ken-Ichi Okamoto, Yasunori Hayashi, and Morgan Sheng. 2004. 'The Importance of Dendritic Mitochondria in the Morphogenesis and Plasticity of Spines and Synapses'. Cell 119 (6): 873–87. https://doi.org/10.1016/j.cell.2004.11.003.

Liao, Dezhi, Neal A. Hessler, and Roberto Malinow. 1995. 'Activation of Postsynaptically Silent Synapses during Pairing-Induced LTP in CA1 Region of Hippocampal Slice'. Nature 375 (6530): 400–404. https://doi.org/10.1038/375400a0.

Lim, Chae-Seok, Hyopil Kim, Nam-Kyung Yu, Sukjae Joshua Kang, TaeHyun Kim, Hyoung-Gon Ko, Jaehyun Lee, et al. 2017. 'Enhancing Inhibitory Synaptic Function Reverses Spatial Memory Deficits in Shank2 Mutant Mice'. Neuropharmacology 112 (January): 104–12. https://doi.org/10.1016/j.neuropharm.2016.08.016.

Lim, Indra A., Michelle A. Merrill, Yucui Chen, and Johannes W. Hell. 2003. 'Disruption of the NMDA Receptor–PSD-95 Interaction in Hippocampal Neurons with No Obvious Physiological Short-Term Effect'. Neuropharmacology 45 (6): 738–54. https://doi.org/10.1016/S0028-3908(03)00276-4.

Lim, Sangmi, Scott Naisbitt, Jiyoung Yoon, Jong-Ik Hwang, Pann-Ghill Suh, Morgan Sheng, and Eunjoon Kim. 1999. 'Characterization of the Shank Family of Synaptic Proteins MULTIPLE GENES, ALTERNATIVE SPLICING, AND DIFFERENTIAL EXPRESSION IN BRAIN AND DEVELOPMENT'. Journal of Biological Chemistry 274 (41): 29510–18. https://doi.org/10.1074/jbc.274.41.29510.

Lin, Bin, Enikö A. Kramár, Xiaoning Bi, Fernando A. Brucher, Christine M. Gall, and Gary Lynch. 2005. 'Theta Stimulation Polymerizes Actin in Dendritic Spines of Hippocampus'. Journal of Neuroscience 25 (8): 2062–69. https://doi.org/10.1523/JNEUROSCI.4283-04.2005.

Lipscombe, Diane. 2005. 'Neuronal Proteins Custom Designed by Alternative Splicing'. Current Opinion in Neurobiology 15 (3): 358–63. https://doi.org/10.1016/j.conb.2005.04.002.

Lisman, J. 1989. 'A Mechanism for the Hebb and the Anti-Hebb Processes Underlying Learning and Memory'. Proceedings of the National Academy of Sciences 86 (23): 9574–78. https://doi.org/10.1073/pnas.86.23.9574.

Lisman, John, Ryohei Yasuda, and Sridhar Raghavachari. 2012. 'Mechanisms of CaMKII Action in Long-Term Potentiation'. Nature Reviews. Neuroscience 13 (3): 169–82. https://doi.org/10.1038/nrn3192.

Lledo, Pierre-Marie, and Françoise Lazarini. 2007. 'Neuronal Replacement in Microcircuits of the Adult Olfactory System'. Comptes Rendus Biologies, Thérapie cellulaire régénérative / Regenerative cell therapy, 330 (6): 510–20. https://doi.org/10.1016/j.crvi.2007.01.002.

Losonczy, Attila, Judit K. Makara, and Jeffrey C. Magee. 2008. 'Compartmentalized Dendritic Plasticity and Input Feature Storage in Neurons'. Nature 452 (7186): 436–41. https://doi.org/10.1038/nature06725.

Louros, Susana R., and Emily K. Osterweil. 2016. 'Perturbed Proteostasis in Autism Spectrum Disorders'. Journal of Neurochemistry 139 (6): 1081–92. https://doi.org/10.1111/jnc.13723.

Lowenthal, Mark S., Sanford P. Markey, and Ayse Dosemeci. 2015. 'Quantitative Mass Spectrometry Measurements Reveal Stoichiometry of Principal Postsynaptic Density Proteins'. Journal of Proteome Research 14 (6): 2528–38. https://doi.org/10.1021/acs.jproteome.5b00109.

Lu, B., G. Nagappan, and Y. Lu. 2014. 'BDNF and Synaptic Plasticity, Cognitive Function, and Dysfunction'. In Neurotrophic Factors, edited by Gary R. Lewin and Bruce D. Carter, 223–50. Handbook of Experimental Pharmacology. Berlin, Heidelberg: Springer Berlin Heidelberg. https://doi.org/10.1007/978-3-642-45106-5_9.

Lu, Wei, Yun Shi, Alexander C. Jackson, Kirsten Bjorgan, Matthew J. During, Rolf Sprengel, Peter H. Seeburg, and Roger A. Nicoll. 2009. 'Subunit Composition of Synaptic AMPA Receptors Revealed by a Single-Cell Genetic Approach'. Neuron 62 (2): 254–68. https://doi.org/10.1016/j.neuron.2009.02.027.

Luckasson, R., and A. Reeve. 2001. 'Naming, Defining, and Classifying in Mental Retardation'. Mental Retardation 39 (1): 47–52. https://doi.org/10.1352/0047-6765(2001)039<0047:NDACIM>2.0.CO;2.

Luco, Reini F., Qun Pan, Kaoru Tominaga, Benjamin J. Blencowe, Olivia M. Pereira-Smith, and Tom Misteli. 2010. 'Regulation of Alternative Splicing by Histone Modifications'. Science (New York, N.Y.) 327 (5968): 996–1000. https://doi.org/10.1126/science.1184208.

Luján, R., R. Shigemoto, and G. López-Bendito. 2005. 'Glutamate and GABA Receptor Signalling in the Developing Brain'. Neuroscience 130 (3): 567–80. https://doi.org/10.1016/j.neuroscience.2004.09.042.

Luo, Jiao-hua, Zhi-qun Qiu, Liang Zhang, and Wei-qun Shu. 2012. 'Arsenite Exposure Altered the Expression of NMDA Receptor and Postsynaptic Signaling Proteins in Rat Hippocampus'. Toxicology Letters 211 (1): 39–44. https://doi.org/10.1016/j.toxlet.2012.02.021.

Ly, Cindy V., and Patrik Verstreken. 2006. 'Mitochondria at the Synapse'. The Neuroscientist 12 (4): 291–99. https://doi.org/10.1177/1073858406287661.

MacAskill, Andrew F., Talia A. Atkin, and Josef T. Kittler. 2010. 'Mitochondrial Trafficking and the Provision of Energy and Calcium Buffering at Excitatory Synapses'. The European Journal of Neuroscience 32 (2): 231–40. https://doi.org/10.1111/j.1460-9568.2010.07345.x.

MacLean, Brendan, Daniela M. Tomazela, Nicholas Shulman, Matthew Chambers, Gregory L. Finney, Barbara Frewen, Randall Kern, David L. Tabb, Daniel C. Liebler, and Michael J. MacCoss. 2010. 'Skyline: An

Open Source Document Editor for Creating and Analyzing Targeted Proteomics Experiments'. Bioinformatics 26 (7): 966–68. https://doi.org/10.1093/bioinformatics/btq054.

Maere, Steven, Karel Heymans, and Martin Kuiper. 2005. 'BiNGO: A Cytoscape Plugin to Assess Overrepresentation of Gene Ontology Categories in Biological Networks'. Bioinformatics (Oxford, England) 21 (16): 3448–49. https://doi.org/10.1093/bioinformatics/bti551.

Magri, Chiara, Rita Gardella, Stefano Davide Barlati, Damiano Podavini, Paraskevas Iatropoulos, Silvia Bonomi, Paolo Valsecchi, Emilio Sacchetti, and Sergio Barlati. 2006. 'Glutamate AMPA Receptor Subunit 1 Gene (GRIA1) and DSM-IV-TR Schizophrenia: A Pilot Case-Control Association Study in an Italian Sample'. American Journal of Medical Genetics. Part B, Neuropsychiatric Genetics: The Official Publication of the International Society of Psychiatric Genetics 141B (3): 287–93. https://doi.org/10.1002/ajmg.b.30294.

Maiti, Panchanan, Jayeeta Manna, G. Ilavazhagan, Julien Rossignol, and Gary L. Dunbar. 2015. 'Molecular Regulation of Dendritic Spine Dynamics and Their Potential Impact on Synaptic Plasticity and Neurological Diseases'. Neuroscience & Biobehavioral Reviews 59 (December): 208–37. https://doi.org/10.1016/j.neubiorev.2015.09.020.

Majewska, Ania K., Jessica R. Newton, and Mriganka Sur. 2006. 'Remodeling of Synaptic Structure in Sensory Cortical Areas in Vivo'. The Journal of Neuroscience: The Official Journal of the Society for Neuroscience 26 (11): 3021–29. https://doi.org/10.1523/JNEUROSCI.4454-05.2006.

Malenka, Robert C., and Mark F. Bear. 2004. 'LTP and LTD: An Embarrassment of Riches'. Neuron 44 (1): 5–21. https://doi.org/10.1016/j.neuron.2004.09.012.

Malinow, Roberto, and Robert C. Malenka. 2002. 'AMPA Receptor Trafficking and Synaptic Plasticity'. Annual Review of Neuroscience 25 (1): 103–26. https://doi.org/10.1146/annurev.neuro.25.112701.142758.

Mar Masdeu, Maria del, Beatriz G. Armendáriz, Anna La Torre, Eduardo Soriano, Ferran Burgaya, and Jesús Mariano Ureña. 2017. 'Identification of Novel Ack1-Interacting Proteins and Ack1 Phosphorylated Sites in Mouse Brain by Mass Spectrometry'. Oncotarget 8 (60): 101146–57. https://doi.org/10.18632/oncotarget.20929.

Maravall, Miguel, Edward A. Stern, and Karel Svoboda. 2004. 'Development of Intrinsic Properties and Excitability of Layer 2/3 Pyramidal Neurons During a Critical Period for Sensory Maps in Rat Barrel Cortex'. Journal of Neurophysiology 92 (1): 144–56. https://doi.org/10.1152/jn.00598.2003.

Marcello, Elena, Monica Di Luca, and Fabrizio Gardoni. 2018. 'Synapse-to-Nucleus Communication: From Developmental Disorders to Alzheimer's Disease'. Current Opinion in Neurobiology, Neurobiology of Disease, 48 (February): 160–66. https://doi.org/10.1016/j.conb.2017.12.017.

Marrs, G. S., S. H. Green, and M. E. Dailey. 2001. 'Rapid Formation and Remodeling of Postsynaptic Densities in Developing Dendrites'. Nature Neuroscience 4 (10): 1006–13. https://doi.org/10.1038/nn717.

Marsden, Kurt C., Adi Shemesh, K. Ulrich Bayer, and Reed C. Carroll. 2010. 'Selective Translocation of Ca2+/Calmodulin Protein Kinase IIα (CaMKIIα) to Inhibitory Synapses'. Proceedings of the National Academy of Sciences of the United States of America 107 (47): 20559–64. https://doi.org/10.1073/pnas.1010346107.

Marsden, Kurt C., Adi Shemesh, K. Ulrich Bayer, and Reed C. Carroll. 2010. 'Selective Translocation of Ca2+/Calmodulin Protein Kinase IIα (CaMKIIα) to Inhibitory Synapses'. Proceedings of the National Academy of Sciences of the United States of America 107 (47): 20559–64. https://doi.org/10.1073/pnas.1010346107.

Marson, A. G., and D. W. Chadwick. 2001. 'New Drug Treatments for Epilepsy'. Journal of Neurology, Neurosurgery & Psychiatry 70 (2): 143–47. https://doi.org/10.1136/jnnp.70.2.143.

Masdeu, Maria del Mar, Beatriz G. Armendáriz, Eduardo Soriano, Jesús Mariano Ureña, and Ferran Burgaya. 2016. 'New Partners and Phosphorylation Sites of Focal Adhesion Kinase Identified by Mass Spectrometry'. Biochimica et Biophysica Acta (BBA) - General Subjects 1860 (7): 1388–94. https://doi.org/10.1016/j.bbagen.2016.02.019.

Matson, Johnny L., and Marie S. Nebel-Schwalm. 2007. 'Comorbid Psychopathology with Autism Spectrum Disorder in Children: An Overview'. Research in Developmental Disabilities 28 (4): 341–52. https://doi.org/10.1016/j.ridd.2005.12.004.

Matson, Johnny L., and Mary Shoemaker. 2009. 'Intellectual Disability and Its Relationship to Autism Spectrum Disorders'. Research in Developmental Disabilities 30 (6): 1107–14. https://doi.org/10.1016/j.ridd.2009.06.003.

Matsuda, Shinji, Thomas Launey, Sumiko Mikawa, and Hirokazu Hirai. 2000. 'Disruption of AMPA Receptor GluR2 Clusters Following Long-term Depression Induction in Cerebellar Purkinje Neurons'. The EMBO Journal 19 (12): 2765–74. https://doi.org/10.1093/emboj/19.12.2765.

Mattson, Mark P., Marc Gleichmann, and Aiwu Cheng. 2008. 'Mitochondria in Neuroplasticity and Neurological Disorders'. Neuron 60 (5): 748–66. https://doi.org/10.1016/j.neuron.2008.10.010.

Maxwell, Christina R., Michele E. Villalobos, Robert T. Schultz, Beate Herpertz-Dahlmann, Kerstin Konrad, and Gregor Kohls. 2015. 'Atypical Laterality of Resting Gamma Oscillations in Autism Spectrum Disorders'. Journal of Autism and Developmental Disorders 45 (2): 292–97. https://doi.org/10.1007/s10803-013-1842-7.

McAllister, A. Kimberley, Lawrence C. Katz, and Donald C. Lo. 1999. 'Neurotrophins and Synaptic Plasticity'. Annual Review of Neuroscience 22 (1): 295–318. https://doi.org/10.1146/annurev.neuro.22.1.295.

McCarthy, S. E., J. Gillis, M. Kramer, J. Lihm, S. Yoon, Y. Berstein, M. Mistry, et al. 2014. 'De Novo Mutations in Schizophrenia Implicate Chromatin Remodeling and Support a Genetic Overlap with Autism and Intellectual Disability'. Molecular Psychiatry 19 (6): 652–58. https://doi.org/10.1038/mp.2014.29.

McCormack, Stefanie G., Ruth L. Stornetta, and J. Julius Zhu. 2006. 'Synaptic AMPA Receptor Exchange Maintains Bidirectional Plasticity'. Neuron 50 (1): 75–88. https://doi.org/10.1016/j.neuron.2006.02.027.

McLaren, J., and S. E. Bryson. 1987. 'Review of Recent Epidemiological Studies of Mental Retardation: Prevalence, Associated Disorders, and Etiology'. American Journal of Mental Retardation: AJMR 92 (3): 243–54.

McLeod, Faye, Alessandro Bossio, Aude Marzo, Lorenza Ciani, Sara Sibilla, Saad Hannan, Gemma A. Wilson, et al. 2018. 'Wnt Signaling Mediates LTP-Dependent Spine Plasticity and AMPAR Localization through Frizzled-7 Receptors'. Cell Reports 23 (4): 1060–71. https://doi.org/10.1016/j.celrep.2018.03.119.

McMahon, A.C., Barnett, M.W., O'Leary, T.S., Stoney, P.N., Collins, M.O., Papadia, S., Choudhary, J.S., Komiyama, N.H., Grant, S.G.N., Hardingham, G.E., et al. (2012). SynGAP isoforms exert opposing effects on synaptic strength. Nat. Commun. 3, 900.

McMahon, A.C., M.W. Barnett, T.S. O'Leary, P.N. Stoney, M.O. Collins, S. Papadia, J.S. Choudhary, et al. 2012. 'SynGAP Isoforms Exert Opposing Effects on Synaptic Strength'. Nature Communications 3 (June): 900. https://doi.org/10.1038/ncomms1900.

McPheeters, Melissa L., Zachary Warren, Nila Sathe, Jennifer L. Bruzek, Shanthi Krishnaswami, Rebecca N. Jerome, and Jeremy Veenstra-Vanderweele. 2011. 'A Systematic Review of Medical Treatments for Children with Autism Spectrum Disorders'. Pediatrics 127 (5): e1312-1321. https://doi.org/10.1542/peds.2011-0427.

Mehregan, Hoda, Hossein Najmabadi, and Kimia Kahrizi. 2016. 'Genetic Studies in Intellectual Disability and Behavioral Impairment'. Archives of Iranian Medicine 19 (5): 363–75. https://doi.org/0161905/AIM.0012.

Mei, Yuan, Patricia Monteiro, Yang Zhou, Jin-Ah Kim, Xian Gao, Zhanyan Fu, and Guoping Feng. 2016. 'Adult Restoration of Shank3 Expression Rescues Selective Autistic-like Phenotypes'. Nature 530 (7591): 481–84. https://doi.org/10.1038/nature16971.

Meng, Fanjie, Jun Guo, Quanguang Zhang, Bo Song, and Guangyi Zhang. 2003. 'Autophosphorylated Calcium/Calmodulin-Dependent Protein Kinase II Alpha (CaMKII Alpha) Reversibly Targets to and Phosphorylates N-Methyl-D-Aspartate Receptor Subunit 2B (NR2B) in Cerebral Ischemia and Reperfusion in Hippocampus of Rats'. Brain Research 967 (1–2): 161–69.

Meng, Linyan, Amanda J. Ward, Seung Chun, C. Frank Bennett, Arthur L. Beaudet, and Frank Rigo. 2015. 'Towards a Therapy for Angelman Syndrome by Targeting a Long Non-Coding RNA'. Nature 518 (7539): 409–12. https://doi.org/10.1038/nature13975.

Meng, Yanghong, Yu Zhang, Vitali Tregoubov, Christopher Janus, Luis Cruz, Mike Jackson, Wei Yang Lu, et al. 2002. 'Abnormal Spine Morphology and Enhanced LTP in LIMK-1 Knockout Mice'. Neuron 35 (1): 121–33.

Meredith, R.M. 2015. 'Sensitive and Critical Periods during Neurotypical and Aberrant Neurodevelopment: A Framework for Neurodevelopmental Disorders'. Neuroscience & Biobehavioral Reviews 50 (March): 180–88. https://doi.org/10.1016/j.neubiorev.2014.12.001.

Merkin, Jason, Caitlin Russell, Ping Chen, and Christopher B. Burge. 2012. 'Evolutionary Dynamics of Gene and Isoform Regulation in Mammalian Tissues'. Science (New York, N.Y.) 338 (6114): 1593–99. https://doi.org/10.1126/science.1228186.

Metsalu, Tauno, and Jaak Vilo. 2015. 'ClustVis: A Web Tool for Visualizing Clustering of Multivariate Data Using Principal Component Analysis and Heatmap'. Nucleic Acids Research 43 (W1): W566-570. https://doi.org/10.1093/nar/gkv468.

Mi, Huaiyu, Xiaosong Huang, Anushya Muruganujan, Haiming Tang, Caitlin Mills, Diane Kang, and Paul D. Thomas. 2017. 'PANTHER Version 11: Expanded Annotation Data from Gene Ontology and Reactome Pathways, and Data Analysis Tool Enhancements'. Nucleic Acids Research 45 (Database issue): D183–89. https://doi.org/10.1093/nar/gkw1138.

Michaelson, Sheldon D., Emin D. Ozkan, Massimiliano Aceti, Sabyasachi Maity, Nerea Llamosas, Monica Weldon, Elisa Mizrachi, et al. 2018. 'SYNGAP1 Heterozygosity Disrupts Sensory Processing by Reducing Touch-Related Activity within Somatosensory Cortex Circuits'. Nature Neuroscience 21 (12): 1. https://doi.org/10.1038/s41593-018-0268-0.

Michel, George F., and Amber N. Tyler. 2005. 'Critical Period: A History of the Transition from Questions of When, to What, to How'. Developmental Psychobiology 46 (3): 156–62. https://doi.org/10.1002/dev.20058.

Mignot, Cyril, Celina von Stülpnagel, Caroline Nava, Dorothée Ville, Damien Sanlaville, Gaetan Lesca, Agnès Rastetter, et al. 2016. 'Genetic and Neurodevelopmental Spectrum of SYNGAP1-Associated Intellectual Disability and Epilepsy'. Journal of Medical Genetics 53 (8): 511–22. https://doi.org/10.1136/jmedgenet-2015-103451.

Miles, Judith H. 2011. 'Autism Spectrum Disorders—A Genetics Review'. Genetics in Medicine 13 (4): 278–94. https://doi.org/10.1097/GIM.0b013e3181ff67ba.

Miller, M. W. 1988. 'Development of Projection and Local Circuit Neurons in Neocortex'. Cerebral Cortex, Vol. 7, Development and Maturation of Cerebral Cortex, 133–75.

Millier, A., U. Schmidt, M. C. Angermeyer, D. Chauhan, V. Murthy, M. Toumi, and N. Cadi-Soussi. 2014. 'Humanistic Burden in Schizophrenia: A Literature Review'. Journal of Psychiatric Research 54 (July): 85–93. https://doi.org/10.1016/j.jpsychires.2014.03.021.

Missler, Markus, and Thomas C. Südhof. 1998. 'Neurexins: Three Genes and 1001 Products'. Trends in Genetics 14 (1): 20–26. https://doi.org/10.1016/S0168-9525(97)01324-3.

Mizrahi, Adi. 2007. 'Dendritic Development and Plasticity of Adult-Born Neurons in the Mouse Olfactory Bulb'. Nature Neuroscience 10 (March): 444.

Moga, D. E., M. E. Calhoun, A. Chowdhury, P. Worley, J. H. Morrison, and M. L. Shapiro. 2004. 'Activity-Regulated Cytoskeletal-Associated Protein Is Localized to Recently Activated Excitatory Synapses'. Neuroscience 125 (1): 7–11. https://doi.org/10.1016/j.neuroscience.2004.02.004.

Monteiro, Patricia, and Guoping Feng. 2017. 'SHANK Proteins: Roles at the Synapse and in Autism Spectrum Disorder'. Nature Reviews Neuroscience 18 (3): 147–57. https://doi.org/10.1038/nrn.2016.183.

Montgomery, Johanna M., and Daniel V. Madison. 2002. 'State-Dependent Heterogeneity in Synaptic Depression between Pyramidal Cell Pairs'. Neuron 33 (5): 765–77. https://doi.org/10.1016/S0896-6273(02)00606-2.

Montoliu, Lluís. 2012. 'Mendel: A Simple Excel Workbook to Compare the Observed and Expected Distributions of Genotypes/Phenotypes in Transgenic and Knockout Mouse Crosses Involving up to Three Unlinked Loci by Means of a X2 Test'. Transgenic Research 21 (3): 677–81. https://doi.org/10.1007/s11248-011-9544-4.

Moon, Il Soo, Hiroyuki Sakagami, Jun Nakayama, and Tatsuo Suzuki. 2008. 'Differential Distribution of SynGAPα1 and SynGAPβ Isoforms in Rat Neurons'. Brain Research 1241 (November): 62–75. https://doi.org/10.1016/j.brainres.2008.09.033.

Morgan Sheng, and Myung Jong Kim. 2002. 'Postsynaptic Signaling and Plasticity Mechanisms'. Science, New Series 298 (5594): 776–80.

Motazacker, Mohammad Mahdi, Benjamin Rainer Rost, Tim Hucho, Masoud Garshasbi, Kimia Kahrizi, Reinhard Ullmann, Seyedeh Sedigheh Abedini, et al. 2007. 'A Defect in the Ionotropic Glutamate Receptor 6 Gene (GRIK2) Is Associated with Autosomal Recessive Mental Retardation'. The American Journal of Human Genetics 81 (4): 792–98. https://doi.org/10.1086/521275.

Muhia, M., J. Feldon, I. Knuesel, and B. K. Yee. 2009. 'Appetitively Motivated Instrumental Learning in SynGAP Heterozygous Knockout Mice'. Behavioral Neuroscience 123 (5): 1114–28. https://doi.org/info:doi/10.1037/a0017118.

Muhia, Mary, Benjamin K. Yee, Joram Feldon, Foivos Markopoulos, and Irene Knuesel. 2010. 'Disruption of Hippocampus-Regulated Behavioural and Cognitive Processes by Heterozygous Constitutive Deletion of SynGAP'. European Journal of Neuroscience 31 (3): 529–43. https://doi.org/10.1111/j.1460-9568.2010.07079.x.

Muhia, Mary, Silvia Willadt, Benjamin K. Yee, Joram Feldon, Jean-Charles Paterna, Severin Schwendener, Kaspar Vogt, Mary B. Kennedy, and Irene Knuesel. 2012. 'Molecular and Behavioral Changes Associated with Adult Hippocampus-Specific SynGAP1 Knockout'. Learning & Memory 19 (7): 268–81. https://doi.org/10.1101/lm.026351.112.

Muro, Ryunosuke, Takeshi Nitta, Toshiyuki Okada, Hitoshi Ideta, Takeshi Tsubata, and Harumi Suzuki. 2015. 'The Ras GTPase-Activating Protein Rasal3 Supports Survival of Naive T Cells'. PLoS ONE 10 (3). https://doi.org/10.1371/journal.pone.0119898.

Musacchio, Andrea, Toby Gibson, Peter Rice, Julie Thompson, and Matti Saraste. 1993. 'The PH Domain: A Common Piece in the Structural Pathcwork of Signalling Proteins'. Trends in Biochemical Sciences 18 (9): 343–48. https://doi.org/10.1016/0968-0004(93)90071-T.

Naisbitt, S., J. Valtschanoff, D. W. Allison, C. Sala, E. Kim, A. M. Craig, R. J. Weinberg, and M. Sheng. 2000. 'Interaction of the Postsynaptic Density-95/Guanylate Kinase Domain-Associated Protein Complex with a Light Chain of Myosin-V and Dynein'. The Journal of Neuroscience: The Official Journal of the Society for Neuroscience 20 (12): 4524–34.

Naisbitt, Scott, Eunjoon Kim, Jian Cheng Tu, Bo Xiao, Carlo Sala, Juli Valtschanoff, Richard J. Weinberg, Paul F. Worley, and Morgan Sheng. 1999. 'Shank, a Novel Family of Postsynaptic Density Proteins That Binds to the NMDA Receptor/PSD-95/GKAP Complex and Cortactin'. Neuron 23 (3): 569–82. https://doi.org/10.1016/S0896-6273(00)80809-0.

Nakamoto, Masaru. 2000. 'Eph Receptors and Ephrins'. The International Journal of Biochemistry & Cell Biology 32 (1): 7–12. https://doi.org/10.1016/S1357-2725(99)00096-5.

Nakase, Taizen, and Christian C. G. Naus. 2004. 'Gap Junctions and Neurological Disorders of the Central Nervous System'. Biochimica et Biophysica Acta (BBA) - Biomembranes, The Connexins, 1662 (1): 149–58. https://doi.org/10.1016/j.bbamem.2004.01.009.

Nalefski, E. A., and J. J. Falke. 1996. 'The C2 Domain Calcium-Binding Motif: Structural and Functional Diversity'. Protein Science: A Publication of the Protein Society 5 (12): 2375–90. https://doi.org/10.1002/pro.5560051201.

Nethe, Micha, and Peter L. Hordijk. 2010. 'The Role of Ubiquitylation and Degradation in RhoGTPase Signalling'. J Cell Sci 123 (23): 4011–18. https://doi.org/10.1242/jcs.078360.

Neves, Guilherme, Sam F. Cooke, and Tim V. P. Bliss. 2008. 'Synaptic Plasticity, Memory and the Hippocampus: A Neural Network Approach to Causality'. Nature Reviews Neuroscience 9 (1): 65–75. https://doi.org/10.1038/nrn2303.

Newpher, Thomas M., and Michael D. Ehlers. 2008. 'Glutamate Receptor Dynamics in Dendritic Microdomains'. Neuron 58 (4): 472–97. https://doi.org/10.1016/j.neuron.2008.04.030.

Nicolas, Céline S., Stéphane Peineau, Mascia Amici, Zsolt Csaba, Assia Fafouri, Charlotte Javalet, Valerie J. Collett, et al. 2012. 'The JAK/STAT Pathway Is Involved in Synaptic Plasticity'. Neuron 73 (2): 374–90. https://doi.org/10.1016/j.neuron.2011.11.024.

Nilsen, Timothy W., and Brenton R. Graveley. 2010. 'Expansion of the Eukaryotic Proteome by Alternative Splicing'. Nature 463 (7280): 457–63. https://doi.org/10.1038/nature08909.

Nonaka, Mio, Tomoko Doi, Yoshinori Fujiyoshi, Sayaka Takemoto-Kimura, and Haruhiko Bito. 2006. 'Essential Contribution of the Ligand-Binding BB/BC Loop of PDZ1 and PDZ2 in the Regulation of Postsynaptic Clustering, Scaffolding, and Localization of Postsynaptic Density-95'. Journal of Neuroscience 26 (3): 763–74. https://doi.org/10.1523/JNEUROSCI.2489-05.2006.

Nourry, Claire, Seth G. N. Grant, and Jean-Paul Borg. 2003. 'PDZ Domain Proteins: Plug and Play!' Science's STKE: Signal Transduction Knowledge Environment 2003 (179): RE7. https://doi.org/10.1126/stke.2003.179.re7.

Nusser, Zoltan. 2000. 'AMPA Amd NMDA Receptors: Similarities and Differences in Their Synaptic Distribution'. Current Opinion in Neurobiology 10 (3): 337–41. https://doi.org/10.1016/S0959-4388(00)00086-6.

Nusser, Zoltan. 2018. 'Creating Diverse Synapses from the Same Molecules'. Current Opinion in Neurobiology 51 (August): 8–15. https://doi.org/10.1016/j.conb.2018.01.001.

Nwabuisi-Heath, Evelyn, Mary Jo LaDu, and Chunjiang Yu. 2012. 'Simultaneous Analysis of Dendritic Spine Density, Morphology and Excitatory Glutamate Receptors during Neuron Maturation in Vitro by Quantitative Immunocytochemistry'. Journal of Neuroscience Methods 207 (2): 137–47. https://doi.org/10.1016/j.jneumeth.2012.04.003.

Oh, Jeong S., Pasquale Manzerra, and Mary B. Kennedy. 2004. 'Regulation of the Neuron-Specific Ras GTPase-Activating Protein, SynGAP, by Ca2+/Calmodulin-Dependent Protein Kinase II'. The Journal of Biological Chemistry 279 (17): 17980–88. https://doi.org/10.1074/jbc.M314109200.

Okabe, Shigeo. 2007. 'Molecular Anatomy of the Postsynaptic Density'. Molecular and Cellular Neuroscience 34 (4): 503–18. https://doi.org/10.1016/j.mcn.2007.01.006.

Okamoto, Kenichi, Miquel Bosch, and Yasunori Hayashi. 2009. 'The Roles of CaMKII and F-Actin in the Structural Plasticity of Dendritic Spines: A Potential Molecular Identity of a Synaptic Tag?' Physiology 24 (6): 357–66. https://doi.org/10.1152/physiol.00029.2009.

Opazo, Patricio, Matthieu Sainlos, and Daniel Choquet. 2012. 'Regulation of AMPA Receptor Surface Diffusion by PSD-95 Slots'. Current Opinion in Neurobiology, Synaptic structure and function, 22 (3): 453–60. https://doi.org/10.1016/j.conb.2011.10.010.

Orban, Paul C, Paul F Chapman, and Riccardo Brambilla. 1999. 'Is the Ras-MAPK Signalling Pathway Necessary for Long-Term Memory Formation?' Trends in Neurosciences 22 (1): 38–44. https://doi.org/10.1016/S0166-2236(98)01306-X.

Ortuño-Sahagún, Daniel, Martha C. Rivera-Cervantes, Graciela Gudiño-Cabrera, Felix Junyent, Ester Verdaguer, Carme Auladell, Mercè Pallàs, Antoni Camins, and Carlos Beas-Zárate. 2012. 'Microarray Analysis of Rat Hippocampus Exposed to Excitotoxicity: Reversal Na(+)/Ca(2+) Exchanger NCX3 Is Overexpressed in Glial Cells'. Hippocampus 22 (2): 128–40. https://doi.org/10.1002/hipo.20869.

Ostroff, Linnaea E, John C Fiala, Brenda Allwardt, and Kristen M Harris. 2002. 'Polyribosomes Redistribute from Dendritic Shafts into Spines with Enlarged Synapses during LTP in Developing Rat Hippocampal Slices'. Neuron 35 (3): 535–45. https://doi.org/10.1016/S0896-6273(02)00785-7.

Otmakhov, Nikolai, Jung-Hwa Tao-Cheng, Stephen Carpenter, Brent Asrican, Ayse Dosemeci, Thomas S. Reese, and John Lisman. 2004. 'Persistent Accumulation of Calcium/Calmodulin-Dependent Protein Kinase II in Dendritic Spines after Induction of NMDA Receptor-Dependent Chemical Long-Term Potentiation'. Journal of Neuroscience 24 (42): 9324–31. https://doi.org/10.1523/JNEUROSCI.2350-04.2004.

Ozkan, Emin D., Thomas K. Creson, Enikö A. Kramár, Camilo Rojas, Ron R. Seese, Alex H. Babyan, Yulin Shi, et al. 2014. 'Reduced Cognition in Syngap1 Mutants Is Caused by Isolated Damage within Developing Forebrain Excitatory Neurons'. Neuron 82 (6): 1317–33. https://doi.org/10.1016/j.neuron.2014.05.015.

Paavilainen, Ville O, Enni Bertling, Sandra Falck, and Pekka Lappalainen. 2004. 'Regulation of Cytoskeletal Dynamics by Actin-Monomer-Binding Proteins'. Trends in Cell Biology 14 (7): 386–94. https://doi.org/10.1016/j.tcb.2004.05.002.

Pablo, M. A. de, S. A. Susin, E. Jacotot, N. Larochette, P. Costantini, L. Ravagnan, N. Zamzami, and G. Kroemer. 1999. 'Palmitate Induces Apoptosis via a Direct Effect on Mitochondria'. Apoptosis 4 (2): 81–87. https://doi.org/10.1023/A:1009694124241.

Pak, Daniel T. S., Soyoung Yang, Sheila Rudolph-Correia, Eunjoon Kim, and Morgan Sheng. 2001. 'Regulation of Dendritic Spine Morphology by SPAR, a PSD-95-Associated RapGAP'. Neuron 31 (2): 289–303. https://doi.org/10.1016/S0896-6273(01)00355-5.

Palay, Sanford L. 1956. 'SYNAPSES IN THE CENTRAL NERVOUS SYSTEM'. The Journal of Biophysical and Biochemical Cytology 2 (4): 193. https://doi.org/10.1083/jcb.2.4.193.

Palay, Sanford L., and George E. Palade. 1955. 'THE FINE STRUCTURE OF NEURONS'. The Journal of Biophysical and Biochemical Cytology 1 (1): 69–88.

Pan, Feng, Georgina M. Aldridge, William T. Greenough, and Wen-Biao Gan. 2010. 'Dendritic Spine Instability and Insensitivity to Modulation by Sensory Experience in a Mouse Model of Fragile X Syndrome'.

Proceedings of the National Academy of Sciences of the United States of America 107 (41): 17768–73. https://doi.org/10.1073/pnas.1012496107.

Pan, Qun, Ofer Shai, Leo J. Lee, Brendan J. Frey, and Benjamin J. Blencowe. 2008. 'Deep Surveying of Alternative Splicing Complexity in the Human Transcriptome by High-Throughput Sequencing'. Nature Genetics 40 (12): 1413–15. https://doi.org/10.1038/ng.259.

Pandis, C., E. Sotiriou, E. Kouvaras, E. Asprodini, C. Papatheodoropoulos, and F. Angelatou. 2006. 'Differential Expression of NMDA and AMPA Receptor Subunits in Rat Dorsal and Ventral Hippocampus'. Neuroscience 140 (1): 163–75. https://doi.org/10.1016/j.neuroscience.2006.02.003.

Paoletti, Pierre, Camilla Bellone, and Qiang Zhou. 2013. 'NMDA Receptor Subunit Diversity: Impact on Receptor Properties, Synaptic Plasticity and Disease'. Nature Reviews. Neuroscience 14 (6): 383–400. https://doi.org/10.1038/nrn3504.

Papa, M., M. C. Bundman, V. Greenberger, and M. Segal. 1995. 'Morphological Analysis of Dendritic Spine Development in Primary Cultures of Hippocampal Neurons'. Journal of Neuroscience 15 (1): 1–11. https://doi.org/10.1523/JNEUROSCI.15-01-00001.1995.

Papadopoulos, Theofilos, Volker Eulenburg, Suneel Reddy-Alla, Isabelle M. Mansuy, Yuqing Li, and Heinrich Betz. 2008. 'Collybistin Is Required for Both the Formation and Maintenance of GABAergic Postsynapses in the Hippocampus'. Molecular and Cellular Neuroscience 39 (2): 161–69. https://doi.org/10.1016/j.mcn.2008.06.006.

Park, Mikyoung, Jennifer M. Salgado, Linnaea Ostroff, Thomas D. Helton, Camenzind G. Robinson, Kristen M. Harris, and Michael D. Ehlers. 2006. 'Plasticity-Induced Growth of Dendritic Spines by Exocytic Trafficking from Recycling Endosomes'. Neuron 52 (5): 817–30. https://doi.org/10.1016/j.neuron.2006.09.040.

Parker, Michael J., Alan E. Fryer, Deborah J. Shears, Katherine L. Lachlan, Shane A. McKee, Alex C. Magee, Shehla Mohammed, et al. 2015. 'De Novo, Heterozygous, Loss-of-function Mutations in SYNGAP1 Cause a Syndromic Form of Intellectual Disability'. American Journal of Medical Genetics. Part A 167 (10): 2231–37. https://doi.org/10.1002/ajmg.a.37189.

Pathan, Mohashin, Shivakumar Keerthikumar, Ching-Seng Ang, Lahiru Gangoda, Camelia Y. J. Quek, Nicholas A. Williamson, Dmitri Mouradov, et al. 2015. 'FunRich: An Open Access Standalone Functional Enrichment and Interaction Network Analysis Tool'. Proteomics 15 (15): 2597–2601. https://doi.org/10.1002/pmic.201400515.

Paul, Abhik, Bharti Nawalpuri, Shruthi Sateesh, Ravi S Muddashetty, and James P Clement. 2018. 'Translational Regulation of Syngap1 by FMRP Modulates NMDAR Mediated Signalling'. BioRxiv, October. https://doi.org/10.1101/345058.

Pavlowsky, A, J Chelly, and P Billuart. 2012. 'Major Synaptic Signaling Pathways Involved in Intellectual Disability'. Molecular Psychiatry 17 (7): 663–663. https://doi.org/10.1038/mp.2012.79.

Payne, Helen L. 2008. 'The Role of Transmembrane AMPA Receptor Regulatory Proteins (TARPs) in Neurotransmission and Receptor Trafficking (Review)'. Molecular Membrane Biology 25 (4): 353–62. https://doi.org/10.1080/09687680801986480.

Pei, Lin, R. Lucy Teves, M. Christopher Wallace, and James W. Gurd. 2001. 'Transient Cerebral Ischemia Increases Tyrosine Phosphorylation of the Synaptic RAS-GTPase Activating Protein, SynGAP , Transient Cerebral Ischemia Increases Tyrosine Phosphorylation of the Synaptic RAS-GTPase Activating Protein, SynGAP'. Journal of Cerebral Blood Flow & Metabolism 21 (8): 955–63. https://doi.org/10.1097/00004647-200108000-00008.

Pena, Vladimir, Michael Hothorn, Alexander Eberth, Nikolai Kaschau, Annabel Parret, Lothar Gremer, Fabien Bonneau, Mohammad Reza Ahmadian, and Klaus Scheffzek. 2008. 'The C2 Domain of SynGAP Is Essential for Stimulation of the Rap GTPase Reaction'. EMBO Reports 9 (4): 350–55. https://doi.org/10.1038/embor.2008.20.

Peng, Junmin, Myung Jong Kim, Dongmei Cheng, Duc M. Duong, Steven P. Gygi, and Morgan Sheng. 2004. 'Semiquantitative Proteomic Analysis of Rat Forebrain Postsynaptic Density Fractions by Mass Spectrometry'. Journal of Biological Chemistry 279 (20): 21003–11. https://doi.org/10.1074/jbc.M400103200.

Penzes, Peter, and Kelly A. Jones. 2008. 'Dendritic Spine Dynamics--a Key Role for Kalirin-7'. Trends in Neurosciences 31 (8): 419–27. https://doi.org/10.1016/j.tins.2008.06.001.

Penzes, Peter, Andres Buonanno, Maria Passafaro, Carlo Sala, and Robert A. Sweet. 2013. 'Developmental Vulnerability of Synapses and Circuits Associated with Neuropsychiatric Disorders'. Journal of Neurochemistry 126 (2): 165–82. https://doi.org/10.1111/jnc.12261.

Penzes, Peter, Michael E Cahill, Kelly A Jones, Jon-Eric VanLeeuwen, and Kevin M Woolfrey. 2011. 'Dendritic Spine Pathology in Neuropsychiatric Disorders'. Nature Neuroscience 14 (3): 285–93. https://doi.org/10.1038/nn.2741.

Penzes, Peter, Richard C. Johnson, Rita Sattler, Xiaoqun Zhang, Richard L. Huganir, Vikram Kambampati, Richard E. Mains, and Betty A. Eipper. 2001. 'The Neuronal Rho-GEF Kalirin-7 Interacts with PDZ Domain–Containing Proteins and Regulates Dendritic Morphogenesis'. Neuron 29 (1): 229–42. https://doi.org/10.1016/S0896-6273(01)00193-3.

Pereda, Alberto E. 2014. 'Electrical Synapses and Their Functional Interactions with Chemical Synapses'. Nature Reviews. Neuroscience 15 (4): 250–63. https://doi.org/10.1038/nrn3708.

Petanjek, Zdravko, Miloš Judaš, Goran Šimić, Mladen Roko Rašin, Harry B. M. Uylings, Pasko Rakic, and Ivica Kostović. 2011. 'Extraordinary Neoteny of Synaptic Spines in the Human Prefrontal Cortex'. Proceedings of the National Academy of Sciences 108 (32): 13281. https://doi.org/10.1073/pnas.1105108108.

Peters, A. 1991. 'The Fine Structure of the Nervous System'. Neurons and Their Supporting Cells. https://ci.nii.ac.jp/naid/10023899762/.

Peters, A., and I. R. Kaiserman-Abramof. 1970. 'The Small Pyramidal Neuron of the Rat Cerebral Cortex. The Perikaryon, Dendrites and Spines'. The American Journal of Anatomy 127 (4): 321–55. https://doi.org/10.1002/aja.1001270402.

Petersen, Jennifer D., Xiaobing Chen, Lucia Vinade, Ayse Dosemeci, John E. Lisman, and Thomas S. Reese. 2003. 'Distribution of Postsynaptic Density (PSD)-95 and Ca2+/Calmodulin-Dependent Protein Kinase II at the PSD'. Journal of Neuroscience 23 (35): 11270–78. https://doi.org/10.1523/JNEUROSCI.23-35-11270.2003.

Petralia Ronald S., Ya-Xian Wang, Mark P. Mattson, Pamela J. Yao 2016. 'Diversity of Spine Synapses in Animals'. Neuromolecular Medicine 18 (4): 497–539. https://doi.org/10.1007/s12017-016-8405-y.

Petralia, R.S., Sans, N., Wang, Y.-X., and Wenthold, R.J. (2005). Ontogeny of Postsynaptic Density Proteins at Glutamatergic Synapses. Mol. Cell. Neurosci. 29, 436–452.

Petralia, Ronald S., Nathalie Sans, Ya-Xian Wang, and Robert J. Wenthold. 2005. 'Ontogeny of Postsynaptic Density Proteins at Glutamatergic Synapses'. Molecular and Cellular Neurosciences 29 (3): 436–52. https://doi.org/10.1016/j.mcn.2005.03.013.

Petralia, Ronald S., Ya-Xian Wang, Mark P. Mattson, and Pamela J. Yao. 2015. 'Structure, Distribution, and Function of Neuronal/Synaptic Spinules and Related Invaginating Projections'. Neuromolecular Medicine 17 (3): 211–40. https://doi.org/10.1007/s12017-015-8358-6.

Petralia, Ronald S., Ya-Xian Wang, Mark P. Mattson, and Pamela J. Yao. 2016. 'Diversity of Spine Synapses in Animals'. Neuromolecular Medicine 18 (4): 497–539. https://doi.org/10.1007/s12017-016-8405-y.

Petreanu, Leopoldo, and Arturo Alvarez-Buylla. 2002. 'Maturation and Death of Adult-Born Olfactory Bulb Granule Neurons: Role of Olfaction'. Journal of Neuroscience 22 (14): 6106–13. https://doi.org/10.1523/JNEUROSCI.22-14-06106.2002.

Pettitt, Stephen J., Qi Liang, Xin Y. Rairdan, Jennifer L. Moran, Haydn M. Prosser, David R. Beier, Kent Lloyd, Allan Bradley, and William C. Skarnes. 2009. 'Agouti C57BL/6N Embryonic Stem Cells for Mouse Genetic Resources'. Nature Methods 6 (7): 493–95. https://doi.org/10.1038/nmeth.1342.

Pickett, Eleanor K., Jamie Rose, Caoimhe McCrory, Chris-Anne McKenzie, Declan King, Colin Smith, Thomas H. Gillingwater, Christopher M. Henstridge, and Tara L. Spires-Jones. 2018. 'Region-Specific Depletion of Synaptic Mitochondria in the Brains of Patients with Alzheimer's Disease'. Acta Neuropathologica 136 (5): 747–57. https://doi.org/10.1007/s00401-018-1903-2.

Pinto, Dalila, Alistair T. Pagnamenta, Lambertus Klei, Richard Anney, Daniele Merico, Regina Regan, Judith Conroy, et al. 2010. 'Functional Impact of Global Rare Copy Number Variation in Autism Spectrum Disorder'. Nature 466 (7304): 368–72. https://doi.org/10.1038/nature09146.

Plachez, Céline, and Linda J. Richards. 2005. 'Mechanisms of Axon Guidance in the Developing Nervous System'. In Current Topics in Developmental Biology, 69:267–346. Neural Development. Academic Press. https://doi.org/10.1016/S0070-2153(05)69010-2.

Pocklington, Andrew J., Mark Cumiskey, J. Douglas Armstrong, and Seth G. N. Grant. 2006. 'The Proteomes of Neurotransmitter Receptor Complexes Form Modular Networks with Distributed Functionality Underlying Plasticity and Behaviour'. Molecular Systems Biology 2: 2006.0023. https://doi.org/10.1038/msb4100041.

Poduri, Annapurna, and Daniel Lowenstein. 2011. 'Epilepsy Genetics—Past, Present, and Future'. Current Opinion in Genetics & Development, Molecular and genetic bases of disease, 21 (3): 325–32. https://doi.org/10.1016/j.gde.2011.01.005.

Pol, AN van den. 1991. 'Glutamate and Aspartate Immunoreactivity in Hypothalamic Presynaptic Axons'. Journal of Neuroscience 11 (7): 2087–2101. https://doi.org/10.1523/JNEUROSCI.11-07-02087.1991.

Polzin, Atsuko, Michail Shipitsin, Takanori Goi, Larry A. Feig, and Timothy J. Turner. 2002. 'Ral-GTPase Influences the Regulation of the Readily Releasable Pool of Synaptic Vesicles'. Molecular and Cellular Biology 22 (6): 1714–22.

Poo, Mu-ming. 2001. 'Neurotrophins as Synaptic Modulators'. Nature Reviews Neuroscience 2 (1): 24–32. https://doi.org/10.1038/35049004.

Popov, Victor, Nikolai I. Medvedev, Heather A. Davies, and Michael G. Stewart. 2005. 'Mitochondria Form a Filamentous Reticular Network in Hippocampal Dendrites but Are Present as Discrete Bodies in Axons: A Three-Dimensional Ultrastructural Study'. The Journal of Comparative Neurology 492 (1): 50–65. https://doi.org/10.1002/cne.20682.

Porter, Karen, Noboru H. Komiyama, Tania Vitalis, Peter C. Kind, and Seth G. N. Grant. 2005. 'Differential Expression of Two NMDA Receptor Interacting Proteins, PSD-95 and SynGAP during Mouse Development'. European Journal of Neuroscience 21 (2): 351–62. https://doi.org/10.1111/j.1460-9568.2005.03874.x.

Prange, Oliver, Tak Pan Wong, Kimberly Gerrow, Yu Tian Wang, and Alaa El-Husseini. 2004. 'A Balance between Excitatory and Inhibitory Synapses Is Controlled by PSD-95 and Neuroligin'. Proceedings of the National Academy of Sciences 101 (38): 13915–20. https://doi.org/10.1073/pnas.0405939101.

Purves, Dale, George J. Augustine, David Fitzpatrick, William C. Hall, Anthony-Samuel LaMantia, James O. McNamara, and Leonard E. White. 2007. Neuroscience. Edición: 4th Edition. Sunderland, Mass: Sinauer Associates.

Racine. 2012 'RStudio: A Platform-Independent IDE for R and Sweave´- Journal of Applied Econometrics - Wiley Online Library'

Racz, B., and R.J. Weinberg. 2006. 'Spatial Organization of Cofilin in Dendritic Spines'. Neuroscience 138 (2): 447–56. https://doi.org/10.1016/j.neuroscience.2005.11.025.

Rácz, Bence, and Richard J. Weinberg. 2008. 'Organization of the Arp2/3 Complex in Hippocampal Spines'. Journal of Neuroscience 28 (22): 5654–59. https://doi.org/10.1523/JNEUROSCI.0756-08.2008.

Rai, Dheeraj, Brian K. Lee, Christina Dalman, Jean Golding, Glyn Lewis, and Cecilia Magnusson. 2013. 'Parental Depression, Maternal Antidepressant Use during Pregnancy, and Risk of Autism Spectrum Disorders: Population Based Case-Control Study'. BMJ 346 (April): f2059. https://doi.org/10.1136/bmj.f2059.

Raj, Bushra, and Benjamin J. Blencowe. 2015. 'Alternative Splicing in the Mammalian Nervous System: Recent Insights into Mechanisms and Functional Roles'. Neuron 87 (1): 14–27. https://doi.org/10.1016/j.neuron.2015.05.004.

Rama, Sylvain, Grigory Krapivinsky, David E. Clapham, and Igor Medina. 2008. 'The MUPP1–SynGAPα Protein Complex Does Not Mediate Activity-Induced LTP'. Molecular and Cellular Neurosciences 38 (2): 183–88. https://doi.org/10.1016/j.mcn.2008.02.007.

Ramaratnam, S., G. A. Baker, and L. H. Goldstein. 2005. 'Psychological Treatments for Epilepsy.' The Cochrane Database of Systematic Reviews, no. 4: CD002029–CD002029. https://doi.org/10.1002/14651858.CD002029.pub2.

Ramos-Quiroga, Josep A., Cristina Sánchez-Mora, Margarida Corominas, Iris Martínez, Víctor Barrau, Laura Prats, Miguel Casas, and Marta Ribasés. 2014. '[Neurotrophic factors and their importance in attention deficit hyperactivity disorde]'. Revista De Neurologia 58 Suppl 1 (February): S19-24.

Rangaraju, Vidhya, Marcel Lauterbach, and Erin M. Schuman. 2019. 'Spatially Stable Mitochondrial Compartments Fuel Local Translation during Plasticity'. Cell 176 (1–2): 73-84.e15. https://doi.org/10.1016/j.cell.2018.12.013.

Rauch, Anita, Dagmar Wieczorek, Elisabeth Graf, Thomas Wieland, Sabine Endele, Thomas Schwarzmayr, Beate Albrecht, et al. 2012. 'Range of Genetic Mutations Associated with Severe Non-Syndromic Sporadic Intellectual Disability: An Exome Sequencing Study'. The Lancet 380 (9854): 1674–82. https://doi.org/10.1016/S0140-6736(12)61480-9.

Rauch, Anita, Dagmar Wieczorek, Elisabeth Graf, Thomas Wieland, Sabine Endele, Thomas Schwarzmayr, Beate Albrecht, et al. 2012. 'Range of Genetic Mutations Associated with Severe Non-Syndromic Sporadic Intellectual Disability: An Exome Sequencing Study'. The Lancet 380 (9854): 1674–82. https://doi.org/10.1016/S0140-6736(12)61480-9.

Rauch, Anita, Juliane Hoyer, Sabine Guth, Christiane Zweier, Cornelia Kraus, Christian Becker, Martin Zenker, et al. 2006. 'Diagnostic Yield of Various Genetic Approaches in Patients with Unexplained Developmental Delay or Mental Retardation'. American Journal of Medical Genetics Part A 140A (19): 2063–74. https://doi.org/10.1002/ajmg.a.31416.

Reble, E., A. Dineen, and C. L. Barr. 2018. 'The Contribution of Alternative Splicing to Genetic Risk for Psychiatric Disorders'. Genes, Brain, and Behavior 17 (3): e12430. https://doi.org/10.1111/gbb.12430.

Redin, Claire, Bénédicte Gérard, Julia Lauer, Yvan Herenger, Jean Muller, Angélique Quartier, Alice Masurel-Paulet, et al. 2014. 'Efficient Strategy for the Molecular Diagnosis of Intellectual Disability Using Targeted High-Throughput Sequencing'. Journal of Medical Genetics 51 (11): 724–36. https://doi.org/10.1136/jmedgenet-2014-102554.

Redin, Claire, Bénédicte Gérard, Julia Lauer, Yvan Herenger, Jean Muller, Angélique Quartier, Alice Masurel-Paulet, et al. 2014. 'Efficient Strategy for the Molecular Diagnosis of Intellectual Disability Using Targeted High-Throughput Sequencing'. Journal of Medical Genetics 51 (11): 724–36. https://doi.org/10.1136/jmedgenet-2014-102554.

Risch, N. J. 2000. 'Searching for Genetic Determinants in the New Millennium'. Nature 405 (6788): 847–56. https://doi.org/10.1038/35015718.

Risch, N., and M. Baron. 1984. 'Segregation Analysis of Schizophrenia and Related Disorders'. American Journal of Human Genetics 36 (5): 1039–59.

Risher, W. Christopher, Tuna Ustunkaya, Jonnathan Singh Alvarado, and Cagla Eroglu. 2014. 'Rapid Golgi Analysis Method for Efficient and Unbiased Classification of Dendritic Spines'. PloS One 9 (9): e107591. https://doi.org/10.1371/journal.pone.0107591.

Rochefort, Nathalie L., and Arthur Konnerth. 2012. 'Dendritic Spines: From Structure to in Vivo Function'. EMBO Reports 13 (8): 699–708. https://doi.org/10.1038/embor.2012.102.

Ronsein, Graziella E., Nathalie Pamir, Priska D. von Haller, Daniel S. Kim, Michael N. Oda, Gail P. Jarvik, Tomas Vaisar, and Jay W. Heinecke. 2015. 'Parallel Reaction Monitoring (PRM) and Selected Reaction Monitoring (SRM) Exhibit Comparable Linearity, Dynamic Range and Precision for Targeted Quantitative HDL Proteomics'. Journal of Proteomics 113 (January): 388–99. https://doi.org/10.1016/j.jprot.2014.10.017.

Ropers, H.-Hilger, and Ben C. J. Hamel. 2005. 'X-Linked Mental Retardation'. Nature Reviews Genetics 6 (January): 46.

Ropers, Hans Hilger. 2010. 'Genetics of Early Onset Cognitive Impairment'. Annual Review of Genomics and Human Genetics 11 (1): 161–87. https://doi.org/10.1146/annurev-genom-082509-141640.

Rossmann, Maxim, Madhav Sukumaran, Andrew C. Penn, Dmitry B. Veprintsev, M. Madan Babu, and Ingo H. Greger. 2011. 'Subunit-selective N-terminal Domain Associations Organize the Formation of AMPA Receptor Heteromers'. The EMBO Journal 30 (5): 959–71. https://doi.org/10.1038/emboj.2011.16.

Rozental, R., A. F. Andrade-Rozental, X. Zheng, M. Urban, D. C. Spray, and F. C. Chiu. 2001. 'Gap Junction-Mediated Bidirectional Signaling between Human Fetal Hippocampal Neurons and Astrocytes'. Developmental Neuroscience 23 (6): 420–31. https://doi.org/10.1159/000048729.

Rubenstein, J. L. R., and M. M. Merzenich. 2003. 'Model of Autism: Increased Ratio of Excitation/Inhibition in Key Neural Systems'. Genes, Brain, and Behavior 2 (5): 255–67.

Rumbaugh, Gavin, J. Paige Adams, Jee H. Kim, and Richard L. Huganir. 2006. 'SynGAP Regulates Synaptic Strength and Mitogen-Activated Protein Kinases in Cultured Neurons'. Proceedings of the National Academy of Sciences of the United States of America 103 (12): 4344–51. https://doi.org/10.1073/pnas.0600084103.

Rust, Marco B. 2015. ‘ADF/Cofilin: A Crucial Regulator of Synapse Physiology and Behavior’. Cellular and Molecular Life Sciences: CMLS 72 (18): 3521–29. https://doi.org/10.1007/s00018-015-1941-z.

Rust, Marco B. 2015. ‘ADF/Cofilin: A Crucial Regulator of Synapse Physiology and Behavior’. Cellular and Molecular Life Sciences: CMLS 72 (18): 3521–29. https://doi.org/10.1007/s00018-015-1941-z.

Ryan, Tomás J., and Seth G. N. Grant. 2009. ‘The Origin and Evolution of Synapses’. Nature Reviews. Neuroscience 10 (10): 701–12. https://doi.org/10.1038/nrn2717.

Sakamoto, Masayuki, Ryoichiro Kageyama, and Itaru Imayoshi. 2014. ‘The Functional Significance of Newly Born Neurons Integrated into Olfactory Bulb Circuits’. Frontiers in Neuroscience 8. https://doi.org/10.3389/fnins.2014.00121.

Sala, Carlo, and Chiara Verpelli. 2016. Neuronal and Synaptic Dysfunction in Autism Spectrum Disorder and Intellectual Disability. 1st ed. Academic Press. http://gen.lib.rus.ec/book/index.php?md5=595e907e5cc395a134feaeecc4a0f29a.

Sala, Carlo, Ilaria Cambianica, and Francesca Rossi. 2008. ‘Molecular Mechanisms of Dendritic Spine Development and Maintenance’. Acta Neurobiologiae Experimentalis 68 (2): 289–304.

Sala, Carlo, Kensuke Futai, Kenji Yamamoto, Paul F. Worley, Yasunori Hayashi, and Morgan Sheng. 2003. ‘Inhibition of Dendritic Spine Morphogenesis and Synaptic Transmission by Activity-Inducible Protein Homer1a’. The Journal of Neuroscience: The Official Journal of the Society for Neuroscience 23 (15): 6327–37.

Sala, Carlo, Valentin Piëch, Nathan R. Wilson, Maria Passafaro, Guosong Liu, and Morgan Sheng. 2001. ‘Regulation of Dendritic Spine Morphology and Synaptic Function by Shank and Homer’. Neuron 31 (1): 115–30. https://doi.org/10.1016/S0896-6273(01)00339-7.

Salinas, Patricia C. 2012. ‘Wnt Signaling in the Vertebrate Central Nervous System: From Axon Guidance to Synaptic Function’. Cold Spring Harbor Perspectives in Biology 4 (2). https://doi.org/10.1101/cshperspect.a008003.

San Martín, Alvaro, and Mario Rafael Pagani. 2014. ‘Understanding Intellectual Disability through RASopathies’. Journal of Physiology, Paris 108 (4–6): 232–39. https://doi.org/10.1016/j.jphysparis.2014.05.003.

Sans, N., R. S. Petralia, Y. X. Wang, J. Blahos, J. W. Hell, and R. J. Wenthold. 2000. ‘A Developmental Change in NMDA Receptor-Associated Proteins at Hippocampal Synapses’. The Journal of Neuroscience: The Official Journal of the Society for Neuroscience 20 (3): 1260–71.

Santini, Emanuela, and Eric Klann. 2014. ‘Reciprocal Signaling between Translational Control Pathways and Synaptic Proteins in Autism Spectrum Disorders’. Science Signaling 7 (349): re10. https://doi.org/10.1126/scisignal.2005832.

Santini, Emanuela, and Eric Klann. 2014. ‘Reciprocal Signaling between Translational Control Pathways and Synaptic Proteins in Autism Spectrum Disorders’. Science Signaling 7 (349): re10. https://doi.org/10.1126/scisignal.2005832.

Santuy, A., M. Turégano-López, J. R. Rodríguez, L. Alonso-Nanclares, J. DeFelipe, and A. Merchán-Pérez. 2018. ‘A Quantitative Study on the Distribution of Mitochondria in the Neuropil of the Juvenile Rat Somatosensory Cortex’. Cerebral Cortex (New York, N.Y.: 1991) 28 (10): 3673–84. https://doi.org/10.1093/cercor/bhy159.

Sato, Daisuke, Anath C. Lionel, Claire S. Leblond, Aparna Prasad, Dalila Pinto, Susan Walker, Irene O’Connor, et al. 2012. ‘SHANK1 Deletions in Males with Autism Spectrum Disorder’. American Journal of Human Genetics 90 (5): 879–87. https://doi.org/10.1016/j.ajhg.2012.03.017.

Savitski, Mikhail M., Mathias WIlhelm, Hannes Hahne, Bernhard Kuster, and Marcus Bantscheff. 2015. ‘A Scalable Approach for Protein False Discovery Rate Estimation in Large Proteomic Data Sets’. Molecular & Cellular Proteomics, May, mcp.M114.046995. https://doi.org/10.1074/mcp.M114.046995.

Sawicka, Kirsty, and R. Suzanne Zukin. 2012. ‘Dysregulation of MTOR Signaling in Neuropsychiatric Disorders: Therapeutic Implications’. Neuropsychopharmacology: Official Publication of the American College of Neuropsychopharmacology 37 (1): 305–6. https://doi.org/10.1038/npp.2011.210.

Scheuss, Volker, and Tobias Bonhoeffer. 2014. ‘Function of Dendritic Spines on Hippocampal Inhibitory Neurons’. Cerebral Cortex 24 (12): 3142–53. https://doi.org/10.1093/cercor/bht171.

Schmeisser, Michael J., Elodie Ey, Stephanie Wegener, Juergen Bockmann, A. Vanessa Stempel, Angelika Kuebler, Anna-Lena Janssen, et al. 2012. 'Autistic-like Behaviours and Hyperactivity in Mice Lacking ProSAP1/Shank2'. Nature 486 (7402): 256–60. https://doi.org/10.1038/nature11015.

Schwartz, Samantha L., Canhong Cao, Olena Pylypenko, Alexey Rak, and Angela Wandinger-Ness. 2007. 'Rab GTPases at a Glance'. Journal of Cell Science 120 (22): 3905–10. https://doi.org/10.1242/jcs.015909.

Schweizer, Felix E. 2001. 'Synapses'. In ELS. American Cancer Society. https://doi.org/10.1038/npg.els.0000207.

Seabra, Miguel C., Emilie H. Mules, and Alistair N. Hume. 2002. 'Rab GTPases, Intracellular Traffic and Disease'. Trends in Molecular Medicine 8 (1): 23–30. https://doi.org/10.1016/S1471-4914(01)02227-4.

Segal, Menahem, and Per Andersen. 2000. 'Dendritic Spines Shaped by Synaptic Activity'. Current Opinion in Neurobiology 10 (5): 582–86. https://doi.org/10.1016/S0959-4388(00)00123-9.

Segal, Menahem. 2010. 'Dendritic Spines, Synaptic Plasticity and Neuronal Survival: Activity Shapes Dendritic Spines to Enhance Neuronal Viability'. European Journal of Neuroscience 31 (12): 2178–84. https://doi.org/10.1111/j.1460-9568.2010.07270.x.

Semple, Bridgette D., Klas Blomgren, Kayleen Gimlin, Donna M. Ferriero, and Linda J. Noble-Haeusslein. 2013. 'Brain Development in Rodents and Humans: Identifying Benchmarks of Maturation and Vulnerability to Injury across Species'. Progress in Neurobiology 106–107 (July): 1–16. https://doi.org/10.1016/j.pneurobio.2013.04.001.

Shapira, Mika, R. Grace Zhai, Thomas Dresbach, Tal Bresler, Viviana I Torres, Eckart D Gundelfinger, Noam E Ziv, and Craig C Garner. 2003. 'Unitary Assembly of Presynaptic Active Zones from Piccolo-Bassoon Transport Vesicles'. Neuron 38 (2): 237–52. https://doi.org/10.1016/S0896-6273(03)00207-1.

Shen, K., and T. Meyer. 1999. 'Dynamic Control of CaMKII Translocation and Localization in Hippocampal Neurons by NMDA Receptor Stimulation'. Science (New York, N.Y.) 284 (5411): 162–66.

Sheng, M., and E. Kim. 2000. 'The Shank Family of Scaffold Proteins'. J Cell Sci 113 (11): 1851–56

Sheng, Morgan, and Carlo Sala. 2001. 'PDZ Domains and the Organization of Supramolecular Complexes'. Annual Review of Neuroscience 24 (1): 1–29. https://doi.org/10.1146/annurev.neuro.24.1.1.

Sheng, Morgan, and Casper C. Hoogenraad. 2007. 'The Postsynaptic Architecture of Excitatory Synapses: A More Quantitative View'. Annual Review of Biochemistry 76 (1): 823–47. https://doi.org/10.1146/annurev.biochem.76.060805.160029.

Sheng, Morgan, and Casper C. Hoogenraad. 2007. 'The Postsynaptic Architecture of Excitatory Synapses: A More Quantitative View'. Annual Review of Biochemistry 76 (1): 823–47. https://doi.org/10.1146/annurev.biochem.76.060805.160029.

Sheng, Morgan, and Eunjoon Kim. 2011. 'The Postsynaptic Organization of Synapses'. Cold Spring Harbor Perspectives in Biology 3 (12). https://doi.org/10.1101/cshperspect.a005678.

Sheng, Zu-Hang, and Qian Cai. 2012. 'Mitochondrial Transport in Neurons: Impact on Synaptic Homeostasis and Neurodegeneration'. Nature Reviews. Neuroscience 13 (2): 77–93. https://doi.org/10.1038/nrn3156.

Shepherd, Gordon M. G., and Kristen M. Harris. 1998. 'Three-Dimensional Structure and Composition of CA3→CA1 Axons in Rat Hippocampal Slices: Implications for Presynaptic Connectivity and Compartmentalization'. The Journal of Neuroscience 18 (20): 8300. https://doi.org/10.1523/JNEUROSCI.18-20-08300.1998.

Sherstnev, V. V., O. N. Golubeva, M. A. Gruden, Z. I. Storozheva, and E. V. Guseva. 2012. 'Neurogenesis and Neuroapoptosis in Different Brain Structures of Adult Wistar Rats'. Neurochemical Journal 6 (3): 179–84. https://doi.org/10.1134/S1819712412020092.

Shi, Yu, and Matthias Gaestel. 2002. 'In the Cellular Garden of Forking Paths: How P38 MAPKs Signal for Downstream Assistance'. Biological Chemistry 383 (10): 1519–36. https://doi.org/10.1515/BC.2002.173.

Shiraishi-Yamaguchi, Yoko, and Teiichi Furuichi. 2007. 'The Homer Family Proteins'. Genome Biology 8 (February): 206. https://doi.org/10.1186/gb-2007-8-2-206.

Sík, Attila, Norbert Hájos, Alexandra Gulácsi, Istvan Mody, and Tamás F. Freund. 1998. 'The Absence of a Major Ca2+ Signaling Pathway in GABAergic Neurons of the Hippocampus'. Proceedings of the National Academy of Sciences 95 (6): 3245–50. https://doi.org/10.1073/pnas.95.6.3245.

Silverthorn, Dee Unglaub, and Dee Unglaub Silverthorn. 2007. Human Physiology : An Integrated Approach. 4th ed. San Francisco, Calif. ; London : Pearson/Benjamin Cummings. https://trove.nla.gov.au/version/24672298.

Simon, David M., and Mark T. Wallace. 2016. 'Dysfunction of Sensory Oscillations in Autism Spectrum Disorder'. Neuroscience & Biobehavioral Reviews 68 (September): 848–61. https://doi.org/10.1016/j.neubiorev.2016.07.016.

Sjöström, Martin, Reto Ossola, Thomas Breslin, Oliver Rinner, Lars Malmström, Alexander Schmidt, Ruedi Aebersold, Johan Malmström, and Emma Niméus. 2015. 'A Combined Shotgun and Targeted Mass Spectrometry Strategy for Breast Cancer Biomarker Discovery'. Journal of Proteome Research 14 (7): 2807–18. https://doi.org/10.1021/acs.jproteome.5b00315.

Sloan, Steven A, and Ben A Barres. 2014. 'Mechanisms of Astrocyte Development and Their Contributions to Neurodevelopmental Disorders'. Current Opinion in Neurobiology 27 (August): 75–81. https://doi.org/10.1016/j.conb.2014.03.005.

Söding, Johannes, and Andrei N. Lupas. 2003. 'More than the Sum of Their Parts: On the Evolution of Proteins from Peptides'. BioEssays 25 (9): 837–46. https://doi.org/10.1002/bies.10321.

Somerville, Shahza M., Adrienne C. Lahti, Robert R. Conley, and Rosalinda C. Roberts. 2011. 'Mitochondria in the Striatum of Subjects with Schizophrenia: Relationship to Treatment Response'. Synapse (New York, N.Y.) 65 (3): 215–24. https://doi.org/10.1002/syn.20838.

Song, Bo, Xue-Bo Yan, and Guang-Yi Zhang. 2004. 'PSD-95 Promotes CaMKII-Catalyzed Serine Phosphorylation of the Synaptic RAS-GTPase Activating Protein SynGAP after Transient Brain Ischemia in Rat Hippocampus'. Brain Research 1005 (1): 44–50. https://doi.org/10.1016/j.brainres.2004.01.032.

Song, Ji-Ying, Konstantin Ichtchenko, Thomas C. Südhof, and Nils Brose. 1999. 'Neuroligin 1 Is a Postsynaptic Cell-Adhesion Molecule of Excitatory Synapses'. Proceedings of the National Academy of Sciences 96 (3): 1100–1105. https://doi.org/10.1073/pnas.96.3.1100.

Sorra, K. E., A. Mishra, S. A. Kirov, and K. M. Harris. 2006. 'Dense Core Vesicles Resemble Active-Zone Transport Vesicles and Are Diminished Following Synaptogenesis in Mature Hippocampal Slices'. Neuroscience 141 (4): 2097–2106. https://doi.org/10.1016/j.neuroscience.2006.05.033.

Sorra, K. E., and K. M. Harris. 2000. 'Overview on the Structure, Composition, Function, Development, and Plasticity of Hippocampal Dendritic Spines'. Hippocampus 10 (5): 501–11. https://doi.org/10.1002/1098-1063(2000)10:5<501::AID-HIPO1>3.0.CO;2-T.

Sotelo, Constantino. 1978. 'Purkinje Cell Ontogeny: Formation and Maintenance of Spines'. In Progress in Brain Research, edited by M. A. Corner, R. E. Baker, N. E. Vandepoll, D. F. Swaab, and H. B. M. Uylings, 48:149–70. Maturation of the Nervous System. Elsevier. https://doi.org/10.1016/S0079-6123(08)61021-3.

Spacek, J. 1982. '"Free" Postsynaptic-like Densities in Normal Adult Brain: Their Occurrence, Distribution, Structure and Association with Subsurface Cisterns'. Journal of Neurocytology 11 (5): 693–706.

Spijker, Sabine. 2011. 'Dissection of Rodent Brain Regions'. In , 57:13–26. https://doi.org/10.1007/978-1-61779-111-6_2.

Spijker, Sabine. 2011. 'Dissection of Rodent Brain Regions'. In Neuroproteomics, 13–26. Neuromethods. Humana Press, Totowa, NJ. https://doi.org/10.1007/978-1-61779-111-6_2.

Spilker, Christina, Gustavo A. Acuña Sanhueza, Tobias M. Böckers, Michael R. Kreutz, and Eckart D. Gundelfinger. 2008. 'SPAR2, a Novel SPAR-Related Protein with GAP Activity for Rap1 and Rap2'. Journal of Neurochemistry 104 (1): 187–201. https://doi.org/10.1111/j.1471-4159.2007.04991.x.

Spronsen, Myrrhe van, and Casper C. Hoogenraad. 2010. 'Synapse Pathology in Psychiatric and Neurologic Disease'. Current Neurology and Neuroscience Reports 10 (3): 207–14. https://doi.org/10.1007/s11910-010-0104-8.

Srivastava, Pranay, Yogesh K. Dhuriya, Vivek Kumar, Akriti Srivastava, Richa Gupta, Rajendra K. Shukla, Rajesh S. Yadav, Hari N. Dwivedi, Aditya B. Pant, and Vinay K. Khanna. 2018. 'PI3K/Akt/GSK3β Induced CREB Activation Ameliorates Arsenic Mediated Alterations in NMDA Receptors and

Associated Signaling in Rat Hippocampus: Neuroprotective Role of Curcumin'. Neurotoxicology 67 (April): 190–205. https://doi.org/10.1016/j.neuro.2018.04.018.

Stafstrom, Carl E. 2010. 'Mechanisms of Action of Antiepileptic Drugs: The Search for Synergy'. Current Opinion in Neurology 23 (2): 157–63. https://doi.org/10.1097/WCO.0b013e32833735b5.

Stafstrom, Carl E., and Lionel Carmant. 2015. 'Seizures and Epilepsy: An Overview for Neuroscientists'. Cold Spring Harbor Perspectives in Medicine 5 (6). https://doi.org/10.1101/cshperspect.a022426.

Stenmark, Harald, and Vesa M. Olkkonen. 2001. 'The Rab GTPase Family'. Genome Biology 2 (April): reviews3007. https://doi.org/10.1186/gb-2001-2-5-reviews3007.

Stepanyants, Armen, Patrick R. Hof, and Dmitri B. Chklovskii. 2002. 'Geometry and Structural Plasticity of Synaptic Connectivity'. Neuron 34 (2): 275–88. https://doi.org/10.1016/S0896-6273(02)00652-9.

Stevens, Craig, Yao Lin, Ben Harrison, Lindsay Burch, Rachel A. Ridgway, Owen Sansom, and Ted Hupp. 2009. 'Peptide Combinatorial Libraries Identify TSC2 as a Death-Associated Protein Kinase (DAPK) Death Domain-Binding Protein and Reveal a Stimulatory Role for DAPK in MTORC1 Signaling'. Journal of Biological Chemistry 284 (1): 334–44. https://doi.org/10.1074/jbc.M805165200.

Stornetta, Ruth L., and J. Julius Zhu. 2011. 'Ras and Rap Signaling in Synaptic Plasticity and Mental Disorders'. The Neuroscientist : A Review Journal Bringing Neurobiology, Neurology and Psychiatry 17 (1): 54–78. https://doi.org/10.1177/1073858410365562.

Strack, S., M. A. Barban, B. E. Wadzinski, and R. J. Colbran. 1997. 'Differential Inactivation of Postsynaptic Density-Associated and Soluble Ca2+/Calmodulin-Dependent Protein Kinase II by Protein Phosphatases 1 and 2A'. Journal of Neurochemistry 68 (5): 2119–28.

Sturgill, James F., Pascal Steiner, Brian L. Czervionke, and Bernardo L. Sabatini. 2009. 'Distinct Domains within PSD-95 Mediate Synaptic Incorporation, Stabilization, and Activity-Dependent Trafficking'. Journal of Neuroscience 29 (41): 12845–54. https://doi.org/10.1523/JNEUROSCI.1841-09.2009.

Südhof, Thomas C. 2012. 'The Presynaptic Active Zone'. Neuron 75 (1): 11–25. https://doi.org/10.1016/j.neuron.2012.06.012.

Südhof, Thomas C. 2017. 'Synaptic Neurexin Complexes: A Molecular Code for the Logic of Neural Circuits'. Cell 171 (4): 745–69. https://doi.org/10.1016/j.cell.2017.10.024.

Südhof, Thomas C., and Josep Rizo. 2011. 'Synaptic Vesicle Exocytosis'. Cold Spring Harbor Perspectives in Biology, October, a005637. https://doi.org/10.1101/cshperspect.a005637.

Sugiyama, Yoshiko, Izumi Kawabata, Kenji Sobue, and Shigeo Okabe. 2005. 'Determination of Absolute Protein Numbers in Single Synapses by a GFP-Based Calibration Technique'. Nature Methods 2 (9): 677–84. https://doi.org/10.1038/nmeth783.

Sumita, Kazutaka, Yuji Sato, Junko Iida, Akira Kawata, Mamiko Hamano, Susumu Hirabayashi, Kikuo Ohno, Elior Peles, and Yutaka Hata. n.d. 'Synaptic Scaffolding Molecule (S-SCAM) Membrane-Associated Guanylate Kinase with Inverted Organization (MAGI)-2 Is Associated with Cell Adhesion Molecules at Inhibitory Synapses in Rat Hippocampal Neurons'. Journal of Neurochemistry 100 (1): 154–66. https://doi.org/10.1111/j.1471-4159.2006.04170.x.

Sung, Hyeran, Krishna L. Kanchi, Xue Wang, Kristen S. Hill, Jane L. Messina, Ji-Hyun Lee, Youngchul Kim, et al. 2016. 'Inactivation of RASA1 Promotes Melanoma Tumorigenesis via R-Ras Activation'. Oncotarget 7 (17): 23885–96. https://doi.org/10.18632/oncotarget.8127.

Supek, Fran, Matko Bošnjak, Nives Škunca, and Tomislav Šmuc. 2011. 'REVIGO Summarizes and Visualizes Long Lists of Gene Ontology Terms'. PLoS ONE 6 (7). https://doi.org/10.1371/journal.pone.0021800.

Suzuki, Nobuchika, Nicole Hajicek, and Tohru Kozasa. 2009. 'Regulation and Physiological Functions of G12/13-Mediated Signaling Pathways'. Neurosignals 17 (1): 55–70. https://doi.org/10.1159/000186690.

Sweatt, J. D. 2001. 'The Neuronal MAP Kinase Cascade: A Biochemical Signal Integration System Subserving Synaptic Plasticity and Memory'. Journal of Neurochemistry 76 (1): 1–10.

Swulius, Matthew T., Yoshihisa Kubota, Amélie Forest, and M. Neal Waxham. 2010. 'Structure and Composition of the Postsynaptic Density during Development'. The Journal of Comparative Neurology 518 (20): 4243–60. https://doi.org/10.1002/cne.22451.

Szklarczyk, Damian, John H. Morris, Helen Cook, Michael Kuhn, Stefan Wyder, Milan Simonovic, Alberto Santos, et al. 2017. 'The STRING Database in 2017: Quality-Controlled Protein–Protein Association

Networks, Made Broadly Accessible'. Nucleic Acids Research 45 (D1): D362–68. https://doi.org/10.1093/nar/gkw937.

Sztainberg, Yehezkel, and Huda Y Zoghbi. 2016. 'Lessons Learned from Studying Syndromic Autism Spectrum Disorders'. Nature Neuroscience 19 (October): 1408.

Sztainberg, Yehezkel, Hong-mei Chen, John W. Swann, Shuang Hao, Bin Tang, Zhenyu Wu, Jianrong Tang, et al. 2015. 'Reversal of Phenotypes in MECP2 Duplication Mice Using Genetic Rescue or Antisense Oligonucleotides'. Nature 528 (7580): 123–26. https://doi.org/10.1038/nature16159.

Tabuchi, Katsuhiko, Jacqueline Blundell, Mark R. Etherton, Robert E. Hammer, Xinran Liu, Craig M. Powell, and Thomas C. Südhof. 2007. 'A Neuroligin-3 Mutation Implicated in Autism Increases Inhibitory Synaptic Transmission in Mice'. Science (New York, N.Y.) 318 (5847): 71–76. https://doi.org/10.1126/science.1146221.

Tabuchi, Katsuhiko, Jacqueline Blundell, Mark R. Etherton, Robert E. Hammer, Xinran Liu, Craig M. Powell, and Thomas C. Südhof. 2007. 'A Neuroligin-3 Mutation Implicated in Autism Increases Inhibitory Synaptic Transmission in Mice'. Science (New York, N.Y.) 318 (5847): 71–76. https://doi.org/10.1126/science.1146221.

Tada, Tomoko, and Morgan Sheng. 2006. 'Molecular Mechanisms of Dendritic Spine Morphogenesis'. Current Opinion in Neurobiology 16 (1): 95–101. https://doi.org/10.1016/j.conb.2005.12.001.

Takahashi, Hideto, Yuko Sekino, Satoshi Tanaka, Toshiyuki Mizui, Shoji Kishi, and Tomoaki Shirao. 2003. 'Drebrin-Dependent Actin Clustering in Dendritic Filopodia Governs Synaptic Targeting of Postsynaptic Density-95 and Dendritic Spine Morphogenesis'. The Journal of Neuroscience: The Official Journal of the Society for Neuroscience 23 (16): 6586–95.

Takai, Yoshimi, Takuya Sasaki, and Takashi Matozaki. 2001. 'Small GTP-Binding Proteins'. Physiological Reviews 81 (1): 153–208. https://doi.org/10.1152/physrev.2001.81.1.153.

Tallafuss, Alexandra, John R. L. Constable, and Philip Washbourne. 2010. 'Organization of Central Synapses by Adhesion Molecules'. The European Journal of Neuroscience 32 (2): 198–206. https://doi.org/10.1111/j.1460-9568.2010.07340.x.

Tallez-Zenteno et al. 2007 Epilepsia temporal: aspectos clínicos, diagnósticos y de tratamiento. Téllez-Zenteno and Ladino. Rev Neurol 2013; 56 (4): 229-242.

Tam, See-Ying, Jennifer N. Lilla, Ching-Cheng Chen, Janet Kalesnikoff, and Mindy Tsai. 2015. 'RabGEF1/Rabex-5 Regulates TrkA-Mediated Neurite Outgrowth and NMDA-Induced Signaling Activation in NGF-Differentiated PC12 Cells'. PLoS ONE 10 (11). https://doi.org/10.1371/journal.pone.0142935.

Tapias, Alicia, and Zhao-Qi Wang. 2017. 'Lysine Acetylation and Deacetylation in Brain Development and Neuropathies'. Genomics, Proteomics & Bioinformatics 15 (1): 19–36. https://doi.org/10.1016/j.gpb.2016.09.002.

Taylor, M., I. Chaudhry, M. Cross, E. McDonald, P. Miller, L. Pilowsky, P. Strickland, and Relapse Prevention in Schizophrenia Consensus Group. 2005. 'Towards Consensus in the Long-Term Management of Relapse Prevention in Schizophrenia'. Human Psychopharmacology 20 (3): 175–81. https://doi.org/10.1002/hup.675.

Taylor, Stephan F., K. Luan Phan, Jennifer C. Britton, and Israel Liberzon. 2005. 'Neural Response to Emotional Salience in Schizophrenia'. Neuropsychopharmacology 30 (5): 984–95. https://doi.org/10.1038/sj.npp.1300679.

Teodoro, Rita O., Gulçin Pekkurnaz, Abdullah Nasser, Misao E. Higashi-Kovtun, Maria Balakireva, Ian G. McLachlan, Jacques Camonis, and Thomas L. Schwarz. 2013. 'Ral Mediates Activity-dependent Growth of Postsynaptic Membranes via Recruitment of the Exocyst'. The EMBO Journal 32 (14): 2039–55. https://doi.org/10.1038/emboj.2013.147.

Thein, Soe, Jung-Hwa Tao-Cheng, Yan Li, K. Ulrich Bayer, Thomas S. Reese, and Ayse Dosemeci. 2014. 'CaMKII Mediates Recruitment and Activation of the Deubiquitinase CYLD at the Postsynaptic Density'. PLOS ONE 9 (3): e91312. https://doi.org/10.1371/journal.pone.0091312.

Tidyman, William E, and Katherine A Rauen. 2009. 'The RASopathies: Developmental Syndromes of Ras/MAPK Pathway Dysregulation'. Current Opinion in Genetics & Development 19 (3): 230–36. https://doi.org/10.1016/j.gde.2009.04.001.

Tidyman, William E., and Katherine A. Rauen. 2016. 'Expansion of the RASopathies'. Current Genetic Medicine Reports 4 (3): 57–64. https://doi.org/10.1007/s40142-016-0100-7.

Tobimatsu, T., and H. Fujisawa. 1989. 'Tissue-Specific Expression of Four Types of Rat Calmodulin-Dependent Protein Kinase II MRNAs.' Journal of Biological Chemistry 264 (30): 17907–12.

Tolias, Kimberley F., Jay B. Bikoff, Christina G. Kane, Christos S. Tolias, Linda Hu, and Michael E. Greenberg. 2007. 'The Rac1 Guanine Nucleotide Exchange Factor Tiam1 Mediates EphB Receptor-Dependent Dendritic Spine Development'. Proceedings of the National Academy of Sciences 104 (17): 7265–70. https://doi.org/10.1073/pnas.0702044104.

Toll-Riera, Macarena, Núria Radó-Trilla, Florian Martys, and M. Mar Albà. 2012. 'Role of Low-Complexity Sequences in the Formation of Novel Protein Coding Sequences'. Molecular Biology and Evolution 29 (3): 883–86. https://doi.org/10.1093/molbev/msr263.

Tomoda, T., Kim, J.H., Zhan, C., and Hatten, M.E. (2004). Role of Unc51.1 and its binding partners in CNS axon outgrowth. Genes Dev. 18, 541–558.

Tomoda, Toshifumi, Jee Hae Kim, Caixin Zhan, and Mary E. Hatten. 2004. 'Role of Unc51.1 and Its Binding Partners in CNS Axon Outgrowth'. Genes & Development 18 (5): 541–58. https://doi.org/10.1101/gad.1151204.

Torres, Viviana I., and Nibaldo C. Inestrosa. 2018. 'Vertebrate Presynaptic Active Zone Assembly: A Role Accomplished by Diverse Molecular and Cellular Mechanisms'. Molecular Neurobiology 55 (6): 4513–28. https://doi.org/10.1007/s12035-017-0661-9.

Torre-Ubieta, Luis de la, Hyejung Won, Jason L. Stein, and Daniel H. Geschwind. 2016. 'Advancing the Understanding of Autism Disease Mechanisms through Genetics'. Nature Medicine 22 (4): 345–61. https://doi.org/10.1038/nm.4071.

Traynelis, Stephen F., Lonnie P. Wollmuth, Chris J. McBain, Frank S. Menniti, Katie M. Vance, Kevin K. Ogden, Kasper B. Hansen, Hongjie Yuan, Scott J. Myers, and Ray Dingledine. 2010. 'Glutamate Receptor Ion Channels: Structure, Regulation, and Function'. Pharmacological Reviews 62 (3): 405–96. https://doi.org/10.1124/pr.109.002451.

Trinidad, Jonathan C., Agnes Thalhammer, Christian G. Specht, Aenoch J. Lynn, Peter R. Baker, Ralf Schoepfer, and Alma L. Burlingame. 2008. 'Quantitative Analysis of Synaptic Phosphorylation and Protein Expression'. Molecular & Cellular Proteomics 7 (4): 684–96. https://doi.org/10.1074/mcp.M700170-MCP200.

Tsai, M. H., C. L. Yu, and D. W. Stacey. 1990. 'A Cytoplasmic Protein Inhibits the GTPase Activity of H-Ras in a Phospholipid-Dependent Manner'. Science 250 (4983): 982–85. https://doi.org/10.1126/science.2237442.

Tsai, M. H., C. L. Yu, F. S. Wei, and D. W. Stacey. 1989. 'The Effect of GTPase Activating Protein upon Ras Is Inhibited by Mitogenically Responsive Lipids'. Science (New York, N.Y.) 243 (4890): 522–26.

Turrigiano, Gina G. 2008. 'The Self-Tuning Neuron: Synaptic Scaling of Excitatory Synapses'. Cell 135 (3): 422–35. https://doi.org/10.1016/j.cell.2008.10.008.

Turrigiano, Gina G., Kenneth R. Leslie, Niraj S. Desai, Lana C. Rutherford, and Sacha B. Nelson. 1998. 'Activity-Dependent Scaling of Quantal Amplitude in Neocortical Neurons'. Nature 391 (6670): 892–96. https://doi.org/10.1038/36103.

Turrigiano, Gina. 2011. 'Too Many Cooks? Intrinsic and Synaptic Homeostatic Mechanisms in Cortical Circuit Refinement'. Annual Review of Neuroscience 34 (1): 89–103. https://doi.org/10.1146/annurev-neuro-060909-153238.

Tyzio, Roman, Gregory L. Holmes, Yehezkiel Ben-Ari, and Roustem Khazipov. 2007. 'Timing of the Developmental Switch in GABA(A) Mediated Signaling from Excitation to Inhibition in CA3 Rat Hippocampus Using Gramicidin Perforated Patch and Extracellular Recordings'. Epilepsia 48 Suppl 5: 96–105. https://doi.org/10.1111/j.1528-1167.2007.01295.x.

Ustianenko, Dmytro, Sebastien M. Weyn-Vanhentenryck, and Chaolin Zhang. 2017. 'Microexons: Discovery, Regulation, and Function'. Wiley Interdisciplinary Reviews. RNA 8 (4). https://doi.org/10.1002/wrna.1418.

Valenti, Daniela, Lidia de Bari, Bianca De Filippis, Alexandra Henrion-Caude, and Rosa Anna Vacca. 2014. 'Mitochondrial Dysfunction as a Central Actor in Intellectual Disability-Related Diseases: An Overview of Down Syndrome, Autism, Fragile X and Rett Syndrome'. Neuroscience & Biobehavioral Reviews, Common mechanisms in intellectual disabilities: a challenge for translational outlooks, 46 (October): 202–17. https://doi.org/10.1016/j.neubiorev.2014.01.012.

Vallejo, Daniela, Juan F. Codocedo, and Nibaldo C. Inestrosa. 2017. 'Posttranslational Modifications Regulate the Postsynaptic Localization of PSD-95'. Molecular Neurobiology 54 (3): 1759–76. https://doi.org/10.1007/s12035-016-9745-1.

Van Esch, Hilde, Marijke Bauters, Jaakko Ignatius, Mieke Jansen, Martine Raynaud, Karen Hollanders, Dorien Lugtenberg, et al. 2005. 'Duplication of the MECP2 Region Is a Frequent Cause of Severe Mental Retardation and Progressive Neurological Symptoms in Males'. American Journal of Human Genetics 77 (3): 442–53. https://doi.org/10.1086/444549.

Vaquero, J., T. H. Nguyen Ho-Bouldoires, A. Clapéron, and L. Fouassier. 2017. 'Role of the PDZ-Scaffold Protein NHERF1/EBP50 in Cancer Biology: From Signaling Regulation to Clinical Relevance'. Oncogene 36 (22): 3067–79. https://doi.org/10.1038/onc.2016.462.

Varghese, Merina, Neha Keshav, Sarah Jacot-Descombes, Tahia Warda, Bridget Wicinski, Dara L. Dickstein, Hala Harony-Nicolas, et al. 2017. 'Autism Spectrum Disorder: Neuropathology and Animal Models'. Acta Neuropathologica 134 (4): 537–66. https://doi.org/10.1007/s00401-017-1736-4.

Varoqueaux, Frédérique, Stéphane Jamain, and Nils Brose. 2004. 'Neuroligin 2 Is Exclusively Localized to Inhibitory Synapses'. European Journal of Cell Biology 83 (9): 449–56. https://doi.org/10.1078/0171-9335-00410.

Vaughn, J. E., C. K. Henrikson, and J. A. Grieshaber. 1974. 'A Quantitative Study of Synapses on Motor Neuron Dendritic Growth Cones in Developing Mouse Spinal Cord'. The Journal of Cell Biology 60 (3): 664–72.

Vazquez, Luis E., Hong-Jung Chen, Irina Sokolova, Irene Knuesel, and Mary B. Kennedy. 2004. 'SynGAP Regulates Spine Formation'. Journal of Neuroscience 24 (40): 8862–72. https://doi.org/10.1523/JNEUROSCI.3213-04.2004.

Verkerk, A. J., M. Pieretti, J. S. Sutcliffe, Y. H. Fu, D. P. Kuhl, A. Pizzuti, O. Reiner, S. Richards, M. F. Victoria, and F. P. Zhang. 1991. 'Identification of a Gene (FMR-1) Containing a CGG Repeat Coincident with a Breakpoint Cluster Region Exhibiting Length Variation in Fragile X Syndrome'. Cell 65 (5): 905–14.

Vilariño-Güell, Carles, Christian Wider, Owen A. Ross, Justus C. Dachsel, Jennifer M. Kachergus, Sarah J. Lincoln, Alexandra I. Soto-Ortolaza, et al. 2011. 'VPS35 Mutations in Parkinson Disease'. The American Journal of Human Genetics 89 (1): 162–67. https://doi.org/10.1016/j.ajhg.2011.06.001.

Vincent, Sylvie, and Jeffrey Settleman. 1999. 'Inhibition of RhoGAP Activity Is Sufficient for the Induction of Rho-Mediated Actin Reorganization'. European Journal of Cell Biology 78 (8): 539–48. https://doi.org/10.1016/S0171-9335(99)80019-3.

Visan, Ioana. 2017. 'Neuroimmune Interactions: Astrocytes'. Nature Immunology 18 (February): 254. https://doi.org/10.1038/ni.3700.

Vissers, Lisenka E. L. M., Joep de Ligt, Christian Gilissen, Irene Janssen, Marloes Steehouwer, Petra de Vries, Bart van Lier, et al. 2010. 'A de Novo Paradigm for Mental Retardation'. Nature Genetics 42 (12): 1109–12. https://doi.org/10.1038/ng.712.

Vlaskamp, Danique R. M., Benjamin J. Shaw, Rosemary Burgess, Davide Mei, Martino Montomoli, Han Xie, Candace T. Myers, et al. 2019. 'SYNGAP1 Encephalopathy: A Distinctive Generalized Developmental and Epileptic Encephalopathy'. Neurology 92 (2): e96–107. https://doi.org/10.1212/WNL.0000000000006729.

Walkup, Ward G., Lorraine Washburn, Michael J. Sweredoski, Holly J. Carlisle, Robert L. Graham, Sonja Hess, and Mary B. Kennedy. 2015. 'Phosphorylation of Synaptic GTPase-Activating Protein (SynGAP) by Ca2+/Calmodulin-Dependent Protein Kinase II (CaMKII) and Cyclin-Dependent Kinase 5 (CDK5) Alters the Ratio of Its GAP Activity toward Ras and Rap GTPases'. The Journal of Biological Chemistry 290 (8): 4908–27. https://doi.org/10.1074/jbc.M114.614420.

Walkup, Ward G., Tara L. Mastro, Leslie T. Schenker, Jost Vielmetter, Rebecca Hu, Ariella Iancu, Meera Reghunathan, Barry Dylan Bannon, and Mary B. Kennedy. 2016. 'A Model for Regulation by SynGAP-A1 of Binding of Synaptic Proteins to PDZ-Domain "Slots" in the Postsynaptic Density'. ELife 5. https://doi.org/10.7554/eLife.16813.

Walsh, Michael J., and Norbert Kuruc. 1992. 'The Postsynaptic Density: Constituent and Associated Proteins Characterized by Electrophoresis, Immunoblotting, and Peptide Sequencing'. Journal of Neurochemistry 59 (2): 667–78. https://doi.org/10.1111/j.1471-4159.1992.tb09421.x.

Walsh, Tony G., Yong Li, Andreas Wersäll, and Alastair W. Poole. 2019. 'Small GTPases in Platelet Membrane Trafficking'. Platelets 30 (1): 31–40. https://doi.org/10.1080/09537104.2018.1535703.

Wang, Chih-Chieh, Richard G. Held, and Benjamin J. Hall. 2013. 'SynGAP Regulates Protein Synthesis and Homeostatic Synaptic Plasticity in Developing Cortical Networks'. PLoS ONE 8 (12). https://doi.org/10.1371/journal.pone.0083941.

Wang, D. S., R. Shaw, J. C. Winkelmann, and G. Shaw. 1994. 'Binding of PH Domains of Beta-Adrenergic Receptor Kinase and Beta-Spectrin to WD40/Beta-Transducin Repeat Containing Regions of the Beta-Subunit of Trimeric G-Proteins'. Biochemical and Biophysical Research Communications 203 (1): 29–35. https://doi.org/10.1006/bbrc.1994.2144.

Wang, Jie, Zhi-Jian Lin, Liu Liu, Hai-Qing Xu, Yi-Wu Shi, Yong-Hong Yi, Na He, and Wei-Ping Liao. 2017. 'Epilepsy-Associated Genes'. Seizure, 25th Anniversary Issue, 44 (January): 11–20. https://doi.org/10.1016/j.seizure.2016.11.030.

Wang, Xinjun, Chunzhao Zhang, Gábor Szábo, and Qian-Quan Sun. 2013. 'Distribution of CaMKIIα Expression in the Brain in Vivo, Studied by CaMKIIα-GFP Mice'. Brain Research 1518 (June): 9–25. https://doi.org/10.1016/j.brainres.2013.04.042.

Wang, Xinxing, Rachel Kery, and Qiaojie Xiong. 2018. 'Synaptopathology in Autism Spectrum Disorders: Complex Effects of Synaptic Genes on Neural Circuits'. Progress in Neuro-Psychopharmacology and Biological Psychiatry, Synaptic Basis of Mental Illness, 84 (June): 398–415. https://doi.org/10.1016/j.pnpbp.2017.09.026.

Wang, Yun, Henry Markram, Philip H Goodman, Thomas K Berger, Junying Ma, and Patricia S Goldman-Rakic. 2006. 'Heterogeneity in the Pyramidal Network of the Medial Prefrontal Cortex'. Nature Neuroscience 9 (March): 534.

Watson, Charles, George Paxinos, and Luis Puelles. 2012. The Mouse Nervous System. Academic Press.

Weldon, Monica, Murat Kilinc, J. Lloyd Holder, and Gavin Rumbaugh. 2018. 'The First International Conference on SYNGAP1-Related Brain Disorders: A Stakeholder Meeting of Families, Researchers, Clinicians, and Regulators'. Journal of Neurodevelopmental Disorders 10 (February). https://doi.org/10.1186/s11689-018-9225-1.

Welsh, John P., Edward S. Ahn, and Dimitris G. Placantonakis. 2005. 'Is Autism Due to Brain Desynchronization?' International Journal of Developmental Neuroscience, Autism: Modeling Human Brain Abnormalities in Developing Animal Systems, 23 (2): 253–63. https://doi.org/10.1016/j.ijdevneu.2004.09.002.

Weng, S. -M., F. McLeod, M. E. S. Bailey, and S. R. Cobb. 2011. 'Synaptic Plasticity Deficits in an Experimental Model of Rett Syndrome: Long-Term Potentiation Saturation and Its Pharmacological Reversal'. Neuroscience 180 (April): 314–21. https://doi.org/10.1016/j.neuroscience.2011.01.061.

Wennerberg, K. 2005. 'The Ras Superfamily at a Glance'. Journal of Cell Science 118 (5): 843–46. https://doi.org/10.1242/jcs.01660.

Westfall, Jane A. 1996. 'Ultrastructure of Synapses in the First-Evolved Nervous Systems'. Journal of Neurocytology 25 (1): 735–46. https://doi.org/10.1007/BF02284838.

Westphal, Ryan S., Steven J. Tavalin, Jerry W. Lin, Neal M. Alto, Iain D. C. Fraser, Lorene K. Langeberg, Morgan Sheng, and John D. Scott. 1999. 'Regulation of NMDA Receptors by an Associated Phosphatase-Kinase Signaling Complex'. Science 285 (5424): 93–96. https://doi.org/10.1126/science.285.5424.93.

Whittaker, V. P. 1984. 'The Synaptosome'. In Structural Elements of the Nervous System, edited by Abel Lajtha, 1–39. Boston, MA: Springer US. https://doi.org/10.1007/978-1-4684-4586-2_1.

Wilkinson, Brent, Jing Li, and Marcelo P. Coba. 2017. 'Synaptic GAP and GEF Complexes Cluster Proteins Essential for GTP Signaling'. Scientific Reports 7 (July). https://doi.org/10.1038/s41598-017-05588-3.

Wilkinson, Kevin A., Yasuko Nakamura, and Jeremy M. Henley. 2010. 'Targets and Consequences of Protein SUMOylation in Neurons'. Brain Research Reviews 64 (1): 195–212. https://doi.org/10.1016/j.brainresrev.2010.04.002.

Willard, Stacey S., and Shahriar Koochekpour. 2013. 'Glutamate, Glutamate Receptors, and Downstream Signaling Pathways'. International Journal of Biological Sciences 9 (9): 948–59. https://doi.org/10.7150/ijbs.6426.

Williams, Sylvain, and Patricia Boksa. 2010. 'Gamma Oscillations and Schizophrenia'. Journal of Psychiatry & Neuroscience : JPN 35 (2): 75–77. https://doi.org/10.1503/jpn.100021.

Wit, Joris de, Emily Sylwestrak, Matthew L. O'Sullivan, Stefanie Otto, Katie Tiglio, Jeffrey N. Savas, John R. Yates, Davide Comoletti, Palmer Taylor, and Anirvan Ghosh. 2009. 'LRRTM2 Interacts with Neurexin1 and Regulates Excitatory Synapse Formation'. Neuron 64 (6): 799–806. https://doi.org/10.1016/j.neuron.2009.12.019.

Wolf, Nicole I., Thomas Bast, and Robert Surtees. 2005. 'Epilepsy in Inborn Errors of Metabolism'. Epileptic Disorders: International Epilepsy Journal with Videotape 7 (2): 67–81.

Won, Hyejung, Hye-Ryeon Lee, Heon Yung Gee, Won Mah, Jae-Ick Kim, Jiseok Lee, Seungmin Ha, et al. 2012. 'Autistic-like Social Behaviour in Shank2-Mutant Mice Improved by Restoring NMDA Receptor Function'. Nature 486 (7402): 261–65. https://doi.org/10.1038/nature11208.

Won, Hyejung, Won Mah, and Eunjoon Kim. 2013. 'Autism Spectrum Disorder Causes, Mechanisms, and Treatments: Focus on Neuronal Synapses'. Frontiers in Molecular Neuroscience 6 (August). https://doi.org/10.3389/fnmol.2013.00019.

Wong, Rachel O. L., and Anirvan Ghosh. 2002. 'Activity-Dependent Regulation of Dendritic Growth and Patterning'. Nature Reviews. Neuroscience 3 (10): 803–12. https://doi.org/10.1038/nrn941.

Woo, Jooyeon, Seok-Kyu Kwon, Jungyong Nam, Seungwon Choi, Hideto Takahashi, Dilja Krueger, Joohyun Park, et al. 2013. 'The Adhesion Protein IgSF9b Is Coupled to Neuroligin 2 via S-SCAM to Promote Inhibitory Synapse Development'. The Journal of Cell Biology 201 (6): 929–44. https://doi.org/10.1083/jcb.201209132.

Wood, Sandra L., Bruce K. Beyer, and Gregg D. Cappon. 2003. 'Species Comparison of Postnatal CNS Development: Functional Measures'. Birth Defects Research. Part B, Developmental and Reproductive Toxicology 68 (5): 391–407. https://doi.org/10.1002/bdrb.10037.

Workman, Alan D., Christine J. Charvet, Barbara Clancy, Richard B. Darlington, and Barbara L. Finlay. 2013. 'Modeling Transformations of Neurodevelopmental Sequences across Mammalian Species'. The Journal of Neuroscience: The Official Journal of the Society for Neuroscience 33 (17): 7368–83. https://doi.org/10.1523/JNEUROSCI.5746-12.2013.

Writzl, Karin, and Alida C. Knegt. 2013. '6p21.3 Microdeletion Involving the SYNGAP1 Gene in a Patient with Intellectual Disability, Seizures, and Severe Speech Impairment'. American Journal of Medical Genetics Part A 161 (7): 1682–85. https://doi.org/10.1002/ajmg.a.35930.

Wu, Min, Hong-Lei Tian, Xiaobo Liu, John Ho Chun Lai, Shengwang Du, and Jun Xia. 2018. 'Impairment of Inhibitory Synapse Formation and Motor Behavior in Mice Lacking the NL2 Binding Partner LHFPL4/GARLH4'. Cell Reports 23 (6): 1691–1705. https://doi.org/10.1016/j.celrep.2018.04.015.

Wu, Yingjie, Chunxin Wang, Hui Sun, Derek LeRoith, and Shoshana Yakar. 2009. 'High-Efficient FLPo Deleter Mice in C57BL/6J Background'. PloS One 4 (11): e8054. https://doi.org/10.1371/journal.pone.0008054.

Wu, Yong, Yong-Gang Yao, and Xiong-Jian Luo. 2017. 'SZDB: A Database for Schizophrenia Genetic Research'. Schizophrenia Bulletin 43 (2): 459–71. https://doi.org/10.1093/schbul/sbw102.

Xin, Dedong, Landian Hu, and Xiangyin Kong. 2008. 'Alternative Promoters Influence Alternative Splicing at the Genomic Level'. PloS One 3 (6): e2377. https://doi.org/10.1371/journal.pone.0002377.

Xing, Jingrui, Hiroki Kimura, Chenyao Wang, Kanako Ishizuka, Itaru Kushima, Yuko Arioka, Akira Yoshimi, et al. 2016. 'Resequencing and Association Analysis of Six PSD-95-Related Genes as Possible Susceptibility Genes for Schizophrenia and Autism Spectrum Disorders'. Scientific Reports 6 (June). https://doi.org/10.1038/srep27491.

Xu, Bin, Iuliana Ionita-Laza, J Louw Roos, Braden Boone, Scarlet Woodrick, Yan Sun, Shawn Levy, Joseph A Gogos, and Maria Karayiorgou. 2012. 'De Novo Gene Mutations Highlight Patterns of Genetic and Neural Complexity in Schizophrenia'. Nature Genetics 44 (12): 1365–69. https://doi.org/10.1038/ng.2446.

Xu, Bin, Iuliana Ionita-Laza, J Louw Roos, Braden Boone, Scarlet Woodrick, Yan Sun, Shawn Levy, Joseph A Gogos, and Maria Karayiorgou. 2012. 'De Novo Gene Mutations Highlight Patterns of Genetic and Neural Complexity in Schizophrenia'. Nature Genetics 44 (12): 1365–69. https://doi.org/10.1038/ng.2446.

Xu, Gangfeng, Peter O'Connell, David Viskochil, Richard Cawthon, Margaret Robertson, Melanie Culver, Diane Dunn, et al. 1990. 'The Neurofibromatosis Type 1 Gene Encodes a Protein Related to GAP'. Cell 62 (3): 599–608. https://doi.org/10.1016/0092-8674(90)90024-9.

Xu, Qiang, Barmak Modrek, and Christopher Lee. 2002. 'Genome-Wide Detection of Tissue-Specific Alternative Splicing in the Human Transcriptome'. Nucleic Acids Research 30 (17): 3754–66.

Xue, Bin, Roland L. Dunbrack, Robert W. Williams, A. Keith Dunker, and Vladimir N. Uversky. 2010. 'PONDR-FIT: A Meta-Predictor of Intrinsically Disordered Amino Acids'. Biochimica Et Biophysica Acta 1804 (4): 996–1010. https://doi.org/10.1016/j.bbapap.2010.01.011.

Yagami, T., H. Kohma, and Y. Yamamoto. 2012. 'L-Type Voltage-Dependent Calcium Channels As Therapeutic Targets for Neurodegenerative Diseases'. Text. October 2012. https://doi.org/info:doi/10.2174/092986712803341430.

Yamagata, Yoko, Shizuka Kobayashi, Tatsuya Umeda, Akihiro Inoue, Hiroyuki Sakagami, Masahiro Fukaya, Masahiko Watanabe, et al. 2009. 'Kinase-Dead Knock-In Mouse Reveals an Essential Role of Kinase Activity of Ca2+/Calmodulin-Dependent Protein Kinase IIα in Dendritic Spine Enlargement, Long-Term Potentiation, and Learning'. Journal of Neuroscience 29 (23): 7607–18. https://doi.org/10.1523/JNEUROSCI.0707-09.2009.

Yamasaki, Nobuyuki, Motoko Maekawa, Katsunori Kobayashi, Yasushi Kajii, Jun Maeda, Miho Soma, Keizo Takao, et al. 2008. 'Alpha-CaMKII Deficiency Causes Immature Dentate Gyrus, a Novel Candidate Endophenotype of Psychiatric Disorders'. Molecular Brain 1 (September): 6. https://doi.org/10.1186/1756-6606-1-6.

Yamashita, Shigeko, Naoki Mochizuki, Yusuke Ohba, Minoru Tobiume, Yuki Okada, Hirofumi Sawa, Kazuo Nagashima, and Michiyuki Matsuda. 2000. 'CalDAG-GEFIII Activation of Ras, R-Ras, and Rap1'. Journal of Biological Chemistry 275 (33): 25488–93. https://doi.org/10.1074/jbc.M003414200.

Yang, S.-N., Huang, C.-B., Yang, C.-H., Lai, M.-C., Chen, W.-F., Wang, C.-L., Wu, C.-L., and Huang, L.-T. (2004). Impaired SynGAP expression and long-term spatial learning and memory in hippocampal CA1 area from rats previously exposed to perinatal hypoxia-induced insults: beneficial effects of A68930. Neurosci. Lett. 371, 73–78.

Yang, San-Nan, Chung-Bin Huang, Chin-Hwa Yang, Ming-Chi Lai, Wu-Fu Chen, Chih-Lu Wang, Chia-Lu Wu, and Li-Tung Huang. 2004. 'Impaired SynGAP Expression and Long-Term Spatial Learning and Memory in Hippocampal CA1 Area from Rats Previously Exposed to Perinatal Hypoxia-Induced Insults: Beneficial Effects of A68930'. Neuroscience Letters 371 (1): 73–78. https://doi.org/10.1016/j.neulet.2004.08.044.

Yang, Yijung, Jung-Hwa Tao-Cheng, K. Ulrich Bayer, Thomas S. Reese, and Ayse Dosemeci. 2013. 'Camkii-Mediated Phosphorylation Regulates Distributions of Syngap-A1 and –A2 at the Postsynaptic Density'. PLoS ONE 8 (8). https://doi.org/10.1371/journal.pone.0071795.

Yang, Yijung, Jung-Hwa Tao-Cheng, Thomas S. Reese, and Ayse Dosemeci. 2011. 'SynGAP Moves out of the Core of the Postsynaptic Density upon Depolarization'. Neuroscience 192 (September): 132–39. https://doi.org/10.1016/j.neuroscience.2011.06.061.

Yao, L., Y. Kawakami, and T. Kawakami. 1994. 'The Pleckstrin Homology Domain of Bruton Tyrosine Kinase Interacts with Protein Kinase C'. Proceedings of the National Academy of Sciences of the United States of America 91 (19): 9175–79.

Ye, Jian, George Coulouris, Irena Zaretskaya, Ioana Cutcutache, Steve Rozen, and Thomas L. Madden. 2012. 'Primer-BLAST: A Tool to Design Target-Specific Primers for Polymerase Chain Reaction'. BMC Bioinformatics 13 (1): 134. https://doi.org/10.1186/1471-2105-13-134.

Ye, Xiaojing, and Thomas J. Carew. 2010. 'Small G Protein Signaling in Neuronal Plasticity and Memory Formation: The Specific Role of Ras Family Proteins'. Neuron 68 (3): 340–61. https://doi.org/10.1016/j.neuron.2010.09.013.

Yeo, Gene, Dirk Holste, Gabriel Kreiman, and Christopher B. Burge. 2004. 'Variation in Alternative Splicing across Human Tissues'. Genome Biology 5 (10): R74. https://doi.org/10.1186/gb-2004-5-10-r74.

Yeung, Natalie, Melissa S. Cline, Allan Kuchinsky, Michael E. Smoot, and Gary D. Bader. 2008. 'Exploring Biological Networks with Cytoscape Software'. In Current Protocols in Bioinformatics, edited by Alex Bateman, William R. Pearson, Lincoln D. Stein, Gary D. Stormo, and John R. Yates, 8.13.1-8.13.20. Hoboken, NJ, USA: John Wiley & Sons, Inc. https://doi.org/10.1002/0471250953.bi0813s23.

Yizhar, Ofer, Lief E. Fenno, Matthias Prigge, Franziska Schneider, Thomas J. Davidson, Daniel J. O'Shea, Vikaas S. Sohal, et al. 2011. 'Neocortical Excitation/Inhibition Balance in Information Processing and Social Dysfunction'. Nature 477 (7363): 171–78. https://doi.org/10.1038/nature10360.

Yokoi, Satoshi, Tsuyoshi Udagawa, Yusuke Fujioka, Daiyu Honda, Haruo Okado, Hirohisa Watanabe, Masahisa Katsuno, Shinsuke Ishigaki, and Gen Sobue. 2017. '3′UTR Length-Dependent Control of SynGAP Isoform A2 MRNA by FUS and ELAV-like Proteins Promotes Dendritic Spine Maturation and Cognitive Function'. Cell Reports 20 (13): 3071–84. https://doi.org/10.1016/j.celrep.2017.08.100.

Yoshii, Akira, Morgan H. Sheng, and Martha Constantine-Paton. 2003. 'Eye Opening Induces a Rapid Dendritic Localization of PSD-95 in Central Visual Neurons'. Proceedings of the National Academy of Sciences 100 (3): 1334–39. https://doi.org/10.1073/pnas.0335785100.

Yoshimura, Yoshiyuki, Takashi Shinkawa, Masato Taoka, Kana Kobayashi, Toshiaki Isobe, and Takashi Yamauchi. 2002. 'Identification of Protein Substrates of Ca2+/Calmodulin-Dependent Protein Kinase II in the Postsynaptic Density by Protein Sequencing and Mass Spectrometry'. Biochemical and Biophysical Research Communications 290 (3): 948–54. https://doi.org/10.1006/bbrc.2001.6320.

Yoshimura, Yoshiyuki, Yoshio Yamauchi, Takashi Shinkawa, Masato Taoka, Hitomi Donai, Nobuhiro Takahashi, Toshiaki Isobe, and Takashi Yamauchi. 2004. 'Molecular Constituents of the Postsynaptic Density Fraction Revealed by Proteomic Analysis Using Multidimensional Liquid Chromatography-Tandem Mass Spectrometry'. Journal of Neurochemistry 88 (3): 759–68. https://doi.org/10.1046/j.1471-4159.2003.02136.x.

Yu, Lily MY, and Yukiko Goda. 2009. 'Dendritic Signalling and Homeostatic Adaptation'. Current Opinion in Neurobiology, Signalling mechanisms, 19 (3): 327–35. https://doi.org/10.1016/j.conb.2009.07.002.

Yuste, 2011. 'Dendritic Spines and Distributed Circuits'. Neuron 71 (5): 772–81. https://doi.org/10.1016/j.neuron.2011.07.024.

Yuste, R., and T. Bonhoeffer. 2001. 'Morphological Changes in Dendritic Spines Associated with Long-Term Synaptic Plasticity'. Annual Review of Neuroscience 24: 1071–89. https://doi.org/10.1146/annurev.neuro.24.1.1071.

Yuste, R., and W. Denk. 1995. 'Dendritic Spines as Basic Functional Units of Neuronal Integration'. Nature 375 (6533): 682–84. https://doi.org/10.1038/375682a0.

Yuste, Rafael, and Tobias Bonhoeffer. 2004. Yuste, R. & Bonhoeffer, T. Genesis of Dendritic Spines: Insights from Ultrastructural and Imaging Studies. Nat. Rev. Neurosci. 5, 24-34. Vol. 5. https://doi.org/10.1038/nrn1300.

Yuste, Rafael, and Tobias Bonhoeffer. 2004. Yuste, R. & Bonhoeffer, T. Genesis of Dendritic Spines: Insights from Ultrastructural and Imaging Studies. Nat. Rev. Neurosci. 5, 24-34. Vol. 5. https://doi.org/10.1038/nrn1300.

Yuste, Rafael. 2010. Dendritic Spines. Cambridge, Mass.; London: MIT Press. http://dx.doi.org/10.7551/mitpress/9780262013505.001.0001.

Yuste, Rafael. 2011. 'Dendritic Spines and Distributed Circuits'. Neuron 71 (5): 772–81. https://doi.org/10.1016/j.neuron.2011.07.024.

Zeng, M., Bai, G., and Zhang, M. (2017). Anchoring high concentrations of SynGAP at postsynaptic densities via liquid-liquid phase separation. Small GTPases 0, 1–9

Zeng, Menglong, Guanhua Bai, and Mingjie Zhang. 2017. 'Anchoring High Concentrations of SynGAP at Postsynaptic Densities via Liquid-Liquid Phase Separation'. Small GTPases 0 (0): 1–9. https://doi.org/10.1080/21541248.2017.1320350.

Zeng, Menglong, Yuan Shang, Tingfeng Guo, Qinghai He, Wing-Ho Yung, Kai Liu, and Mingjie Zhang. 2016. 'A Binding Site Outside the Canonical PDZ Domain Determines the Specific Interaction between Shank and SAPAP and Their Function'. Proceedings of the National Academy of Sciences of the United States of America 113 (22): E3081-3090. https://doi.org/10.1073/pnas.1523265113.

Zhai, Rong Grace, Hagit Vardinon-Friedman, Claudia Cases-Langhoff, Birgit Becker, Eckart D. Gundelfinger, Noam E. Ziv, and Craig C. Garner. 2001. 'Assembling the Presynaptic Active Zone: A Characterization of an Active Zone Precursor Vesicle'. Neuron 29 (1): 131–43. https://doi.org/10.1016/S0896-6273(01)00185-4.

Zhang, Guoan, Thomas A. Neubert, and Bryen A. Jordan. 2012. 'RNA Binding Proteins Accumulate at the Postsynaptic Density with Synaptic Activity'. Journal of Neuroscience 32 (2): 599–609. https://doi.org/10.1523/JNEUROSCI.2463-11.2012.

Zhang, Jichuan, Ya Yang, Hongbin Li, Jun Cao, and Lin Xu. 2005. 'Amplitude/Frequency of Spontaneous MEPSC Correlates to the Degree of Long-Term Depression in the CA1 Region of the Hippocampal Slice'. Brain Research 1050 (1): 110–17. https://doi.org/10.1016/j.brainres.2005.05.032.

Zhang, Jingping, Tai-Xiang Xu, Penelope J. Hallett, Masahiko Watanabe, Seth G. N. Grant, Ole Isacson, and Wei-Dong Yao. 2009. 'PSD-95 Uncouples Dopamine-Glutamate Interaction in the D1/PSD-95/NMDA Receptor Complex'. The Journal of Neuroscience: The Official Journal of the Society for Neuroscience 29 (9): 2948–60. https://doi.org/10.1523/JNEUROSCI.4424-08.2009.

Zhang, Wandong, and Deanna Benson. 2000. Development and Molecular Organization of Dendritic Spines and Their Synapses. Vol. 10. https://doi.org/10.1002/1098-1063(2000)10:5<512::AID-HIPO2>3.0.CO;2-M.

Zhang, Wandong, Luis Vazquez, Michelle Apperson, and Mary B. Kennedy. 1999. 'Citron Binds to PSD-95 at Glutamatergic Synapses on Inhibitory Neurons in the Hippocampus'. Journal of Neuroscience 19 (1): 96–108. https://doi.org/10.1523/JNEUROSCI.19-01-00096.1999.

Zheng, Sika, Erin E. Gray, Geetanjali Chawla, Bo Torben Porse, Thomas J. O'Dell, and Douglas L. Black. 2012. 'Psd-95 Is Post-Transcriptionally Repressed during Early Neural Development by PTBP1 and PTBP2'. Nature Neuroscience 15 (3): 381-S1. https://doi.org/10.1038/nn.3026.

Zhou, Shanglin, and Yuguo Yu. 2018. 'Synaptic E-I Balance Underlies Efficient Neural Coding'. Frontiers in Neuroscience 12 (February). https://doi.org/10.3389/fnins.2018.00046.

Zhu, Fei, Mélissa Cizeron, Zhen Qiu, Ruth Benavides-Piccione, Maksym V. Kopanitsa, Nathan G. Skene, Babis Koniaris, et al. 2018. 'Architecture of the Mouse Brain Synaptome'. Neuron 99 (4): 781-799.e10. https://doi.org/10.1016/j.neuron.2018.07.007.

Zhu, J. Julius, Yi Qin, Mingming Zhao, Linda Van Aelst, and Roberto Malinow. 2002. 'Ras and Rap Control AMPA Receptor Trafficking during Synaptic Plasticity'. Cell 110 (4): 443–55. https://doi.org/10.1016/S0092-8674(02)00897-8.

Zhu, Yinghua, Daniel Pak, Yi Qin, Stefanie G. McCormack, Myung J. Kim, Joel P. Baumgart, Vanisree Velamoor, et al. 2005. 'Rap2-JNK Removes Synaptic AMPA Receptors during Depotentiation'. Neuron 46 (6): 905–16. https://doi.org/10.1016/j.neuron.2005.04.037.

Zimmer, Manuel, Amparo Palmer, Jenny Köhler, and Rüdiger Klein. 2003. 'EphB-EphrinB Bi-Directional Endocytosis Terminates Adhesion Allowing Contact Mediated Repulsion'. Nature Cell Biology 5 (10): 869–78. https://doi.org/10.1038/ncb1045.

Ziv, Noam E., and Naama Brenner. 2018. 'Synaptic Tenacity or Lack Thereof: Spontaneous Remodeling of Synapses'. Trends in Neurosciences 41 (2): 89–99. https://doi.org/10.1016/j.tins.2017.12.003.

Ziv, Noam E., and Stephen J Smith. 1996. 'Evidence for a Role of Dendritic Filopodia in Synaptogenesis and Spine Formation'. Neuron 17 (1): 91–102. https://doi.org/10.1016/S0896-6273(00)80283-4.

Zoghbi, H. Y., and M. F. Bear. 2012. 'Synaptic Dysfunction in Neurodevelopmental Disorders Associated with Autism and Intellectual Disabilities'. Cold Spring Harbor Perspectives in Biology 4 (3): a009886–a009886. https://doi.org/10.1101/cshperspect.a009886.

Zollino, Marcella, Fiorella Gurrieri, Daniela Orteschi, Giuseppe Marangi, Vincenzo Leuzzi, and Giovanni Neri. 2011. 'Integrated Analysis of Clinical Signs and Literature Data for the Diagnosis and Therapy of a Previously Undescribed 6p21.3 Deletion Syndrome'. European Journal of Human Genetics 19 (2): 239–42. https://doi.org/10.1038/ejhg.2010.172.